Landolt-Börnstein
Numerical Data and Functional Relationships in Science and Technology
New Series / Editor in Chief: W. Martienssen

Group I: Elementary Particles, Nuclei and Atoms
Volume 17

Photon and Electron Interactions with Atoms, Molecules and Ions

Subvolume B
Collisions of Electrons with Atomic Ions

Y. Hahn, A.K. Pradhan,
H. Tawara, H.L. Zhang

Edited by Y. Itikawa

Springer

ISSN 1615-1844 (Elementary Particles, Nuclei and Atoms)

ISBN 3-540-65347-3 Springer-Verlag Berlin Heidelberg New York

Library of Congress Cataloging in Publication Data
Zahlenwerte und Funktionen aus Naturwissenschaften und Technik, Neue Serie
Editor in Chief: W. Martienssen
Vol. I/17B: Editor: Y. Itikawa
At head of title: Landolt-Börnstein. Added t.p.: Numerical data and functional relationships in science and technology.
Tables chiefly in English.
Intended to supersede the Physikalisch-chemische Tabellen by H. Landolt and R. Börnstein of which the 6th ed. began publication in 1950 under title: Zahlenwerte und Funktionen aus Physik, Chemie, Astronomie, Geophysik und Technik.
Vols. published after v. 1 of group I have imprint: Berlin, New York, Springer-Verlag
Includes bibliographies.
1. Physics--Tables. 2. Chemistry--Tables. 3. Engineering--Tables.
I. Börnstein, R. (Richard), 1852-1913. II. Landolt, H. (Hans), 1831-1910.
III. Physikalisch-chemische Tabellen. IV. Title: Numerical data and functional relationships in science and technology.
QC61.23 502'.12 62-53136

Springer-Verlag Berlin Heidelberg New York
a member of BertelsmannSpringer Science+Business Media GmbH

Printed in Germany

Cover layout: Erich Kirchner, Heidelberg
Typesetting: Redaktion Landolt-Börnstein, Darmstadt
Printing: Computer to plate, Mercedes-Druck, Berlin
Binding: Lüderitz & Bauer, Berlin

SPIN: 1070 6187 63/3020 - 5 4 3 2 1 0 – Printed on acid-free paper

Editor

Y. Itikawa
Institute of Space and Astronautical Science,
3-1-1 Yoshinodai, Sagamihara, Kanagawa 229-8510, Japan
e-mail: itikawa@pub.isas.ac.jp

Contributers

Y. Hahn
Department of Physics,
University of Connecticut,
2152 Hillside Road, Storrs, CT 06269-3046,
USA
e-mail: hahn3@uconnvm.uconn.edu
Electron ion recombination processes

A.K. Pradhan
Department of Astronomy,
4017 McPherson Laboratory,
The Ohio State University,
140 West 18th Avenue.,
Columbus, OH 43210-1106, USA
e-mail: pradhan@astronomy.ohio-state.edu
Excitation

H. Tawara
National Institute for Fusion Science,
Toki 509-5292, Japan
e-mail: tawara@nifs.ac.jp

Physics Department, Kansas State University,
Manhattan, KS 66506-2601, USA
e-mail: tawara@phys.ksu.edu
Ionization
Electron detachment from negative ions

H.L. Zhang
Group X-5, MS F663,
Los Alamos National Laboratory,
Los Alamos, NM 87545, USA
e-mail: zhang@lanl.gov
Excitation

Landolt-Börnstein

Editorial Office
Gagernstr. 8, D-64283 Darmstadt, Germany
fax: +49 (6151) 171760
e-mail: lb@springer.de

Internet
http://www.landolt-boernstein.com/

Preface

Interactions of photons and electrons with atoms, molecules, and ions are fundamental elementary processes in a wide variety of neutral or ionized gases in nature or laboratory. The data on the cross sections or related quantities for those processes are eagerly needed in many fields of application such as astrophysics, atmospheric science, plasma science, radiation physics and chemistry, etc. They are also important in understanding physical or chemical properties of atoms, molecules, and their ions.

Volume I/17 provides cross section data and related quantitative information on the collisions of (*1*) photons with atoms, (*2*) electrons with atoms, (*3*) electrons with atomic ions, (*4*) photons with molecules, and (*5*) electrons with molecules. In particular subvolume B of volume I/17 deals with the interactions of electrons with atomic ions. The scope and the outline of the contents are given in the General Introduction of subvolume A . With the continuing development of experimental technique, as well as with the increasing demands from the application fields, the relevant data are constantly produced. The present volume includes the data available as of early summer of 1999.

I thank all the authors for their enormous efforts to survey uncounted number of publications and to critically compile data from them to be assembled in this volume.

Sagamihara, September 2001 **The Editor**

3 Electron collisions with atomic ions

3.1 Excitation

3.1.1 Introduction

Electron impact excitation of ions is one of the primary processes for spectral formation in laboratory and astrophysical plasmas. The cross sections and rates for a large number of ions are therefore required for the diagnostics and modeling of plasma sources as diverse as the interstellar medium, with temperatures as low as a few degrees Kelvin, and X-ray objects such as supernova remnants or nuclear fusion plasmas at a few million degrees. Owing to the wide range of temperatures a large variety of atomic ions in various ionization stages need to be studied.

Nearly all atomic data for practical applications is obtained theoretically. Experimental measurements are difficult and have been done for a relatively small number of ions and transitions essentially to ascertain the accuracy of theoretical calculations. Theoretical methods have been developed or improved in recent years to meet many of the needs with high precision, although much work remains to be done. Most of the excitation data available is still from earlier works. It is therefore necessary to determine the accuracy of the excitation data in literature. A very large number of theoretical calculations have been carried, but mostly in relatively simple approximations that exclude one or the other of the important atomic effects determining the accuracy of the cross sections. On the ohter hand practical applications increasingly require a large number of atomic transitions to be taken into account, such as in non-local thermodynamic equilibrium (NLTE) atomic models for astrophysical spectroscopy. A huge amount of data is required and the users therefore need to be aware of the uncertainties in the available data.

Related to the requirement of theoretical calculations, appropriate methods need to be employed depending on the electronic structure and nuclear charge of the ion and associated atomic effects. Theoretical methods must, in principle, be able to accurately account for both the extensive electron correlation effects and the effect of relativity generally important in multiply charged ions when fine structure must be considered. A brief introduction to the methods and atomic effects, important in the assessment of a given calculation, is given.

In this review we present results from some recent calculations, as well an assessment of recent theoretical data sources compiled in the bibliographies by Itikawa 1996,1998). A comprehensive compilation and evaluation of data up to 1990 was carried out by Pradhan and Gallagher [92P1], including a discussion of the primary methods and atomic effects. The present review is therefore concerned with progress made since 1990 in the theoretical methods and atomic effects (subsection 3.1.2), comparison with new experiments (subsection 3.1.3), scaling laws, analysis of data, and databases (subsection 3.1.4), and data tables and accuracy ratings (subsection 3.1.5). Only those data are presented herein that are of reliable accuracy. For some important ions the data given may be of uncertain accuracy but are the only ones available. A special effort is made to present the data, as compleletly as possible, for all iron ions; these are of special importance in both laboratory and astrophysical sources and comprehensive datasets for the complex low-ionization stages of iron have recently been calculated.

3.1.2 Theory

A number of approximations are usually employed to satisfy the two criteria of correlation and relativistic effects, respectively stated as: (i) coupling between the excited states as manifested, for example, in autoionizing resonances in the energy regions between states, and (ii) angular momenta and spin coupling schemes for the fine structure and relativistic operators in the hamiltonian for the (e + ion) system. Some of the major approximations for (i) are (a) the close coupling (CC) approximation that allows for strong coupling between the states of the target ion, and (b) weak-coupling approximation such as the distorted wave (DW) which accounts only for coupling between the initial and the final target states. Some of the approximations for fine structure transitions are: (a) non-relativisitic re-coupling of the total L and S of the (e + ion) system to yield the total J symmetry, i.e. $\mathbf{L} + \mathbf{S} \longrightarrow \mathbf{J}$, (b) a term-coupling scheme allowing for relativistic atomic structure effects in the target ion alone, (c) intermediate coupling scheme via the Breit-Pauli hamiltonian for the (e + ion), (d) a fully relativistic Dirac hamiltonian.

In electron scattering calculations over the past three decades or so the CC approximation has been widely employed to account for the coupling between the electron scattering channels. The most powerful CC method has proven to be the R-matrix method [93B7] that is particularly suited for calculations for cross sections at a large number of energies needed to resolve resonance structures. The R-matrix method has been extended for cases (a), (b), (c), and (d) to include fine structure and relativistic effects. For exmaple a number of calculations have been carried out in recent years using the Breit-Pauli R-matrix (BPRM) method under the Iron Project [93H1].

For sufficiently highly charged ions the coupling between channels is weak, since the scattering is dominated by the coulomb potential, and the DW approximation yields accurate results. Several formulations of the DW approximation have been developed, for example a package developed by Eissner & Seaton [72E1]. Relativistic effects have also been incorporated into the DW formulation and relativistic distorted wave (RDW) codes have been developed (e.g. Zhang et al. [89Z1]).

Although most of the calculations for electron scattering cross sections have been carried out using the CC or the DW methods, a number of calculations using other approximations are also found in literature.

3.1.2.1 Definitions and formulae

The total (electron + ion) wave function may be represented as

$$\Psi = A \sum_{i=1}^{NF} \psi_i \theta_i + \sum_{j=1} C_j \Phi_J, \tag{1}$$

where ψ_i is a target ion wave function in a specific state $S_i\ L_i$ and θ_i is the wave function for the free electron in a channel labeled as $S_i L_i k_i^2 \ell_i (SL\pi)$, k_i^2 being its incident kinetic energy relative to $E(S_i L_i)$ and ℓ_i its orbital angular momentum. The total number of free channels is NF ("open" or "closed" according to whether $k_i^2 <$ or $> E(S_i L_i)$. A is the antisymmetrization operator for all $N + 1$ electron bound states, with C_j as variational coefficients. The second sum in Eq. (1) represents short-range correlation effects and orthogonality constraints between the continuum electron and the one-electron orbitals in the target. The radial asymptotic form of θ_i is expressed as follows:

$$F_i(r) \underset{r\to\infty}{\sim} \sin(\xi r) + \cos(\xi r)\, \tilde{K}, \tag{2}$$

where ξ is the Coulomb phase and $\tilde{K}$ is a real matrix called the *reactance* matrix. The *scattering matrix*, which is complex, is given by

$$\tilde{S} = (1 + \mathrm{i}\tilde{K})(1 - \mathrm{i}\tilde{K})^{-1}, \tag{3}$$

and the *collision strength* for the transition from the initial state of the target ion S_iL_i to the final state S_jL_j is

$$\Omega(S_iL_i - S_jL_j) = \frac{1}{2}\sum_{SL\pi}\sum_{\ell_i\ell_j}(2S+1)(2L+1)|S^{SL\pi}(S_iL_i\ell_i - S_jL_j\ell_j)|^2, \tag{4}$$

where $SL\pi$ is the total (e + ion) symmetry, i.e. the total spin and orbital angular momenta and parity, and $\ell_i\ell_j$ are contributing partial waves of the incident, scattering electron. The *cross section* Q is expressed in terms of the collision strength as

$$Q(i,j) = \frac{\Omega(i,j)}{\omega_i k_i^2}(\pi a_o^2), \tag{5}$$

in units of Bohr area, ($\omega_i = (2S_i+1)(2L_i+1)$ and $\pi a_0^2 = 8.797\times10^{-17}\text{cm}^2$); k_i^2 is the energy of the incident electron in Rydbergs (1 Ryd = 13.61 eV). For practical applications the quantity of interest is the *Maxwellian averaged collision strength*, sometimes referred to as the rate parameter or the *effective collision strength*, given by

$$\Upsilon(T) \text{ or } \gamma(T) = \int_0^\infty \Omega_{ij}(\epsilon_j)e^{-\epsilon_j/kT}d(\epsilon_j/kT). \tag{6}$$

Finally, the excitation *rate coefficient* is given by

$$q_{ij}(T) = \frac{8.63(-6)}{\omega_i T^{1/2}}e^{-E_{ij}/kT}\gamma(T)\ \text{cm}^3\text{s}^{-1}, \tag{7}$$

with T in K and $E_{ij} = E_j - E_i, E_i < E_j$ in Rydbergs ($1/kT = 157885/T$); j is the excited upper state.

It follows from detailed balance that the *de-excitation* rate coefficient ($E_i < E_j$) is given by

$$q_{ji} = q_{ij}\frac{\omega_i}{\omega_j}e^{E_{ij}/kT}. \tag{8}$$

In general Ω is an energy dependent function which consists of a slowly varying part, the background or nonresonant Ω, and a rapidly varying part due to autoionizing resonances that can significantly affect the scattering rate.

3.1.2.2 Principal methods

This section describes briefly the principal methods, the R-matrix and the DW methods, employed in most of the computations.

3.1.2.2.1 The close coupling approximation and the R-matrix method

The Schrödinger equation for the electron-ion collision problem may be expressed in terms of the scattering electron moving in the potential of the target ion. The radial part of the wave function of the scattering electron is written as

$$[\frac{d^2}{dr_i^2} - \frac{\ell_i(\ell_i+1)}{r_i^2} + k_i^2]F(i,r) = 2\sum_{i'}\{V_{ii'} \pm W_{ii'}\}F(i',r), \tag{9}$$

where F is the radial function in a given channel (represented by i or i'). The summation on the RHS of Eq. (9) is over all discrete and continuum states. $V_{ii'}$ and $W_{ii'}$ are direct and exchange potential operators respectively. The $W_{ii'}$ are integral operators and therefore Eq. (9) represents

an infinite set of coupled integro-differential equations. The following sections discuss the various approximations found in literature for solving Eq. (9).

Truncating the sum on the RHS of Eq. (9) to a finite number of excited states of the target ion and solving the remaining coupled equations exactly yields the nCC approximation, where n is the number of states included. The method of solution based on the R-matrix method has been computerized in the RMATRX package of codes developed at the Queen's University of Belfast by P. G. Burke and associates [93B7]. It is important to ensure that the basis set of eigenfunctions that represent the n states of the target ion be obtained with high precision. These atomic structure calculations may be carried out using the computer program CIV3 [75H1], based on the Hartree-Fock method (with configuration interaction) for computing one- electron orbitals, or the program SUPERSTRUCTURE based on a Thomas-Fermi-Dirac-Amaldi type potential [74E1].

The Breit-Pauli R-matrix method [82S1] considers the scattering problem in intermediate coupling to take account of relativistic effects. The $(N+1)$-electron Breit-Pauli hamiltonian includes the one-body, non-fine structure mass-velocity and Darwin terms, and the spin-orbit interaction leading to fine structure. The one-body non-fine- structure operators and may be included in R-matrix calculations in an otherwise LS-coupling non-relativistic calculation. In the full BPRM calculations the total angular momenta states are LSJ and parity.

3.1.2.2.2 The distorted wave and the relativistic distorted wave approximations

Usually for ions more than two or three times ionized, the distorted wave (DW) method can be used, since coupling is not very strong. In the DW method the relavant matrix elements need include only the initial and final states. However, the method allows for the distortion of the channel wave functions, from their asymptotic Coulomb form, in the target potential. The collision strength in terms of the transition matrix $\tilde{T}$ is

$$\Omega(i-j) = \frac{1}{2}\sum_{s_i,s_j} \omega |T(s_i;s_j)|^2, \tag{10}$$

where i and j are the initial and final target states in appropriate representation, s_i and s_j represent the overall quantum numbers of the $(N+1)$-electron ion, obtained by coupling the continuum functions to the target states, and ω is the corresponding statistical weight, such as $(2S+1)(2L+1)$ in Eq. (4) for LS coupling. The $\tilde{T}$-matrix elements are obtained from the $\tilde{S}$ matrix as

$$\tilde{T} = 1 - \tilde{S} = -2\mathrm{i}\tilde{K}(1-\mathrm{i}\tilde{K})^{-1} \simeq -2\mathrm{i}\tilde{K}, \tag{11}$$

where the last expression indicates that the unitarity constraint is neglected, valid for highly-charged ions in which $\tilde{K}$-matrix elements are usually much smaller than unity. It is generally accepted that, for ion charge $Z > 30$, a fully relativistic treatment is preferred.

The DW results for electron-ion scattering are usually accurate for highly charged ions or for high energies and should be a good complement to the CC results. Most DW results in literacture usually do not include resonance contributions. However, there are a number of ways to include the resonance contributions. In the UCL formulation, bound channel wave functions can be introduced in the total eigenfunction expansion for the (e + ion) system. These give rise to poles in the scattering matrix in the continuum energy region and thus account for a limited number of resonances in the cross sections. Another way to implement the resonances is that described by Cowan [80C1] as a two step process of electron capture followed by autoionization with radiative decay of the continuum included.

For ions with very high Z, i.e., $Z > 50$, the lowest order of QED corrections, in particular the generalized Breit interaction, to the Coulomb interaction in the scattering matrix, could be important, especially for excitation of the $1s$ orbital. The effect of the generalized Breit interaction on electon-ion scattering was first studied by Walker [75W1] for H-like ions. Fontes et al. [93F1]

studied this effect for more complex ions and included it as an option in the general RDW codes of Sampson et al. and Zhang et al. [89S1, 89Z1].

In addition to the total cross section for excitation by electron impact, the differential cross section and the partial cross section for transitions between the magnetic sublevels can also be calculated, e.g., Zhang et al. [90Z1] and Inal & Dubau [93I1]. The results for the transitions between the magnetic sublevels are useful for comparison with and interpretation of experimental results in the electron-beam ion-trap (EBIT) experiments. These can also be used to study the polarization of emmision lines. It should be mentioned that results for the hyperfine structrure transitions may also be of astrophysical interest and can be obtained readily [01Z1].

3.1.2.2.3 High partial waves and the Coulomb-Bethe approximation

The basis of the Coulomb-Bethe (CBe) approximation is that the collisional transition may be treated as an induced radiative process. It is employed for optically allowed transitions where, due to the long-range dipole potential involved, it is usually necessary to sum over a large number of orbital angular momenta (ℓ) of the incident electron. The method is valid for ℓ-waves higher than a given ℓ_o, which depends on the ionic charge, and is often used in conjunction with DW or CC approximations for low ℓ-waves. If one takes $\bar{r}$ to be the mean radius of the target ion of charge z, the condition for the validity of the CBe approximation is

$$\ell > (k^2\bar{r}^2 + 2z\bar{r} + \frac{1}{4})^{1/2} - \frac{1}{2} \equiv \ell_0. \tag{12}$$

Thus, for allowed transitions the scattering calculations may be divided according to the sets of partial waves $\ell \leq \ell_o$ and $\ell_o < \ell < \infty$; the former are treated in the DW or CC approximations that take account of the detailed close-range interaction and the latter in the CBe approximation. The partial wave summation for forbidden transitions usually converges for $\ell \geq \ell_0$. A discussion of the general forms of the Born and the Bethe approximations is given by Burgess and Tully [92B5]. The CBe approximation overestimates the cross sections due to the fact that the approximation is invalid for close encounters, i.e. low ℓ-waves and the neglect of coupling among target states. The contribution due to high partial waves is further discussed by Burke and Seaton [86B1] who describe a "top-up" scheme, in LS coupling, implemented as an option in the R-matrix codes.

3.1.2.2.4 The Iron Project

Employing the R-matrix method large-scale close coupling calculations for radiative transitions, oscillator strengths and photoionization cross sections, were carried out under the Opacity Project for astrophysically abundant elements with $Z = 1-14, 16, 18, 20, 26$ in all ionization stages [95O1, 94S5]. Collisional calculations using the BPRM method are now being carried out in a systematic manner under the Iron Project [93H1]. The primary emphasis is on fine structure transitions in all ions of iron and iron-peak elements, although a number of calculations for other atomic systems are also being done. The close coupling calculations may be complemented, for high energies and partial waves, by the other methods discussed above such as the DW, RDW, or CBe. This is often necessary since the close coupling method is intended for low energies and partial waves (typically $\ell \sim 10$) requiring a detailed consideration of short range electron interactions. However for many transitions, such as electric dipole and quadrupole, the partial wave expansion needs to be more extensive for the convergence of the collision strengths, i.e. up to $\ell \sim 10 - 100$.

The Iron Project data is being made available electronically, together with data from the the Opacity Project, in a database called TOPbase/TIPbase [93C3]. Links to the Iron Project work, papers, and data are available from the Web site www.astronomy.ohio-state.edu/∼pradhan.

3.1.2.3 Atomic effects

The primary atomic effects that determine the accuarcy of theoeretical calculation for electron impact excitation, and are usually incoportated in the theoretical methods employed are: (a) electron exchange, (b) coupling between the scattering channels, (c) accuracy of the eigenfunction expansion, i.e. the configuration interaction included to represent the basis of target states, (d) relativistic effects and fine structure when necessary. The uncertainty in a given calculation depends not only on the principal method employed but also on these contributing atomic effects included. The relative importance and magnitude of these effects varies widely from ion to ion. Even within an iso-electronic sequence large variations with Z may be found; for example, pure LS coupling calculations become invalid for some transitions in high Z ions. Another example is where, for the same ion, a close-coupling calculation may be less accurate than a distorted-wave calculation if the target wave functions in the latter take into account configuration interaction but the former do not. Also, at high energies a close-coupling calculation may not be accurate if the target states corresponding to the incident electron energies are not explicitly included in the target eigenfunction expansion, although otherwise it may represent short range electron correlation accurately and the low-lying transition cross sections may be reliable at low energies.

Following is brief description of the atomic effects.

3.1.2.3.1 Electron exchange

Almost all present day calculations fully include electron exchange. However, there are still many older sources of data in literature that are from calculations neglecting exchange [92P1]. The total (e + ion) wave function should be an antisymmetrized product of the $N+1$ electron wave function in the system with N electrons in a bound state of the target ion and one free electron. It has been shown that apart from spin-flip transitions, which proceed only through electron exchange, it may be necessary to include exchange even for optically allowed transitions when the low ℓ-wave contribution is significant, e.g., $1\,^1\mathrm{S} - 2\,^1\mathrm{P}$ in He-like ions where neglect of exchange leads to an error of about 50% (see Fig. 1 in [92P1]).

3.1.2.3.2 Channel-coupling

For low-stages of ionization, with energetically closely spaced energy levels, electron scattering couples the probabilities of excitation of more than one level. When the coupling between the initial and the final levels is comparable to or weaker than the coupling with other levels included in the target expansion, then the scattered electron flux is diverted to those other states and coupling effects may significantly affect the cross sections. Thus the weak-coupling approximations such as the Born or the CB tend to overestimate the cross sections. As the ion charge increases, the nuclear Coulomb potential dominates the electron-electron interaction and correlation effects (such as exchange and coupling) decrease in importance. Whereas for neutrals and once or twice charged ions coupling between several states is usually strong and only a close-coupling calculation may yield accurate results, for multiply charged ions a distorted-wave treatment often suffices. Optically allowed transitions are generally not affected much, however, although there are exceptions such as in Li-like ions where the $2\mathrm{p} - 3\mathrm{s}$ transition is strongly influenced by the stronger coupling between the 2p and the 3d. In such cases, resonance contributions to the cross sections are also large [81H1].

3.1.2.3.3 Target representation

An accurate representation for the wave functions of the target ion is essential to obtain accurate cross sections since the error is of the first order with respect to the error in the target ion wave functions. For complex atomic systems (e.g. low ionization stages of iron; see Refs. in Bautista and Pradhan 1998 [98B5]) it is necessary to include a large configuraton interaction (CI) basis in order to obtain the proper wave functions for states of various target (angular + spin) symmetries $SL\pi$. The accuracy may be judged by comparing the calculated eigenenergies and the oscillator strengths (in the length and the velocity formulation) with experimental or other theoretical data for the states of interest in the collision. The advent of increasingly powerful serial and massively parallel supercomputers has enabled some very large atomic systems to be dealt with, e.g. Fe II [95Z1]. To circumvent the problem of computer memory restrictions, the target state expansion may include pseudo-states, with adjustable parameters in the total eigenfunction expansion over the target states for additional CI. Transitions involving the pseudo-states themselves are ignored. Single configuration (SC) calculations are generally less accurate than the ones including CI. In the asymptotic region the coupling potentials are proportional to $\sqrt{f}$ where f is the corresponding oscillator strength. It is therefore particularly important that the wavefunctions used should give accurate results for these oscillator strengths.

3.1.2.3.4 Relativistic effects

As mentioned earlier, the relativistic effects may be taken into account in several ways. However, the necessity to include these, and the method to be employed, depends on the ion under consideration. As the ion charge increases, relativistic effects may become prominent and have to be considered explicitly. For low-Z or z (nuclear charge or ionization state) ions the cross sections for fine structure transitions may be obtained by a pure algebraic transformation from the LS to LSJ or an intermediate-coupling scheme e.g., through programs JAJOM or STGFJ as part of the R-matrix package of codes [93H1]. In general, the ratio of the fine structure collision strengths to multiplet collision strengths depends on the recoupling coefficients, but for the case of $S_i = 0$ or $L_i = 0$ we have

$$\frac{\Omega(S_iL_iJ_i, S_jL_jJ_j)}{\Omega(S_iL_i, S_jL_j)} = \frac{(2J_j+1)}{(2S_j+1))(2L_j+1)}. \tag{13}$$

For example, consider the transitions in p^3 open-shell ions where the terms dominated by the ground configuration are: $^4S_{3/2}$, $^2D_{3/2,5/2}$, $^2P_{1/2,3/2}$. The ratio $\Omega(\,^4S_{3/2} - \,^2D_{3/2})/\Omega(\,^4S - \,^2D) = 4/10$ and $\Omega(\,^4S_{3/2} - \,^2D_{5/2})/\Omega(\,^4S - \,^2D) = 6/10$.

As the relativistic effects become larger one may employ three different approaches. The first one, for high-Z and z, is based on the Dirac equation. The Dirac R-matrix package of codes (DARC) has been developed by Norrington and Grant [87N1]. The second method is to generate term coupling coefficients $< S_iL_iJ_i|\Delta_iJ_i >$ which diagonalize the target Hamiltonian including relativistic terms (Breit-Pauli Hamiltonian); Δ_iJ_i is the target state representation in intermediate coupling. These coefficients are then used together with the transformation procedure mentioned above to account for relativistic effects. The second method is incorporated in the program JAJOM or STGFJ [93H1]. The third approach, the BPRM method is by Scott and Taylor [82S1] who extended the close-coupling nonrelativistic RMATRX package to treat the entire electron-ion scattering process in the Breti-Pauli scheme. The BPRM method appears particularly well suited for elements up to the iron group ($Z < 30$) to account for both the electron correlation and the relativistic effects accurately. However, for very heavy and highly charge systems the DARC approach may be needed and further studies are required to determine the precise validity of each of the methods.

A comparison of the various relativisitic approximations, the Dirac R-matrix, BPRM, and term-coupling, for electron scattering with boron-like Fe XXII shows that the term-coupling approximation is not particularly accurate but that there is good agreement between the DARC and the BPRM calculations including the fine structure resonances that are important for several transitions [95Z2, 96A1].

3.1.2.3.5 Radiation damping of autoionizing resonances

In the close coupling approximation the channels corresponding to each target state and angular momemtum of the incident electron, are coupled together. Resonances occur at energies below a target threshold due to coupling between the 'open' channels, corresponding to the excitation of energetically accessible target states, and the 'closed' channels corresponding to higher, energetically inaccessible target states that may be excited during electron collision but leaving the free electron temporarily bound in an autoionising resonant state. The R-matrix calculations include the resonance effects in an ab initio manner and the resonance profiles are obtained in detail by calculating the cross section directly at a large number of energies. The autoionizing resonances may enhance the excitation rates by up to several factors, with some reduction due to radiation damping in the continuum for highly charged ions (discussed below).

Electron scattering flux may undergo recombination with the target ion with emission of a photon. Such recombination may take place both through direct recombination, i.e. radiative recombination (RR), or indirectly through autoionizing resonances, i.e. dielectronic recombination (DR). The DR process thus diminishes the influence of resonances in electron impact excitation (EIE) cross section via radiation damping (e.g. Pradhan [81P1]). In a combined study of fine structure, autoionization, and radiative decays of *high-n* resonances up to the Rydberg series limits at target thresholds, Pradhan [83P1, 83P2] found maximum reductions in the EIE rate coefficients for the metastable $1\,^1S_0 - 2\,^3S_1$ transition of 9% for He-like Fe XXV and 19% for Mo XLI. Fig. 1 shows the cross sections for EIE of He-like Ti XXI including relativistic and radiative damping effects [95Z6]; Fig. 2 compares the theoretical results with the experimentally measured values from the Electron-Beam-Ion-Trap (EBIT) at Livermore.

Thus DR and EIE are complementary processes and related through the unitarity of the generalized scattering matrix including both the electron and the photon channels. This follows from the conservation of (photon + electron) flux during the scattering process. A general theory of DR was developed by Bell and Seaton [85B1] that provided a rigorous theoretical framework for radiation damping, and precise expressions for practical calculations, combined with multi-channel quantum defect theory, appropriate for Rydberg series of atomic states, and coupled-channel wavefunctions that allow for resonances in an *ab initio* manner.

As is physically evident, the RR and the DR processes are unified in nature. Extending the CC approximation and the R-matrix method to electron-ion recombination, Nahar and Pradhan [92N2] have developed a computationally unified approach to obtain total (e + ion) recombination cross sections and rate coefficients. Further, employing BPRM method the calculations have been extended to highly charged ions including relativistic effects and associated couplings (Zhang and Pradhan [97Z4, 97P2]). Fig. 3 illustrates the unification process, and relation to EIE, for electron scattering and recombination with He-like carbon: e + C V → C IV. The photo-recombination cross sections labeled 'PR' are unified elctron-ion recombination cross sections, including both RR and DR, obtained via the detailed balance relation from photoionization cross sections. At sufficiently high-n the resonant contribution (DR) is very large compared to the background, non-resonant part and the total recombination cross section may be approximated accurately by simply the DR cross section. This is verified in Fig. 3 where the PR (including RR and DR) matches the DR cross section precisely at about $n = 10$. Finally, the DR cross section merges with the EIE cross section at the threshold for excitation of the dipole transition $1\,^1S_0 - 2\,^1P^o_1$ It may be noted that the resonances are completely damped out radiatively as $n \longrightarrow \infty$, even as the DR cross section rises to equal the EIE cross section at the threshold [99Z2].

3.1.3 Comparison with experiments

Although experimental measurements of electron-ion scattering cross sections are difficult, a number of advances have been made in recent years. The advent of merged-beam techniques, synchrotron ion storage rings, and electron-beam-ion-traps (EBIT) have made it possible to measure the cross sections to unprecedented accuracy.

Most of the recent experimental work employs the merged beam technique and cross sections for a number of ions have been measured. In nearly all cases the experimental results agree with the most sophisticated coupled channel calculations to within the typical experimental uncertainties of 10–15% – the range of uncertainty often quoted for such theoretical calculations. However, it needs to be emphasized that the details of resonance structures in the experimental data are subject to beam resolution; the theoretical data are convolved over the FWHM beam width in comparing with experiments. A few of the merged-beam cross sections and corresponding theoretical works are presented below.

The cross sections for C II in Fig. 4 are for the three lowest transitions from the ground state: the intercombination transition $1s^2 2s^2 2p\ ^2P^o \longrightarrow 1s2s2p^2\ ^4P^o$ (Fig. 4a), and the next two dipole allowed transitions to $1s^2 2s2p^2$ (^2D, ^2S) (Figs. 4b, 4c). The latter two final states lie relatively close together in energy and are coupled, as indicated by the fact that the proportion of the collision strengths is quite different from that of the oscillator strengths [90L1]. It follows that simple formulae such as the Van Regemorter formula, or the "g-bar" approximation, for the collision strengths gives incorrect collision strengths [90L1]. All three cross sections in Fig. 4 show considerable resonance structures; therefore approximations neglecting channel couplings, such as the distorted wave, are also likely to yield inaccurate collision strengths.

The measured cross sections in Figs. 4b and 4c for C II are for relatively strong dipole allowed transitions and therefore not as sensitive to channel coupling effects and resonances as the weaker intercombination or LS forbidden transitions. However, recent experimental work has also been carried out for the LS-forbidden transitions in O II [95Z6] and S II [97L1]. Both ions have the same LS-term structure. The measured cross sections are from the ground state $^4S^o \longrightarrow (^2D^o, ^2P^o)$, and for the dipole allowed transitions up to the higher ^4P terms. Figs. 5a and 5b show the experimental and theoretical results for the forbidden transition ($2s^2 2p^3\ ^4S^o \longrightarrow\ ^2D^o$), and the dipole allowed transition ($2s^2 2p^3\ ^4S^o \longrightarrow 2s2p^4\ ^4P$) in O II. Theoretical data from two different sets of R-matrix calculations [95Z6] agree with experiment well within experimental error bars.

Fig. 6 presents the measured and theoretical collision strengths for the dipole allowed transition 3s – 3p in Mg II [95S5]. All experimental points except the last one agree with theoretical results within experimental uncertainties. It might be noted that the agreement holds true even at energies that span a number of excited $n = 4$ and $n = 5$ thresholds.

Fig. 7 shows the results for three transitions in S II [97L1]: $3s^2 3p^3\ ^4S^o \longrightarrow 3s^2 3p^3\ ^2D^o$ and $^2P^o$, and $3s^2 3p^3\ ^4S^o \longrightarrow 3s3p^4\ ^4P$. The theoretical data curves are based on two 19-state close coupling calculations (solid line and dash-dot line) and a 12-state close coupling calculation (dashed curve). While the all theoretical results agree with experiment for the first transition $^4S^o \longrightarrow\ ^2D^o$ (Fig. 7a), there is considerable disagreement for the transition $^4S^o \longrightarrow\ ^2P^o$ (Fig. 7b) between the 12-state calculation and experiment owing to the presence of a near-threshold resonance structure that is delineated by the 19-state, but not by the 12-state, close coupling calculation. This illustrates the importance of the configuration interaction expansion used in close coupling calculations; although the transition in question is only to the second excited state, the 12-state target expansion is not sufficiently accurate to reproduce the large resonance structure. Similarly, the 12-state results are also considerbly lower than experiment for the even higher transition up to $3s3p^4\ ^4P$ (Fig. 7c).

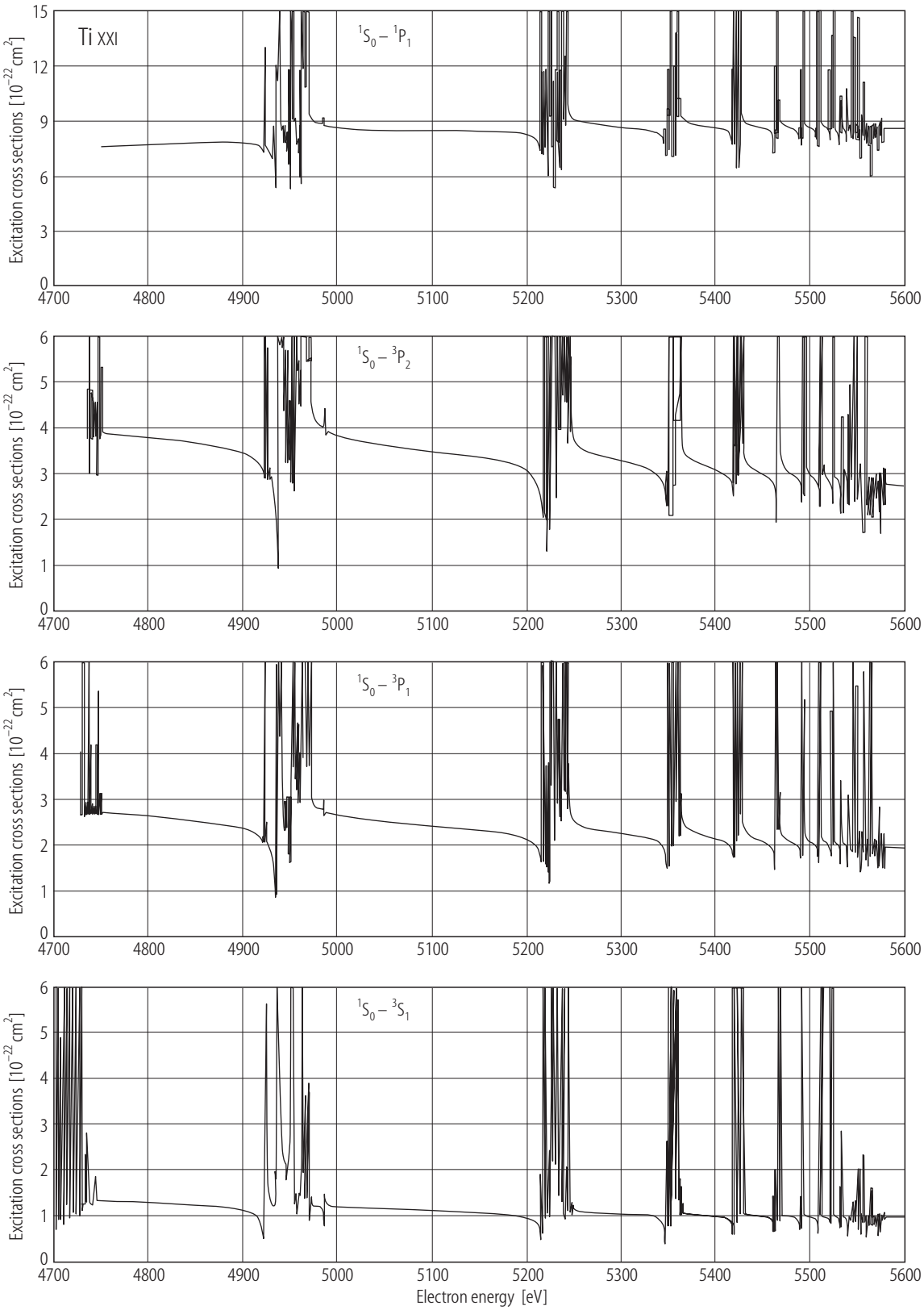

Fig. 1 (left panels). For caption see p. 3-13.

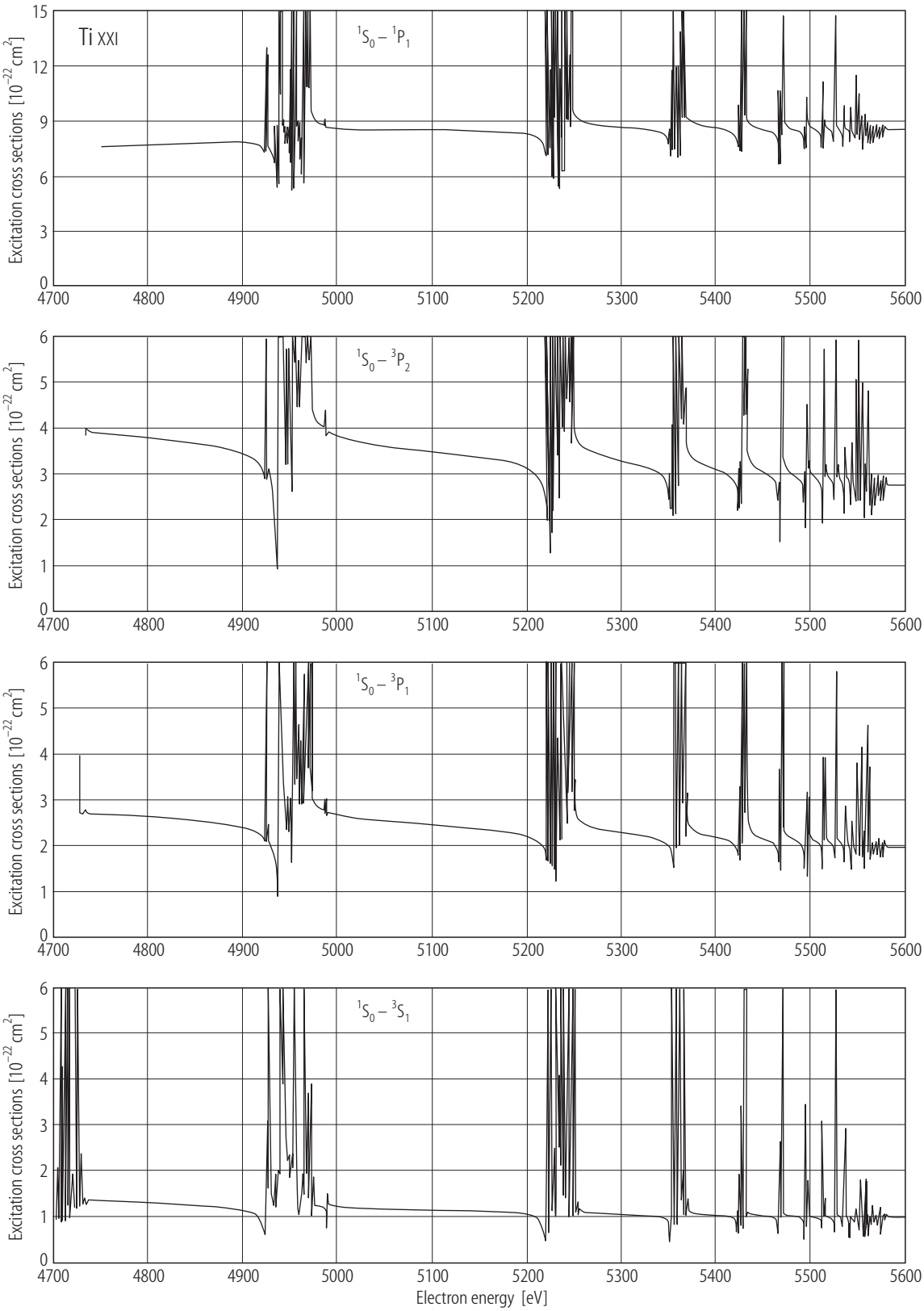

Fig. 1 (right panels). For caption see p. 3-13.

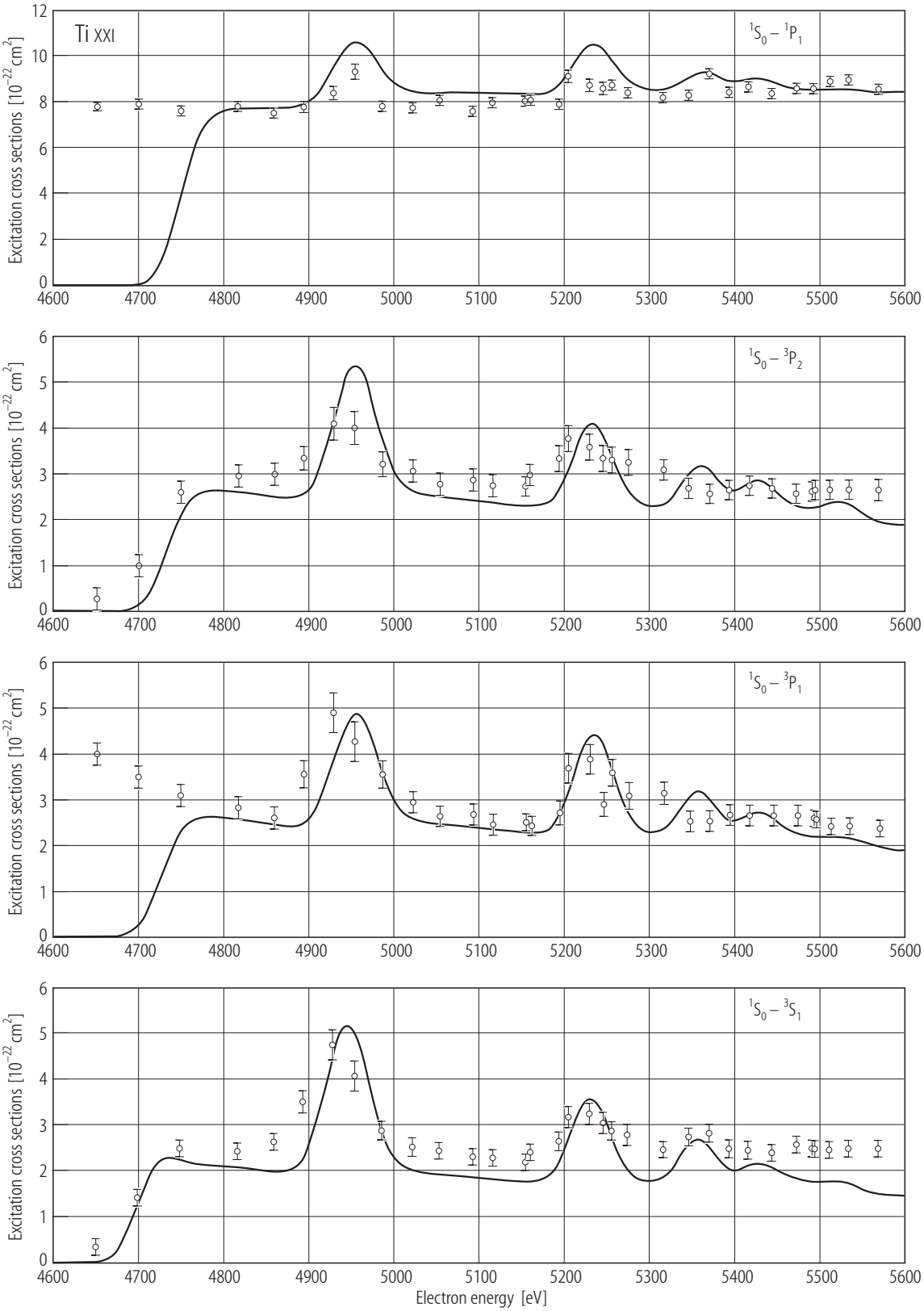

Fig. 2. For caption see p. 3-13.

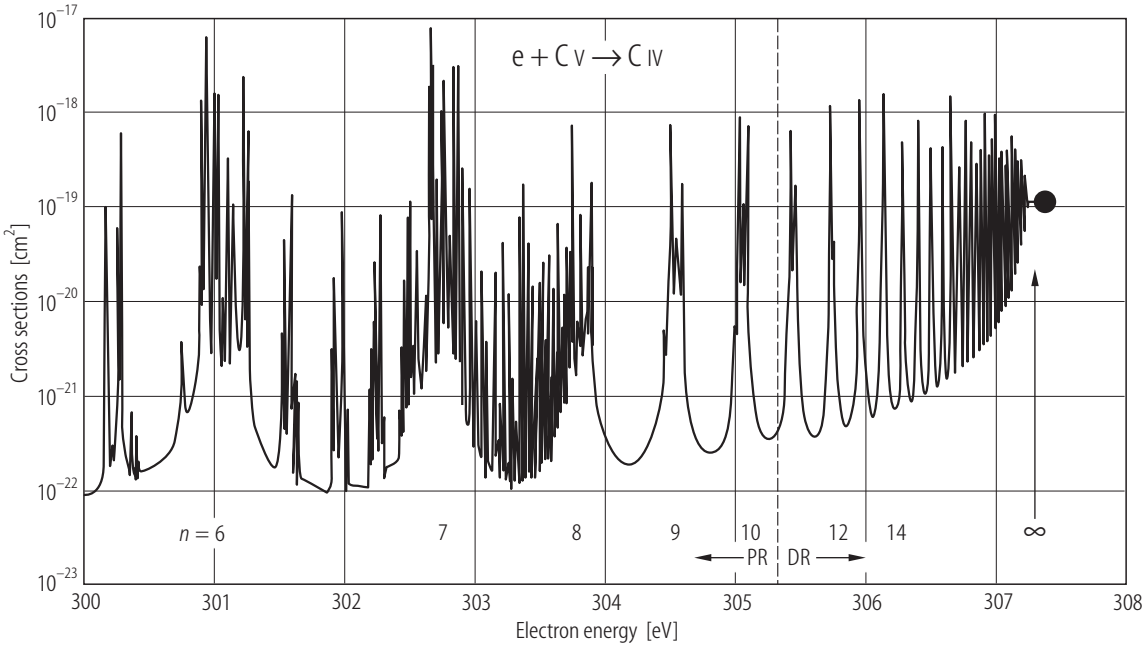

Fig. 3. Correspondence between photo-recombination (PR), dielectronic recombination (DR), and electron impact excitation. The PR cross sections are derived from photoionization cross section via detailed balance and include both resonant and non-resonant (background) recombination; the DR cross sections are computed using the coupled-channel theory of DR [85B1]; and the filled circle represents the near-threshold value of electron impact excitation cross section for the dipole transition $1\,^1S_0 - 2\,^1P_1$ in C V (Zhang et al. 1998 [99Z2]).

Fig. 1. Electron impact excitation cross sections for the transitions $1\,^1S_0 - 2\,^1P_1$, $1\,^1S_0 - 2\,^3P_2$, $1\,^1S_0 - 2\,^3P_1$, and $1\,^1S_0 - 2\,^3S_1$ in Ti XXI; left panels: without radiation damping, right panels: with radiation damping (Zhang and Pradhan 1995 [95Z4]).

Fig. 2. Comparison of the convolved theoretical electron impact excitation cross sections, solid lines (Zhang and Pradhan 1995 [95Z4]) with the EBIT experimental data, circles with error bars (Chantrenne et al. 1992 [92C3]) for the transitions in Ti XXI in Fig. 1.

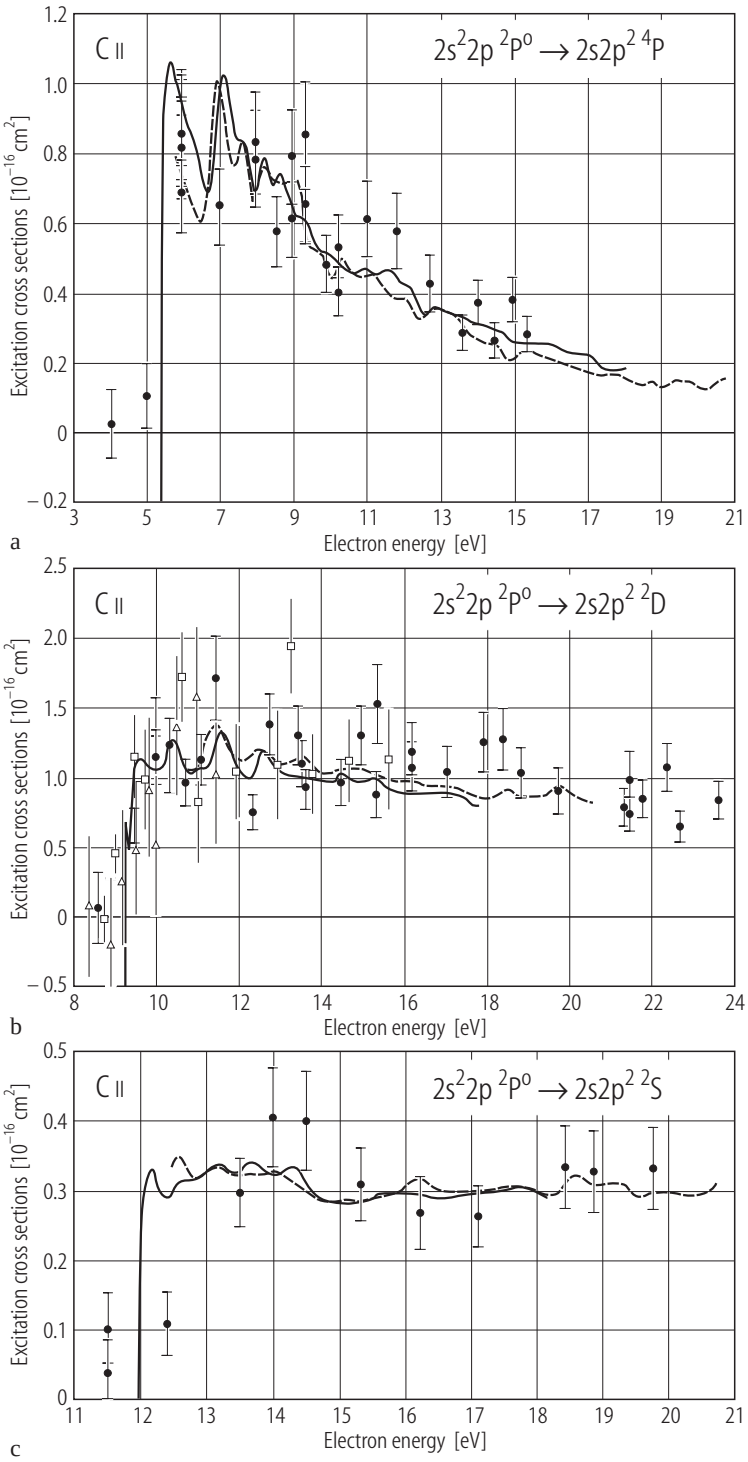

Fig. 4. Experimental (filled circles) and theoretical R-matrix cross sections for C II convoluted with a 250 MeV FWHM resolution (Smith et al. 1996 [96S3]); solid line [96S3], dashed line (Luo and Pradhan [90L1]) for the excitation of the (a) $^2P^o - {}^4P$ (intercombination) transition, (b) $^2P^o - {}^2D$ (allowed) transition, and (c) $^2P^o - {}^2S$ (allowed) transition.

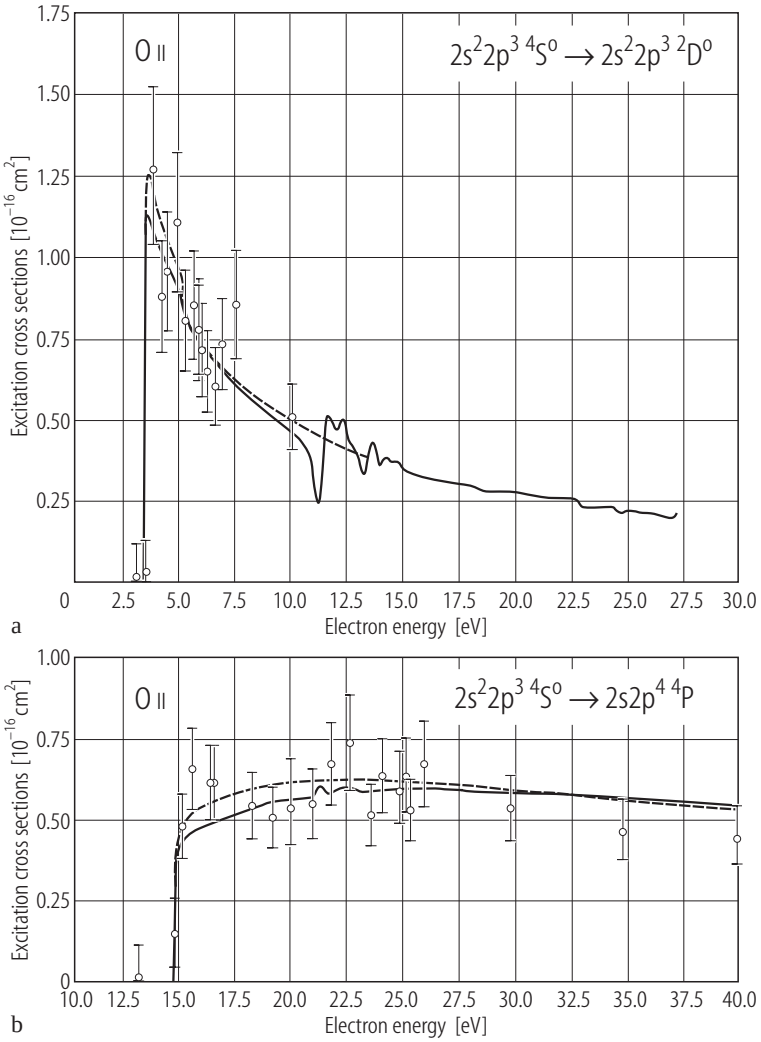

Fig. 5. Experimental (circles) and theoretical R-matrix cross sections (solid line, Zuo et al. 1996 [95Z6]) for O II for excitation of the (a) $2s^2 2p^3\ ^4S^o - {}^2D^o$ (forbidden) transition and (b) $^4S^o - 2s2p^4\ ^4P$ (resonance) transition.

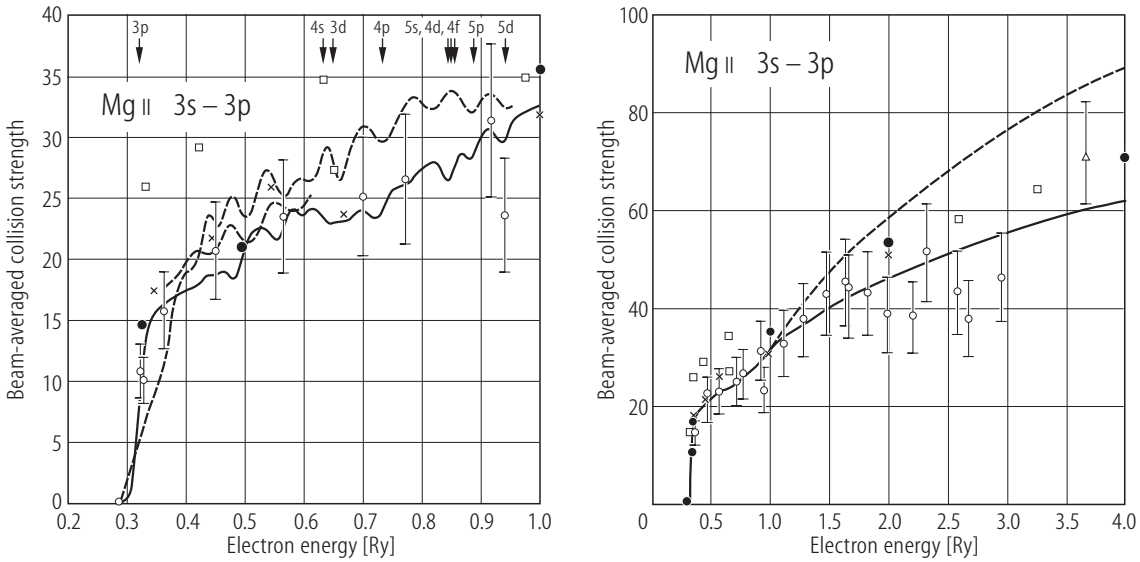

Fig. 6. Comparison of the 3s – 3p collision strength for Mg II with experiment (Smith et al. 1993, 93S1); the full curve is the ten-state close coupling (R-matrix) calculation averaged over a Gaussian electron beam of 0.3 eV FWHM (Sigut and Pradhan [95S5]).

Fig. 7. Experimental (circles) and theoretical cross sections for excitation of S II. Theoretical results are convoluted with a 250 meV (FWHM) electron energy width: solid line, 19-state R-matrix calculation; dash-dot line, Ramsbottom et al. (1996) 19-state R-matrix calculation; dashed line, Cai and Pradhan (1993) 12-state R-matrix calculation; dotted line, Tayal et al. (1987) 6-state R-matrix calculation (as reported in Liao et al. 1997 [97L1]) – (a) $^4S^o \rightarrow {}^2D^o$ transition, (b) $^4S^o \rightarrow {}^2P^o$ transition and (c) $^4S^o \rightarrow {}^4P$ transition.

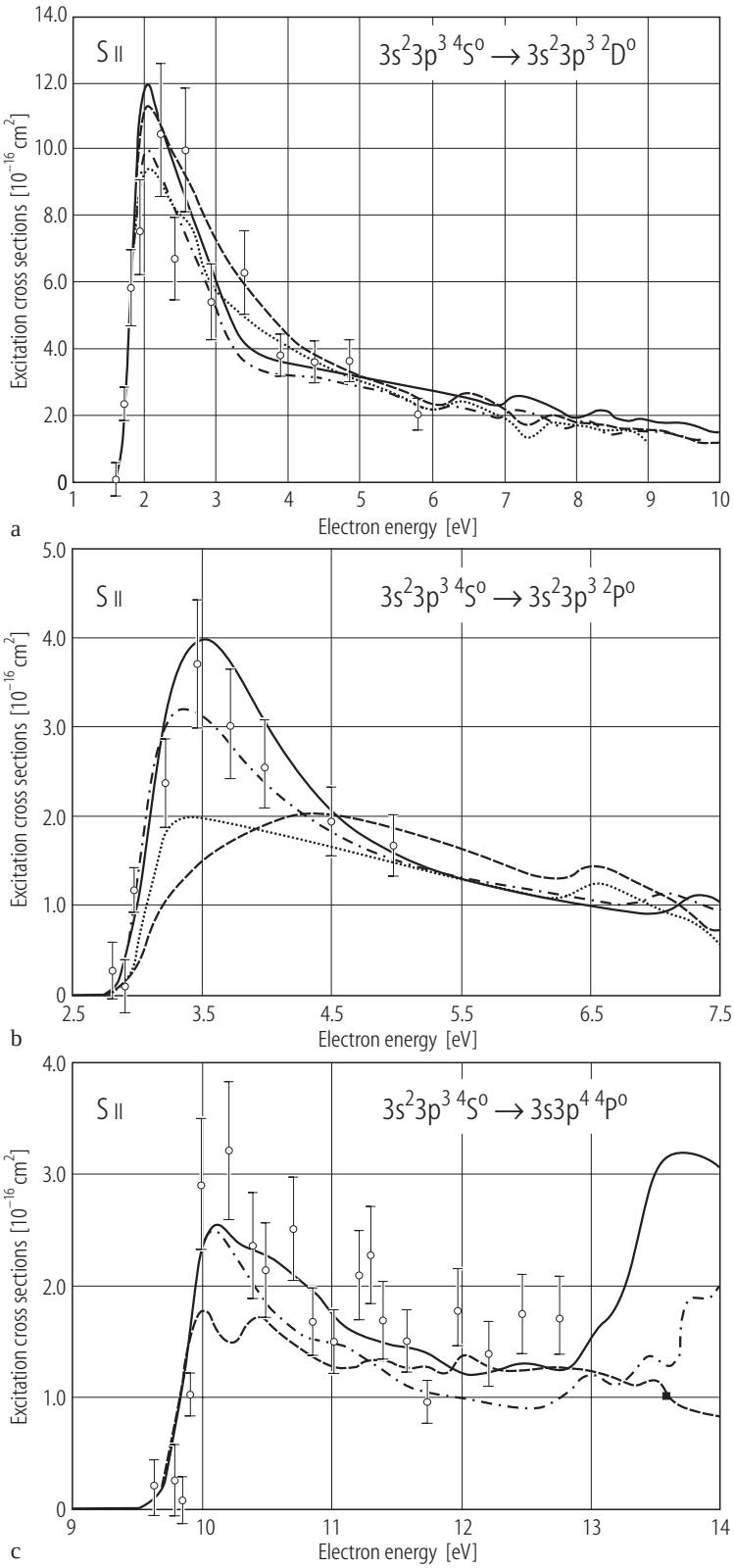

Fig. 7. For caption see p. 3-16

Electron impact excitation cross sections for multicharged ions have also been measured using the Merged Electron-ion Beams Energy Loss (MEIBEL) technique [94B7]. Measured cross sections include: C^{3+} 2s ^{2}S – 2p ^{2}P, O^{5+} 2s ^{2}S – 2p ^{2}P, Si^{2+} 3s^2 ^{1}S – 3s3p ^{1}P, Si^{2+} 3s^2 ^{1}S – 3s3p ^{3}P, Si^{3+} 3s ^{2}S – 3p ^{2}P, Ar^{6+} 3s^2 ^{1}S – 3s3p ^{1}P, Ar^{6+} 3s^2 ^{1}S – 3s3p ^{3}P, Ar^{7+} 3s ^{2}S – 3p ^{2}P, and Kr^{6+} 4s^2 ^{1}S – 4s4p ^{3}P. References to the experimental works and comparisons with theory may be obtained from at: www-cfadc.phy.ornl.gov/meibel/meibel.html. There is good agreement, usually within experimental uncertainties, between experimental values and theoretical close coupling calculations using the R-matrix method. It might be noted that the measured transitions are the lowest dipole allowed or intercombination transitions. Some discrepancies between theory and experiment are evident in the figures given, although the overall structures agree.

In summary, the most elaborate theoretical calculations for up to the third row elements generally agree with experiments for the low-lying transitions that have been experimentally studied. However, detailed comparisons show that several prior theoretical results were in error.

3.1.4 Scaling laws, analysis of data, and databases

Transitions may be classified according to the range of the potential interaction ($V_{ii'} \pm W_{ii'}$) in Eq. (9). Spin change transitions depend entirely on the exchange term $W_{ii'}$ which is very short range since the colliding electron must penetrate the ion for exchange to occur. Therefore, only the first few partial waves are likely to contribute to the cross section, but these involve quite an elaborate treatment (e.g. close-coupling). For allowed transitions, on the other hand, a fairly large number of partial waves contribute and simpler approximations (e.g. Coulomb-Born) often yield acceptable results. The asymptotic behavior of the collision strengths for allowed and forbidden transitions is as follows (x is in threshold units of energy):

(A) $\Omega(i,j) \underset{x\to\infty}{\sim}$ constant, for forbidden (electric quadrupole) transitions, $\Delta L \neq 1, \Delta S = 0$

(B) $\Omega(i,j) \underset{x\to\infty}{\sim} x^{-2}$, for spin-change transitions, $\Delta S \neq 0$

(C) $\Omega(i,j) \underset{x\to\infty}{\sim} a\ln(4x)$, allowed transitions, $\Delta\ell = 0, \pm 1, \Delta S = 0$.

The slope a in the last equation is proportional to the dipole oscillator strength. The above forms are valid for transitions in LS coupling. For highly charged ions where one must allow for relativistic effects, through say an intermediate coupling scheme, sharp deviations may occur from these asymptotic forms particularly for transitions labeled as intercombination type (e.g., the transition $1\,^1$S $-$ $2\,^3$P in He-like ions). For low-Z ions ($Z < 15$) when LS coupling is usually valid, $\Omega(1\,^1\mathrm{S} - 2\,^3\mathrm{P})$ behaves as (B). With increasing Z, the fine structure splitting between $2\,^3$P ($J = 0, 1, 2$) becomes significant and the collision strength $\Omega(1\,^1\mathrm{S}_0 - 2\,^3\mathrm{P}_1)$ gradually assumes form (C).

A useful fact for isosequence interpolation or extrapolation is that $Z^2\Omega(i,j)$ tends to a finite limit, as $Z \to \infty$, as a function of k^2/Z^2; i.e., at the Z^2 reduced incident electron energy, $\Omega(i,j)$ is constant or a slowly varying function for large Z. For highly ionized atoms (e.g. H-like, He-like) the Z^2 behavior is valid even for $Z < 10$, but for many-electron ions (e.g. Ne-like) one needs to go to much higher values of Z.

Faced with the huge volume of atomic data, calculated with different methods, it is important to be able to analyze, evaluate, compile, and disseminate it in efficient ways. One such approach is to adopt scaling procedures and examine systematic trends in the collision strengths. Burgess and Tully have implemented this approach to fit and extrapolate or interpolate effective (maxwellian averaged) collision strengths in a computer program called OMEUPS [92B5]. Although useful in many cases, the limiting values(i.e as E or $T \longrightarrow \infty$) adopted in this approach may not always be accurate, particularly for non-dipole transitions where coupling effects, such as n-complexes of

Electron impact excitation cross sections for multicharged ions have also been measured using the Merged Electron-ion Beams Energy Loss (MEIBEL) technique [94B7]. Measured cross sections include: C^{3+} 2s ^{2}S – 2p ^{2}P, O^{5+} 2s ^{2}S – 2p ^{2}P, Si^{2+} 3s^2 ^{1}S – 3s3p ^{1}P, Si^{2+} 3s^2 ^{1}S – 3s3p ^{3}P, Si^{3+} 3s ^{2}S – 3p ^{2}P, Ar^{6+} 3s^2 ^{1}S – 3s3p ^{1}P, Ar^{6+} 3s^2 ^{1}S – 3s3p ^{3}P, Ar^{7+} 3s ^{2}S – 3p ^{2}P, and Kr^{6+} 4s^2 ^{1}S – 4s4p ^{3}P. References to the experimental works and comparisons with theory may be obtained from at: www-cfadc.phy.ornl.gov/meibel/meibel.html. There is good agreement, usually within experimental uncertainties, between experimental values and theoretical close coupling calculations using the R-matrix method. It might be noted that the measured transitions are the lowest dipole allowed or intercombination transitions. Some discrepancies between theory and experiment are evident in the figures given, although the overall structures agree.

In summary, the most elaborate theoretical calculations for up to the third row elements generally agree with experiments for the low-lying transitions that have been experimentally studied. However, detailed comparisons show that several prior theoretical results were in error.

3.1.4 Scaling laws, analysis of data, and databases

Transitions may be classified according to the range of the potential interaction ($V_{ii'} \pm W_{ii'}$) in Eq. (9). Spin change transitions depend entirely on the exchange term $W_{ii'}$ which is very short range since the colliding electron must penetrate the ion for exchange to occur. Therefore, only the first few partial waves are likely to contribute to the cross section, but these involve quite an elaborate treatment (e.g. close-coupling). For allowed transitions, on the other hand, a fairly large number of partial waves contribute and simpler approximations (e.g. Coulomb-Born) often yield acceptable results. The asymptotic behavior of the collision strengths for allowed and forbidden transitions is as follows (x is in threshold units of energy):

(A) $\Omega(i,j) \underset{x\to\infty}{\sim}$ constant, for forbidden (electric quadrupole) transitions, $\Delta L \neq 1, \Delta S = 0$

(B) $\Omega(i,j) \underset{x\to\infty}{\sim} x^{-2}$, for spin-change transitions, $\Delta S \neq 0$

(C) $\Omega(i,j) \underset{x\to\infty}{\sim} a\ln(4x)$, allowed transitions, $\Delta\ell = 0, \pm 1, \Delta S = 0$.

The slope a in the last equation is proportional to the dipole oscillator strength. The above forms are valid for transitions in LS coupling. For highly charged ions where one must allow for relativistic effects, through say an intermediate coupling scheme, sharp deviations may occur from these asymptotic forms particularly for transitions labeled as intercombination type (e.g., the transition $1\,^1$S $-$ $2\,^3$P in He-like ions). For low-Z ions ($Z < 15$) when LS coupling is usually valid, $\Omega(1\,^1\mathrm{S} - 2\,^3\mathrm{P})$ behaves as (B). With increasing Z, the fine structure splitting between $2\,^3$P ($J = 0, 1, 2$) becomes significant and the collision strength $\Omega(1\,^1\mathrm{S}_0 - 2\,^3\mathrm{P}_1)$ gradually assumes form (C).

A useful fact for isosequence interpolation or extrapolation is that $Z^2\Omega(i,j)$ tends to a finite limit, as $Z \to \infty$, as a function of k^2/Z^2; i.e., at the Z^2 reduced incident electron energy, $\Omega(i,j)$ is constant or a slowly varying function for large Z. For highly ionized atoms (e.g. H-like, He-like) the Z^2 behavior is valid even for $Z < 10$, but for many-electron ions (e.g. Ne-like) one needs to go to much higher values of Z.

Faced with the huge volume of atomic data, calculated with different methods, it is important to be able to analyze, evaluate, compile, and disseminate it in efficient ways. One such approach is to adopt scaling procedures and examine systematic trends in the collision strengths. Burgess and Tully have implemented this approach to fit and extrapolate or interpolate effective (maxwellian averaged) collision strengths in a computer program called OMEUPS [92B5]. Although useful in many cases, the limiting values(i.e as E or $T \longrightarrow \infty$) adopted in this approach may not always be accurate, particularly for non-dipole transitions where coupling effects, such as n-complexes of

resonances, may attenuate the collision strengths even to very high energies and the Coulomb-Born or Coulomb-Bethe limits may not be applicable. Nonetheless the scaled collision strength data can be visualized in a systematic manner, for example along iso-electronic sequences. Deviations from the fits may be investigated to explore possible errors, presence of resonances, convergence of partial wave expansion, etc.

A number of databases are listed in a review article on atomic data by Pradhan and Peng [95P2]. As mentioned above a new database, TIPbase, has been developed to include the high precision data from the Iron Project [93H1].

3.1.5 Data tables and accuracy ratings

Three sets of data tables are presented:

Table 1, an evaluated compilation of theoretical data sources since 1990 (similar to the one by Pradhan and Gallager [92P1] for sources before 1990),

Table 2, recommended data for a number of ions containing the maxwellian averaged or effective collision strengths $\Upsilon(T)$ at a range of electron temperatures, the wavelengths and transition probabilities of associated transitions, and

Table 3, effective collision strengths for all iron ions, for a large number of transitions, taken from the recent Iron Project work or relativistic distorted-wave calculations.

Most of the data chosen are of high accuracy, rated A or B (10–20 % estimated uncertainty). Data rated lower, with higher uncertainties, are not included in the data tables 2 and 3 (with some exceptions), as many of these are being recalculated at the present time.

3.1.5.1 Theoretical data sources

As mentioned earlier, a comprehesive survey and evaluation of theoretical calculations up to 1990 was carried out by Pradhan and Gallagher [92P1]. Further compilations of data have been done by Itikawa for theoretical data sources appearing between 1990-1994 [96I1], and from 1995- [98I1]. The papers listed in the annotated bibliographies in the latter two publications have been evaluated according to the basic criteria of (i) theoretical method employed and (ii) atomic effects included (these are explained in greater detail in [92P1]).

An approximate accuracy rating is assigned according to estimated uncertainties within 10% (A), 20% (B), 30% (C), 50% (D), $>$ 50% (E), and uncertain (U). Table 1 presents the data sources along with these ratings. It is noted that unlike most of the calculations prior to 1990, nearly all of the recent calculations for electron impact excitation have been carried out in the close coupling approximation using the R-matrix method, or the distorted wave (relativistic and non-relativistic) approximation. Also, unlike previous calculations the often dominant effect of autoionzing resonances is now well established and most calculations for low-ionization species include or estimate these effects.

It should be emphasized that the accuracy rating assigned is only an overall estimate of the theoretical calculations reported in the corresponding publication. It does not attempt to represent the accuracy of each individual transition or range of energies for which the uncertainties may well vary even for the same method with the same effects included for the same ion. As such, the ratings are meant only as a rough criterion to provide some assessment of the overall reliability of the data, and whether the data needs to be recalculated with improved accuracy.

Sections of Table 1 are divided according to isoelectronic sequences, with the number of electrons in the ion, $N = 1$, etc., and in order of the atomic number the elements listed. The first author's name is listed. Soemtimes it is not possible to list all the transitions in detail and users should consult the data source(s) before deciding to use a given set of data.

resonances, may attenuate the collision strengths even to very high energies and the Coulomb-Born or Coulomb-Bethe limits may not be applicable. Nonetheless the scaled collision strength data can be visualized in a systematic manner, for example along iso-electronic sequences. Deviations from the fits may be investigated to explore possible errors, presence of resonances, convergence of partial wave expansion, etc.

A number of databases are listed in a review article on atomic data by Pradhan and Peng [95P2]. As mentioned above a new database, TIPbase, has been developed to include the high precision data from the Iron Project [93H1].

3.1.5 Data tables and accuracy ratings

Three sets of data tables are presented:

Table 1, an evaluated compilation of theoretical data sources since 1990 (similar to the one by Pradhan and Gallager [92P1] for sources before 1990),

Table 2, recommended data for a number of ions containing the maxwellian averaged or effective collision strengths $\Upsilon(T)$ at a range of electron temperatures, the wavelengths and transition probabilities of associated transitions, and

Table 3, effective collision strengths for all iron ions, for a large number of transitions, taken from the recent Iron Project work or relativistic distorted-wave calculations.

Most of the data chosen are of high accuracy, rated A or B (10–20 % estimated uncertainty). Data rated lower, with higher uncertainties, are not included in the data tables 2 and 3 (with some exceptions), as many of these are being recalculated at the present time.

3.1.5.1 Theoretical data sources

As mentioned earlier, a comprehesive survey and evaluation of theoretical calculations up to 1990 was carried out by Pradhan and Gallagher [92P1]. Further compilations of data have been done by Itikawa for theoretical data sources appearing between 1990-1994 [96I1], and from 1995- [98I1]. The papers listed in the annotated bibliographies in the latter two publications have been evaluated according to the basic criteria of (i) theoretical method employed and (ii) atomic effects included (these are explained in greater detail in [92P1]).

An approximate accuracy rating is assigned according to estimated uncertainties within 10% (A), 20% (B), 30% (C), 50% (D), $>$ 50% (E), and uncertain (U). Table 1 presents the data sources along with these ratings. It is noted that unlike most of the calculations prior to 1990, nearly all of the recent calculations for electron impact excitation have been carried out in the close coupling approximation using the R-matrix method, or the distorted wave (relativistic and non-relativistic) approximation. Also, unlike previous calculations the often dominant effect of autoionzing resonances is now well established and most calculations for low-ionization species include or estimate these effects.

It should be emphasized that the accuracy rating assigned is only an overall estimate of the theoretical calculations reported in the corresponding publication. It does not attempt to represent the accuracy of each individual transition or range of energies for which the uncertainties may well vary even for the same method with the same effects included for the same ion. As such, the ratings are meant only as a rough criterion to provide some assessment of the overall reliability of the data, and whether the data needs to be recalculated with improved accuracy.

Sections of Table 1 are divided according to isoelectronic sequences, with the number of electrons in the ion, $N = 1$, etc., and in order of the atomic number the elements listed. The first author's name is listed. Soemtimes it is not possible to list all the transitions in detail and users should consult the data source(s) before deciding to use a given set of data.

The symbols used to represent the available "Data" are as follows:

Ω - collision strength, ϒ - maxwellian averaged collision strength, Q - cross section, q - rate coefficient, f - oscillator strength, DCS - differential cross section, Pol. - polarization data.

The theoretical methods listed in Table 1 are:

RM – R-matrix, BPRM – Breit-Pauli R-matrix, CC – close coupling (R-matrix or others), CCC – convergent close coupling, DW – distorted wave, RDW – relativistic DW, CB – Coulomb Born, CBe – Coulomb Bethe, CDW – Coulomb DW, CBR - Coulomb Born relativistic, QDT – quantum defect theory.

Table 1. Evaluation of theoretical data sources, 1990-

Ion	Ref.	Author	Method	Transitions	Data	Rating
			$N = 1$ (H-like)			
H-like	94C1	Callaway	review	many	Ω,ϒ	A-C
H-like	93C2	Chidichimo	CB scaling	many	Q	U
H-like	93J1	Jung	semi-class	many	Q	U
H-like	97F1	Fisher	CCC, CB	$1s-2s, 2p; n-n'$ fits	Q	A
He II	93B6	Bray	CC	$1s-2s$	Q	A
He II	91A5	Aggarwal	RM	$n = 1-5$	ϒ	A
He II	92A4	Aggarwal	RM	$n = 1-3$	ϒ	A
He II	91U1	Unnikrishnan	CC	$n = 1-3$	Ω	A
He II	94F1	Fon	RM	$1s-2s$	Ω	A
Be IV	92B1	Berrington	fits	$n = 1-3\ell$	Ω,ϒ	A,B
Be IV	96C2	Clark	DW fits	many	Q	C
B V	92B1	Berrington	fits	$n = 1-3\ell$	Ω,ϒ	A,B
B V	96C2	Clark	DW fits	many	Q	C
C VI	91A6	Aggarwal	RM	$n = 1-5$	ϒ	A
O VIII	94C4	Cornille	DW	$1s-2p$	ϒ,f	B
Ne X	92S3	Shevelko	approx.	$1s-2p$	Q	B
Ne X	91A6	Aggarwal	RM	$n = 1-5$	ϒ	A
Si XIV	92A2	Aggarwal	RM	$n = 1-5$	Ω,ϒ	A
Ca XX	92A3	Aggarwal	RM	$n = 1-5$	Ω,ϒ	A
Fe XXVI	96K2	Kisielius	BPRM	$n \leq 4, \ell \leq 3$	Ω,ϒ	A
Fe XXVI	93A2	Aggarwal	RM	n = 1-5	ϒ	A
Fe XXVI	93F1	Fontes	RDW	$n = 1, 2-2, 3;$	Ω	C
Fe XXVI, U XCII						
	91M3	Moores	RDW	$1s-2s, 2p$	Ω	C
H-like, Z = 2, 26, 92						
	95K1	Kisielius	BPRM	$n = 1-2$	Ω	A
H-like, Z = 3, 10, 26						
	90C2	Clark	DW	$n = 3-n' = 9$	Ω	C
H-like, Z = 13, 18, 22, 42, 56, 79, 92						
	93R1	Reed	RDW	$n = 1, 2$ mag. levels	Pol.	U
H-like, Z = 26, 54, 67, 79, 92						
	92M1	Moores	RDW	$1s-2s, 2p$	Ω	C
H-like, Z = 50, 54						
	93F1	Fontes	RDW	$n = 1, 2-2, 3;$	Ω,Q	B

Table 1 (continued)

Ion	Ref.	Author	Method	Transitions	Data	Rating
H-like, $Z = 92, 100$						
	93F1	Fontes	RDW	$n = 1, 2 - 2, 3;$	Ω,Q	A
			$N = 2$ (He-like)			
He-like	95I1	Itikawa	review	many	ϒ	A-C
He-like	94D1	Dubau	review	many	Ω,ϒ	A-C
Li II	90G2	Griffin	CC/DW	$1s^2 - 1s2\ell$	Q,DCS	A-C
Li II	91B2	Berrington	RM	$1\,^1S - n = 2, 3$	Q	A
Li II	91N1	Nakazaki	RM	$1\,^1S - 2(^1P, {}^1S, {}^3P, {}^3S)$	DCS	A
Be III	92B1	Berrington	fits	$n = 1 - 3\ell$	Ω,ϒ	A,B
Be III	96C2	Clark	DW fits	many	Q	C
B IV	92B1	Berrington	fits	$n = 1 - 3\ell$	Ω,ϒ	A,B
B IV	96C2	Clark	DW fits	many	Q	C
Ne IX	95Z5	Zhang	RDW	mag. levels	Ω	C
S XV	93N1	Nakazaki	RM	$1\,^1S - n = 2, 3$	q	A
Ti XXI	95G2	Gorczyca	BPRM	$1s^2 - 1s2s, 2p$	Q	A
Ti XXI	95Z4	Zhang	BPRM	$1\,^1S_0 - 2\,^1P^o_1, 2\,^3P^o_{1,2}$	Ω,Q	A
Fe XXV	90Z3	Zhang	RDW	mag. levels	Ω	C
Fe XXV	92I1	Inal	RDW	$1s^2, 1s2\ell, 3\ell$	Pol.	B
Fe XXV	93I1	Inal	RDW	mag. levels	Pol.	B
Fe XXV	95Z2	Zhang	BPRM	$1^1S_0 - 2^3P^o_1$	Ω	A
Fe XXV	93F1	Fontes	RDW	$n = 1 - 2$	Ω	C
Fe XXV	95Z5	Zhang	RDW	mag. levels	Ω	C
Fe XXV	99F1	Fontes	RDW	mag. levels	Ω	C
Ni XXVII	95H1	Harra-Murnion	Rel. RM	$1s^2 - 1s2\ell, 1s3\ell$	ϒ	A
Xe LIII	93F1	Fontes	RDW	$n = 1 - 2$	Ω	B
Xe LIII	99F1	Fontes	RDW	mag. levels	Ω	A
U XCI	93F1	Fontes	RDW	$n = 1 - 2$	Ω	A
He-like, $Z = 6 - 46$						
	92V1	Vainshtein	CB	$1s^2 - 1s2\ell, 1s3\ell$	Q,q	C,D
He-like, $Z = 13, 18, 22, 42, 56, 79, 92$						
	93R1	Reed	RDW	$n = 1, 2$ mag. levels	Pol.	U
He-like, $Z = 56, 79$						
	95Z5	Zhang	RDW	mag. levels	Ω	B,A
			$N = 3$ (Li-like)			
Li-like	94M4	McWhirter	review	many	Ω,ϒ	A-C
Be II	92B1	Berrington	fits	$n = 1 - 3\ell$	Ω,ϒ	A,B
Be II	90G1	Gedeon	CC/CB	$2s - 2p, 3s, 3p, 3d;$ $3s - 3p$	Q,q	B
Be II	91P1	Pan	RM, QDT	$2s - 2p$	Q,DCS	B
Be II	96C2	Clark	DW fits	many	Q	C
Be II	97B1	Bartschat	CCC, RM	$2s - 3\ell, 4\ell$	Q	A
Be II, B III, C IV, N V						
	92S3	Shevelko	approx.	$1s^22s - 1s2s2p$	Q	C
B III	92B1	Berrington	fits	$n = 1 - 3\ell$	Ω,ϒ	A,B
B III	96C2	Clark	DW fits	many	Q	C

Table 1 (continued)

Ion	Ref.	Author	Method	Transitions	Data	Rating
B III	97M1	Marchalant	CCC	$2s-2p, 3\ell, 4\ell'$	Q	C
C IV	92B4	Burke	RM	$2s-2p, 3\ell$	Ω	A
C IV, O VI						
	91B1	Badnell	DW/RM	$2s-2p$	Q	A,B
Fe XXIV	90Z3	Zhang	RDW	mag. levels	Ω	C
Fe XXIV	93F1	Fontes	RDW	$n=1-2$	Ω	C
Fe XXIV	97B3	Berrington	BPRM	$n=2,3,4$	Ω,Υ	A
Xe LII	93F1	Fontes	RDW	$n=1-2$	Ω	B
U XC	93F1	Fontes	RDW	$n=1-2$	Ω	A
Li-like, $6<Z<42$						
	95S1	Safronova	CB	$\Delta n=1$	Q,q	C,D
Li-like, $6<Z<42$						
	96S1	Safronova	CB	$1s^22s-1s2s2p$, $1s2s^2, 1s2p^2$	Q,q	C,D
Li-like, $8\le Z\le 30$						
	90Z1	Zhang	RDW	$n=2-3,4,5$	Ω,f	C
Li-like, $8\le Z\le 40$						
	90Z1	Zhang	RDW	$2s-2p_j$	Ω,f	C
Li-like, $31\le Z\le 50$						
	90Z1	Zhang	RDW	$n=2-3,4,5$	Ω,f	B
Li-like, $41\le Z\le 60$						
	90Z1	Zhang	RDW	$2s-2p_j$	Ω,f	B
Li-like, $51\le Z\le 92$						
	90Z1	Zhang	RDW	$n=2-3,4,5$	Ω,f	A
Li-like, $61\le Z\le 92$						
	90Z1	Zhang	RDW	$2s-2p_j$	Ω,f	A
			$N=4$ (Be-like)			
Be-like	94B4	Berrington	review	many	Ω,Υ	A-C
B II	92B1	Berrington	fits	$n=1-3\ell$	Ω,Υ	A,B
B II	96C2	Clark	DW fits	many	Q	C
C III	92K1	Keenan	RM	$2s^2-2s2p\ {}^3P_J$	Υ	A
N IV	94R1	Ramsbottam	RM	$2s^2, 2s2p, 2s3\ell, 2p^2$	Υ	A
O V	90K1	Kato	review	$n=2,3$	q	A,B
O V, Si XI, Fe XXIII, Mo XXXIX						
	90S1	Safronova	CBR	$2s^2, 2s2p, 2p^2$	Ω	C,D
O V, Si XI, Fe XXIII, Mo XXXIX						
	91K1	Kato	CBR	$2s^2, 2s2p, 2p^2$	Ω,q	C,D
O V, Si XI, Fe XXIII, Mo XXXIX						
	92S1	Safronova	CBR	$2s^2, 2s2p, 2p^2$	Q,q	C,D
Ne VII	94R2	Ramsbottam	RM	$2s^2, 2s2p, 2s3\ell, 2p^2$	Υ	A
Ne VII	95R1	Ramsbottam	RM	$n=2,3$	Υ	A
Fe XXIII	93K1	Keenan	RM	$2s^2, 2s2p, 2p^2$	Υ	A
Fe XXIII	98C2	Chen	RDW	$n=2,3$	Q	C
Mo XXXIX	94C3	Chen	RM	$1s^22s^2-1s2s^22p$	Q	B
Xe LI	93Z1	Zhang	RDW	$2s^2, 2s2p, 2p^2$	Ω	B
U LXXXIX	94F3	Fontes	RDW	$n=2-2$	Ω	A

Table 1 (continued)

Ion	Ref.	Author	Method	Transitions	Data	Rating
Be-like, $6 \le Z \le 54$						
	95S2	Safronova	CB	$2s^2, 2s2p, 2p^2$	Q,q	C,D
Be-like, $Z = 8, 10, 26$						
	93Z1	Zhang	RDW	$2s^2, 2s2p, 2p^2$	Ω	C
Be-like, $8 \le Z \le 40$						
	92Z1	Zhang	RDW	$2s^2, 2s2p, 2p^2$	Ω,f	C
Be-like, $Z = 21 - 30$						
	94O1	O'Mahoney	fits	$2s^2, 2s2p, 2p^2$	Υ	C
Be-like, $41 \le Z \le 60$						
	92Z1	Zhang	RDW	$2s^2, 2s2p, 2p^2$	Ω,f	B
Be-like, $61 \le Z \le 92$						
	92Z1	Zhang	RDW	$2s^2, 2s2p, 2p^2$	Ω,f	A
			$N = 5$ (B-like)			
B-like	94S1	Sampson	review	many	Ω,Υ	A-C
C II	91B4	Blum	RM	$^2P^o_{1/2-3/2}$; $^2P^o - {}^2D$	Ω	A
C II	96S3	Smith	RM, Exp	$2s^22p, 2s2p^2$	Q,DCS	A
C II, N III, O IV						
	90L1	Luo	RM	$n = 2$	Ω	A
C II, N III, O IV						
	92B3	Blum	RM	$2s^22p, 2s2p^2, 2p^3$	Υ	A
N III	92S4	Stafford	RM	n = 2,3	Ω,Υ	A
N III	94S3	Stafford	fits	n = 2,3	Ω,Υ	A,B
Ne VI	92H1	Hayes	CC	n = 2,3	Υ	A
Fe XXII	95Z2	Zhang	BPRM	$^2P^o_{1/2} - {}^4P_{5/2}$	Ω	A
Fe XXII	96A1	Ait-Tahar	Rel. RM	$2s^22p, 2s2p^2, 2p^3$	Ω	A
Fe XXII	97Z1	Zhang	BPRM	n = 2,3; J-levels	Ω,Υ	A
Mo XXXVIII	94Z3	Zhang	RDW	$n = 2 - 3$; J-levels	Ω,f	B
Gd LX	94Z3	Zhang	RDW	$n = 2 - 3$; J-levels	Ω,f	A
B-like, $Z = 8 - 14, 18, 20, 26$						
	94Z1	Zhang	RM	$2s^2p, 2s2p^2, 2p^3$	Ω	A,B
B-like, $Z = 8 - 14, 18, 20, 26$						
	94Z4	Zhang	RM	$2s^2p, 2s2p^2, 2p^3$	Υ	A,B
B-like, $8 \le Z \le 42$						
	94Z2	Zhang	RDW	$2s^2p, 2s2p^2, 2p^3$	Ω,f	C
B-like, $Z = 14, 26$						
	94Z3	Zhang	RDW	$n = 2 - 3$; J-levels	Ω,f	C
B-like, $43 \le Z \le 62$						
	94Z2	Zhang	RDW	$2s^2p, 2s2p^2, 2p^3$	Ω,f	B
B-like, $63 \le Z \le 92$						
	94Z2	Zhang	RDW	$2s^2p, 2s2p^2, 2p^3$	Ω,f	A
			$N = 6$ (C-like)			
C-like	94F2	Fossi	review	many	Ω,Υ	A-C
N II	94S4	Stafford	RM	$2p^2, 2s2p^3, 2p3p$	Ω,Υ	A
O III	91A1	Aggarwal	RM	$2s^22p^2, 2s2p^3, 2p^4$	q,f	A
O III	93A1	Aggarwal	RM	$2s^22p^2, 2s2p^3, 2p^4$	Υ	A

Table 1 (continued)

Ion	Ref.	Author	Method	Transitions	Data	Rating
O III	93B1	Bhatia	DW	$n = 2, 3$	Ω,f	C
F IV, Na VI, Al VIII, P X, S XI, Cl XII, Ar XIII, K XIV						
	92C2	Conlon	RM	$2s^22p^2, 2s2p^3$	Υ	B
Ne V	91L1	Lennon	RM	$2s^22p^2\ {}^3P_J,\ {}^1D,\ {}^1S$	Υ	A
Ne V	93B4	Bhatia	DW	$n = 2,3$	Ω,f	C
Mg VII	91B5	Burgess	RM, DW	$2s^22p^2, 2s2p^3$	Ω	A,B
Mg VII	95B4	Bhatia	DW	$2p^2, 2s2p^3, 2p^4, 2p3\ell$	Ω,f	C,D
Si IX	93B3	Bhatia	DW	$n = 2,3$	Ω,f	C
Ca XV	91A2	Aggarwal	RM	$2s^22p^2, 2s2p^3, 2p^4$	Υ	A
Ca XV	91A3	Aggarwal	Rel. RM/DW	$2s^22p^2, 2s2p^3, 2p^4$	Ω	A
Ca XV	92A1	Aggarwal	Rel. RM/DW	$2s^22p^2, 2s2p^3, 2p^4$	Υ	A
Ca XV	93B5	Bhatia	DW	$n = 2,3$	Ω,f	C
Fe XXI	91A4	Aggarwal	RM	$2s^22p^2, 2s2p^3, 2p^4$	q	A
Xe XLIX	97Z3	Zhang	RDW	$n = 2 - n = 3$	Ω,f	B
C-like, $Z = 7 - 16$						
	94L2	Lennon	RM	$2p^2\ {}^3P_J,\ {}^1D_2,\ {}^1S_0$	Υ	A
C-like, $9 \le Z \le 44$						
	96Z2	Zhang	RDW	$2p^2, 2s2p^3, 2p^4$	Ω,f	C
C-like, $Z = 12, 26$						
	97Z3	Zhang	RDW	$n = 2 - n = 3$	Ω,f	C
C-like, $Z = 21 - 28$						
	94W1	Warren	fits	$2p^2, 2s2p^3$	Υ	B,C
C-like, $45 \le Z \le 54$						
	96Z2	Zhang	RDW	$2p^2, 2s2p^3, 2p^4$	Ω,f	B
			$N = 7$ (N-like)			
N-like	94K1	Kato	review	many	Ω,Υ	A-C
O II	93M1	McLaughlin	RM	$2p^3, 2s2p^4, 2p^23s$	Ω,Υ	A
O II	93M2	McLaughlin	RM	$2p^3, 2s2p^4$	Υ	A
O II	93M3	McLaughlin	RM	$2p^3, 2s2p^4$	Ω,Υ	A
O II	94M2	McLaughlin	RM	$2p^3, 2s2p^4, 2p^23s$	Υ	A
O II	94M3	McLaughlin	RM	", fits	Υ	A
O II	95Z6	Zuo	RM, Exp	$2p^3, 2s2p^4$	Q	A
Mg VI	98B4	Bhatia	DW	$2p^3, 2s2p^4, 2p^5, 2p^23s$	Ω	C
N-like, $Z = 12 - 46$						
	99Z1	Zhang	RDW	$2p^2, 2s2p^3, 2p^4$	Ω,f	C
N-like, $Z = 47 - 64$						
	99Z1	Zhang	RDW	$2p^2, 2s2p^3, 2p^4$	Ω,f	B
N-like, $Z = 65 - 92$						
	99Z1	Zhang	RDW	$2p^2, 2s2p^3, 2p^4$	Ω,f	A
			$N = 8$ (O-like)			
O-like	94L1	Lang	review	many	Ω,Υ	A-C
O-like	94B6	Butler	BPRM	gd. state Js	Ω,Υ	A
F II	92N1	Nasser	DW	$2p^4, 2s2p^5$	Q	C
Ca XIII	94B3	Baliyan	RM	$n = 2,3$	Ω	A,B
Kr XXIX	91W2	Wijesundera	Rel. RM	$2s^22p^4, 2s2p^5, 2p^6$	Ω	A

Table 1 (continued)

Ion	Ref.	Author	Method	Transitions	Data	Rating
			$N = 9$ (F-like)			
F-like	98B1	Berrington	BPRM	$^2P_{3/2} - {}^2P_{1/2}$	Ω,Υ	A
F-like	94B5	Bhatia	review	many	Ω,Υ	A-E
Si VI	90M1	Mohan	RM	$2p^5\ {}^2P^o - 2p^4 3s, 3p$	Υ	A
Si VI	90M2	Mohan	RM	$2p^5\ {}^2P^o_{3/2} - {}^2P^o_{1/2}$	Υ	A
Cl IX	91M2	Mohan	RM	$2p^5, 2sp^6, 2p^4 3s$	Υ	B
Fe XVIII	93H1	Hummer	BPRM	$^2P^o_{3/2} - {}^2P^o_{1/2}$	Ω	A
Ni XX	90M3	Mohan	RM	$2p^5\ {}^2P^o_{3/2} - {}^2P^o_{1/2}$	Υ	B
Ni XX	90M5	Mohan	RM	$2s^2 2p5 - 2s2p^6, 2p^4 3s$	Υ	B
Se XXVI	98C1	Chen	RDWB	$2s^2p^5, 2s2p^6$, J-levels	Q	D
F-like, $Z = 10 - 26$						
	94S2	Saraph	RM	$2p^5\ {}^2P^o_{1/2} - {}^2P^o_{3/2}$	Υ	A
F-like, $22 \le Z \le 42$						
	91S1	Sampson	RDW	$n = 2 - 3$, J-levels	Ω,f	C-D
F-like, $22 \le Z \le 50$						
	91S1	Sampson	RDW	$n = 2 - 2$, J-levels	Ω,f	C-D
F-like, $Z = 26, 34, 42, 47, 54, 63$						
	94C2	Chen	RDW	$^2P^o_{1/2} - {}^2P^o_{3/2}$	Υ,f	C
F-like, $46 \le Z \le 62$						
	91S1	Sampson	RDW	$n = 2 - 3$, J-levels	Ω,f	B
F-like, $54 \le Z \le 66$						
	91S1	Sampson	RDW	$n = 2 - 2$, J-levels	Ω,f	B
F-like, $66 \le Z \le 92$						
	91S1	Sampson	RDW	$n = 2 - 3$, J-levels	Ω,f	A
F-like, $70 \le Z \le 92$						
	91S1	Sampson	RDW	$n = 2 - 2$, J-levels	Ω,f	A
			$N = 10$ (Ne-like)			
S VII	90M4	Mohan	RM	$2p^6 - 2p^5 3\ell$	Υ	C
Cl VIII	94M5	Mohan	RM	$2p^6\ {}^1S - 2p^5 3\ell$	Υ	C
Ar IX	91M1	Mohan	RM	$2p^6\ {}^1S - 2p^5 3\ell$	Υ	C
Ar IX, Fe XVII						
	93I2	Ivanov	QED	$2p^6 - 2p^5 3\ell, 2s2p^6 3\ell$	Q,q	C
Ca XI	95M2	Mohan	RM	$2p^6 - 2p^5 3\ell$	Υ	C
Ti XIII	97M2	Mohan	RM	$2p^6 - 2p^5 3\ell$	Υ	C
Fe XVII	94B2	Badnell	review	many	Ω,Υ	A-E
Fe XVII	90Z3	Zhang	RDW	mag. levels	Ω	C
Fe XVII	92B2	Bhatia	DW	$2p^6 - 2p^5 3\ell$	Ω,f	C,D
Fe XVII	94C5	Cornille	DW	$2p^6 - 2p^5 3\ell, 2s2p^6 3\ell$	Υ,f	C
Fe XVII	97M3	Mohan	RM	$2p^6 - 2p^5 3\ell$	Υ	C
Fe XVII, Cu XX, Ge XXIII, Se XXV, Sr XXIX, Mo XXXIII, Ag XXXVIII						
	94C4	Cornille	DW	$2p^6 - 2p^5 3\ell, 4\ell$	Υ,f	C
Cu XX	95M1	Mohan	RM	$2p^6 - 2p^5 3\ell$	Ω,Υ	B
Se XXV	90C1	Chen	RDW	$n = 3$	Υ	C
Se XXV	91W1	Wijesundera	Rel.RM	$2p^6 - 2p^5 3\ell$	Ω	A
Mo XXXIII	90Z3	Zhang	RDW	mag. levels	Ω	B

Table 1 (continued)

Ion	Ref.	Author	Method	Transitions	Data	Rating
Xe XLV	94F3	Fontes	RDW	$n = 2 - n = 3$	Ω	B
U LXXXIII	94F3	Fontes	RDW	$n = 2 - n = 3$	Ω	A
			$N = 11$ (Na-like)			
Na-like	96K1	Keenan	fits	3s, 3p, 4s, 4p	Υ	C
Mg II	91P1	Pan	RM, QDT	$3s - 3p$	Q,DCS	B
Mg II	93S1	Smith	CC	$ns^2S - np^2P$	Q	A
Mg II	95S5	Sigut	RM	$3\ell, 4\ell, 5\ell$	Ω,Υ	A,B
Mg II, Si IV						
Si IV	94D2	Dufton	review	many	Ω,Υ	A-C
	92S3	Shevelko	approx.	$3s - 3p$	Q	B
Si IV, Ar VIII, Ti XII						
	91B1	Badnell	DW/RM	$3s - 3p, 3d$	Q	A,B
Ar VIII	93P1	Pindzola	DW	$3s - 3p$	Q,DCS	B
Ar VIII	96N1	Nakazaki	RM	$3s - 3p, 3d, 4s, 4p, 4d$	Q,DCS	A
Fe XVI	94B2	Badnell	review	many	Ω,Υ	A-E
Fe XVI	94C5	Cornille	DW	$3s\ ^2S_{1/2} - 3p\ ^2P_J$	Υ,f	C
Fe XVI	94T1	Tayal	RM	$3s - 4d$; J-levels	Ω,Υ	B
Fe XVI	92S2	Sampson	RDW	many	Ω	D
Ni XVIII	96M1	Mohan	RM	3s, 3p, 3d, 4s, 4p, 4d, 4f	Υ	B,C
Cu XIX	96Y1	Ying	RM	$3s - 3p, 3d$; $3p - 3d$	q	A
Na-like, $Z = 15, 17, 18, 19, 20, 21, 23, 24, 25, 27$						
	97E1	Eissner	BPRM	$n \leq 4$	Ω,Υ	A
Na-like, $22 \leq Z \leq 42$						
	90S2	Sampson	RDW	$n = 3 - n = 4, 5$	Ω,f	C-D
Na-like, $22 \leq Z \leq 52$						
	90S2	Sampson	RDW	$3s - 3p, 3d$; $3p - 3d$	Ω,f	C-D
Na-like, $43 \leq Z \leq 64$						
	90S2	Sampson	RDW	$n = 3 - n = 4, 5$	Ω,f	B
Na-like, $53 \leq Z \leq 70$						
	90S2	Sampson	RDW	$3s - 3p, 3d$; $3p - 3d$	Ω,f	B
Na-like, $65 \leq Z \leq 92$						
	90S2	Sampson	RDW	$n = 3 - n = 4, 5$	Ω,f	A
Na-like, $71 \leq Z \leq 92$						
	90S2	Sampson	RDW	$3s - 3p, 3d$; $3p - 3d$	Ω,f	A
			$N = 12$ (Mg-like)			
Al II	92D1	Doyle	RM	$3s^2, 3s3p, 3p^2$	Υ	A
Al II	92K2	Keenan	RM	$3s^2 - 3s3p\ ^3P_J$	Υ	A
Al II	94A2	Aggarwal	RM	$3s^2, 3p^2, 3s(3d, 4s, 4p)$	Ω	A
Al II	94A1	Aggarwal	RM	$3s^2, 3p^2, 3s(3d, 4s, 4p)$	Υ	A
Si III, Ar VII						
Si III	94D2	Dufton	review	many	Ω,Υ	A-C
	93G1	Griffin	RM	$3s^2 - 3s3p$	Q,DCS	A,B
Ar VII, Ti XI, Fe XV, Se XXIII						
	94B1	Badnell	RM	$3s^2\ ^1S - 3s3p\ ^3P$	Ω	B

Table 1 (continued)

Ion	Ref.	Author	Method	Transitions	Data	Rating
Fe XV	94B2	Badnell	review	many	Ω,Υ	A-E
Fe XV	97B2	Bhatia	DW	$3s^2, 3s3p, 3p^2,$ $3s4\ell, 3p4\ell$	Ω, f	C
			$N = 13$ (Al-like)			
Si II	94D2	Dufton	review	many	Ω,Υ	A-C
Si II	91D1	Dufton	RM	$3s^23p\ ^2P,\ 3s3p^2,$ $^4P,\ ^2D$	Υ	A
P III, S IV, Cl V						
	98S1	Saraph	BPRM	$3s^23p\ ^2P^o_{1/2} - {}^2P^o_{3/2}$	Ω,Υ	A
S IV	94D2	Dufton	review	many	Ω,Υ	A-C
Ar VI, K VII, Ca VIII						
	96S2	Saraph	BPRM	$3s^23p\ ^2P^o_{1/2} - {}^2P^o_{3/2}$	Ω,Υ	A
Fe XIV	94M1	Mason	review	many	Ω,Υ	C,D
Fe XIV	91D2	Dufton	RM	$3s^23p, 3s3p^2, 3s^23d$	Υ	A
Fe XIV	93B2	Bhatia	DW	$n = 3$	Ω, f	C
Fe XIV	96B2	Bhatia	DW	$n = 3$	Ω, f	C
Fe XIV	96S4	Storey	BPRM	$3s^23p\ ^2P^o_{1/2} - {}^2P^o_{3/2}$	Ω,Υ	A
			$N = 14$ (Si-like)			
S III	94D2	Dufton	review	many	Ω,Υ	A-C
S III	97T1	Tayal	RM	$n = 3,4$	Υ	A,B
Fe XIII	94M1	Mason	review	many	Ω,Υ	C,D
Fe XIII	95T1	Tayal	RM	$n = 3$; J-levels	Υ	B
Si-like, $Z = 16 - 20$						
	95G4	Galavis	BPRM	$3s^23p^2$,J-levels	Υ	A
			$N = 15$ (P-like)			
S II	94D2	Dufton	review	many	Ω,Υ	A-C
S II	90H1	Ho	RM	$3p^3, 3s3p^4, 3p^23d, 4s$	Ω,Υ	B,C
S II	93C1	Cai	RM	$n = 3, 4$	Υ	A-D
S II	96R1	Ramsbottom	RM	$3p^3, 3s3p^4, 3p^23d$	Υ	A,B
S II	96R2	Ramsbottom	RM	$3p^3, 3s3p^4, 3p^23d, 3p^24\ell$	Υ	A,B
S II	97L1	Liao	RM,Exp	$3p^3, 3s3p^4$	Q	A
S II	97T2	Tayal	RM	$n = 3,4$	Υ	A,B
Ar IV	97R1	Ramsbottom	RM	$3p^3, 3s3p^4, 3p^23d$	Υ	A,B
Fe XII	94M1	Mason	review	many	Ω,Υ	C,D
Fe XII	98B2	Binello	BPRM	$3s^23p^3$	Ω,Υ	A
Fe XII	98B3	Binello	BPRM	E1 Trans.	Ω,Υ	A
			$N = 16$ (S-like)			
Ar III	90J1	Johnson	RM	$3s^23p^4$	Υ	A
Ar III	98G1	Galavis	BPRM	E2 Trans.	Ω,Υ	A
Ti VII	91C2	Clark	DW	$3p^4-$	Ω	D
Fe XI	94M1	Mason	review	many	Ω,Υ	C,D

Table 1 (continued)

Ion	Ref.	Author	Method	Transitions	Data	Rating
Fe XI	99G1	Gupta	RM	$3s3p^4, 3s3p^5$, J-levels	Υ	B,C
S-like, $Z = 18 - 20$						
	95G4	Galavis	BPRM	$3s^23p^4$,J-levels	Υ	A
			$N = 17$	(Cl-like)		
Ar II	96T1	Tayal	RM	$3p^5, 3s3p^6, 3p^43d$	Ω,Υ	B
Ar II	97G1	Griffin	RM	$3p^5, 3p^44s, 4p$	Q	B
Fe X	94M1	Mason	review	many	Ω,Υ	C,D
Fe X	94M6	Mohan	RM	$3p^5, 3s3p^6, 3p^43d$	Υ	B
Fe X	95B3	Bhatia	DW	$n = 3$	Ω,f	C,D
Cl-like, $Z = 18 - 28$, Ar II – Ni XII						
	95P1	Pelan	BPRM	$^2P^o_{3/2} - {}^2P^o_{1/2}$	Υ	A
			$N = 18$	(Ar-like)		
Fe IX	94M1	Mason	review	many	Ω,Υ	C,D
Fe IX	91F1	Fawcett	DW	$3s^23p^6, 3s^23p^53d$, $3s^23p^54s$	Ω,f	C,D
Mo XXV, Xe XXXVII, Eu XLVI						
	91C1	Chen	DW	$3p - 3d$	q	C
			$N = 19$	(K-like)		
Ca II	91P1	Pan	RM, QDT	$4s - 4p$	Q,DCS	A
Ca II	91Z1	Zatsarinny	CC	$4s - 4p$	Q	A
Ca II	92C1	Chidichimo	CDW	$4s - 5f, 5s - 4f$	Ω	B
Ca II	95B5	Burgess	DW	$3d, 4s, 4p, 4d, 5s$	Ω,Υ	C
Ti IV	91G1	Griffin	RM	$3d, 4s, 4p$	Ω	B
			$N = 21$	(Sc-like)		
Fe VI	99C1	Chen	BPRM	$3d^3, 3d^4s, 4p$	Ω,Υ	A,B
Fe VI	99C2	Chen	BPRM	$3d^3, 3d^4s, 4p$	Ω	A
			$N = 22$	(Ti-like)		
V II, Cr III, Mn IV, Fe V, Co VI, Ni VII						
Ti-like	95B1	Berrington	RM	$3d^4\ {}^5D_J$, ${}^5D'_J$	Ω,Υ	B,C
			$N = 23$	(V-like)		
Mn III, Fe IV, Co V, Ni VI						
V-like	95B2	Berrington	RM	$3d^5\ {}^4G_J$, ${}^4P_J$, ${}^4D_J$	Υ	B,C
Fe IV	97Z3	Zhang	RM	$3d^5, 3d^44s, 3d^44p$	Υ	B,C
			$N = 24$	(Cr-like)		
Fe III	91B3	Berrington	RM	$3d^6\ {}^5D_J$	Ω	B,C
Fe III	95Z3	Zhang	RM	$3d^6\ {}^5D_J$	Ω,Υ	A,B
Fe III	96Z1	Zhang	RM	$3d^6, 3d^54s, 3d^54p$	Υ	B,C

Table 1 (continued)

Ion	Ref.	Author	Method	Transitions	Data	Rating
			$N = 25$ (Mn-like)			
Fe II	93P2	Pradhan	RM	many	Ω	C,D
Fe II	93P3	Pradhan	RM	^6D_J, ^4F_J, ^4D_J, ^4P_J	Ω	A,B
Fe II	95Z1	Zhang	RM	$3d^64s, 3d^7, 3d^64p$	Υ	B,C
Fe II	96B1	Bautista	RM	$3d^64s$	Υ	C,D
			$N = 27$ (Co-like)			
Ni II	96B1	Bautista	RM	$3d^9 - 3d^84s$	Ω,Υ	U
Ni II	96W1	Watts	RM	$3d^9 - 3d^84s$	Ω,Υ	U
			$N = 28$ (Ni-like)			
Cu II	95G3	Griffin	RM	$3d^{10} - 3d^94s, 4p$	Q	C
Zr XIII, Mo XV						
	96F1	Fournier	reson.	$3d^{10} - 3d^94s, 4p$	Q	C
Ta XLVI	95C1	Chen	RDW	$3d^{10} - 3d^94\ell$	q	C,D
Gd XXXVII, U LXV						
	96C1	Chen	RDW	$3d^{10} - 3d^94\ell$	q	C,D
Ni-like, $60 \le Z \le 72$						
	91Z2	Zhang	RDW	$n = 3 - n = 4, 5$	Ω,f	C,D
Ni-like, $73 \le Z \le 92$						
	91Z2	Zhang	RDW	$n = 3 - n = 4, 5$	Ω,f	A,B
			$N = 29$ (Cu-like)			
Zn II	91P2	Pindzola	CC	$4s - 4p, 4d, 5s$	Q,DCS	B
Gd XXXVI	92S2	Sampson	RDW	many	Ω	B
Cu-like, $60 \le Z \le 74$						
	90Z2	Zhang	RDW	$n = 4 - 4, 5$	Ω,f	C,D
Cu-like, $75 \le Z \le 92$						
	90Z2	Zhang	RDW	$n = 4 - 4, 5$	Ω,f	A,B
			$N = 30$ (Zn-like)			
Kr VII	95G1	Gorczyca	BPRM	$4s^2\ ^1S - 4s4p\ ^3P$	Ω	B
			$N = 32$ (Ge-like)			
Kr V	97S1	Schöning	RM	$4p^2$; J-levels	Υ	C
			$N = 33$ (As-like)			
Kr IV	95S4	Schöning	RM	$4p^3$; J-levels	Ω,Υ	C
Kr IV	97S1	Schöning	RM	$4p^3$; J-levels	Υ	C
			$N = 34$ (Se-like)			
Kr III	97S1	Schöning	RM	$4p^4$; J-levels	Υ	C

Table 1 (continued)

Ion	Ref.	Author	Method	Transitions	Data	Rating
			$N = 37$ (Rb-like)			
Sr II	92C1	Chidichimo	CDW	$4s - 5f, 5s - 4f$	Ω	B
			$N = 51$ (Sb-like)			
Xe IV	95S3	Schoning	CC	$5s^2 5p^3$; J-levels	Ω, Υ	C

3.1.5.2 Effective collision strengths, wavelengths, and A-values

At electron temperatures around 10000 K the elements in a plasma source are in low ionization stages and low levels of excitation. In astronomy such sources are often "nebular" plasmas such as found in supernova remnants, diffuse and planetary nebulae, stellar atmospheres, active galactic nuclei, and the interstellar medium. In Table 2 we present the maxwellian averaged collision strengths $\Upsilon(T)$, and the observed wavelengths and Einstein A-coefficients, for low-lying transitions in a number of ions. These recommended data are taken from the best available sources and have been interpolated where necessary to obtain the $\Upsilon(T)$ at 5000 K, 10000K, 15000 K, and 20000 K (data sources are listed in the review article by Pradhan and Peng [95P2]).

The decimal and exponent notation for the effective collision strength $\Upsilon(T)$ is 'a.bc-x', where 'x' is the exponent in 10^x. The "$\Downarrow$" after the *first* fine structure transition within a multiplet indicates that the available value is for the whole LS multiplet, which may be divided according to the fine structure statistical weights among the other transitions as described above for cases *when one of the levels has only one associated J-value* (see subsection 3.2.3.4), i.e. for levels with $L = 0$ or $S = 0$. For transitions such as ^{1}D $-$ ^{3}P, such division is not possible in a straightforward manner and only the total multiplet value may be used (although Table 2 lists the fine structure levels). The "–" indicate that the data is not available for those transitions.

The order of transitions in Table 2 with respect to the upper and lower levels is mixed, and the initial levels under the column 'Transition' is not usually the lower one. Therefore care must be exercised in using Eq. (7) or (8) to determine the lower and the upper levels E_i or E_j. Wavelengths may be converted into excitation energy as E_{ij}[Ryd] = 911.26708/λ[Å] or E_{ij}[eV] = 12399/λ[Å] (assuming the Rydberg constant for infinite mass $R_\infty = 911.26708$).

Table 2. Effective collision strengths and A-values.

Ion	Transition	λ [Å]	A [s^{-1}]	$\Upsilon(T)$			
				5000 K	10000 K	15000 K	20000 K
H I	$1s - 2s$	1215.67	$8.23 + 0$	$2.55 - 1$	$2.74 - 1$	$2.81 - 1$	$2.84 - 1$
	$1s - 2p$	1215.66	$6.265 + 8$	$4.16 - 1$	$4.72 - 1$	$5.28 - 1$	$5.85 - 1$
He I	$1^1S - 2^3S$	625.48	$1.13 - 4$	$6.50 - 2$	$6.87 - 2$	$6.81 - 2$	$6.72 - 2$
	$1^1S - 2^1S$	601.30	$5.13 + 1$	$3.11 - 2$	$3.61 - 2$	$3.84 - 2$	$4.01 - 2$
	$1^1S - 2^3P^o$	591.29	$1.76 + 2$	$1.60 - 2$	$2.27 - 2$	$2.71 - 2$	$3.07 - 2$
	$1^1S - 2^1P^o$	584.21	$1.80 + 9$	$9.92 - 3$	$1.54 - 2$	$1.98 - 2$	$2.40 - 2$
	$2^3S - 2^1S$	15553.7	$1.51 - 7$	$2.24 + 0$	$2.40 + 0$	$2.32 + 0$	$2.20 + 0$
	$2^3S - 2^3P^o$	10817.0	$1.02 + 7$	$1.50 + 1$	$2.69 + 1$	$3.74 + 1$	$4.66 + 1$

Table 1 (continued)

Ion	Ref.	Author	Method	Transitions	Data	Rating
			$N = 37$ (Rb-like)			
Sr II	92C1	Chidichimo	CDW	$4s - 5f, 5s - 4f$	Ω	B
			$N = 51$ (Sb-like)			
Xe IV	95S3	Schoning	CC	$5s^2 5p^3$; J-levels	Ω, Υ	C

3.1.5.2 Effective collision strengths, wavelengths, and A-values

At electron temperatures around 10000 K the elements in a plasma source are in low ionization stages and low levels of excitation. In astronomy such sources are often "nebular" plasmas such as found in supernova remnants, diffuse and planetary nebulae, stellar atmospheres, active galactic nuclei, and the interstellar medium. In Table 2 we present the maxwellian averaged collision strengths $\Upsilon(T)$, and the observed wavelengths and Einstein A-coefficients, for low-lying transitions in a number of ions. These recommended data are taken from the best available sources and have been interpolated where necessary to obtain the $\Upsilon(T)$ at 5000 K, 10000K, 15000 K, and 20000 K (data sources are listed in the review article by Pradhan and Peng [95P2]).

The decimal and exponent notation for the effective collision strength $\Upsilon(T)$ is 'a.bc-x', where 'x' is the exponent in 10^x. The "$\Downarrow$" after the *first* fine structure transition within a multiplet indicates that the available value is for the whole LS multiplet, which may be divided according to the fine structure statistical weights among the other transitions as described above for cases *when one of the levels has only one associated J-value* (see subsection 3.2.3.4), i.e. for levels with $L = 0$ or $S = 0$. For transitions such as ^{1}D $-$ ^{3}P, such division is not possible in a straightforward manner and only the total multiplet value may be used (although Table 2 lists the fine structure levels). The "–" indicate that the data is not available for those transitions.

The order of transitions in Table 2 with respect to the upper and lower levels is mixed, and the initial levels under the column 'Transition' is not usually the lower one. Therefore care must be exercised in using Eq. (7) or (8) to determine the lower and the upper levels E_i or E_j. Wavelengths may be converted into excitation energy as E_{ij}[Ryd] = 911.26708/λ[Å] or E_{ij}[eV] = 12399/λ[Å] (assuming the Rydberg constant for infinite mass $R_\infty = 911.26708$).

Table 2. Effective collision strengths and A-values.

Ion	Transition	λ [Å]	A [s^{-1}]	$\Upsilon(T)$			
				5000 K	10000 K	15000 K	20000 K
H I	$1s - 2s$	1215.67	$8.23 + 0$	$2.55 - 1$	$2.74 - 1$	$2.81 - 1$	$2.84 - 1$
	$1s - 2p$	1215.66	$6.265 + 8$	$4.16 - 1$	$4.72 - 1$	$5.28 - 1$	$5.85 - 1$
He I	$1^1S - 2^3S$	625.48	$1.13 - 4$	$6.50 - 2$	$6.87 - 2$	$6.81 - 2$	$6.72 - 2$
	$1^1S - 2^1S$	601.30	$5.13 + 1$	$3.11 - 2$	$3.61 - 2$	$3.84 - 2$	$4.01 - 2$
	$1^1S - 2^3P^o$	591.29	$1.76 + 2$	$1.60 - 2$	$2.27 - 2$	$2.71 - 2$	$3.07 - 2$
	$1^1S - 2^1P^o$	584.21	$1.80 + 9$	$9.92 - 3$	$1.54 - 2$	$1.98 - 2$	$2.40 - 2$
	$2^3S - 2^1S$	15553.7	$1.51 - 7$	$2.24 + 0$	$2.40 + 0$	$2.32 + 0$	$2.20 + 0$
	$2^3S - 2^3P^o$	10817.0	$1.02 + 7$	$1.50 + 1$	$2.69 + 1$	$3.74 + 1$	$4.66 + 1$

Table 2 (continued)

Ion	Transition	λ [Å]	A [s^{-1}]	$\Upsilon(T)$			
				5000 K	10000 K	15000 K	20000 K
	$2^3S - 2^1P^o$	8854.5	1.29 + 0	7.70 − 1	9.75 − 1	1.05 + 0	1.08 + 0
	$2^1S - 2^3P^o$	35519.5	2.70 − 2	1.50 + 0	1.70 + 0	1.74 + 0	1.72 + 0
	$2^1S - 2^1P^o$	20557.7	1.98 + 6	9.73 + 0	1.86 + 1	2.58 + 1	3.32 + 1
	$2^3P^o - 2^1P^o$	48804.3	−−	1.45 + 0	2.07 + 0	2.40 + 0	2.60 + 0
He II	1s − 2s	303.92	5.66 + 2	1.60 − 1	1.59 − 1	1.57 − 1	1.56 − 1
	1s − 2p	303.92	1.0 + 10	3.40 − 1	3.53 − 1	3.63 − 1	3.73 − 1
Li II	$1^1S - 2^3S$	210.11	2.039 − 2	5.54 − 2	5.49 − 2	5.43 − 2	5.38 − 2
	$1^1S - 2^1S$	−−	1.95 + 3	3.81 − 2	3.83 − 2	3.85 − 2	3.86 − 2
	$1^1S - 2^3P^o$	202.55	3.289 − 7	9.07 − 2	9.17 − 2	9.26 − 2	9.34 − 2
	$1^1S - 2^1P^o$	199.30	2.56 + 2	3.82 − 2	4.05 − 2	4.28 − 2	4.50 − 2
C I	$^1D_2 - {}^3P_0$	9811.03	7.77 − 8	6.03 − 1	1.14 + 0	1.60 + 0	1.96 + 0
	$^1D_2 - {}^3P_1$	9824.12	8.21 − 5	⇓	⇓	⇓	⇓
	$^1D_2 - {}^3P_2$	9850.28	2.44 − 4	⇓	⇓	⇓	⇓
	$^1S_0 - {}^3P_1$	4621.57	2.71 − 3	1.49 − 1	2.52 − 1	3.20 − 1	3.65 − 1
	$^1S_0 - {}^3P_2$	4628.64	2.00 − 5				
	$^1S_0 - {}^1D_2$	8727.18	5.28 − 1	1.96 − 1	2.77 − 1	3.40 − 1	3.92 − 1
	$^3P_1 - {}^3P_0$	6.094 + 6	7.95 − 8	2.43 − 1	3.71 − 1	−−	−−
	$^3P_2 - {}^3P_0$	2304147	1.71 − 14	1.82 − 1	2.46 − 1	−−	−−
	$^3P_2 - {}^3P_1$	3704140	2.65 − 7	7.14 − 1	1.02 + 0	−−	−−
	$^5S^o_2 - {}^3P_1$	2965.70	6.94 + 0	4.75 − 1	6.71 − 1	8.22 − 1	9.50 − 1
	$^5S^o_2 - {}^3P_2$	2968.08	1.56 + 1	⇓	⇓	⇓	⇓
C II	$^2P^o_{3/2} - {}^2P^o_{1/2}$	1.5774 + 5	2.29 − 6	1.89 + 0	2.15 + 0	2.26 + 0	2.28 + 0
	$^4P_{1/2} - {}^2P^o_{1/2}$	2325	7.0 + 1	2.43 − 1	2.42 − 1	2.46 − 1	2.48 − 1
	$^4P_{1/2} - {}^2P^o_{3/2}$	2329	6.3 + 1	1.74 − 1	1.77 − 1	1.82 − 1	1.84 − 1
	$^4P_{3/2} - {}^2P^o_{1/2}$	2324	1.4 + 0	3.61 − 1	3.62 − 1	3.68 − 1	3.70 − 1
	$^4P_{3/2} - {}^2P^o_{3/2}$	2328	9.4 + 0	4.72 − 1	4.77 − 1	4.88 − 1	4.93 − 1
	$^4P_{3/2} - {}^4P_{1/2}$	4.55 + 6	2.39 − 7	6.60 − 1	8.24 − 1	9.64 − 1	1.06 + 0
	$^4P_{5/2} - {}^2P^o_{1/2}$	2323	−−	2.29 − 1	2.34 − 1	2.42 − 1	2.45 − 1
	$^4P_{5/2} - {}^2P^o_{3/2}$	2326	5.1 + 1	1.02 + 0	1.02 + 0	1.04 + 0	1.05 + 0
	$^4P_{5/2} - {}^4P_{1/2}$	1.99 + 6	3.49 − 14	7.30 − 1	8.53 − 1	9.32 − 1	9.71 − 1
	$^4P_{5/2} - {}^4P_{3/2}$	3.53 + 6	3.67 − 7	1.65 + 0	1.98 + 0	2.23 + 0	2.39 + 0
C III	$^3P^o_2 - {}^1S_0$	1907	5.19 − 3	1.12 + 0	1.01 + 0	9.90 − 1	9.96 − 1
	$^3P^o_1 - {}^1S_0$	1909	1.21 + 2	⇓	⇓	⇓	⇓
	$^3P^o_0 - {}^1S_0$	1909.6	−−	⇓	⇓	⇓	⇓
	$^1P^o_1 - {}^1S_0$	977.02	1.79 + 9	3.85 + 0	4.34 + 0	4.56 + 0	4.69 + 0
	$^3P^o_1 - {}^3P^o_0$	4.22 + 6	3.00 − 7	8.48 − 1	9.11 − 1	9.75 − 1	1.03 + 0
	$^3P^o_2 - {}^3P^o_0$	1.25 + 6	−−	5.79 − 1	6.77 − 1	7.76 − 1	8.67 − 1
	$^3P^o_2 - {}^3P^o_1$	1.774 + 6	2.10 − 6	2.36 + 0	2.66 + 0	2.97 + 0	3.23 + 0
C IV	$^2P^o_{3/2} - {}^2S_{1/2}$	1548.2	2.65 + 8	−−	8.88 + 0	−−	8.95 + 0
	$^2P^o_{1/2} - {}^2S_{1/2}$	1550.8	2.63 + 8	−−	⇓	−−	⇓

Table 2 (continued)

Ion	Transition	λ [Å]	A [s^{-1}]	$\Upsilon(T)$			
				5000 K	10000 K	15000 K	20000 K
N I	$^2D^o_{5/2} - {}^4S^o_{3/2}$	5200.4	6.13 − 6	1.55 − 1	2.90 − 1	−−	4.76 − 1
	$^2D^o_{3/2} - {}^4S^o_{3/2}$	5197.9	2.28 − 5	1.03 − 1	1.94 − 1	−−	3.18 − 1
	$^2P^o_{3/2} - {}^4S^o_{3/2}$	3466.5	6.60 − 3	5.97 − 2	1.13 − 1	−−	1.89 − 1
	$^2P^o_{1/2} - {}^4S^o_{3/2}$	3466.5	2.72 − 3	2.98 − 2	5.67 − 2	−−	9.47 − 2
	$^2D^o_{5/2} - {}^2D^o_{3/2}$	1.148 + 7	1.24 − 8	1.28 − 1	2.69 − 1	−−	4.65 − 1
	$^2P^o_{3/2} - {}^2P^o_{1/2}$	2.59 + 8	5.17 − 13	3.29 − 2	7.10 − 2	−−	1.53 − 1
	$^2P^o_{3/2} - {}^2D^o_{5/2}$	10397.7	5.59 − 2	1.62 − 1	2.66 − 1	−−	4.38 − 1
	$^2P^o_{3/2} - {}^2D^o_{3/2}$	10407.2	2.52 − 2	8.56 − 2	1.47 − 1	−−	2.52 − 1
	$^2P^o_{1/2} - {}^2D^o_{5/2}$	1040.1	3.14 − 2	6.26 − 2	1.09 − 1	−−	1.90 − 1
	$^2P^o_{1/2} - {}^2D^o_{3/2}$	10407.6	4.80 − 2	6.01 − 2	9.70 − 2	−−	1.57 − 1
N II	$^1D_2 - {}^3P_0$	6529.0	5.35 − 7	2.57 + 0	2.64 + 0	2.70 + 0	2.73 + 0
	$^1D_2 - {}^3P_1$	6548.1	1.01 − 3	⇓	⇓	⇓	⇓
	$^1D_2 - {}^3P_2$	6583.4	2.99 − 3	⇓	⇓	⇓	⇓
	$^1S_0 - {}^3P_1$	3062.9	3.38 − 2	2.87 − 1	2.93 − 1	3.00 − 1	3.05 − 1
	$^1S_0 - {}^3P_2$	3071.4	1.51 − 4				
	$^1S_0 - {}^1D_2$	5754.6	1.12 + 0	9.59 − 1	8.34 − 1	7.61 − 1	7.34 − 1
	$^3P_1 - {}^3P_0$	2.055 + 6	2.08 − 6	3.71 − 1	4.08 − 1	4.29 − 1	4.43 − 1
	$^3P_2 - {}^3P_0$	7.65 + 5	1.16 − 12	2.43 − 1	2.72 − 1	3.01 − 1	3.16 − 1
	$^3P_2 - {}^3P_1$	1.22 + 6	7.46 − 6	1.01 + 0	1.12 + 0	1.21 + 0	1.26 + 0
	$^5S^o_2 - {}^3P_1$	2144	4.80 + 1	1.19 + 0	1.19 + 0	1.21 + 0	1.21 + 0
	$^5S^o_2 - {}^3P_2$	2140	1.07 + 2				
N III	$^2P^o_{3/2} - {}^2P^o_{1/2}$	5.73 + 5	4.77 − 5	1.32 + 0	1.45 + 0	1.55 + 0	1.64 + 0
	$^4P_{1/2} - {}^2P^o_{1/2}$	1748	3.39 + 2	1.89 − 1	1.98 − 1	2.04 − 1	2.07 − 1
	$^4P_{1/2} - {}^2P^o_{3/2}$	1754	3.64 + 2	1.35 − 1	1.51 − 1	1.62 − 1	1.68 − 1
	$^4P_{3/2} - {}^2P^o_{1/2}$	1747	8.95 + 2	2.81 − 1	2.98 − 1	3.09 − 1	3.16 − 1
	$^4P_{3/2} - {}^2P^o_{3/2}$	1752	5.90 + 1	3.67 − 1	3.99 − 1	4.23 − 1	4.35 − 1
	$^4P_{3/2} - {}^4P_{1/2}$	1.68 + 6	−−	1.01 + 0	1.10 + 0	1.14 + 0	1.16 + 0
	$^4P_{5/2} - {}^2P^o_{1/2}$	1744.4	−−	1.78 − 1	2.01 − 1	2.19 − 1	2.29 − 1
	$^4P_{5/2} - {}^2P^o_{3/2}$	1747	3.08 + 2	7.93 − 1	8.44 − 1	8.80 − 1	8.98 − 1
	$^4P_{5/2} - {}^4P_{1/2}$	7.10 + 5	−−	6.12 − 1	6.67 − 1	6.95 − 1	7.11 − 1
	$^4P_{5/2} - {}^4P_{3/2}$	1.23 + 6	−−	1.88 + 0	2.04 + 0	2.12 + 0	2.16 + 0
N IV	$^3P^o_2 - {}^1S_0$	1483.3	1.15 − 2	9.37 − 1	9.05 − 1	8.79 − 1	8.58 − 1
	$^3P^o_1 - {}^1S_0$	1486.4	5.77 + 2	⇓	⇓	⇓	⇓
	$^3P^o_0 - {}^1S_0$	1487.9	−−	⇓	⇓	⇓	⇓
	$^1P^o_1 - {}^1S_0$	765.15	2.40 + 9	3.84 + 0	3.53 + 0	3.41 + 0	3.36 + 0
	$^3P^o_1 - {}^3P^o_0$	1.585 + 6	6.00 − 6	−−	−−	−−	−−
	$^3P^o_2 - {}^3P^o_0$	4.83 + 5	−−	−−	−−	−−	−−
	$^3P^o_2 - {}^3P^o_1$	6.94 + 5	3.63 − 5	−−	−−	−−	−−
N V	$^2P^o_{3/2} - {}^2S_{1/2}$	1238.8	3.41 + 8	6.61 + 0	6.65 + 0	6.69 + 0	6.72 + 0
	$^2P^o_{1/2} - {}^2S_{1/2}$	1242.8	3.38 + 8	−−	⇓	−−	⇓

Table 2 (continued)

Ion	Transition	λ [Å]	A [s^{-1}]	$\Upsilon(T)$			
				5000 K	10000 K	15000 K	20000 K
O I	$^1D_2 - {}^3P_0$	6393.5	7.23 − 7	1.24 − 1	2.66 − 1	−−	5.01 − 1
	$^1D_2 - {}^3P_1$	6363.8	2.11 − 3	⇓	⇓		⇓
	$^1D_2 - {}^3P_2$	6300.3	6.34 − 3	⇓	⇓		⇓
	$^1S_0 - {}^3P_1$	2972.3	7.32 − 2	1.53 − 2	3.24 − 2	−−	6.07 − 2
	$^1S_0 - {}^3P_2$	2959.2	2.88 − 4	⇓	⇓		⇓
	$^1S_0 - {}^1D_2$	5577.3	1.22 + 0	7.32 − 2	1.05 − 1	−−	1.48 − 1
	$^3P_0 - {}^3P_1$	1.46 + 6	1.74 − 5	1.12 − 2	2.65 − 2	−−	6.93 − 2
	$^3P_0 - {}^3P_2$	4.41 + 5	1.00 − 10	1.48 − 2	2.92 − 2	−−	5.36 − 2
	$^3P_1 - {}^3P_2$	6.32 + 5	8.92 − 5	4.74 − 2	9.87 − 2	−−	2.07 − 1
O II	$^2D^o_{5/2} - {}^4S^o_{3/2}$	3728.8	3.50 − 5	7.95 − 1	8.01 − 1	8.10 − 1	8.18 − 1
	$^2D^o_{3/2} - {}^4S^o_{3/2}$	3726.0	1.79 − 4	5.30 − 1	5.34 − 1	5.41 − 1	5.45 − 1
	$^2P^o_{3/2} - {}^4S^o_{3/2}$	2470.3	5.70 − 2	2.65 − 1	2.70 − 1	2.75 − 1	2.80 − 1
	$^2P^o_{1/2} - {}^4S^o_{3/2}$	2470.2	2.34 − 2	1.33 − 1	1.35 − 1	1.37 − 1	1.40 − 1
	$^2D^o_{5/2} - {}^2D^o_{3/2}$	4.97 + 6	1.30 − 7	1.22 + 0	1.17 + 0	1.14 + 0	1.11 + 0
	$^2P^o_{3/2} - {}^2P^o_{1/2}$	5.00 + 7	2.08 − 11	2.80 − 1	2.87 − 1	2.93 − 1	3.00 − 1
	$^2P^o_{3/2} - {}^2D^o_{5/2}$	7319.9	1.07 − 1	7.18 − 1	7.30 − 1	7.41 − 1	7.55 − 1
	$^2P^o_{3/2} - {}^2D^o_{3/2}$	7330.7	5.78 − 2	4.01 − 1	4.08 − 1	4.14 − 1	4.22 − 1
	$^2P^o_{1/2} - {}^2D^o_{5/2}$	7321.8	6.15 − 2	2.90 − 1	2.95 − 1	3.00 − 1	3.05 − 1
	$^2P^o_{1/2} - {}^2D^o_{3/2}$	7329.6	1.02 − 1	2.70 − 1	2.75 − 1	2.81 − 1	2.84 − 1
O III	$^1D_2 - {}^3P_0$	4932.6	2.74 − 6	2.13 + 0	2.29 + 0	2.45 + 0	2.52 + 0
	$^1D_2 - {}^3P_1$	4958.9	6.74 − 3	⇓	⇓	⇓	⇓
	$^1D_2 - {}^3P_2$	5006.7	1.96 − 2	⇓	⇓	⇓	⇓
	$^1S_0 - {}^3P_1$	2321.0	2.23 − 1	2.72 − 1	2.93 − 1	3.17 − 1	3.29 − 1
	$^1S_0 - {}^3P_2$	2332.1	7.85 − 4	⇓	⇓	⇓	⇓
	$^1S_0 - {}^1D_2$	4363.2	1.78 + 0	4.94 − 1	5.82 − 1	6.10 − 1	6.10 − 1
	$^3P_1 - {}^3P_0$	883562	2.62 − 5	5.24 − 1	5.45 − 1	5.59 − 1	5.63 − 1
	$^3P_2 - {}^3P_0$	326611	3.02 − 11	2.58 − 1	2.71 − 1	2.83 − 1	2.89 − 1
	$^3P_2 - {}^3P_1$	518145	9.76 − 5	1.23 + 0	1.29 + 0	1.34 + 0	1.35 + 0
	$^5S^o_2 - {}^3P_1$	1660.8	2.12 + 2	1.07 + 0	1.21 + 0	1.25 + 0	1.26 + 0
	$^5S^o_2 - {}^3P_2$	1666.1	5.22 + 2	⇓	⇓	⇓	⇓
O IV	$^2P^o_{3/2} - {}^2P^o_{1/2}$	2.587 + 5	5.18 − 4	2.02 + 0	2.40 + 0	2.53 + 0	2.57 + 0
	$^4P_{1/2} - {}^2P^o_{1/2}$	1426.46	1.81 + 3	1.21 − 1	1.33 − 1	1.42 − 1	1.48 − 1
	$^4P_{1/2} - {}^2P^o_{3/2}$	1434.07	1.77 + 3	8.67 − 2	1.02 − 1	1.15 − 1	1.24 − 1
	$^4P_{3/2} - {}^2P^o_{1/2}$	1423.84	2.28 + 1	1.80 − 1	2.00 − 1	2.16 − 1	2.28 − 1
	$^4P_{3/2} - {}^2P^o_{3/2}$	1431.42	3.28 + 2	2.36 − 1	2.68 − 1	2.98 − 1	3.18 − 1
	$^4P_{3/2} - {}^4P_{1/2}$	1.68 + 6	−−	1.04 + 0	1.09 + 0	1.13 + 0	1.16 + 0
	$^4P_{5/2} - {}^2P^o_{1/2}$	1420.19	−−	1.15 − 1	1.36 − 1	1.55 − 1	1.69 − 1
	$^4P_{5/2} - {}^2P^o_{3/2}$	1427.78	1.04 + 3	5.08 − 1	5.67 − 1	6.15 − 1	6.48 − 1
	$^4P_{5/2} - {}^4P_{1/2}$	3.26 + 5	−−	7.14 − 1	6.88 − 1	7.06 − 1	7.36 − 1
	$^4P_{5/2} - {}^4P_{3/2}$	5.62 + 5	1.02 − 4	2.04 + 0	2.05 + 0	2.12 + 0	2.20 + 0

Table 2 (continued)

Ion	Transition	λ [Å]	A [s^{-1}]	$\Upsilon(T)$			
				5000 K	10000 K	15000 K	20000 K
O V	$^3P^o_2 - {}^1S_0$	1213.8	2.16 − 2	7.33 − 1	7.21 − 1	6.74 − 1	6.39 − 1
	$^3P^o_1 - {}^1S_0$	1218.3	2.25 + 3	⇓	⇓	⇓	⇓
	$^3P^o_0 - {}^1S_0$	1220.4	−−	⇓	⇓	⇓	⇓
	$^1P^o_1 - {}^1S_0$	629.7	2.80 + 9	2.66 + 0	2.76 + 0	2.82 + 0	2.85 + 0
	$^3P^o_1 - {}^3P^o_0$	7.35 + 5	5.81 − 5	7.26 − 1	8.39 − 1	8.65 − 1	8.66 − 1
	$^3P^o_2 - {}^3P^o_0$	2.26 + 5	−−	2.74 − 1	6.02 − 1	7.51 − 1	8.16 − 1
	$^3P^o_2 - {}^3P^o_1$	3.26 + 5	3.55 − 4	3.19 + 0	2.86 + 0	2.80 + 0	2.77 + 0
O VI	$^2P^o_{3/2} - {}^2S_{1/2}$	1031.9	4.15 + 8	4.98 + 0	5.00 + 0	5.03 + 0	5.05 + 0
	$^2P^o_{1/2} - {}^2S_{1/2}$	1037.6	4.08 + 8	⇓	⇓	⇓	⇓
Ne II	$^2P^o_{1/2} - {}^2P^o_{3/2}$	1.28 + 5	8.55 − 3	2.96 − 1	3.03 − 1	3.10 − 1	3.17 − 1
Ne III	$^1D_2 - {}^3P_0$	4012.8	8.51 − 6	1.63 + 0	1.65 + 0	1.65 + 0	1.64 + 0
	$^1D_2 - {}^3P_1$	3967.5	5.42 − 2	⇓	⇓	⇓	⇓
	$^1D_2 - {}^3P_2$	3868.8	1.71 − 1	⇓	⇓	⇓	⇓
	$^1S_0 - {}^3P_1$	1814.6	2.00 + 0	1.51 − 1	1.69 − 1	1.75 − 1	1.79 − 1
	$^1S_0 - {}^3P_2$	1793.7	3.94 − 3	⇓	⇓	⇓	⇓
	$^1S_0 - {}^1D_2$	3342.5	2.71 + 0	2.00 − 1	2.26 − 1	2.43 − 1	2.60 − 1
	$^3P_0 - {}^3P_1$	3.60 + 5	1.15 − 3	3.31 − 1	3.50 − 1	3.51 − 1	3.50 − 1
	$^3P_0 - {}^3P_2$	1.07 + 5	2.18 − 8	3.00 − 1	3.07 − 1	3.03 − 1	2.98 − 1
	$^3P_1 - {}^3P_2$	1.56 + 5	5.97 − 3	1.09 + 0	1.65 + 0	1.65 + 0	1.64 + 0
Ne IV	$^2D^o_{5/2} - {}^4S^o_{3/2}$	2420.9	4.58 − 4	8.45 − 1	8.43 − 1	8.32 − 1	8.24 − 1
	$^2D^o_{3/2} - {}^4S^o_{3/2}$	2418.2	5.77 − 3	5.63 − 1	5.59 − 1	5.55 − 1	5.50 − 1
	$^2P^o_{3/2} - {}^4S^o_{3/2}$	1601.5	1.27 + 0	3.07 − 1	3.13 − 1	3.12 − 1	3.09 − 1
	$^2P^o_{1/2} - {}^4S^o_{3/2}$	1601.7	5.21 − 1	1.53 − 1	1.56 − 1	1.56 − 1	1.55 − 1
	$^2D^o_{5/2} - {}^2D^o_{3/2}$	2.237 + 6	1.48 − 6	1.37 + 0	1.36 + 0	1.35 + 0	1.33 + 0
	$^2P^o_{3/2} - {}^2P^o_{1/2}$	1.56 + 7	2.82 − 9	3.17 − 1	3.43 − 1	3.58 − 1	3.70 − 1
	$^2P^o_{3/2} - {}^2D^o_{5/2}$	4714.3	3.88 − 1	8.56 − 1	9.00 − 1	9.08 − 1	9.09 − 1
	$^2P^o_{3/2} - {}^2D^o_{3/2}$	4724.2	4.37 − 1	4.73 − 1	5.09 − 1	5.15 − 1	5.16 − 1
	$^2P^o_{1/2} - {}^2D^o_{5/2}$	4717.0	1.15 − 2	3.40 − 1	3.68 − 1	3.73 − 1	3.74 − 1
	$^2P^o_{1/2} - {}^2D^o_{3/2}$	4725.6	3.93 − 1	3.24 − 1	3.36 − 1	3.39 − 1	3.39 − 1
Ne V	$^1D_2 - {}^3P_0$	3301.3	2.37 − 5	2.13 + 0	2.09 + 0	2.11 + 0	2.14 + 0
	$^1D_2 - {}^3P_1$	3345.8	1.31 − 1	⇓	⇓	⇓	⇓
	$^1D_2 - {}^3P_2$	3425.9	3.65 − 1	⇓	⇓	⇓	⇓
	$^1S_0 - {}^3P_1$	1574.8	4.21 + 0	2.54 − 1	2.46 − 1	2.49 − 1	2.51 − 1
	$^1S_0 - {}^3P_2$	1592.3	6.69 − 3	⇓	⇓	⇓	⇓
	$^1S_0 - {}^1D_2$	2972.8	2.85 + 0	6.63 − 1	5.77 − 1	6.10 − 1	6.49 − 1
	$^3P_1 - {}^3P_0$	2.428 + 5	1.28 − 3	1.68 + 0	1.41 + 0	1.19 + 0	1.10 + 0
	$^3P_2 - {}^3P_0$	90082	5.08 − 9	2.44 + 0	1.81 + 0	1.42 + 0	1.26 + 0
	$^3P_2 - {}^3P_1$	1.432 + 5	4.59 − 3	7.59 + 0	5.82 + 0	4.68 + 0	4.20 + 0
	$^5S^o_2 - {}^3P_1$	1137.0	2.37 + 3	1.11 + 0	1.43 + 0	1.39 + 0	1.34 + 0
	$^5S^o_2 - {}^3P_2$	1146.1	6.06 + 3	⇓	⇓	⇓	⇓

Table 2 (continued)

Ion	Transition	λ [Å]	A [s^{-1}]	$\Upsilon(T)$			
				5000 K	10000 K	15000 K	20000 K
Ne VI	$^2P^o_{3/2} - {}^2P^o_{1/2}$	7.642 + 4	2.02 − 2	3.22 + 0	2.72 + 0	2.37 + 0	2.15 + 0
	$^4P_{1/2} - {}^2P^o_{1/2}$	1003.6	1.59 + 4	1.54 − 1	1.37 − 1	1.26 − 1	1.18 − 1
	$^4P_{1/2} - {}^2P^o_{3/2}$	1016.6	1.43 + 4	1.85 − 1	1.53 − 1	1.36 − 1	1.27 − 1
	$^4P_{3/2} - {}^2P^o_{1/2}$	999.13	3.20 + 2	2.69 − 1	2.32 − 1	2.10 − 1	1.96 − 1
	$^4P_{3/2} - {}^2P^o_{3/2}$	1012.0	3.33 + 3	4.51 − 1	3.73 − 1	3.32 − 1	3.08 − 1
	$^4P_{3/2} - {}^4P_{1/2}$	2.24 + 5	−−	5.34 − 1	5.73 − 1	5.95 − 1	6.22 − 1
	$^4P_{5/2} - {}^2P^o_{1/2}$	992.76	−−	2.56 − 1	2.11 − 1	1.89 − 1	1.76 − 1
	$^4P_{5/2} - {}^2P^o_{3/2}$	1005.5	1.14 + 4	7.88 + 0	6.75 − 1	6.09 − 1	5.68 − 1
	$^4P_{5/2} - {}^4P_{1/2}$	92166	−−	4.12 − 1	4.23 − 1	4.36 − 2	4.56 − 1
	$^4P_{5/2} - {}^4P_{3/2}$	1.56 + 5	−−	1.10 + 0	1.16 + 0	1.20 + 0	1.26 + 0
Ne VII	$^3P^o_2 - {}^1S_0$	887.22	5.78 − 2	1.29 − 1	1.72 − 1	2.05 − 1	2.28 − 1
	$^3P^o_1 - {}^1S_0$	895.12	1.98 + 4	⇓	⇓	⇓	⇓
	$^3P^o_0 - {}^1S_0$	898.76	−−	⇓	⇓	⇓	⇓
	$^1P^o_1 - {}^1S_0$	465.22	4.09 + 9	1.39 + 0	1.56 + 0	1.63 + 0	1.66 + 0
	$^3P^o_1 - {}^3P^o_0$	2.20 + 5	1.99 − 3	−−	−−	−−	−−
	$^3P^o_2 - {}^3P^o_0$	69127.6	−−	−−	−−	−−	−−
	$^3P^o_2 - {}^3P^o_1$	1.01 + 5	1.25 − 2	−−	−−	−−	−−
Na III	$^2P^o_{1/2} - {}^2P^o_{3/2}$	7.319 + 4	4.59 − 2	3.00 − 1			
Na IV	$^1D_2 - {}^3P_0$	3417.2	2.24 − 5	1.17 + 0			
	$^1D_2 - {}^3P_1$	3362.2	1.86 − 1	⇓			
	$^1D_2 - {}^3P_2$	3241.7	6.10 − 1	⇓			
	$^1S_0 - {}^3P_1$	1529.3	7.10 + 0	1.63 − 1			
	$^1S_0 - {}^3P_2$	1503.8	1.05 − 2	⇓			
	$^1S_0 - {}^1D_2$	2803.7	3.46 + 0	1.57 − 1			
	$^3P_0 - {}^3P_1$	2.129 + 5	5.57 − 3	1.77 − 1			
	$^3P_0 - {}^3P_2$	62467.9	1.67 − 7	1.11 − 1			
	$^3P_1 - {}^3P_2$	90391.4	3.04 − 2	4.71 − 1			
Na V	$^2D^o_{5/2} - {}^4S^o_{3/2}$	2068.4	1.39 − 3	5.51 − 1			
	$^2D^o_{3/2} - {}^4S^o_{3/2}$	2066.9	2.70 − 2	3.68 − 1			
	$^2P^o_{3/2} - {}^4S^o_{3/2}$	1365.1	4.23 + 0	2.39 − 1			
	$^2P^o_{1/2} - {}^4S^o_{3/2}$	1365.8	1.76 + 0	1.20 − 1			
	$^2D^o_{5/2} - {}^2D^o_{3/2}$	2.78 + 6	1.56 − 6	6.96 − 1			
	$^2P^o_{3/2} - {}^2P^o_{1/2}$	2.70 + 6	3.66 − 7	4.38 − 1			
	$^2P^o_{3/2} - {}^2D^o_{5/2}$	4010.9	9.07 − 1	5.02 − 1			
	$^2P^o_{3/2} - {}^2D^o_{3/2}$	4016.7	1.28 + 0	2.79 − 1			
	$^2P^o_{1/2} - {}^2D^o_{5/2}$	4017.9	1.35 − 1	2.01 − 1			
	$^2P^o_{1/2} - {}^2D^o_{3/2}$	4022.7	9.75 − 1	1.90 − 1			
Na VI	$^1D_2 - {}^3P_0$	2816.1	−−	1.55 + 0	1.45 + 0	1.39 + 0	1.38 + 0
	$^1D_2 - {}^3P_1$	2872.7	4.06 − 1	⇓	⇓	⇓	⇓
	$^1D_2 - {}^3P_2$	2971.9	1.27 + 0	⇓	⇓	⇓	⇓
	$^1S_0 - {}^3P_1$	1356.6	1.69 + 1	1.73 − 1	1.72 − 1	1.72 − 1	1.73 − 1

Table 2 (continued)

Ion	Transition	λ [Å]	A [s^{-1}]	$\Upsilon(T)$			
				5000 K	10000 K	15000 K	20000 K
	$^1S_0 - {}^3P_2$	1343.9	−−	⇓	⇓	⇓	⇓
	$^1S_0 - {}^1D_2$	2568.9	5.27 + 0	1.07 − 1	1.16 − 1	1.28 − 1	1.39 − 1
	$^3P_1 - {}^3P_0$	1.43 + 5	6.14 − 3	7.24 − 1	7.70 − 1	7.73 − 1	7.58 − 1
	$^3P_2 - {}^3P_0$	5.37 + 4	−−	5.02 − 1	5.21 − 1	5.08 − 1	4.94 − 1
	$^3P_2 - {}^3P_1$	8.61 + 4	2.11 − 2	2.03 + 0	2.13 + 0	2.10 + 0	2.05 + 0
Mg II	$^2P^o_{3/2} - {}^2S_{1/2}$	2795.5	2.6 + 8	1.59 + 1	1.69 + 1	1.78 + 1	1.86 + 1
	$^2P^o_{1/2} - {}^2S_{1/2}$	2802.7	2.6 + 8	⇓	⇓	⇓	⇓
Mg IV	$^2P^o_{1/2} - {}^2P^o_{3/2}$	4.487 + 4	1.99 − 1	3.44 − 1	3.46 − 1	3.49 − 1	3.51 − 1
Mg V	$^1D_2 - {}^3P_0$	2993.1	5.20 − 5	1.31 + 0	1.33 + 0	1.32 + 0	1.30 + 0
	$^1D_2 - {}^3P_1$	2928.0	5.41 − 1	⇓	⇓	⇓	⇓
	$^1D_2 - {}^3P_2$	2782.7	1.85 + 0	⇓	⇓	⇓	⇓
	$^1S_0 - {}^3P_1$	1324.4	2.14 + 1	1.42 − 1	1.48 − 1	1.46 − 1	1.44 − 1
	$^1S_0 - {}^3P_2$	1293.9	2.45 − 2	⇓	⇓	⇓	⇓
	$^1S_0 - {}^1D_2$	2417.5	4.23 + 0	1.91 − 1	1.97 − 1	2.02 − 1	2.08 − 1
	$^3P_0 - {}^3P_1$	1.354 + 5	2.17 − 2	2.48 − 1	3.00 − 1	3.18 − 1	3.18 − 1
	$^3P_0 - {}^3P_2$	39654.2	1.01 − 6	2.31 − 1	2.92 − 1	3.04 − 1	2.99 − 1
	$^3P_1 - {}^3P_2$	5.608 + 4	1.27 − 1	8.30 − 1	1.03 + 0	1.08 + 0	1.07 + 0
Mg VII	$^1D_2 - {}^3P_0$	2441.4	−−	7.96 − 1	8.57 − 1	9.11 − 1	9.42 − 1
	$^1D_2 - {}^3P_1$	2509.2	1.17 + 0	⇓	⇓	⇓	⇓
	$^1D_2 - {}^3P_2$	2629.1	3.36 + 0	⇓	⇓	⇓	⇓
	$^1S_0 - {}^3P_1$	1189.8	4.58 + 1	2.08 − 1	1.85 − 1	1.75 − 1	1.73 − 1
	$^1S_0 - {}^3P_2$	1174.3	−−	⇓	⇓	⇓	⇓
	$^1S_0 - {}^1D_2$	2261.5	6.16 + 0	5.25 − 1	4.46 − 1	3.90 − 1	3.82 − 1
	$^3P_1 - {}^3P_0$	9.03 + 4	2.44 − 2	2.75 − 1	3.37 − 1	3.95 − 1	4.14 − 1
	$^3P_2 - {}^3P_0$	3.42 + 4	−−	1.90 − 1	3.01 − 1	3.88 − 1	4.09 − 1
	$^3P_2 - {}^3P_1$	5.50 + 4	8.09 − 2	7.69 + 0	1.08 + 0	1.32 + 0	1.39 + 0
Al II	$^3P^o_2 - {}^1S_0$	2661.1	−−	3.062 + 0	3.564 + 0	3.612 + 0	3.54 + 0
	$^3P^o_1 - {}^1S_0$	2669.9	−−	⇓	⇓	⇓	⇓
	$^3P^o_0 - {}^1S_0$	2674.3	−−	⇓	⇓	⇓	⇓
	$^1P^o_1 - {}^1S_0$	1670.8	1.46 + 9	2.045 + 0	3.251 + 0	4.096 + 0	4.717 + 0
	$^3P^o_1 - {}^3P^o_0$	1.6426 + 6	4.10 − 6	−−	−−	−−	−−
	$^3P^o_2 - {}^3P^o_0$	5.4124 + 5	− − −	−−	−−	−−	−−
	$^3P^o_2 - {}^3P^o_1$	8.072 + 5	2.45 − 5	−−	−−	−−	−−
Si II	$^2P^o_{3/2} - {}^2P^o_{1/2}$	3.48 + 5	2.17 − 4	5.59 + 0	5.70 + 0	5.78 + 0	5.77 + 0
	$^4P_{1/2} - {}^2P^o_{1/2}$	2335	4.55 + 3	5.50 − 1	5.16 − 1	4.88 − 1	4.67 − 1
	$^4P_{1/2} - {}^2P^o_{3/2}$	2350	4.41 + 3	4.33 − 1	4.02 − 1	3.81 − 1	3.65 − 1
	$^4P_{3/2} - {}^2P^o_{1/2}$	2329	1.32 + 1	8.32 − 1	7.80 − 1	7.37 − 1	7.06 − 1
	$^4P_{3/2} - {}^2P^o_{3/2}$	2344	1.22 + 3	1.13 + 0	1.05 + 0	9.97 − 1	9.56 − 1
	$^4P_{3/2} - {}^4P_{1/2}$	9.23 + 5	−−	4.92 + 0	4.51 + 0	4.18 + 0	3.94 + 0
	$^4P_{5/2} - {}^2P^o_{1/2}$	2319.8	−−	5.71 − 1	5.34 − 1	5.08 − 1	4.88 − 1

Table 2 (continued)

Ion	Transition	λ [Å]	A [s^{-1}]	$\Upsilon(T)$			
				5000 K	10000 K	15000 K	20000 K
	$^4P_{5/2} - {}^2P^o_{3/2}$	2335	2.46 + 3	2.33 + 0	2.19 + 0	2.08 + 0	1.99 + 0
	$^4P_{5/2} - {}^4P_{1/2}$	3.53 + 5	−−	1.68 + 0	1.67 + 0	1.63 + 0	1.57 + 0
	$^4P_{5/2} - {}^4P_{3/2}$	5.70 + 5	−−	7.36 + 0	6.94 + 0	6.58 + 0	6.32 + 0
Si III	$^3P^o_2 - {}^1S_0$	1882.7	1.20 − 2	6.96 + 0	5.46 + 0	4.82 + 0	4.41 + 0
	$^3P^o_1 - {}^1S_0$	1892.0	1.67 + 4	⇓	⇓	⇓	⇓
	$^3P^o_0 - {}^1S_0$	1896.6	−−	⇓	⇓	⇓	⇓
	$^1P^o_1 - {}^1S_0$	1206.5	2.59 + 9	5.30 + 0	5.60 + 0	5.93 + 0	6.22 + 0
	$^3P^o_1 - {}^3P^o_0$	7.78 + 5	3.86 − 5	1.78 + 0	1.81 + 0	1.83 + 0	1.83 + 0
	$^3P^o_2 - {}^3P^o_0$	2.56 + 5	3.20 − 9	3.66 + 0	3.62 + 0	3.53 + 0	3.43 + 0
	$^3P^o_2 - {}^3P^o_1$	3.82 + 5	2.42 − 4	1.04 + 1	1.04 + 1	1.02 + 1	1.00 + 1
Si IV	$^2P^o_{3/2} - {}^2S_{1/2}$	1393.8	7.73 + 8	1.69 + 1	1.60 + 1	1.61 + 1	1.62 + 1
	$^2P^o_{1/2} - {}^2S_{1/2}$	1402.8	7.58 + 8	⇓	⇓	⇓	⇓
Si VI	$^2P^o_{1/2} - {}^2P^o_{3/2}$	1.964 + 4	2.38 + 0	2.42 − 1			
S II	$^2D^o_{5/2} - {}^4S^o_{3/2}$	6716.5	2.60 − 4	4.90 + 0	4.66 + 0	4.44 + 0	4.26 + 0
	$^2D^o_{3/2} - {}^4S^o_{3/2}$	6730.8	8.82 − 4	3.27 + 0	3.11 + 0	2.97 + 0	2.84 + 0
	$^2P^o_{3/2} - {}^4S^o_{3/2}$	4068.6	2.25 − 1	1.67 + 0	2.07 + 0	1.98 + 0	2.07 + 0
	$^2P^o_{1/2} - {}^4S^o_{3/2}$	4076.4	9.06 − 2	8.31 − 1	8.97 − 1	9.87 − 1	1.03 + 0
	$^2D^o_{5/2} - {}^2D^o_{3/2}$	3.145 + 6	3.35 − 7	7.90 + 0	7.46 + 0	7.11 + 0	8.65 + 0
	$^2P^o_{3/2} - {}^2P^o_{1/2}$	2.14 + 6	1.03 − 6	2.02 + 0	2.54 + 0	2.13 + 0	2.22 + 0
	$^2P^o_{3/2} - {}^2D^o_{5/2}$	10320.4	1.79 − 1	5.93 + 0	4.77 + 0	4.75 + 0	4.68 + 0
	$^2P^o_{3/2} - {}^2D^o_{3/2}$	10286.7	1.33 − 1	3.41 + 0	2.74 + 0	2.74 + 0	2.71 + 0
	$^2P^o_{1/2} - {}^2D^o_{5/2}$	10373.3	7.79 − 2	2.47 + 0	1.99 + 0	1.99 + 0	1.97 + 0
	$^2P^o_{1/2} - {}^2D^o_{3/2}$	10336.3	1.63 − 1	2.20 + 0	1.76 + 0	1.76 + 0	1.73 + 0
S III	$^1D_2 - {}^3P_0$	8833.9	5.82 − 6	9.07 + 0	8.39 + 0	8.29 + 0	8.20 + 0
	$^1D_2 - {}^3P_1$	9068.9	2.21 − 2	⇓	⇓	⇓	⇓
	$^1D_2 - {}^3P_2$	9531.0	5.76 − 2	⇓	⇓	⇓	⇓
	$^1S_0 - {}^3P_1$	3721.7	7.96 − 1	1.16 + 0	1.19 + 0	1.21 + 0	1.24 + 0
	$^1S_0 - {}^3P_2$	3797.8	1.05 − 2	⇓	⇓	⇓	⇓
	$^1S_0 - {}^1D_2$	6312.1	2.22 + 0	1.42 + 0	1.88 + 0	2.02 + 0	2.08 + 0
	$^3P_1 - {}^3P_0$	3.347 + 5	4.72 − 4	2.64 + 0	2.59 + 0	2.38 + 0	2.20 + 0
	$^3P_2 - {}^3P_0$	1.20 + 5	4.61 − 8	1.11 + 0	1.15 + 0	1.15 + 0	1.14 + 0
	$^3P_2 - {}^3P_1$	187129	2.07 − 3	5.79 + 0	5.81 + 0	5.56 + 0	5.32 + 0
	$^5S^o_2 - {}^3P_1$	1683.5	6.22 + 3	−−	3.8 + 0	3.7 + 0	3.6 + 0
	$^5S^o_2 - {}^3P_2$	1698.86	1.70 + 4	⇓	⇓	⇓	⇓
S IV	$^2P^o_{3/2} - {}^2P^o_{1/2}$	1.05 + 5	7.73 − 3	−−	6.42 + 0	6.41 + 0	6.40 + 0
	$^4P_{1/2} - {}^2P^o_{1/2}$	1404.9	5.50 + 4	−−	5.50 − 1	4.80 − 1	4.60 − 1
	$^4P_{1/2} - {}^2P^o_{3/2}$	1423.9	3.39 + 4	−−	6.60 − 1	6.30 − 1	6.10 − 1
	$^4P_{3/2} - {}^2P^o_{1/2}$	1398.1	1.40 + 2	−−	8.70 − 1	8.30 − 1	8.00 − 1
	$^4P_{3/2} - {}^2P^o_{3/2}$	1017.0	1.95 + 4	−−	1.47 + 0	1.40 + 0	1.34 + 0
	$^4P_{3/2} - {}^4P_{1/2}$	2.91 + 5	−−	−−	3.04 + 0	2.85 + 0	2.72 + 0

Table 2 (continued)

Ion	Transition	λ [Å]	A [s^{-1}]	$\Upsilon(T)$			
				5000 K	10000 K	15000 K	20000 K
	$^4P_{5/2} - {}^2P^o_{1/2}$	1387.5	−−	−−	9.5 − 1	9.1 − 1	8.8 − 1
	$^4P_{5/2} - {}^2P^o_{3/2}$	1406.1	3.95 + 4	−−	2.53 + 0	2.41 + 0	2.33 + 0
	$^4P_{5/2} - {}^4P_{1/2}$	1.12 + 5	−−	−−	2.92 + 0	2.71 + 0	2.56 + 0
	$^4P_{5/2} - {}^4P_{3/2}$	1.85 + 5	−−	−−	7.01 + 0	6.57 + 0	6.20 + 0
S V	$^3P^o_2 - {}^1S_0$	1188.3	6.59 − 2	9.11 − 1	9.10 − 1	9.14 − 1	9.05 − 1
	$^3P^o_1 - {}^1S_0$	1199.1	1.26 + 5	⇓	⇓	⇓	⇓
	$^3P^o_0 - {}^1S_0$	1204.5	−−	⇓	⇓	⇓	
	$^1P^o_1 - {}^1S_0$	786.48	5.25 + 9	7.30 + 0	7.30 + 0	7.29 + 0	7.27 + 0
	$^3P^o_1 - {}^3P^o_0$	2.71 + 5	9.16 − 4		2.72 − 1		
	$^3P^o_2 - {}^3P^o_0$	88401.7	−−		4.00 − 1		
	$^3P^o_2 - {}^3P^o_1$	1.312 + 5	5.49 − 3		1.24 + 0		
S VI	$^2P^o_{3/2} - {}^2S_{1/2}$	933.38	1.7 + 9	1.18 + 1	1.19 + 1	1.19 + 1	1.19 + 1
	$^2P^o_{1/2} - {}^2S_{1/2}$	944.52	1.6 + 9	⇓	⇓	⇓	⇓
	$^2P^o_{1/2} - {}^2P^o_{3/2}$	1.0846 + 5	7.75 − 3	5.85 + 0	6.67 + 0	7.10 + 0	7.27 + 0
Cl II	$^1D_2 - {}^3P_0$	9383.4	9.82 − 6		3.86 + 0		
	$^1D_2 - {}^3P_1$	9123.6	2.92 − 2		⇓		
	$^1D_2 - {}^3P_2$	8578.7	1.04 − 1		⇓		
	$^1S_0 - {}^3P_1$	3677.9	1.31 + 0		4.56 − 1		
	$^1S_0 - {}^3P_2$	3587.1	1.97 − 2		⇓		
	$^1S_0 - {}^1D_2$	6161.8	2.06 + 0		1.15 + 0		
	$^3P_0 - {}^3P_1$	3.328 + 5	1.46 − 3		9.33 − 1		
	$^3P_0 - {}^3P_2$	1.004 + 5	4.57 − 7		4.43 − 1		
	$^3P_1 - {}^3P_2$	1.437 + 5	7.57 − 3		2.17 + 0		
Cl III	$^2D^o_{5/2} - {}^4S^o_{3/2}$	5517.7	7.04 − 4	1.94 + 0	2.05 + 0	2.04 + 0	2.04 + 0
	$^2D^o_{3/2} - {}^4S^o_{3/2}$	5537.9	4.83 − 3	1.29 + 0	1.36 + 0	1.36 + 0	1.35 + 0
	$^2P^o_{3/2} - {}^4S^o_{3/2}$	3342.9	7.54 − 1	7.69 − 1	8.37 − 1	8.88 − 1	9.20 − 1
	$^2P^o_{1/2} - {}^4S^o_{3/2}$	3353.3	3.05 − 1	3.85 − 1	4.18 − 1	4.44 − 1	4.61 − 1
	$^2D^o_{5/2} - {}^2D^o_{3/2}$	1.516 + 6	3.22 − 6	4.45 + 0	4.52 + 0	4.51 + 0	4.48 + 0
	$^2P^o_{3/2} - {}^2P^o_{1/2}$	1.081 + 6	7.65 − 6	1.73 + 0	1.76 + 0	1.81 + 0	1.86 + 0
	$^2P^o_{3/2} - {}^2D^o_{5/2}$	8480.9	3.16 − 1	3.75 + 0	4.20 + 0	4.33 + 0	4.32 + 0
	$^2P^o_{3/2} - {}^2D^o_{3/2}$	8433.7	3.23 − 1	2.01 + 0	2.19 + 0	2.34 + 0	2.25 + 0
	$^2P^o_{1/2} - {}^2D^o_{5/2}$	8552.1	1.00 − 1	1.44 + 0	1.56 + 0	1.60 + 0	1.60 + 0
	$^2P^o_{1/2} - {}^2D^o_{3/2}$	8500.0	3.03 − 1	1.45 + 0	1.65 + 0	1.71 + 0	1.72 + 0
Cl IV	$^1D_2 - {}^3P_0$	7263.4	1.54 − 5	5.10 + 0	5.42 + 0	5.88 + 0	6.19 + 0
	$^1D_2 - {}^3P_1$	7529.9	5.57 − 2	⇓	⇓	⇓	⇓
	$^1D_2 - {}^3P_2$	8045.6	2.08 − 1	⇓	⇓	⇓	⇓
	$^1S_0 - {}^3P_1$	3118.6	2.19 + 0	2.04 + 0	2.27 + 0	2.32 + 0	2.30 + 0
	$^1S_0 - {}^3P_2$	3204.5	2.62 − 2	⇓	⇓	⇓	⇓
	$^1S_0 - {}^1D_2$	5323.3	4.14 + 0	9.35 − 1	1.39 + 0	1.73 + 0	1.92 + 0
	$^3P_1 - {}^3P_0$	2.035 + 5	2.13 − 3		4.75 − 1		
	$^3P_2 - {}^3P_0$	74521	2.70 − 7		4.00 − 1		

Table 2 (continued)

Ion	Transition	λ [Å]	A [s^{-1}]	$\Upsilon(T)$			
				5000 K	10000 K	15000 K	20000 K
	$^3P_2 - {}^3P_1$	1.1741 + 5	8.32 − 3		1.50 + 0		
Cl V	$^2P^o_{3/2} - {}^2P^o_{1/2}$	67049	2.98 − 2		1.05 + 0		
Ar II	$^2P^o_{1/2} - {}^2P^o_{3/2}$	69851.9	5.27 − 2		6.35 − 1		
Ar III	$^1D_2 - {}^3P_0$	8038.7	2.21 − 5		4.74 + 0		
	$^1D_2 - {}^3P_1$	7751.1	8.23 − 2	⇓	⇓	⇓	⇓
	$^1D_2 - {}^3P_2$	7135.8	3.14 − 1	⇓	⇓	⇓	⇓
	$^1S_0 - {}^3P_1$	3109.1	3.91 + 0		6.80 − 1		
	$^1S_0 - {}^3P_2$	3006.1	4.17 − 2	⇓	⇓	⇓	⇓
	$^1S_0 - {}^1D_2$	5191.8	2.59 + 0		8.23 − 1		
	$^3P_0 - {}^3P_1$	2.184 + 5	5.17 − 3		1.18 + 0		
	$^3P_0 - {}^3P_2$	63686.2	2.37 − 6		5.31 − 1		
	$^3P_1 - {}^3P_2$	89910	3.08 − 2		2.24 + 0		
Ar IV	$^2D^o_{5/2} - {}^4S^o_{3/2}$	4711.3	1.77 − 3	2.56 + 0	6.13 + 0	1.64 + 0	1.46 + 1
	$^2D^o_{3/2} - {}^4S^o_{3/2}$	4740.2	2.23 − 2	1.71 + 0	1.30 + 0	1.14 + 0	9.70 − 1
	$^2P^o_{3/2} - {}^4S^o_{3/2}$	2853.7	2.11 + 0	3.01 − 1	2.93 − 1	3.06 − 1	3.25 − 1
	$^2P^o_{1/2} - {}^4S^o_{3/2}$	2868.2	8.62 − 1	1.49 − 1	1.46 − 1	1.53 − 1	1.63 − 1
	$^2D^o_{5/2} - {}^2D^o_{3/2}$	7.741 + 5	2.30 − 5	6.35 + 0	6.13 + 0	6.03 + 0	5.93 + 0
	$^2P^o_{3/2} - {}^2P^o_{1/2}$	564721	4.94 − 5	2.24 + 0	2.33 + 0	2.53 + 0	2.72 + 0
	$^2P^o_{3/2} - {}^2D^o_{5/2}$	7237.3	5.98 − 1	4.29 + 0	4.44 + 0	4.40 + 0	4.34 + 0
	$^2P^o_{3/2} - {}^2D^o_{3/2}$	7170.6	7.89 − 1	2.45 + 0	2.47 + 0	2.44 + 0	2.39 + 0
	$^2P^o_{1/2} - {}^2D^o_{5/2}$	7333.4	1.19 − 1	1.78 + 0	1.79 + 0	1.76 + 0	1.72 + 0
	$^2P^o_{1/2} - {}^2D^o_{3/2}$	7262.8	6.03 − 1	1.61 + 0	1.69 + 0	1.68 + 0	1.66 + 0
Ar V	$^1D_2 - {}^3P_0$	6135.2	3.50 − 5	4.37 + 0	3.72 + 0	3.52 + 0	3.42 + 0
	$^1D_2 - {}^3P_1$	6435.1	1.61 − 1	⇓	⇓	⇓	⇓
	$^1D_2 - {}^3P_2$	7005.7	4.70 − 1	4.37 + 0	3.72 + 0	3.52 + 0	3.42 + 0
	$^1S_0 - {}^3P_1$	2691.0	5.89 + 0	1.17 + 0	1.18 + 0	1.11 + 0	1.03 + 0
	$^1S_0 - {}^3P_2$	2686.8	5.69 − 2	⇓	⇓	⇓	⇓
	$^1S_0 - {}^1D_2$	4625.5	5.18 + 0	1.26 + 0	1.25 + 0	1.24 + 0	1.23 + 0
	$^3P_1 - {}^3P_0$	1.307 + 5	8.03 − 3		2.57 − 1		
	$^3P_2 - {}^3P_0$	49280.5	1.24 − 6		3.20 − 1		
	$^3P_2 - {}^3P_1$	79040	2.72 − 2		1.04 + 0		
Ar VI	$^2P^o_{3/2} - {}^2P^o_{1/2}$	45275	9.69 − 2		7.98 − 2		
K III	$^2P^o_{1/2} - {}^2P^o_{3/2}$	46153.2	1.83 − 1		1.78 + 0		
K IV	$^1D_2 - {}^3P_0$	7110.9	4.54 − 5		1.90 + 0		
	$^1D_2 - {}^3P_1$	6795.0	1.98 − 1		⇓		
	$^1D_2 - {}^3P_2$	6101.8	8.14 − 1		⇓		
	$^1S_0 - {}^3P_1$	2711.1	1.00 + 1		2.92 − 1		
	$^1S_0 - {}^3P_2$	2594.3	8.17 − 2		⇓		
	$^1S_0 - {}^1D_2$	4510.9	3.18 + 0		7.98 − 1		

Table 2 (continued)

Ion	Transition	λ [Å]	A [s^{-1}]	$\Upsilon(T)$			
				5000 K	10000 K	15000 K	20000 K
	$^3P_0 - {}^3P_1$	1.539 + 5	1.48 − 2		4.21 − 1		
	$^3P_0 - {}^3P_2$	43081.2	1.01 − 5		2.90 − 1		
	$^3P_1 - {}^3P_2$	59830.0	1.04 − 1		1.16 + 0		
K V	$^2D^o_{5/2} - {}^4S^o_{3/2}$	4122.6	4.59 − 3	9.25 − 1	8.51 − 1	8.24 − 1	8.18 − 1
	$^2D^o_{3/2} - {}^4S^o_{3/2}$	4163.3	8.84 − 2	6.17 − 1	5.67 − 1	5.50 − 1	5.45 − 1
	$^2P^o_{3/2} - {}^4S^o_{3/2}$	2494.2	5.19 + 0	1.49 − 1	3.68 − 1	4.94 − 1	5.47 − 1
	$^2P^o_{1/2} - {}^4S^o_{3/2}$	2514.5	2.14 + 0	7.40 − 2	1.84 − 1	2.47 − 1	2.73 − 1
	$^2D^o_{5/2} - {}^2D^o_{3/2}$	4.22 + 5	1.42 − 4	5.24 + 0	5.31 + 0	5.13 + 0	4.96 + 0
	$^2P^o_{3/2} - {}^2P^o_{1/2}$	3.11 + 5	2.96 − 4	4.43 − 1	6.27 − 1	7.83 − 1	9.02 − 1
	$^2P^o_{3/2} - {}^2D^o_{5/2}$	6315.1	1.21 + 0	2.56 + 0	3.07 + 0	3.31 + 0	3.40 + 0
	$^2P^o_{3/2} - {}^2D^o_{3/2}$	6221.9	1.86 + 0	1.39 + 0	1.76 + 0	1.93 + 0	2.00 + 0
	$^2P^o_{1/2} - {}^2D^o_{5/2}$	6448.1	1.41 − 1	9.92 − 1	1.28 + 0	1.41 + 0	1.46 + 0
	$^2P^o_{1/2} - {}^2D^o_{3/2}$	6349.2	1.25 + 0	9.83 − 1	1.14 + 0	1.21 + 0	1.24 + 0
Ca II	$^2P^o_{3/2} - {}^2S_{1/2}$	3933.7	1.47 + 8	1.56 + 1	1.75 + 1	1.92 + 1	2.08 + 1
	$^2P^o_{1/2} - {}^2S_{1/2}$	3968.5	1.4 + 8	⇓	⇓	⇓	⇓
Ca IV	$^2P^o_{1/2} - {}^2P^o_{3/2}$	32061.9	5.45 − 1		1.06 + 0		
Ca V	$^1D_2 - {}^3P_0$	6428.9	8.42 − 5		9.04 − 1		
	$^1D_2 - {}^3P_1$	6086.4	4.26 − 1		⇓		
	$^1D_2 - {}^3P_2$	5309.2	1.90 + 0		⇓		
	$^1S_0 - {}^3P_1$	2412.9	2.31 + 1		1.16 − 1		
	$^1S_0 - {}^3P_2$	2281.2	1.45 − 1		⇓		
	$^1S_0 - {}^1D_2$	3997.9	3.73 + 0		7.93 − 1		
	$^3P_0 - {}^3P_1$	1.1482 + 5	3.54 − 2		2.02 − 1		
	$^3P_0 - {}^3P_2$	30528.8	3.67 − 5		2.24 − 1		
	$^3P_1 - {}^3P_2$	41574.2	3.10 − 1		7.60 − 1		
Fe II	$a^6D_{9/2} - a^6D_{7/2}$	2.598 + 5	2.13 − 3	7.41 − 3	5.52 + 0	5.46 + 0	5.48 + 0
	$a^6D_{9/2} - a^6D_{5/2}$	1.479 + 5		6.14 + 0	1.49 + 0	1.55 + 0	1.64 + 0
	$a^6D_{9/2} - a^6D_{3/2}$	1.159 + 5		4.25 − 1	6.75 − 1	6.83 − 1	7.15 − 1
	$a^6D_{9/2} - a^6D_{1/2}$	1.023 + 5		1.63 − 1	2.84 − 1	2.84 − 1	2.95 − 1
	$a^6D_{9/2} - a^4F_{9/2}$	5.339 + 4	4.17 − 5	4.77 − 2	3.60 + 0	3.19 + 0	2.89 + 0
	$a^6D_{9/2} - a^4D_{7/2}$	1.257 + 4	4.83 − 3	3.10 + 0	1.10 + 1	9.65 + 0	8.77 + 0
	$a^6D_{5/2} - a^4D_{5/2}$	1.294 + 4	1.94 − 3	3.46 + 0	2.85 + 0	2.56 + 0	2.36 + 0
	$a^6D_{3/2} - a^4D_{5/2}$	1.328 + 4	1.21 − 3	7.11 − 1	6.26 − 1	6.05 − 1	5.87 − 1
	$a^6D_{1/2} - a^4D_{1/2}$	1.270 + 4	2.91 − 3	2.06 + 0	1.65 + 0	1.44 + 0	1.30 + 0
	$a^4F_{9/2} - a^4D_{7/2}$	1.644 + 4	4.65 − 3	2.28 + 0	2.11 + 0	2.14 + 0	2.18 + 0
	$a^4F_{9/2} - a^4D_{5/2}$	1.533 + 4	2.44 − 3	7.77 − 1	7.25 − 1	7.54 − 1	7.83 − 1
	$a^4F_{9/2} - a^4P_{5/2}$	8617.0	2.73 − 2	1.22 + 0	1.23 + 0	1.27 + 0	1.29 + 0
	$a^4F_{7/2} - a^4P_{3/2}$	8892.0	1.74 − 2	5.53 + 0	5.54 − 1	5.64 − 1	5.71 + 0
	$a^4F_{9/2} - a^4H_{13/2}$	5157	4.4 − 1	1.03 + 0	1.13 + 0	1.33 + 0	1.51 + 0
	$a^4F_{9/2} - a^4G_{11/2}$	4244	9.0 − 1	6.45 − 1	8.24 − 1	1.02 + 0	1.16 + 0
	$a^4F_{7/2} - a^4H_{11/2}$	5262	3.1 − 1	5.21 − 1	5.66 − 1	6.69 − 1	7.64 − 1

Table 2 (continued)

Ion	Transition	λ [Å]	A [s^{-1}]	$\Upsilon(T)$			
				5000 K	10000 K	15000 K	20000 K
	$a^4F_{7/2} - a^4G_{9/2}$	4277	6.5 − 1	3.67 − 1	4.47 − 1	5.35 − 1	5.97 − 1
	$a^4F_{5/2} - a^4H_{9/2}$	5334	2.6 − 1	3.22 − 1	3.57 − 1	4.32 − 1	5.01 − 1
	$a^4F_{9/2} - b^4F_{9/2}$	4815	4.0 − 1	1.06 + 0	1.21 + 0	1.42 + 0	1.60 + 0
Fe III	$^5D_4 - {}^5D_3$	229146		2.38 + 0	2.87 + 0	3.02 + 0	3.01 + 0
	$^5D_4 - {}^5D_2$	135513		9.70 − 1	1.23 + 0	1.31 + 0	1.32 + 0
	$^5D_4 - {}^5D_1$	107294		4.75 − 1	5.91 − 1	6.29 − 1	6.36 − 1
	$^5D_4 - {}^5D_0$	97436		1.43 − 1	1.78 − 1	1.90 − 1	1.94 − 1
	$^5D_3 - {}^5D_2$	331636		1.65 + 0	2.03 + 0	2.16 + 0	2.18 + 0
	$^5D_3 - {}^5D_1$	201769		6.12 − 1	7.94 − 1	8.45 − 1	8.46 − 1
	$^5D_3 - {}^5D_0$	169516		1.70 − 1	2.23 − 1	2.36 − 1	2.35 − 1
	$^5D_2 - {}^5D_1$	515254		1.04 + 0	1.28 + 0	1.36 + 0	1.36 + 0
	$^5D_2 - {}^5D_0$	346768		2.35 − 1	3.09 − 1	3.31 − 1	3.33 − 1
	$^5D_1 - {}^5D_0$	1060465		4.00 − 1	4.85 − 1	5.15 − 1	5.20 − 1
	$^3H_6 - {}^3G_5$	22189.8		2.80 + 0	2.72 + 0	2.67 + 0	2.60 + 0
	$^3H_6 - {}^3G_4$	20448.4		1.18 + 0	1.20 + 0	1.19 + 0	1.16 + 0
	$^3H_6 - {}^3G_3$	19655.2		2.77 − 1	2.90 − 1	2.97 − 1	2.96 − 1
	$^3H_5 - {}^3G_5$	23505.2		1.26 + 0	1.28 + 0	1.26 + 0	1.23 + 0
	$^3H_5 - {}^3G_4$	21560.3		1.60 + 0	1.69 + 0	1.70 + 0	1.66 + 0
	$^3H_5 - {}^3G_3$	20680.3		1.07 + 0	1.12 + 0	1.12 + 0	1.10 + 0
	$^3H_4 - {}^3G_5$	24516.1		3.43 − 1	3.75 − 1	3.88 − 1	3.88 − 1
	$^3H_4 - {}^3G_4$	22407.9		1.18 + 0	1.23 + 0	1.23 + 0	1.21 + 0
	$^3H_4 - {}^3G_3$	21458.8		1.80 + 0	1.94 + 0	1.96 + 0	1.92 + 0

3.1.5.3 Excitation data for iron ions

Electron-impact excitation data for iron ions are very important for astrophysical and other plasam modeling applications. The Iron Project (IP) [93H1] is mostly devoted to calculating reliable collisional data for all iron ions using the most accurate method, the Breit-Pauli R-matrix close-coupling method, with relativistic fine structure effects. The effective, or maxwellian-averaged, collision strengths tabulated in this section are mostly taken from the collective efforts by the IP. Because this is an on-going endeavor, data for some iron ions by the IP are currently not available. For some of these ions data calculated by the RDW method are also tabulated. It is noted that these RDW data contain only the background, or non-resonant, contribution. It should be accurate if the resonance contributions, by using the method described in subsection 3.1.2.2.2, is added.

In Table 3 the data tables for the iron ions are summarized. It also lists the methods and the data sources. The theoretical methods listed in Table 3 are:

DARC – relativistic Dirac R-matix [87N1], BPRM – Breit-Pauli R-matrix,
FARM – FARM package of the R-matrix method [95B2],
ARRM – R-matrix with algebraic recoupling to obtain fine-structure results,
TCC – same as ARRM but with inclusion of term coupling coefficients, and
RDW – relativistic distorted wave.

Table 2 (continued)

Ion	Transition	λ [Å]	A [s^{-1}]	$\Upsilon(T)$			
				5000 K	10000 K	15000 K	20000 K
	$a^4F_{7/2} - a^4G_{9/2}$	4277	6.5 − 1	3.67 − 1	4.47 − 1	5.35 − 1	5.97 − 1
	$a^4F_{5/2} - a^4H_{9/2}$	5334	2.6 − 1	3.22 − 1	3.57 − 1	4.32 − 1	5.01 − 1
	$a^4F_{9/2} - b^4F_{9/2}$	4815	4.0 − 1	1.06 + 0	1.21 + 0	1.42 + 0	1.60 + 0
Fe III	$^5D_4 - {}^5D_3$	229146		2.38 + 0	2.87 + 0	3.02 + 0	3.01 + 0
	$^5D_4 - {}^5D_2$	135513		9.70 − 1	1.23 + 0	1.31 + 0	1.32 + 0
	$^5D_4 - {}^5D_1$	107294		4.75 − 1	5.91 − 1	6.29 − 1	6.36 − 1
	$^5D_4 - {}^5D_0$	97436		1.43 − 1	1.78 − 1	1.90 − 1	1.94 − 1
	$^5D_3 - {}^5D_2$	331636		1.65 + 0	2.03 + 0	2.16 + 0	2.18 + 0
	$^5D_3 - {}^5D_1$	201769		6.12 − 1	7.94 − 1	8.45 − 1	8.46 − 1
	$^5D_3 - {}^5D_0$	169516		1.70 − 1	2.23 − 1	2.36 − 1	2.35 − 1
	$^5D_2 - {}^5D_1$	515254		1.04 + 0	1.28 + 0	1.36 + 0	1.36 + 0
	$^5D_2 - {}^5D_0$	346768		2.35 − 1	3.09 − 1	3.31 − 1	3.33 − 1
	$^5D_1 - {}^5D_0$	1060465		4.00 − 1	4.85 − 1	5.15 − 1	5.20 − 1
	$^3H_6 - {}^3G_5$	22189.8		2.80 + 0	2.72 + 0	2.67 + 0	2.60 + 0
	$^3H_6 - {}^3G_4$	20448.4		1.18 + 0	1.20 + 0	1.19 + 0	1.16 + 0
	$^3H_6 - {}^3G_3$	19655.2		2.77 − 1	2.90 − 1	2.97 − 1	2.96 − 1
	$^3H_5 - {}^3G_5$	23505.2		1.26 + 0	1.28 + 0	1.26 + 0	1.23 + 0
	$^3H_5 - {}^3G_4$	21560.3		1.60 + 0	1.69 + 0	1.70 + 0	1.66 + 0
	$^3H_5 - {}^3G_3$	20680.3		1.07 + 0	1.12 + 0	1.12 + 0	1.10 + 0
	$^3H_4 - {}^3G_5$	24516.1		3.43 − 1	3.75 − 1	3.88 − 1	3.88 − 1
	$^3H_4 - {}^3G_4$	22407.9		1.18 + 0	1.23 + 0	1.23 + 0	1.21 + 0
	$^3H_4 - {}^3G_3$	21458.8		1.80 + 0	1.94 + 0	1.96 + 0	1.92 + 0

3.1.5.3 Excitation data for iron ions

Electron-impact excitation data for iron ions are very important for astrophysical and other plasam modeling applications. The Iron Project (IP) [93H1] is mostly devoted to calculating reliable collisional data for all iron ions using the most accurate method, the Breit-Pauli R-matrix close-coupling method, with relativistic fine structure effects. The effective, or maxwellian-averaged, collision strengths tabulated in this section are mostly taken from the collective efforts by the IP. Because this is an on-going endeavor, data for some iron ions by the IP are currently not available. For some of these ions data calculated by the RDW method are also tabulated. It is noted that these RDW data contain only the background, or non-resonant, contribution. It should be accurate if the resonance contributions, by using the method described in subsection 3.1.2.2.2, is added.

In Table 3 the data tables for the iron ions are summarized. It also lists the methods and the data sources. The theoretical methods listed in Table 3 are:

DARC – relativistic Dirac R-matix [87N1], BPRM – Breit-Pauli R-matrix,
FARM – FARM package of the R-matrix method [95B2],
ARRM – R-matrix with algebraic recoupling to obtain fine-structure results,
TCC – same as ARRM but with inclusion of term coupling coefficients, and
RDW – relativistic distorted wave.

The symbols used in the data tables are:

J – the total angular momentum for the fine-structure level,
T – temperature, and
Υ – the effective or maxwellian-averaged collision strength.

The decimal and exponent notation for Υ is '$a.bc[x]$', where 'x' is the exponent in 10^x. For most ions there are two tables, **a** and **b**, where, for instance, for Fe II Table 3.2a lists the fine-structure energy levels and the observed and theoretical energies, and Table 3.2b gives the effective collision strengths Υ as a function of temperatures T[K].

Table 3. List of the data tables for the iron ions included.

Tables		Ion	Method	Ref.
3.1a	3.1b	Fe I	FARM	97P1
3.2a	3.2b	Fe II	ARRM	95Z1
3.3a	3.3b	Fe III	ARRM	96Z1
3.4a	3.4b	Fe IV	ARRM	97Z2
3.5		Fe V	BPRM	95B1
3.6		Fe X	ARRM	95P1
3.7a	3.7b	Fe XII	TCC	98B2, 98B3
3.8		Fe XIV	TCC	96S1
3.9a	3.9b	Fe XVI	RDW	90S2
3.10a	3.10b	Fe XVII	RDW	89Z2
3.11		Fe XVIII	ARRM	98B1
3.12a	3.12b	Fe XXI	RDW	96Z2
3.13a	3.13b	Fe XXII	BPRM	97Z1
3.14a	3.14b	Fe XXIII	RDW	92Z1
3.15a	3.15b	Fe XXIV	BPRM	97B3
3.16a	3.16b	Fe XXVI	DARC	96K2

Table 3.1a. Fe I. Lowest 10 fine-structure energy levels of the states included in the calculation [97P1] and their observed energies E [Ry] in rydbergs [75R1]. The index i is used in Table 3.1b for transition keys; J is the total angular momentum for specifying the fine-structure level.

i	LS Term	J	E [Ry]	i	LS Term	J	E [Ry]
1	$3d^6 4s^2\ ^5D$	4	0.0	6	$3d^7 4s\ ^5F$	5	0.0760
2		3	0.0046	7		4	0.0810
3		2	0.0077	8		3	0.0848
4		1	0.0097	9		2	0.0876
5		0	0.0107	10		1	0.0895

Table 3.1b. Fe I. Effective collision strengths $\Upsilon(i,j)$ as a function of temperature T [K] for the transitions between the first 10 metastable levels as specified in Table 3.1a [97P1].

Levels		$\log T$				
i	j	2.0	2.4	2.8	3.2	3.6
1	2	2.010[-2]	3.380[-2]	7.050[-2]	2.440[-1]	7.650[-1]
1	3	4.270[-2]	9.470[-2]	1.550[-1]	2.280[-1]	3.440[-1]
1	4	1.060[-4]	4.300[-4]	1.740[-3]	1.310[-2]	3.350[-2]
1	5	2.390[-7]	1.140[-6]	3.720[-5]	1.020[-3]	2.720[-3]
1	6	2.620[-2]	7.720[-2]	1.830[-1]	4.300[-1]	8.240[-1]
1	7	1.840[-2]	4.320[-2]	9.150[-2]	1.920[-1]	3.320[-1]
1	8	8.610[-3]	1.840[-2]	3.790[-2]	7.780[-2]	1.260[-1]
1	9	2.560[-3]	5.960[-3]	1.250[-2]	2.380[-2]	3.440[-2]
1	10	6.730[-5]	2.000[-4]	4.860[-4]	1.020[-3]	1.500[-3]
2	3	1.760[-2]	4.750[-2]	1.070[-1]	2.730[-1]	7.200[-1]
2	4	1.090[-2]	2.160[-2]	3.410[-2]	8.070[-2]	2.350[-1]
2	5	3.970[-5]	1.710[-4]	8.710[-4]	1.060[-2]	3.380[-2]
2	6	9.050[-3]	2.560[-2]	5.690[-2]	1.310[-1]	2.640[-1]
2	7	1.510[-2]	3.490[-2]	7.380[-2]	1.640[-1]	3.040[-1]
2	8	1.720[-2]	3.760[-2]	7.980[-2]	1.670[-1]	2.780[-1]
2	9	9.570[-3]	2.190[-2]	4.630[-2]	9.650[-2]	1.570[-1]
2	10	2.310[-3]	6.130[-3]	1.280[-2]	2.460[-2]	3.680[-2]
3	4	7.720[-3]	2.250[-2]	5.390[-2]	1.460[-1]	4.020[-1]
3	5	2.110[-4]	9.840[-4]	4.390[-3]	3.240[-2]	1.450[-1]
3	6	2.560[-3]	6.770[-3]	1.310[-2]	2.540[-2]	4.820[-2]
3	7	7.910[-3]	1.880[-2]	4.170[-2]	1.000[-1]	2.030[-1]
3	8	1.500[-2]	2.960[-2]	5.510[-2]	1.080[-1]	1.830[-1]
3	9	1.510[-2]	3.600[-2]	7.620[-2]	1.450[-1]	2.180[-1]
3	10	6.070[-3]	1.650[-2]	3.590[-2]	7.630[-2]	1.270[-1]
4	5	1.860[-4]	5.940[-4]	2.420[-3]	2.060[-2]	9.760[-2]
4	6	8.990[-7]	2.910[-6]	8.260[-6]	2.460[-5]	5.720[-5]
4	7	5.550[-3]	1.160[-2]	2.040[-2]	3.720[-2]	6.550[-2]
4	8	4.430[-3]	1.010[-2]	2.370[-2]	5.780[-2]	1.130[-1]
4	9	1.210[-2]	2.440[-2]	4.360[-2]	8.000[-2]	1.290[-1]
4	10	9.670[-3]	2.740[-2]	5.820[-2]	1.050[-1]	1.520[-1]
5	6	3.660[-9]	3.480[-8]	2.970[-7]	1.400[-6]	4.130[-6]
5	7	2.850[-8]	1.640[-7]	1.210[-6]	7.800[-6]	2.660[-5]
5	8	4.490[-3]	8.310[-3]	1.400[-2]	2.560[-2]	4.460[-2]
5	9	1.930[-3]	5.200[-3]	1.290[-2]	3.070[-2]	5.700[-2]
5	10	1.890[-3]	4.770[-3]	9.320[-3]	1.840[-2]	3.100[-2]
6	7	2.470[-2]	5.410[-2]	1.020[-1]	2.000[-1]	3.750[-1]
6	8	8.890[-4]	2.180[-3]	5.530[-3]	1.460[-2]	2.910[-2]
6	9	1.100[-5]	4.390[-5]	1.860[-4]	7.270[-4]	1.770[-3]
6	10	1.300[-8]	1.410[-7]	2.240[-6]	2.710[-5]	1.020[-4]

Table 3.1b. Fe I (continued)

Levels		$\log T$				
i	j	2.0	2.4	2.8	3.2	3.6
7	8	5.530[-2]	1.080[-1]	1.870[-1]	3.270[-1]	5.330[-1]
7	9	8.570[-4]	2.250[-3]	5.790[-3]	1.560[-2]	3.160[-2]
7	10	6.360[-6]	2.810[-5]	1.230[-4]	5.270[-4]	1.380[-3]
8	9	5.730[-2]	1.190[-1]	2.120[-1]	3.700[-1]	5.890[-1]
8	10	4.440[-4]	1.440[-3]	3.970[-3]	1.120[-2]	2.310[-2]
9	10	2.930[-2]	7.640[-2]	1.490[-1]	2.780[-1]	4.490[-1]

Table 3.2a. Fe II. Lowest 49 fine-structure levels from the 142 levels included in the calculation [95Z1] and their observed energies E [Ry] in rydbergs [85S1]. The index i is used in Table 3.2b for transition keys; J is the total angular momentum for specifying the fine-structure level.

i	LS Term		J	E [Ry]	i	LS Term		J	E [Ry]
1	$3d^6(^5D)4s$	a^6D	9/2	0.00000	28	$3d^6(^3G)4s$	a^4G	11/2	0.23172
2			7/2	0.00351	29			9/2	0.23516
3			5/2	0.00608	30			7/2	0.23676
4			3/2	0.00786	31			5/2	0.23743
5			1/2	0.00890	32	$3d^6(^3D)4s$	b^4D	7/2	0.28690
6	$3d^7$	a^4F	9/2	0.01706	33			5/2	0.28603
7			7/2	0.02214	34			3/2	0.28581
8			5/2	0.02586	35			1/2	0.28585
9			3/2	0.02841	36	$3d^6(^5D)4p$	z^6D^o	9/2	0.35046
10	$3d^6(^5D)4s$	a^4D	7/2	0.07249	37			7/2	0.35230
11			5/2	0.07647	38			5/2	0.35411
12			3/2	0.07910	39			3/2	0.35551
13			1/2	0.08062	40			1/2	0.35639
14	$3d^7$	a^4P	5/2	0.12279	41	$3d^6(^5D)4p$	z^6F^o	11/2	0.38244
15			3/2	0.12460	42			9/2	0.38378
16			1/2	0.12671	43			7/2	0.38489
17	$3d^6(^3P_2)4s$	b^4P	5/2	0.18982	44			5/2	0.38578
18			3/2	0.19877	45			3/2	0.38639
19			1/2	0.20421	46			1/2	0.38674
20	$3d^6(^3H)4s$	a^4H	13/2	0.19366	47	$3d^6(^5D)4p$	z^6P^o	7/2	0.38873
21			11/2	0.19529	48			5/2	0.39402
22			9/2	0.19667	49			3/2	0.39750
23			7/2	0.19785					
24	$3d^6(^3F_2)4s$	b^4F	9/2	0.20629					
25			7/2	0.20786					
26			5/2	0.20904					
27			3/2	0.20988					

Table 3.2b. Fe II. Effective collision strengths $\Upsilon(i,j)$ as a function of temperature T [K] for the transitions between the first 16 metastable levels and the transitions between the five levels of the ground term $3d^6 5s\ ^6D$ and the higher 33 levels, i = 17–49 as specified in Table 3.2a [95Z1].

Levels		T [K]							
i	j	1000	3000	5000	10000	15000	20000	30000	40000
1	2	6.97	6.27	5.97	5.52	5.46	5.48	5.40	5.18
1	3	2.02	1.85	1.68	1.49	1.55	1.64	1.73	1.71
1	4	8.65[-1]	8.60[-1]	7.82[-1]	6.75[-1]	6.83[-1]	7.15[-1]	7.50[-1]	7.44[-1]
1	5	3.37[-1]	3.60[-1]	3.30[-1]	2.84[-1]	2.84[-1]	2.95[-1]	3.08[-1]	3.07[-1]
1	6	3.81	4.00	4.05	3.60	3.19	2.89	2.48	2.18
1	7	1.66	1.70	1.71	1.51	1.33	1.21	1.03	9.09[-1]
1	8	5.98[-1]	5.91[-1]	5.85[-1]	4.97[-1]	4.31[-1]	3.85[-1]	3.23[-1]	2.80[-1]
1	9	1.63[-1]	1.65[-1]	1.64[-1]	1.37[-1]	1.17[-1]	1.03[-1]	8.51[-2]	7.30[-2]
1	10	1.74[+1]	1.53[+1]	1.36[+1]	1.10[+1]	9.65	8.77	7.55	6.67
1	11	7.86[-1]	6.21[-1]	5.47[-1]	5.60[-1]	6.16[-1]	6.43[-1]	6.35[-1]	5.94[-1]
1	12	2.40[-1]	2.08[-1]	1.86[-1]	1.91[-1]	2.12[-1]	2.22[-1]	2.22[-1]	2.09[-1]
1	13	6.24[-2]	6.06[-2]	5.63[-2]	6.10[-2]	7.00[-2]	7.51[-2]	7.67[-2]	7.33[-2]
1	14	7.89[-1]	8.64[-1]	9.01[-1]	9.48[-1]	9.52[-1]	9.28[-1]	8.54[-1]	7.79[-1]
1	15	4.06[-1]	4.41[-1]	4.67[-1]	5.02[-1]	5.11[-1]	5.02[-1]	4.67[-1]	4.30[-1]
1	16	7.03[-3]	1.46[-2]	2.10[-2]	3.28[-2]	3.85[-2]	4.01[-2]	3.85[-2]	3.52[-2]
2	3	6.31	5.80	5.69	5.44	5.42	5.43	5.31	5.07
2	4	1.62	1.42	1.30	1.20	1.29	1.39	1.50	1.49
2	5	5.89[-1]	5.27[-1]	4.75[-1]	4.19[-1]	4.38[-1]	4.68[-1]	4.96[-1]	4.92[-1]
2	6	1.79	1.84	1.85	1.63	1.45	1.31	1.12	9.92[-1]
2	7	1.58	1.67	1.69	1.48	1.31	1.18	1.00	8.79[-1]
2	8	1.07	1.12	1.14	1.03	9.21[-1]	8.43[-1]	7.29[-1]	6.49[-1]
2	9	5.37[-1]	5.29[-1]	5.22[-1]	4.46[-1]	3.88[-1]	3.47[-1]	2.92[-1]	2.55[-1]
2	10	3.84	3.31	2.93	2.48	2.29	2.16	1.93	1.74
2	11	1.03[+1]	9.13	8.10	6.54	5.74	5.22	4.50	3.99
2	12	4.97[-1]	3.85[-1]	3.40[-1]	3.55[-1]	3.95[-1]	4.16[-1]	4.13[-1]	3.87[-1]
2	13	1.74[-1]	1.42[-1]	1.24[-1]	1.23[-1]	1.33[-1]	1.38[-1]	1.35[-1]	1.26[-1]
2	14	5.53[-1]	6.08[-1]	6.40[-1]	6.81[-1]	6.87[-1]	6.72[-1]	6.21[-1]	5.69[-1]
2	15	1.69[-1]	1.96[-1]	2.09[-1]	2.28[-1]	2.32[-1]	2.27[-1]	2.08[-1]	1.88[-1]
2	16	2.40[-1]	2.58[-1]	2.70[-1]	2.87[-1]	2.90[-1]	2.84[-1]	2.64[-1]	2.43[-1]
3	4	4.94	4.55	4.50	4.32	4.25	4.20	4.04	3.83
3	5	1.02	8.54[-1]	7.71[-1]	7.25[-1]	8.03[-1]	8.85[-1]	9.67[-1]	9.72[-1]
3	6	7.42[-1]	7.43[-1]	7.40[-1]	6.37[-1]	5.57[-1]	5.01[-1]	4.24[-1]	3.71[-1]
3	7	1.15	1.22	1.24	1.11	9.95[-1]	9.07[-1]	7.82[-1]	6.93[-1]
3	8	1.06	1.10	1.10	9.58[-1]	8.40[-1]	7.55[-1]	6.38[-1]	5.59[-1]
3	9	7.84[-1]	8.13[-1]	8.23[-1]	7.37[-1]	6.60[-1]	6.03[-1]	5.20[-1]	4.62[-1]
3	10	7.19[-1]	6.07[-1]	5.38[-1]	5.03[-1]	5.16[-1]	5.19[-1]	4.96[-1]	4.59[-1]
3	11	4.45	3.90	3.46	2.85	2.56	2.36	2.07	1.85
3	12	5.66	5.00	4.44	3.58	3.15	2.86	2.47	2.18
3	13	2.85[-1]	2.16[-1]	1.89[-1]	1.96[-1]	2.16[-1]	2.26[-1]	2.22[-1]	2.08[-1]
3	14	3.03[-1]	3.35[-1]	3.56[-1]	3.85[-1]	3.92[-1]	3.85[-1]	3.57[-1]	3.28[-1]
3	15	2.13[-1]	2.39[-1]	2.52[-1]	2.68[-1]	2.71[-1]	2.64[-1]	2.43[-1]	2.21[-1]
3	16	2.06[-1]	2.23[-1]	2.33[-1]	2.45[-1]	2.46[-1]	2.40[-1]	2.21[-1]	2.02[-1]

Table 3.2b. Fe II (continued)

Levels		T [K]							
i	j	1000	3000	5000	10000	15000	20000	30000	40000
4	5	2.97	2.74	2.73	2.64	2.59	2.55	2.44	2.30
4	6	2.57[-1]	2.54[-1]	2.52[-1]	2.11[-1]	1.81[-1]	1.61[-1]	1.34[-1]	1.16[-1]
4	7	6.65[-1]	6.83[-1]	6.89[-1]	6.08[-1]	5.40[-1]	4.91[-1]	4.21[-1]	3.72[-1]
4	8	8.27[-1]	8.61[-1]	8.68[-1]	7.65[-1]	6.77[-1]	6.12[-1]	5.22[-1]	4.60[-1]
4	9	7.42[-1]	7.86[-1]	7.98[-1]	7.14[-1]	6.37[-1]	5.80[-1]	4.99[-1]	4.42[-1]
4	10	1.80[-1]	1.57[-1]	1.41[-1]	1.47[-1]	1.64[-1]	1.74[-1]	1.74[-1]	1.65[-1]
4	11	9.51[-1]	8.04[-1]	7.11[-1]	6.26[-1]	6.05[-1]	5.87[-1]	5.41[-1]	4.92[-1]
4	12	3.86	3.40	3.01	2.44	2.16	1.97	1.71	1.52
4	13	2.42	2.13	1.89	1.53	1.36	1.24	1.08	9.56[-1]
4	14	1.25[-1]	1.41[-1]	1.53[-1]	1.71[-1]	1.76[-1]	1.74[-1]	1.62[-1]	1.49[-1]
4	15	2.47[-1]	2.69[-1]	2.82[-1]	2.97[-1]	2.98[-1]	2.91[-1]	2.69[-1]	2.46[-1]
4	16	1.09[-1]	1.21[-1]	1.26[-1]	1.32[-1]	1.32[-1]	1.28[-1]	1.17[-1]	1.06[-1]
5	6	6.83[-2]	6.97[-2]	6.98[-2]	5.80[-2]	4.92[-2]	4.33[-2]	3.56[-2]	3.04[-2]
5	7	2.79[-1]	2.70[-1]	2.65[-1]	2.23[-1]	1.93[-1]	1.72[-1]	1.43[-1]	1.24[-1]
5	8	4.57[-1]	4.83[-1]	4.93[-1]	4.47[-1]	4.02[-1]	3.69[-1]	3.20[-1]	2.85[-1]
5	9	4.42[-1]	4.72[-1]	4.79[-1]	4.24[-1]	3.75[-1]	3.40[-1]	2.89[-1]	2.55[-1]
5	10	5.91[-2]	5.54[-2]	5.09[-2]	5.43[-2]	6.17[-2]	6.59[-2]	6.68[-2]	6.37[-2]
5	11	1.71[-1]	1.35[-1]	1.18[-1]	1.18[-1]	1.28[-1]	1.32[-1]	1.30[-1]	1.21[-1]
5	12	8.60[-1]	7.34[-1]	6.50[-1]	5.54[-1]	5.16[-1]	4.89[-1]	4.40[-1]	3.97[-1]
5	13	2.62	2.32	2.06	1.65	1.44	1.30	1.11	9.80[-1]
5	14	3.43[-2]	4.07[-2]	4.54[-2]	5.33[-2]	5.63[-2]	5.64[-2]	5.29[-2]	4.86[-2]
5	15	1.68[-1]	1.80[-1]	1.87[-1]	1.97[-1]	1.97[-1]	1.93[-1]	1.78[-1]	1.64[-1]
5	16	3.84[-2]	4.43[-2]	4.59[-2]	4.77[-2]	4.74[-2]	4.57[-2]	4.11[-2]	3.66[-2]
6	7	6.17	8.80	9.51	8.36	7.53	7.54	9.07	1.13[+1]
6	8	1.81	2.36	2.53	2.23	2.04	2.11	2.68	3.46
6	9	4.04[-1]	6.55[-1]	7.62[-1]	7.01[-1]	6.55[-1]	6.96[-1]	9.66[-1]	1.36
6	10	2.92	2.53	2.28	2.11	2.14	2.18	2.19	2.15
6	11	1.04	8.72[-1]	7.77[-1]	7.25[-1]	7.54[-1]	7.83[-1]	7.98[-1]	7.82[-1]
6	12	2.00[-1]	1.67[-1]	1.48[-1]	1.48[-1]	1.67[-1]	1.82[-1]	1.92[-1]	1.88[-1]
6	13	1.87[-2]	1.85[-2]	1.72[-2]	2.12[-2]	2.91[-2]	3.52[-2]	4.08[-2]	4.14[-2]
6	14	9.40[-1]	1.19	1.22	1.23	1.27	1.29	1.31	1.30
6	15	2.36[-1]	3.21[-1]	3.60[-1]	4.11[-1]	4.50[-1]	4.77[-1]	5.03[-1]	5.10[-1]
6	16	8.63[-2]	1.10[-1]	1.23[-1]	1.40[-1]	1.53[-1]	1.62[-1]	1.71[-1]	1.75[-1]
7	8	5.04	7.60	8.31	7.39	6.84	7.20	9.52	1.25[+1]
7	9	1.86	2.28	2.38	2.07	1.91	2.00	2.60	3.38
7	10	1.27	1.07	9.58[-1]	8.91[-1]	9.22[-1]	9.53[-1]	9.70[-1]	9.51[-1]
7	11	1.19	1.03	9.25[-1]	8.51[-1]	8.67[-1]	8.87[-1]	8.93[-1]	8.72[-1]
7	12	7.54[-1]	6.63[-1]	5.99[-1]	5.56[-1]	5.69[-1]	5.84[-1]	5.93[-1]	5.85[-1]
7	13	2.31[-1]	1.81[-1]	1.58[-1]	1.47[-1]	1.56[-1]	1.64[-1]	1.67[-1]	1.60[-1]
7	14	4.70[-1]	6.11[-1]	6.48[-1]	6.88[-1]	7.27[-1]	7.54[-1]	7.79[-1]	7.82[-1]
7	15	4.30[-1]	5.40[-1]	5.53[-1]	5.54[-1]	5.64[-1]	5.71[-1]	5.73[-1]	5.68[-1]
7	16	1.11[-1]	1.55[-1]	1.75[-1]	1.99[-1]	2.17[-1]	2.30[-1]	2.41[-1]	2.41[-1]

Table 3.2b. Fe II (continued)

Levels		T [K]							
i	j	1000	3000	5000	10000	15000	20000	30000	40000
8	9	3.97	5.85	6.35	5.63	5.23	5.54	7.43	9.91
8	10	4.49[-1]	3.59[-1]	3.14[-1]	2.94[-1]	3.14[-1]	3.32[-1]	3.43[-1]	3.35[-1]
8	11	9.34[-1]	8.21[-1]	7.41[-1]	6.86[-1]	7.01[-1]	7.19[-1]	7.29[-1]	7.18[-1]
8	12	7.22[-1]	6.09[-1]	5.43[-1]	5.00[-1]	5.11[-1]	5.23[-1]	5.23[-1]	5.06[-1]
8	13	4.89[-1]	4.36[-1]	3.96[-1]	3.67[-1]	3.73[-1]	3.81[-1]	3.84[-1]	3.77[-1]
8	14	2.36[-1]	3.11[-1]	3.40[-1]	3.78[-1]	4.08[-1]	4.28[-1]	4.48[-1]	4.54[-1]
8	15	3.33[-1]	4.27[-1]	4.42[-1]	4.49[-1]	4.61[-1]	4.69[-1]	4.73[-1]	4.67[-1]
8	16	1.89[-1]	2.45[-1]	2.55[-1]	2.60[-1]	2.68[-1]	2.73[-1]	2.75[-1]	2.72[-1]
9	10	7.85[-2]	6.82[-2]	6.13[-2]	6.48[-2]	7.82[-2]	8.87[-2]	9.74[-2]	9.69[-2]
9	11	4.63[-1]	3.82[-1]	3.38[-1]	3.15[-1]	3.28[-1]	3.41[-1]	3.46[-1]	3.36[-1]
9	12	6.97[-1]	6.18[-1]	5.60[-1]	5.18[-1]	5.26[-1]	5.36[-1]	5.41[-1]	5.33[-1]
9	13	4.48[-1]	3.94[-1]	3.56[-1]	3.27[-1]	3.30[-1]	3.35[-1]	3.35[-1]	3.26[-1]
9	14	1.20[-1]	1.56[-1]	1.73[-1]	1.97[-1]	2.15[-1]	2.27[-1]	2.39[-1]	2.43[-1]
9	15	1.82[-1]	2.45[-1]	2.62[-1]	2.81[-1]	2.97[-1]	3.08[-1]	3.17[-1]	3.19[-1]
9	16	2.04[-1]	2.57[-1]	2.57[-1]	2.48[-1]	2.46[-1]	2.46[-1]	2.42[-1]	2.36[-1]
10	11	3.07	2.62	2.33	2.23	2.52	3.00	4.51	6.58
10	12	1.02	8.98[-1]	8.26[-1]	8.18[-1]	9.24[-1]	1.08	1.52	2.11
10	13	4.52[-1]	4.12[-1]	3.82[-1]	3.69[-1]	4.00[-1]	4.51[-1]	6.19[-1]	8.57[-1]
10	14	8.10[-1]	8.92[-1]	8.97[-1]	1.01	1.14	1.22	1.25	1.22
10	15	4.04[-1]	4.20[-1]	4.26[-1]	4.69[-1]	5.18[-1]	5.48[-1]	5.64[-1]	5.56[-1]
10	16	5.90[-2]	6.22[-2]	6.55[-2]	7.63[-2]	8.56[-2]	9.00[-2]	8.93[-2]	8.41[-2]
11	12	2.51	2.13	1.88	1.75	2.01	2.53	4.22	6.44
11	13	4.88[-1]	4.07[-1]	3.67[-1]	3.78[-1]	4.61[-1]	5.84[-1]	9.28[-1]	1.33
11	14	4.89[-1]	5.20[-1]	5.26[-1]	5.87[-1]	6.56[-1]	6.97[-1]	7.19[-1]	7.06[-1]
11	15	2.24[-1]	2.51[-1]	2.52[-1]	2.90[-1]	3.35[-1]	3.58[-1]	3.62[-1]	3.43[-1]
11	16	2.47[-1]	2.61[-1]	2.63[-1]	2.88[-1]	3.17[-1]	3.35[-1]	3.47[-1]	3.45[-1]
12	13	1.50	1.27	1.10	1.01	1.17	1.50	2.62	4.11
12	14	2.18[-1]	2.25[-1]	2.29[-1]	2.56[-1]	2.86[-1]	3.03[-1]	3.10[-1]	3.03[-1]
12	15	2.59[-1]	2.83[-1]	2.84[-1]	3.18[-1]	3.58[-1]	3.81[-1]	3.91[-1]	3.82[-1]
12	16	1.63[-1]	1.81[-1]	1.82[-1]	2.03[-1]	2.29[-1]	2.44[-1]	2.51[-1]	2.45[-1]
13	14	6.70[-2]	6.63[-2]	6.80[-2]	7.69[-2]	8.57[-2]	9.03[-2]	9.09[-2]	8.71[-2]
13	15	1.91[-1]	2.04[-1]	2.06[-1]	2.26[-1]	2.50[-1]	2.66[-1]	2.76[-1]	2.74[-1]
13	16	6.30[-2]	7.45[-2]	7.42[-2]	8.60[-2]	1.00[-1]	1.08[-1]	1.09[-1]	1.04[-1]
14	15	1.42	1.47	1.41	1.28	1.21	1.16	1.08	1.01
14	16	5.23[-1]	5.35[-1]	5.16[-1]	4.84[-1]	4.69[-1]	4.56[-1]	4.32[-1]	4.11[-1]
15	16	7.01[-1]	7.40[-1]	7.07[-1]	6.29[-1]	5.83[-1]	5.49[-1]	4.97[-1]	4.56[-1]

Table 3.2b. Fe II (continued)

Levels		T [K]							
i	j	1000	3000	5000	10000	15000	20000	30000	40000
1	17	3.66[-1]	3.49[-1]	3.30[-1]	3.08[-1]	2.98[-1]	2.92[-1]	2.83[-1]	2.77[-1]
1	18	1.14[-1]	1.14[-1]	1.08[-1]	9.92[-2]	9.43[-2]	9.08[-2]	8.57[-2]	8.19[-2]
1	19	5.02[-3]	6.72[-3]	7.43[-3]	7.99[-3]	8.14[-3]	8.07[-3]	7.59[-3]	6.98[-3]
1	20	6.64[-1]	6.68[-1]	6.49[-1]	6.31[-1]	6.32[-1]	6.37[-1]	6.47[-1]	6.54[-1]
1	21	3.22[-1]	3.26[-1]	3.19[-1]	3.11[-1]	3.12[-1]	3.14[-1]	3.19[-1]	3.22[-1]
1	22	9.59[-2]	9.81[-2]	9.62[-2]	9.51[-2]	9.59[-2]	9.69[-2]	9.81[-2]	9.87[-2]
1	23	1.52[-2]	1.61[-2]	1.61[-2]	1.65[-2]	1.69[-2]	1.71[-2]	1.73[-2]	1.72[-2]
1	24	2.55[-1]	3.32[-1]	3.65[-1]	4.02[-1]	4.18[-1]	4.27[-1]	4.35[-1]	4.36[-1]
1	25	1.96[-1]	2.13[-1]	2.15[-1]	2.15[-1]	2.16[-1]	2.17[-1]	2.16[-1]	2.16[-1]
1	26	9.89[-2]	1.09[-1]	1.11[-1]	1.12[-1]	1.13[-1]	1.14[-1]	1.14[-1]	1.14[-1]
1	27	3.21[-2]	3.57[-2]	3.70[-2]	3.82[-2]	3.87[-2]	3.88[-2]	3.89[-2]	3.89[-2]
1	28	9.81[-2]	1.77[-1]	2.44[-1]	3.44[-1]	3.99[-1]	4.32[-1]	4.70[-1]	4.90[-1]
1	29	1.70[-1]	2.00[-1]	2.07[-1]	2.15[-1]	2.22[-1]	2.26[-1]	2.32[-1]	2.34[-1]
1	30	6.56[-2]	7.64[-2]	7.78[-2]	7.98[-2]	8.16[-2]	8.31[-2]	8.47[-2]	8.56[-2]
1	31	1.69[-2]	1.99[-2]	1.99[-2]	1.98[-2]	1.98[-2]	1.97[-2]	1.96[-2]	1.94[-2]
1	32	2.71[-1]	2.56[-1]	2.62[-1]	2.76[-1]	2.84[-1]	2.88[-1]	2.92[-1]	2.92[-1]
1	33	1.46[-1]	1.46[-1]	1.50[-1]	1.54[-1]	1.57[-1]	1.59[-1]	1.61[-1]	1.62[-1]
1	34	6.66[-2]	6.79[-2]	7.01[-2]	7.31[-2]	7.48[-2]	7.60[-2]	7.75[-2]	7.85[-2]
1	35	3.42[-2]	3.46[-2]	3.55[-2]	3.69[-2]	3.78[-2]	3.86[-2]	3.96[-2]	4.03[-2]
1	36	1.67[+1]	1.98[+1]	2.13[+1]	2.30[+1]	2.44[+1]	2.57[+1]	2.84[+1]	3.10[+1]
1	37	1.08[+1]	8.53	7.81	7.06	6.90	6.95	7.33	7.83
1	38	4.11	2.11	1.54	9.60[-1]	7.18[-1]	5.84[-1]	4.38[-1]	3.59[-1]
1	39	2.31	1.03	7.08[-1]	4.08[-1]	2.89[-1]	2.26[-1]	1.58[-1]	1.23[-1]
1	40	9.91[-1]	4.14[-1]	2.76[-1]	1.55[-1]	1.08[-1]	8.39[-2]	5.81[-2]	4.48[-2]
1	41	3.21[+1]	3.00[+1]	2.94[+1]	2.96[+1]	3.05[+1]	3.17[+1]	3.42[+1]	3.66[+1]
1	42	5.93	5.38	5.19	5.13	5.27	5.47	5.93	6.40
1	43	8.81[-1]	7.17[-1]	6.53[-1]	6.00[-1]	5.91[-1]	5.97[-1]	6.23[-1]	6.58[-1]
1	44	1.74[-1]	1.16[-1]	9.37[-2]	7.27[-2]	6.43[-2]	5.97[-2]	5.47[-2]	5.20[-2]
1	45	6.95[-2]	4.58[-2]	3.73[-2]	2.94[-2]	2.63[-2]	2.46[-2]	2.31[-2]	2.24[-2]
1	46	2.98[-2]	1.97[-2]	1.63[-2]	1.32[-2]	1.20[-2]	1.13[-2]	1.08[-2]	1.06[-2]
1	47	1.13[+1]	1.16[+1]	1.18[+1]	1.24[+1]	1.32[+1]	1.41[+1]	1.58[+1]	1.75[+1]
1	48	2.53[-1]	2.26[-1]	2.11[-1]	1.93[-1]	1.84[-1]	1.78[-1]	1.68[-1]	1.61[-1]
1	49	6.21[-2]	5.35[-2]	4.95[-2]	4.55[-2]	4.37[-2]	4.25[-2]	4.06[-2]	3.93[-2]
2	17	2.09[-1]	2.03[-1]	1.92[-1]	1.78[-1]	1.71[-1]	1.66[-1]	1.60[-1]	1.55[-1]
2	18	1.14[-1]	1.09[-1]	1.04[-1]	9.91[-2]	9.71[-2]	9.57[-2]	9.36[-2]	9.19[-2]
2	19	6.65[-2]	6.60[-2]	6.20[-2]	5.64[-2]	5.34[-2]	5.14[-2]	4.85[-2]	4.65[-2]
2	20	2.88[-1]	2.92[-1]	2.85[-1]	2.79[-1]	2.80[-1]	2.83[-1]	2.87[-1]	2.90[-1]
2	21	2.45[-1]	2.46[-1]	2.37[-1]	2.28[-1]	2.28[-1]	2.29[-1]	2.31[-1]	2.32[-1]
2	22	2.54[-1]	2.56[-1]	2.49[-1]	2.42[-1]	2.42[-1]	2.44[-1]	2.47[-1]	2.49[-1]
2	23	1.01[-1]	1.03[-1]	1.01[-1]	9.90[-2]	9.97[-2]	1.01[-1]	1.02[-1]	1.03[-1]
2	24	1.49[-1]	1.87[-1]	2.00[-1]	2.13[-1]	2.19[-1]	2.22[-1]	2.25[-1]	2.26[-1]
2	25	2.10[-1]	2.21[-1]	2.23[-1]	2.26[-1]	2.28[-1]	2.30[-1]	2.30[-1]	2.29[-1]
2	26	9.48[-2]	1.03[-1]	1.03[-1]	1.03[-1]	1.03[-1]	1.03[-1]	1.02[-1]	1.00[-1]
2	27	8.40[-2]	9.18[-2]	9.30[-2]	9.39[-2]	9.45[-2]	9.49[-2]	9.53[-2]	9.54[-2]
2	28	6.70[-2]	9.66[-2]	1.19[-1]	1.55[-1]	1.76[-1]	1.89[-1]	2.03[-1]	2.11[-1]

Table 3.2b. Fe II (continued)

Levels		T [K]							
i	j	1000	3000	5000	10000	15000	20000	30000	40000
2	29	1.56[-1]	1.94[-1]	2.06[-1]	2.18[-1]	2.24[-1]	2.27[-1]	2.30[-1]	2.32[-1]
2	30	1.11[-1]	1.33[-1]	1.39[-1]	1.46[-1]	1.50[-1]	1.53[-1]	1.56[-1]	1.57[-1]
2	31	6.33[-2]	7.36[-2]	7.52[-2]	7.75[-2]	7.97[-2]	8.13[-2]	8.33[-2]	8.44[-2]
2	32	1.60[-1]	1.59[-1]	1.64[-1]	1.72[-1]	1.77[-1]	1.80[-1]	1.84[-1]	1.85[-1]
2	33	1.45[-1]	1.34[-1]	1.35[-1]	1.37[-1]	1.38[-1]	1.38[-1]	1.38[-1]	1.38[-1]
2	34	1.02[-1]	1.00[-1]	1.02[-1]	1.05[-1]	1.07[-1]	1.08[-1]	1.10[-1]	1.10[-1]
2	35	2.55[-2]	2.62[-2]	2.72[-2]	2.82[-2]	2.87[-2]	2.90[-2]	2.93[-2]	2.94[-2]
2	36	6.26	6.13	6.14	6.10	6.18	6.35	6.76	7.20
2	37	1.15[+1]	1.11[+1]	1.10[+1]	1.11[+1]	1.14[+1]	1.18[+1]	1.29[+1]	1.40[+1]
2	38	9.51	8.81	8.55	8.30	8.41	8.68	9.41	1.02[+1]
2	39	2.84	1.70	1.31	8.72[-1]	6.77[-1]	5.67[-1]	4.44[-1]	3.77[-1]
2	40	1.34	6.75[-1]	4.85[-1]	2.91[-1]	2.10[-1]	1.65[-1]	1.17[-1]	9.18[-2]
2	41	1.14	8.62[-1]	7.41[-1]	6.14[-1]	5.57[-1]	5.23[-1]	4.79[-1]	4.51[-1]
2	42	2.08[+1]	1.95[+1]	1.92[+1]	1.95[+1]	2.03[+1]	2.13[+1]	2.33[+1]	2.53[+1]
2	43	7.70	7.12	6.94	6.98	7.25	7.59	8.34	9.09
2	44	1.46	1.26	1.18	1.14	1.15	1.18	1.26	1.35
2	45	2.13[-1]	1.45[-1]	1.18[-1]	9.13[-2]	8.04[-2]	7.42[-2]	6.71[-2]	6.29[-2]
2	46	4.65[-2]	2.95[-2]	2.29[-2]	1.69[-2]	1.46[-2]	1.33[-2]	1.19[-2]	1.12[-2]
2	47	3.39	3.45	3.50	3.68	3.89	4.12	4.59	5.03
2	48	5.71	5.86	5.97	6.32	6.74	7.18	8.06	8.93
2	49	1.56[-1]	1.39[-1]	1.30[-1]	1.20[-1]	1.14[-1]	1.10[-1]	1.04[-1]	1.00[-1]
3	17	1.02[-1]	1.01[-1]	9.62[-2]	8.92[-2]	8.56[-2]	8.31[-2]	7.92[-2]	7.63[-2]
3	18	1.13[-1]	1.08[-1]	1.02[-1]	9.63[-2]	9.36[-2]	9.18[-2]	8.93[-2]	8.75[-2]
3	19	7.77[-2]	7.50[-2]	7.06[-2]	6.50[-2]	6.23[-2]	6.06[-2]	5.82[-2]	5.65[-2]
3	20	7.95[-2]	8.14[-2]	8.00[-2]	7.94[-2]	8.02[-2]	8.11[-2]	8.22[-2]	8.27[-2]
3	21	2.21[-1]	2.22[-1]	2.16[-1]	2.10[-1]	2.10[-1]	2.11[-1]	2.14[-1]	2.16[-1]
3	22	1.66[-1]	1.66[-1]	1.60[-1]	1.55[-1]	1.54[-1]	1.55[-1]	1.56[-1]	1.57[-1]
3	23	2.03[-1]	2.05[-1]	1.99[-1]	1.94[-1]	1.94[-1]	1.96[-1]	1.98[-1]	2.00[-1]
3	24	1.01[-1]	1.14[-1]	1.18[-1]	1.21[-1]	1.22[-1]	1.23[-1]	1.23[-1]	1.24[-1]
3	25	1.14[-1]	1.21[-1]	1.22[-1]	1.22[-1]	1.23[-1]	1.23[-1]	1.22[-1]	1.21[-1]
3	26	1.51[-1]	1.60[-1]	1.61[-1]	1.63[-1]	1.65[-1]	1.66[-1]	1.67[-1]	1.67[-1]
3	27	7.51[-2]	8.12[-2]	8.13[-2]	8.09[-2]	8.09[-2]	8.08[-2]	8.02[-2]	7.95[-2]
3	28	5.11[-2]	6.16[-2]	6.52[-2]	7.08[-2]	7.46[-2]	7.71[-2]	8.01[-2]	8.16[-2]
3	29	1.07[-1]	1.30[-1]	1.36[-1]	1.42[-1]	1.46[-1]	1.49[-1]	1.52[-1]	1.54[-1]
3	30	1.10[-1]	1.35[-1]	1.43[-1]	1.51[-1]	1.55[-1]	1.58[-1]	1.60[-1]	1.61[-1]
3	31	9.11[-2]	1.08[-1]	1.12[-1]	1.18[-1]	1.21[-1]	1.24[-1]	1.27[-1]	1.28[-1]
3	32	9.36[-2]	9.48[-2]	9.80[-2]	1.03[-1]	1.05[-1]	1.07[-1]	1.09[-1]	1.10[-1]
3	33	1.23[-1]	1.17[-1]	1.19[-1]	1.21[-1]	1.23[-1]	1.23[-1]	1.24[-1]	1.24[-1]
3	34	6.84[-2]	6.32[-2]	6.37[-2]	6.44[-2]	6.45[-2]	6.44[-2]	6.38[-2]	6.31[-2]
3	35	4.78[-2]	4.68[-2]	4.74[-2]	4.83[-2]	4.90[-2]	4.95[-2]	5.01[-2]	5.04[-2]
3	36	1.88	1.14	8.98[-1]	6.09[-1]	4.75[-1]	3.98[-1]	3.12[-1]	2.64[-1]
3	37	8.71	8.23	8.11	8.02	8.19	8.46	9.14	9.84
3	38	5.08	4.37	4.14	3.88	3.85	3.91	4.14	4.41
3	39	7.60	7.40	7.32	7.27	7.46	7.76	8.50	9.30
3	40	1.45	1.01	8.20[-1]	5.74[-1]	4.60[-1]	3.93[-1]	3.18[-1]	2.75[-1]

Table 3.2b. Fe II (continued)

Levels		T [K]							
i	j	1000	3000	5000	10000	15000	20000	30000	40000
3	41	2.27[-1]	1.42[-1]	1.11[-1]	8.07[-2]	6.91[-2]	6.28[-2]	5.62[-2]	5.30[-2]
3	42	1.01	8.16[-1]	7.23[-1]	6.20[-1]	5.71[-1]	5.40[-1]	5.00[-1]	4.72[-1]
3	43	1.30[+1]	1.21[+1]	1.19[+1]	1.22[+1]	1.27[+1]	1.34[+1]	1.48[+1]	1.62[+1]
3	44	7.40	6.89	6.75	6.85	7.16	7.53	8.33	9.14
3	45	1.69	1.52	1.45	1.43	1.46	1.52	1.64	1.78
3	46	2.02[-1]	1.41[-1]	1.16[-1]	9.05[-2]	8.00[-2]	7.39[-2]	6.66[-2]	6.22[-2]
3	47	6.82[-1]	6.78[-1]	6.80[-1]	7.01[-1]	7.32[-1]	7.66[-1]	8.35[-1]	9.00[-1]
3	48	4.10	4.20	4.28	4.52	4.81	5.12	5.73	6.31
3	49	2.16	2.21	2.24	2.37	2.51	2.67	2.99	3.30
4	17	4.00[-2]	4.08[-2]	3.93[-2]	3.69[-2]	3.55[-2]	3.45[-2]	3.27[-2]	3.12[-2]
4	18	9.35[-2]	9.05[-2]	8.53[-2]	7.86[-2]	7.54[-2]	7.33[-2]	7.04[-2]	6.84[-2]
4	19	6.18[-2]	5.81[-2]	5.49[-2]	5.14[-2]	4.99[-2]	4.91[-2]	4.79[-2]	4.71[-2]
4	20	1.07[-2]	1.15[-2]	1.15[-2]	1.19[-2]	1.23[-2]	1.25[-2]	1.25[-2]	1.24[-2]
4	21	1.05[-1]	1.07[-1]	1.05[-1]	1.03[-1]	1.03[-1]	1.04[-1]	1.05[-1]	1.06[-1]
4	22	1.42[-1]	1.43[-1]	1.39[-1]	1.35[-1]	1.35[-1]	1.36[-1]	1.37[-1]	1.38[-1]
4	23	1.87[-1]	1.88[-1]	1.82[-1]	1.76[-1]	1.76[-1]	1.76[-1]	1.79[-1]	1.80[-1]
4	24	4.73[-2]	5.21[-2]	5.35[-2]	5.48[-2]	5.53[-2]	5.55[-2]	5.57[-2]	5.58[-2]
4	25	7.46[-2]	8.14[-2]	8.21[-2]	8.22[-2]	8.23[-2]	8.24[-2]	8.21[-2]	8.18[-2]
4	26	1.02[-1]	1.08[-1]	1.08[-1]	1.09[-1]	1.10[-1]	1.10[-1]	1.11[-1]	1.10[-1]
4	27	7.59[-2]	7.97[-2]	7.99[-2]	8.00[-2]	8.04[-2]	8.06[-2]	8.05[-2]	8.00[-2]
4	28	1.93[-2]	2.25[-2]	2.26[-2]	2.26[-2]	2.29[-2]	2.30[-2]	2.32[-2]	2.32[-2]
4	29	5.91[-2]	6.91[-2]	7.10[-2]	7.36[-2]	7.57[-2]	7.72[-2]	7.92[-2]	8.02[-2]
4	30	8.30[-2]	1.01[-1]	1.06[-1]	1.11[-1]	1.14[-1]	1.16[-1]	1.19[-1]	1.20[-1]
4	31	8.66[-2]	1.06[-1]	1.12[-1]	1.18[-1]	1.22[-1]	1.24[-1]	1.26[-1]	1.28[-1]
4	32	5.54[-2]	5.63[-2]	5.81[-2]	6.07[-2]	6.22[-2]	6.32[-2]	6.46[-2]	6.55[-2]
4	33	6.88[-2]	6.77[-2]	6.90[-2]	7.10[-2]	7.21[-2]	7.27[-2]	7.34[-2]	7.37[-2]
4	34	5.91[-2]	5.49[-2]	5.52[-2]	5.58[-2]	5.60[-2]	5.60[-2]	5.57[-2]	5.53[-2]
4	35	4.10[-2]	3.79[-2]	3.78[-2]	3.80[-2]	3.82[-2]	3.82[-2]	3.81[-2]	3.79[-2]
4	36	8.25[-1]	4.49[-1]	3.34[-1]	2.07[-1]	1.52[-1]	1.21[-1]	8.74[-2]	6.93[-2]
4	37	2.58	1.52	1.17	7.87[-1]	6.16[-1]	5.19[-1]	4.11[-1]	3.51[-1]
4	38	7.09	6.99	7.01	7.08	7.31	7.62	8.34	9.07
4	39	1.82	1.41	1.21	9.52[-1]	8.29[-1]	7.58[-1]	6.82[-1]	6.41[-1]
4	40	4.34	4.53	4.56	4.61	4.76	4.98	5.47	5.99
4	41	7.71[-2]	5.13[-2]	4.21[-2]	3.35[-2]	3.02[-2]	2.84[-2]	2.67[-2]	2.60[-2]
4	42	2.20[-1]	1.33[-1]	1.01[-1]	6.98[-2]	5.78[-2]	5.13[-2]	4.44[-2]	4.09[-2]
4	43	6.84[-1]	5.70[-1]	5.13[-1]	4.49[-1]	4.17[-1]	3.97[-1]	3.70[-1]	3.50[-1]
4	44	7.36	6.86	6.73	6.86	7.18	7.57	8.39	9.19
4	45	5.89	5.49	5.38	5.48	5.74	6.05	6.72	7.39
4	46	1.44	1.32	1.28	1.27	1.31	1.36	1.49	1.61
4	47	7.50[-2]	6.58[-2]	6.12[-2]	5.62[-2]	5.38[-2]	5.21[-2]	4.96[-2]	4.78[-2]
4	48	1.43	1.45	1.48	1.55	1.64	1.74	1.93	2.11
4	49	3.13	3.20	3.27	3.45	3.68	3.91	4.39	4.84
5	17	1.13[-2]	1.20[-2]	1.18[-2]	1.14[-2]	1.11[-2]	1.08[-2]	1.02[-2]	9.65[-3]
5	18	5.30[-2]	5.17[-2]	4.85[-2]	4.42[-2]	4.20[-2]	4.06[-2]	3.86[-2]	3.74[-2]

Table 3.2b. Fe II (continued)

Levels		T [K]							
i	j	1000	3000	5000	10000	15000	20000	30000	40000
5	19	3.34[-2]	3.08[-2]	2.92[-2]	2.76[-2]	2.71[-2]	2.69[-2]	2.65[-2]	2.63[-2]
5	20	3.19[-4]	4.90[-4]	5.95[-4]	8.08[-4]	9.19[-4]	9.57[-4]	9.35[-4]	8.70[-4]
5	21	1.78[-2]	1.85[-2]	1.84[-2]	1.85[-2]	1.88[-2]	1.91[-2]	1.93[-2]	1.93[-2]
5	22	1.03[-1]	1.04[-1]	1.01[-1]	9.86[-2]	9.88[-2]	9.96[-2]	1.01[-1]	1.02[-1]
5	23	1.02[-1]	1.02[-1]	9.85[-2]	9.47[-2]	9.43[-2]	9.47[-2]	9.57[-2]	9.64[-2]
5	24	1.39[-2]	1.55[-2]	1.61[-2]	1.68[-2]	1.69[-2]	1.70[-2]	1.70[-2]	1.70[-2]
5	25	4.75[-2]	5.19[-2]	5.26[-2]	5.31[-2]	5.35[-2]	5.38[-2]	5.40[-2]	5.42[-2]
5	26	3.46[-2]	3.76[-2]	3.74[-2]	3.68[-2]	3.65[-2]	3.63[-2]	3.58[-2]	3.52[-2]
5	27	5.37[-2]	5.56[-2]	5.58[-2]	5.65[-2]	5.70[-2]	5.74[-2]	5.76[-2]	5.75[-2]
5	28	3.68[-3]	4.42[-3]	4.33[-3]	4.13[-3]	3.99[-3]	3.88[-3]	3.69[-3]	3.55[-3]
5	29	2.43[-2]	2.80[-2]	2.83[-2]	2.90[-2]	2.98[-2]	3.04[-2]	3.12[-2]	3.17[-2]
5	30	4.39[-2]	5.16[-2]	5.34[-2]	5.58[-2]	5.75[-2]	5.88[-2]	6.04[-2]	6.13[-2]
5	31	5.21[-2]	6.51[-2]	6.96[-2]	7.39[-2]	7.59[-2]	7.71[-2]	7.83[-2]	7.88[-2]
5	32	2.72[-2]	2.76[-2]	2.84[-2]	2.96[-2]	3.04[-2]	3.09[-2]	3.16[-2]	3.21[-2]
5	33	2.36[-2]	2.40[-2]	2.48[-2]	2.57[-2]	2.61[-2]	2.63[-2]	2.65[-2]	2.66[-2]
5	34	4.14[-2]	3.96[-2]	4.00[-2]	4.07[-2]	4.11[-2]	4.14[-2]	4.17[-2]	4.18[-2]
5	35	2.02[-2]	1.74[-2]	1.71[-2]	1.69[-2]	1.67[-2]	1.65[-2]	1.61[-2]	1.57[-2]
5	36	2.11[-1]	1.21[-1]	9.15[-2]	5.73[-2]	4.21[-2]	3.35[-2]	2.42[-2]	1.91[-2]
5	37	1.34	6.75[-1]	4.84[-1]	2.90[-1]	2.10[-1]	1.65[-1]	1.17[-1]	9.17[-2]
5	38	1.45	1.01	8.19[-1]	5.73[-1]	4.59[-1]	3.93[-1]	3.17[-1]	2.75[-1]
5	39	4.33	4.52	4.55	4.60	4.76	4.96	5.44	5.93
5	40	1.34	1.41	1.42	1.43	1.47	1.53	1.66	1.80
5	41	3.52[-2]	2.33[-2]	1.93[-2]	1.56[-2]	1.42[-2]	1.35[-2]	1.28[-2]	1.26[-2]
5	42	3.67[-2]	2.44[-2]	1.97[-2]	1.54[-2]	1.37[-2]	1.28[-2]	1.19[-2]	1.14[-2]
5	43	1.46[-1]	8.66[-2]	6.42[-2]	4.32[-2]	3.51[-2]	3.06[-2]	2.58[-2]	2.33[-2]
5	44	4.06[-1]	3.29[-1]	2.92[-1]	2.52[-1]	2.33[-1]	2.20[-1]	2.04[-1]	1.93[-1]
5	45	3.34	3.11	3.05	3.09	3.22	3.39	3.75	4.10
5	46	3.88	3.64	3.58	3.66	3.85	4.07	4.54	5.01
5	47	2.48[-2]	2.14[-2]	1.98[-2]	1.82[-2]	1.75[-2]	1.70[-2]	1.62[-2]	1.57[-2]
5	48	8.07[-2]	7.24[-2]	6.77[-2]	6.22[-2]	5.92[-2]	5.71[-2]	5.40[-2]	5.15[-2]
5	49	2.21	2.27	2.31	2.45	2.61	2.78	3.11	3.43

⟹

Table 3.3a. Fe III. Selected 94 fine-structure levels from the 219 levels included in the calculation [96Z1] and their observed energies E [Ry] in rydbergs [85S1]. The index i is used in Table 3.3b for transition keys; J is the total angular momentum for specifying the fine-structure level.

Table 3.3a. Fe III. For caption see previous page.

i	LS Term		J	E [Ry]	i	LS Term		J	E [Ry]
1	$3d^6$	a^5D	4	0.0000	48	$3d^5(^4D)4s$	b^3D	3	7.0128[-1]
2			3	3.9749[-3]	49			2	7.0261[-1]
3			2	6.7334[-3]	50			1	7.0236[-1]
4			1	8.4967[-3]	51	$3d^5(^2I)4s$	a^3I	7	7.2756[-1]
5			0	9.3614[-3]	52			6	7.2760[-1]
6	$3d^6$	a^3P	2	1.7683[-1]	53			5	7.2774[-1]
7			1	1.8853[-1]	54	$3d^5(^6S)4p$	z^7P^o	4	7.5495[-1]
8			0	1.9327[-1]	55			3	7.5028[-1]
9	$3d^6$	a^3H	6	1.8272[-1]	56			2	7.4725[-1]
10			5	1.8499[-1]	57	$3d^5(^2D3)4s$	c^3D	3	7.5073[-1]
11			4	1.8664[-1]	58			2	7.5098[-1]
12	$3d^6$	a^3F	4	1.9558[-1]	59			1	7.5175[-1]
13			3	1.9774[-1]	60	$3d^5(^4F3)4s$	a^5F	5	7.5761[-1]
14			2	1.9918[-1]	61			4	7.5782[-1]
15	$3d^6$	a^3G	5	2.2380[-1]	62			3	7.5852[-1]
16			4	2.2728[-1]	63			2	7.5962[-1]
17			3	2.2911[-1]	64			1	7.6225[-1]
18	$3d^5(^6S)4s$	a^7S	3	2.7419[-1]	65	$3d^5(^2F2)4s$	c^3F	4	7.6692[-1]
19	$3d^6$	a^3D	3	2.8120[-1]	66			3	7.7159[-1]
20			2	2.7991[-1]	67			2	7.6884[-1]
21			1	2.7999[-1]	68	$3d^5(^2H)4s$	b^3H	6	8.1033[-1]
22	$3d^5(^6S)4s$	a^5S	2	3.7362[-1]	69			5	8.0825[-1]
23	$3d^6$	b^3P	2	4.5939[-1]	70			4	8.0796[-1]
24			1	4.5178[-1]	71	$3d^5(^6S)4p$	z^5P^o	3	8.1180[-1]
25			0	4.4787[-1]	72			2	8.1408[-1]
26	$3d^6$	b^3F	4	4.5815[-1]	73			1	8.1551[-1]
27			3	4.5832[-1]	74	$3d^5(^4G)4p$	z^5G^o	6	1.0365
28	$3d^5(^4G)4s$	a^5G	6	5.7797[-1]	75			5	1.0359
29			2	4.5732[-1]	76			4	1.0355
30			5	5.7835[-1]	77			3	1.0352
31			4	5.7853[-1]	78			2	1.0351
32			3	5.7860[-1]	79	$3d^5(^4G)4p$	z^5H^o	7	1.0538
33			2	5.7861[-1]	80			6	1.0523
34	$3d^5(^4P)4s$	a^5P	3	6.0567[-1]	81			5	1.0506
35			2	6.0620[-1]	82			4	1.0490
36			1	6.0683[-1]	83			3	1.0475
37	$3d^5(^4D)4s$	b^5D	4	6.3511[-1]	84	$3d^5(^4G)4p$	z^5F^o	5	1.0600
38			3	6.3640[-1]	85			4	1.0613
39			2	6.3641[-1]	86			3	1.0614
40			1	6.3596[-1]	87			2	1.0660
41			0	6.3559[-1]	88			1	1.0656
42	$3d^5(^4G)4s$	b^3G	5	6.4421[-1]	89	$3d^5(^4P)4p$	z^5S^o	2	1.0653
43			4	6.4453[-1]	90	$3d^5(^4P)4p$	z^5D^o	4	1.0709
44			3	6.4449[-1]	91			3	1.0668
45	$3d^5(^4P)4s$	c^3P	2	6.7186[-1]	92			2	1.0609
46			1	6.7296[-1]	93			1	1.0605
47			0	6.7375[-1]	94			0	1.0604

Table 3.3b. Fe III. Effective collision strengths $\Upsilon(i,j)$ as a function of temperature T [K] for the transitions between the first 17 metastable levels and the transitions between the five levels of the ground term $3d^6\ ^5D$ and the 77 higher levels, $i = 18 - 94$ as specified in Table 3.3a [96Z1].

Levels		T [K]							
i	j	1000	3000	5000	10000	15000	20000	30000	40000
1	2	2.85	2.29	2.48	2.92	3.05	3.04	2.92	2.79
1	3	8.41[-1]	8.41[-1]	1.00	1.24	1.32	1.33	1.29	1.24
2	3	1.57	1.50	1.70	2.06	2.18	2.19	2.14	2.06
1	4	4.18[-1]	4.14[-1]	4.84[-1]	5.95[-1]	6.31[-1]	6.39[-1]	6.29[-1]	6.13[-1]
2	4	3.98[-1]	4.89[-1]	6.21[-1]	7.99[-1]	8.48[-1]	8.49[-1]	8.17[-1]	7.83[-1]
3	4	9.43[-1]	9.29[-1]	1.06	1.29	1.36	1.37	1.33	1.29
1	5	1.33[-1]	1.29[-1]	1.48[-1]	1.80[-1]	1.92[-1]	1.96[-1]	1.95[-1]	1.92[-1]
2	5	1.01[-1]	1.33[-1]	1.74[-1]	2.25[-1]	2.38[-1]	2.37[-1]	2.27[-1]	2.18[-1]
3	5	1.31[-1]	1.85[-1]	2.39[-1]	3.12[-1]	3.33[-1]	3.34[-1]	3.22[-1]	3.08[-1]
4	5	4.10[-1]	3.79[-1]	4.16[-1]	4.93[-1]	5.20[-1]	5.24[-1]	5.13[-1]	4.98[-1]
1	6	6.28[-1]	6.47[-1]	6.24[-1]	5.80[-1]	5.55[-1]	5.40[-1]	5.32[-1]	5.41[-1]
2	6	3.70[-1]	3.82[-1]	3.64[-1]	3.35[-1]	3.20[-1]	3.11[-1]	3.05[-1]	3.07[-1]
3	6	1.91[-1]	2.00[-1]	1.90[-1]	1.73[-1]	1.64[-1]	1.59[-1]	1.54[-1]	1.53[-1]
4	6	8.27[-2]	8.85[-2]	8.45[-2]	7.67[-2]	7.29[-2]	7.05[-2]	6.78[-2]	6.68[-2]
5	6	2.19[-2]	2.41[-2]	2.31[-2]	2.11[-2]	2.01[-2]	1.94[-2]	1.86[-2]	1.82[-2]
1	7	1.93[-1]	1.99[-1]	1.86[-1]	1.65[-1]	1.55[-1]	1.49[-1]	1.43[-1]	1.41[-1]
2	7	1.95[-1]	2.09[-1]	2.05[-1]	1.95[-1]	1.88[-1]	1.83[-1]	1.80[-1]	1.83[-1]
3	7	1.91[-1]	1.98[-1]	1.92[-1]	1.79[-1]	1.72[-1]	1.67[-1]	1.65[-1]	1.69[-1]
4	7	1.43[-1]	1.45[-1]	1.38[-1]	1.26[-1]	1.20[-1]	1.17[-1]	1.15[-1]	1.18[-1]
5	7	5.34[-2]	5.33[-2]	5.01[-2]	4.53[-2]	4.31[-2]	4.18[-2]	4.13[-2]	4.21[-2]
6	7	1.93	1.43	1.26	1.10	1.02	9.51[-1]	8.46[-1]	7.67[-1]
1	8	1.69[-2]	2.22[-2]	2.24[-2]	2.13[-2]	2.06[-2]	1.99[-2]	1.86[-2]	1.75[-2]
2	8	8.70[-2]	8.60[-2]	7.90[-2]	6.98[-2]	6.60[-2]	6.40[-2]	6.25[-2]	6.27[-2]
3	8	8.36[-2]	8.48[-2]	8.07[-2]	7.41[-2]	7.08[-2]	6.89[-2]	6.86[-2]	7.06[-2]
4	8	5.33[-2]	5.61[-2]	5.53[-2]	5.28[-2]	5.09[-2]	4.97[-2]	5.00[-2]	5.22[-2]
5	8	1.77[-2]	1.91[-2]	1.93[-2]	1.89[-2]	1.82[-2]	1.77[-2]	1.70[-2]	1.66[-2]
6	8	4.45[-1]	3.45[-1]	3.15[-1]	2.82[-1]	2.60[-1]	2.42[-1]	2.12[-1]	1.89[-1]
7	8	7.50[-1]	5.24[-1]	4.46[-1]	3.77[-1]	3.50[-1]	3.31[-1]	3.02[-1]	2.80[-1]
1	9	1.38	1.45	1.40	1.34	1.32	1.32	1.37	1.46
2	9	5.95[-1]	5.99[-1]	5.77[-1]	5.55[-1]	5.54[-1]	5.58[-1]	5.86[-1]	6.24[-1]
3	9	1.92[-1]	1.92[-1]	1.85[-1]	1.78[-1]	1.79[-1]	1.81[-1]	1.92[-1]	2.05[-1]
4	9	3.64[-2]	3.70[-2]	3.58[-2]	3.48[-2]	3.53[-2]	3.62[-2]	3.86[-2]	4.15[-2]
5	9	9.22[-4]	1.08[-3]	1.08[-3]	1.22[-3]	1.44[-3]	1.62[-3]	1.85[-3]	2.00[-3]
6	9	5.98[-1]	5.10[-1]	4.54[-1]	4.03[-1]	3.92[-1]	3.92[-1]	4.09[-1]	4.38[-1]
7	9	1.38[-1]	1.15[-1]	1.01[-1]	8.76[-2]	8.36[-2]	8.18[-2]	8.10[-2]	8.19[-2]
8	9	4.62[-3]	6.53[-3]	7.30[-3]	8.07[-3]	8.38[-3]	8.43[-3]	8.26[-3]	8.02[-3]

Table 3.3b. Fe III (continued)

Levels		T [K]							
i	j	1000	3000	5000	10000	15000	20000	30000	40000
1	10	5.21[-1]	5.29[-1]	5.10[-1]	4.89[-1]	4.86[-1]	4.90[-1]	5.14[-1]	5.49[-1]
2	10	6.83[-1]	6.67[-1]	6.36[-1]	6.09[-1]	6.02[-1]	6.02[-1]	6.23[-1]	6.58[-1]
3	10	4.81[-1]	4.72[-1]	4.51[-1]	4.30[-1]	4.25[-1]	4.25[-1]	4.41[-1]	4.66[-1]
4	10	2.43[-1]	2.41[-1]	2.31[-1]	2.23[-1]	2.23[-1]	2.25[-1]	2.36[-1]	2.52[-1]
5	10	6.90[-2]	6.93[-2]	6.70[-2]	6.53[-2]	6.62[-2]	6.77[-2]	7.22[-2]	7.75[-2]
6	10	3.20[-1]	2.71[-1]	2.40[-1]	2.13[-1]	2.07[-1]	2.05[-1]	2.06[-1]	2.11[-1]
7	10	2.22[-1]	1.96[-1]	1.79[-1]	1.67[-1]	1.68[-1]	1.68[-1]	1.71[-1]	1.74[-1]
8	10	8.78[-2]	7.00[-2]	6.00[-2]	5.26[-2]	5.15[-2]	5.11[-2]	5.08[-2]	5.08[-2]
9	10	3.01	3.00	2.97	2.84	2.71	2.59	2.39	2.24
1	11	9.69[-2]	9.81[-2]	9.48[-2]	9.26[-2]	9.41[-2]	9.63[-2]	1.03[-1]	1.10[-1]
2	11	3.97[-1]	3.94[-1]	3.79[-1]	3.67[-1]	3.68[-1]	3.73[-1]	3.89[-1]	4.10[-1]
3	11	5.37[-1]	5.28[-1]	5.05[-1]	4.86[-1]	4.84[-1]	4.85[-1]	4.92[-1]	5.04[-1]
4	11	4.47[-1]	4.37[-1]	4.17[-1]	4.01[-1]	3.99[-1]	3.98[-1]	4.03[-1]	4.12[-1]
5	11	1.72[-1]	1.68[-1]	1.60[-1]	1.54[-1]	1.53[-1]	1.53[-1]	1.55[-1]	1.59[-1]
6	11	1.28[-1]	1.11[-1]	1.01[-1]	9.39[-2]	9.41[-2]	9.44[-2]	9.52[-2]	9.63[-2]
7	11	2.72[-1]	2.26[-1]	2.00[-1]	1.81[-1]	1.80[-1]	1.80[-1]	1.84[-1]	1.89[-1]
8	11	1.19[-1]	1.03[-1]	9.30[-2]	8.54[-2]	8.50[-2]	8.55[-2]	8.82[-2]	9.18[-2]
9	11	3.55[-1]	3.74[-1]	3.77[-1]	3.79[-1]	3.77[-1]	3.70[-1]	3.48[-1]	3.28[-1]
10	11	2.95	3.07	3.10	3.07	2.97	2.86	2.64	2.47
1	12	1.67	1.27	1.15	1.07	1.02	9.87[-1]	9.24[-1]	8.77[-1]
2	12	7.61[-1]	6.10[-1]	5.65[-1]	5.38[-1]	5.29[-1]	5.18[-1]	4.96[-1]	4.77[-1]
3	12	3.17[-1]	2.70[-1]	2.55[-1]	2.49[-1]	2.48[-1]	2.47[-1]	2.40[-1]	2.33[-1]
4	12	1.17[-1]	1.06[-1]	1.02[-1]	1.01[-1]	1.03[-1]	1.03[-1]	1.02[-1]	1.00[-1]
5	12	2.86[-2]	2.69[-2]	2.63[-2]	2.65[-2]	2.72[-2]	2.75[-2]	2.75[-2]	2.71[-2]
6	12	1.03	1.02	9.96[-1]	9.42[-1]	9.03[-1]	8.68[-1]	8.08[-1]	7.60[-1]
7	12	6.42[-1]	6.71[-1]	6.50[-1]	6.03[-1]	5.71[-1]	5.46[-1]	5.07[-1]	4.77[-1]
8	12	2.22[-1]	2.45[-1]	2.37[-1]	2.16[-1]	2.03[-1]	1.93[-1]	1.78[-1]	1.67[-1]
9	12	2.59	2.34	2.13	1.85	1.70	1.59	1.48	1.42
10	12	1.13	1.03	9.42[-1]	8.14[-1]	7.46[-1]	7.02[-1]	6.50[-1]	6.24[-1]
11	12	2.12[-1]	2.13[-1]	2.00[-1]	1.80[-1]	1.70[-1]	1.62[-1]	1.52[-1]	1.47[-1]
1	13	5.82[-1]	4.84[-1]	4.53[-1]	4.35[-1]	4.31[-1]	4.24[-1]	4.10[-1]	3.96[-1]
2	13	7.44[-1]	5.66[-1]	5.16[-1]	4.84[-1]	4.67[-1]	4.51[-1]	4.24[-1]	4.04[-1]
3	13	5.45[-1]	4.20[-1]	3.85[-1]	3.62[-1]	3.51[-1]	3.41[-1]	3.23[-1]	3.10[-1]
4	13	2.92[-1]	2.34[-1]	2.17[-1]	2.07[-1]	2.03[-1]	1.99[-1]	1.92[-1]	1.86[-1]
5	13	8.73[-2]	7.25[-2]	6.78[-2]	6.54[-2]	6.50[-2]	6.44[-2]	6.28[-2]	6.13[-2]
6	13	8.23[-1]	8.46[-1]	8.21[-1]	7.68[-1]	7.33[-1]	7.03[-1]	6.56[-1]	6.18[-1]
7	13	4.98[-1]	5.18[-1]	5.03[-1]	4.72[-1]	4.50[-1]	4.31[-1]	3.99[-1]	3.74[-1]
8	13	1.55[-1]	1.46[-1]	1.43[-1]	1.37[-1]	1.34[-1]	1.30[-1]	1.24[-1]	1.18[-1]
9	13	9.35[-1]	8.54[-1]	7.77[-1]	6.67[-1]	6.08[-1]	5.70[-1]	5.27[-1]	5.06[-1]
10	13	1.09	1.00	9.25[-1]	8.37[-1]	7.88[-1]	7.51[-1]	6.99[-1]	6.69[-1]
11	13	1.06	9.56[-1]	8.76[-1]	7.78[-1]	7.28[-1]	6.93[-1]	6.44[-1]	6.13[-1]
12	13	1.22	1.23	1.23	1.25	1.24	1.21	1.14	1.07

Table 3.3b. Fe III (continued)

Levels		T [K]							
i	j	1000	3000	5000	10000	15000	20000	30000	40000
1	14	1.79[-1]	1.63[-1]	1.58[-1]	1.57[-1]	1.60[-1]	1.61[-1]	1.59[-1]	1.56[-1]
2	14	3.85[-1]	3.16[-1]	2.95[-1]	2.85[-1]	2.83[-1]	2.79[-1]	2.71[-1]	2.63[-1]
3	14	4.88[-1]	3.76[-1]	3.44[-1]	3.24[-1]	3.15[-1]	3.07[-1]	2.93[-1]	2.84[-1]
4	14	4.02[-1]	3.00[-1]	2.71[-1]	2.53[-1]	2.43[-1]	2.34[-1]	2.21[-1]	2.14[-1]
5	14	1.54[-1]	1.14[-1]	1.03[-1]	9.50[-2]	9.08[-2]	8.72[-2]	8.19[-2]	7.88[-2]
6	14	6.03[-1]	6.45[-1]	6.25[-1]	5.79[-1]	5.49[-1]	5.25[-1]	4.88[-1]	4.59[-1]
7	14	3.36[-1]	3.21[-1]	3.13[-1]	3.02[-1]	2.94[-1]	2.86[-1]	2.70[-1]	2.57[-1]
8	14	1.15[-1]	1.12[-1]	1.10[-1]	1.06[-1]	1.03[-1]	9.93[-2]	9.28[-2]	8.73[-2]
9	14	9.40[-2]	1.04[-1]	9.94[-2]	9.05[-2]	8.58[-2]	8.23[-2]	7.76[-2]	7.49[-2]
10	14	8.56[-1]	7.74[-1]	7.08[-1]	6.26[-1]	5.84[-1]	5.56[-1]	5.20[-1]	4.99[-1]
11	14	1.25	1.13	1.04	9.41[-1]	8.89[-1]	8.48[-1]	7.85[-1]	7.39[-1]
12	14	2.73[-1]	2.83[-1]	2.83[-1]	2.92[-1]	2.95[-1]	2.91[-1]	2.75[-1]	2.58[-1]
13	14	1.04	1.04	1.05	1.10	1.11	1.10	1.04	9.87[-1]
1	15	8.39[-1]	1.03	1.07	1.10	1.09	1.08	1.04	1.02
2	15	3.82[-1]	4.74[-1]	4.89[-1]	4.98[-1]	4.97[-1]	4.92[-1]	4.81[-1]	4.72[-1]
3	15	1.48[-1]	1.81[-1]	1.85[-1]	1.87[-1]	1.87[-1]	1.86[-1]	1.83[-1]	1.81[-1]
4	15	4.81[-2]	5.51[-2]	5.54[-2]	5.49[-2]	5.48[-2]	5.46[-2]	5.43[-2]	5.40[-2]
5	15	1.01[-2]	1.05[-2]	1.02[-2]	9.94[-3]	9.91[-3]	9.92[-3]	9.97[-3]	1.00[-2]
6	15	6.00[-1]	6.95[-1]	6.65[-1]	6.07[-1]	5.72[-1]	5.47[-1]	5.17[-1]	5.01[-1]
7	15	2.47[-1]	2.80[-1]	2.66[-1]	2.42[-1]	2.26[-1]	2.14[-1]	1.96[-1]	1.84[-1]
8	15	4.45[-2]	4.28[-2]	3.98[-2]	3.79[-2]	3.73[-2]	3.64[-2]	3.42[-2]	3.20[-2]
9	15	2.87	2.86	2.80	2.72	2.67	2.61	2.50	2.40
10	15	1.23	1.24	1.26	1.28	1.26	1.24	1.18	1.13
11	15	3.37[-1]	3.35[-1]	3.43[-1]	3.75[-1]	3.88[-1]	3.90[-1]	3.81[-1]	3.71[-1]
12	15	1.67	1.71	1.67	1.71	1.72	1.69	1.59	1.49
13	15	6.45[-1]	6.80[-1]	6.74[-1]	6.85[-1]	6.89[-1]	6.78[-1]	6.41[-1]	6.04[-1]
14	15	1.41[-1]	1.58[-1]	1.57[-1]	1.60[-1]	1.61[-1]	1.59[-1]	1.50[-1]	1.42[-1]
1	16	3.25[-1]	4.05[-1]	4.19[-1]	4.28[-1]	4.27[-1]	4.24[-1]	4.16[-1]	4.09[-1]
2	16	3.84[-1]	4.66[-1]	4.85[-1]	5.11[-1]	5.16[-1]	5.13[-1]	4.99[-1]	4.87[-1]
3	16	2.77[-1]	3.40[-1]	3.54[-1]	3.70[-1]	3.74[-1]	3.71[-1]	3.63[-1]	3.56[-1]
4	16	1.48[-1]	1.87[-1]	1.95[-1]	2.01[-1]	2.02[-1]	2.01[-1]	1.99[-1]	1.97[-1]
5	16	4.44[-2]	5.70[-2]	5.96[-2]	6.12[-2]	6.15[-2]	6.14[-2]	6.12[-2]	6.11[-2]
6	16	3.95[-1]	4.52[-1]	4.33[-1]	3.99[-1]	3.78[-1]	3.60[-1]	3.35[-1]	3.19[-1]
7	16	2.21[-1]	2.44[-1]	2.35[-1]	2.28[-1]	2.22[-1]	2.16[-1]	2.06[-1]	2.00[-1]
8	16	1.14[-1]	1.38[-1]	1.35[-1]	1.27[-1]	1.20[-1]	1.13[-1]	1.03[-1]	9.52[-2]
9	16	1.15	1.16	1.18	1.20	1.19	1.16	1.11	1.07
10	16	1.43	1.52	1.60	1.69	1.70	1.67	1.58	1.51
11	16	1.11	1.13	1.17	1.23	1.23	1.21	1.16	1.11
12	16	7.21[-1]	7.61[-1]	7.56[-1]	7.74[-1]	7.80[-1]	7.69[-1]	7.28[-1]	6.86[-1]
13	16	7.39[-1]	7.64[-1]	7.62[-1]	8.13[-1]	8.32[-1]	8.22[-1]	7.72[-1]	7.19[-1]
14	16	5.52[-1]	5.83[-1]	5.86[-1]	6.14[-1]	6.26[-1]	6.22[-1]	5.95[-1]	5.64[-1]
15	16	1.60	1.75	1.76	1.75	1.70	1.64	1.52	1.42

Table 3.3b. Fe III (continued)

Levels		T [K]							
i	j	1000	3000	5000	10000	15000	20000	30000	40000
1	17	9.40[-2]	1.08[-1]	1.09[-1]	1.09[-1]	1.09[-1]	1.09[-1]	1.08[-1]	1.08[-1]
2	17	2.28[-1]	2.86[-1]	2.98[-1]	3.08[-1]	3.10[-1]	3.09[-1]	3.07[-1]	3.04[-1]
3	17	2.77[-1]	3.45[-1]	3.63[-1]	3.83[-1]	3.88[-1]	3.88[-1]	3.87[-1]	3.87[-1]
4	17	2.22[-1]	2.74[-1]	2.90[-1]	3.10[-1]	3.15[-1]	3.15[-1]	3.13[-1]	3.12[-1]
5	17	8.43[-2]	1.04[-1]	1.10[-1]	1.18[-1]	1.20[-1]	1.20[-1]	1.19[-1]	1.18[-1]
6	17	2.21[-1]	2.41[-1]	2.31[-1]	2.18[-1]	2.09[-1]	2.00[-1]	1.85[-1]	1.74[-1]
7	17	2.61[-1]	3.11[-1]	3.04[-1]	2.90[-1]	2.77[-1]	2.64[-1]	2.45[-1]	2.31[-1]
8	17	8.50[-2]	9.71[-2]	9.46[-2]	9.31[-2]	9.10[-2]	8.84[-2]	8.35[-2]	7.99[-2]
9	17	2.79[-1]	2.75[-1]	2.77[-1]	2.90[-1]	2.97[-1]	2.97[-1]	2.92[-1]	2.87[-1]
10	17	1.02	1.04	1.07	1.12	1.12	1.10	1.05	1.01
11	17	1.59	1.70	1.80	1.94	1.96	1.92	1.83	1.74
12	17	1.92[-1]	2.12[-1]	2.12[-1]	2.16[-1]	2.17[-1]	2.14[-1]	2.02[-1]	1.90[-1]
13	17	6.29[-1]	6.63[-1]	6.66[-1]	6.99[-1]	7.13[-1]	7.08[-1]	6.78[-1]	6.45[-1]
14	17	7.47[-1]	7.70[-1]	7.75[-1]	8.37[-1]	8.65[-1]	8.62[-1]	8.28[-1]	7.89[-1]
15	17	2.72[-1]	2.88[-1]	2.82[-1]	2.95[-1]	2.96[-1]	2.88[-1]	2.64[-1]	2.41[-1]
16	17	1.46	1.61	1.65	1.67	1.64	1.59	1.47	1.37
1	18	8.98[-1]	1.20	1.35	1.36	1.28	1.20	1.07	9.70[-1]
2	18	5.19[-1]	8.00[-1]	9.43[-1]	9.86[-1]	9.34[-1]	8.79[-1]	7.86[-1]	7.11[-1]
3	18	5.66[-1]	7.31[-1]	8.03[-1]	7.96[-1]	7.43[-1]	6.95[-1]	6.19[-1]	5.60[-1]
4	18	3.35[-1]	4.32[-1]	4.76[-1]	4.73[-1]	4.42[-1]	4.14[-1]	3.69[-1]	3.34[-1]
5	18	1.20[-1]	1.56[-1]	1.71[-1]	1.67[-1]	1.56[-1]	1.45[-1]	1.29[-1]	1.17[-1]
1	19	6.26[-1]	6.07[-1]	6.58[-1]	7.27[-1]	7.27[-1]	7.08[-1]	6.65[-1]	6.31[-1]
2	19	4.41[-1]	3.83[-1]	4.00[-1]	4.36[-1]	4.38[-1]	4.29[-1]	4.08[-1]	3.90[-1]
3	19	2.36[-1]	2.13[-1]	2.25[-1]	2.47[-1]	2.51[-1]	2.48[-1]	2.38[-1]	2.29[-1]
4	19	1.13[-1]	1.07[-1]	1.14[-1]	1.26[-1]	1.29[-1]	1.29[-1]	1.25[-1]	1.21[-1]
5	19	3.45[-2]	3.32[-2]	3.54[-2]	3.91[-2]	4.02[-2]	4.01[-2]	3.90[-2]	3.79[-2]
1	20	3.05[-1]	2.83[-1]	2.99[-1]	3.29[-1]	3.34[-1]	3.30[-1]	3.16[-1]	3.05[-1]
2	20	4.83[-1]	3.54[-1]	3.54[-1]	3.70[-1]	3.66[-1]	3.56[-1]	3.35[-1]	3.18[-1]
3	20	3.43[-1]	2.58[-1]	2.60[-1]	2.74[-1]	2.71[-1]	2.63[-1]	2.47[-1]	2.34[-1]
4	20	1.68[-1]	1.38[-1]	1.43[-1]	1.54[-1]	1.54[-1]	1.50[-1]	1.42[-1]	1.35[-1]
5	20	4.57[-2]	4.13[-2]	4.35[-2]	4.78[-2]	4.82[-2]	4.73[-2]	4.50[-2]	4.31[-2]
1	21	1.33[-1]	1.28[-1]	1.36[-1]	1.50[-1]	1.53[-1]	1.53[-1]	1.49[-1]	1.45[-1]
2	21	1.62[-1]	1.49[-1]	1.57[-1]	1.73[-1]	1.75[-1]	1.72[-1]	1.64[-1]	1.58[-1]
3	21	2.27[-1]	1.72[-1]	1.74[-1]	1.84[-1]	1.82[-1]	1.77[-1]	1.65[-1]	1.57[-1]
4	21	2.04[-1]	1.41[-1]	1.39[-1]	1.44[-1]	1.40[-1]	1.35[-1]	1.25[-1]	1.18[-1]
5	21	8.14[-2]	5.46[-2]	5.33[-2]	5.42[-2]	5.27[-2]	5.05[-2]	4.67[-2]	4.39[-2]
1	22	1.08	1.57	1.68	1.61	1.54	1.49	1.40	1.30
2	22	8.54[-1]	1.27	1.36	1.30	1.25	1.21	1.13	1.06
3	22	6.37[-1]	9.16[-1]	9.75[-1]	9.30[-1]	8.93[-1]	8.65[-1]	8.09[-1]	7.56[-1]
4	22	3.78[-1]	5.45[-1]	5.81[-1]	5.54[-1]	5.33[-1]	5.16[-1]	4.83[-1]	4.51[-1]
5	22	1.37[-1]	1.96[-1]	2.08[-1]	1.97[-1]	1.89[-1]	1.83[-1]	1.72[-1]	1.60[-1]

Table 3.3b. Fe III (continued)

Levels		T [K]							
i	j	1000	3000	5000	10000	15000	20000	30000	40000
1	23	5.82[-1]	4.46[-1]	3.84[-1]	3.23[-1]	2.95[-1]	2.78[-1]	2.56[-1]	2.43[-1]
2	23	2.77[-1]	2.37[-1]	2.18[-1]	2.01[-1]	1.94[-1]	1.88[-1]	1.80[-1]	1.75[-1]
3	23	1.24[-1]	1.21[-1]	1.20[-1]	1.20[-1]	1.20[-1]	1.19[-1]	1.18[-1]	1.16[-1]
4	23	5.10[-2]	5.70[-2]	5.99[-2]	6.37[-2]	6.52[-2]	6.58[-2]	6.59[-2]	6.56[-2]
5	23	1.37[-2]	1.67[-2]	1.81[-2]	1.99[-2]	2.06[-2]	2.09[-2]	2.12[-2]	2.12[-2]
1	24	7.73[-2]	9.53[-2]	1.04[-1]	1.14[-1]	1.18[-1]	1.21[-1]	1.22[-1]	1.21[-1]
2	24	2.25[-1]	1.76[-1]	1.53[-1]	1.31[-1]	1.21[-1]	1.15[-1]	1.07[-1]	1.02[-1]
3	24	1.87[-1]	1.44[-1]	1.25[-1]	1.05[-1]	9.63[-2]	9.07[-2]	8.36[-2]	7.93[-2]
4	24	1.06[-1]	8.40[-2]	7.41[-2]	6.44[-2]	6.01[-2]	5.74[-2]	5.36[-2]	5.12[-2]
5	24	3.24[-2]	2.66[-2]	2.39[-2]	2.14[-2]	2.03[-2]	1.96[-2]	1.85[-2]	1.78[-2]
1	25	1.89[-2]	2.56[-2]	2.89[-2]	3.26[-2]	3.40[-2]	3.47[-2]	3.53[-2]	3.54[-2]
2	25	2.61[-2]	3.06[-2]	3.27[-2]	3.53[-2]	3.65[-2]	3.70[-2]	3.71[-2]	3.68[-2]
3	25	6.56[-2]	5.11[-2]	4.44[-2]	3.79[-2]	3.50[-2]	3.31[-2]	3.07[-2]	2.91[-2]
4	25	6.99[-2]	4.90[-2]	3.95[-2]	2.99[-2]	2.55[-2]	2.29[-2]	1.98[-2]	1.80[-2]
5	25	2.96[-2]	2.01[-2]	1.58[-2]	1.13[-2]	9.34[-3]	8.15[-3]	6.77[-3]	5.99[-3]
1	26	8.13[-1]	7.07[-1]	6.64[-1]	6.13[-1]	5.79[-1]	5.56[-1]	5.27[-1]	5.10[-1]
2	26	3.92[-1]	3.75[-1]	3.68[-1]	3.56[-1]	3.43[-1]	3.34[-1]	3.22[-1]	3.16[-1]
3	26	1.67[-1]	1.74[-1]	1.79[-1]	1.79[-1]	1.74[-1]	1.69[-1]	1.63[-1]	1.59[-1]
4	26	6.23[-2]	6.71[-2]	7.06[-2]	7.07[-2]	6.85[-2]	6.64[-2]	6.37[-2]	6.19[-2]
5	26	1.55[-2]	1.62[-2]	1.69[-2]	1.67[-2]	1.61[-2]	1.55[-2]	1.48[-2]	1.43[-2]
1	27	3.03[-1]	3.15[-1]	3.25[-1]	3.26[-1]	3.17[-1]	3.09[-1]	2.99[-1]	2.92[-1]
2	27	3.84[-1]	3.20[-1]	2.90[-1]	2.56[-1]	2.36[-1]	2.23[-1]	2.07[-1]	1.98[-1]
3	27	2.82[-1]	2.52[-1]	2.40[-1]	2.21[-1]	2.08[-1]	1.98[-1]	1.86[-1]	1.79[-1]
4	27	1.54[-1]	1.54[-1]	1.54[-1]	1.52[-1]	1.47[-1]	1.43[-1]	1.38[-1]	1.35[-1]
5	27	4.72[-2]	5.07[-2]	5.26[-2]	5.37[-2]	5.30[-2]	5.23[-2]	5.13[-2]	5.07[-2]
1	28	9.63[-2]	1.04[-1]	1.09[-1]	1.09[-1]	1.05[-1]	1.02[-1]	9.70[-2]	9.39[-2]
2	28	2.06[-1]	2.18[-1]	2.26[-1]	2.27[-1]	2.20[-1]	2.14[-1]	2.05[-1]	2.00[-1]
3	28	2.57[-1]	2.38[-1]	2.32[-1]	2.19[-1]	2.08[-1]	1.99[-1]	1.88[-1]	1.82[-1]
4	28	2.09[-1]	1.77[-1]	1.62[-1]	1.45[-1]	1.35[-1]	1.28[-1]	1.20[-1]	1.15[-1]
5	28	8.01[-2]	6.46[-2]	5.71[-2]	4.93[-2]	4.53[-2]	4.27[-2]	3.97[-2]	3.80[-2]
1	29	1.29	1.12	1.07	1.01	1.05	1.14	1.29	1.36
2	29	4.79[-1]	4.16[-1]	3.93[-1]	3.59[-1]	3.75[-1]	4.18[-1]	4.92[-1]	5.25[-1]
3	29	2.09[-1]	2.03[-1]	1.96[-1]	1.74[-1]	1.77[-1]	1.94[-1]	2.26[-1]	2.40[-1]
4	29	1.16[-1]	1.00[-1]	9.19[-2]	7.83[-2]	7.67[-2]	8.16[-2]	9.19[-2]	9.63[-2]
5	29	4.37[-2]	3.89[-2]	3.62[-2]	3.04[-2]	2.80[-2]	2.76[-2]	2.80[-2]	2.78[-2]
1	30	7.62[-1]	7.13[-1]	6.87[-1]	6.21[-1]	6.18[-1]	6.52[-1]	7.17[-1]	7.42[-1]
2	30	7.35[-1]	8.65[-1]	8.75[-1]	8.15[-1]	8.04[-1]	8.30[-1]	8.86[-1]	9.06[-1]
3	30	4.86[-1]	4.77[-1]	4.70[-1]	4.26[-1]	4.10[-1]	4.13[-1]	4.25[-1]	4.23[-1]
4	30	1.44[-1]	1.31[-1]	1.24[-1]	1.10[-1]	1.09[-1]	1.17[-1]	1.31[-1]	1.37[-1]

Table 3.3b. Fe III (continued)

Levels		T [K]							
i	j	1000	3000	5000	10000	15000	20000	30000	40000
5	30	4.93[-2]	4.44[-2]	4.13[-2]	3.52[-2]	3.52[-2]	3.83[-2]	4.45[-2]	4.73[-2]
1	31	4.36[-1]	4.14[-1]	3.99[-1]	3.57[-1]	3.52[-1]	3.70[-1]	4.07[-1]	4.21[-1]
2	31	6.69[-1]	7.49[-1]	7.63[-1]	7.10[-1]	6.86[-1]	6.90[-1]	7.07[-1]	7.05[-1]
3	31	5.20[-1]	5.98[-1]	6.11[-1]	5.69[-1]	5.55[-1]	5.64[-1]	5.88[-1]	5.92[-1]
4	31	3.05[-1]	2.68[-1]	2.56[-1]	2.29[-1]	2.24[-1]	2.29[-1]	2.42[-1]	2.44[-1]
5	31	6.08[-2]	7.02[-2]	7.22[-2]	6.64[-2]	6.34[-2]	6.32[-2]	6.38[-2]	6.27[-2]
1	32	2.51[-1]	2.32[-1]	2.20[-1]	1.92[-1]	1.88[-1]	1.99[-1]	2.22[-1]	2.31[-1]
2	32	3.99[-1]	4.11[-1]	4.08[-1]	3.73[-1]	3.65[-1]	3.75[-1]	3.97[-1]	4.02[-1]
3	32	5.29[-1]	5.61[-1]	5.61[-1]	5.15[-1]	5.00[-1]	5.09[-1]	5.31[-1]	5.34[-1]
4	32	3.49[-1]	4.12[-1]	4.26[-1]	4.01[-1]	3.87[-1]	3.89[-1]	3.96[-1]	3.94[-1]
5	32	1.68[-1]	1.65[-1]	1.65[-1]	1.51[-1]	1.43[-1]	1.40[-1]	1.38[-1]	1.33[-1]
1	33	1.62[-1]	1.47[-1]	1.37[-1]	1.17[-1]	1.11[-1]	1.15[-1]	1.23[-1]	1.26[-1]
2	33	2.18[-1]	2.19[-1]	2.14[-1]	1.91[-1]	1.90[-1]	2.01[-1]	2.24[-1]	2.32[-1]
3	33	3.68[-1]	4.00[-1]	4.07[-1]	3.75[-1]	3.59[-1]	3.59[-1]	3.65[-1]	3.62[-1]
4	33	4.28[-1]	4.82[-1]	4.96[-1]	4.64[-1]	4.44[-1]	4.41[-1]	4.44[-1]	4.37[-1]
5	33	1.73[-1]	2.19[-1]	2.31[-1]	2.20[-1]	2.12[-1]	2.11[-1]	2.13[-1]	2.11[-1]
1	34	7.21[-1]	8.91[-1]	8.81[-1]	7.92[-1]	7.58[-1]	7.46[-1]	7.22[-1]	6.86[-1]
2	34	5.22[-1]	6.28[-1]	6.16[-1]	5.46[-1]	5.12[-1]	4.97[-1]	4.72[-1]	4.45[-1]
3	34	3.05[-1]	3.75[-1]	3.77[-1]	3.37[-1]	3.15[-1]	3.04[-1]	2.87[-1]	2.69[-1]
4	34	1.60[-1]	1.93[-1]	1.92[-1]	1.67[-1]	1.53[-1]	1.45[-1]	1.34[-1]	1.23[-1]
5	34	6.17[-2]	7.49[-2]	7.32[-2]	6.20[-2]	5.53[-2]	5.14[-2]	4.62[-2]	4.20[-2]
1	35	4.50[-1]	6.18[-1]	6.26[-1]	5.50[-1]	5.03[-1]	4.76[-1]	4.39[-1]	4.07[-1]
2	35	3.78[-1]	4.66[-1]	4.59[-1]	4.03[-1]	3.77[-1]	3.65[-1]	3.45[-1]	3.22[-1]
3	35	3.07[-1]	3.98[-1]	4.00[-1]	3.55[-1]	3.34[-1]	3.24[-1]	3.08[-1]	2.89[-1]
4	35	2.05[-1]	2.75[-1]	2.79[-1]	2.49[-1]	2.32[-1]	2.24[-1]	2.12[-1]	1.99[-1]
5	35	7.46[-2]	1.09[-1]	1.14[-1]	1.02[-1]	9.43[-2]	9.00[-2]	8.39[-2]	7.85[-2]
1	36	1.63[-1]	2.23[-1]	2.26[-1]	1.96[-1]	1.77[-1]	1.66[-1]	1.50[-1]	1.37[-1]
2	36	2.53[-1]	3.49[-1]	3.55[-1]	3.14[-1]	2.88[-1]	2.74[-1]	2.54[-1]	2.37[-1]
3	36	1.98[-1]	2.70[-1]	2.77[-1]	2.51[-1]	2.37[-1]	2.30[-1]	2.19[-1]	2.06[-1]
4	36	1.28[-1]	1.62[-1]	1.65[-1]	1.51[-1]	1.46[-1]	1.45[-1]	1.41[-1]	1.34[-1]
5	36	5.14[-2]	6.31[-2]	6.26[-2]	5.66[-2]	5.51[-2]	5.51[-2]	5.41[-2]	5.14[-2]
1	37	1.17	1.49	1.55	1.45	1.37	1.31	1.22	1.14
2	37	7.95[-1]	8.80[-1]	8.81[-1]	7.98[-1]	7.37[-1]	6.99[-1]	6.43[-1]	5.96[-1]
3	37	5.24[-1]	5.16[-1]	4.92[-1]	4.25[-1]	3.86[-1]	3.64[-1]	3.33[-1]	3.07[-1]
4	37	2.10[-1]	2.16[-1]	2.08[-1]	1.81[-1]	1.64[-1]	1.55[-1]	1.41[-1]	1.29[-1]
5	37	8.31[-2]	8.29[-2]	7.81[-2]	6.55[-2]	5.81[-2]	5.35[-2]	4.73[-2]	4.25[-2]
1	38	8.10[-1]	9.23[-1]	9.22[-1]	8.31[-1]	7.67[-1]	7.28[-1]	6.70[-1]	6.20[-1]
2	38	1.28	1.14	1.03	8.66[-1]	7.89[-1]	7.47[-1]	6.88[-1]	6.35[-1]

Table 3.3b. Fe III (continued)

Levels		T [K]							
i	j	1000	3000	5000	10000	15000	20000	30000	40000
3	38	8.51[-1]	7.72[-1]	7.11[-1]	6.04[-1]	5.53[-1]	5.26[-1]	4.87[-1]	4.52[-1]
4	38	3.73[-1]	3.65[-1]	3.47[-1]	2.98[-1]	2.71[-1]	2.56[-1]	2.35[-1]	2.18[-1]
5	38	1.03[-1]	1.12[-1]	1.11[-1]	9.73[-2]	8.81[-2]	8.24[-2]	7.44[-2]	6.80[-2]
1	39	5.20[-1]	5.25[-1]	5.08[-1]	4.45[-1]	4.05[-1]	3.81[-1]	3.48[-1]	3.20[-1]
2	39	8.34[-1]	7.77[-1]	7.30[-1]	6.33[-1]	5.81[-1]	5.51[-1]	5.08[-1]	4.70[-1]
3	39	8.75[-1]	7.62[-1]	6.89[-1]	5.74[-1]	5.18[-1]	4.87[-1]	4.45[-1]	4.10[-1]
4	39	4.90[-1]	4.53[-1]	4.27[-1]	3.71[-1]	3.41[-1]	3.24[-1]	2.98[-1]	2.76[-1]
5	39	2.54[-1]	2.22[-1]	2.02[-1]	1.66[-1]	1.48[-1]	1.37[-1]	1.22[-1]	1.12[-1]
1	40	2.06[-1]	2.14[-1]	2.09[-1]	1.84[-1]	1.68[-1]	1.58[-1]	1.44[-1]	1.32[-1]
2	40	3.65[-1]	3.68[-1]	3.58[-1]	3.16[-1]	2.88[-1]	2.72[-1]	2.49[-1]	2.30[-1]
3	40	4.90[-1]	4.53[-1]	4.27[-1]	3.72[-1]	3.42[-1]	3.25[-1]	2.99[-1]	2.77[-1]
4	40	7.33[-1]	5.77[-1]	4.92[-1]	3.82[-1]	3.33[-1]	3.06[-1]	2.72[-1]	2.48[-1]
5	40	2.32[-1]	1.76[-1]	1.53[-1]	1.25[-1]	1.14[-1]	1.08[-1]	9.90[-2]	9.12[-2]
1	41	8.35[-2]	8.36[-2]	7.88[-2]	6.61[-2]	5.87[-2]	5.41[-2]	4.78[-2]	4.30[-2]
2	41	1.03[-1]	1.12[-1]	1.11[-1]	9.78[-2]	8.86[-2]	8.29[-2]	7.49[-2]	6.85[-2]
3	41	2.55[-1]	2.24[-1]	2.05[-1]	1.69[-1]	1.50[-1]	1.39[-1]	1.25[-1]	1.14[-1]
4	41	2.32[-1]	1.77[-1]	1.53[-1]	1.25[-1]	1.14[-1]	1.08[-1]	9.94[-2]	9.15[-2]
5	41	1.51[-1]	1.13[-1]	9.13[-2]	6.62[-2]	5.58[-2]	5.03[-2]	4.37[-2]	3.92[-2]
1	42	4.69[-1]	5.40[-1]	5.38[-1]	5.18[-1]	5.41[-1]	5.68[-1]	5.90[-1]	5.81[-1]
2	42	1.79[-1]	2.25[-1]	2.32[-1]	2.32[-1]	2.52[-1]	2.73[-1]	2.91[-1]	2.88[-1]
3	42	4.59[-2]	6.54[-2]	7.09[-2]	7.71[-2]	9.13[-2]	1.04[-1]	1.17[-1]	1.19[-1]
4	42	1.01[-2]	1.73[-2]	2.00[-2]	2.42[-2]	3.15[-2]	3.80[-2]	4.48[-2]	4.60[-2]
5	42	2.73[-3]	4.60[-3]	5.35[-3]	6.65[-3]	8.74[-3]	1.06[-2]	1.25[-2]	1.28[-2]
1	43	9.56[-2]	1.36[-1]	1.47[-1]	1.58[-1]	1.82[-1]	2.04[-1]	2.26[-1]	2.27[-1]
2	43	3.60[-1]	4.00[-1]	3.90[-1]	3.64[-1]	3.68[-1]	3.78[-1]	3.81[-1]	3.69[-1]
3	43	1.98[-1]	2.26[-1]	2.23[-1]	2.15[-1]	2.25[-1]	2.37[-1]	2.47[-1]	2.42[-1]
4	43	5.96[-2]	7.79[-2]	8.13[-2]	8.37[-2]	9.41[-2]	1.04[-1]	1.14[-1]	1.14[-1]
5	43	8.07[-3]	1.48[-2]	1.70[-2]	1.92[-2]	2.32[-2]	2.70[-2]	3.08[-2]	3.12[-2]
1	44	2.38[-2]	3.90[-2]	4.45[-2]	5.22[-2]	6.53[-2]	7.70[-2]	8.90[-2]	9.07[-2]
2	44	9.63[-2]	1.24[-1]	1.29[-1]	1.31[-1]	1.45[-1]	1.60[-1]	1.73[-1]	1.73[-1]
3	44	1.85[-1]	2.16[-1]	2.16[-1]	2.08[-1]	2.18[-1]	2.29[-1]	2.37[-1]	2.33[-1]
4	44	2.15[-1]	2.40[-1]	2.34[-1]	2.16[-1]	2.17[-1]	2.22[-1]	2.22[-1]	2.15[-1]
5	44	9.74[-2]	1.07[-1]	1.03[-1]	9.38[-2]	9.26[-2]	9.32[-2]	9.21[-2]	8.84[-2]
1	45	1.46[-1]	1.69[-1]	1.75[-1]	1.73[-1]	1.75[-1]	1.76[-1]	1.74[-1]	1.66[-1]
2	45	1.06[-1]	1.28[-1]	1.36[-1]	1.38[-1]	1.45[-1]	1.53[-1]	1.57[-1]	1.54[-1]
3	45	6.19[-2]	7.60[-2]	8.08[-2]	8.26[-2]	8.79[-2]	9.31[-2]	9.71[-2]	9.53[-2]
4	45	3.20[-2]	3.82[-2]	4.04[-2]	4.12[-2]	4.43[-2]	4.73[-2]	4.97[-2]	4.89[-2]
5	45	1.01[-2]	1.16[-2]	1.21[-2]	1.24[-2]	1.34[-2]	1.44[-2]	1.53[-2]	1.51[-2]

Table 3.3b. Fe III (continued)

Levels		T [K]							
i	j	1000	3000	5000	10000	15000	20000	30000	40000
1	46	6.22[-2]	7.38[-2]	7.69[-2]	7.56[-2]	7.73[-2]	7.93[-2]	8.00[-2]	7.74[-2]
2	46	4.38[-2]	5.09[-2]	5.39[-2]	5.61[-2]	6.06[-2]	6.46[-2]	6.74[-2]	6.60[-2]
3	46	4.56[-2]	5.54[-2]	5.87[-2]	5.99[-2]	6.31[-2]	6.60[-2]	6.78[-2]	6.61[-2]
4	46	4.07[-2]	4.95[-2]	5.21[-2]	5.21[-2]	5.38[-2]	5.56[-2]	5.64[-2]	5.48[-2]
5	46	1.67[-2]	2.03[-2]	2.12[-2]	2.10[-2]	2.16[-2]	2.22[-2]	2.24[-2]	2.17[-2]
1	47	1.05[-2]	1.15[-2]	1.22[-2]	1.34[-2]	1.61[-2]	1.86[-2]	2.10[-2]	2.12[-2]
2	47	3.52[-2]	4.23[-2]	4.40[-2]	4.33[-2]	4.47[-2]	4.63[-2]	4.74[-2]	4.62[-2]
3	47	2.36[-2]	2.86[-2]	3.02[-2]	3.04[-2]	3.14[-2]	3.23[-2]	3.26[-2]	3.16[-2]
4	47	8.88[-3]	1.10[-2]	1.20[-2]	1.29[-2]	1.35[-2]	1.40[-2]	1.40[-2]	1.34[-2]
5	47	1.63[-3]	2.08[-3]	2.44[-3]	2.87[-3]	3.12[-3]	3.24[-3]	3.21[-3]	3.02[-3]
1	48	2.94[-1]	2.91[-1]	2.78[-1]	2.54[-1]	2.45[-1]	2.37[-1]	2.21[-1]	2.05[-1]
2	48	1.93[-1]	1.91[-1]	1.83[-1]	1.67[-1]	1.60[-1]	1.54[-1]	1.43[-1]	1.32[-1]
3	48	1.05[-1]	1.03[-1]	9.81[-2]	8.81[-2]	8.29[-2]	7.90[-2]	7.20[-2]	6.58[-2]
4	48	4.79[-2]	4.79[-2]	4.55[-2]	4.03[-2]	3.71[-2]	3.47[-2]	3.09[-2]	2.77[-2]
5	48	1.35[-2]	1.38[-2]	1.32[-2]	1.16[-2]	1.05[-2]	9.70[-3]	8.45[-3]	7.48[-3]
1	49	1.66[-1]	1.57[-1]	1.47[-1]	1.31[-1]	1.23[-1]	1.17[-1]	1.06[-1]	9.72[-2]
2	49	1.50[-1]	1.45[-1]	1.37[-1]	1.24[-1]	1.20[-1]	1.16[-1]	1.08[-1]	9.91[-2]
3	49	1.23[-1]	1.18[-1]	1.11[-1]	1.00[-1]	9.59[-2]	9.28[-2]	8.62[-2]	7.97[-2]
4	49	8.98[-2]	8.44[-2]	7.85[-2]	6.97[-2]	6.61[-2]	6.35[-2]	5.87[-2]	5.44[-2]
5	49	3.42[-2]	3.16[-2]	2.92[-2]	2.57[-2]	2.41[-2]	2.31[-2]	2.13[-2]	1.97[-2]
1	50	5.04[-2]	5.11[-2]	4.88[-2]	4.31[-2]	3.94[-2]	3.65[-2]	3.19[-2]	2.82[-2]
2	50	1.02[-1]	9.53[-2]	8.89[-2]	7.92[-2]	7.51[-2]	7.21[-2]	6.65[-2]	6.14[-2]
3	50	1.04[-1]	9.84[-2]	9.17[-2]	8.17[-2]	7.78[-2]	7.51[-2]	6.97[-2]	6.45[-2]
4	50	7.29[-2]	6.97[-2]	6.52[-2]	5.89[-2]	5.68[-2]	5.52[-2]	5.16[-2]	4.78[-2]
5	50	2.58[-2]	2.48[-2]	2.33[-2]	2.12[-2]	2.06[-2]	2.02[-2]	1.90[-2]	1.76[-2]
1	51	5.48[-2]	4.41[-2]	4.12[-2]	6.51[-2]	1.04[-1]	1.32[-1]	1.56[-1]	1.57[-1]
2	51	2.33[-2]	2.16[-2]	2.15[-2]	3.41[-2]	5.36[-2]	6.75[-2]	7.89[-2]	7.93[-2]
3	51	6.87[-3]	6.45[-3]	6.41[-3]	1.21[-2]	2.09[-2]	2.73[-2]	3.26[-2]	3.30[-2]
4	51	1.86[-3]	1.61[-3]	1.55[-3]	3.71[-3]	7.02[-3]	9.40[-3]	1.15[-2]	1.17[-2]
5	51	5.05[-4]	4.40[-4]	4.31[-4]	9.40[-4]	1.71[-3]	2.27[-3]	2.73[-3]	2.78[-3]
1	52	3.38[-2]	2.78[-2]	2.52[-2]	3.52[-2]	5.39[-2]	6.74[-2]	7.86[-2]	7.90[-2]
2	52	5.77[-2]	4.93[-2]	4.49[-2]	5.20[-2]	6.93[-2]	8.20[-2]	9.16[-2]	9.06[-2]
3	52	3.51[-2]	3.01[-2]	2.73[-2]	3.78[-2]	5.78[-2]	7.25[-2]	8.46[-2]	8.50[-2]
4	52	1.53[-2]	1.32[-2]	1.23[-2]	2.07[-2]	3.47[-2]	4.50[-2]	5.36[-2]	5.43[-2]
5	52	4.00[-3]	3.51[-3]	3.39[-3]	6.38[-3]	1.11[-2]	1.46[-2]	1.75[-2]	1.77[-2]
1	53	1.20[-2]	1.08[-2]	9.68[-3]	1.32[-2]	2.02[-2]	2.54[-2]	2.96[-2]	2.97[-2]
2	53	3.19[-2]	2.72[-2]	2.51[-2]	3.62[-2]	5.61[-2]	7.07[-2]	8.27[-2]	8.32[-2]
3	53	4.29[-2]	3.67[-2]	3.46[-2]	6.03[-2]	1.03[-1]	1.34[-1]	1.60[-1]	1.62[-1]
4	53	4.00[-2]	3.35[-2]	3.12[-2]	5.08[-2]	8.37[-2]	1.08[-1]	1.28[-1]	1.29[-1]

Table 3.3b. Fe III (continued)

Levels		T [K]							
i	j	1000	3000	5000	10000	15000	20000	30000	40000
5	53	1.66[-2]	1.37[-2]	1.27[-2]	1.91[-2]	3.03[-2]	3.84[-2]	4.51[-2]	4.55[-2]
1	54	7.04[-1]	4.66[-1]	4.27[-1]	4.21[-1]	4.20[-1]	4.14[-1]	3.96[-1]	3.78[-1]
2	54	3.96[-1]	2.85[-1]	2.60[-1]	2.44[-1]	2.36[-1]	2.30[-1]	2.17[-1]	2.07[-1]
3	54	2.68[-1]	2.14[-1]	2.05[-1]	2.02[-1]	2.00[-1]	1.97[-1]	1.88[-1]	1.80[-1]
4	54	1.67[-1]	1.36[-1]	1.30[-1]	1.27[-1]	1.25[-1]	1.23[-1]	1.18[-1]	1.13[-1]
5	54	6.08[-2]	4.95[-2]	4.71[-2]	4.58[-2]	4.51[-2]	4.42[-2]	4.25[-2]	4.09[-2]
1	55	3.32[-1]	2.30[-1]	2.08[-1]	1.95[-1]	1.90[-1]	1.85[-1]	1.77[-1]	1.69[-1]
2	55	4.44[-1]	3.07[-1]	2.79[-1]	2.67[-1]	2.63[-1]	2.59[-1]	2.49[-1]	2.40[-1]
3	55	2.90[-1]	2.11[-1]	1.96[-1]	1.93[-1]	1.91[-1]	1.88[-1]	1.79[-1]	1.71[-1]
4	55	1.23[-1]	9.74[-2]	9.41[-2]	9.49[-2]	9.44[-2]	9.24[-2]	8.72[-2]	8.22[-2]
5	55	3.13[-2]	2.68[-2]	2.67[-2]	2.76[-2]	2.75[-2]	2.68[-2]	2.50[-2]	2.33[-2]
1	56	2.96[-1]	2.40[-1]	2.28[-1]	2.21[-1]	2.17[-1]	2.12[-1]	2.04[-1]	1.95[-1]
2	56	2.03[-1]	1.63[-1]	1.58[-1]	1.58[-1]	1.56[-1]	1.53[-1]	1.44[-1]	1.36[-1]
3	56	2.05[-1]	1.47[-1]	1.37[-1]	1.36[-1]	1.35[-1]	1.33[-1]	1.26[-1]	1.19[-1]
4	56	1.67[-1]	1.12[-1]	1.01[-1]	9.96[-2]	9.90[-2]	9.73[-2]	9.26[-2]	8.80[-2]
5	56	6.56[-2]	4.25[-2]	3.82[-2]	3.72[-2]	3.70[-2]	3.64[-2]	3.48[-2]	3.32[-2]
1	57	1.31[-1]	9.12[-2]	7.96[-2]	6.86[-2]	6.35[-2]	5.93[-2]	5.20[-2]	4.59[-2]
2	57	8.31[-2]	5.86[-2]	5.17[-2]	4.52[-2]	4.24[-2]	4.00[-2]	3.54[-2]	3.13[-2]
3	57	4.86[-2]	3.49[-2]	3.09[-2]	2.72[-2]	2.55[-2]	2.40[-2]	2.12[-2]	1.88[-2]
4	57	2.55[-2]	1.87[-2]	1.67[-2]	1.46[-2]	1.37[-2]	1.29[-2]	1.14[-2]	1.00[-2]
5	57	8.01[-3]	5.99[-3]	5.33[-3]	4.68[-3]	4.37[-3]	4.11[-3]	3.63[-3]	3.21[-3]
1	58	6.23[-2]	4.52[-2]	4.06[-2]	3.60[-2]	3.36[-2]	3.16[-2]	2.77[-2]	2.44[-2]
2	58	6.36[-2]	4.60[-2]	4.13[-2]	3.80[-2]	3.69[-2]	3.55[-2]	3.20[-2]	2.86[-2]
3	58	5.04[-2]	3.59[-2]	3.21[-2]	2.95[-2]	2.88[-2]	2.79[-2]	2.52[-2]	2.26[-2]
4	58	3.19[-2]	2.28[-2]	2.04[-2]	1.85[-2]	1.78[-2]	1.71[-2]	1.54[-2]	1.38[-2]
5	58	1.09[-2]	7.83[-3]	7.02[-3]	6.30[-3]	6.00[-3]	5.72[-3]	5.13[-3]	4.57[-3]
1	59	2.99[-2]	2.23[-2]	1.98[-2]	1.72[-2]	1.59[-2]	1.48[-2]	1.29[-2]	1.14[-2]
2	59	3.86[-2]	2.74[-2]	2.44[-2]	2.14[-2]	1.99[-2]	1.87[-2]	1.65[-2]	1.46[-2]
3	59	3.63[-2]	2.60[-2]	2.33[-2]	2.13[-2]	2.08[-2]	2.01[-2]	1.82[-2]	1.63[-2]
4	59	2.56[-2]	1.87[-2]	1.68[-2]	1.58[-2]	1.58[-2]	1.54[-2]	1.42[-2]	1.28[-2]
5	59	9.23[-3]	6.82[-3]	6.15[-3]	5.84[-3]	5.87[-3]	5.77[-3]	5.33[-3]	4.80[-3]
1	60	6.35[-1]	5.87[-1]	6.10[-1]	6.81[-1]	7.19[-1]	7.31[-1]	7.16[-1]	6.82[-1]
2	60	2.53[-1]	2.45[-1]	2.57[-1]	2.86[-1]	3.02[-1]	3.07[-1]	3.00[-1]	2.84[-1]
3	60	8.36[-2]	8.91[-2]	1.02[-1]	1.25[-1]	1.36[-1]	1.39[-1]	1.32[-1]	1.22[-1]
4	60	1.93[-2]	2.16[-2]	2.68[-2]	3.71[-2]	4.26[-2]	4.43[-2]	4.28[-2]	3.93[-2]
5	60	4.61[-3]	5.42[-3]	7.08[-3]	9.89[-3]	1.13[-2]	1.17[-2]	1.13[-2]	1.04[-2]
1	61	3.29[-1]	3.13[-1]	3.37[-1]	3.77[-1]	3.93[-1]	3.95[-1]	3.80[-1]	3.58[-1]
2	61	2.50[-1]	2.52[-1]	2.85[-1]	3.46[-1]	3.74[-1]	3.81[-1]	3.69[-1]	3.46[-1]

Table 3.3b. Fe III (continued)

Levels		T [K]							
i	j	1000	3000	5000	10000	15000	20000	30000	40000
3	61	1.97[-1]	2.04[-1]	2.26[-1]	2.59[-1]	2.73[-1]	2.76[-1]	2.69[-1]	2.55[-1]
4	61	7.04[-2]	7.20[-2]	7.86[-2]	9.24[-2]	9.92[-2]	1.00[-1]	9.60[-2]	8.88[-2]
5	61	1.29[-2]	1.61[-2]	2.02[-2]	2.62[-2]	2.83[-2]	2.84[-2]	2.64[-2]	2.38[-2]
1	62	1.33[-1]	1.33[-1]	1.52[-1]	1.83[-1]	1.96[-1]	1.99[-1]	1.90[-1]	1.77[-1]
2	62	2.26[-1]	2.38[-1]	2.64[-1]	3.06[-1]	3.25[-1]	3.30[-1]	3.20[-1]	3.03[-1]
3	62	1.68[-1]	1.73[-1]	1.98[-1]	2.41[-1]	2.59[-1]	2.62[-1]	2.50[-1]	2.31[-1]
4	62	1.36[-1]	1.36[-1]	1.46[-1]	1.63[-1]	1.71[-1]	1.73[-1]	1.68[-1]	1.60[-1]
5	62	5.08[-2]	5.12[-2]	5.56[-2]	6.20[-2]	6.38[-2]	6.33[-2]	5.94[-2]	5.48[-2]
1	63	4.79[-2]	5.24[-2]	6.43[-2]	8.31[-2]	9.14[-2]	9.33[-2]	8.89[-2]	8.15[-2]
2	63	1.46[-1]	1.60[-1]	1.81[-1]	2.08[-1]	2.16[-1]	2.16[-1]	2.05[-1]	1.90[-1]
3	63	1.73[-1]	1.86[-1]	2.09[-1]	2.41[-1]	2.52[-1]	2.53[-1]	2.41[-1]	2.25[-1]
4	63	1.32[-1]	1.33[-1]	1.48[-1]	1.72[-1]	1.81[-1]	1.81[-1]	1.71[-1]	1.58[-1]
5	63	6.48[-2]	7.00[-2]	7.71[-2]	8.46[-2]	8.67[-2]	8.66[-2]	8.36[-2]	7.94[-2]
1	64	1.64[-2]	1.86[-2]	2.36[-2]	3.24[-2]	3.67[-2]	3.79[-2]	3.63[-2]	3.32[-2]
2	64	5.78[-2]	6.45[-2]	7.51[-2]	8.94[-2]	9.38[-2]	9.34[-2]	8.71[-2]	7.95[-2]
3	64	1.33[-1]	1.38[-1]	1.51[-1]	1.66[-1]	1.70[-1]	1.69[-1]	1.61[-1]	1.50[-1]
4	64	1.13[-1]	1.20[-1]	1.33[-1]	1.49[-1]	1.54[-1]	1.55[-1]	1.48[-1]	1.40[-1]
5	64	3.40[-2]	3.49[-2]	4.03[-2]	4.96[-2]	5.33[-2]	5.38[-2]	5.11[-2]	4.71[-2]
1	65	6.42[-2]	5.52[-2]	5.37[-2]	5.82[-2]	6.22[-2]	6.31[-2]	5.97[-2]	5.44[-2]
2	65	6.04[-2]	4.57[-2]	4.16[-2]	4.18[-2]	4.36[-2]	4.37[-2]	4.10[-2]	3.73[-2]
3	65	3.93[-2]	2.77[-2]	2.43[-2]	2.35[-2]	2.42[-2]	2.42[-2]	2.26[-2]	2.06[-2]
4	65	2.07[-2]	1.41[-2]	1.21[-2]	1.15[-2]	1.18[-2]	1.18[-2]	1.10[-2]	1.00[-2]
5	65	6.35[-3]	4.31[-3]	3.70[-3]	3.47[-3]	3.56[-3]	3.55[-3]	3.32[-3]	3.02[-3]
1	66	5.28[-2]	3.90[-2]	3.54[-2]	3.61[-2]	3.80[-2]	3.84[-2]	3.62[-2]	3.30[-2]
2	66	4.96[-2]	3.74[-2]	3.36[-2]	3.29[-2]	3.38[-2]	3.37[-2]	3.15[-2]	2.86[-2]
3	66	3.90[-2]	2.99[-2]	2.68[-2]	2.54[-2]	2.55[-2]	2.50[-2]	2.30[-2]	2.07[-2]
4	66	2.59[-2]	2.03[-2]	1.84[-2]	1.73[-2]	1.71[-2]	1.66[-2]	1.51[-2]	1.36[-2]
5	66	9.29[-3]	7.40[-3]	6.75[-3]	6.37[-3]	6.26[-3]	6.06[-3]	5.50[-3]	4.92[-3]
1	67	3.68[-2]	2.39[-2]	2.03[-2]	1.92[-2]	1.98[-2]	1.99[-2]	1.87[-2]	1.70[-2]
2	67	4.09[-2]	3.10[-2]	2.80[-2]	2.70[-2]	2.73[-2]	2.69[-2]	2.49[-2]	2.25[-2]
3	67	3.61[-2]	2.84[-2]	2.58[-2]	2.46[-2]	2.46[-2]	2.41[-2]	2.21[-2]	1.99[-2]
4	67	2.40[-2]	1.93[-2]	1.76[-2]	1.69[-2]	1.69[-2]	1.66[-2]	1.52[-2]	1.37[-2]
5	67	8.35[-3]	6.81[-3]	6.24[-3]	6.01[-3]	6.05[-3]	5.95[-3]	5.48[-3]	4.95[-3]
1	68	4.52[-2]	3.67[-2]	3.51[-2]	3.33[-2]	3.20[-2]	3.04[-2]	2.70[-2]	2.40[-2]
2	68	3.85[-2]	2.86[-2]	2.53[-2]	2.18[-2]	2.02[-2]	1.89[-2]	1.65[-2]	1.46[-2]
3	68	1.15[-2]	9.37[-3]	8.60[-3]	7.84[-3]	7.52[-3]	7.18[-3]	6.41[-3]	5.71[-3]
4	68	2.63[-3]	2.60[-3]	2.55[-3]	2.53[-3]	2.54[-3]	2.48[-3]	2.27[-3]	2.04[-3]
5	68	8.54[-4]	8.11[-4]	7.69[-4]	7.36[-4]	7.30[-4]	7.08[-4]	6.42[-4]	5.74[-4]

Table 3.3b. Fe III (continued)

Levels		T [K]							
i	j	1000	3000	5000	10000	15000	20000	30000	40000
1	69	2.23[-2]	1.86[-2]	1.77[-2]	1.67[-2]	1.61[-2]	1.54[-2]	1.37[-2]	1.22[-2]
2	69	5.46[-2]	3.88[-2]	3.27[-2]	2.67[-2]	2.42[-2]	2.24[-2]	1.95[-2]	1.72[-2]
3	69	2.36[-2]	1.81[-2]	1.62[-2]	1.45[-2]	1.38[-2]	1.31[-2]	1.17[-2]	1.04[-2]
4	69	1.27[-2]	9.88[-3]	8.99[-3]	8.12[-3]	7.74[-3]	7.37[-3]	6.59[-3]	5.88[-3]
5	69	5.49[-3]	4.05[-3]	3.55[-3]	3.04[-3]	2.83[-3]	2.66[-3]	2.34[-3]	2.08[-3]
1	70	9.12[-3]	7.84[-3]	7.27[-3]	6.77[-3]	6.60[-3]	6.35[-3]	5.73[-3]	5.11[-3]
2	70	2.53[-2]	1.92[-2]	1.71[-2]	1.52[-2]	1.45[-2]	1.38[-2]	1.23[-2]	1.10[-2]
3	70	3.10[-2]	2.29[-2]	2.04[-2]	1.83[-2]	1.74[-2]	1.65[-2]	1.48[-2]	1.31[-2]
4	70	3.71[-2]	2.59[-2]	2.18[-2]	1.81[-2]	1.65[-2]	1.54[-2]	1.35[-2]	1.19[-2]
5	70	1.76[-2]	1.20[-2]	9.88[-3]	7.85[-3]	7.04[-3]	6.47[-3]	5.59[-3]	4.90[-3]
1	71	3.21	3.40	3.43	3.54	3.64	3.70	3.78	3.84
2	71	9.73[-1]	1.01	1.01	1.05	1.08	1.09	1.10	1.11
3	71	3.11[-1]	3.11[-1]	3.07[-1]	3.17[-1]	3.24[-1]	3.25[-1]	3.21[-1]	3.16[-1]
4	71	1.40[-1]	1.37[-1]	1.32[-1]	1.34[-1]	1.35[-1]	1.33[-1]	1.28[-1]	1.23[-1]
5	71	5.05[-2]	4.94[-2]	4.74[-2]	4.68[-2]	4.66[-2]	4.58[-2]	4.38[-2]	4.22[-2]
1	72	2.72[-1]	2.56[-1]	2.52[-1]	2.71[-1]	2.82[-1]	2.83[-1]	2.73[-1]	2.62[-1]
2	72	1.74	1.86	1.87	1.92	1.96	1.99	2.02	2.05
3	72	1.04	1.09	1.10	1.13	1.15	1.16	1.18	1.20
4	72	3.01[-1]	3.05[-1]	3.05[-1]	3.14[-1]	3.22[-1]	3.26[-1]	3.30[-1]	3.34[-1]
5	72	2.98[-2]	2.55[-2]	2.46[-2]	2.66[-2]	2.79[-2]	2.81[-2]	2.74[-2]	2.64[-2]
1	73	1.97[-1]	1.92[-1]	1.86[-1]	1.87[-1]	1.87[-1]	1.84[-1]	1.76[-1]	1.69[-1]
2	73	1.34[-1]	1.21[-1]	1.18[-1]	1.28[-1]	1.35[-1]	1.35[-1]	1.31[-1]	1.25[-1]
3	73	6.69[-1]	7.07[-1]	7.13[-1]	7.36[-1]	7.56[-1]	7.67[-1]	7.80[-1]	7.90[-1]
4	73	7.74[-1]	8.30[-1]	8.37[-1]	8.57[-1]	8.75[-1]	8.87[-1]	9.03[-1]	9.17[-1]
5	73	3.38[-1]	3.64[-1]	3.68[-1]	3.76[-1]	3.83[-1]	3.88[-1]	3.96[-1]	4.03[-1]
1	74	2.97[-1]	2.73[-1]	2.46[-1]	2.01[-1]	1.76[-1]	1.61[-1]	1.43[-1]	1.32[-1]
2	74	9.05[-2]	8.16[-2]	7.21[-2]	5.63[-2]	4.75[-2]	4.21[-2]	3.59[-2]	3.25[-2]
3	74	2.70[-2]	2.39[-2]	2.06[-2]	1.54[-2]	1.25[-2]	1.07[-2]	8.57[-3]	7.38[-3]
4	74	6.00[-3]	5.43[-3]	4.62[-3]	3.30[-3]	2.59[-3]	2.16[-3]	1.66[-3]	1.37[-3]
5	74	1.22[-3]	1.17[-3]	1.01[-3]	7.29[-4]	5.78[-4]	4.85[-4]	3.78[-4]	3.16[-4]
1	75	1.75[-1]	1.60[-1]	1.43[-1]	1.14[-1]	9.76[-2]	8.72[-2]	7.51[-2]	6.83[-2]
2	75	2.33[-1]	2.18[-1]	1.95[-1]	1.57[-1]	1.35[-1]	1.21[-1]	1.05[-1]	9.60[-2]
3	75	9.66[-2]	9.00[-2]	8.04[-2]	6.34[-2]	5.36[-2]	4.75[-2]	4.04[-2]	3.65[-2]
4	75	2.23[-2]	2.03[-2]	1.78[-2]	1.36[-2]	1.12[-2]	9.70[-3]	7.94[-3]	6.92[-3]
5	75	5.51[-3]	5.37[-3]	4.68[-3]	3.46[-3]	2.76[-3]	2.32[-3]	1.78[-3]	1.46[-3]
1	76	8.34[-2]	7.48[-2]	6.56[-2]	5.05[-2]	4.21[-2]	3.69[-2]	3.07[-2]	2.72[-2]
2	76	1.83[-1]	1.68[-1]	1.50[-1]	1.19[-1]	1.01[-1]	9.01[-2]	7.73[-2]	7.02[-2]
3	76	1.69[-1]	1.55[-1]	1.38[-1]	1.09[-1]	9.25[-2]	8.22[-2]	7.00[-2]	6.30[-2]
4	76	6.87[-2]	6.37[-2]	5.68[-2]	4.47[-2]	3.77[-2]	3.34[-2]	2.84[-2]	2.56[-2]

Table 3.3b. Fe III (continued)

Levels		T [K]							
i	j	1000	3000	5000	10000	15000	20000	30000	40000
5	76	1.26[-2]	1.19[-2]	1.07[-2]	8.44[-3]	7.11[-3]	6.26[-3]	5.25[-3]	4.67[-3]
1	77	3.39[-2]	3.01[-2]	2.59[-2]	1.93[-2]	1.57[-2]	1.34[-2]	1.08[-2]	9.32[-3]
2	77	1.01[-1]	9.17[-2]	8.11[-2]	6.34[-2]	5.34[-2]	4.71[-2]	3.99[-2]	3.57[-2]
3	77	1.56[-1]	1.43[-1]	1.27[-1]	1.00[-1]	8.49[-2]	7.54[-2]	6.41[-2]	5.77[-2]
4	77	1.13[-1]	1.04[-1]	9.17[-2]	7.21[-2]	6.12[-2]	5.43[-2]	4.63[-2]	4.17[-2]
5	77	3.40[-2]	3.27[-2]	2.96[-2]	2.36[-2]	2.01[-2]	1.79[-2]	1.53[-2]	1.39[-2]
1	78	1.30[-2]	1.11[-2]	9.29[-3]	6.64[-3]	5.26[-3]	4.41[-3]	3.44[-3]	2.88[-3]
2	78	4.56[-2]	4.03[-2]	3.49[-2]	2.64[-2]	2.16[-2]	1.87[-2]	1.53[-2]	1.33[-2]
3	78	9.76[-2]	8.78[-2]	7.76[-2]	6.06[-2]	5.11[-2]	4.51[-2]	3.81[-2]	3.42[-2]
4	78	1.26[-1]	1.15[-1]	1.02[-1]	8.06[-2]	6.84[-2]	6.07[-2]	5.17[-2]	4.66[-2]
5	78	5.78[-2]	5.41[-2]	4.82[-2]	3.85[-2]	3.29[-2]	2.94[-2]	2.52[-2]	2.27[-2]
1	79	2.60[-1]	2.74[-1]	2.69[-1]	2.57[-1]	2.51[-1]	2.50[-1]	2.49[-1]	2.49[-1]
2	79	4.20[-2]	4.54[-2]	4.12[-2]	3.45[-2]	3.11[-2]	2.91[-2]	2.68[-2]	2.54[-2]
3	79	8.89[-3]	9.83[-3]	8.24[-3]	5.84[-3]	4.65[-3]	3.94[-3]	3.14[-3]	2.69[-3]
4	79	1.72[-3]	1.88[-3]	1.54[-3]	1.06[-3]	8.30[-4]	7.04[-4]	5.76[-4]	5.16[-4]
5	79	3.82[-4]	4.25[-4]	3.52[-4]	2.45[-4]	1.94[-4]	1.65[-4]	1.35[-4]	1.21[-4]
1	80	9.38[-2]	9.60[-2]	9.06[-2]	8.20[-2]	7.78[-2]	7.56[-2]	7.34[-2]	7.23[-2]
2	80	1.22[-1]	1.19[-1]	1.15[-1]	1.11[-1]	1.08[-1]	1.07[-1]	1.07[-1]	1.07[-1]
3	80	3.70[-2]	3.90[-2]	3.66[-2]	3.23[-2]	2.99[-2]	2.85[-2]	2.69[-2]	2.60[-2]
4	80	5.88[-3]	6.20[-3]	5.11[-3]	3.58[-3]	2.84[-3]	2.40[-3]	1.89[-3]	1.60[-3]
5	80	1.68[-3]	1.86[-3]	1.55[-3]	1.11[-3]	9.06[-4]	7.92[-4]	6.65[-4]	5.90[-4]
1	81	3.87[-2]	4.02[-2]	3.68[-2]	3.12[-2]	2.84[-2]	2.67[-2]	2.48[-2]	2.38[-2]
2	81	1.07[-1]	1.10[-1]	1.06[-1]	9.81[-2]	9.41[-2]	9.20[-2]	9.00[-2]	8.90[-2]
3	81	9.53[-2]	9.68[-2]	9.32[-2]	8.62[-2]	8.26[-2]	8.08[-2]	7.93[-2]	7.86[-2]
4	81	2.50[-2]	2.66[-2]	2.47[-2]	2.15[-2]	1.98[-2]	1.88[-2]	1.78[-2]	1.73[-2]
5	81	4.59[-3]	5.06[-3]	4.28[-3]	3.06[-3]	2.43[-3]	2.05[-3]	1.60[-3]	1.34[-3]
1	82	1.40[-2]	1.51[-2]	1.33[-2]	1.06[-2]	9.27[-3]	8.48[-3]	7.59[-3]	7.09[-3]
2	82	5.51[-2]	5.78[-2]	5.42[-2]	4.78[-2]	4.46[-2]	4.27[-2]	4.08[-2]	3.97[-2]
3	82	9.06[-2]	9.28[-2]	8.93[-2]	8.21[-2]	7.84[-2]	7.64[-2]	7.47[-2]	7.39[-2]
4	82	6.65[-2]	6.79[-2]	6.50[-2]	5.93[-2]	5.64[-2]	5.48[-2]	5.33[-2]	5.25[-2]
5	82	1.56[-2]	1.69[-2]	1.61[-2]	1.45[-2]	1.36[-2]	1.30[-2]	1.24[-2]	1.21[-2]
1	83	4.52[-3]	4.98[-3]	4.25[-3]	3.15[-3]	2.62[-3]	2.33[-3]	2.01[-3]	1.84[-3]
2	83	2.05[-2]	2.22[-2]	1.99[-2]	1.62[-2]	1.44[-2]	1.33[-2]	1.21[-2]	1.14[-2]
3	83	5.48[-2]	5.74[-2]	5.41[-2]	4.81[-2]	4.48[-2]	4.30[-2]	4.09[-2]	3.98[-2]
4	83	8.16[-2]	8.35[-2]	8.08[-2]	7.48[-2]	7.15[-2]	6.97[-2]	6.80[-2]	6.70[-2]
5	83	4.09[-2]	4.19[-2]	4.10[-2]	3.87[-2]	3.74[-2]	3.67[-2]	3.61[-2]	3.58[-2]
1	84	1.20	1.30	1.42	1.68	1.88	2.03	2.29	2.49
2	84	5.80[-2]	6.44[-2]	6.14[-2]	5.32[-2]	4.84[-2]	4.56[-2]	4.30[-2]	4.20[-2]

Table 3.3b. Fe III (continued)

Levels		T [K]							
i	j	1000	3000	5000	10000	15000	20000	30000	40000
3	84	2.07[-2]	2.30[-2]	2.13[-2]	1.78[-2]	1.60[-2]	1.50[-2]	1.41[-2]	1.38[-2]
4	84	7.43[-3]	8.28[-3]	7.76[-3]	6.94[-3]	6.66[-3]	6.62[-3]	6.79[-3]	7.06[-3]
5	84	2.33[-3]	2.68[-3]	2.52[-3]	2.27[-3]	2.21[-3]	2.23[-3]	2.35[-3]	2.48[-3]
1	85	3.76[-1]	3.94[-1]	3.92[-1]	3.84[-1]	3.83[-1]	3.86[-1]	4.01[-1]	4.17[-1]
2	85	1.33	1.38	1.41	1.48	1.54	1.59	1.71	1.82
3	85	6.04[-2]	6.48[-2]	6.22[-2]	5.55[-2]	5.15[-2]	4.91[-2]	4.70[-2]	4.62[-2]
4	85	1.57[-2]	1.78[-2]	1.65[-2]	1.37[-2]	1.21[-2]	1.11[-2]	9.96[-3]	9.37[-3]
5	85	3.76[-3]	4.22[-3]	3.80[-3]	3.09[-3]	2.74[-3]	2.54[-3]	2.34[-3]	2.24[-3]
1	86	6.27[-2]	6.69[-2]	6.38[-2]	5.74[-2]	5.41[-2]	5.24[-2]	5.14[-2]	5.15[-2]
2	86	5.45[-1]	5.67[-1]	5.65[-1]	5.51[-1]	5.45[-1]	5.47[-1]	5.62[-1]	5.81[-1]
3	86	1.06	1.10	1.10	1.09	1.09	1.11	1.15	1.20
4	86	3.70[-2]	3.91[-2]	3.73[-2]	3.31[-2]	3.07[-2]	2.93[-2]	2.81[-2]	2.78[-2]
5	86	9.27[-3]	1.08[-2]	1.00[-2]	8.30[-3]	7.21[-3]	6.49[-3]	5.60[-3]	5.07[-3]
1	87	1.56[-2]	1.73[-2]	1.60[-2]	1.36[-2]	1.24[-2]	1.17[-2]	1.11[-2]	1.08[-2]
2	87	8.98[-2]	9.44[-2]	9.21[-2]	8.59[-2]	8.24[-2]	8.07[-2]	8.01[-2]	8.10[-2]
3	87	5.20[-1]	5.37[-1]	5.35[-1]	5.23[-1]	5.17[-1]	5.19[-1]	5.32[-1]	5.50[-1]
4	87	6.48[-1]	6.72[-1]	6.72[-1]	6.58[-1]	6.54[-1]	6.58[-1]	6.79[-1]	7.06[-1]
5	87	1.95[-2]	2.03[-2]	1.97[-2]	1.80[-2]	1.70[-2]	1.64[-2]	1.60[-2]	1.60[-2]
1	88	6.88[-3]	7.73[-3]	7.17[-3]	6.30[-3]	5.99[-3]	5.93[-3]	6.07[-3]	6.30[-3]
2	88	1.55[-2]	1.70[-2]	1.54[-2]	1.27[-2]	1.12[-2]	1.03[-2]	9.24[-3]	8.69[-3]
3	88	8.50[-2]	8.94[-2]	8.76[-2]	8.24[-2]	7.95[-2]	7.82[-2]	7.80[-2]	7.90[-2]
4	88	3.97[-1]	4.09[-1]	4.08[-1]	3.97[-1]	3.93[-1]	3.94[-1]	4.02[-1]	4.15[-1]
5	88	3.75[-1]	3.85[-1]	3.85[-1]	3.77[-1]	3.74[-1]	3.75[-1]	3.85[-1]	3.98[-1]
1	89	3.70[-2]	4.24[-2]	3.98[-2]	3.29[-2]	2.88[-2]	2.64[-2]	2.36[-2]	2.21[-2]
2	89	3.33[-2]	3.78[-2]	3.55[-2]	2.94[-2]	2.59[-2]	2.39[-2]	2.16[-2]	2.03[-2]
3	89	2.59[-2]	2.91[-2]	2.73[-2]	2.25[-2]	1.98[-2]	1.82[-2]	1.65[-2]	1.55[-2]
4	89	1.56[-2]	1.77[-2]	1.65[-2]	1.37[-2]	1.20[-2]	1.10[-2]	9.96[-3]	9.34[-3]
5	89	5.44[-3]	6.14[-3]	5.73[-3]	4.70[-3]	4.12[-3]	3.78[-3]	3.40[-3]	3.18[-3]
1	90	1.63[-1]	1.71[-1]	1.55[-1]	1.26[-1]	1.10[-1]	1.01[-1]	9.21[-2]	8.81[-2]
2	90	1.10[-1]	1.08[-1]	9.86[-2]	8.17[-2]	7.28[-2]	6.78[-2]	6.25[-2]	6.00[-2]
3	90	6.67[-2]	6.63[-2]	6.06[-2]	5.05[-2]	4.51[-2]	4.21[-2]	3.88[-2]	3.71[-2]
4	90	2.38[-2]	2.44[-2]	2.24[-2]	1.86[-2]	1.65[-2]	1.53[-2]	1.39[-2]	1.32[-2]
5	90	5.40[-3]	5.56[-3]	4.95[-3]	3.87[-3]	3.27[-3]	2.91[-3]	2.50[-3]	2.28[-3]
1	91	1.23[-1]	1.22[-1]	1.11[-1]	9.06[-2]	8.00[-2]	7.39[-2]	6.75[-2]	6.42[-2]
2	91	8.19[-2]	8.35[-2]	7.51[-2]	5.98[-2]	5.19[-2]	4.74[-2]	4.29[-2]	4.07[-2]
3	91	6.36[-2]	6.43[-2]	5.72[-2]	4.49[-2]	3.85[-2]	3.49[-2]	3.10[-2]	2.92[-2]
4	91	4.39[-2]	4.46[-2]	4.14[-2]	3.50[-2]	3.15[-2]	2.96[-2]	2.75[-2]	2.64[-2]
5	91	2.03[-2]	2.04[-2]	1.92[-2]	1.67[-2]	1.54[-2]	1.47[-2]	1.40[-2]	1.37[-2]

Table 3.3b. Fe III (continued)

Levels		T [K]							
i	j	1000	3000	5000	10000	15000	20000	30000	40000
1	92	6.38[-2]	6.36[-2]	5.86[-2]	4.94[-2]	4.45[-2]	4.16[-2]	3.85[-2]	3.69[-2]
2	92	6.47[-2]	6.48[-2]	5.77[-2]	4.54[-2]	3.91[-2]	3.54[-2]	3.16[-2]	2.98[-2]
3	92	6.19[-2]	6.24[-2]	5.70[-2]	4.72[-2]	4.20[-2]	3.91[-2]	3.61[-2]	3.47[-2]
4	92	4.63[-2]	4.66[-2]	4.24[-2]	3.49[-2]	3.10[-2]	2.89[-2]	2.67[-2]	2.58[-2]
5	92	1.22[-2]	1.23[-2]	1.08[-2]	8.16[-3]	6.79[-3]	5.97[-3]	5.08[-3]	4.59[-3]
1	93	2.90[-2]	2.85[-2]	2.57[-2]	2.10[-2]	1.85[-2]	1.71[-2]	1.55[-2]	1.46[-2]
2	93	4.95[-2]	4.91[-2]	4.48[-2]	3.73[-2]	3.33[-2]	3.11[-2]	2.87[-2]	2.74[-2]
3	93	5.09[-2]	5.09[-2]	4.61[-2]	3.76[-2]	3.33[-2]	3.09[-2]	2.85[-2]	2.74[-2]
4	93	1.98[-2]	2.07[-2]	1.83[-2]	1.39[-2]	1.16[-2]	1.02[-2]	8.63[-3]	7.82[-3]
5	93	1.37[-2]	1.38[-2]	1.23[-2]	9.70[-3]	8.41[-3]	7.71[-3]	7.05[-3]	6.80[-3]
1	94	4.71[-3]	5.00[-3]	4.52[-3]	3.60[-3]	3.08[-3]	2.75[-3]	2.39[-3]	2.18[-3]
2	94	2.09[-2]	2.07[-2]	1.93[-2]	1.68[-2]	1.55[-2]	1.48[-2]	1.41[-2]	1.37[-2]
3	94	1.19[-2]	1.21[-2]	1.07[-2]	8.08[-3]	6.73[-3]	5.93[-3]	5.05[-3]	4.58[-3]
4	94	1.25[-2]	1.30[-2]	1.17[-2]	9.35[-3]	8.15[-3]	7.49[-3]	6.87[-3]	6.64[-3]
5	94	1.30[-3]	1.52[-3]	1.36[-3]	9.94[-4]	7.90[-4]	6.65[-4]	5.19[-4]	4.36[-4]

Table 3.4a. Fe IV. Selected 68 fine-structure levels from the 140 levels included in the calculation [97Z2] and their observed energies E [Ry] in rydbergs [85S1]. The index i is used in Table 3.4b for transition keys; J is the total angular momentum for specifying the fine-structure level.

i	LS Term		J	E [Ry]	i	LS Term		J	E [Ry]
1	$3d^5$	^6S	5/2	0.00000	37	$3d^4(^3G\ )4s$	^4G	11/2	1.45200
2	$3d^5$	^4G	11/2	0.29384	38			9/2	1.45100
3			9/2	0.29427	39			7/2	1.44900
4			7/2	0.29439	40			5/2	1.44650
5			5/2	0.29435	41	$3d^4(^3D\ )4s$	^4D	7/2	1.50810
6	$3d^5$	^4P	5/2	0.32126	42			5/2	1.50910
7			3/2	0.32198	43			3/2	1.51020
8			1/2	0.32265	44			1/2	1.51090
9	$3d^5$	^4D	7/2	0.35338	45	$3d^4(^5D\ )4p$	$^6F^o$	11/2	1.73390
10			5/2	0.35480	46			9/2	1.72700
11			3/2	0.35483	47			7/2	1.72140
12			1/2	0.35445	48			5/2	1.71710
13	$3d^5$	^4F	9/2	0.47952	49			3/2	1.71400
14			7/2	0.48020	50			1/2	1.71210
15			5/2	0.48150	51	$3d^4(^5D\ )4p$	$^6P^o$	7/2	1.73350
16			3/2	0.48149	52			5/2	1.73150
17	$3d^4(^5D\ )4s$	^6D	9/2	1.17520	53			3/2	1.73040
18			7/2	1.17140	54	$3d^4(^3P1)4s$	^4P	5/2	1.73120
19			5/2	1.16820	55			3/2	1.73880
20			3/2	1.16580	56			1/2	1.74360
21			1/2	1.16430	57	$3d^4(^3F1)4s$	^4F	9/2	1.73430
22	$3d^4(^5D\ )4s$	^4D	7/2	1.26520	58			7/2	1.73530
23			5/2	1.26060	59			5/2	1.73540
24			3/2	1.25710	60			3/2	1.73510
25			1/2	1.25480	61	$3d^4(^5D\ )4p$	$^4P^o$	5/2	1.76380
26	$3d^4(^3P2)4s$	^4P	5/2	1.41930	62			3/2	1.74680
27			3/2	1.40770	63			1/2	1.74070
28			1/2	1.40020	64	$3d^4(^5D\ )4p$	$^6D^o$	9/2	1.76590
29	$3d^4(^3H\ )4s$	^4H	13/2	1.41000	65			7/2	1.76230
30			11/2	1.40800	66			5/2	1.75510
31			9/2	1.40630	67			3/2	1.76120
32			7/2	1.40500	68			1/2	1.75980
33	$3d^4(^3F2)4s$	^4F	9/2	1.42360					
34			7/2	1.42270					
35			5/2	1.42200					
36			3/2	1.42170					

Table 3.4b. Fe IV. Effective collision strengths $\Upsilon(i,j)$ as a function of temperature T [K] for the transitions between the first 12 metastable levels and the transitions between the ground level $3d^5\ {}^6S_{5/2}$ and the 56 higher levels, $i = 13 - 68$ as specified in Table 3.4a [97Z2].

Levels		T [K]							
i	j	2000	4000	6000	10000	15000	20000	30000	50000
1	2	1.60	1.38	1.26	1.15	1.09	1.06	1.02	9.88[-1]
1	3	1.34	1.15	1.05	9.58[-1]	9.08[-1]	8.82[-1]	8.54[-1]	8.24[-1]
2	3	3.86	3.45	3.27	3.05	2.83	2.66	2.41	2.15
1	4	1.07	9.20[-1]	8.43[-1]	7.67[-1]	7.26[-1]	7.06[-1]	6.83[-1]	6.59[-1]
2	4	8.99[-1]	7.75[-1]	7.14[-1]	6.48[-1]	5.93[-1]	5.50[-1]	4.92[-1]	4.31[-1]
3	4	3.55	3.21	3.06	2.88	2.69	2.53	2.32	2.10
1	5	8.01[-1]	6.90[-1]	6.32[-1]	5.75[-1]	5.45[-1]	5.29[-1]	5.12[-1]	4.94[-1]
2	5	1.98[-1]	1.62[-1]	1.44[-1]	1.26[-1]	1.14[-1]	1.05[-1]	9.61[-2]	9.25[-2]
3	5	9.44[-1]	8.21[-1]	7.61[-1]	6.94[-1]	6.36[-1]	5.92[-1]	5.34[-1]	4.94[-1]
4	5	2.95	2.66	2.54	2.38	2.22	2.09	1.92	1.75
1	6	5.99[-1]	5.91[-1]	5.95[-1]	5.87[-1]	5.62[-1]	5.37[-1]	5.03[-1]	4.69[-1]
2	6	6.84[-1]	7.28[-1]	7.50[-1]	7.63[-1]	7.44[-1]	7.14[-1]	6.59[-1]	5.82[-1]
3	6	5.01[-1]	5.23[-1]	5.34[-1]	5.37[-1]	5.22[-1]	5.01[-1]	4.65[-1]	4.16[-1]
4	6	2.98[-1]	3.07[-1]	3.11[-1]	3.12[-1]	3.02[-1]	2.91[-1]	2.70[-1]	2.43[-1]
5	6	1.37[-1]	1.39[-1]	1.40[-1]	1.40[-1]	1.36[-1]	1.31[-1]	1.22[-1]	1.10[-1]
1	7	3.99[-1]	3.94[-1]	3.97[-1]	3.92[-1]	3.75[-1]	3.58[-1]	3.36[-1]	3.13[-1]
2	7	3.56[-1]	3.64[-1]	3.68[-1]	3.65[-1]	3.53[-1]	3.39[-1]	3.17[-1]	2.87[-1]
3	7	1.92[-1]	2.06[-1]	2.14[-1]	2.22[-1]	2.18[-1]	2.10[-1]	1.92[-1]	1.66[-1]
4	7	2.37[-1]	2.52[-1]	2.60[-1]	2.65[-1]	2.59[-1]	2.49[-1]	2.29[-1]	2.02[-1]
5	7	2.97[-1]	3.10[-1]	3.16[-1]	3.16[-1]	3.06[-1]	2.94[-1]	2.73[-1]	2.46[-1]
6	7	9.22[-1]	8.70[-1]	8.75[-1]	8.81[-1]	8.55[-1]	8.18[-1]	7.53[-1]	6.69[-1]
1	8	2.00[-1]	1.97[-1]	1.98[-1]	1.96[-1]	1.87[-1]	1.79[-1]	1.68[-1]	1.56[-1]
2	8	4.18[-2]	4.00[-2]	3.98[-2]	4.01[-2]	3.95[-2]	3.82[-2]	3.54[-2]	3.12[-2]
3	8	2.08[-1]	2.14[-1]	2.17[-1]	2.15[-1]	2.07[-1]	1.99[-1]	1.86[-1]	1.69[-1]
4	8	1.85[-1]	1.95[-1]	2.00[-1]	2.02[-1]	1.96[-1]	1.88[-1]	1.74[-1]	1.56[-1]
5	8	1.06[-1]	1.16[-1]	1.22[-1]	1.27[-1]	1.25[-1]	1.20[-1]	1.10[-1]	9.43[-2]
6	8	3.36[-1]	3.06[-1]	3.03[-1]	3.04[-1]	2.96[-1]	2.84[-1]	2.61[-1]	2.30[-1]
7	8	4.56[-1]	4.43[-1]	4.52[-1]	4.56[-1]	4.41[-1]	4.21[-1]	3.88[-1]	3.47[-1]
1	9	5.64[-1]	5.47[-1]	5.46[-1]	5.57[-1]	5.68[-1]	5.76[-1]	5.84[-1]	5.89[-1]
2	9	1.88	1.88	1.85	1.79	1.71	1.64	1.54	1.43
3	9	1.01	1.00	9.93[-1]	9.74[-1]	9.46[-1]	9.19[-1]	8.76[-1]	8.22[-1]
4	9	4.98[-1]	4.84[-1]	4.79[-1]	4.75[-1]	4.67[-1]	4.58[-1]	4.44[-1]	4.23[-1]
5	9	2.07[-1]	1.96[-1]	1.92[-1]	1.90[-1]	1.88[-1]	1.86[-1]	1.82[-1]	1.78[-1]
6	9	8.40[-1]	8.86[-1]	9.16[-1]	9.30[-1]	9.12[-1]	8.86[-1]	8.41[-1]	7.77[-1]
7	9	4.39[-1]	4.55[-1]	4.67[-1]	4.74[-1]	4.67[-1]	4.56[-1]	4.35[-1]	4.04[-1]
8	9	1.49[-1]	1.53[-1]	1.57[-1]	1.58[-1]	1.54[-1]	1.48[-1]	1.37[-1]	1.22[-1]

Table 3.4b. Fe IV (continued)

Levels		T [K]							
i	j	1000	3000	5000	10000	15000	20000	30000	40000
1	10	4.23[-1]	4.10[-1]	4.10[-1]	4.17[-1]	4.26[-1]	4.32[-1]	4.38[-1]	4.42[-1]
2	10	7.76[-1]	7.64[-1]	7.59[-1]	7.50[-1]	7.34[-1]	7.17[-1]	6.88[-1]	6.50[-1]
3	10	8.08[-1]	7.99[-1]	7.84[-1]	7.52[-1]	7.15[-1]	6.86[-1]	6.46[-1]	5.99[-1]
4	10	6.48[-1]	6.44[-1]	6.36[-1]	6.15[-1]	5.89[-1]	5.66[-1]	5.33[-1]	4.94[-1]
5	10	4.67[-1]	4.60[-1]	4.58[-1]	4.54[-1]	4.45[-1]	4.35[-1]	4.19[-1]	3.96[-1]
6	10	5.35[-1]	5.57[-1]	5.74[-1]	5.83[-1]	5.73[-1]	5.58[-1]	5.31[-1]	4.93[-1]
7	10	3.21[-1]	3.40[-1]	3.52[-1]	3.56[-1]	3.46[-1]	3.32[-1]	3.09[-1]	2.77[-1]
8	10	2.15[-1]	2.23[-1]	2.30[-1]	2.34[-1]	2.32[-1]	2.28[-1]	2.20[-1]	2.08[-1]
9	10	1.27	1.25	1.23	1.20	1.15	1.10	1.03	9.32[-1]
1	11	2.82[-1]	2.74[-1]	2.73[-1]	2.78[-1]	2.84[-1]	2.88[-1]	2.92[-1]	2.95[-1]
2	11	2.73[-1]	2.61[-1]	2.58[-1]	2.57[-1]	2.56[-1]	2.53[-1]	2.48[-1]	2.40[-1]
3	11	4.66[-1]	4.62[-1]	4.58[-1]	4.48[-1]	4.32[-1]	4.18[-1]	3.96[-1]	3.69[-1]
4	11	5.61[-1]	5.54[-1]	5.46[-1]	5.30[-1]	5.09[-1]	4.92[-1]	4.67[-1]	4.37[-1]
5	11	5.00[-1]	5.01[-1]	4.96[-1]	4.80[-1]	4.59[-1]	4.40[-1]	4.13[-1]	3.81[-1]
6	11	2.90[-1]	3.00[-1]	3.08[-1]	3.12[-1]	3.06[-1]	2.97[-1]	2.81[-1]	2.58[-1]
7	11	2.68[-1]	2.82[-1]	2.91[-1]	2.96[-1]	2.90[-1]	2.82[-1]	2.68[-1]	2.48[-1]
8	11	1.57[-1]	1.66[-1]	1.71[-1]	1.74[-1]	1.71[-1]	1.66[-1]	1.58[-1]	1.47[-1]
9	11	4.66[-1]	4.47[-1]	4.38[-1]	4.25[-1]	4.06[-1]	3.87[-1]	3.57[-1]	3.15[-1]
10	11	9.69[-1]	9.55[-1]	9.44[-1]	9.21[-1]	8.85[-1]	8.51[-1]	7.99[-1]	7.35[-1]
1	12	1.41[-1]	1.37[-1]	1.37[-1]	1.39[-1]	1.42[-1]	1.44[-1]	1.46[-1]	1.47[-1]
2	12	6.95[-2]	6.37[-2]	6.15[-2]	6.02[-2]	5.97[-2]	5.93[-2]	5.88[-2]	5.82[-2]
3	12	2.12[-1]	2.07[-1]	2.06[-1]	2.07[-1]	2.06[-1]	2.03[-1]	1.98[-1]	1.90[-1]
4	12	2.93[-1]	2.94[-1]	2.92[-1]	2.85[-1]	2.75[-1]	2.65[-1]	2.50[-1]	2.31[-1]
5	12	3.25[-1]	3.25[-1]	3.20[-1]	3.05[-1]	2.88[-1]	2.74[-1]	2.56[-1]	2.34[-1]
6	12	1.20[-1]	1.24[-1]	1.27[-1]	1.29[-1]	1.26[-1]	1.21[-1]	1.13[-1]	1.02[-1]
7	12	1.62[-1]	1.69[-1]	1.74[-1]	1.77[-1]	1.75[-1]	1.72[-1]	1.67[-1]	1.58[-1]
8	12	7.50[-2]	8.07[-2]	8.42[-2]	8.53[-2]	8.26[-2]	7.93[-2]	7.37[-2]	6.63[-2]
9	12	2.01[-1]	1.88[-1]	1.84[-1]	1.79[-1]	1.72[-1]	1.65[-1]	1.52[-1]	1.33[-1]
10	12	2.35[-1]	2.34[-1]	2.30[-1]	2.21[-1]	2.09[-1]	2.00[-1]	1.84[-1]	1.63[-1]
11	12	5.59[-1]	5.55[-1]	5.49[-1]	5.37[-1]	5.16[-1]	4.97[-1]	4.69[-1]	4.35[-1]
1	13	6.41[-1]	5.29[-1]	4.67[-1]	4.13[-1]	3.91[-1]	3.85[-1]	3.88[-1]	3.95[-1]
1	14	5.13[-1]	4.23[-1]	3.73[-1]	3.30[-1]	3.13[-1]	3.08[-1]	3.10[-1]	3.16[-1]
1	15	3.85[-1]	3.17[-1]	2.80[-1]	2.48[-1]	2.34[-1]	2.31[-1]	2.33[-1]	2.37[-1]
1	16	2.56[-1]	2.11[-1]	1.87[-1]	1.65[-1]	1.56[-1]	1.54[-1]	1.55[-1]	1.58[-1]
1	17	1.99	2.00	1.90	1.71	1.58	1.51	1.42	1.26
1	18	1.59	1.61	1.52	1.37	1.27	1.22	1.14	1.01
1	19	1.20	1.20	1.14	1.03	9.54[-1]	9.13[-1]	8.58[-1]	7.62[-1]
1	20	7.97[-1]	8.03[-1]	7.62[-1]	6.87[-1]	6.36[-1]	6.09[-1]	5.73[-1]	5.08[-1]
1	21	3.98[-1]	4.01[-1]	3.81[-1]	3.43[-1]	3.18[-1]	3.04[-1]	2.86[-1]	2.54[-1]
1	22	7.36[-1]	6.33[-1]	5.81[-1]	5.29[-1]	4.98[-1]	4.78[-1]	4.44[-1]	3.83[-1]
1	23	5.52[-1]	4.75[-1]	4.36[-1]	3.97[-1]	3.74[-1]	3.59[-1]	3.32[-1]	2.86[-1]
1	24	3.68[-1]	3.17[-1]	2.91[-1]	2.65[-1]	2.49[-1]	2.39[-1]	2.21[-1]	1.90[-1]
1	25	1.84[-1]	1.58[-1]	1.45[-1]	1.32[-1]	1.25[-1]	1.19[-1]	1.10[-1]	9.45[-2]

Table 3.4b. Fe IV (continued)

Levels		T [K]							
i	j	1000	3000	5000	10000	15000	20000	30000	40000
1	26	1.85[-2]	1.64[-2]	1.59[-2]	1.60[-2]	1.58[-2]	1.53[-2]	1.39[-2]	1.12[-2]
1	27	1.23[-2]	1.09[-2]	1.06[-2]	1.06[-2]	1.06[-2]	1.02[-2]	9.31[-3]	7.51[-3]
1	28	6.17[-3]	5.47[-3]	5.32[-3]	5.32[-3]	5.26[-3]	5.08[-3]	4.59[-3]	3.68[-3]
1	29	1.20[-2]	1.02[-2]	9.30[-3]	9.03[-3]	9.17[-3]	9.11[-3]	8.53[-3]	7.10[-3]
1	30	1.02[-2]	8.76[-3]	7.97[-3]	7.74[-3]	7.86[-3]	7.80[-3]	7.30[-3]	6.07[-3]
1	31	8.54[-3]	7.30[-3]	6.64[-3]	6.45[-3]	6.55[-3]	6.50[-3]	6.08[-3]	5.05[-3]
1	32	6.83[-3]	5.84[-3]	5.31[-3]	5.16[-3]	5.24[-3]	5.20[-3]	4.86[-3]	4.03[-3]
1	33	1.63[-2]	1.42[-2]	1.32[-2]	1.28[-2]	1.31[-2]	1.31[-2]	1.26[-2]	1.07[-2]
1	34	1.31[-2]	1.14[-2]	1.05[-2]	1.03[-2]	1.05[-2]	1.05[-2]	1.00[-2]	8.50[-3]
1	35	9.81[-3]	8.54[-3]	7.89[-3]	7.69[-3]	7.85[-3]	7.88[-3]	7.52[-3]	6.40[-3]
1	36	6.54[-3]	5.69[-3]	5.26[-3]	5.13[-3]	5.22[-3]	5.23[-3]	4.98[-3]	4.23[-3]
1	37	2.94[-2]	1.96[-2]	1.79[-2]	1.89[-2]	1.98[-2]	1.98[-2]	1.82[-2]	1.47[-2]
1	38	2.45[-2]	1.63[-2]	1.49[-2]	1.57[-2]	1.66[-2]	1.66[-2]	1.54[-2]	1.26[-2]
1	39	1.96[-2]	1.30[-2]	1.20[-2]	1.26[-2]	1.33[-2]	1.34[-2]	1.25[-2]	1.02[-2]
1	40	1.47[-2]	9.78[-3]	8.97[-3]	9.45[-3]	1.00[-2]	1.00[-2]	9.37[-3]	7.65[-3]
1	41	1.52[-2]	1.13[-2]	1.02[-2]	9.46[-3]	8.87[-3]	8.32[-3]	7.32[-3]	5.82[-3]
1	42	1.14[-2]	8.45[-3]	7.67[-3]	7.08[-3]	6.60[-3]	6.15[-3]	5.34[-3]	4.18[-3]
1	43	7.58[-3]	5.63[-3]	5.11[-3]	4.72[-3]	4.39[-3]	4.09[-3]	3.54[-3]	2.76[-3]
1	44	3.79[-3]	2.82[-3]	2.56[-3]	2.35[-3]	2.18[-3]	2.03[-3]	1.75[-3]	1.36[-3]
1	45	2.04[-1]	1.95[-1]	1.87[-1]	1.77[-1]	1.69[-1]	1.64[-1]	1.59[-1]	1.56[-1]
1	46	1.59[-1]	1.46[-1]	1.37[-1]	1.27[-1]	1.20[-1]	1.16[-1]	1.11[-1]	1.09[-1]
1	47	1.26[-1]	1.15[-1]	1.08[-1]	1.00[-1]	9.39[-2]	9.03[-2]	8.68[-2]	8.44[-2]
1	48	9.63[-2]	8.85[-2]	8.35[-2]	7.72[-2]	7.26[-2]	6.98[-2]	6.70[-2]	6.51[-2]
1	49	6.70[-2]	6.26[-2]	5.95[-2]	5.55[-2]	5.23[-2]	5.04[-2]	4.85[-2]	4.72[-2]
1	50	3.45[-2]	3.27[-2]	3.13[-2]	2.94[-2]	2.78[-2]	2.69[-2]	2.59[-2]	2.52[-2]
1	51	1.67	1.68	1.69	1.70	1.70	1.71	1.75	1.85
1	52	1.22	1.22	1.22	1.22	1.22	1.23	1.25	1.33
1	53	8.09[-1]	7.99[-1]	7.99[-1]	7.98[-1]	7.95[-1]	7.96[-1]	8.11[-1]	8.55[-1]
1	54	3.23[-4]	3.72[-4]	4.03[-4]	4.49[-4]	4.82[-4]	5.00[-4]	5.12[-4]	4.99[-4]
1	55	2.48[-4]	2.88[-4]	3.12[-4]	3.47[-4]	3.71[-4]	3.83[-4]	3.91[-4]	3.80[-4]
1	56	1.22[-4]	1.37[-4]	1.45[-4]	1.54[-4]	1.59[-4]	1.60[-4]	1.60[-4]	1.52[-4]
1	57	4.31[-4]	4.55[-4]	4.58[-4]	4.44[-4]	4.27[-4]	4.19[-4]	4.15[-4]	4.10[-4]
1	58	3.06[-4]	3.36[-4]	3.56[-4]	3.71[-4]	3.69[-4]	3.64[-4]	3.55[-4]	3.40[-4]
1	59	2.35[-4]	2.57[-4]	2.71[-4]	2.78[-4]	2.68[-4]	2.55[-4]	2.34[-4]	2.06[-4]
1	60	1.51[-4]	1.62[-4]	1.68[-4]	1.70[-4]	1.63[-4]	1.54[-4]	1.40[-4]	1.22[-4]
1	61	1.41[-1]	1.41[-1]	1.38[-1]	1.29[-1]	1.21[-1]	1.15[-1]	1.09[-1]	1.04[-1]
1	62	8.07[-2]	8.02[-2]	7.80[-2]	7.35[-2]	6.92[-2]	6.63[-2]	6.32[-2]	6.06[-2]
1	63	3.57[-2]	3.55[-2]	3.47[-2]	3.29[-2]	3.12[-2]	3.02[-2]	2.91[-2]	2.85[-2]
1	64	9.18[-2]	9.03[-2]	8.86[-2]	8.52[-2]	8.17[-2]	7.94[-2]	7.68[-2]	7.44[-2]
1	65	8.45[-2]	8.33[-2]	8.19[-2]	7.90[-2]	7.60[-2]	7.40[-2]	7.17[-2]	6.96[-2]
1	66	6.18[-2]	6.08[-2]	5.97[-2]	5.75[-2]	5.51[-2]	5.36[-2]	5.18[-2]	5.01[-2]
1	67	3.50[-2]	3.44[-2]	3.37[-2]	3.24[-2]	3.11[-2]	3.02[-2]	2.92[-2]	2.83[-2]
1	68	1.55[-2]	1.52[-2]	1.49[-2]	1.42[-2]	1.36[-2]	1.31[-2]	1.27[-2]	1.22[-2]

Table 3.5. Fe V. Effective collision strengths $\Upsilon(i,j)$ as a function of temperature T [K] for the transitions between the five fine-structure $3d^4\ {}^5D_J$ levels [95B1]. The observed energies are 0.0, 0.0013, 0.0038, 0.0073, and 0.0117 Ry for $J = 0, 1, 2, 3$, and 4, respectively [75R1].

Levels		$\log T$							
J_i	J_j	4.0	4.2	4.4	4.6	4.8	5.0	5.2	5.4
0	1	8.61[-1]	7.28[-1]	6.09[-1]	5.15[-1]	4.47[-1]	4.00[-1]	3.70[-1]	3.50[-1]
0	2	4.61[-1]	3.67[-1]	2.85[-1]	2.21[-1]	1.76[-1]	1.46[-1]	1.27[-1]	1.15[-1]
0	3	3.92[-1]	3.01[-1]	2.24[-1]	1.67[-1]	1.26[-1]	9.80[-2]	7.90[-2]	6.00[-2]
0	4	3.38[-1]	2.56[-1]	1.93[-1]	1.49[-1]	1.18[-1]	9.70[-2]	8.20[-2]	7.00[-2]
1	2	2.44	1.95	1.55	1.26	1.05	9.09[-1]	8.20[-1]	7.61[-1]
1	3	1.44	1.11	8.33[-1]	6.28[-1]	4.84[-1]	3.86[-1]	3.22[-1]	2.79[-1]
1	4	1.27	9.41[-1]	6.98[-1]	5.24[-1]	4.05[-1]	3.23[-1]	2.67[-1]	2.26[-1]
2	3	3.21	2.62	2.11	1.73	1.46	1.28	1.16	1.08
2	4	2.43	1.81	1.34	1.00	7.73[-1]	6.18[-1]	5.13[-1]	4.40[-1]
3	4	6.73	5.07	3.79	2.86	2.22	1.80	1.53	1.35

Table 3.6. Fe X. Effective collision strengths Υ as a function of temperature T [K] for the transition between the fine-structure levels $^2P_{3/2}$ and $^2P_{1/2}$ of the ground configuration $3s^23p^5$ [95P1]. The transition energy is 0.143 Ry.

$\log T$	5.0	5.2	5.4	5.6	5.8	6.0	6.2	6.4	6.6	6.8	7.0
Υ	3.38	3.15	2.97	2.69	2.27	1.79	1.35	0.99	0.73	0.54	0.40

Table 3.7a. Fe XII. 41 fine-structure levels for the three lowest configurations included in the calculation [98B2, 98B3] and their calculated and observed energies E [Ry] in rydbergs [85S1]. The index i is used in Table 3.7b for transition keys.

i	Level		E [Ry]		i	Level		E [Ry]	
			obs.	calc.				obs.	calc.
1	$3s^2\,3p^3$	$^4S^o_{3/2}$	0.00000	0.00000	22	$3s^2\,3p^2\,3d$	$(^3P)\,^4D_{5/2}$	4.06475	4.20646
2		$^2D^o_{3/2}$	0.37868	0.40530	23		$(^1D)\,^2F_{7/2}$	4.15435	4.29484
3		$^2D^o_{5/2}$	0.41998	0.44697	24		$(^1D)\,^2G_{7/2}$	4.48255	4.62304
4		$^2P^o_{1/2}$	0.67532	0.70856	25		$(^1D)\,^2G_{9/2}$	4.50967	4.65016
5		$^2P^o_{3/2}$	0.73371	0.76600	26		$(^3P)\,^2P_{3/2}$	4.57274	4.68104
6	$3s\,3p^4$	$^4P_{5/2}$	2.50027	2.49772	27		$(^3P)\,^4P_{5/2}$	4.67033	4.78306
7		$^4P_{3/2}$	2.58804	2.58617	28		$(^3P)\,^2P_{1/2}$	4.68255	4.79089
8		$^4P_{1/2}$	2.62725	2.62622	29		$(^3P)\,^4P_{3/2}$	4.70888	4.82004
9		$^2D_{3/2}$	3.09613	3.12817	30		$(^3P)\,^4P_{1/2}$	4.73649	4.84375
10		$^2D_{5/2}$	3.11383	3.14543	31		$(^1S)\,^2D_{3/2}$	4.79436	4.91741
11		$^2P_{3/2}$	3.55092	3.61480	32		$(^1S)\,^2D_{5/2}$	4.90298	5.01586
12		$^2P_{1/2}$	3.59360	3.65671	33		$(^1D)\,^2D_{3/2}$	5.04869	5.17481
13		$^2S_{1/2}$	3.73985	3.80195	34		$(^1D)\,^2D_{5/2}$	5.05398	5.18534
14	$3s^2\,3p^2\,3d$	$(^3P)\,^4F_{3/2}$	3.82967	3.97138	35		$(^1D)\,^2P_{1/2}$	5.18456	5.35194
15		$(^3P)\,^4F_{5/2}$	3.86397	4.00568	36		$(^3P)\,^2F_{5/2}$	5.25564	5.40762
16		$(^3P)\,^4F_{7/2}$	3.91417	4.05588	37		$(^1D)\,^2P_{3/2}$	5.26475	5.42483
17		$(^3P)\,^4F_{9/2}$	3.97663	4.11834	38		$(^1D)\,^2S_{1/2}$	5.28198	5.41253
18		$(^1D)\,^2F_{5/2}$	3.98400	4.12450	39		$(^3P)\,^2F_{7/2}$	5.29610	5.44754
19		$(^3P)\,^4D_{1/2}$	4.01245	4.15417	40		$(^3P)\,^2D_{5/2}$	5.50342	5.65921
20		$(^3P)\,^4D_{7/2}$	4.01815	4.15986	41		$(^3P)\,^2D_{3/2}$	5.51754	5.67384
21		$(^3P)\,^4D_{3/2}$	4.02246	4.16418					

Table 3.7b. Fe XII. Effective collision strengths $\Upsilon(i,j)$ as a function of temperature T [K] for the transitions among the five fine-structure levels of the ground configuration, and the transitions between these five levels to the eight levels of the first excited configuration. The level indices are as specified in Table 3.7a [98B2, 98B3].

Levels		T [$\times 10^6$ K]								
i	j	0.4	0.8	1.2	1.6	2.0	3.0	5.0	7.0	10.0
1	2	0.2680	0.1960	0.1570	0.1320	0.1150	0.0880	0.0631	0.0505	0.0401
1	3	0.2680	0.2070	0.1710	0.1480	0.1310	0.1060	0.0796	0.0663	0.0549
1	4	0.0740	0.0550	0.0430	0.0350	0.0300	0.0220	0.0147	0.0111	0.0083
1	5	0.3040	0.2190	0.1680	0.1360	0.1140	0.0820	0.0529	0.0392	0.0283
2	3	2.3750	1.6990	1.3150	1.0780	0.9180	0.6800	0.4655	0.3658	0.2872
2	4	0.7630	0.6170	0.5350	0.4850	0.4510	0.4030	0.3600	0.3407	0.3258
2	5	1.4180	1.0840	0.8740	0.7400	0.6500	0.5140	0.3929	0.3370	0.2934
3	4	0.5560	0.4440	0.3850	0.3500	0.3270	0.2930	0.2638	0.2505	0.2403
3	5	1.7790	1.4210	1.2270	1.1100	1.0320	0.9190	0.8199	0.7752	0.7407

Table 3.7b. Fe XII (continued)

Levels		T [$\times 10^6$ K]								
i	j	0.4	0.8	1.2	1.6	2.0	3.0	5.0	7.0	10.0
4	5	1.2410	0.9400	0.7360	0.6040	0.5140	0.3780	0.2538	0.1960	0.1505
1	6	0.8614	0.9203	0.9688	1.0090	1.0440	1.1150	1.2190	1.2950	1.3810
1	7	0.5652	0.6009	0.6312	0.6568	0.6790	0.7248	0.7918	0.8410	0.8969
1	8	0.2837	0.3018	0.3171	0.3299	0.3411	0.3640	0.3976	0.4223	0.4502
1	9	0.0049	0.0042	0.0038	0.0036	0.0033	0.0030	0.0026	0.0024	0.0022
1	10	0.0045	0.0036	0.0033	0.0031	0.0031	0.0030	0.0031	0.0032	0.0033
1	11	0.0771	0.0675	0.0612	0.0565	0.0527	0.0456	0.0372	0.0322	0.0277
1	12	0.0264	0.0230	0.0209	0.0194	0.0182	0.0161	0.0135	0.0120	0.0107
1	13	0.0124	0.0116	0.0111	0.0107	0.0104	0.0099	0.0093	0.0090	0.0088
2	6	0.0457	0.0394	0.0362	0.0342	0.0327	0.0302	0.0277	0.0264	0.0254
2	7	0.0331	0.0262	0.0226	0.0202	0.0183	0.0152	0.0117	0.0098	0.0080
2	8	0.0163	0.0129	0.0112	0.0101	0.0093	0.0080	0.0065	0.0057	0.0049
2	9	0.8267	0.9183	0.9841	1.0360	1.0790	1.1660	1.2870	1.3750	1.4730
2	10	0.0844	0.0703	0.0633	0.0589	0.0556	0.0502	0.0445	0.0415	0.0390
2	11	0.1869	0.1869	0.1918	0.1973	0.2026	0.2145	0.2334	0.2477	0.2642
2	12	0.5174	0.5672	0.6045	0.6349	0.6610	0.7141	0.7910	0.8469	0.9101
2	13	0.0463	0.0432	0.0428	0.0430	0.0435	0.0448	0.0472	0.0492	0.0517
3	6	0.0824	0.0715	0.0662	0.0628	0.0603	0.0563	0.0522	0.0503	0.0489
3	7	0.0305	0.0235	0.0203	0.0182	0.0167	0.0143	0.0118	0.0104	0.0093
3	9	0.1041	0.0848	0.0756	0.0697	0.0655	0.0584	0.0510	0.0470	0.0438
3	10	1.1570	1.2500	1.3230	1.3830	1.4330	1.5360	1.6830	1.7900	1.9110
3	11	1.2540	1.3530	1.4320	1.4990	1.5560	1.6740	1.8460	1.9720	2.1150
4	7	0.0213	0.0171	0.0149	0.0133	0.0122	0.0101	0.0078	0.0064	0.0052
4	8	0.0170	0.0157	0.0148	0.0142	0.0136	0.0127	0.0116	0.0110	0.0105
4	9	0.1308	0.1330	0.1375	0.1417	0.1456	0.1538	0.1662	0.1755	0.1862
4	11	0.0932	0.0962	0.0994	0.1024	0.1051	0.1108	0.1195	0.1262	0.1338
4	12	0.3362	0.3782	0.4061	0.4277	0.4457	0.4812	0.5312	0.5669	0.6069
4	13	0.0742	0.0810	0.0861	0.0903	0.0940	0.1014	0.1121	0.1199	0.1287
5	6	0.0480	0.0371	0.0320	0.0288	0.0265	0.0227	0.0186	0.0164	0.0145
5	7	0.0440	0.0375	0.0342	0.0322	0.0306	0.0281	0.0255	0.0242	0.0231
5	8	0.0222	0.0174	0.0150	0.0134	0.0122	0.0103	0.0082	0.0070	0.0059
5	9	0.0719	0.0557	0.0487	0.0445	0.0416	0.0372	0.0327	0.0305	0.0287
5	10	0.3843	0.4026	0.4211	0.4370	0.4507	0.4789	0.5198	0.5497	0.5836
5	11	0.1752	0.1820	0.1892	0.1956	0.2012	0.2131	0.2308	0.2439	0.2591
5	12	0.0377	0.0238	0.0183	0.0152	0.0132	0.0101	0.0072	0.0057	0.0044
5	13	0.7153	0.7716	0.8148	0.8504	0.8810	0.9436	1.0350	1.1020	1.1780

Table 3.8. Fe XIV. Effective collision strengths Υ as a function of temperature T [K] for the transition between the fine-structure levels $^2P^o_{1/2}$ and $^2P^o_{3/2}$ of the ground configuration $3s^23p$ [96S4]. The transition energy is 0.1718 Ry.

$\log T$	5.0	5.2	5.4	5.6	5.8	6.0	6.2	6.4	6.6	6.8	7.0
Υ	3.13	2.98	2.74	2.35	1.88	1.43	1.05	0.768	0.565	0.427	0.335

Table 3.9a. Fe XVI. 12 fine-structure $n = 3$ and 4 levels included in the calculation [90S2] and their calculated and observed energies E [Ry] in rydbergs [85S1]. The index i is used in Table 3.9b for transition keys.

i	Level	E [Ry]		i	Level	E [Ry]	
		obs.	calc.			obs.	calc.
1	3s $^2S_{1/2}$	0.00000	0.00000	7	4p $^2P_{1/2}$	18.02523	18.00200
2	3p $^2P_{1/2}$	2.52596	2.53472	8	4p $^2P_{3/2}$	18.09868	18.07618
3	3p $^2P_{3/2}$	2.71688	2.72460	9	4d $^2D_{3/2}$	19.35704	19.33858
4	3d $^2D_{3/2}$	6.15544	6.16600	10	4d $^2D_{5/2}$	19.36771	19.35048
5	3d $^2D_{5/2}$	6.18198	6.19134	11	4f $^2F_{5/2}$	19.90772	19.88518
6	4s $^2S_{1/2}$	17.01828	16.99770	12	4f $^2F_{7/2}$	19.91255	19.88958

Table 3.9b. Fe XVI. Effective collision strengths $\Upsilon(i, j)$ as a function of temperature T [K] for transitions among the five $n = 3$ levels and transitions from these five levels to the seven $n = 4$ levels as specified in Table 3.9a [90S2].

Levels		T [$\times 10^6$ K]							
i	j	0.1	0.2	0.5	1.0	2.0	5.0	10.0	20.0
1	2	1.23	1.23	1.25	1.31	1.40	1.59	1.78	2.02
1	3	2.48	2.46	2.49	2.58	2.75	3.12	3.51	3.98
1	4	1.20[-1]	1.20[-1]	1.21[-1]	1.23[-1]	1.26[-1]	1.30[-1]	1.34[-1]	1.36[-1]
1	5	1.80[-1]	1.80[-1]	1.82[-1]	1.85[-1]	1.89[-1]	1.96[-1]	2.01[-1]	2.05[-1]
2	3	2.18[-1]	2.17[-1]	2.13[-1]	2.08[-1]	2.01[-1]	1.91[-1]	1.85[-1]	1.80[-1]
2	4	1.76	1.77	1.80	1.88	2.01	2.28	2.57	2.94
2	5	4.49[-2]	4.45[-2]	4.29[-2]	4.09[-2]	3.82[-2]	3.48[-2]	3.31[-2]	3.24[-2]
3	4	4.09[-1]	4.11[-1]	4.19[-1]	4.32[-1]	4.55[-1]	5.07[-1]	5.65[-1]	6.38[-1]
3	5	3.23	3.26	3.34	3.48	3.71	4.21	4.75	5.42
4	5	2.23[-1]	2.20[-1]	2.07[-1]	1.89[-1]	1.66[-1]	1.33[-1]	1.13[-1]	9.82[-2]
1	6	9.85[-2]	9.90[-2]	1.00[-1]	1.02[-1]	1.04[-1]	1.07[-1]	1.10[-1]	1.13[-1]
1	7	5.91[-3]	6.05[-3]	6.54[-3]	7.45[-3]	9.39[-3]	1.49[-2]	2.24[-2]	3.31[-2]
1	8	1.12[-2]	1.14[-2]	1.22[-2]	1.39[-2]	1.73[-2]	2.73[-2]	4.10[-2]	6.09[-2]
1	9	1.63[-2]	1.65[-2]	1.70[-2]	1.77[-2]	1.92[-2]	2.23[-2]	2.56[-2]	2.94[-2]
1	10	2.43[-2]	2.45[-2]	2.52[-2]	2.64[-2]	2.85[-2]	3.32[-2]	3.81[-2]	4.36[-2]

Table 3.9b. Fe XVI (continued)

Levels		T [$\times 10^6$ K]							
i	j	0.1	0.2	0.5	1.0	2.0	5.0	10.0	20.0
1	11	3.39[-2]	3.39[-2]	3.39[-2]	3.41[-2]	3.44[-2]	3.53[-2]	3.61[-2]	3.70[-2]
1	12	4.52[-2]	4.52[-2]	4.52[-2]	4.55[-2]	4.59[-2]	4.70[-2]	4.82[-2]	4.93[-2]
2	6	9.08[-3]	9.28[-3]	1.00[-2]	1.13[-2]	1.38[-2]	2.04[-2]	2.88[-2]	4.03[-2]
2	7	1.14[-1]	1.14[-1]	1.15[-1]	1.17[-1]	1.18[-1]	1.21[-1]	1.23[-1]	1.25[-1]
2	8	1.59[-2]	1.58[-2]	1.58[-2]	1.60[-2]	1.64[-2]	1.76[-2]	1.90[-2]	2.07[-2]
2	9	3.48[-2]	3.59[-2]	3.92[-2]	4.47[-2]	5.52[-2]	8.20[-2]	1.16[-1]	1.61[-1]
2	10	1.53[-2]	1.52[-2]	1.48[-2]	1.44[-2]	1.39[-2]	1.32[-2]	1.28[-2]	1.25[-2]
2	11	1.07[-1]	1.09[-1]	1.12[-1]	1.18[-1]	1.27[-1]	1.47[-1]	1.65[-1]	1.84[-1]
2	12	2.37[-2]	2.32[-2]	2.19[-2]	2.04[-2]	1.86[-2]	1.64[-2]	1.54[-2]	1.50[-2]
3	6	1.97[-2]	2.02[-2]	2.19[-2]	2.48[-2]	3.05[-2]	4.50[-2]	6.31[-2]	8.78[-2]
3	7	1.70[-2]	1.70[-2]	1.71[-2]	1.73[-2]	1.78[-2]	1.92[-2]	2.09[-2]	2.27[-2]
3	8	2.47[-1]	2.48[-1]	2.50[-1]	2.52[-1]	2.57[-1]	2.64[-1]	2.69[-1]	2.74[-1]
3	9	2.68[-2]	2.69[-2]	2.72[-2]	2.79[-2]	2.95[-2]	3.44[-2]	4.11[-2]	5.06[-2]
3	10	8.05[-2]	8.24[-2]	8.86[-2]	9.89[-2]	1.19[-1]	1.69[-1]	2.33[-1]	3.20[-1]
3	11	6.24[-2]	6.21[-2]	6.15[-2]	6.13[-2]	6.17[-2]	6.45[-2]	6.85[-2]	7.35[-2]
3	12	2.05[-1]	2.07[-1]	2.13[-1]	2.22[-1]	2.37[-1]	2.70[-1]	3.01[-1]	3.34[-1]
4	6	1.45[-2]	1.45[-2]	1.45[-2]	1.45[-2]	1.48[-2]	1.55[-2]	1.63[-2]	1.72[-2]
4	7	1.99[-2]	2.03[-2]	2.16[-2]	2.38[-2]	2.81[-2]	3.87[-2]	5.14[-2]	6.81[-2]
4	8	2.06[-2]	2.03[-2]	1.98[-2]	1.92[-2]	1.87[-2]	1.89[-2]	2.01[-2]	2.24[-2]
4	9	2.94[-1]	2.94[-1]	2.94[-1]	2.94[-1]	2.95[-1]	2.96[-1]	2.97[-1]	2.97[-1]
4	10	4.49[-2]	4.36[-2]	4.04[-2]	3.66[-2]	3.19[-2]	2.56[-2]	2.20[-2]	1.96[-2]
4	11	8.97[-1]	9.11[-1]	9.52[-1]	1.01	1.13	1.39	1.69	2.07
4	12	7.32[-2]	7.06[-2]	6.44[-2]	5.72[-2]	4.84[-2]	3.69[-2]	3.01[-2]	2.55[-2]
5	6	2.19[-2]	2.19[-2]	2.19[-2]	2.20[-2]	2.23[-2]	2.34[-2]	2.47[-2]	2.61[-2]
5	7	1.43[-2]	1.41[-2]	1.34[-2]	1.26[-2]	1.15[-2]	9.98[-3]	9.02[-3]	8.34[-3]
5	8	4.54[-2]	4.59[-2]	4.75[-2]	5.06[-2]	5.70[-2]	7.37[-2]	9.47[-2]	1.23[-1]
5	9	4.51[-2]	4.37[-2]	4.05[-2]	3.67[-2]	3.20[-2]	2.58[-2]	2.22[-2]	1.99[-2]
5	10	4.64[-1]	4.64[-1]	4.62[-1]	4.61[-1]	4.59[-1]	4.57[-1]	4.57[-1]	4.56[-1]
5	11	1.43[-1]	1.41[-1]	1.38[-1]	1.35[-1]	1.33[-1]	1.39[-1]	1.54[-1]	1.76[-1]
5	12	1.32	1.34	1.39	1.48	1.64	2.01	2.44	2.98

⟹

Table 3.10a. Fe XVII. 89 fine-structure $n = 2$, 3 and 4 levels included in the calculation [89Z2] and their calculated and observed energies E [Ry] in rydbergs [85S1]. The index i is used in Table 3.10b for transition keys.

Table 3.10a. Fe XVII. For caption see previous page.

i	Level	E [Ry]		i	Level	E [Ry]	
		obs.	calc.			obs.	calc.
1	$2s^2\ 2p^6\ {}^1S_0$	0.00000	0.00000	46	$2s^2\ 2p^5\ 4p\ {}^3P_2$		72.86972
2	$2s^2\ 2p^5\ 3s\ {}^3P_2$	53.29655	53.23584	47	$2s^2\ 2p^5\ 4p\ {}^3P_0$		73.15410
3	$2s^2\ 2p^5\ 3s\ {}^1P_1$	53.43670	53.38548	48	$2s^2\ 2p^5\ 4p\ {}^3D_1$		73.66470
4	$2s^2\ 2p^5\ 3s\ {}^3P_0$	54.22686	54.16750	49	$2s^2\ 2p^5\ 4p\ {}^3P_1$		73.75198
5	$2s^2\ 2p^5\ 3s\ {}^3P_1$	54.31398	54.26352	50	$2s^2\ 2p^5\ 4p\ {}^1D_2$		73.76776
6	$2s^2\ 2p^5\ 3p\ {}^3S_1$	55.52177	55.45052	51	$2s^2\ 2p^5\ 4d\ {}^3P_0$		73.91878
7	$2s^2\ 2p^5\ 3p\ {}^3D_2$	55.77875	55.72620	52	$2s^2\ 2p^5\ 4d\ {}^3P_1$	73.95844	73.94986
8	$2s^2\ 2p^5\ 3p\ {}^3D_3$	55.89740	55.84066	53	$2s^2\ 2p^5\ 4d\ {}^3F_4$		73.98824
9	$2s^2\ 2p^5\ 3p\ {}^1P_1$	55.98041	55.93104	54	$2s^2\ 2p^5\ 4d\ {}^3P_2$		74.00070
10	$2s^2\ 2p^5\ 3p\ {}^3P_2$	56.11373	56.06446	55	$2s^2\ 2p^5\ 4p\ {}^1S_0$		74.00698
11	$2s^2\ 2p^5\ 3p\ {}^3P_0$	56.51551	56.47704	56	$2s^2\ 2p^5\ 4d\ {}^3F_3$		74.00786
12	$2s^2\ 2p^5\ 3p\ {}^3D_1$	56.66724	56.61730	57	$2s^2\ 2p^5\ 4d\ {}^1D_2$		74.05190
13	$2s^2\ 2p^5\ 3p\ {}^3P_1$	56.90608	56.85468	58	$2s^2\ 2p^5\ 4d\ {}^3D_3$		74.07894
14	$2s^2\ 2p^5\ 3p\ {}^1D_2$	56.93369	56.88462	59	$2s^2\ 2p^5\ 4d\ {}^3D_1$	74.30472	74.26912
15	$2s^2\ 2p^5\ 3p\ {}^1S_0$	57.88943	58.03326	60	$2s^2\ 2p^5\ 4f\ {}^3D_1$		74.57186
16	$2s^2\ 2p^5\ 3d\ {}^3P_0$	58.89829	58.84048	61	$2s^2\ 2p^5\ 4f\ {}^1G_4$		74.57360
17	$2s^2\ 2p^5\ 3d\ {}^3P_1$	58.98176	58.91248	62	$2s^2\ 2p^5\ 4f\ {}^3G_5$		74.57500
18	$2s^2\ 2p^5\ 3d\ {}^3P_2$	59.09768	59.04986	63	$2s^2\ 2p^5\ 4f\ {}^3D_2$		74.58210
19	$2s^2\ 2p^5\ 3d\ {}^3F_4$	59.10415	59.05848	64	$2s^2\ 2p^5\ 4f\ {}^3D_3$		74.60650
20	$2s^2\ 2p^5\ 3d\ {}^3F_3$	59.16119	59.11976	65	$2s^2\ 2p^5\ 4f\ {}^3F_2$		74.61038
21	$2s^2\ 2p^5\ 3d\ {}^1D_2$	59.28758	59.24910	66	$2s^2\ 2p^5\ 4f\ {}^1F_3$		74.61314
22	$2s^2\ 2p^5\ 3d\ {}^3D_3$	59.36659	59.33030	67	$2s^2\ 2p^5\ 4f\ {}^3F_4$		74.61876
23	$2s^2\ 2p^5\ 3d\ {}^3D_1$	59.70804	59.68620	68	$2s^2\ 2p^5\ 4d\ {}^3F_2$		74.93436
24	$2s^2\ 2p^5\ 3d\ {}^3F_2$	60.08768	60.04864	69	$2s^2\ 2p^5\ 4d\ {}^3D_2$		74.95288
25	$2s^2\ 2p^5\ 3d\ {}^3D_2$	60.16176	60.10738	70	$2s^2\ 2p^5\ 4d\ {}^1F_3$		74.97430
26	$2s^2\ 2p^5\ 3d\ {}^1F_3$	60.19739	60.15014	71	$2s^2\ 2p^5\ 4d\ {}^1P_1$	75.17042	75.13268
27	$2s^2\ 2p^5\ 3d\ {}^1P_1$	60.69039	60.72882	72	$2s^2\ 2p^5\ 4f\ {}^3G_3$		75.52322
28	$2s\ 2p^6\ 3s\ {}^3S_1$		63.24164	73	$2s^2\ {}^5\ 4f\ {}^3G_4$		75.53134
29	$2s\ 2p^6\ 3s\ {}^1S_0$		63.73804	74	$2s^2\ {}^5\ 4f\ {}^3F_3$		75.53918
30	$2s\ 2p^6\ 3p\ {}^3P_0$		65.65782	75	$2s^2\ {}^5\ 4f\ {}^1D_2$		75.53992
31	$2s\ 2p^6\ 3p\ {}^3P_1$	65.60121	65.69168	76	$2s\ 2p^6\ 4s\ {}^3S_1$		81.62174
32	$2s\ 2p^6\ 3p\ {}^3P_2$		65.86124	77	$2s\ 2p^6\ 4s\ {}^1S_0$		81.78526
33	$2s\ 2p^6\ 3p\ {}^1P_1$	65.92380	66.00920	78	$2s\ 2p^6\ 4p\ {}^3P_0$		82.59652
34	$2s\ 2p^6\ 3d\ {}^3D_1$		68.94956	79	$2s\ 2p^6\ 4p\ {}^3P_1$	82.52435	82.60820
35	$2s\ 2p^6\ 3d\ {}^3D_2$		68.95962	80	$2s\ 2p^6\ 4p\ {}^3P_2$		82.67778
36	$2s\ 2p^6\ 3d\ {}^3D_3$		68.97878	81	$2s\ 2p^6\ 4p\ {}^1P_1$	82.67015	82.72356
37	$2s\ 2p^6\ 3d\ {}^1D_2$		69.35794	82	$2s\ 2p^6\ 4d\ {}^3D_1$		83.83876
38	$2s^2\ 2p^5\ 4s\ {}^3P_2$		71.75930	83	$2s\ 2p^6\ 4d\ {}^3D_2$		83.84350
39	$2s^2\ 2p^5\ 4s\ {}^1P_1$	71.86070	71.80538	84	$2s\ 2p^6\ 4d\ {}^3D_3$		83.85244
40	$2s^2\ 2p^5\ 4p\ {}^3S_1$		72.68730	85	$2s\ 2p^6\ 4d\ {}^1D_2$		83.97676
41	$2s^2\ 2p^5\ 4s\ {}^3P_0$		72.69488	86	$2s\ 2p^6\ 4f\ {}^3F_2$		84.41184
42	$2s^2\ 2p^5\ 4s\ {}^3P_1$	72.74645	72.71850	87	$2s\ 2p^6\ 4f\ {}^3F_3$		84.41306
43	$2s^2\ 2p^5\ 4p\ {}^3D_2$		72.74812	88	$2s\ 2p^6\ 4f\ {}^3F_4$		84.41676
44	$2s^2\ 2p^5\ 4p\ {}^3D_3$		72.79862	89	$2s\ 2p^6\ 4f\ {}^1F_3$		84.42732
45	$2s^2\ 2p^5\ 4p\ {}^1P_1$		72.82728				

Table 3.10b. Fe XVII. Effective collision strengths $\Upsilon(i,j)$ as a function of temperature T [K] for excitation from the ground level to the 88 $n = 3$ and 4 levels as specified in Table 3.10a [89Z2].

Levels		T [$\times 10^6$ K]							
i	j	0.1	0.2	0.5	1.0	2.0	5.0	10.0	20.0
1	2	1.72[-3]	1.70[-3]	1.66[-3]	1.60[-3]	1.48[-3]	1.24[-3]	9.87[-4]	7.20[-4]
1	3	1.66[-3]	1.68[-3]	1.75[-3]	1.88[-3]	2.14[-3]	2.90[-3]	4.04[-3]	5.90[-3]
1	4	3.39[-4]	3.36[-4]	3.27[-4]	3.14[-4]	2.92[-4]	2.44[-4]	1.95[-4]	1.42[-4]
1	5	1.53[-3]	1.55[-3]	1.60[-3]	1.70[-3]	1.90[-3]	2.52[-3]	3.46[-3]	5.01[-3]
1	6	4.67[-3]	4.63[-3]	4.50[-3]	4.31[-3]	3.98[-3]	3.29[-3]	2.61[-3]	1.90[-3]
1	7	3.91[-3]	3.89[-3]	3.84[-3]	3.77[-3]	3.66[-3]	3.49[-3]	3.39[-3]	3.38[-3]
1	8	5.02[-3]	4.96[-3]	4.80[-3]	4.56[-3]	4.16[-3]	3.35[-3]	2.59[-3]	1.83[-3]
1	9	1.76[-3]	1.74[-3]	1.68[-3]	1.60[-3]	1.46[-3]	1.17[-3]	9.04[-4]	6.36[-4]
1	10	3.12[-3]	3.12[-3]	3.09[-3]	3.06[-3]	3.03[-3]	2.99[-3]	3.03[-3]	3.17[-3]
1	11	2.83[-3]	2.83[-3]	2.83[-3]	2.84[-3]	2.84[-3]	2.86[-3]	2.88[-3]	2.90[-3]
1	12	1.92[-3]	1.89[-3]	1.83[-3]	1.74[-3]	1.59[-3]	1.28[-3]	9.92[-4]	7.01[-4]
1	13	1.96[-3]	1.93[-3]	1.87[-3]	1.79[-3]	1.64[-3]	1.33[-3]	1.03[-3]	7.32[-4]
1	14	3.70[-3]	3.69[-3]	3.66[-3]	3.62[-3]	3.56[-3]	3.50[-3]	3.52[-3]	3.65[-3]
1	15	4.13[-2]	4.14[-2]	4.17[-2]	4.21[-2]	4.28[-2]	4.43[-2]	4.58[-2]	4.75[-2]
1	16	2.27[-3]	2.24[-3]	2.16[-3]	2.04[-3]	1.85[-3]	1.46[-3]	1.11[-3]	7.75[-4]
1	17	6.70[-3]	6.62[-3]	6.40[-3]	6.08[-3]	5.57[-3]	4.58[-3]	3.71[-3]	2.93[-3]
1	18	8.79[-3]	8.68[-3]	8.36[-3]	7.89[-3]	7.12[-3]	5.63[-3]	4.27[-3]	2.96[-3]
1	19	7.71[-3]	7.60[-3]	7.30[-3]	6.87[-3]	6.17[-3]	4.81[-3]	3.61[-3]	2.47[-3]
1	20	5.23[-3]	5.18[-3]	5.04[-3]	4.84[-3]	4.53[-3]	3.96[-3]	3.52[-3]	3.16[-3]
1	21	3.12[-3]	3.07[-3]	2.94[-3]	2.75[-3]	2.45[-3]	1.88[-3]	1.39[-3]	9.31[-4]
1	22	3.55[-3]	3.52[-3]	3.45[-3]	3.35[-3]	3.20[-3]	2.99[-3]	2.89[-3]	2.88[-3]
1	23	2.20[-2]	2.22[-2]	2.27[-2]	2.35[-2]	2.52[-2]	2.97[-2]	3.59[-2]	4.56[-2]
1	24	3.52[-3]	3.47[-3]	3.33[-3]	3.13[-3]	2.80[-3]	2.17[-3]	1.62[-3]	1.10[-3]
1	25	4.61[-3]	4.54[-3]	4.36[-3]	4.10[-3]	3.68[-3]	2.87[-3]	2.15[-3]	1.47[-3]
1	26	4.23[-3]	4.19[-3]	4.11[-3]	3.98[-3]	3.80[-3]	3.51[-3]	3.33[-3]	3.24[-3]
1	27	8.45[-2]	8.53[-2]	8.76[-2]	9.15[-2]	9.88[-2]	1.18[-1]	1.45[-1]	1.85[-1]
1	28	1.20[-3]	1.19[-3]	1.15[-3]	1.09[-3]	9.89[-4]	7.92[-4]	6.10[-4]	4.32[-4]
1	29	1.53[-2]	1.53[-2]	1.55[-2]	1.57[-2]	1.60[-2]	1.68[-2]	1.77[-2]	1.86[-2]
1	30	2.75[-4]	2.72[-4]	2.65[-4]	2.54[-4]	2.35[-4]	1.95[-4]	1.55[-4]	1.13[-4]
1	31	9.66[-4]	9.65[-4]	9.61[-4]	9.59[-4]	9.65[-4]	1.03[-3]	1.17[-3]	1.48[-3]
1	32	1.35[-3]	1.33[-3]	1.30[-3]	1.25[-3]	1.15[-3]	9.61[-4]	7.66[-4]	5.59[-4]
1	33	1.89[-3]	1.93[-3]	2.05[-3]	2.27[-3]	2.72[-3]	4.05[-3]	6.11[-3]	9.56[-3]
1	34	2.04[-3]	2.01[-3]	1.95[-3]	1.85[-3]	1.68[-3]	1.35[-3]	1.04[-3]	7.34[-4]
1	35	3.41[-3]	3.37[-3]	3.26[-3]	3.09[-3]	2.82[-3]	2.28[-3]	1.77[-3]	1.27[-3]
1	36	4.73[-3]	4.67[-3]	4.52[-3]	4.29[-3]	3.90[-3]	3.13[-3]	2.41[-3]	1.70[-3]
1	37	1.36[-2]	1.37[-2]	1.41[-2]	1.48[-2]	1.60[-2]	1.91[-2]	2.27[-2]	2.74[-2]
1	38	5.11[-4]	5.07[-4]	4.94[-4]	4.74[-4]	4.41[-4]	3.68[-4]	2.94[-4]	2.15[-4]
1	39	2.83[-4]	2.85[-4]	2.91[-4]	3.01[-4]	3.26[-4]	4.10[-4]	5.47[-4]	7.82[-4]
1	40	1.12[-3]	1.11[-3]	1.08[-3]	1.03[-3]	9.53[-4]	7.89[-4]	6.26[-4]	4.55[-4]
1	41	1.02[-4]	1.01[-4]	9.83[-5]	9.44[-5]	8.77[-5]	7.33[-5]	5.86[-5]	4.28[-5]
1	42	3.02[-4]	3.02[-4]	3.03[-4]	3.06[-4]	3.16[-4]	3.55[-4]	4.30[-4]	5.69[-4]
1	43	1.05[-3]	1.04[-3]	1.02[-3]	9.87[-4]	9.35[-4]	8.39[-4]	7.60[-4]	6.98[-4]
1	44	1.63[-3]	1.61[-3]	1.56[-3]	1.48[-3]	1.35[-3]	1.10[-3]	8.50[-4]	6.03[-4]
1	45	5.76[-4]	5.70[-4]	5.51[-4]	5.24[-4]	4.79[-4]	3.87[-4]	2.99[-4]	2.11[-4]
1	46	8.25[-4]	8.19[-4]	8.03[-4]	7.79[-4]	7.42[-4]	6.73[-4]	6.19[-4]	5.83[-4]

Table 3.10b. Fe XVII (continued)

Levels		T [$\times 10^6$ K]							
i	j	0.1	0.2	0.5	1.0	2.0	5.0	10.0	20.0
1	47	4.51[-3]	4.52[-3]	4.55[-3]	4.60[-3]	4.67[-3]	4.84[-3]	5.01[-3]	5.21[-3]
1	48	6.58[-4]	6.51[-4]	6.30[-4]	6.00[-4]	5.49[-4]	4.44[-4]	3.45[-4]	2.45[-4]
1	49	7.08[-4]	7.01[-4]	6.80[-4]	6.49[-4]	5.97[-4]	4.88[-4]	3.82[-4]	2.73[-4]
1	50	1.01[-3]	9.99[-4]	9.78[-4]	9.49[-4]	9.02[-4]	8.14[-4]	7.44[-4]	6.92[-4]
1	51	7.17[-4]	7.08[-4]	6.83[-4]	6.47[-4]	5.87[-4]	4.68[-4]	3.59[-4]	2.51[-4]
1	52	2.02[-3]	2.00[-3]	1.93[-3]	1.84[-3]	1.69[-3]	1.40[-3]	1.14[-3]	9.10[-4]
1	53	2.55[-3]	2.51[-3]	2.42[-3]	2.28[-3]	2.06[-3]	1.62[-3]	1.22[-3]	8.40[-4]
1	54	2.42[-3]	2.39[-3]	2.30[-3]	2.17[-3]	1.97[-3]	1.56[-3]	1.18[-3]	8.22[-4]
1	55	8.46[-3]	8.48[-3]	8.54[-3]	8.63[-3]	8.78[-3]	9.12[-3]	9.48[-3]	9.87[-3]
1	56	1.52[-3]	1.50[-3]	1.45[-3]	1.38[-3]	1.28[-3]	1.09[-3]	9.30[-4]	8.04[-4]
1	57	1.05[-3]	1.04[-3]	9.96[-4]	9.34[-4]	8.34[-4]	6.42[-4]	4.74[-4]	3.19[-4]
1	58	1.10[-3]	1.09[-3]	1.05[-3]	1.00[-3]	9.20[-4]	7.83[-4]	6.83[-4]	6.15[-4]
1	59	1.29[-2]	1.30[-2]	1.33[-2]	1.39[-2]	1.49[-2]	1.74[-2]	2.10[-2]	2.63[-2]
1	60	2.99[-4]	2.94[-4]	2.80[-4]	2.60[-4]	2.30[-4]	1.73[-4]	1.25[-4]	8.23[-5]
1	61	3.54[-4]	3.50[-4]	3.38[-4]	3.22[-4]	2.99[-4]	2.62[-4]	2.40[-4]	2.28[-4]
1	62	5.36[-4]	5.26[-4]	4.99[-4]	4.61[-4]	4.03[-4]	2.99[-4]	2.14[-4]	1.40[-4]
1	63	5.78[-4]	5.75[-4]	5.66[-4]	5.57[-4]	5.47[-4]	5.52[-4]	5.90[-4]	6.68[-4]
1	64	4.22[-4]	4.14[-4]	3.93[-4]	3.64[-4]	3.19[-4]	2.37[-4]	1.70[-4]	1.11[-4]
1	65	5.71[-4]	5.78[-4]	5.98[-4]	6.31[-4]	6.98[-4]	8.78[-4]	1.11[-3]	1.44[-3]
1	66	2.49[-4]	2.44[-4]	2.31[-4]	2.13[-4]	1.84[-4]	1.34[-4]	9.45[-5]	6.06[-5]
1	67	2.77[-4]	2.72[-4]	2.59[-4]	2.41[-4]	2.14[-4]	1.68[-4]	1.34[-4]	1.09[-4]
1	68	1.28[-3]	1.26[-3]	1.21[-3]	1.14[-3]	1.03[-3]	8.04[-4]	6.04[-4]	4.14[-4]
1	69	1.94[-3]	1.91[-3]	1.84[-3]	1.74[-3]	1.57[-3]	1.24[-3]	9.37[-4]	6.48[-4]
1	70	1.33[-3]	1.32[-3]	1.27[-3]	1.22[-3]	1.13[-3]	9.65[-4]	8.40[-4]	7.45[-4]
1	71	1.45[-2]	1.46[-2]	1.50[-2]	1.56[-2]	1.67[-2]	1.96[-2]	2.36[-2]	2.97[-2]
1	72	2.90[-4]	2.85[-4]	2.70[-4]	2.49[-4]	2.17[-4]	1.61[-4]	1.15[-4]	7.48[-5]
1	73	3.17[-4]	3.13[-4]	3.00[-4]	2.82[-4]	2.57[-4]	2.14[-4]	1.83[-4]	1.62[-4]
1	74	4.48[-4]	4.40[-4]	4.19[-4]	3.88[-4]	3.41[-4]	2.54[-4]	1.83[-4]	1.20[-4]
1	75	4.82[-4]	4.84[-4]	4.91[-4]	5.05[-4]	5.37[-4]	6.32[-4]	7.68[-4]	9.63[-4]
1	76	4.51[-4]	4.46[-4]	4.31[-4]	4.08[-4]	3.72[-4]	2.98[-4]	2.30[-4]	1.63[-4]
1	77	3.09[-3]	3.10[-3]	3.14[-3]	3.18[-3]	3.26[-3]	3.45[-3]	3.64[-3]	3.87[-3]
1	78	1.07[-4]	1.06[-4]	1.03[-4]	9.80[-5]	9.03[-5]	7.44[-5]	5.88[-5]	4.25[-5]
1	79	3.90[-4]	3.89[-4]	3.88[-4]	3.87[-4]	3.90[-4]	4.13[-4]	4.68[-4]	5.83[-4]
1	80	5.18[-4]	5.13[-4]	4.98[-4]	4.76[-4]	4.40[-4]	3.63[-4]	2.87[-4]	2.08[-4]
1	81	6.97[-4]	7.10[-4]	7.49[-4]	8.15[-4]	9.48[-4]	1.34[-3]	1.93[-3]	2.91[-3]
1	82	5.95[-4]	5.89[-4]	5.71[-4]	5.44[-4]	5.00[-4]	4.07[-4]	3.18[-4]	2.27[-4]
1	83	9.97[-4]	9.87[-4]	9.58[-4]	9.14[-4]	8.40[-4]	6.88[-4]	5.43[-4]	3.95[-4]
1	84	1.39[-3]	1.37[-3]	1.33[-3]	1.27[-3]	1.16[-3]	9.47[-4]	7.39[-4]	5.27[-4]
1	85	2.81[-3]	2.84[-3]	2.92[-3]	3.05[-3]	3.29[-3]	3.89[-3]	4.62[-3]	5.59[-3]
1	86	2.58[-4]	2.54[-4]	2.43[-4]	2.27[-4]	2.02[-4]	1.55[-4]	1.14[-4]	7.65[-5]
1	87	3.64[-4]	3.59[-4]	3.45[-4]	3.25[-4]	2.94[-4]	2.37[-4]	1.90[-4]	1.48[-4]
1	88	4.63[-4]	4.56[-4]	4.36[-4]	4.08[-4]	3.62[-4]	2.77[-4]	2.04[-4]	1.37[-4]
1	89	4.03[-4]	4.08[-4]	4.22[-4]	4.46[-4]	4.89[-4]	5.97[-4]	7.20[-4]	8.66[-4]

Table 3.11. Fe XVIII. Effective collision strengths Υ as a function of temperature T [K] for the transition between the fine-structure levels $^2P_{3/2}$ and $^2P_{1/2}$ of the ground configuration $2s^2 2p^5$ [98B1]. The observed transition energy is 9.3895 Ry [82C1].

$\log T$	3.0	3.2	3.4	3.6	3.8	4.0	4.2	4.4	4.6	4.8	5.0
Υ	1.09[-1]	1.05[-1]	9.81[-2]	9.69[-2]	1.06[-1]	1.17[-1]	1.19[-1]	1.09[-1]	9.17[-2]	7.32[-2]	5.72[-2]

Table 3.12a. Fe XXI. 20 fine-structure $n = 2$ levels included in the calculation [96Z2] and their calculated and observed energies E [Ry] in rydbergs [85S1]. The index i is used in Table 3.12b for transition keys.

i	Level	E [Ry]		i	Level	E [Ry]	
		obs.	calc.			obs.	calc.
1	$2p^2\ ^3P_0$	0.00000	0.00000	11	$2s\ 2p^3\,(2P)\,^3P^o_1$	8.42813	8.44762
2	$2p^2\ ^3P_1$	0.67297	0.67615	12	$2s\ 2p^3\,(2P)\,^3P^o_2$	8.58705	8.60964
3	$2p^2\ ^3P_2$	1.06940	1.07803	13	$2s\ 2p^3\,(4S)\,^3S^o_1$	9.98384	10.11770
4	$2p^2\ ^1D_2$	2.22859	2.24847	14	$2s\ 2p^3\,(2D)\,^1D^o_2$	10.26816	10.41071
5	$2p^2\ ^1S_0$	3.38900	3.35864	15	$2s\ 2p^3\,(2P)\,^1P^o_1$	11.49108	11.62571
6	$2s\ 2p^3\,(4S)\,^5S^o_2$	4.43742	4.32957	16	$2p^4\ ^3P_2$	15.00219	15.12820
7	$2s\ 2p^3\,(2D)\,^3D^o_1$	7.07854	7.10322	17	$2p^4\ ^3P_0$	15.81686	15.94688
8	$2s\ 2p^3\,(2D)\,^3D^o_2$	7.08373	7.10353	18	$2p^4\ ^3P_1$	15.86060	15.97580
9	$2s\ 2p^3\,(2D)\,^3D^o_3$	7.32595	7.34391	19	$2p^4\ ^1D_2$	16.56046	16.74414
10	$2s\ 2p^3\,(2P)\,^3P^o_0$	8.05367	8.36301	20	$2p^4\ ^1S_0$	18.66457	18.86922

Table 3.12b. Fe XXI. Effective collision strengths $\Upsilon(i,j)$ as a function of temperature T [K] for the transitions between the 20 $n = 2$ levels as specified in Table 3.12a [96Z2].

Levels		T [$\times 10^6$ K]							
i	j	0.05	0.25	0.5	1.25	2.5	5.0	10.0	25.0
1	2	1.87[-2]	1.86[-2]	1.84[-2]	1.75[-2]	1.61[-2]	1.41[-2]	1.14[-2]	7.54[-3]
1	3	1.69[-2]	1.69[-2]	1.68[-2]	1.63[-2]	1.57[-2]	1.47[-2]	1.36[-2]	1.23[-2]
1	4	1.99[-3]	2.92[-3]	3.17[-3]	3.22[-3]	3.03[-3]	2.65[-3]	2.14[-3]	1.40[-3]
1	5	2.33[-4]	4.00[-4]	4.57[-4]	4.78[-4]	4.50[-4]	3.92[-4]	3.12[-4]	1.98[-4]
1	6	2.76[-3]	3.03[-3]	3.11[-3]	3.07[-3]	2.91[-3]	2.62[-3]	2.18[-3]	1.49[-3]
1	7	1.76[-1]	1.76[-1]	1.77[-1]	1.83[-1]	1.91[-1]	2.05[-1]	2.24[-1]	2.58[-1]
1	8	2.62[-3]	2.68[-3]	2.68[-3]	2.60[-3]	2.45[-3]	2.19[-3]	1.82[-3]	1.25[-3]
1	10	7.81[-5]	7.89[-5]	7.85[-5]	7.55[-5]	7.06[-5]	6.27[-5]	5.16[-5]	3.48[-5]
1	11	3.50[-2]	3.52[-2]	3.55[-2]	3.67[-2]	3.83[-2]	4.10[-2]	4.50[-2]	5.19[-2]
1	12	4.95[-4]	5.00[-4]	4.97[-4]	4.80[-4]	4.51[-4]	4.02[-4]	3.34[-4]	2.28[-4]
1	13	4.59[-2]	4.62[-2]	4.67[-2]	4.81[-2]	5.01[-2]	5.35[-2]	5.85[-2]	6.75[-2]
1	14	6.23[-4]	6.23[-4]	6.17[-4]	5.93[-4]	5.57[-4]	4.97[-4]	4.14[-4]	2.83[-4]
1	15	1.46[-4]	1.46[-4]	1.45[-4]	1.43[-4]	1.40[-4]	1.37[-4]	1.32[-4]	1.27[-4]
1	16	2.62[-4]	2.62[-4]	2.61[-4]	2.60[-4]	2.59[-4]	2.58[-4]	2.60[-4]	2.69[-4]
1	17	1.16[-4]	1.13[-4]	1.12[-4]	1.09[-4]	1.06[-4]	1.02[-4]	9.64[-5]	8.94[-5]
1	18	6.31[-6]	6.21[-6]	6.08[-6]	5.70[-6]	5.19[-6]	4.43[-6]	3.47[-6]	2.18[-6]
1	19	2.49[-5]	2.45[-5]	2.40[-5]	2.25[-5]	2.05[-5]	1.75[-5]	1.37[-5]	8.66[-6]

Table 3.12b. Fe XXI (continued)

Levels		T [$\times 10^6$ K]							
i	j	0.05	0.25	0.5	1.25	2.5	5.0	10.0	25.0
1	20	6.51[-6]	6.20[-6]	5.98[-6]	5.66[-6]	5.35[-6]	4.92[-6]	4.38[-6]	3.68[-6]
2	3	5.09[-2]	5.09[-2]	5.05[-2]	4.86[-2]	4.56[-2]	4.12[-2]	3.56[-2]	2.79[-2]
2	4	2.94[-2]	2.93[-2]	2.90[-2]	2.76[-2]	2.57[-2]	2.27[-2]	1.89[-2]	1.36[-2]
2	5	3.39[-3]	4.28[-3]	4.51[-3]	4.48[-3]	4.17[-3]	3.62[-3]	2.88[-3]	1.85[-3]
2	6	1.32[-2]	1.36[-2]	1.38[-2]	1.40[-2]	1.39[-2]	1.38[-2]	1.36[-2]	1.34[-2]
2	7	2.08[-2]	2.05[-2]	2.06[-2]	2.10[-2]	2.16[-2]	2.26[-2]	2.40[-2]	2.64[-2]
2	8	3.45[-1]	3.38[-1]	3.38[-1]	3.48[-1]	3.65[-1]	3.91[-1]	4.29[-1]	4.91[-1]
2	9	2.52[-3]	2.60[-3]	2.61[-3]	2.54[-3]	2.40[-3]	2.15[-3]	1.79[-3]	1.22[-3]
2	10	8.69[-2]	8.70[-2]	8.78[-2]	9.06[-2]	9.47[-2]	1.01[-1]	1.11[-1]	1.28[-1]
2	11	1.76[-1]	1.77[-1]	1.78[-1]	1.84[-1]	1.92[-1]	2.06[-1]	2.26[-1]	2.60[-1]
2	12	8.39[-3]	8.42[-3]	8.49[-3]	8.68[-3]	8.94[-3]	9.37[-3]	1.00[-2]	1.12[-2]
2	13	1.54[-1]	1.55[-1]	1.56[-1]	1.61[-1]	1.68[-1]	1.79[-1]	1.96[-1]	2.25[-1]
2	14	6.39[-3]	6.43[-3]	6.44[-3]	6.43[-3]	6.40[-3]	6.35[-3]	6.31[-3]	6.32[-3]
2	15	1.85[-2]	1.86[-2]	1.88[-2]	1.93[-2]	2.00[-2]	2.13[-2]	2.32[-2]	2.66[-2]
2	16	5.56[-4]	5.55[-4]	5.55[-4]	5.54[-4]	5.55[-4]	5.58[-4]	5.67[-4]	5.95[-4]
2	17	4.56[-5]	4.49[-5]	4.40[-5]	4.13[-5]	3.75[-5]	3.20[-5]	2.51[-5]	1.57[-5]
2	18	4.84[-4]	4.83[-4]	4.81[-4]	4.76[-4]	4.69[-4]	4.60[-4]	4.50[-4]	4.42[-4]
2	19	1.82[-4]	1.80[-4]	1.77[-4]	1.69[-4]	1.58[-4]	1.42[-4]	1.22[-4]	9.73[-5]
2	20	1.74[-5]	1.72[-5]	1.68[-5]	1.57[-5]	1.43[-5]	1.22[-5]	9.60[-6]	6.03[-6]
3	4	6.50[-2]	6.48[-2]	6.42[-2]	6.19[-2]	5.84[-2]	5.31[-2]	4.66[-2]	3.78[-2]
3	5	5.85[-3]	7.50[-3]	7.94[-3]	8.00[-3]	7.65[-3]	6.99[-3]	6.13[-3]	5.01[-3]
3	6	1.71[-2]	1.79[-2]	1.82[-2]	1.84[-2]	1.84[-2]	1.83[-2]	1.81[-2]	1.79[-2]
3	7	2.83[-3]	2.84[-3]	2.85[-3]	2.86[-3]	2.88[-3]	2.89[-3]	2.91[-3]	2.96[-3]
3	8	4.82[-3]	5.01[-3]	5.05[-3]	4.95[-3]	4.69[-3]	4.25[-3]	3.61[-3]	2.61[-3]
3	9	3.57[-1]	3.50[-1]	3.51[-1]	3.60[-1]	3.76[-1]	4.02[-1]	4.39[-1]	5.00[-1]
3	10	1.15[-3]	1.18[-3]	1.18[-3]	1.14[-3]	1.07[-3]	9.55[-4]	7.92[-4]	5.39[-4]
3	11	4.34[-2]	4.34[-2]	4.38[-2]	4.51[-2]	4.69[-2]	4.98[-2]	5.41[-2]	6.15[-2]
3	12	4.21[-1]	4.21[-1]	4.25[-1]	4.39[-1]	4.59[-1]	4.91[-1]	5.38[-1]	6.20[-1]
3	13	4.16[-1]	4.18[-1]	4.23[-1]	4.36[-1]	4.55[-1]	4.87[-1]	5.34[-1]	6.16[-1]
3	14	8.94[-2]	9.00[-2]	9.09[-2]	9.34[-2]	9.70[-2]	1.03[-1]	1.12[-1]	1.28[-1]
3	15	3.77[-3]	3.77[-3]	3.75[-3]	3.67[-3]	3.55[-3]	3.36[-3]	3.10[-3]	2.73[-3]
3	16	1.02[-3]	1.03[-3]	1.03[-3]	1.02[-3]	1.01[-3]	9.89[-4]	9.74[-4]	9.69[-4]
3	17	1.79[-4]	1.80[-4]	1.81[-4]	1.86[-4]	1.93[-4]	2.04[-4]	2.21[-4]	2.51[-4]
3	18	3.67[-4]	3.68[-4]	3.69[-4]	3.73[-4]	3.80[-4]	3.92[-4]	4.12[-4]	4.51[-4]
3	19	6.61[-4]	6.53[-4]	6.44[-4]	6.24[-4]	5.99[-4]	5.63[-4]	5.20[-4]	4.66[-4]
3	20	4.77[-5]	4.70[-5]	4.61[-5]	4.35[-5]	4.00[-5]	3.49[-5]	2.85[-5]	2.00[-5]
4	5	2.03[-2]	2.12[-2]	2.14[-2]	2.15[-2]	2.15[-2]	2.16[-2]	2.20[-2]	2.33[-2]
4	6	2.59[-3]	2.81[-3]	2.89[-3]	2.95[-3]	2.97[-3]	2.97[-3]	2.95[-3]	2.91[-3]
4	7	1.45[-2]	1.45[-2]	1.45[-2]	1.47[-2]	1.49[-2]	1.52[-2]	1.56[-2]	1.64[-2]
4	8	1.01[-2]	1.05[-2]	1.06[-2]	1.06[-2]	1.03[-2]	9.84[-3]	9.11[-3]	7.99[-3]
4	9	1.15[-1]	1.12[-1]	1.12[-1]	1.14[-1]	1.18[-1]	1.25[-1]	1.36[-1]	1.53[-1]
4	10	2.62[-4]	2.73[-4]	2.76[-4]	2.69[-4]	2.53[-4]	2.26[-4]	1.88[-4]	1.28[-4]
4	11	9.88[-3]	9.83[-3]	9.86[-3]	1.00[-2]	1.02[-2]	1.05[-2]	1.09[-2]	1.15[-2]

Table 3.12b. Fe XXI (continued)

Levels		T [$\times 10^6$ K]							
i	j	0.05	0.25	0.5	1.25	2.5	5.0	10.0	25.0
4	12	1.72[-2]	1.73[-2]	1.74[-2]	1.74[-2]	1.73[-2]	1.71[-2]	1.68[-2]	1.63[-2]
4	13	3.51[-3]	3.53[-3]	3.55[-3]	3.62[-3]	3.71[-3]	3.86[-3]	4.09[-3]	4.49[-3]
4	14	7.30[-1]	7.32[-1]	7.40[-1]	7.63[-1]	7.97[-1]	8.54[-1]	9.36[-1]	1.08
4	15	4.05[-1]	4.08[-1]	4.12[-1]	4.25[-1]	4.44[-1]	4.74[-1]	5.20[-1]	6.00[-1]
4	16	5.77[-4]	5.86[-4]	5.88[-4]	5.78[-4]	5.56[-4]	5.21[-4]	4.77[-4]	4.16[-4]
4	17	6.96[-5]	6.86[-5]	6.73[-5]	6.34[-5]	5.80[-5]	5.02[-5]	4.04[-5]	2.73[-5]
4	18	3.74[-4]	3.71[-4]	3.66[-4]	3.53[-4]	3.35[-4]	3.10[-4]	2.80[-4]	2.43[-4]
4	19	1.40[-3]	1.41[-3]	1.42[-3]	1.44[-3]	1.47[-3]	1.52[-3]	1.60[-3]	1.75[-3]
4	20	1.89[-4]	1.90[-4]	1.90[-4]	1.91[-4]	1.94[-4]	1.99[-4]	2.07[-4]	2.24[-4]
5	6	2.17[-5]	2.17[-5]	2.15[-5]	2.07[-5]	1.93[-5]	1.72[-5]	1.42[-5]	9.55[-6]
5	7	6.48[-3]	6.11[-3]	6.04[-3]	6.15[-3]	6.43[-3]	6.91[-3]	7.63[-3]	8.83[-3]
5	8	1.87[-4]	2.09[-4]	2.15[-4]	2.14[-4]	2.04[-4]	1.84[-4]	1.53[-4]	1.06[-4]
5	10	1.28[-3]	1.37[-3]	1.39[-3]	1.36[-3]	1.29[-3]	1.16[-3]	9.69[-4]	6.66[-4]
5	11	1.02[-2]	1.01[-2]	1.02[-2]	1.03[-2]	1.05[-2]	1.07[-2]	1.11[-2]	1.18[-2]
5	12	3.32[-3]	3.51[-3]	3.56[-3]	3.49[-3]	3.30[-3]	2.96[-3]	2.47[-3]	1.70[-3]
5	13	1.25[-2]	1.23[-2]	1.23[-2]	1.27[-2]	1.32[-2]	1.41[-2]	1.54[-2]	1.76[-2]
5	14	7.60[-4]	7.79[-4]	7.81[-4]	7.59[-4]	7.15[-4]	6.40[-4]	5.33[-4]	3.66[-4]
5	15	1.61[-1]	1.62[-1]	1.63[-1]	1.68[-1]	1.76[-1]	1.88[-1]	2.07[-1]	2.38[-1]
5	16	2.02[-5]	2.00[-5]	1.96[-5]	1.84[-5]	1.68[-5]	1.44[-5]	1.14[-5]	7.37[-6]
5	17	5.11[-5]	5.14[-5]	5.12[-5]	4.97[-5]	4.71[-5]	4.30[-5]	3.80[-5]	3.10[-5]
5	18	5.71[-5]	5.64[-5]	5.52[-5]	5.18[-5]	4.71[-5]	4.02[-5]	3.15[-5]	1.97[-5]
5	19	1.87[-4]	1.87[-4]	1.88[-4]	1.91[-4]	1.96[-4]	2.04[-4]	2.17[-4]	2.40[-4]
5	20	2.81[-4]	2.87[-4]	2.90[-4]	2.91[-4]	2.89[-4]	2.85[-4]	2.80[-4]	2.71[-4]
6	7	1.33[-2]	1.62[-2]	1.69[-2]	1.68[-2]	1.57[-2]	1.38[-2]	1.11[-2]	7.36[-3]
6	8	1.95[-2]	2.54[-2]	2.70[-2]	2.72[-2]	2.56[-2]	2.25[-2]	1.84[-2]	1.25[-2]
6	9	2.50[-2]	3.38[-2]	3.65[-2]	3.72[-2]	3.52[-2]	3.12[-2]	2.57[-2]	1.76[-2]
6	10	3.19[-3]	3.44[-3]	3.48[-3]	3.34[-3]	3.06[-3]	2.62[-3]	2.05[-3]	1.29[-3]
6	11	1.01[-2]	1.09[-2]	1.10[-2]	1.05[-2]	9.68[-3]	8.30[-3]	6.55[-3]	4.15[-3]
6	12	1.55[-2]	1.69[-2]	1.72[-2]	1.66[-2]	1.53[-2]	1.31[-2]	1.04[-2]	6.61[-3]
6	13	1.44[-3]	1.48[-3]	1.48[-3]	1.42[-3]	1.32[-3]	1.16[-3]	9.52[-4]	6.47[-4]
6	14	3.14[-4]	3.24[-4]	3.24[-4]	3.08[-4]	2.82[-4]	2.41[-4]	1.89[-4]	1.19[-4]
6	15	1.12[-4]	1.13[-4]	1.11[-4]	1.06[-4]	9.86[-5]	8.67[-5]	7.13[-5]	4.88[-5]
6	16	1.91[-2]	1.91[-2]	1.91[-2]	1.89[-2]	1.87[-2]	1.83[-2]	1.79[-2]	1.74[-2]
6	17	1.80[-3]	1.79[-3]	1.77[-3]	1.69[-3]	1.58[-3]	1.41[-3]	1.17[-3]	7.92[-4]
6	18	5.70[-3]	5.67[-3]	5.61[-3]	5.43[-3]	5.16[-3]	4.73[-3]	4.14[-3]	3.25[-3]
6	19	5.27[-4]	5.24[-4]	5.20[-4]	5.10[-4]	4.96[-4]	4.75[-4]	4.47[-4]	4.11[-4]
6	20	2.35[-5]	2.32[-5]	2.28[-5]	2.18[-5]	2.04[-5]	1.81[-5]	1.51[-5]	1.03[-5]
7	8	3.79[-2]	3.77[-2]	3.73[-2]	3.54[-2]	3.26[-2]	2.84[-2]	2.29[-2]	1.52[-2]
7	9	9.54[-3]	9.52[-3]	9.43[-3]	9.12[-3]	8.67[-3]	8.00[-3]	7.19[-3]	6.13[-3]
7	10	3.01[-3]	3.00[-3]	2.96[-3]	2.81[-3]	2.58[-3]	2.24[-3]	1.79[-3]	1.17[-3]
7	11	1.02[-2]	1.81[-2]	2.02[-2]	2.14[-2]	2.13[-2]	2.06[-2]	1.96[-2]	1.84[-2]
7	12	7.13[-3]	1.15[-2]	1.27[-2]	1.35[-2]	1.34[-2]	1.30[-2]	1.25[-2]	1.19[-2]
7	13	4.20[-3]	5.01[-3]	5.23[-3]	5.22[-3]	4.95[-3]	4.46[-3]	3.81[-3]	2.90[-3]

Table 3.12b. Fe XXI (continued)

Levels		T [$\times 10^6$ K]							
i	j	0.05	0.25	0.5	1.25	2.5	5.0	10.0	25.0
7	14	6.11[-3]	7.92[-3]	8.48[-3]	8.55[-3]	8.05[-3]	7.10[-3]	5.78[-3]	3.85[-3]
7	15	1.66[-3]	1.97[-3]	2.06[-3]	2.03[-3]	1.89[-3]	1.63[-3]	1.30[-3]	8.25[-4]
7	16	6.25[-2]	6.27[-2]	6.33[-2]	6.51[-2]	6.76[-2]	7.18[-2]	7.79[-2]	8.85[-2]
7	17	8.74[-2]	8.79[-2]	8.89[-2]	9.16[-2]	9.56[-2]	1.02[-1]	1.12[-1]	1.29[-1]
7	18	1.08[-1]	1.09[-1]	1.10[-1]	1.13[-1]	1.18[-1]	1.26[-1]	1.38[-1]	1.59[-1]
7	19	2.91[-3]	2.92[-3]	2.89[-3]	2.79[-3]	2.62[-3]	2.35[-3]	1.97[-3]	1.38[-3]
7	20	2.20[-4]	2.21[-4]	2.22[-4]	2.25[-4]	2.30[-4]	2.39[-4]	2.53[-4]	2.80[-4]
8	9	5.42[-2]	5.41[-2]	5.36[-2]	5.15[-2]	4.81[-2]	4.30[-2]	3.66[-2]	2.78[-2]
8	10	1.53[-2]	1.65[-2]	1.68[-2]	1.70[-2]	1.69[-2]	1.70[-2]	1.72[-2]	1.79[-2]
8	11	3.67[-3]	6.30[-3]	7.03[-3]	7.45[-3]	7.44[-3]	7.26[-3]	7.00[-3]	6.73[-3]
8	12	1.06[-2]	1.95[-2]	2.20[-2]	2.34[-2]	2.32[-2]	2.21[-2]	2.07[-2]	1.89[-2]
8	13	4.83[-3]	6.28[-3]	6.71[-3]	6.75[-3]	6.34[-3]	5.58[-3]	4.54[-3]	3.05[-3]
8	14	1.41[-2]	1.66[-2]	1.73[-2]	1.72[-2]	1.62[-2]	1.44[-2]	1.20[-2]	8.47[-3]
8	15	3.93[-3]	4.15[-3]	4.16[-3]	3.99[-3]	3.67[-3]	3.16[-3]	2.51[-3]	1.61[-3]
8	16	2.38[-1]	2.39[-1]	2.41[-1]	2.49[-1]	2.59[-1]	2.77[-1]	3.02[-1]	3.47[-1]
8	17	8.21[-4]	8.28[-4]	8.22[-4]	7.92[-4]	7.42[-4]	6.60[-4]	5.46[-4]	3.70[-4]
8	18	1.60[-1]	1.61[-1]	1.63[-1]	1.68[-1]	1.75[-1]	1.87[-1]	2.04[-1]	2.35[-1]
8	19	1.24[-2]	1.25[-2]	1.25[-2]	1.25[-2]	1.24[-2]	1.24[-2]	1.23[-2]	1.25[-2]
8	20	2.09[-4]	2.07[-4]	2.03[-4]	1.95[-4]	1.82[-4]	1.61[-4]	1.33[-4]	9.03[-5]
9	11	2.07[-2]	2.34[-2]	2.41[-2]	2.44[-2]	2.44[-2]	2.44[-2]	2.47[-2]	2.57[-2]
9	12	3.30[-2]	4.55[-2]	4.88[-2]	5.07[-2]	5.06[-2]	4.98[-2]	4.90[-2]	4.87[-2]
9	13	7.27[-3]	8.69[-3]	9.04[-3]	8.96[-3]	8.42[-3]	7.47[-3]	6.21[-3]	4.43[-3]
9	14	2.50[-2]	2.90[-2]	3.01[-2]	2.98[-2]	2.81[-2]	2.51[-2]	2.10[-2]	1.53[-2]
9	15	6.37[-3]	6.77[-3]	6.81[-3]	6.53[-3]	6.00[-3]	5.15[-3]	4.08[-3]	2.61[-3]
9	16	5.55[-1]	5.56[-1]	5.61[-1]	5.79[-1]	6.04[-1]	6.47[-1]	7.08[-1]	8.15[-1]
9	18	2.03[-3]	2.05[-3]	2.04[-3]	1.97[-3]	1.85[-3]	1.65[-3]	1.37[-3]	9.29[-4]
9	19	6.68[-2]	6.72[-2]	6.77[-2]	6.89[-2]	7.06[-2]	7.34[-2]	7.76[-2]	8.54[-2]
10	11	1.48[-2]	1.48[-2]	1.46[-2]	1.39[-2]	1.28[-2]	1.12[-2]	9.03[-3]	5.97[-3]
10	12	6.89[-3]	6.88[-3]	6.82[-3]	6.64[-3]	6.37[-3]	6.00[-3]	5.56[-3]	5.05[-3]
10	13	1.91[-3]	1.91[-3]	1.89[-3]	1.80[-3]	1.65[-3]	1.43[-3]	1.14[-3]	7.37[-4]
10	14	8.51[-4]	1.52[-3]	1.71[-3]	1.76[-3]	1.66[-3]	1.45[-3]	1.15[-3]	7.48[-4]
10	15	1.34[-3]	2.00[-3]	2.22[-3]	2.30[-3]	2.18[-3]	1.93[-3]	1.57[-3]	1.04[-3]
10	16	1.60[-4]	1.65[-4]	1.66[-4]	1.61[-4]	1.52[-4]	1.36[-4]	1.13[-4]	7.76[-5]
10	17	8.53[-4]	8.68[-4]	8.67[-4]	8.40[-4]	7.90[-4]	7.06[-4]	5.87[-4]	4.02[-4]
10	18	5.94[-2]	5.94[-2]	6.00[-2]	6.19[-2]	6.46[-2]	6.92[-2]	7.59[-2]	8.73[-2]
10	19	1.70[-3]	1.72[-3]	1.71[-3]	1.66[-3]	1.56[-3]	1.39[-3]	1.16[-3]	7.92[-4]
10	20	2.78[-4]	2.77[-4]	2.73[-4]	2.62[-4]	2.44[-4]	2.17[-4]	1.78[-4]	1.20[-4]
11	12	2.98[-2]	2.97[-2]	2.93[-2]	2.79[-2]	2.57[-2]	2.23[-2]	1.80[-2]	1.18[-2]
11	13	3.46[-3]	3.46[-3]	3.44[-3]	3.28[-3]	3.01[-3]	2.62[-3]	2.11[-3]	1.38[-3]
11	14	8.53[-3]	8.51[-3]	8.40[-3]	7.95[-3]	7.26[-3]	6.24[-3]	4.95[-3]	3.17[-3]
11	15	6.69[-3]	8.12[-3]	8.52[-3]	8.48[-3]	7.97[-3]	7.05[-3]	5.82[-3]	4.06[-3]
11	16	1.19[-1]	1.17[-1]	1.17[-1]	1.21[-1]	1.26[-1]	1.36[-1]	1.49[-1]	1.71[-1]

Table 3.12b. Fe XXI (continued)

Levels		T [$\times 10^6$ K]							
i	j	0.05	0.25	0.5	1.25	2.5	5.0	10.0	25.0
11	17	8.31[-2]	8.31[-2]	8.38[-2]	8.64[-2]	9.03[-2]	9.66[-2]	1.06[-1]	1.22[-1]
11	18	4.64[-3]	4.70[-3]	4.71[-3]	4.64[-3]	4.51[-3]	4.28[-3]	3.97[-3]	3.50[-3]
11	19	2.20[-2]	2.22[-2]	2.23[-2]	2.28[-2]	2.34[-2]	2.43[-2]	2.58[-2]	2.83[-2]
11	20	6.83[-3]	6.87[-3]	6.93[-3]	7.06[-3]	7.25[-3]	7.57[-3]	8.07[-3]	8.99[-3]
12	13	6.61[-3]	6.60[-3]	6.52[-3]	6.20[-3]	5.70[-3]	4.96[-3]	4.00[-3]	2.68[-3]
12	14	1.78[-2]	1.78[-2]	1.76[-2]	1.67[-2]	1.53[-2]	1.33[-2]	1.08[-2]	7.24[-3]
12	15	1.32[-2]	1.52[-2]	1.57[-2]	1.54[-2]	1.45[-2]	1.29[-2]	1.09[-2]	7.95[-3]
12	16	1.29[-1]	1.26[-1]	1.26[-1]	1.30[-1]	1.36[-1]	1.45[-1]	1.59[-1]	1.80[-1]
12	17	2.76[-4]	2.81[-4]	2.81[-4]	2.73[-4]	2.57[-4]	2.30[-4]	1.92[-4]	1.32[-4]
12	18	2.25[-1]	2.24[-1]	2.26[-1]	2.33[-1]	2.44[-1]	2.61[-1]	2.86[-1]	3.29[-1]
12	19	4.44[-2]	4.46[-2]	4.50[-2]	4.60[-2]	4.74[-2]	4.96[-2]	5.29[-2]	5.88[-2]
12	20	3.54[-3]	3.54[-3]	3.50[-3]	3.36[-3]	3.14[-3]	2.80[-3]	2.31[-3]	1.57[-3]
13	14	3.39[-2]	3.39[-2]	3.36[-2]	3.24[-2]	3.05[-2]	2.78[-2]	2.44[-2]	1.99[-2]
13	15	1.55[-2]	1.55[-2]	1.53[-2]	1.45[-2]	1.33[-2]	1.15[-2]	9.20[-3]	5.96[-3]
13	16	5.25[-1]	5.06[-1]	5.04[-1]	5.17[-1]	5.41[-1]	5.81[-1]	6.40[-1]	7.37[-1]
13	17	1.76[-1]	1.72[-1]	1.71[-1]	1.76[-1]	1.85[-1]	1.99[-1]	2.18[-1]	2.51[-1]
13	18	3.91[-1]	3.81[-1]	3.80[-1]	3.91[-1]	4.10[-1]	4.40[-1]	4.84[-1]	5.55[-1]
13	19	1.25[-3]	1.27[-3]	1.27[-3]	1.26[-3]	1.24[-3]	1.19[-3]	1.11[-3]	1.01[-3]
13	20	1.47[-2]	1.48[-2]	1.50[-2]	1.55[-2]	1.61[-2]	1.73[-2]	1.89[-2]	2.18[-2]
14	15	4.39[-2]	4.59[-2]	4.64[-2]	4.66[-2]	4.67[-2]	4.70[-2]	4.79[-2]	5.03[-2]
14	16	7.70[-2]	7.43[-2]	7.39[-2]	7.56[-2]	7.89[-2]	8.43[-2]	9.23[-2]	1.06[-1]
14	17	9.55[-4]	1.01[-3]	1.02[-3]	1.00[-3]	9.45[-4]	8.46[-4]	7.03[-4]	4.80[-4]
14	18	1.43[-2]	1.41[-2]	1.41[-2]	1.44[-2]	1.47[-2]	1.52[-2]	1.60[-2]	1.73[-2]
14	19	1.29	1.26	1.27	1.30	1.36	1.47	1.61	1.85
14	20	7.70[-4]	7.78[-4]	7.74[-4]	7.47[-4]	7.00[-4]	6.24[-4]	5.16[-4]	3.51[-4]
15	16	2.86[-2]	2.70[-2]	2.67[-2]	2.72[-2]	2.83[-2]	3.02[-2]	3.32[-2]	3.81[-2]
15	17	9.24[-4]	1.00[-3]	1.03[-3]	1.02[-3]	9.79[-4]	8.98[-4]	7.80[-4]	5.94[-4]
15	18	5.48[-2]	5.25[-2]	5.22[-2]	5.33[-2]	5.55[-2]	5.94[-2]	6.50[-2]	7.44[-2]
15	19	3.63[-1]	3.51[-1]	3.49[-1]	3.58[-1]	3.75[-1]	4.03[-1]	4.44[-1]	5.11[-1]
15	20	3.75[-1]	3.74[-1]	3.77[-1]	3.89[-1]	4.07[-1]	4.36[-1]	4.79[-1]	5.52[-1]
16	17	1.26[-2]	1.25[-2]	1.25[-2]	1.22[-2]	1.18[-2]	1.12[-2]	1.07[-2]	1.01[-2]
16	18	4.22[-2]	4.21[-2]	4.17[-2]	4.03[-2]	3.81[-2]	3.49[-2]	3.09[-2]	2.56[-2]
16	19	5.02[-2]	5.00[-2]	4.95[-2]	4.74[-2]	4.42[-2]	3.94[-2]	3.34[-2]	2.52[-2]
16	20	3.76[-3]	4.10[-3]	4.15[-3]	4.02[-3]	3.72[-3]	3.24[-3]	2.63[-3]	1.82[-3]
17	18	1.63[-2]	1.62[-2]	1.60[-2]	1.53[-2]	1.41[-2]	1.23[-2]	1.00[-2]	6.67[-3]
17	19	1.18[-2]	1.18[-2]	1.17[-2]	1.11[-2]	1.03[-2]	9.09[-3]	7.52[-3]	5.32[-3]
17	20	1.48[-3]	1.48[-3]	1.46[-3]	1.38[-3]	1.26[-3]	1.07[-3]	8.41[-4]	5.26[-4]
18	19	3.81[-2]	3.81[-2]	3.77[-2]	3.60[-2]	3.32[-2]	2.90[-2]	2.36[-2]	1.59[-2]
18	20	5.36[-3]	6.49[-3]	6.76[-3]	6.67[-3]	6.19[-3]	5.35[-3]	4.25[-3]	2.71[-3]

Table 3.12b. Fe XXI (continued)

Levels		T [$\times 10^6$ K]							
i	j	0.05	0.25	0.5	1.25	2.5	5.0	10.0	25.0
19	20	2.27[-2]	2.24[-2]	2.22[-2]	2.21[-2]	2.22[-2]	2.25[-2]	2.31[-2]	2.47[-2]

Table 3.13a. Fe XXII. 45 fine-structure $n = 2$ and $n = 3$ levels included in the calculation [97Z1] and their calculated and observed energies E [Ry] in rydbergs [85S1]. The index i is used in Table 3.13b for transition keys.

i	Level	E [Ry]		i	Level	E [Ry]	
		obs.	calc.			obs.	calc.
1	$2s^2 2p\ ^2P^o_{1/2}$	0.00000	0.00000	24	$2s2p(^3P)3s\ ^2P^o_{1/2}$		78.37193
2	$2s^2 2p\ ^2P^o_{3/2}$	1.07776	1.05629	25	$2s2p(^3P)3p\ ^4D_{1/2}$		78.83664
3	$2s\ 2p^2\ ^4P_{1/2}$	3.68653	3.63439	26	$2s2p(^3P)3p\ ^4D_{3/2}$		79.07484
4	$2s\ 2p^2\ ^4P_{3/2}$	4.19365	4.13075	27	$2s2p(^3P)3s\ ^2P^o_{3/2}$		79.11491
5	$2s\ 2p^2\ ^4P_{5/2}$	4.67717	4.64059	28	$2s2p(^3P)3p\ ^4D_{5/2}$		79.52481
6	$2s\ 2p^2\ ^2D_{3/2}$	6.71166	6.73858	29	$2s2p(^3P)3p\ ^2P_{1/2}$	78.22317	79.52855
7	$2s\ 2p^2\ ^2D_{5/2}$	6.92217	6.94497	30	$2s2p(^3P)3p\ ^2P_{3/2}$	79.17089	79.41152
8	$2s\ 2p^2\ ^2P_{1/2}$	7.77748	7.82265	31	$2s2p(^3P)3p\ ^4P_{1/2}$		79.79154
9	$2s\ 2p^2\ ^2S_{1/2}$	8.91420	8.93489	32	$2s2p(^3P)3p\ ^2D_{3/2}$	79.64474	79.90941
10	$2s\ 2p^2\ ^2P_{3/2}$	9.04241	9.09880	33	$2s2p(^3P)3p\ ^4D_{7/2}$		80.16203
11	$2p^3\ ^4S^o_{3/2}$	11.44278	11.43474	34	$2s2p(^3P)3p\ ^4P_{3/2}$		80.27484
12	$2p^3\ ^2D^o_{3/2}$	12.72512	12.77092	35	$2s2p(^3P)3p\ ^4S_{3/2}$		80.39784
13	$2p^3\ ^2D^o_{5/2}$	13.00269	13.07500	36	$2s2p(^3P)3p\ ^4P_{5/2}$		80.44491
14	$2p^3\ ^2P^o_{1/2}$	14.30352	14.37056	37	$2s2p(^3P)3p\ ^2D_{5/2}$	80.60158	80.87084
15	$2p^3\ ^2P^o_{3/2}$	14.83288	14.88660	38	$2s2p(^3P)3p\ ^2S_{1/2}$		81.14805
16	$2s^2 3s\ ^2S_{1/2}$		74.08994	39	$2s2p(^1P)3s\ ^2P^o_{1/2}$		81.18313
17	$2s^2 3p\ ^2P^o_{1/2}$		75.74732	40	$2s2p(^1P)3s\ ^2P^o_{3/2}$		81.21893
18	$2s^2 3p\ ^2P^o_{3/2}$		76.01977	41	$2s2p(^1P)3p\ ^2P_{1/2}$		82.82656
19	$2s2p(^3P)3s\ ^4P^o_{1/2}$		77.41721	42	$2s2p(^1P)3p\ ^2D_{3/2}$		82.83533
20	$2s^2 3d\ ^2D_{3/2}$	77.43948	77.57156	43	$2s2p(^1P)3p\ ^2D_{5/2}$		83.03150
21	$2s^2 3d\ ^2D_{5/2}$	77.52149	77.65898	44	$2s2p(^1P)3p\ ^2P_{3/2}$		83.11559
22	$2s2p(^3P)3s\ ^4P^o_{3/2}$		77.69215	45	$2s2p(^1P)3p\ ^2S_{1/2}$		83.47909
23	$2s2p(^3P)3s\ ^4P^o_{5/2}$		78.31381				

Table 3.13b. Fe XXII. Effective collision strengths $\Upsilon(i,j)$ as a function of temperature T [K] for the transitions between the 15 $n = 2$ levels and the transitions between the five $n = 2$ levels and the 30 $n = 3$ levels, i = 16-45 as specified in Table 3.13a [97Z1]. The temperatures are in z^2K, where $z = 21$ is the ion charge.

Levels		$T\,[z^2\mathrm{K}]$							
i	j	100	500	1000	2500	5000	10000	20000	50000
1	2	1.35[-1]	1.47[-1]	1.51[-1]	1.17[-1]	8.89[-2]	6.94[-2]	5.38[-2]	3.62[-2]
1	3	1.46[-2]	1.37[-2]	1.23[-2]	1.13[-2]	1.18[-2]	1.24[-2]	1.27[-2]	1.25[-2]
2	3	9.10[-3]	9.58[-3]	8.11[-3]	6.69[-3]	6.74[-3]	7.09[-3]	7.17[-3]	6.86[-3]
1	4	1.63[-2]	1.59[-2]	1.31[-2]	9.82[-3]	9.00[-3]	8.47[-3]	7.14[-3]	4.74[-3]
2	4	1.92[-2]	2.30[-2]	1.94[-2]	1.48[-2]	1.37[-2]	1.30[-2]	1.16[-2]	8.98[-3]
3	4	1.06[-1]	7.19[-2]	6.31[-2]	5.13[-2]	4.62[-2]	4.01[-2]	3.18[-2]	2.08[-2]
1	5	1.45[-2]	1.57[-2]	1.29[-2]	9.28[-3]	7.99[-3]	7.01[-3]	5.62[-3]	3.59[-3]
2	5	4.39[-2]	4.68[-2]	4.05[-2]	3.46[-2]	3.46[-2]	3.59[-2]	3.62[-2]	3.48[-2]
3	5	9.29[-2]	6.10[-2]	5.31[-2]	4.15[-2]	3.53[-2]	3.03[-2]	2.54[-2]	1.96[-2]
4	5	2.00[-1]	1.40[-1]	1.24[-1]	9.82[-2]	8.34[-2]	7.08[-2]	5.77[-2]	4.16[-2]
1	6	2.02[-1]	1.90[-1]	1.97[-1]	2.22[-1]	2.52[-1]	2.85[-1]	3.22[-1]	3.65[-1]
2	6	2.45[-2]	2.37[-2]	1.87[-2]	1.41[-2]	1.32[-2]	1.27[-2]	1.12[-2]	8.35[-3]
3	6	2.15[-2]	1.92[-2]	1.74[-2]	1.61[-2]	1.69[-2]	1.61[-2]	1.32[-2]	8.49[-3]
4	6	3.91[-2]	3.89[-2]	3.28[-2]	2.81[-2]	2.91[-2]	2.76[-2]	2.21[-2]	1.35[-2]
5	6	3.36[-2]	3.43[-2]	2.94[-2]	2.49[-2]	2.56[-2]	2.44[-2]	1.96[-2]	1.22[-2]
1	7	1.42[-2]	1.42[-2]	1.09[-2]	7.48[-3]	6.31[-3]	5.45[-3]	4.34[-3]	2.76[-3]
2	7	2.33[-1]	2.37[-1]	2.49[-1]	2.90[-1]	3.35[-1]	3.80[-1]	4.26[-1]	4.80[-1]
3	7	8.65[-3]	8.49[-3]	7.41[-3]	7.24[-3]	8.94[-3]	9.20[-3]	7.51[-3]	4.62[-3]
4	7	4.16[-2]	4.44[-2]	3.78[-2]	3.19[-2]	3.14[-2]	2.90[-2]	2.37[-2]	1.57[-2]
5	7	7.38[-2]	7.80[-2]	7.01[-2]	6.13[-2]	5.94[-2]	5.56[-2]	4.72[-2]	3.32[-2]
6	7	1.77[-1]	2.33[-1]	1.77[-1]	1.10[-1]	7.85[-2]	5.73[-2]	4.14[-2]	2.68[-2]
1	8	2.60[-1]	2.46[-1]	2.44[-1]	2.65[-1]	2.92[-1]	3.24[-1]	3.62[-1]	4.06[-1]
2	8	2.60[-3]	2.67[-3]	2.57[-3]	2.94[-3]	3.82[-3]	4.09[-3]	3.49[-3]	2.26[-3]
3	8	5.28[-3]	6.34[-3]	5.71[-3]	5.50[-3]	6.43[-3]	6.27[-3]	4.95[-3]	2.97[-3]
4	8	8.09[-3]	1.07[-2]	9.40[-3]	8.97[-3]	1.09[-2]	1.07[-2]	8.16[-3]	4.56[-3]
5	8	9.33[-3]	1.14[-2]	1.03[-2]	9.29[-3]	9.91[-3]	9.34[-3]	7.35[-3]	4.40[-3]
6	8	3.45[-2]	4.71[-2]	4.22[-2]	3.30[-2]	2.88[-2]	2.51[-2]	2.09[-2]	1.62[-2]
7	8	3.05[-2]	4.26[-2]	3.88[-2]	3.10[-2]	2.75[-2]	2.44[-2]	2.09[-2]	1.68[-2]
1	9	1.18[-2]	1.12[-2]	1.10[-2]	1.19[-2]	1.33[-2]	1.48[-2]	1.64[-2]	1.82[-2]
2	9	2.36[-1]	2.20[-1]	2.16[-1]	2.35[-1]	2.60[-1]	2.89[-1]	3.22[-1]	3.60[-1]
3	9	1.51[-3]	1.88[-3]	1.63[-3]	1.86[-3]	2.78[-3]	2.93[-3]	2.27[-3]	1.25[-3]
4	9	5.69[-3]	6.50[-3]	5.83[-3]	5.74[-3]	6.80[-3]	6.68[-3]	5.31[-3]	3.22[-3]
5	9	1.00[-2]	1.06[-2]	9.81[-3]	9.20[-3]	9.55[-3]	9.00[-3]	7.39[-3]	4.91[-3]
6	9	4.48[-2]	5.90[-2]	5.23[-2]	3.76[-2]	2.91[-2]	2.28[-2]	1.77[-2]	1.30[-2]
7	9	3.64[-2]	4.21[-2]	3.88[-2]	3.31[-2]	3.09[-2]	2.87[-2]	2.58[-2]	2.19[-2]
8	9	2.93[-2]	3.97[-2]	3.48[-2]	2.56[-2]	2.16[-2]	1.77[-2]	1.29[-2]	7.23[-3]

Table 3.13b. Fe XXII (continued)

Levels		$T\,[z^2\mathrm{K}]$							
i	j	100	500	1000	2500	5000	10000	20000	50000
1	10	5.58[-2]	5.28[-2]	5.20[-2]	5.51[-2]	5.99[-2]	6.56[-2]	7.21[-2]	8.00[-2]
2	10	5.80[-1]	5.39[-1]	5.30[-1]	5.69[-1]	6.23[-1]	6.88[-1]	7.65[-1]	8.56[-1]
3	10	2.48[-3]	3.84[-3]	3.24[-3]	2.69[-3]	3.07[-3]	2.99[-3]	2.31[-3]	1.31[-3]
4	10	8.42[-3]	1.23[-2]	1.07[-2]	8.76[-3]	9.04[-3]	8.47[-3]	6.59[-3]	3.84[-3]
5	10	1.53[-2]	2.17[-2]	1.90[-2]	1.48[-2]	1.40[-2]	1.26[-2]	9.82[-3]	5.99[-3]
6	10	6.48[-2]	9.34[-2]	8.29[-2]	6.00[-2]	4.78[-2]	3.81[-2]	2.87[-2]	1.82[-2]
7	10	9.03[-2]	1.28[-1]	1.11[-1]	7.72[-2]	5.89[-2]	4.50[-2]	3.24[-2]	1.87[-2]
8	10	4.80[-2]	6.01[-2]	5.20[-2]	3.94[-2]	3.54[-2]	3.10[-2]	2.43[-2]	1.58[-2]
9	10	6.62[-2]	8.27[-2]	6.98[-2]	5.01[-2]	4.19[-2]	3.52[-2]	2.77[-2]	1.91[-2]
1	11	3.98[-4]	3.59[-4]	3.34[-4]	3.61[-4]	4.38[-4]	4.41[-4]	3.71[-4]	2.57[-4]
2	11	6.36[-4]	5.86[-4]	5.41[-4]	6.56[-4]	8.92[-4]	9.22[-4]	7.50[-4]	4.76[-4]
3	11	1.28[-1]	1.24[-1]	1.31[-1]	1.47[-1]	1.61[-1]	1.76[-1]	1.93[-1]	2.15[-1]
4	11	2.32[-1]	2.25[-1]	2.40[-1]	2.71[-1]	2.98[-1]	3.27[-1]	3.62[-1]	4.03[-1]
5	11	3.72[-1]	3.59[-1]	3.85[-1]	4.39[-1]	4.89[-1]	5.42[-1]	6.02[-1]	6.68[-1]
6	11	1.46[-2]	1.23[-2]	1.14[-2]	1.19[-2]	1.34[-2]	1.42[-2]	1.44[-2]	1.46[-2]
7	11	1.00[-2]	7.86[-3]	5.64[-3]	4.11[-3]	4.25[-3]	4.05[-3]	3.38[-3]	2.55[-3]
8	11	2.45[-2]	2.12[-2]	2.08[-2]	2.31[-2]	2.65[-2]	2.84[-2]	2.92[-2]	2.99[-2]
9	11	1.15[-2]	8.88[-3]	8.24[-3]	8.96[-3]	1.06[-2]	1.13[-2]	1.12[-2]	1.09[-2]
10	11	3.84[-2]	3.22[-2]	2.99[-2]	3.05[-2]	3.36[-2]	3.51[-2]	3.51[-2]	3.45[-2]
1	12	1.05[-3]	9.92[-4]	9.89[-4]	1.07[-3]	1.19[-3]	1.20[-3]	1.12[-3]	9.76[-4]
2	12	8.83[-4]	8.42[-4]	8.13[-4]	9.58[-4]	1.19[-3]	1.20[-3]	1.04[-3]	7.79[-4]
3	12	4.19[-3]	4.12[-3]	4.08[-3]	4.86[-3]	5.82[-3]	5.65[-3]	4.60[-3]	3.03[-3]
4	12	2.65[-2]	2.59[-2]	2.66[-2]	2.88[-2]	3.14[-2]	3.32[-2]	3.44[-2]	3.55[-2]
5	12	2.78[-3]	2.66[-3]	2.70[-3]	3.84[-3]	5.50[-3]	5.99[-3]	5.50[-3]	4.69[-3]
6	12	2.30[-1]	2.19[-1]	2.33[-1]	2.58[-1]	2.81[-1]	3.06[-1]	3.37[-1]	3.73[-1]
7	12	1.70[-1]	1.63[-1]	1.73[-1]	1.94[-1]	2.13[-1]	2.33[-1]	2.55[-1]	2.79[-1]
8	12	3.44[-1]	3.23[-1]	3.51[-1]	3.95[-1]	4.31[-1]	4.70[-1]	5.20[-1]	5.81[-1]
9	12	1.00[-1]	9.48[-2]	1.04[-1]	1.20[-1]	1.32[-1]	1.46[-1]	1.62[-1]	1.82[-1]
10	12	1.74[-2]	1.48[-2]	1.34[-2]	1.43[-2]	1.72[-2]	1.79[-2]	1.68[-2]	1.51[-2]
11	12	3.48[-2]	3.41[-2]	3.35[-2]	3.79[-2]	4.51[-2]	4.39[-2]	3.59[-2]	2.37[-2]
1	13	6.20[-4]	5.85[-4]	5.70[-4]	6.31[-4]	7.38[-4]	7.47[-4]	6.65[-4]	5.32[-4]
2	13	2.00[-3]	1.89[-3]	1.85[-3]	1.96[-3]	2.13[-3]	2.14[-3]	2.01[-3]	1.77[-3]
3	13	4.49[-4]	4.30[-4]	4.17[-4]	7.66[-4]	1.30[-3]	1.38[-3]	1.07[-3]	5.96[-4]
4	13	4.38[-3]	4.24[-3]	4.15[-3]	4.86[-3]	6.15[-3]	6.29[-3]	5.33[-3]	3.77[-3]
5	13	4.15[-2]	4.05[-2]	4.14[-2]	4.44[-2]	4.84[-2]	5.10[-2]	5.24[-2]	5.31[-2]
6	13	1.44[-1]	1.37[-1]	1.42[-1]	1.53[-1]	1.65[-1]	1.78[-1]	1.94[-1]	2.14[-1]
7	13	5.48[-1]	5.23[-1]	5.56[-1]	6.16[-1]	6.71[-1]	7.32[-1]	8.06[-1]	8.94[-1]
8	13	3.48[-3]	2.93[-3]	2.22[-3]	2.30[-3]	3.23[-3]	3.25[-3]	2.45[-3]	1.34[-3]
9	13	5.93[-3]	4.90[-3]	3.45[-3]	2.34[-3]	2.34[-3]	2.06[-3]	1.47[-3]	7.72[-4]
10	13	5.26[-1]	5.05[-1]	5.54[-1]	6.29[-1]	6.89[-1]	7.57[-1]	8.40[-1]	9.40[-1]
11	13	4.26[-2]	4.18[-2]	4.08[-2]	4.13[-2]	4.39[-2]	4.20[-2]	3.57[-2]	2.54[-2]
12	13	5.62[-2]	5.46[-2]	5.30[-2]	5.70[-2]	6.76[-2]	6.77[-2]	5.68[-2]	3.90[-2]

Table 3.13b. Fe XXII (continued)

Levels		$T\,[z^2\mathrm{K}]$							
i	j	100	500	1000	2500	5000	10000	20000	50000
1	14	7.72[-4]	7.69[-4]	7.71[-4]	8.46[-4]	9.36[-4]	9.36[-4]	8.56[-4]	7.04[-4]
2	14	5.30[-4]	5.22[-4]	5.23[-4]	6.09[-4]	7.07[-4]	7.05[-4]	6.25[-4]	5.02[-4]
3	14	1.13[-3]	1.13[-3]	1.14[-3]	1.41[-3]	1.70[-3]	1.70[-3]	1.52[-3]	1.27[-3]
4	14	2.02[-3]	2.00[-3]	2.01[-3]	2.51[-3]	3.06[-3]	2.97[-3]	2.43[-3]	1.66[-3]
5	14	1.73[-3]	1.71[-3]	1.71[-3]	2.34[-3]	3.05[-3]	2.95[-3]	2.30[-3]	1.37[-3]
6	14	2.08[-1]	2.11[-1]	2.16[-1]	2.30[-1]	2.47[-1]	2.70[-1]	2.98[-1]	3.32[-1]
7	14	1.51[-3]	1.50[-3]	1.50[-3]	2.09[-3]	2.82[-3]	2.80[-3]	2.18[-3]	1.29[-3]
8	14	3.06[-2]	3.13[-2]	3.20[-2]	3.43[-2]	3.69[-2]	3.95[-2]	4.23[-2]	4.57[-2]
9	14	2.62[-1]	2.66[-1]	2.73[-1]	2.89[-1]	3.09[-1]	3.35[-1]	3.68[-1]	4.08[-1]
10	14	5.35[-2]	5.47[-2]	5.63[-2]	6.19[-2]	6.84[-2]	7.42[-2]	8.04[-2]	8.75[-2]
11	14	8.96[-3]	8.81[-3]	8.70[-3]	1.08[-2]	1.39[-2]	1.35[-2]	1.05[-2]	6.21[-3]
12	14	2.06[-2]	2.06[-2]	2.06[-2]	2.42[-2]	2.94[-2]	3.02[-2]	2.75[-2]	2.31[-2]
13	14	2.12[-2]	2.11[-2]	2.10[-2]	2.32[-2]	2.69[-2]	2.72[-2]	2.45[-2]	2.02[-2]
1	15	1.12[-4]	1.10[-4]	1.13[-4]	1.89[-4]	2.80[-4]	2.86[-4]	2.28[-4]	1.46[-4]
2	15	2.27[-3]	2.26[-3]	2.26[-3]	2.40[-3]	2.58[-3]	2.56[-3]	2.37[-3]	2.01[-3]
3	15	1.19[-4]	1.18[-4]	1.32[-4]	4.58[-4]	8.44[-4]	8.78[-4]	6.61[-4]	3.65[-4]
4	15	2.29[-3]	2.29[-3]	2.35[-3]	3.37[-3]	4.55[-3]	4.71[-3]	4.15[-3]	3.36[-3]
5	15	5.62[-3]	5.59[-3]	5.57[-3]	6.54[-3]	7.73[-3]	7.58[-3]	6.41[-3]	4.66[-3]
6	15	5.98[-2]	6.11[-2]	6.23[-2]	6.63[-2]	7.16[-2]	7.73[-2]	8.41[-2]	9.23[-2]
7	15	1.84[-1]	1.89[-1]	1.94[-1]	2.06[-1]	2.22[-1]	2.41[-1]	2.64[-1]	2.90[-1]
8	15	7.35[-2]	7.51[-2]	7.67[-2]	8.11[-2]	8.66[-2]	9.28[-2]	1.01[-1]	1.11[-1]
9	15	6.19[-2]	6.29[-2]	6.39[-2]	6.71[-2]	7.12[-2]	7.59[-2]	8.16[-2]	8.85[-2]
10	15	6.95[-1]	7.07[-1]	7.24[-1]	7.66[-1]	8.19[-1]	8.87[-1]	9.76[-1]	1.09
11	15	1.23[-2]	1.21[-2]	1.19[-2]	1.50[-2]	1.95[-2]	1.92[-2]	1.49[-2]	8.60[-3]
12	15	2.41[-2]	2.39[-2]	2.38[-2]	3.08[-2]	4.13[-2]	4.20[-2]	3.49[-2]	2.42[-2]
13	15	5.47[-2]	5.44[-2]	5.42[-2]	6.09[-2]	7.19[-2]	7.34[-2]	6.67[-2]	5.56[-2]
14	15	2.05[-2]	2.02[-2]	2.00[-2]	2.26[-2]	2.67[-2]	2.62[-2]	2.20[-2]	1.54[-2]
1	16	3.13[-2]	2.35[-2]	1.72[-2]	9.65[-3]	5.92[-3]	3.74[-3]	2.63[-3]	2.14[-3]
2	16	8.22[-2]	5.91[-2]	4.27[-2]	2.37[-2]	1.43[-2]	8.81[-3]	6.07[-3]	4.85[-3]
3	16	5.76[-3]	2.94[-3]	1.90[-3]	9.47[-4]	5.18[-4]	2.72[-4]	1.40[-4]	5.74[-5]
4	16	1.13[-2]	6.01[-3]	3.82[-3]	1.86[-3]	1.00[-3]	5.23[-4]	2.68[-4]	1.09[-4]
5	16	6.70[-3]	4.35[-3]	3.02[-3]	1.58[-3]	8.76[-4]	4.65[-4]	2.42[-4]	1.02[-4]
1	17	2.68[-2]	2.88[-2]	2.40[-2]	1.70[-2]	1.36[-2]	1.16[-2]	1.05[-2]	9.30[-3]
2	17	2.78[-2]	2.78[-2]	2.16[-2]	1.33[-2]	9.24[-3]	6.73[-3]	5.19[-3]	3.78[-3]
3	17	2.90[-3]	4.06[-3]	3.15[-3]	1.71[-3]	9.58[-4]	5.13[-4]	2.70[-4]	1.15[-4]
4	17	6.12[-3]	7.20[-3]	5.54[-3]	3.00[-3]	1.68[-3]	8.99[-4]	4.72[-4]	2.04[-4]
5	17	4.12[-3]	6.59[-3]	5.22[-3]	2.84[-3]	1.59[-3]	8.42[-4]	4.36[-4]	1.80[-4]
1	18	2.66[-2]	2.63[-2]	2.04[-2]	1.27[-2]	8.90[-3]	6.53[-3]	5.02[-3]	3.59[-3]
2	18	1.36[-1]	1.16[-1]	8.76[-2]	5.62[-2]	4.19[-2]	3.37[-2]	2.92[-2]	2.51[-2]
3	18	4.79[-3]	4.41[-3]	3.26[-3]	1.75[-3]	9.80[-4]	5.24[-4]	2.76[-4]	1.24[-4]
4	18	1.38[-2]	1.22[-2]	8.68[-3]	4.57[-3]	2.54[-3]	1.35[-3]	7.04[-4]	2.93[-4]
5	18	2.25[-2]	1.87[-2]	1.32[-2]	6.78[-3]	3.75[-3]	2.00[-3]	1.07[-3]	5.03[-4]

Table 3.13b. Fe XXII (continued)

Levels		$T\,[z^2\mathrm{K}]$							
i	j	100	500	1000	2500	5000	10000	20000	50000
1	19	1.67[-2]	8.77[-3]	5.75[-3]	3.23[-3]	2.21[-3]	1.62[-3]	1.25[-3]	9.09[-4]
2	19	7.02[-3]	3.40[-3]	2.09[-3]	9.94[-4]	5.55[-4]	3.14[-4]	1.82[-4]	9.08[-5]
3	19	6.78[-3]	5.31[-3]	3.62[-3]	1.99[-3]	1.31[-3]	9.70[-4]	8.48[-4]	8.57[-4]
4	19	1.81[-2]	1.24[-2]	8.65[-3]	5.09[-3]	3.69[-3]	3.11[-3]	3.21[-3]	3.87[-3]
5	19	7.79[-3]	4.48[-3]	2.81[-3]	1.37[-3]	7.82[-4]	4.55[-4]	2.72[-4]	1.38[-4]
1	20	7.60[-2]	5.90[-2]	5.38[-2]	5.10[-2]	5.20[-2]	5.59[-2]	6.39[-2]	7.72[-2]
2	20	3.53[-2]	2.64[-2]	2.37[-2]	2.15[-2]	2.07[-2]	2.04[-2]	2.07[-2]	2.16[-2]
3	20	6.75[-5]	7.21[-5]	5.71[-5]	3.73[-5]	2.80[-5]	2.29[-5]	2.03[-5]	1.79[-5]
4	20	1.77[-4]	2.40[-4]	1.88[-4]	1.04[-4]	6.24[-5]	3.76[-5]	2.41[-5]	1.49[-5]
5	20	1.23[-4]	1.31[-4]	9.64[-5]	5.14[-5]	3.00[-5]	1.75[-5]	1.06[-5]	5.74[-6]
1	21	1.52[-2]	1.14[-2]	1.02[-2]	9.06[-3]	8.28[-3]	7.37[-3]	6.29[-3]	4.72[-3]
2	21	1.50[-1]	1.17[-1]	1.06[-1]	1.00[-1]	1.02[-1]	1.08[-1]	1.21[-1]	1.42[-1]
3	21	5.59[-5]	4.65[-5]	3.89[-5]	3.12[-5]	2.76[-5]	2.51[-5]	2.31[-5]	2.00[-5]
4	21	5.82[-5]	5.49[-5]	4.25[-5]	2.61[-5]	1.80[-5]	1.27[-5]	8.99[-6]	5.49[-6]
5	21	2.70[-4]	1.99[-4]	1.65[-4]	1.34[-4]	1.23[-4]	1.17[-4]	1.14[-4]	1.08[-4]
1	22	6.90[-3]	4.53[-3]	3.22[-3]	1.98[-3]	1.41[-3]	1.04[-3]	7.62[-4]	4.78[-4]
2	22	3.70[-2]	1.90[-2]	1.23[-2]	6.73[-3]	4.53[-3]	3.34[-3]	2.71[-3]	2.22[-3]
3	22	1.41[-2]	1.08[-2]	7.55[-3]	4.53[-3]	3.34[-3]	2.86[-3]	2.92[-3]	3.39[-3]
4	22	1.41[-2]	1.09[-2]	7.72[-3]	4.24[-3]	2.68[-3]	1.84[-3]	1.48[-3]	1.37[-3]
5	22	3.74[-2]	2.36[-2]	1.55[-2]	8.39[-3]	5.62[-3]	4.34[-3]	4.13[-3]	4.70[-3]
1	23	1.57[-3]	1.27[-3]	8.45[-4]	4.11[-4]	2.23[-4]	1.19[-4]	6.29[-5]	2.72[-5]
2	23	1.26[-2]	8.35[-3]	5.98[-3]	3.84[-3]	2.88[-3]	2.20[-3]	1.65[-3]	1.04[-3]
3	23	3.10[-3]	2.18[-3]	1.41[-3]	7.03[-4]	4.09[-4]	2.44[-4]	1.49[-4]	7.83[-5]
4	23	2.50[-2]	1.66[-2]	1.13[-2]	6.40[-3]	4.42[-3]	3.50[-3]	3.33[-3]	3.63[-3]
5	23	1.11[-1]	5.86[-2]	3.67[-2]	1.90[-2]	1.22[-2]	9.08[-3]	8.27[-3]	8.98[-3]
1	24	4.71[-2]	3.48[-2]	3.07[-2]	2.77[-2]	2.68[-2]	2.67[-2]	2.71[-2]	2.70[-2]
2	24	3.33[-3]	1.72[-3]	1.11[-3]	5.82[-4]	3.65[-4]	2.40[-4]	1.62[-4]	9.69[-5]
3	24	5.69[-3]	4.12[-3]	2.83[-3]	1.59[-3]	1.05[-3]	7.19[-4]	5.02[-4]	3.02[-4]
4	24	1.07[-2]	8.60[-3]	6.08[-3]	3.27[-3]	1.97[-3]	1.21[-3]	7.67[-4]	4.30[-4]
5	24	5.32[-3]	3.50[-3]	2.44[-3]	1.44[-3]	9.93[-4]	7.11[-4]	5.13[-4]	3.14[-4]
1	25	1.10[-3]	1.07[-3]	1.05[-3]	1.06[-3]	1.11[-3]	1.20[-3]	1.40[-3]	1.76[-3]
2	25	8.59[-5]	1.09[-4]	1.14[-4]	1.20[-4]	1.32[-4]	1.54[-4]	1.97[-4]	2.68[-4]
3	25	9.16[-4]	9.04[-4]	8.81[-4]	8.51[-4]	8.16[-4]	7.52[-4]	6.55[-4]	4.93[-4]
4	25	2.49[-3]	2.48[-3]	2.43[-3]	2.40[-3]	2.39[-3]	2.35[-3]	2.27[-3]	2.02[-3]
5	25	2.53[-4]	2.35[-4]	2.30[-4]	2.30[-4]	2.32[-4]	2.30[-4]	2.24[-4]	2.04[-4]
1	26	1.12[-3]	1.10[-3]	1.07[-3]	1.03[-3]	9.98[-4]	9.92[-4]	1.06[-3]	1.24[-3]
2	26	9.59[-4]	9.27[-4]	9.05[-4]	9.02[-4]	9.21[-4]	9.74[-4]	1.15[-3]	1.57[-3]
3	26	1.80[-3]	1.75[-3]	1.73[-3]	1.67[-3]	1.60[-3]	1.49[-3]	1.36[-3]	1.12[-3]
4	26	1.93[-3]	1.91[-3]	1.86[-3]	1.80[-3]	1.76[-3]	1.71[-3]	1.68[-3]	1.55[-3]

Table 3.13b. Fe XXII (continued)

Levels		$T\,[z^2\mathrm{K}]$							
i	j	100	500	1000	2500	5000	10000	20000	50000
5	26	2.64[-3]	2.48[-3]	2.39[-3]	2.30[-3]	2.22[-3]	2.11[-3]	1.97[-3]	1.71[-3]
1	27	5.64[-3]	2.64[-3]	1.65[-3]	8.15[-4]	4.78[-4]	2.90[-4]	1.85[-4]	1.06[-4]
2	27	1.12[-1]	7.26[-2]	5.99[-2]	5.02[-2]	4.70[-2]	4.59[-2]	4.60[-2]	4.54[-2]
3	27	6.14[-3]	4.20[-3]	2.69[-3]	1.32[-3]	7.48[-4]	4.34[-4]	2.66[-4]	1.55[-4]
4	27	1.03[-2]	6.33[-3]	4.28[-3]	2.40[-3]	1.60[-3]	1.12[-3]	8.11[-4]	5.32[-4]
5	27	2.58[-2]	1.60[-2]	1.05[-2]	5.69[-3]	3.68[-3]	2.50[-3]	1.74[-3]	1.05[-3]
1	28	1.09[-3]	1.07[-3]	1.04[-3]	9.92[-4]	9.30[-4]	8.26[-4]	6.81[-4]	4.57[-4]
2	28	1.56[-3]	9.81[-4]	8.58[-4]	7.60[-4]	7.15[-4]	6.74[-4]	6.34[-4]	5.90[-4]
3	28	3.37[-3]	3.33[-3]	3.25[-3]	3.22[-3]	3.23[-3]	3.23[-3]	3.19[-3]	2.88[-3]
4	28	1.81[-3]	1.76[-3]	1.70[-3]	1.62[-3]	1.54[-3]	1.39[-3]	1.19[-3]	8.61[-4]
5	28	1.10[-2]	1.09[-2]	1.07[-2]	1.07[-2]	1.08[-2]	1.10[-2]	1.11[-2]	1.06[-2]
1	29	3.08[-3]	2.62[-3]	2.55[-3]	2.64[-3]	2.95[-3]	3.63[-3]	5.00[-3]	7.60[-3]
2	29	7.88[-4]	6.80[-4]	6.61[-4]	6.47[-4]	6.59[-4]	7.04[-4]	8.15[-4]	1.02[-3]
3	29	2.00[-3]	1.68[-3]	1.60[-3]	1.50[-3]	1.40[-3]	1.25[-3]	1.07[-3]	8.02[-4]
4	29	1.30[-3]	1.20[-3]	1.16[-3]	1.11[-3]	1.05[-3]	9.71[-4]	8.74[-4]	6.98[-4]
5	29	1.57[-3]	1.41[-3]	1.33[-3]	1.25[-3]	1.16[-3]	1.02[-3]	8.38[-4]	5.58[-4]
1	30	2.63[-3]	2.58[-3]	2.56[-3]	2.62[-3]	2.74[-3]	3.02[-3]	3.67[-3]	4.94[-3]
2	30	9.49[-4]	9.30[-4]	8.99[-4]	8.89[-4]	9.23[-4]	1.04[-3]	1.35[-3]	2.02[-3]
3	30	1.24[-3]	1.21[-3]	1.19[-3]	1.16[-3]	1.12[-3]	1.04[-3]	9.20[-4]	7.16[-4]
4	30	1.46[-2]	1.45[-2]	1.43[-2]	1.43[-2]	1.44[-2]	1.44[-2]	1.43[-2]	1.35[-2]
5	30	5.72[-4]	4.42[-4]	4.06[-4]	3.75[-4]	3.46[-4]	3.08[-4]	2.67[-4]	2.08[-4]
1	31	5.62[-4]	5.05[-4]	4.86[-4]	4.66[-4]	4.52[-4]	4.36[-4]	4.40[-4]	5.01[-4]
2	31	4.62[-4]	2.98[-4]	2.45[-4]	2.12[-4]	2.06[-4]	2.11[-4]	2.28[-4]	2.70[-4]
3	31	2.32[-2]	2.32[-2]	2.30[-2]	2.33[-2]	2.41[-2]	2.54[-2]	2.71[-2]	2.78[-2]
4	31	1.03[-3]	1.00[-3]	9.67[-4]	9.23[-4]	8.71[-4]	7.86[-4]	6.65[-4]	4.68[-4]
5	31	1.76[-3]	1.62[-3]	1.57[-3]	1.53[-3]	1.52[-3]	1.51[-3]	1.49[-3]	1.38[-3]
1	32	3.82[-3]	3.91[-3]	4.11[-3]	4.49[-3]	4.91[-3]	5.68[-3]	7.38[-3]	1.10[-2]
2	32	6.69[-4]	5.99[-4]	5.63[-4]	5.24[-4]	4.80[-4]	4.04[-4]	3.14[-4]	2.34[-4]
3	32	1.19[-3]	1.15[-3]	1.08[-3]	1.01[-3]	9.36[-4]	8.28[-4]	6.87[-4]	4.73[-4]
4	32	7.86[-3]	8.04[-3]	8.00[-3]	7.90[-3]	7.71[-3]	7.44[-3]	7.20[-3]	6.80[-3]
5	32	2.54[-3]	2.51[-3]	2.44[-3]	2.32[-3]	2.19[-3]	1.99[-3]	1.74[-3]	1.33[-3]
1	33	8.00[-7]	7.70[-7]	7.43[-7]	6.96[-7]	6.40[-7]	5.51[-7]	4.34[-7]	2.71[-7]
2	33	2.45[-3]	2.40[-3]	2.32[-3]	2.20[-3]	2.06[-3]	1.82[-3]	1.50[-3]	1.00[-3]
3	33	2.35[-4]	2.30[-4]	2.23[-4]	2.13[-4]	2.00[-4]	1.78[-4]	1.45[-4]	9.66[-5]
4	33	3.92[-3]	3.87[-3]	3.78[-3]	3.73[-3]	3.70[-3]	3.64[-3]	3.50[-3]	3.04[-3]
5	33	7.28[-3]	7.16[-3]	6.99[-3]	6.83[-3]	6.71[-3]	6.48[-3]	6.11[-3]	5.18[-3]

Table 3.13b. Fe XXII (continued)

Levels		$T\,[z^2\mathrm{K}]$							
i	j	100	500	1000	2500	5000	10000	20000	50000
1	34	1.85[-3]	1.76[-3]	1.69[-3]	1.74[-3]	1.93[-3]	2.25[-3]	2.71[-3]	3.18[-3]
2	34	3.38[-3]	3.26[-3]	3.21[-3]	3.26[-3]	3.38[-3]	3.73[-3]	4.62[-3]	6.30[-3]
3	34	4.24[-4]	4.38[-4]	4.27[-4]	4.12[-4]	4.04[-4]	3.79[-4]	3.22[-4]	2.18[-4]
4	34	2.46[-2]	2.44[-2]	2.40[-2]	2.40[-2]	2.41[-2]	2.43[-2]	2.49[-2]	2.50[-2]
5	34	2.62[-3]	2.50[-3]	2.54[-3]	2.50[-3]	2.36[-3]	2.17[-3]	1.95[-3]	1.57[-3]
1	35	1.26[-3]	1.21[-3]	1.19[-3]	1.30[-3]	1.52[-3]	1.88[-3]	2.41[-3]	3.11[-3]
2	35	2.16[-3]	2.12[-3]	2.11[-3]	2.06[-3]	2.05[-3]	2.22[-3]	3.00[-3]	5.34[-3]
3	35	4.89[-4]	4.96[-4]	4.96[-4]	5.07[-4]	5.12[-4]	4.84[-4]	4.12[-4]	2.78[-4]
4	35	1.84[-2]	1.83[-2]	1.80[-2]	1.80[-2]	1.82[-2]	1.84[-2]	1.86[-2]	1.79[-2]
5	35	2.44[-3]	2.40[-3]	2.32[-3]	2.21[-3]	2.09[-3]	1.89[-3]	1.64[-3]	1.26[-3]
1	36	2.42[-4]	2.15[-4]	2.06[-4]	1.97[-4]	1.88[-4]	1.69[-4]	1.40[-4]	9.36[-5]
2	36	5.20[-3]	4.57[-3]	4.43[-3]	4.45[-3]	4.68[-3]	5.21[-3]	6.25[-3]	8.05[-3]
3	36	8.28[-4]	8.11[-4]	7.87[-4]	7.58[-4]	7.28[-4]	6.79[-4]	6.07[-4]	4.77[-4]
4	36	2.81[-3]	2.77[-3]	2.69[-3]	2.59[-3]	2.48[-3]	2.30[-3]	2.03[-3]	1.57[-3]
5	36	7.36[-2]	7.41[-2]	7.34[-2]	7.38[-2]	7.50[-2]	7.64[-2]	7.82[-2]	7.71[-2]
1	37	3.28[-5]	1.72[-5]	1.43[-5]	1.18[-5]	1.05[-5]	9.06[-6]	7.46[-6]	5.20[-6]
2	37	1.17[-2]	1.12[-2]	1.10[-2]	1.14[-2]	1.25[-2]	1.48[-2]	1.91[-2]	2.67[-2]
3	37	2.38[-4]	2.30[-4]	2.22[-4]	2.12[-4]	2.01[-4]	1.85[-4]	1.63[-4]	1.25[-4]
4	37	2.40[-3]	2.36[-3]	2.29[-3]	2.20[-3]	2.07[-3]	1.88[-3]	1.61[-3]	1.17[-3]
5	37	1.54[-2]	1.52[-2]	1.49[-2]	1.47[-2]	1.47[-2]	1.46[-2]	1.42[-2]	1.30[-2]
1	38	7.99[-4]	7.62[-4]	7.17[-4]	7.11[-4]	7.60[-4]	8.86[-4]	1.16[-3]	1.69[-3]
2	38	2.80[-3]	2.95[-3]	3.09[-3]	3.43[-3]	3.89[-3]	4.73[-3]	6.34[-3]	9.35[-3]
3	38	1.20[-3]	1.08[-3]	1.01[-3]	9.47[-4]	8.89[-4]	8.18[-4]	7.67[-4]	7.20[-4]
4	38	7.45[-4]	7.11[-4]	6.86[-4]	6.54[-4]	6.08[-4]	5.34[-4]	4.33[-4]	2.85[-4]
5	38	1.07[-3]	1.03[-3]	9.83[-4]	9.27[-4]	8.57[-4]	7.48[-4]	6.05[-4]	3.95[-4]
1	39	2.64[-3]	2.60[-3]	2.58[-3]	2.65[-3]	2.74[-3]	2.85[-3]	2.98[-3]	3.02[-3]
2	39	5.85[-4]	5.69[-4]	5.57[-4]	5.46[-4]	5.28[-4]	4.93[-4]	4.44[-4]	3.58[-4]
3	39	2.26[-5]	2.22[-5]	2.15[-5]	2.07[-5]	1.98[-5]	1.85[-5]	1.70[-5]	1.45[-5]
4	39	5.15[-5]	4.92[-5]	4.74[-5]	4.49[-5]	4.17[-5]	3.69[-5]	3.06[-5]	2.12[-5]
5	39	3.50[-5]	3.06[-5]	2.89[-5]	2.67[-5]	2.42[-5]	2.06[-5]	1.61[-5]	1.03[-5]
1	40	4.07[-4]	3.94[-4]	3.84[-4]	3.72[-4]	3.58[-4]	3.37[-4]	3.10[-4]	2.62[-4]
2	40	1.36[-2]	1.35[-2]	1.34[-2]	1.36[-2]	1.39[-2]	1.43[-2]	1.49[-2]	1.52[-2]
3	40	5.26[-5]	5.11[-5]	4.98[-5]	4.83[-5]	4.61[-5]	4.26[-5]	3.83[-5]	3.17[-5]
4	40	5.61[-5]	5.44[-5]	5.27[-5]	5.04[-5]	4.73[-5]	4.13[-5]	3.30[-5]	2.21[-5]
5	40	1.15[-4]	1.12[-4]	1.08[-4]	1.04[-4]	9.85[-5]	8.82[-5]	7.49[-5]	5.65[-5]
1	41	3.77[-4]	3.83[-4]	3.95[-4]	4.21[-4]	4.53[-4]	5.19[-4]	6.76[-4]	1.03[-3]
2	41	1.03[-3]	1.06[-3]	1.11[-3]	1.21[-3]	1.32[-3]	1.51[-3]	1.91[-3]	2.71[-3]
3	41	3.63[-4]	3.56[-4]	3.51[-4]	3.33[-4]	3.08[-4]	2.70[-4]	2.21[-4]	1.64[-4]
4	41	1.05[-4]	1.04[-4]	1.02[-4]	9.33[-5]	8.10[-5]	6.60[-5]	5.00[-5]	3.05[-5]

Table 3.13b. Fe XXII (continued)

Levels		$T\,[z^2\mathrm{K}]$							
i	j	100	500	1000	2500	5000	10000	20000	50000
5	41	9.93[-5]	9.64[-5]	9.41[-5]	8.87[-5]	8.13[-5]	6.80[-5]	5.13[-5]	3.14[-5]
1	42	1.73[-4]	1.76[-4]	1.81[-4]	1.89[-4]	1.92[-4]	1.94[-4]	1.93[-4]	1.81[-4]
2	42	2.38[-3]	2.47[-3]	2.63[-3]	2.98[-3]	3.36[-3]	3.87[-3]	4.56[-3]	5.40[-3]
3	42	1.34[-4]	1.36[-4]	1.39[-4]	1.43[-4]	1.41[-4]	1.32[-4]	1.11[-4]	7.23[-5]
4	42	3.86[-4]	3.90[-4]	3.99[-4]	4.07[-4]	3.98[-4]	3.70[-4]	3.16[-4]	2.17[-4]
5	42	6.28[-4]	6.37[-4]	6.52[-4]	6.69[-4]	6.61[-4]	6.19[-4]	5.22[-4]	3.40[-4]
1	43	3.00[-4]	3.02[-4]	3.07[-4]	3.08[-4]	2.96[-4]	2.68[-4]	2.27[-4]	1.58[-4]
2	43	1.54[-3]	1.57[-3]	1.63[-3]	1.72[-3]	1.81[-3]	1.99[-3]	2.37[-3]	3.14[-3]
3	43	1.02[-5]	1.03[-5]	1.05[-5]	1.07[-5]	1.03[-5]	9.27[-6]	7.61[-6]	5.08[-6]
4	43	6.42[-5]	6.49[-5]	6.63[-5]	6.70[-5]	6.48[-5]	5.93[-5]	5.08[-5]	3.67[-5]
5	43	4.11[-4]	4.19[-4]	4.31[-4]	4.48[-4]	4.53[-4]	4.50[-4]	4.37[-4]	3.91[-4]
1	44	7.11[-4]	7.11[-4]	7.47[-4]	8.57[-4]	1.01[-3]	1.25[-3]	1.58[-3]	1.93[-3]
2	44	2.77[-3]	2.79[-3]	2.92[-3]	3.32[-3]	3.88[-3]	4.77[-3]	6.04[-3]	7.67[-3]
3	44	6.92[-5]	7.07[-5]	7.33[-5]	7.75[-5]	8.07[-5]	8.32[-5]	7.98[-5]	6.00[-5]
4	44	5.02[-4]	5.15[-4]	5.37[-4]	5.78[-4]	6.17[-4]	6.68[-4]	6.87[-4]	5.63[-4]
5	44	6.83[-4]	6.98[-4]	7.22[-4]	7.60[-4]	7.86[-4]	8.12[-4]	8.05[-4]	6.49[-4]
1	45	3.59[-4]	3.69[-4]	3.84[-4]	4.14[-4]	4.43[-4]	4.89[-4]	5.75[-4]	7.22[-4]
2	45	5.28[-4]	5.36[-4]	5.50[-4]	5.65[-4]	5.65[-4]	5.57[-4]	5.53[-4]	5.44[-4]
3	45	1.31[-4]	1.32[-4]	1.34[-4]	1.38[-4]	1.38[-4]	1.29[-4]	1.07[-4]	7.16[-5]
4	45	6.64[-5]	6.65[-5]	6.69[-5]	6.56[-5]	6.15[-5]	5.37[-5]	4.30[-5]	2.77[-5]
5	45	9.09[-5]	9.14[-5]	9.21[-5]	9.00[-5]	8.41[-5]	7.46[-5]	6.21[-5]	4.35[-5]

Table 3.14a. Fe XXIII. Ten fine-structure $n = 2$ levels included in the calculation [92Z1] and their calculated and observed energies E [Ry] in rydbergs [85S1]. The index i is used in Table 3.14b for transition keys.

i	Level	E [Ry]		i	Level	E [Ry]	
		obs.	calc.			obs.	calc.
1	$2s^2\ ^1S_0$	0.00000	0.00000	6	$2p^2\ ^3P_0$	8.71263	8.75346
2	$2s\ 2p\ ^3P^o_0$	3.17285	3.18393	7	$2p^2\ ^3P_1$	9.36054	9.39077
3	$2s\ 2p\ ^3P^o_1$	3.45489	3.46780	8	$2p^2\ ^3P_2$	9.76605	9.81506
4	$2s\ 2p\ ^3P^o_2$	4.29918	4.30822	9	$2p^2\ ^1D_2$	10.97348	11.05975
5	$2s\ 2p\ ^1P^o_1$	6.86038	6.98700	10	$2p^2\ ^1S_0$	12.96733	13.10207

Table 3.14b. Fe XXIII. Effective collision strengths $\Upsilon(i,j)$ as a function of temperature T [K] for the transitions between the ten $n = 2$ levels as specified in Table 3.14a [92Z1].

Levels		T [$\times 10^6$ K]							
i	j	0.05	0.25	0.5	1.25	2.5	5.0	10.0	25.0
1	2	1.17[-3]	1.28[-3]	1.31[-3]	1.29[-3]	1.23[-3]	1.11[-3]	9.36[-4]	6.52[-4]
1	3	1.04[-2]	1.06[-2]	1.06[-2]	1.08[-2]	1.10[-2]	1.13[-2]	1.17[-2]	1.23[-2]
1	4	6.20[-3]	6.47[-3]	6.51[-3]	6.36[-3]	6.02[-3]	5.42[-3]	4.55[-3]	3.16[-3]
1	5	2.94[-1]	3.00[-1]	3.05[-1]	3.16[-1]	3.31[-1]	3.56[-1]	3.91[-1]	4.54[-1]
1	6	1.22[-4]	1.22[-4]	1.21[-4]	1.18[-4]	1.12[-4]	1.04[-4]	9.39[-5]	7.92[-5]
1	7	1.79[-4]	1.79[-4]	1.76[-4]	1.66[-4]	1.52[-4]	1.31[-4]	1.04[-4]	6.65[-5]
1	8	4.37[-4]	4.36[-4]	4.34[-4]	4.28[-4]	4.19[-4]	4.06[-4]	3.93[-4]	3.82[-4]
1	9	6.14[-4]	6.16[-4]	6.18[-4]	6.27[-4]	6.40[-4]	6.62[-4]	6.98[-4]	7.65[-4]
1	10	3.54[-4]	3.53[-4]	3.53[-4]	3.51[-4]	3.48[-4]	3.43[-4]	3.37[-4]	3.27[-4]
2	3	1.53[-2]	1.53[-2]	1.51[-2]	1.44[-2]	1.33[-2]	1.17[-2]	9.57[-3]	6.43[-3]
2	4	1.00[-2]	1.00[-2]	9.94[-3]	9.76[-3]	9.49[-3]	9.11[-3]	8.69[-3]	8.23[-3]
2	5	3.17[-3]	3.41[-3]	3.45[-3]	3.35[-3]	3.13[-3]	2.74[-3]	2.23[-3]	1.48[-3]
2	6	8.90[-4]	9.08[-4]	9.06[-4]	8.79[-4]	8.29[-4]	7.44[-4]	6.23[-4]	4.31[-4]
2	7	1.41[-1]	1.43[-1]	1.46[-1]	1.51[-1]	1.58[-1]	1.71[-1]	1.87[-1]	2.17[-1]
2	8	2.42[-3]	2.44[-3]	2.43[-3]	2.35[-3]	2.21[-3]	1.99[-3]	1.66[-3]	1.15[-3]
2	9	5.32[-4]	5.34[-4]	5.30[-4]	5.12[-4]	4.82[-4]	4.32[-4]	3.62[-4]	2.51[-4]
2	10	8.25[-5]	8.22[-5]	8.12[-5]	7.78[-5]	7.26[-5]	6.43[-5]	5.29[-5]	3.56[-5]
3	4	4.05[-2]	4.05[-2]	4.01[-2]	3.89[-2]	3.70[-2]	3.42[-2]	3.07[-2]	2.59[-2]
3	5	9.64[-3]	1.05[-2]	1.07[-2]	1.04[-2]	9.79[-3]	8.72[-3]	7.29[-3]	5.21[-3]
3	6	1.50[-1]	1.52[-1]	1.54[-1]	1.59[-1]	1.68[-1]	1.81[-1]	1.99[-1]	2.30[-1]
3	7	1.07[-1]	1.09[-1]	1.11[-1]	1.15[-1]	1.20[-1]	1.29[-1]	1.41[-1]	1.62[-1]
3	8	1.85[-1]	1.88[-1]	1.91[-1]	1.98[-1]	2.07[-1]	2.22[-1]	2.43[-1]	2.80[-1]
3	9	1.07[-2]	1.09[-2]	1.10[-2]	1.12[-2]	1.15[-2]	1.19[-2]	1.24[-2]	1.36[-2]
3	10	6.84[-4]	6.87[-4]	6.86[-4]	6.81[-4]	6.71[-4]	6.55[-4]	6.37[-4]	6.19[-4]
4	5	1.39[-2]	1.68[-2]	1.75[-2]	1.74[-2]	1.64[-2]	1.45[-2]	1.18[-2]	7.96[-3]
4	6	5.47[-4]	5.67[-4]	5.70[-4]	5.56[-4]	5.27[-4]	4.75[-4]	3.99[-4]	2.78[-4]
4	7	1.90[-1]	1.91[-1]	1.94[-1]	2.00[-1]	2.11[-1]	2.28[-1]	2.50[-1]	2.87[-1]
4	8	4.11[-1]	4.17[-1]	4.24[-1]	4.39[-1]	4.61[-1]	4.96[-1]	5.45[-1]	6.30[-1]
4	9	1.39[-1]	1.42[-1]	1.44[-1]	1.48[-1]	1.54[-1]	1.64[-1]	1.78[-1]	2.03[-1]
4	10	1.74[-3]	1.74[-3]	1.72[-3]	1.66[-3]	1.56[-3]	1.39[-3]	1.15[-3]	7.88[-4]
5	6	1.25[-2]	1.00[-2]	9.26[-3]	8.92[-3]	9.23[-3]	1.01[-2]	1.12[-2]	1.31[-2]
5	7	5.81[-3]	5.98[-3]	6.03[-3]	6.07[-3]	6.10[-3]	6.15[-3]	6.20[-3]	6.26[-3]
5	8	1.66[-1]	1.58[-1]	1.56[-1]	1.59[-1]	1.67[-1]	1.82[-1]	2.03[-1]	2.36[-1]
5	9	6.52[-1]	6.48[-1]	6.53[-1]	6.74[-1]	7.10[-1]	7.70[-1]	8.52[-1]	9.80[-1]
5	10	2.41[-1]	2.45[-1]	2.49[-1]	2.58[-1]	2.71[-1]	2.92[-1]	3.21[-1]	3.72[-1]
6	7	1.62[-2]	1.62[-2]	1.60[-2]	1.53[-2]	1.42[-2]	1.25[-2]	1.03[-2]	6.93[-3]
6	8	1.52[-2]	1.52[-2]	1.51[-2]	1.47[-2]	1.42[-2]	1.33[-2]	1.24[-2]	1.11[-2]
6	9	2.00[-3]	2.76[-3]	2.97[-3]	3.00[-3]	2.83[-3]	2.49[-3]	2.02[-3]	1.34[-3]
6	10	5.50[-4]	5.83[-4]	5.86[-4]	5.63[-4]	5.18[-4]	4.47[-4]	3.55[-4]	2.26[-4]

Table 3.14b. Fe XXIII (continued)

Levels		T [$\times 10^6$ K]							
i	j	0.05	0.25	0.5	1.25	2.5	5.0	10.0	25.0
7	8	4.50[-2]	4.49[-2]	4.44[-2]	4.29[-2]	4.05[-2]	3.70[-2]	3.24[-2]	2.58[-2]
7	9	9.34[-3]	1.88[-2]	2.15[-2]	2.27[-2]	2.19[-2]	2.00[-2]	1.70[-2]	1.27[-2]
7	10	3.25[-3]	3.55[-3]	3.60[-3]	3.49[-3]	3.24[-3]	2.81[-3]	2.26[-3]	1.46[-3]
8	9	5.83[-2]	5.81[-2]	5.77[-2]	5.58[-2]	5.31[-2]	4.89[-2]	4.35[-2]	3.62[-2]
8	10	6.85[-3]	7.35[-3]	7.45[-3]	7.35[-3]	7.05[-3]	6.56[-3]	5.94[-3]	5.15[-3]
9	10	1.96[-2]	1.96[-2]	1.95[-2]	1.95[-2]	1.95[-2]	1.96[-2]	2.00[-2]	2.11[-2]

Table 3.15a. Fe XXIV. Fifteen $n = 2$, 3 and 4 fine-structure levels included in the calculation [97B3] and their observed energies E [Ry] in rydbergs [92R1]. $\Delta = E_i(\mathrm{BP}) - E_i(\mathrm{obs.})$, where $E_i(\mathrm{BP})$ is from the Breit-Pauli R-matrix calculation. The index i is used in Table 3.15b for transition keys; J is the total angular momentum for specifying the fine-structure level.

i	LS Term	J	E [Ry]	Δ	i	LS Term	J	E [Ry]	Δ
1	2s ^{2}S	1/2	0.0		9	4s ^{2}S	1/2	113.584	0.035
2	2p ^{2}P	1/2	3.57201	0.004	10	4p ^{2}P	1/2	113.990	0.030
3		3/2	4.74549	−0.014	11		3/2	114.136	0.018
4	3s ^{2}S	1/2	84.497	0.034	12	4d ^{2}D	3/2	114.266	0.050
5	3p ^{2}P	1/2	85.461	0.048	13		5/2	114.321	0.040
6		3/2	85.815	0.024	14	4f ^{2}F	5/2	114.342	0.028
7	3d ^{2}D	3/2	86.197	0.034	15		7/2	114.379	0.014
8		5/2	86.321	0.019					

Table 3.15b. Fe XXIV. Effective collision strengths $\Upsilon(i,j)$ as a function of temperature T [K] for the transitions between the three $n = 2$ levels and fourteen $n' = 2$, 3 and 4 levels as specified in Table 3.15a for [97B3].

Levels		$\log T$									
i	j	6.2	6.4	6.6	6.8	7.0	7.2	7.4	7.6	7.8	8.0
1	2	1.66[-1]	1.75[-1]	1.85[-1]	1.98[-1]	2.12[-1]	2.28[-1]	2.46[-1]	2.66[-1]	2.87[-1]	3.10[-1]
1	3	3.17[-1]	3.33[-1]	3.52[-1]	3.74[-1]	4.00[-1]	4.30[-1]	4.64[-1]	5.03[-1]	5.45[-1]	5.88[-1]
1	4	1.60[-2]	1.56[-2]	1.52[-2]	1.49[-2]	1.48[-2]	1.50[-2]	1.53[-2]	1.58[-2]	1.63[-2]	1.68[-2]
1	5	5.57[-3]	5.53[-3]	5.57[-3]	5.79[-3]	6.33[-3]	7.28[-3]	8.75[-3]	1.08[-2]	1.34[-2]	1.66[-2]
1	6	1.04[-2]	1.04[-2]	1.05[-2]	1.10[-2]	1.20[-2]	1.38[-2]	1.65[-2]	2.03[-2]	2.51[-2]	3.10[-2]
1	7	1.28[-2]	1.27[-2]	1.26[-2]	1.26[-2]	1.28[-2]	1.33[-2]	1.41[-2]	1.50[-2]	1.61[-2]	1.71[-2]
1	8	1.96[-2]	1.95[-2]	1.93[-2]	1.92[-2]	1.94[-2]	2.01[-2]	2.12[-2]	2.26[-2]	2.44[-2]	2.64[-2]
1	9	2.50[-3]	2.51[-3]	2.53[-3]	2.56[-3]	2.62[-3]	2.72[-3]	2.84[-3]	2.98[-3]	3.11[-3]	3.22[-3]
1	10	1.10[-3]	1.13[-3]	1.17[-3]	1.25[-3]	1.37[-3]	1.56[-3]	1.83[-3]	2.20[-3]	2.68[-3]	3.26[-3]

Table 3.15b. Fe XXIV (continued)

Levels		log T									
i	j	6.2	6.4	6.6	6.8	7.0	7.2	7.4	7.6	7.8	8.0
1	11	2.18[-3]	2.23[-3]	2.32[-3]	2.47[-3]	2.71[-3]	3.06[-3]	3.56[-3]	4.27[-3]	5.18[-3]	6.32[-3]
1	12	2.10[-3]	2.09[-3]	2.09[-3]	2.09[-3]	2.10[-3]	2.13[-3]	2.19[-3]	2.28[-3]	2.40[-3]	2.54[-3]
1	13	3.17[-3]	3.16[-3]	3.15[-3]	3.16[-3]	3.18[-3]	3.22[-3]	3.31[-3]	3.44[-3]	3.60[-3]	3.78[-3]
1	14	1.23[-3]	1.21[-3]	1.19[-3]	1.17[-3]	1.15[-3]	1.13[-3]	1.13[-3]	1.14[-3]	1.15[-3]	1.16[-3]
1	15	1.65[-3]	1.62[-3]	1.59[-3]	1.56[-3]	1.53[-3]	1.51[-3]	1.51[-3]	1.52[-3]	1.54[-3]	1.57[-3]
2	3	3.73[-2]	4.12[-2]	4.29[-2]	4.17[-2]	3.81[-2]	3.35[-2]	2.90[-2]	2.52[-2]	2.23[-2]	2.02[-2]
2	4	4.74[-3]	3.72[-3]	2.95[-3]	2.38[-3]	2.00[-3]	1.80[-3]	1.75[-3]	1.85[-3]	2.08[-3]	2.42[-3]
2	5	1.65[-2]	1.60[-2]	1.56[-2]	1.53[-2]	1.51[-2]	1.52[-2]	1.54[-2]	1.57[-2]	1.60[-2]	1.63[-2]
2	6	7.16[-3]	6.70[-3]	6.00[-3]	5.25[-3]	4.57[-3]	4.02[-3]	3.63[-3]	3.36[-3]	3.21[-3]	3.15[-3]
2	7	5.39[-2]	5.53[-2]	5.73[-2]	6.05[-2]	6.52[-2]	7.22[-2]	8.19[-2]	9.46[-2]	1.10[-1]	1.29[-1]
2	8	1.27[-2]	1.19[-2]	1.06[-2]	9.20[-3]	7.83[-3]	6.63[-3]	5.63[-3]	4.86[-3]	4.30[-3]	3.91[-3]
2	9	4.30[-4]	4.13[-4]	3.93[-4]	3.73[-4]	3.55[-4]	3.44[-4]	3.45[-4]	3.63[-4]	3.99[-4]	4.53[-4]
2	10	2.75[-3]	2.73[-3]	2.72[-3]	2.72[-3]	2.74[-3]	2.79[-3]	2.87[-3]	2.96[-3]	3.04[-3]	3.10[-3]
2	11	1.40[-3]	1.34[-3]	1.27[-3]	1.18[-3]	1.08[-3]	9.82[-4]	8.92[-4]	8.18[-4]	7.63[-4]	7.28[-4]
2	12	9.90[-3]	1.01[-2]	1.04[-2]	1.09[-2]	1.16[-2]	1.26[-2]	1.40[-2]	1.57[-2]	1.79[-2]	2.05[-2]
2	13	2.57[-3]	2.43[-3]	2.25[-3]	2.04[-3]	1.79[-3]	1.53[-3]	1.29[-3]	1.07[-3]	8.85[-4]	7.35[-4]
2	14	1.70[-3]	1.71[-3]	1.74[-3]	1.80[-3]	1.90[-3]	2.05[-3]	2.25[-3]	2.49[-3]	2.77[-3]	3.06[-3]
2	15	1.05[-3]	9.84[-4]	8.99[-4]	8.02[-4]	6.97[-4]	5.95[-4]	5.04[-4]	4.30[-4]	3.76[-4]	3.40[-4]
3	4	1.04[-2]	8.31[-3]	6.63[-3]	5.36[-3]	4.48[-3]	4.00[-3]	3.87[-3]	4.08[-3]	4.60[-3]	5.39[-3]
3	5	8.01[-3]	7.34[-3]	6.49[-3]	5.63[-3]	4.89[-3]	4.30[-3]	3.89[-3]	3.62[-3]	3.49[-3]	3.44[-3]
3	6	4.10[-2]	4.00[-2]	3.86[-2]	3.73[-2]	3.62[-2]	3.57[-2]	3.56[-2]	3.58[-2]	3.62[-2]	3.66[-2]
3	7	2.69[-2]	2.62[-2]	2.50[-2]	2.39[-2]	2.32[-2]	2.31[-2]	2.39[-2]	2.55[-2]	2.80[-2]	3.13[-2]
3	8	1.11[-1]	1.13[-1]	1.16[-1]	1.20[-1]	1.28[-1]	1.40[-1]	1.57[-1]	1.80[-1]	2.08[-1]	2.42[-1]
3	9	8.68[-4]	8.34[-4]	7.96[-4]	7.57[-4]	7.23[-4]	7.05[-4]	7.14[-4]	7.58[-4]	8.40[-4]	9.60[-4]
3	10	1.38[-3]	1.32[-3]	1.25[-3]	1.16[-3]	1.07[-3]	9.77[-4]	8.97[-4]	8.36[-4]	8.00[-4]	7.90[-4]
3	11	7.29[-3]	7.22[-3]	7.12[-3]	7.04[-3]	7.02[-3]	7.08[-3]	7.20[-3]	7.35[-3]	7.48[-3]	7.58[-3]
3	12	5.10[-3]	4.97[-3]	4.82[-3]	4.65[-3]	4.50[-3]	4.40[-3]	4.39[-3]	4.50[-3]	4.76[-3]	5.15[-3]
3	13	2.03[-2]	2.06[-2]	2.10[-2]	2.17[-2]	2.28[-2]	2.44[-2]	2.67[-2]	2.98[-2]	3.37[-2]	3.85[-2]
3	14	1.91[-3]	1.82[-3]	1.72[-3]	1.61[-3]	1.50[-3]	1.41[-3]	1.35[-3]	1.33[-3]	1.34[-3]	1.38[-3]
3	15	3.83[-3]	3.81[-3]	3.81[-3]	3.85[-3]	3.95[-3]	4.14[-3]	4.43[-3]	4.82[-3]	5.29[-3]	5.79[-3]

Table 3.16a. Fe XXVI. 16 fine-structure $n = 1$, 2, 3 and 4 levels included in the calculation [96K2] and their theoretical energies E [Ry] in rydbergs. The index i is used in Table 3.16b for transition keys.

i	Level	E [Ry]	i	Level	E [Ry]	i	Level	E [Ry]	i	Level	E [Ry]
1	$1s_{1/2}$	0.00000	5	$3p_{1/2}$	606.09088	9	$3d_{5/2}$	606.70381	13	$4p_{3/2}$	639.52059
2	$2p_{1/2}$	510.95198	6	$3s_{1/2}$	606.10384	10	$4p_{1/2}$	639.32572	14	$4f_{5/2}$	639.58408
3	$2s_{1/2}$	510.99499	7	$3d_{3/2}$	606.55231	11	$4s_{1/2}$	639.33120	15	$4d_{5/2}$	639.58420
4	$2p_{3/2}$	512.51098	8	$3p_{3/2}$	606.55314	12	$4d_{3/2}$	639.52024	16	$4f_{7/2}$	639.61593

Table 5.3.16b. Fe XXVI. Effective collision strengths $\Upsilon(i,j)$ as a function of temperature T [K] for transitions among the 16 n = 1, 2, 3 and 4 levels as specified in Table 3.16a [96K2].

Levels		$\log T$				Levels		$\log T$			
i	j	6.0	6.5	7.0	7.5	i	j	6.0	6.5	7.0	7.5
1	2	1.49[-3]	1.65[-3]	1.74[-3]	1.64[-3]	4	10	2.28[-3]	1.79[-3]	1.24[-3]	7.80[-4]
1	3	1.14[-3]	1.43[-3]	1.42[-3]	1.18[-3]	4	11	1.78[-3]	1.30[-3]	8.69[-4]	5.72[-4]
1	4	3.03[-3]	3.67[-3]	3.66[-3]	3.30[-3]	4	12	6.12[-3]	5.22[-3]	4.33[-3]	3.28[-3]
1	5	3.59[-4]	3.66[-4]	3.52[-4]	3.02[-4]	4	13	7.95[-3]	7.26[-3]	6.54[-3]	5.21[-3]
1	6	2.79[-4]	2.84[-4]	2.61[-4]	2.11[-4]	4	14	3.66[-3]	2.71[-3]	1.82[-3]	1.18[-3]
1	7	1.15[-4]	1.17[-4]	8.74[-5]	5.64[-5]	4	15	1.95[-2]	1.91[-2]	1.99[-2]	1.85[-2]
1	8	6.81[-4]	6.90[-4]	6.74[-4]	5.89[-4]	4	16	5.60[-3]	4.71[-3]	4.05[-3]	3.44[-3]
1	9	1.64[-4]	1.67[-4]	1.24[-4]	8.03[-5]	5	8	1.30[-1]	1.30[-1]	1.14[-1]	8.91[-2]
1	10	1.87[-4]	1.61[-4]	1.40[-4]	1.12[-4]	5	9	5.34[-2]	5.56[-2]	3.58[-2]	2.01[-2]
1	11	1.63[-4]	1.30[-4]	1.05[-4]	7.93[-5]	5	10	5.93[-2]	5.98[-2]	6.09[-2]	5.25[-2]
1	12	7.15[-5]	5.38[-5]	3.83[-5]	2.54[-5]	5	11	7.38[-3]	6.34[-3]	6.05[-3]	6.11[-3]
1	13	2.80[-4]	2.66[-4]	2.56[-4]	2.16[-4]	5	12	7.53[-2]	8.57[-2]	1.16[-1]	1.31[-1]
1	14	2.46[-5]	1.44[-5]	6.55[-6]	2.82[-6]	5	13	1.21[-2]	1.08[-2]	9.98[-3]	8.63[-3]
1	15	7.82[-5]	6.28[-5]	4.92[-5]	3.46[-5]	5	14	8.09[-2]	8.51[-2]	9.54[-2]	9.08[-2]
1	16	2.31[-5]	1.39[-5]	6.65[-6]	3.03[-6]	5	15	1.82[-2]	1.52[-2]	1.21[-2]	9.06[-3]
2	4	2.92[-2]	4.14[-2]	4.02[-2]	2.67[-2]	5	16	2.23[-2]	1.71[-2]	1.24[-2]	8.78[-3]
2	5	1.36[-2]	1.42[-2]	1.39[-2]	1.19[-2]	6	7	9.08[-2]	9.26[-2]	7.76[-2]	5.84[-2]
2	6	1.97[-3]	2.19[-3]	1.67[-3]	1.17[-3]	6	9	1.39[-1]	1.40[-1]	1.17[-1]	8.81[-2]
2	7	4.60[-2]	4.97[-2]	5.66[-2]	5.86[-2]	6	10	1.47[-2]	1.65[-2]	2.29[-2]	2.75[-2]
2	8	5.49[-3]	5.59[-3]	4.27[-3]	2.84[-3]	6	11	5.83[-2]	5.90[-2]	6.07[-2]	5.28[-2]
2	9	1.01[-2]	1.00[-2]	7.33[-3]	4.49[-3]	6	12	2.86[-2]	2.98[-2]	3.35[-2]	3.22[-2]
2	10	3.36[-3]	3.06[-3]	2.77[-3]	2.24[-3]	6	13	2.42[-2]	2.81[-2]	4.11[-2]	5.05[-2]
2	11	1.19[-3]	8.17[-4]	4.95[-4]	3.03[-4]	6	14	3.13[-2]	2.94[-2]	2.77[-2]	2.28[-2]
2	12	9.27[-3]	9.27[-3]	1.00[-2]	9.55[-3]	6	15	4.26[-2]	4.45[-2]	5.00[-2]	4.08[-2]
2	13	2.09[-3]	1.68[-3]	1.18[-3]	7.47[-4]	6	16	4.18[-2]	3.90[-2]	3.68[-2]	3.04[-2]
2	14	2.58[-3]	2.17[-3]	1.94[-3]	1.73[-3]	7	9	2.06[-1]	2.15[-1]	1.35[-1]	7.06[-2]
2	15	3.28[-3]	2.65[-3]	1.84[-3]	1.08[-3]	7	10	1.29[-2]	1.06[-2]	8.70[-3]	7.34[-3]
2	16	1.96[-3]	1.41[-3]	8.65[-4]	4.72[-4]	7	11	8.42[-3]	6.26[-3]	4.17[-3]	2.80[-3]
3	5	5.20[-3]	5.86[-3]	6.79[-3]	7.43[-3]	7	12	1.27[-1]	1.23[-1]	1.20[-1]	1.01[-1]
3	6	1.26[-2]	1.31[-2]	1.34[-2]	1.19[-2]	7	13	1.75[-2]	1.27[-2]	7.87[-3]	4.86[-3]
3	7	1.13[-2]	1.19[-2]	1.21[-2]	1.12[-2]	7	14	5.02[-1]	5.44[-1]	6.55[-1]	6.76[-1]
3	8	9.34[-3]	1.04[-2]	1.23[-2]	1.37[-2]	7	15	3.43[-2]	2.46[-2]	1.52[-2]	8.94[-3]
3	9	1.63[-2]	1.71[-2]	1.78[-2]	1.66[-2]	7	16	5.64[-2]	4.05[-2]	2.46[-2]	1.39[-2]
3	10	1.85[-3]	1.60[-3]	1.55[-3]	1.48[-3]	8	10	1.23[-2]	1.12[-2]	1.06[-2]	9.42[-3]
3	11	3.16[-3]	2.87[-3]	2.69[-3]	2.26[-3]	8	11	1.16[-2]	1.05[-2]	1.17[-2]	1.28[-2]
3	12	2.68[-3]	2.28[-3]	2.00[-3]	1.62[-3]	8	12	3.85[-2]	3.72[-2]	3.98[-2]	3.92[-2]
3	13	2.85[-3]	2.66[-3]	2.79[-3]	2.77[-3]	8	13	1.28[-1]	1.29[-1]	1.32[-1]	1.15[-1]
3	14	2.02[-3]	1.61[-3]	1.31[-3]	1.02[-3]	8	14	5.30[-2]	4.73[-2]	4.41[-2]	3.79[-2]
3	15	3.70[-3]	3.26[-3]	2.94[-3]	2.43[-3]	8	15	1.58[-1]	1.76[-1]	2.29[-1]	2.55[-1]
3	16	2.46[-3]	2.02[-3]	1.70[-3]	1.33[-3]	8	16	1.59[-1]	1.61[-1]	1.76[-1]	1.65[-1]
4	5	5.85[-3]	5.93[-3]	4.52[-3]	3.04[-3]	9	10	1.13[-2]	8.11[-3]	4.90[-3]	2.82[-3]
4	6	3.91[-3]	4.12[-3]	3.18[-3]	2.35[-3]	9	11	1.20[-2]	9.12[-3]	6.21[-3]	4.22[-3]
4	7	2.25[-2]	2.34[-2]	2.13[-2]	1.79[-2]	9	12	3.39[-2]	2.43[-2]	1.51[-2]	9.01[-3]
4	8	3.29[-2]	3.38[-2]	3.20[-2]	2.68[-2]	9	13	3.18[-2]	2.50[-2]	1.92[-2]	1.51[-2]
4	9	9.40[-2]	1.01[-1]	1.12[-1]	1.13[-1]	9	14	9.75[-2]	8.27[-2]	7.35[-2]	6.35[-2]

Table 3.16b. Fe XXVI (continued)

Levels		log T				Levels		log T			
i	j	6.0	6.5	7.0	7.5	i	j	6.0	6.5	7.0	7.5
9	15	2.11[-1]	2.03[-1]	1.91[-1]	1.58[-1]	11	15	5.06[-1]	4.72[-1]	4.33[-1]	3.43[-1]
9	16	7.73[-1]	8.25[-1]	9.96[-1]	9.84[-1]	11	16	1.17[-1]	8.91[-2]	5.86[-2]	3.92[-2]
10	13	4.17[-1]	3.87[-1]	3.56[-1]	2.83[-1]	12	15	3.42[-1]	2.66[-1]	2.00[-1]	1.44[-1]
10	14	2.99[-1]	2.64[-1]	2.29[-1]	1.78[-1]	12	16	2.56[-1]	1.55[-1]	7.75[-2]	4.00[-2]
10	15	1.01[-1]	8.11[-2]	6.60[-2]	5.22[-2]	13	14	2.30[-1]	1.68[-1]	1.14[-1]	7.71[-2]
10	16	9.93[-2]	6.36[-2]	3.49[-2]	1.98[-2]	13	16	6.04[-1]	5.17[-1]	4.26[-1]	3.20[-1]
11	12	3.36[-1]	3.13[-1]	2.87[-1]	2.27[-1]	14	16	7.37[-1]	4.55[-1]	2.33[-1]	1.19[-1]
11	14	8.65[-2]	6.23[-2]	4.14[-2]	2.84[-2]						

3.1.6 References for 3.1

72E1 W. Eissner and M.J. Seaton, J. Phys. B: At. Mol. Opt. Phys. 5, 2187 (1972)
74E1 W. Eissner, M. Jones and H. Nussbaumer, Comput. Phys. Commun. 8, 270 (1974)
75H1 A. Hibbert, Comput. Phys. Commun. 9, 141 (1975)
75R1 J. Reader and J. Sugar, J. Phys. Chem. Ref. Data 4, 353 (1975)
75W1 D.W. Walker, J. Phys. B: At. Mol. Opt. Phys. 8, 760 (1975)
80C1 R. Cowan, J. Phys. B: At. Mol. Opt. Phys. 13, 1471 (1980)
81H1 R.J.W. Henry, Phys. Rep. 68, 1 (1981)
81P1 A.K. Pradhan, Phys. Rev. Lett. 47, 79 (1981)
82C1 C. Corliss and J. Sugar, J. Phys. Chem. Ref. Data 11, 135 (1982)
82S1 N.S. Scott and K.T. Taylor, Comput. Phys. Commun. 25, 347 (1982)
83P1 A.K. Pradhan, Phys. Rev. A 28, 2113 (1983)
83P2 A.K. Pradhan, Phys. Rev. A 28, 2128 (1983)
85B1 R.H. Bell and M.J. Seaton, J. Phys. B: At. Mol. Opt. Phys. 18, 1589 (1985)
85S1 J. Sugar and C. Corliss, J. Phys. Chem. Ref. Data 14, Suppl. 2 (1985)
86B1 V.M. Burke and M.J. Seaton, J.Phys.B 19, L527 (1986)
87N1 P.H. Norrington and I.P. Grant, J. Phys. B: At. Mol. Opt. Phys. 20, 4869 (1987)
89S1 D.H.Sampson, H.L.Zhang, A.K.Mohanty, and R.E.H.Clark, Phys. Rev. A 40, 604 (1989)
89Z1 H.L. Zhang, D.H. Sampson and A.K. Mohanty, Phys. Rev. A 40, 616(1989)
89Z2 H.L. Zhang and D.H. Sampson, Atomic Data Nucl. Data Tables 43, 1 (1989)
90C1 M.H. Chen and K.J. Reed, Phys. Rev. A 41, 4759 (1990)
90C2 R.E.H. Clark, Astrophys. J. 354, 382 (1990)
90G1 V.F. Gedeon, O.I. Zatsarinnyi and E.A. Masalovich, Opt. Spectrosc. 69, 439 (1990)
90G2 D.C. Griffin and M.S. Pindzola, Phys. Rev. A 42, 248 (1990)
90H1 Y.K. Ho and R.J.W. Henry, Astrophys. J. 351, 701 (1990)
90J1 C.T. Johnson and A.E. Kingston, J. Phys. B: At. Mol. Opt. Phys. 23, 3393 (1990)
90K1 T. Kato, J. Lang and K.E. Berrington, Atomic Data Nucl. Data Tables 44, 133 (1990)
90L1 D. Luo and A.K. Pradhan, Phys. Rev. A 41, 165 (1990)
90M1 M. Mohan and M. LeDourneuf, Astron. Astrophys. 227, 285 (1990)
90M2 M. Mohan and M. LeDourneuf, Phys. Rev. A 41, 2862 (1990)
90M3 M. Mohan, M. LeDourneuf, A. Hibbert and P.G. Burke, Mon. Not. R. Astron. Soc. 243, 372 (1990)

Table 3.16b. Fe XXVI (continued)

Levels		log T				Levels		log T			
i	j	6.0	6.5	7.0	7.5	i	j	6.0	6.5	7.0	7.5
9	15	2.11[-1]	2.03[-1]	1.91[-1]	1.58[-1]	11	15	5.06[-1]	4.72[-1]	4.33[-1]	3.43[-1]
9	16	7.73[-1]	8.25[-1]	9.96[-1]	9.84[-1]	11	16	1.17[-1]	8.91[-2]	5.86[-2]	3.92[-2]
10	13	4.17[-1]	3.87[-1]	3.56[-1]	2.83[-1]	12	15	3.42[-1]	2.66[-1]	2.00[-1]	1.44[-1]
10	14	2.99[-1]	2.64[-1]	2.29[-1]	1.78[-1]	12	16	2.56[-1]	1.55[-1]	7.75[-2]	4.00[-2]
10	15	1.01[-1]	8.11[-2]	6.60[-2]	5.22[-2]	13	14	2.30[-1]	1.68[-1]	1.14[-1]	7.71[-2]
10	16	9.93[-2]	6.36[-2]	3.49[-2]	1.98[-2]	13	16	6.04[-1]	5.17[-1]	4.26[-1]	3.20[-1]
11	12	3.36[-1]	3.13[-1]	2.87[-1]	2.27[-1]	14	16	7.37[-1]	4.55[-1]	2.33[-1]	1.19[-1]
11	14	8.65[-2]	6.23[-2]	4.14[-2]	2.84[-2]						

3.1.6 References for 3.1

72E1 W. Eissner and M.J. Seaton, J. Phys. B: At. Mol. Opt. Phys. 5, 2187 (1972)
74E1 W. Eissner, M. Jones and H. Nussbaumer, Comput. Phys. Commun. 8, 270 (1974)
75H1 A. Hibbert, Comput. Phys. Commun. 9, 141 (1975)
75R1 J. Reader and J. Sugar, J. Phys. Chem. Ref. Data 4, 353 (1975)
75W1 D.W. Walker, J. Phys. B: At. Mol. Opt. Phys. 8, 760 (1975)
80C1 R. Cowan, J. Phys. B: At. Mol. Opt. Phys. 13, 1471 (1980)
81H1 R.J.W. Henry, Phys. Rep. 68, 1 (1981)
81P1 A.K. Pradhan, Phys. Rev. Lett. 47, 79 (1981)
82C1 C. Corliss and J. Sugar, J. Phys. Chem. Ref. Data 11, 135 (1982)
82S1 N.S. Scott and K.T. Taylor, Comput. Phys. Commun. 25, 347 (1982)
83P1 A.K. Pradhan, Phys. Rev. A 28, 2113 (1983)
83P2 A.K. Pradhan, Phys. Rev. A 28, 2128 (1983)
85B1 R.H. Bell and M.J. Seaton, J. Phys. B: At. Mol. Opt. Phys. 18, 1589 (1985)
85S1 J. Sugar and C. Corliss, J. Phys. Chem. Ref. Data 14, Suppl. 2 (1985)
86B1 V.M. Burke and M.J. Seaton, J.Phys.B 19, L527 (1986)
87N1 P.H. Norrington and I.P. Grant, J. Phys. B: At. Mol. Opt. Phys. 20, 4869 (1987)
89S1 D.H.Sampson, H.L.Zhang, A.K.Mohanty, and R.E.H.Clark, Phys. Rev. A 40, 604 (1989)
89Z1 H.L. Zhang, D.H. Sampson and A.K. Mohanty, Phys. Rev. A 40, 616(1989)
89Z2 H.L. Zhang and D.H. Sampson, Atomic Data Nucl. Data Tables 43, 1 (1989)
90C1 M.H. Chen and K.J. Reed, Phys. Rev. A 41, 4759 (1990)
90C2 R.E.H. Clark, Astrophys. J. 354, 382 (1990)
90G1 V.F. Gedeon, O.I. Zatsarinnyi and E.A. Masalovich, Opt. Spectrosc. 69, 439 (1990)
90G2 D.C. Griffin and M.S. Pindzola, Phys. Rev. A 42, 248 (1990)
90H1 Y.K. Ho and R.J.W. Henry, Astrophys. J. 351, 701 (1990)
90J1 C.T. Johnson and A.E. Kingston, J. Phys. B: At. Mol. Opt. Phys. 23, 3393 (1990)
90K1 T. Kato, J. Lang and K.E. Berrington, Atomic Data Nucl. Data Tables 44, 133 (1990)
90L1 D. Luo and A.K. Pradhan, Phys. Rev. A 41, 165 (1990)
90M1 M. Mohan and M. LeDourneuf, Astron. Astrophys. 227, 285 (1990)
90M2 M. Mohan and M. LeDourneuf, Phys. Rev. A 41, 2862 (1990)
90M3 M. Mohan, M. LeDourneuf, A. Hibbert and P.G. Burke, Mon. Not. R. Astron. Soc. 243, 372 (1990)

90M4 M. Mohan, A. Hibbert, K.A. Berrington and P.G. Burke, J. Phys. B: At. Mol. Opt. Phys. 23, 989 (1990)
90M5 M. Mohan, A. Hibbert and P.G. Burke, J. Phys. B: At. Mol. Opt. Phys. 23, 997 (1990)
90S1 U.I. Safronova, T. Kato, K. Masai, L.A. Vainshtein and A.S. Shlyapzeva, NIFS-DATA-8 (1990)
90S2 D.H. Sampson, H.L. Zhang and C.J. Fontes, Atomic Data Nucl. Data Tables 44, 209 (1990)
90Z1 H.L. Zhang, D.H. Sampson and C.J. Fontes, Atomic Data Nucl. Data Tables 44, 31 (1990)
90Z2 H.L. Zhang, D.H. Sampson and C.J. Fontes, Atomic Data Nucl. Data Tables 44, 273 (1990)
90Z3 H.L. Zhang, D.H. Sampson and R.E.H. Clark, Phys. Rev. A 41, 198 (1990)
91A1 K.M. Aggarwal, Astrophys. J. Supp. 77, 677 (1991)
91A2 K.M. Aggarwal, K.A. Berrington, W.B. Eissner and P.H. Norrington, J. Phys. B: At. Mol. Opt. Phys. 24, 2201 (1991)
91A3 K.M. Aggarwal and A. Hibbert, J. Phys. B: At. Mol. Opt. Phys. 24, 3445 (1991)
91A4 K.M. Aggarwal and A.E. Kingston, J. Phys. B: At. Mol. Opt. Phys. 24, 4583 (1991)
91A5 K.M. Aggarwal, K.A. Berrington, A.E. Kingston and A. Pathak, J. Phys. B: At. Mol. Opt. Phys. 24, 1757 (1991)
91A6 K.M. Aggarwal and A.E. Kingston, Phys. Scr. 44, 517 (1991)
91B1 N.R. Badnell, M.S. Pindzola and D.C. Griffin, Phys. Rev. A 43, 2250 (1991)
91B2 K.A. Berrington and S. Nakazaki, J. Phys. B: At. Mol. Opt. Phys. 24, 1411 (1991)
91B3 K.A. Berrington, C.J. Zeippen, M. LeDourneuf, W. Eissner and P.G. Burke, J. Phys. B: At. Mol. Opt. Phys. 24, 3467 (1991)
91B4 R.D. Blum and A.K. Pradhan, Phys. Rev. A 44, 6123 (1991)
91B5 A. Burgess, H.E. Mason and J.A. Tully, Astrophys. J. 376, 803 (1991)
91C1 M.H. Chen and B. Crasemann, Phys. Rev. A 43, 5886 (1991)
91C2 R.E.H. Clark and J. Abdallah Jr., Phys. Scr. T37, 28 (1991)
91D1 P.L. Dufton and A.E. Kingston, Mon. Not. R. Astron. Soc. 248, 827 (1991)
91D2 P.L. Dufton and A.E. Kingston, Phys. Scr. 43, 386 (1991)
91F1 B.C. Fawcett and H.E. Mason, Atomic Data Nucl. Data Tables 47, 17 (1991)
91G1 D.C. Griffin, M.S. Pindzola and N.R. Badnell, J. Phys. B: At. Mol. Opt. Phys. 24, L621 (1991)
91K1 T. Kato and U.I. Safronova, Optics and Spectroscopy 70, 291 (1991)
91L1 D.J. Lennon and V.M. Burke, Mon. Not. R. Astron. Soc. 251, 628 (1991)
91M1 M. Mohan, M. LeDourneuf and A. Hibbert, J. Phys. B: At. Mol. Opt. Phys. 24, 299 (1991)
91M2 M. Mohan, K.L. Baluja, V. Prasad and A. Hibbert, J. Phys. B: At. Mol. Opt. Phys. 24, 3889 (1991)
91M3 D.L. Moores and M.S. Pindzola, Z. Phys. D 21, S187 (1991)
91N1 S. Nakazaki and K.A. Berrington, Phys. Rev. A 43, 3509 (1991)
91P1 X. Pan, Phys. Rev. A 44, 7269 (1991)
91P2 M.S. Pindzola, N.R. Badnell, R.J.W. Henry and D.C. Griffin, Phys. Rev. A 44, 5628 (1991)
91S1 D.H. Sampson, H.L. Zhang and C.J. Fontes, Atomic Data Nucl. Data Tables 48, 25 (1991)
91U1 K. Unnikrishnan, J. Callaway and D.H. Oza, Phys. Rev. A 43, 5966 (1991)
91W1 W.P. Wijesundera, I.P. Grant, P.H. Norrington and F.A. Parpia, J. Phys. B: At. Mol. Opt. Phys. 24, 1017 (1991)
91W2 W.P. Wijesundera, F.A. Parpia, I.P. Grant and P.H. Norrington, J. Phys. B: At. Mol. Opt. Phys. 24, 1803 (1991)
91Z1 O.I. Zatsarinny, V.I. Lengyel and E.A. Masalovich, Phys. Rev. A 44, 7343 (1991)

91Z2 H.L. Zhang, D.H. Sampson and C.J. Fontes, Atomic Data Nucl. Data Tables 48, 91 (1991)
92A1 K.M. Aggarwal, Astrophys. J. Supp. 80, 453 (1992)
92A2 K.M. Aggarwal and A.E. Kingston, Phys. Scr. 46, 193 (1992)
92A3 K.M. Aggarwal and A.E. Kingston, J. Phys. B: At. Mol. Opt. Phys. 25, 751 (1992)
92A4 K.M. Aggarwal, J. Callaway, A.E. Kingston and K. Unnikrishnan, Astrophys. J. Supp. 80, 473 (1992)
92B1 K.A. Berrington and R.E.H. Clark, Nucl. Fusion Supp. 3, 87 (1992)
92B2 A.K. Bhatia and G.A. Doschek, Atomic Data Nucl. Data Tables 52, 1 (1992)
92B3 R.D. Blum and A.K.Pradhan, Astrophys. J. Supp. 80, 425 (1992)
92B4 V.M. Burke, J. Phys. B: At. Mol. Opt. Phys. 25, 4917 (1992)
92B5 A. Burgess and J.A. Tully, Astron. Astrophys. 254, 436 (1992)
92C1 M.C. Chidichimo, Phys. Rev. A 45, 1690 (1992)
92C2 E.S. Conlon, F.P. Keenan and K.M. Aggarwal, Phys. Scr. 45, 309 (1992)
92C3 S. Chantrenne, P. Beirsdorfer, R. Cauble, and M.B. Schneider, Phys. Rev. Lett. 69, 265 (1992)
92D1 J.G. Doyle, F.P. Keenan, L.K. Harra, K.M. Aggarwal and S.S. Tayal, Astron. Astrophys. 261, 285 (1992)
92H1 M.A. Hayes, J. Phys. B: At. Mol. Opt. Phys. 25, 2649 (1992)
92I1 M.K. Inal, H.L. Zhang and D.H. Sampson, Phys. Rev. A 46, 2449 (1992)
92K1 F.P. Keenan, W.A. Feibelman and K.A. Berrington, Astrophys. J. 389, 443 (1992)
92K2 F.P. Keenan, L.K. Harra, K.M. Aggarwal and W.A. Feibelman, Astrophys. J. 385, 375 (1992)
92M1 D.L. Moores and M.S. Pindzola, J. Phys. B: At. Mol. Opt. Phys. 25, 4581 (1992)
92N1 I. Nasser and Y. Hahn, J. Phys. B: At. Mol. Opt. Phys. 25, 521 (1992)
92N2 S.N. Nahar and A.K. Pradhan, Phys. Rev. Lett 68, 1488 (1992)
92P1 A.K. Pradhan and J.W. Gallagher, Atomic Data and Nucl. Data Tables 52, 227 (1992)
92R1 J. Reader, J. Sugar, N. Acquista and R. Bahr, J. Opt. Soc. Am. B 11, 1930 (1992)
92S1 U.I. Safronova, A.S. Shlyapzeva, L.A. Vainshtein, T. Kato and K. Masai, Phys. Scr. 46, 409 (1992)
92S2 D.H. Sampson and H.L. Zhang, Phys. Rev. A 45, 1556 (1992)
92S3 V.P. Shevelko, Phys. Scr. 46, 531 (1992)
92S4 R.P. Stafford, K.L. Bell and A. Hibbert, J. Phys. B: At. Mol. Opt. Phys. 25, 5449 (1992)
92V1 L.A. Vainshtein and Y. Itikawa, Inst. Space Astron. Sci. Report No.647 (1992)
92Z1 H.L. Zhang and D.H. Sampson, Atomic Data Nucl. Data Tables 52, 143 (1992)
93A1 K.M. Aggarwal, Astrophys. J. Supp. 85, 197 (1993)
93A2 K.M. Aggarwal and A.E. Kingston, Astrophys. J. Supp. 85, 187 (1993)
93B1 A.K. Bhatia and S.O. Kastner, Atomic Data Nucl. Data Tables 54, 133 (1993)
93B2 A.K. Bhatia and S.O. Kastner, J. Quant. Spectrosc. Radiat. Transfer 49, 609 (1993)
93B3 A.K. Bhatia and G.A. Doschek, Atomic Data Nucl. Data Tables 55, 281 (1993)
93B4 A.K. Bhatia and G.A. Doschek, Atomic Data Nucl. Data Tables 55, 315 (1993)
93B5 A.K. Bhatia and G.A. Doschek, Atomic Data Nucl. Data Tables 53, 195 (1993)
93B6 I. Bray, I.E. McCarthy, J. Wigley and A.T. Stelbovics, J. Phys. B: At. Mol. Opt. Phys. 26, L831 (1993)
93B7 P.G. Burke and K.A. Berrington, *Atomic and Molecular Processes, an R-matrix Approach*, Institute of Physics Publ., Bristol UK, (1993)
93C1 W. Cai and A.K. Pradhan, Astrophys. J. Supp. 88, 329 (1993)
93C2 M.C. Chidichimo, D.W. Schranz and B. Zygelman, Phys. Rev. A 48, 4245 (1993)
93C3 W. Cunto, C. Mendoza, F. Ochsenbein and C.J. Zeippen, Astron. Astrophys. 275, L5 (1993)
93F1 C.J. Fontes, D.H. Sampson and H.L. Zhang, Phys. Rev. A 47, 1009 (1993)

93G1 D.C. Griffin, Phys. Rev. A 47, 2871 (1993)
93H1 D.G. Hummer, K.A. Berrington, W. Eissner, A.K. Pradhan, H.E. Saraph and J.A. Tully, Astron. Astrophys. 279, 298 (1993)
93I1 M.K. Inal and J. Dubau, Phys. Rev. A 47, 4794 (1993)
93I2 L.N. Ivanov, E.P. Ivanova and L.V. Knight, Phys. Rev. A 48, 4365 (1993)
93J1 Y.-D. Jung, Astrophys. J. 409, 841 (1993)
93K1 F.P. Keenan, E.S. Conlon, G.A. Warren, A.W. Boone and P.H. Norrington, Astrophys. J. 406, 350 (1993)
93M1 B.M. McLaughlin and K.L. Bell, J. Phys. B: At. Mol. Opt. Phys. 26, 3313 (1993)
93M2 B.M. McLaughlin and K.L. Bell, Astrophys. J. 408, 753 (1993)
93M3 B.M. McLaughlin and K.L. Bell, J. Phys. B: At. Mol. Opt. Phys. 26, 1797 (1993)
93N1 S. Nakazaki, K. Sakimoto and Y. Itikawa, Phys. Scr. 47, 359 (1993)
93P1 M.S. Pindzola, D.R. Schultz and D.C. Griffin, Phys. Rev. A 48, 4333 (1993)
93P2 A.K. Pradhan and K.A. Berrington, J. Phys. B: At. Mol. Opt. Phys. 26, 157 (1993)
93P3 A.K. Pradhan and H.L. Zhang, Astrophys. J. 409, L77 (1993)
93R1 K.J. Reed and M.H. Chen, Phys. Rev. A 48, 3644 (1993)
93S1 S.J. Smith, A. Chutjian, J. Mitroy, S.S. Tayal, R.J.W. Henry, K.F. Man, R.J. Mawhorter and I.D. Williams, Phys. Rev. A 48, 292 (1993)
93Z1 H.L. Zhang and D.H. Sampson, Phys. Rev. A 47, 208 (1993)
94A1 K.M. Aggarwal and F.P. Keenan, J. Phys. B: At. Mol. Opt. Phys. 27, 2343 (1994)
94A2 K.M. Aggarwal and F.P. Keenan, J. Phys. B: At. Mol. Opt. Phys. 27, 5321 (1994)
94B1 N.R. Badnell, D.C. Griffin, T.W. Gorczyca and M.S. Pindzola, Phys. Rev. A 50, 1231 (1994)
94B2 N.R. Badnell and D.L. Moores, Atomic Data Nucl. Data Tables 57, 329 (1994)
94B3 K.S. Baliyan and A.K. Bhatia, J. Phys. B: At. Mol. Opt. Phys. 27, 4281 (1994)
94B4 K.A. Berrington, Atomic Data Nucl. Data Tables 57, 71 (1994)
94B5 A.K. Bhatia, Atomic Data Nucl. Data Tables 57, 253 (1994)
94B6 K. Butler and C.J. Zeippen, Astron. Astrophys. Supp. 108, 1 (1994)
94B7 M.E. Bannister, X.Q. Guo, T.M. Kojima and G.H. Dunn, Phys. Rev. Lett. 72, 3336 (1994)
94C1 J. Callaway, Atomic Data Nucl. Data Tables 57, 9 (1994)
94C2 M.H. Chen, K.J. Reed and A.U. Hazi, Phys. Rev. A 49, 1782 (1994)
94C3 M.H. Chen and K.J. Reed, Phys. Rev. A 50, 2279 (1994)
94C4 M. Cornille, J. Dubau and S. Jacquemot, Atomic Data Nucl. Data Tables 58, 1 (1994)
94C5 M. Cornille, J. Dubau, P. Faucher, F. Bely-Dubau and C. Blancard, Astron. Astrophys. Suppl. 105, 77 (1994)
94D1 J. Dubau, Atomic Data Nucl. Data Tables 57, 21 (1994)
94D2 P.L. Dufton and A.E. Kingston, Atomic Data Nucl. Data Tables 57, 273 (1994)
94F1 W.C. Fon, K. Ratnavelu, K.M. Aggarwal and K.A. Berrington, J. Phys. B: At. Mol. Opt. Phys. 27, L803 (1994)
94F2 B.C.M. Fossi and M. Landini, Atomic Data Nucl. Data Tables 57, 125 (1994)
94F3 C.J. Fontes, D.H. Sampson and H.L. Zhang, Phys. Rev. A 49, 3704 (1994)
94K1 T. Kato, Atomic Data Nucl. Data Tables 57, 181 (1994)
94L1 J. Lang and H.P. Summers, Atomic Data Nucl. Data Tables 57, 215 (1994)
94L2 D.J. Lennon and V.M. Burke, Astron. Astrophys. Supp. 103, 273 (1994)
94M1 H.E. Mason, Atomic Data Nucl. Data Tables 57, 305 (1994)
94M2 B.M. McLaughlin and K.L. Bell, Mon. Not. R. Astron. Soc. 267, 231 (1994)
94M3 B.M. McLaughlin and K.L. Bell, Astrophys. J. Supp. 94, 825 (1994)
94M4 R.W.P. McWhirter, Atomic Data Nucl. Data Tables 57, 39 (1994)
94M5 M. Mohan and K.M. Aggarwal, Phys. Scr. 49, 62 (1994)
94M6 M. Mohan, A. Hibbert and A.E. Kingston, Astrophys. J. 434, 389 (1994)
94O1 N. O'Mahony, F.P. Keenan and E.S. Conlon, Phys. Scr. 49, 675 (1994)

94R1 C.A. Ramsbottom, K.A. Berrington, A. Hibbert and K.L. Bell, Phys. Scr. 50, 246 (1994)
94R2 C.A. Ramsbottom, K.A. Berrington and K.L. Bell, J. Phys. B: At. Mol. Opt. Phys. 27, L811 (1994)
94S1 D.H. Sampson, H.L. Zhang and C.J. Fontes, Atomic Data Nucl. Data Tables 57, 97 (1994)
94S2 H.E. Saraph and J.A. Tully, Astron. Astrophys. Supp. 107, 29 (1994)
94S3 R.P. Stafford, K.L. Bell and A. Hibbert, Mon. Not. R. Astron. Soc. 266, 715 (1994)
94S4 R.P. Stafford, K.L. Bell, A. Hibbert and W.P. Wijesundera, Mon. Not. R. Astron. Soc. 268, 816 (1994)
94S5 M.J.Seaton, Y. Yu, D. Mihalas and Anil K. Pradhan, Mon. Not. Roy. Astr. Soc 266, 805 (1994)
94T1 S.S. Tayal, Astrophys. J. 426, 449 (1994)
94W1 G.A. Warren, F.P. Keenan, E.S. Conlon and K.M. Aggarwal, Phys. Scr. 49, 91 (1994)
94Z1 H.L. Zhang and A.K. Pradhan, Phys. Rev. A 50, 3105 (1994)
94Z2 H.L. Zhang and D.H. Sampson, Atomic Data Nucl. Data Tables 56, 41 (1994)
94Z3 H.L. Zhang and D.H. Sampson, Atomic Data Nucl. Data Tables 58, 255 (1994)
94Z4 H.L. Zhang, M. Graziani and A.K. Pradhan, Astron. Astrophys. 283, 319 (1994)
95B1 K.A. Berrington, Astron. Astrophys. Supp. 109, 193 (1995)
95B2 K.A. Berrington and J.C. Pelan, Astron. Astrophys. Supp. 114, 367 (1995)
95B3 A.K. Bhatia and G.A. Doschek, Atomic Data Nucl. Data Tables 60, 97 (1995)
95B4 A.K. Bhatia and G.A. Doschek, Atomic Data Nucl. Data Tables 60, 145 (1995)
95B5 A. Burgess, M.C. Chidichimo and J.A. Tully, Astron. Astrophys. 300, 627 (1995)
95C1 M.H. Chen and A.L. Osterheld, Phys. Rev. A 52, 3790 (1995)
95G1 T.W. Gorczyca, M.S. Pindzola, N.R. Badnell and D.C. Griffin, Phys. Rev. A 51, 488 (1995)
95G2 T.W. Gorczyca, F. Robicheaux, M.S. Pindzola and N.R. Badnell, Phys. Rev. A 52, 3852 (1995)
95G3 D.C. Griffin and M.S. Pindzola, J. Phys. B: At. Mol. Opt. Phys. 28, 4347 (1995)
95G4 M.E. Galavis, C. Mendoza and C.J. Zeippen, Astron. Astrophys. Supp. 111, 347 (1995)
95H1 L.K. Harra-Murnion, A.W. Boone, F.P. Keenan, A.E. Kingston and P.H. Norrington, Phys. Scr. 51, 346 (1995)
95I1 Y. Itikawa, T. Kato and K. Sakimoto, Institute of Space and Astronautical Science Report No. 657, (1995)
95K1 R. Kisielius, K.A. Berrington and P.H. Norrington, J. Phys. B: At. Mol. Opt. Phys. 28, 2459 (1995)
95M1 M. Mohan, W. Eissner, A. Hibbert and P.G. Burke, J. Phys. B: At. Mol. Opt. Phys. 28, 2249 (1995)
95M2 M. Mohan, A. Hibbert, R.P. Staford and B. Sharma, Phys. Scr. 52, 162 (1995)
95O1 The Opacity Project Team, *The Opacity Project*, Inst. of Physics Publ., Bristol UK (1995)
95P1 J. Pelan and K.A. Berrington, Astron. Astrophys. Supp. 110, 209 (1995)
95P2 A.K. Pradhan and J. Peng, in *Analysis of Emission Lines*, Ed. R.E. Williams and M. Livio, Cambridge University Press (1995)
95R1 C.A. Ramsbottom, K.A. Berrington and K.L. Bell, Atomic Data Nucl. Data Tables 61, 105 (1995)
95S1 U.I. Safronova, M.S. Safronova and T. Kato, NIFS-DATA 29, (1995)
95S2 U.I. Safronova, A.S. Shlyaptseva, T. Kato, K. Masai and L.A. Vainshtein, Atomic Data Nucl. Data Tables 60, 1 (1995)
95S3 T. Schoning, Astron. Astrophys. 299, L25 (1995)
95S4 T. Schoning and K. Butler, Astron. Astrophys. 296, L29 (1995)
95S5 T.A.A. Sigut and A.K. Pradhan, J. Phys. B: At. Mol. Opt. Phys. 28, 4879 (1995)
95T1 S.S. Tayal, Astrophys. J. 446, 895 (1995)

95Z1 H.L. Zhang and A.K. Pradhan, Astron. Astrophys. 293, 953 (1995)
95Z2 H.L. Zhang and A.K. Pradhan, J. Phys. B: At. Mol. Opt. Phys. 28, L285 (1995)
95Z3 H.L. Zhang and A.K. Pradhan, J. Phys. B: At. Mol. Opt. Phys. 28, 3403 (1995)
95Z4 H.L. Zhang and A.K. Pradhan, Phys. Rev. A 52, 3366 (1995)
95Z5 H.L. Zhang and D.H. Sampson, Phys. Rev. A 52, 3827 (1995)
95Z6 M. Zuo, S.J. Smith, A. Chutjian, I.D. Williams, S.S. Tayal and B.M. McLaughlin, Astrophys. J. 440, 421 (1995)
96A1 S. Ait-Tahar, I.P. Grant and P.H. Norrington, Phys. Rev. A 54, 3984 (1996)
96B1 M.A. Bautista and A.K. Pradhan, Astron. Astrophys. Supp. 115, 551 (1996)
96B2 A.K. Bhatia and G.A. Doschek, Atomic Data Nucl. Data Tables 64, 183 (1996)
96C1 G.-X. Chen, Phys. Rev. A 53, 3227 (1996)
96C2 R.E.H. Clark and J. Abdallah Jr., Phys. Scr. T62, 7 (1996)
96F1 K.B. Fournier, W.H. Goldstein, M. May, M. Finkenthal and J.L. Terry, Phys. Rev. A 53, 3310 (1996)
96I1 Y. Itikawa, Atomic Data and Nucl. Data Tables 63, 315 (1996)
96K1 F.P. Keenan, I.J. Roche, V.J. Foster and M. Mohan, Phys. Scr. 54, 163 (1996)
96K2 R. Kisielius, K.A. Berrington and P.H. Norrington, Astron. Astrophys. Supp. 118, 157 (1996)
96M1 M. Mohan, R. Sharma and A. Hibbert, Phys. Scr. 54, 352 (1996)
96N1 S. Nakazaki, M. Okahara and Y. Itikawa, J. Phys. Soc. Jpn. 65, 2472 (1996)
96R1 C.A. Ramsbottom and K.L. Bell, Phys. Scr. 54, 357 (1996)
96R2 C.A. Ramsbottom, K.L. Bell and R.P. Stafford, Atomic Data Nucl. Data Tables 63, 57 (1996)
96S1 U.I. Safronova, M.S. Safronova and T. Kato, Phys. Scr. 54, 68 (1996)
96S2 H.E. Saraph and P.J. Storey, Astron. Astrophys. Supp. 115, 151 (1996)
96S3 S.J. Smith, M. Zuo, A. Chutjian, S.S. Tayal and I.D. Williams, Astrophys. J. 463, 808 (1996)
96S4 P.J. Storey, H.E. Mason and H.E. Saraph, Astron. Astrophys. 309, 677 (1996)
96T1 S.S. Tayal and R.J.W. Henry, J. Phys. B: At. Mol. Opt. Phys. 29, 3443 (1996)
96W1 M.S. Watts, K.A. Berrington, P.G. Burke and V.M. Burke, J. Phys. B: At. Mol. Opt. Phys. 29, L505 (1996)
96Y1 Z. Ying, Z. Qiren, P. Shoufu and S. Guizhen, Z. Phys. D 36, 1 (1996)
96Z1 H.L. Zhang, Astron. Astrophys. Supp. 119, 523 (1996)
96Z2 H.L. Zhang and D.H. Sampson, Atomic Data Nucl. Data Tables 63, 275 (1996)
97B1 K. Bartschat and I. Bray, J. Phys. B: At. Mol. Opt. Phys. 30, L109 (1997)
97B2 A.K. Bhatia, H.E. Mason and C. Blancard, Atomic Data Nucl. Data Tables 66, 83 (1997)
97B3 K.A. Berrington and J.A. Tully, Astron. Astrophys. Supp. 126, 105 (1997)
97E1 W. Eissner, M.E. Galavis, C. Mendoza and C.J. Zeippen, Astron. Astrophys. Supp. 136, 385 (1997)
97F1 V.I. Fisher, Y.V. Ralchenko, V.A. Bernshtam, A. Goldgirsh, Y. Marcon, L.A. Vainshtein, I. Bray and H. Golten, Phys. Rev. A 55, 329 (1997)
97G1 D.C. Griffin, M.S. Pindzola, J.A. Shaw, N.R. Badnell, M. O'Mullane and H.P. Summers, J. Phys. B: At. Mol. Opt. Phys. 30, 3543 (1997)
97L1 C. Liao, S.J. Smith, D. Hitz, A. Chutjian and S.S. Tayal, Astrophys. J. 484, 979 (1997)
97M1 P.J. Marchalant, K. Bartschat and I. Bray, J. Phys. B: At. Mol. Opt. Phys. 30, L435 (1997)
97M2 M. Mohan, Z. Phys. D 41, 9 (1997)
97M3 M. Mohan, R. Sharma and W. Eissner, Astrophys. J. Supp. 108, 389 (1997)
97P1 J. Pelan and K.A. Berrington, Astron. Astrophys. Supp. 122, 177 (1997)
97P2 A.K. Pradhan and H.L. Zhang, J. Phys. B: At. Mol. Opt. Phys. 30, L571 (1997)
97R1 C.A. Ramsbottom and K.L. Bell, Atomic Data Nucl. Data Tables 66, 65 (1997)
97S1 T. Schoning, Astron. Astrophys. Supp. 122, 277 (1997)

97T1 S.S. Tayal, Astrophys. J. 481, 550 (1997)
97T2 S.S. Tayal, Astrophys. J. Supp. 111, 459 (1997)
97Z1 H.L. Zhang and A.K. Pradhan, Astron. Astrophys. Supp. 123, 575 (1997)
97Z2 H.L. Zhang and A.K. Pradhan, Astron. Astrophys. Supp. 126, 373 (1997)
97Z3 H.L. Zhang and D.H. Sampson, Atomic Data Nucl. Data Tables 65, 183 (1997)
97Z4 H.L. Zhang and A.K. Pradhan, Phys. Rev. Lett 78, 195 (1997)
98B1 K.A. Berrington, H.E. Saraph and J.A. Tully, Astron. Astrophys. Supp. 129, 161 (1998)
98B2 A.M.Binello, H.E. Mason and P.J. Storey, Astron. Astrophys. Supp. 127, 545 (1998)
98B3 A.M.Binello, H.E. Mason and P.J. Storey, Astron. Astrophys. Supp. 131, 153 (1998)
98B4 A.K. Bhatia and P.R. Young, Atomic Data and Nuclear Data Tables, 68, 219 (1998)
98B5 M.A. Bautista and A.K. Pradhan, Astrophys. J. 492, 650 (1998)
98C1 G.X. Chen and P.P. Ong, Atomic Data and Nuclear Data Tables, 70, 93 (1999)
98C2 G.X. Chen, Phys. Rev. A 58, 1183 (1998)
98G1 M.E.Galavis, C.Mendoza and C.J.Zeippen, Astron. Astrophys. Supp., 133, 326 (1998)
98I1 Y. Itikawa, private communication
98S1 H.E. Saraph and P.J. Storey, Astron. Astrophys. Supp. 134, 369 (1999)
99C1 G.X. Chen and A.K. Pradhan, Astron. Astrophys. Supp., 136, 395 (1999)
99C2 G.X. Chen and A.K. Pradhan, J.Phys.B, 32, 1809 (1999)
99F1 C.J. Fontes, H.L. Zhang, D.H. Sampson, Phys. Rev. A, 59, 295 (1999)
99G1 G.P. Gupta and S.S. Tayal, Astrophys. J., 510, 1078 (1999)
99Z1 H.L. Zhang, D.H. Sampson, Atomic Data Nucl. Data Tables, 72, 153 (1999)
99Z2 H.L. Zhang, S.N. Nahar and A.K. Pradhan, J. Phys. B: At. Mol. Opt. Phys. 32, 1459 (1999)
01Z1 H.L. Zhang and D.H. Sampson, Mon. Not. Roy. Astr. Soc 322, 433 (2001)

3.2 Ionization

3.2.1 Introduction and general description

Most of the important features of the ionization phenomena of ions by electron impact are similar to those already given in Section 2.6 and have also been summarized in a number of reviews [71Ino1] and books [85Mär1]. The most recent review on the experimental aspects of the ionization phenomena of ions under electron impact has been given [94Dol1]. The important references on the ionization processes involving ions have been summarized [96Iti1]. Several compilations of the electron impact ionization cross section data of ions in various charge states are available [83Bel1, 87Taw1, 88Len1, 89Hig1] as well as in several databases (for example, NIFS [www1], JAERI [www2], ORNL [www3] and IAEA [www4]).

As described in Section 2.6, the apparent ionization cross sections ($\sigma_i^a = \sum_m m\sigma_i^{m+}$: σ_i^{m+} is the ionization cross section for production of ions with the charge state m) for most of the neutral atoms can relatively easily be determined with reasonable accuracies by crossing the energy-selected incident electrons through gas targets. On the other hand, the ionization cross sections for ions are usually obtained through so-called crossed-beams technique where the target ions provided from an ion source are crossed by the incident electrons and, then, are charge-analyzed to determine the intensities of ions with different charges produced in collisions.

Generally speaking, as the the number of electrons to be ionized increases, the corresponding ionization cross sections decrease due to the increased binding energy, as shown in Fig. 3.2.1a where the observed cross sections of production of multiply charged Xe^{m+} (m = 2-5) ions from Xe^+ ions under electron impact are given as a function of the electron impact energy. Similar features for the ionization of Xe^{2+} ions are also shown in Fig. 3.2.1b. It is easily noted that the cross sections for Xe^{4+} ion production from Xe^{2+} ions are close to those for Xe^{3+} ions at some electron energy region, shown in Fig. 3.2.1b which can be understood to be due to the significant contribution of the indirect processes to total ionization (see Subsect. 3.2.3).

3.2.2 Experimental techniques for ion targets

Collision experiments involving ions as target are very much complicated and highly sophisticated techniques are required to get reliable cross sections. The main reason is the fact that the ion target densities are so low and are of the order of 10^{-10} Torr or less which is generally much less than the residual gas atom densities in the vacuum systems. Thus, ultra-high vacuum techniques are requisite. Even in such ultra-high vacuum systems, the signal-to-noise ratios are often less than 1/10 and sometimes even 1/100. To get reasonable signals, both of the colliding incident electron and target ion beams are chopped. Also the overlapping of the incident ion and target ion beams has to be known accurately.

Another important and more serious aspect in such crossed-beams techniques is the fact that the ions produced in most of the ion sources such as electron cyclotron resonance ion sources include a significant fraction of the metastable state beam whose contribution can clearly be seen in the appearance of the cross sections below the expected threshold energy in the electron impact energy dependence of the ionization cross sections. As the ionization cross sections for the metastable state ion beams are quite large, compared with those for the ground state ion beams, then even a small fraction of such a beam strongly influence the observed ionization cross sections.

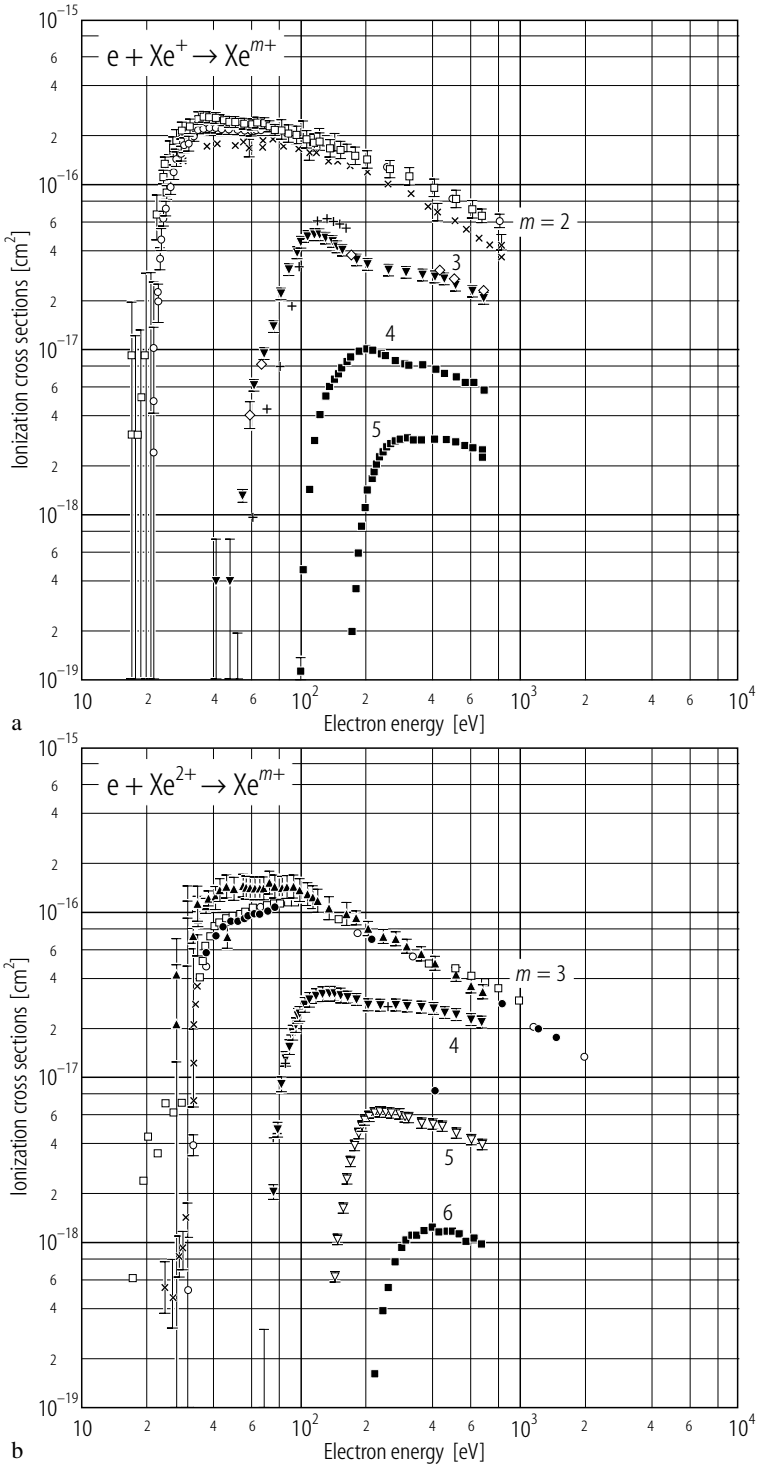

Fig. 3.2.1. Multiple-electron ionization cross sections for various ionization states of Xe^{m+} ions from (**a**) Xe^{+} and (**b**) Xe^{2+} ions under electron impact as a function of the electron impact energy (The data are taken from our database at NIFS).

1. Crossed-beams technique
This has been successfully used over years and is still providing a lot of reliable data for ionization of relatively low charged ions colliding with a powerful electron beam [95Ste1]. But as the effective target ion densities, in particular for highly charged ions, are very low, it is hard to measure the cross sections involving highly charged ions and also not possible to look into the detailed resonance structures in the ionization processes due to the indirect processes (Subsect. 3.2.3).

2. Storage ring technique
Highly and very highly charged ions with sufficient intensities are usually not easy to get directly from any present-day ion source. Instead, they are first accelerated up to MeV/amu energy range through proper accelerator systems and, by combining the electron stripping collisions, a number of the electrons are removed off to get the target ions in the proper charge states. Then, in order to get the ion beam of highly charged ions with very small energy spreads, they are sent into a storage ring (mostly a part of the whole accelerator systems) where they are cooled down through so-called electron cooler, which consists of high density electron beam with the velocity matching with that of the stored ions. Once these ions are stored and sufficiently cooled, they collide with the energy-variable electron beam which was used to cool the ions before [92Kil1, 96Mül1]. Thus, much better energy resolution experiments can be performed using such a cooler electron at the storage rings, as shown later.

3.2.3 Contribution of various processes to ionization

Not only the *direct* ionization processes where some electrons in the outermost-shell as well as in the inner-shell are directly removed from the target ions under electron impact but also the *indirect* ionization processes following the innershell-electron excitation or electron capture (recombination) processes play a role in the overall ionization processes and related fields. In some electronic configurations of the target ions, the contribution of the indirect ionization processes to total ionization are more important than that of the direct processes.

3.2.3.1 Direct processes

In simple target ions (A^{q+}) such as H- or He-like ions, the contribution to the ionization is mostly due to so-called single-electron *direct ionization (DI)* process where one of the outermost-shell electrons is ionized under electron impact as expressed as follows:

$$e + A^{q+} \rightarrow e + A^{(q+1)} + e. \quad (1)$$

When the electron impact energy increases, the cross sections usually show, in addition to the first threshold due to the ionization of the outermost-shell electrons, some shoulders at the threshold energies of the inner-shell electrons. Also it should be noted that not only a single electron but also two (or more) electrons can be ionized simultaneously with relatively high probabilities resulting in the double- (or multiple-) ionization (see Fig. 3.2.1):

$$e + A^{q+} \rightarrow e + A^{(q+m)+} + me. \quad (2)$$

Generally the double-electron ionization ($m = 2$) processes are dominant over higher ($m \geq 3$) ionization processes among multiple-electron ionization. Sometimes, the sum of all multiple-electron ionization becomes comparable to the single-electron ionization.

3.2.3.2 Indirect processes

In many-electron targets, the most significant contribution often comes from so-called indirect processes [94Moo1] which involve mostly the innershell electrons. After one of the inner-shell electrons is excited or ionized under the incident electron impact, are formed the doubly or triply excited states of ions which decay through the secondary (as well as ternary) processes such as a series of the autoionization processes and finally get stabilized into the ground state of highly ionized ions.

Different indirect processes play a role in such ionization process (in the following, "//" indicates the secondary or ternary processes after the intermediate states which are formed in the first collision process).

1. The *excitation//autoionization (EA)* process where one of the inner-shell electrons in the ion is first excited above the threshold of the ionization limit of the next higher charge state ions, forming the intermediate doubly excited state, a part of which is stabilized though the autoionization process:

$$e + A^{q+} \rightarrow e + A^{q+}{**} \rightarrow e + A^{(q+1)+} + e, \tag{3}$$

   resulting in single-electron ionization. The rest is stabilized through *radiative emission process*, just like the simple excitation processes, where, in principle, the charge state of ions does not change before and after collisions. The ratio of the autoionization over the sum of the autoionization and radiative emission, often called the (autoionization) branching ratio, is an important parameter in the formation of highly ionized ions under electron impact processes.
2. Another complicated process, so-called the *resonant-excitation-recombination//double autoioni-zation (RERDAI)*, where firstly the incident electron excites one of the target inner-shell electrons and, after losing its energy, is resonantly captured into high Rydberg state of the target ions (often called dielectronic recombination process) forming the triply excited (one-hole and two-electron excited) state, a part of which in turn is stabilized through two successive (double) autoionization:

$$e + A^{q+} \rightarrow A^{(q-1)+***} \rightarrow Aq^{+**} + e \rightarrow A^{(q+1)+} + 2e. \tag{4}$$

3. The resonant-excitation-recombination//auto-double-ionization (RERADI) process which firstly the incident electron excites one of the target innershell electrons into higher electronic state and, after losing its energy, is resonantly captured into high Rydberg state of the target ions forming the triply excited state, which then is stabilized through the simultaneous two-electron emission via single auto-ionization,

$$e + A^{q+} \rightarrow A^{(q-1)+***} \rightarrow A^{(q+1)+} + 2e. \tag{5}$$

   Generally, RERDAI occurs at the electron energy higher than RERADI as the former needs high excitation energy.

Though depending strongly on the electronic configurations of the target ions under consideration, the contribution of these indirect processes is significant in most of many-electron ion systems. Thus, total ionization cross sections, σ_i, can be given as the sum of the two processes mentioned above, under the assumption that they are the independent processes (though there is a suggestion that strong correlations exist in these processes), namely there is no correlation among the ionizing collision events:

$$\sigma_i = \sum_h \sigma_{di}^h + \sum_j \sigma_{ex}^j B_{SA}^j + \sum_k \sigma_{DR}^k (B_{DA}^k + B_{AD}^k) \tag{6}$$

where σ_{di}^h is the direct ionization cross section from h-th shell, σ_{ex}^j the excitation cross section to the j-state and thus the total cross sections have to be summed over all the possible j-states, σ_{DR}^k the dielectronic recombination (capture) cross section to the k-state and the total cross sections have to be summed over all the possible k-states, B_{SA}^j the branching ratio for the single-autoionization of the j-state,

B^k_{DA} the branching ratio for the double-autoionization of the k-state and B^k_{AD} the branching ratio for the auto-double ionization of the *k*-state.

These branching ratios can be calculated as follows:

$$B^j_{SA} = \frac{\sum_m A^{jm}_{SA}}{\sum_m A^{jm}_{SA} + \sum_n A^{jn}_{R}}, \quad B^k_{DA} = \frac{\sum_{k'} A^{kk'}_{SA} \sum_f A^{k'f}_{SA}}{\left(\sum_n A^{kn}_{SA} + \sum_{n'} A^{kn'}_{R}\right)\left(\sum_n A^{k'n}_{SA} + \sum_{n'} A^{k'n}_{R}\right)}, \tag{7, 8}$$

where A^{jm}_{SA} is the single autoionization probability from the *j*-state to the *m*-state and A^{jn}_{R} the radiative emission probability from the *j*-state to the *n*-state.

In low charged ions, the autoionization rate, A_{SA}, is generally dominant over the radiative transition rate, A_R, and, thus, both B^j_{SA} and B^k_{DA} become equal to unity. Now it is not necessary to know these rates anymore in order to get the ionization cross sections from the indirect processes. Then, the formula given above becomes simpler:

$$\sigma_i = \sum_h \sigma^h_{di} + \sum_j \sigma^j_{ex} + \sum_k \sigma^k_{DR} . \tag{9}$$

On the other hand, in very highly ionized ions such as H- and He-like ions, the situations are reverse and the radiative transitions are more favored and thus both *B* becomes zero. Finally we can discard the effect of the EA and the direct ionization processes dominate the total ionization cross sections:

$$\sigma_i = \sum_h \sigma^h_{di} . \tag{10}$$

The double-electron ionization processes can also be contributed by a series of similar indirect processes mentioned above.

3.2.4 Experimental results of ionization cross sections of ions

3.2.4.1 General features of the ionization cross section behavior

As mentioned in Introduction, there are some compilations and reviews of the ionization data for ion targets under electron impact. Accompanied with the technical and theoretical developments, steady accumulation of the electron impact ionization cross sections of ions up to U^{91+} ions is continuing. The important experimental data sources for ionization cross sections of multiply-charged ions by electron impact obtained after the previous compilation [87Taw1] are given as an appendix at the end of this Section.

Table 3.2.1 shows a summary of the present situations on measurements of the electron impact ionization cross section data of various ions with different charge which are stored and available from our databases at NIFS.

It is quite important to realize that the observed data of the ionization cross sections, in particular for the intermediate-to-high charge ions, have to be handled with precaution by knowing, as already pointed out in Introduction, that most of the primary ions from the ion sources should include some fractions of the metastable state ions whose cross sections are usually much larger (sometimes more than one order of magnitude) than those for the ground state ions. If the threshold energies are significantly different from each other, the contribution of the metastable species is easily distinguished from the appearance of the cross sections at the electron energies lower than expected. But as the charge state of ions becomes large and a number of the excited states are densely populated, the difference among the excited states becomes relatively small and then it is difficult to know their contributions.

B^k_{DA} the branching ratio for the double-autoionization of the k-state and B^k_{AD} the branching ratio for the auto-double ionization of the *k*-state.

These branching ratios can be calculated as follows:

$$B^j_{SA} = \frac{\sum_m A^{jm}_{SA}}{\sum_m A^{jm}_{SA} + \sum_n A^{jn}_{R}}, \quad B^k_{DA} = \frac{\sum_{k'} A^{kk'}_{SA} \sum_f A^{k'f}_{SA}}{\left(\sum_n A^{kn}_{SA} + \sum_{n'} A^{kn'}_{R}\right)\left(\sum_n A^{k'n}_{SA} + \sum_{n'} A^{k'n}_{R}\right)}, \tag{7, 8}$$

where A^{jm}_{SA} is the single autoionization probability from the *j*-state to the *m*-state and A^{jn}_{R} the radiative emission probability from the *j*-state to the *n*-state.

In low charged ions, the autoionization rate, A_{SA}, is generally dominant over the radiative transition rate, A_R, and, thus, both B^j_{SA} and B^k_{DA} become equal to unity. Now it is not necessary to know these rates anymore in order to get the ionization cross sections from the indirect processes. Then, the formula given above becomes simpler:

$$\sigma_i = \sum_h \sigma^h_{di} + \sum_j \sigma^j_{ex} + \sum_k \sigma^k_{DR} . \tag{9}$$

On the other hand, in very highly ionized ions such as H- and He-like ions, the situations are reverse and the radiative transitions are more favored and thus both *B* becomes zero. Finally we can discard the effect of the EA and the direct ionization processes dominate the total ionization cross sections:

$$\sigma_i = \sum_h \sigma^h_{di} . \tag{10}$$

The double-electron ionization processes can also be contributed by a series of similar indirect processes mentioned above.

3.2.4 Experimental results of ionization cross sections of ions

3.2.4.1 General features of the ionization cross section behavior

As mentioned in Introduction, there are some compilations and reviews of the ionization data for ion targets under electron impact. Accompanied with the technical and theoretical developments, steady accumulation of the electron impact ionization cross sections of ions up to U^{91+} ions is continuing. The important experimental data sources for ionization cross sections of multiply-charged ions by electron impact obtained after the previous compilation [87Taw1] are given as an appendix at the end of this Section.

Table 3.2.1 shows a summary of the present situations on measurements of the electron impact ionization cross section data of various ions with different charge which are stored and available from our databases at NIFS.

It is quite important to realize that the observed data of the ionization cross sections, in particular for the intermediate-to-high charge ions, have to be handled with precaution by knowing, as already pointed out in Introduction, that most of the primary ions from the ion sources should include some fractions of the metastable state ions whose cross sections are usually much larger (sometimes more than one order of magnitude) than those for the ground state ions. If the threshold energies are significantly different from each other, the contribution of the metastable species is easily distinguished from the appearance of the cross sections at the electron energies lower than expected. But as the charge state of ions becomes large and a number of the excited states are densely populated, the difference among the excited states becomes relatively small and then it is difficult to know their contributions.

Table 3.2.1. Summaries of the experimental electron impact ionization data in the databases at NIFS. The initial charge of ions is shown on the abscissa (horizontal direction) for each element (vertical direction) and the number in the tables shows the number of the experimental investigations performed so far.

Ion	Initial charge state																
	1+	2+	3+	4+	5+	6+	7+	8+	9+	10+	11+	12+	13+	14+	15+	16+	17+
He	9																
Li	10	2															
Be	2	-	-														
B	1	2	-	-													
C	9	9	10	3	4												
N	12	9	11	11	-	2											
O	11	8	4	8	10	1	1										
F	1	1	-	-	3	-	-	-									
Ne	13	4	8	1	1	2	4	1	4								
Na	11	1	1	-	-	-	-	-	-	-							
Mg	11	6	-	-	-	-	-	-	-	-	-						
Al	4	9	4	1	1	1	1	-	-	-	-	-					
Si	1	1	4	-	-	-	-	-	-	-	-	-	-				
P	1	-	-	5	-	-	-	-	-	-	-	-	-	-			
S	3	1	-	4	-	-	-	-	-	-	-	-	-	-	-		
Cl	2	1	-	-	4	-	-	-	-	-	-	-	-	-	-	-	
Ar	12	10	12	7	5	6	8	5	-	1	1	1	-	3	1	1	1
K	10	3	-	-	-	-	-	-	-	-	-	-	-	-	-	-	-
Ca	6	3	-	-	-	-	-	-	-	-	-	-	-	-	-	-	-
Sc	-	1	6	6	3	3	3	3	1	-	-	-	-	-	-	-	-
Ti	1	2	3	-	1	-	-	-	-	-	-	-	-	-	-	-	-
V	-	-	-	-	3	-	-	-	-	-	-	-	-	-	-	-	-
Cr	1	-	-	-	-	1	1	1	-	-	-	-	-	-	-	-	-
Fe	6	6	6	5	5	5	4	8	7	3	4	3	4	1	9	6	4
Ni	2	1	3	1	2	2	2	2	1	2	2	3	2	2	1	2	2
Cu	-	2	2	-	-	-	-	-	-	-	-	-	-	-	-	-	
Zn	2	-	-	-	-	-	-	-	-	-	-	-	-	-	-	-	
Ga	3	-	-	-	-	-	-	-	-	-	-	-	-	-	-	-	
Kr	6	8	6	4	1	-	1	1	-	-	-	-	-	-	-	-	
Rb	9	-	-	-	-	-	-	-	-	-	-	-	-	-	-	-	
Sr	3	-	-	-	-	-	-	-	-	-	-	-	-	-	-	-	
Zr	-	-	2	-	-	-	-	-	-	-	-	-	-	-	-	-	
Mo	1	-	-	1	6	-	-	-	-	-	-	-	-	-	-	-	
Cd	1	-	-	-	-	-	-	-	-	-	-	-	-	-	-	-	
In	1	-	-	-	-	-	-	-	-	-	-	-	-	-	-	-	
Sb	2	1	3	-	-	-	-	-	-	-	-	-	-	-	-	-	
I	2	-	-	-	-	-	-	-	-	-	-	-	-	-	-	-	
Xe	9	8	5	5	1	4	-	2	-	-	-	-	-	-	-	-	
Cs	7	-	-	-	-	-	-	-	-	-	-	-	-	-	-	-	
Ba	10	2	1	-	-	-	-	-	-	-	-	-	-	-	-	-	
La	-	1	3	1	-	-	-	-	-	-	-	-	-	-	-	-	
Hf	-	-	-	2	-	-	-	-	-	-	-	-	-	-	-	-	
Ta	1	-	1	-	-	-	-	-	-	-	-	-	-	-	-	-	
W	1	-	-	-	-	-	-	-	-	-	-	-	-	-	-	-	

Ion	Initial charge state															
	1+	2+	3+	4+	5+	6+	7+	8+	9+	10+	11+	12+	13+	14+	15+	16+	17+
Au	-	-	1	-	-	-	-	-	-	-	-	-	-	-	-	-	
Hg	4	-	-	-	-	-	-	-	-	-	-	-	-	-	-	-	
Tl	1	-	-	-	-	-	-	-	-	-	-	-	-	-	-	-	
Bi	2	2	2	1	-	-	-	-	-	-	-	-	-	-	-	-	
U	-	-	-	-	-	-	-	-	-	2	-	1	1	-	-	1	

3.2.4.2 High resolution ionization cross section measurements of indirect processes

As mentioned above, not only the direct ionization processes but also the indirect processes (see Subsect. 3.2.3), which often show the broad bumps or resonance-like behavior, contribute to the total ionization cross sections. Only recently such high resolution ionization experiments for highly charged ions could become possible (see Subsect. 3.2.2).

For example, some systematic high resolution experimental investigations on the indirect processes in Li-like ions have been reported using high power electron crossed-beams technique [90Hof1]. The indirect processes can be seen in Fig. 3.2.2 where the energy diagram of the parent Li-like ion, intermediate state ion and the final stabilized state ion is related [90Hof1].

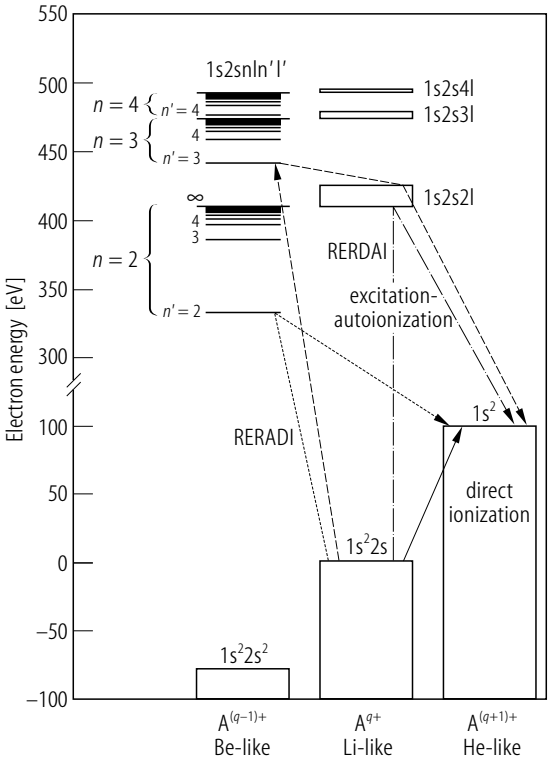

Fig. 3.2.2. Energy diagram of various ions involved in the indirect ionization processes of Li-like ions under electron impact. The energy scale corresponds to N^{4+} ions.

A typical RERADI, where two electrons are emitted simultaneously, can be described as follows:

$$e + C^{3+}(1s^2 2s) \rightarrow C^{2+***}(1s2s2p\,nl) \rightarrow C^{4+}(1s^2) + 2e \quad (11)$$

and contributes to the total ionization less than 1 % in relatively small-Z ions. On the other hand, the contribution of RERDAI, where two electrons are emitted sequentially,

$$e + C^{3+}(1s^2 2s) \rightarrow C^{2+***}(1s2s3\,lnl) \rightarrow C^{3+**}(1s2s2l) + e \rightarrow C^{4+}(1s^2) + 2e \quad (12)$$

is relatively large and indeed comparable to those of EA in the intermediate-to-high-Z ions.

Similar and significant contribution of the indirect processes (EA and RERDAI) to the ionization of the Li-like ions such as Si^{11+} and Cl^{14+} ions has clearly been observed at a storage ring experiment. The observed results for Cl^{14+} ions

$$e + Cl^{14+}(1s^2 2s) \rightarrow e + Cl^{14+**}(1s2s\,nl) \rightarrow e + Cl^{15+}(1s^2) + e \quad (13)$$

$$e + Cl^{14+}(1s^2 2s) \rightarrow Cl^{13+***}(1s2s\,nln'l') \rightarrow Cl^{15+}(1s^2) + 2e. \quad (14)$$

are shown in Fig. 3.2.3 [95Ken1].

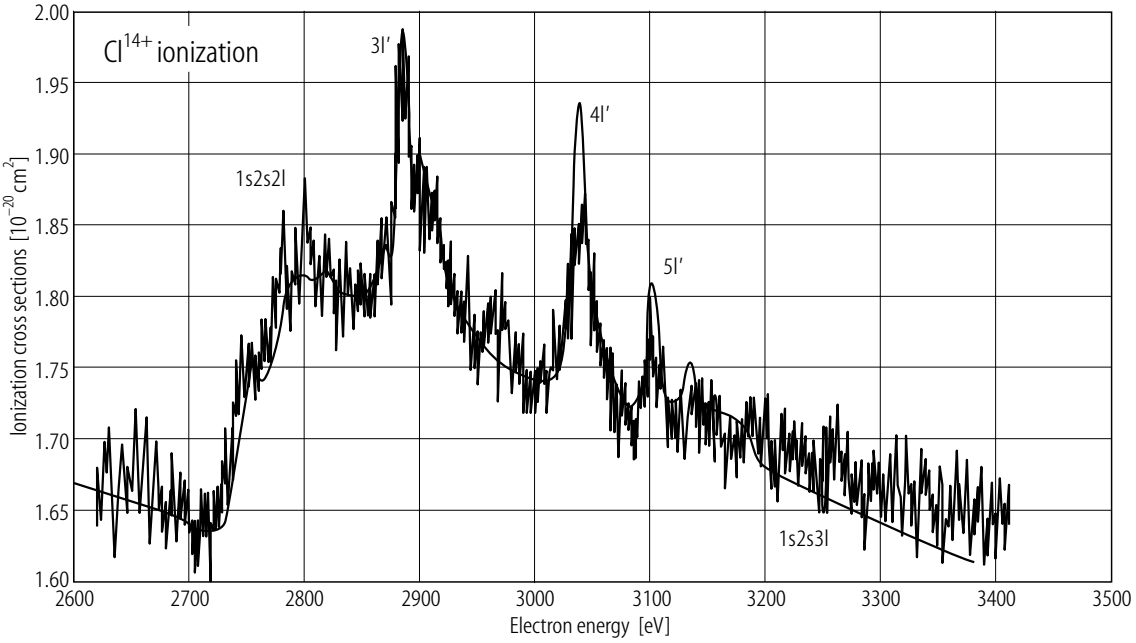

Fig. 3.2.3. The observed structures due to the indirect ionization processes in Cl^{14+} ions by electrons. The continuum background below 2720 eV is due to the direct ionization and that above it is due to the EA process (eq. 13) and a series of the peaks correspond to the RERDAI process (eq. 14).

Theoretical calculations based upon the semi-relativistic distorted-wave approximation show better agreement with the observation [90Hof1, 92Ree1, 95Ken1].
Systematic calculations of the indirect processes (EA and RERDAI) in different isoelectronic sequence of a few atomic species have been performed [93Bad1].

Furthermore, the ionization cross section measurements for more complicated Na-like Fe^{15+} ions performed also at another storage ring experiment can be compared with a previous measurement which had been done using the ordinary crossed-beams technique [87Gre1]. This particular electronic configuration ($1s^2 2s^2 2p^6 3s$) is interesting as it has one-electron at the outermost-shell and also eight electrons in the next inner-shells (2s and 2p). The following processes can be distinguished in the ionization of such Na-like ions, as seen in Fig. 3.2.4.

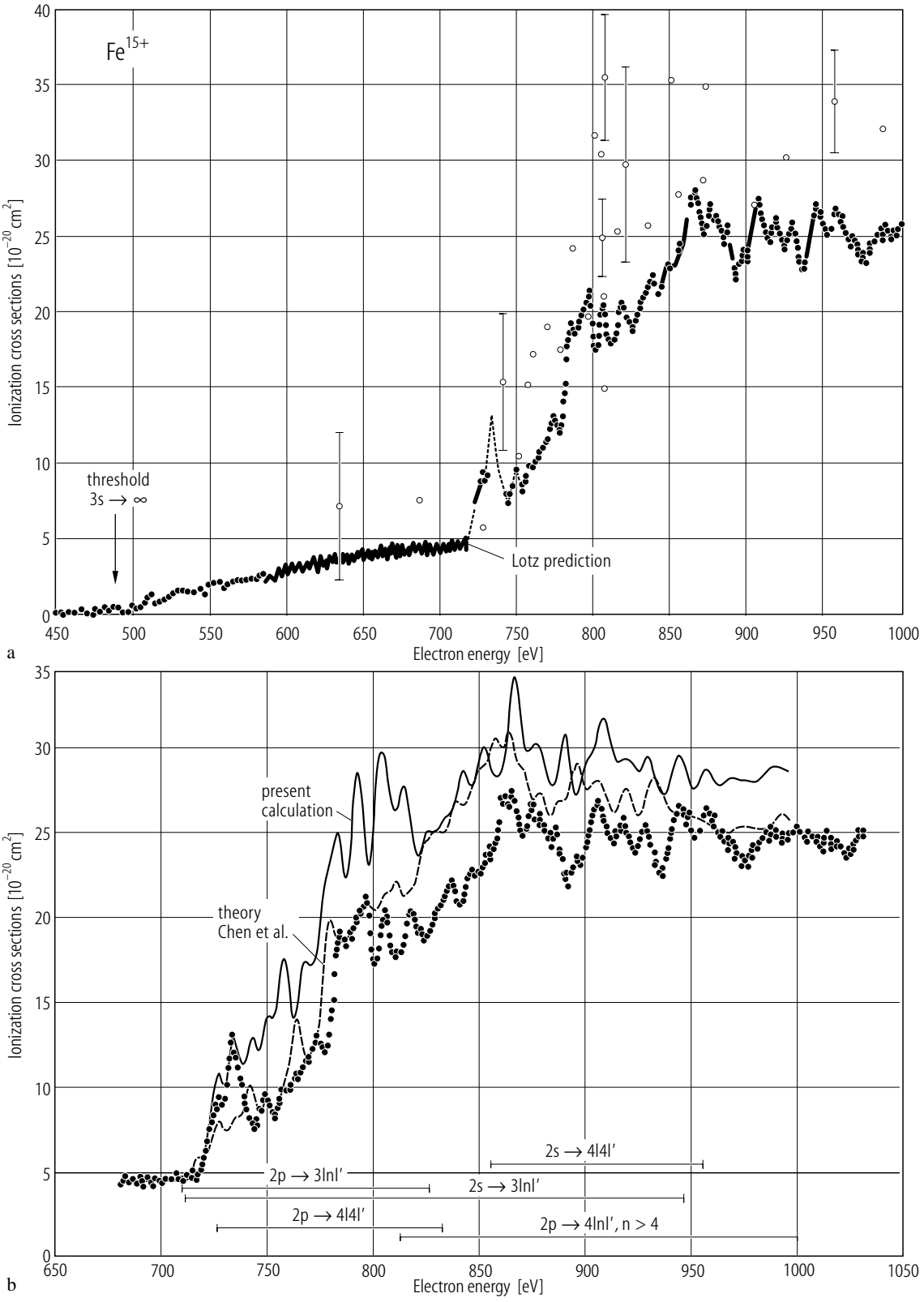

Fig. 3.2.4. For caption see next page.

The direct ionization

$$e + Fe^{15+}(1s^2 2s^2 2p^6 3s) \rightarrow e + Fe^{16+}(1s^2 2s^2 2p^6) + e \quad (15)$$

is varied smoothly from the threshold at 490 eV up to 710 eV as a function of the incident electron energy. Then the sudden increase of the ionization cross sections above 710 eV can be observed which is due to the following EA:

$$e + Fe^{15+}(1s^2 2s^2 2p^6 3s) \rightarrow e + Fe^{15+*}(1s^2 2s^2 2p^5 3snl: n \geq 3) \rightarrow e + Fe^{16+}(1s^2 2s^2 2p^6) + e \quad (16)$$

or

$$e + Fe^{15+}(1s^2 2s^2 2p^6 3s) \rightarrow e + Fe^{15+*}(1s^2 2s 2p^6 3snl: n = 3 \text{ and } 4) \rightarrow e + Fe^{16+}(1s^2 2s^2 2p^6) + e. \quad (17)$$

Another important contribution to the ionization of Fe^{15+} ions is the following RERDAI:

$$e + Fe^{15+}(1s^2 2s^2 2p^6 3s) \rightarrow Fe^{14+**}(1s^2 2s^2 2p^5 3snln'l') \rightarrow Fe^{16+}(1s^2 2s^2 2p^6) + 2e \quad (18)$$

or

$$e + Fe^{15+}(1s^2 2s^2 2p^6 3s) \rightarrow Fe^{14+**}(1s^2 2s^2 p^6 3snln'l') \rightarrow Fe^{16+}(1s^2 2s^2 2p^6) + 2e. \quad (19)$$

This contribution can be seen as a series of the resonance-like structures superposed on the EA curve which generally show step-wise increase of the cross sections. This is a part of the *dielectronic recombination (DR)* processes which can also decay by the radiative process, instead of the autoionization:

$$e + Fe^{15+}(1s^2 2s^2 2p^6 3s) \rightarrow Fe^{14+**}(1s^2 2s^2 2p^5 3snln'l') \rightarrow Fe^{14+}(1s^2 2s^2 2p^6 3s^2) + \hbar\omega. \quad (20)$$

This does not contribute to the ionization as the final charge of the ions does not increase.

The observed results [95Lin1] are shown in Fig. 3.2.4, together with those previous data [87Gre1]. Clearly new data based upon the electron cooler-storage ring experiment show a number of the resonance ionization contributions which had not been distinguished previously. The theoretical calculations based upon different approximations (the Breit-Pauli distorted-wave method (dotted line) [91Bad1] and the Dirac-Fock distorted-wave method (dashed line) [90Che1] seem to be in general agreement with the observed data but their detailed behavior shows some disagreement with each other as well as with the observation. Further theoretical description on the resonant effects on the ionization for Na-like ions has been given [95Che1]. Those for Mg-like ions have also been described [93Che1].

More systematic calculations involving the indirect ionization of ions in various charge states have been reported for isonuclear sequences [87Pin1, 88Gri1]. A set of the calculated cross sections are compared with the experimental data available (see Fig. 3.2.5). It is clear that the as the ion charge increases the contribution of the indirect ionization processes increases significantly. Another important point of this systematic calculation is the fact that the target ions, in particular higher charged ions produced in a particular ion source (namely an electron cyclotron resonance ion source), may include a significant fraction of the metastable state species which change the total ionization cross sections. Indeed, much better agreement has been obtained if the calculated contribution of the metastable species has been included (see Subect. 3.2.2).

←

Fig. 3.2.4. (**a**) The observed ionization cross sections (solid circles) indicating strong contribution of the indirect ionization processes in Fe^{15+} ions under electron impact. The continuous curve below 720 eV is due to the direct ionization of 3s electron, together with the Lotz empirical formula (see Section 2.6) and the open circles correspond to the crossed-beams measurement [87Gre1]. (**b**) Comparison of the measured cross sections with those calculated with different approximations (the dotted and dashed lines correspond to the Breit-Pauli distorted-wave method [91Bad1] and Dirac-Fock distorted-wave calculations [90Che1], respectively).

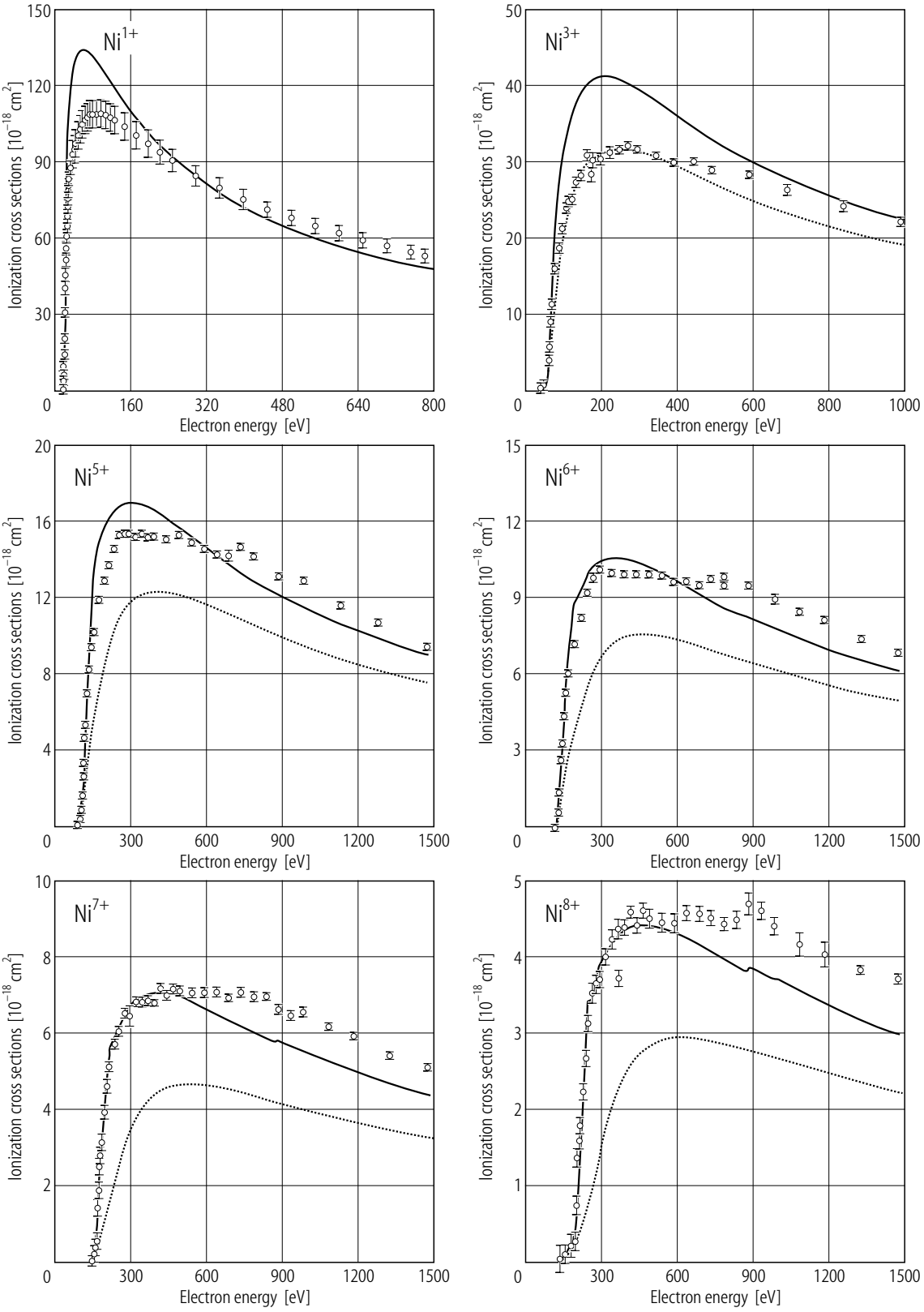

Fig. 3.2.5. Ni^{q+} ions (q = 1 - 8). For caption see next page.

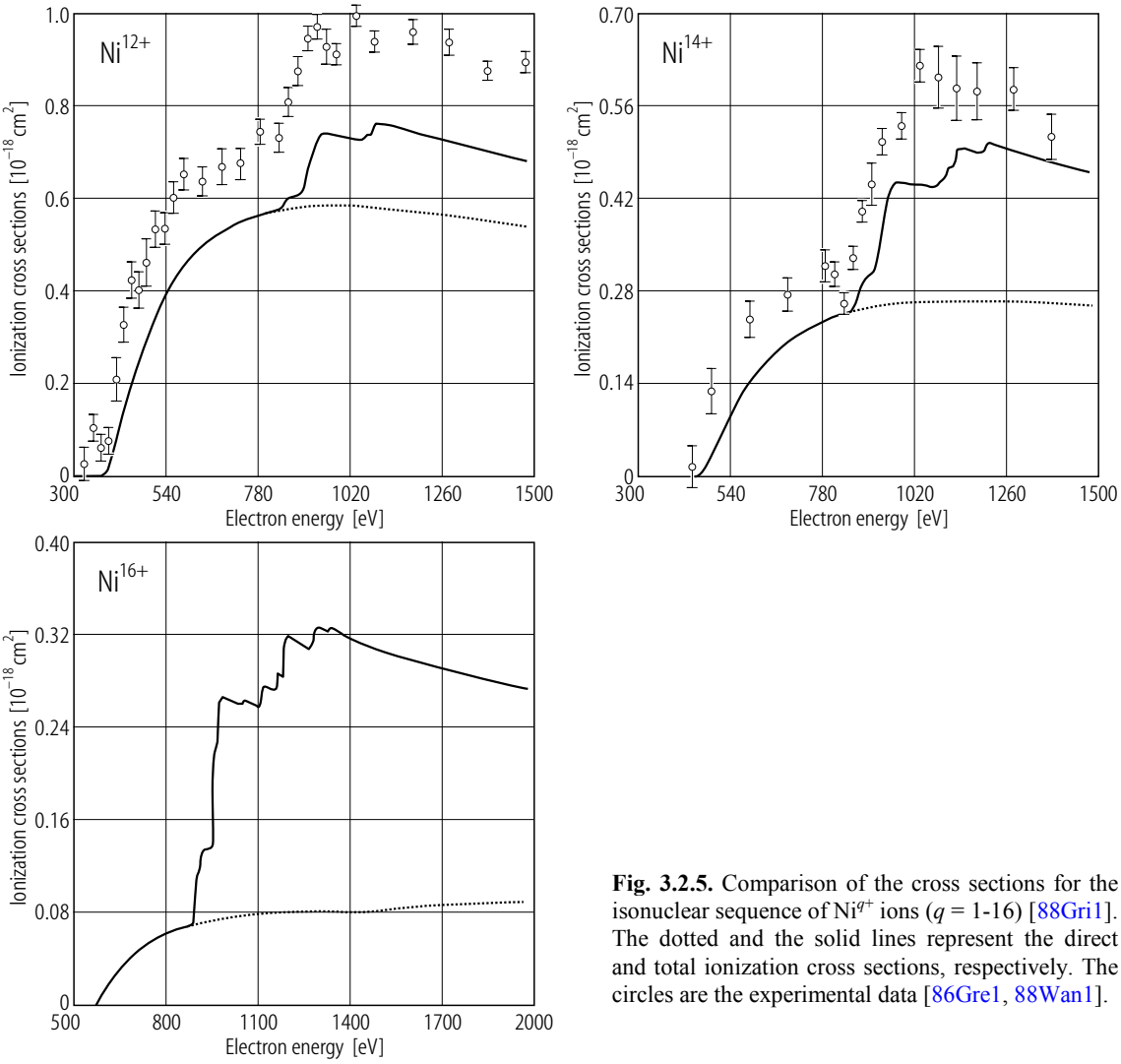

Fig. 3.2.5. Comparison of the cross sections for the isonuclear sequence of Ni^{q+} ions (q = 1-16) [88Gri1]. The dotted and the solid lines represent the direct and total ionization cross sections, respectively. The circles are the experimental data [86Gre1, 88Wan1].

3.2.4.3 Ionization of relativistic electrons

So far few experimental measurements of the ionization cross sections of relativistic electrons in highly ionized heavy ions had been reported, except for those involving the relativistic inner-shell electrons of neutral atoms by relativistic electron impact which have already been described in Section 2.6.

With the advent of powerful ion sources such as electron beam ion trap (EBIT), highly charged ions such as H-like U^{91+} ions are now available. Though their intensities are not sufficient, in principle it is now possible to work on such H-like heavy ions. But the measurements of the cross sections are still limited in the impact energy near the threshold region and data themselves are also scattered. For example, the ionization cross sections for Li-like ions such as Ti^{19+} - Fe^{23+} ions have been measured at a single impact energy of 2.3 times the ionization threshold energy [93Won1]. The observed values are in good agreement with the relativistic distorted-wave calculations. Also measurements of the ionization cross sections of very heavy H-like ions such as U^{91+} ions near the threshold energy region have been reported recently. The theoretical analysis of the ionization of the relativistic electrons with the relativistic distorted-wave approximation with the Møller interaction has been performed and favorably compared with the limited data for H-like very heavy ions obtained so far in the EBIT. It has been found that in such an electron

energy region the exchange effect is quite important and also the Møller interaction increases the cross sections significantly. Some comparison [97Mar1] is given in Table 3.2.2.

It is interesting to note that the most simple Lotz empirical formula (see Section 2.6) provides reasonable values within a factor of two for very heavy ions such as Au^{78+} and U^{91+} ions. However, the Lotz formula, the simplest without any corrections, is not appropriate to apply near the threshold region and the agreement seems to be fortuitous. More systematic data are necessary to test the theories in the ionization of the relativistic electrons [95Moo1].

The observed electron impact energy dependence of H-like Mo^{41+} ions is compared with various theoretical calculations, as shown in Fig. 3.2.6. The full relativistic distorted-wave calculations are clearly in better agreement with the experimental data [95Fon1]. This trend becomes more clear for heavier ions.

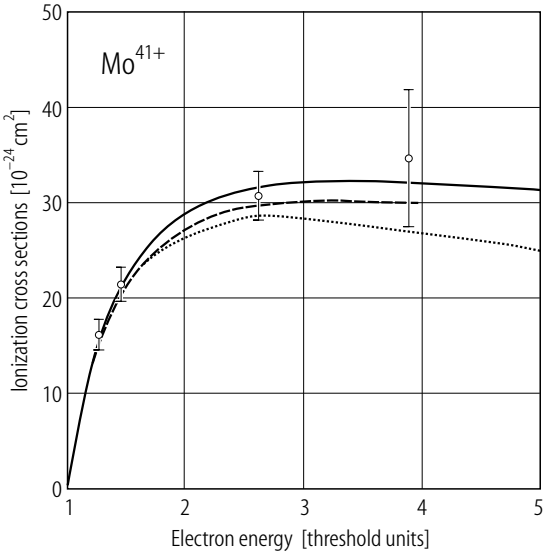

Fig. 3.2.6. Ionization cross sections of relativistic electrons in H-like Mo^{41+} ions as a function of the incident electron energy in units of the ionization threshold energy.

Table 3.2.2. Single-electron ionization cross sections for relativistic electrons in some H-like heavy ions under relativistic electron impact. The cross sections are given in 10^{-24} cm^2 units.

Ion	Energy [1])	Experiment	RDW [2])	RDW [3])	Lotz [4])
Mo^{41+}	1.28	15.9 ± 1.6	15.1	14.8	14.3
	1.47	21.2 ± 1.9	20.8	20.0	19.4
	2.63	30.8 ± 2.6	31.6	29.9	27.3
	3.89	34.7 ± 7.2	32.2	30.2	25.9
Dy^{65+}	1.51	4.17 ± 0.58	4.13	3.47	3.1
	2.43	6.29 ± 0.83	6.11	5.06	4.1
Au^{78+}	1.64	2.33 ± 0.33	2.47	1.91	1.6
Bi^{82+}	1.84	2.37 ± 0.19	2.40	1.76	1.4
U^{91+}	1.50	1.55 ± 0.27	1.44	0.93	0.7

[1]) Energy: electron impact energy divided by ionization energy.
[2]) Relativistic distorted-wave calculation with Møller interaction.
[3]) Relativistic distorted-wave calculation without Møller interaction.
[4]) Lotz formula without any correction.

3.2.5 Short description of theories

A number of different approximations for electron impact ionization of ions have been used (see [85Mär1]). The convergent close-coupling (CCC) method recently developed has been found to be very powerful for neutral atoms and singly charged ions [92Bra1, 93Bra1] but has still not been tested for ionization of highly charged ions.

Recently theories involving the excitation//autoionization (EA), resonant-excitation-capture// autoionization (RERDAI, RERADI) processes have been pursued enthusiastically. There is a nice recent review on such complicated theories [94Moo1].

For many applications, a number of the empirical formulas have been proposed in order to estimate the ionization cross sections for various ions and are going to be described in the following Subsect. 3.2.7.

3.2.6 Evaluated ionization cross sections for ions

Most of the observed cross sections are often scattered to some extent. It is necessary to evaluate the best sets of the ionization cross sections for various ions. As there are many different combinations of the charge states and ions, here are shown the evaluated cross sections only for single-electron ionization of singly-charged ions under electron impact as they are believed to be more applicable in various fields. The basic techniques for evaluating the ionization cross sections for ions are practically the same as those for neutral atoms mentioned in Section 2.6, except for a few important issues which are related with the target ions themselves. The target ions, which are produced through plasma type ion sources or through high energy electron impact ion sources (EBIS, EBIT), usually contain a significant fraction of the metastable state species with the same charge as the ground state ions. As these metastable state ions have low threshold energies, their contribution is easily noted by looking at the cross section-electron impact energy curves where the finite cross sections are observed even before the threshold energy of the ground state ions. The ions which are stored for a sufficiently long period of time, for example in the storage rings or traps, can be effectively in the ground states.

The evaluated single-electron ionization cross sections for singly-charged ions from He^+ to Bi^+ ions under electron impact over the threshold energy to 10^4 eV are given in Table 3.2.3 for He^+ to Na^+ ion, Table 3.2.4 (Mg^+-Ti^+), Table 3.2. 5 (Cr^+-Kr^+), Table 3.2.6 (Rb^+-Xe^+) and Table 3.2.7 (Cs^+-Bi^+). Here the cross section (9.00e-19) in these tables means $9.00 \cdot 10^{-19}$ cm^2. Also these data are shown in Fig. 3.2.7 (He^+-C^+), Fig. 3.2.8 (N^+-Na^+), Fig. 3.2.9 (Mg^+-S^+), Fig. 3.2.10 (Cl^+-Ti^+), Fig. 3.2.11 (Cr^+-Cu+), Fig. 3.2.12 (Zn^+-Kr^+), Fig. 3.2.13 (Rb^+-Cd^+), Fig. 3.2.14 (In^+-Xe^+), Fig. 3.2.15 (Cs^+-Ta^+) and Fig. 3.2.16 (W^+-Bi^+) as a function of the electron impact energy. The readers can find more evaluated data for various ions of different charge states in some references [83Bel1, 88Len1, 89Hig1].

Table 3.2.3. Recommended cross sections for single-electron ionization of singly-charged ions (He^+-Na^+) under electron impact as a function of the electron impact energy (cf. Figs. 3.2.7 and 3.2.8).

Energy [eV]	Cross section [cm^2]									
	He^+	Li^+	Be^+	B^+	C^+	N^+	O^+	F^+	Ne^+	Na^+
10										
12.5										
15										
20			1.15E-17							
25			2.60E-17							
30			3.45E-17	1.30E-17	1.30E-17					
35			4.00E-17	3.20E-17	2.35E-17	1.00E-17				
40			4.30E-17	4.40E-17	3.20E-17	1.80E-17	6.50E-18	4.10E-18		
50			4.50E-17	5.20E-17	4.40E-17	3.00E-17	1.75E-17	1.17E-17	3.60E-18	9.50E-19
60	9.00E-19		4.45E-17	5.60E-17	5.20E-17	3.80E-17	2.70E-17	1.96E-17	8.00E-18	3.80E-18
70	2.00E-18		4.30E-17	5.80E-17	5.60E-17	4.20E-17	3.20E-17	2.56E-17	1.40E-17	6.90E-18
80	2.80E-18	4.00E-19	4.20E-17	5.80E-17	5.70E-17	4.65E-17	3.60E-17	3.00E-17	1.80E-17	9.50E-18
90	3.35E-18	1.15E-18	4.05E-17	5.75E-17	5.65E-17	4.80E-17	3.80E-17	3.35E-17	2.20E-17	1.25E-17
100	3.75E-18	1.75E-18	3.85E-17	5.70E-17	5.50E-17	4.90E-17	4.15E-17	3.66E-17	2.55E-17	1.55E-17
150	4.75E-18	3.60E-18	3.40E-17	5.40E-17	4.85E-17	4.80E-17	4.40E-17	4.40E-17	3.25E-17	2.30E-17
200	4.95E-18	4.30E-18	3.05E-17	4.80E-17	4.40E-17	4.50E-17	4.20E-17	4.45E-17	3.35E-17	2.65E-17
250	4.85E-18	4.40E-18	2.65E-17	4.20E-17	4.00E-17	4.20E17	4.00E-17	4.15E-17	3.30E-17	2.75E-17
300	4.60E-18	4.50E-18	2.40E-17	3.80E-17	3.60E-17	3.70E-17	3.75E-17	3.85E-17	3.15E-17	2.75E-17
400	4.05E-18	4.25E-18	2.00E-17	3.25E-17	3.05E-17	3.20E-17	3.30E-17	3.33E-17	2.70E-17	2.55E-17
600	3.25E-18	3.60E-18	1.55E-17	2.50E-17	2.35E-17	2.50E-17	2.70E-17	2.63E-17	2.20E-17	2.15E-17
800	2.80E-18	3.15E-18	1.30E-17	2.05E-17	1.85E-17	2.05E-17	2.20E-17	2.20E-17	1.85E-17	1.80E-17
1000	2.35E-18	2.70E-18	1.10E-17	1.70E-17	1.70E-17	1.75E-17	1.85E-17	1.82E-17	1.60E-17	1.60E-17
2000	1.35E-18	1.70E-18	6.50E-18	1.05E-17	1.00E-17	1.05E-17	1.20E-17		1.00E-17	9.80E-18
4000	7.65E-19	1.05E-18	3.80E-18	6.30E-18	5.80E-18	6.20E-18	8.10E-18		6.40E-18	5.90E-18
6000	5.15E-19	7.80E-19	2.80E-18	4.50E-18	4.20E-18	4.50E-18	6.30E-18		4.60E-18	4.35E-18
10000	3.15E-19	5.30E-19	1.85E-18	3.00E-18	2.80E-18	2.95E-18	4.70E-18		3.20E-18	2.90E-18

Table 3.2.4. Recommended cross sections for single-electron ionization of singly-charged ions (Mg^+-Ti^+) under electron impact as a function of the electron impact energy (cf. Figs. 3.2.9 and 3.2.10).

Energy [eV]	Cross section [cm^2]									
	Mg^+	Al^+	Si^+	P^+	S^+	Cl^+	Ar^+	K^+	Ca^+	Ti^+
12.50									6.50E-18	
15									2.90E-17	5.40E-17
20	2.90E-17	1.10E-17	9.50E-17						4.80E-17	9.46E-17
25	4.32E-17	5.40E-17	1.41E-16	9.00E-17	8.00E-18	1.30E-17	1.30E-17		5.90E-17	1.16E-16
30	4.78E-17	6.95E-17	1.52E-16	1.35E-16	5.55E-17	8.85E-17	5.10E-17		2.50E-16	1.26E-16
35	4.80E-17	7.30E-17	1.55E-16	1.55E-16	1.05E-16	1.25E-16	9.70E-17	1.60E-17	2.50E-16	1.76E-16
40	4.75E-17	7.30E-17	1.53E-16	1.60E-16	1.28E-16	1.40E-16	1.12E-16	3.80E-17	2.20E-16	1.86E-16
50	4.38E-17	6.90E-17	1.43E-16	1.58E-16	1.38E-16	1.45E-16	1.16E-16	6.30E-17	1.80E-16	1.81E-16
60	4.40E-17	6.40E-17	1.35E-16	1.52E-16	1.38E-16	1.50E-16	1.18E-16	7.60E-17	1.75E-16	1.72E-16
70	4.35E-17	6.00E-17	1.24E-16	1.45E-16	1.35E-16	1.50E-16	1.18E-16	8.20E-17	1.70E-16	1.63E-16
80	4.29E-17	5.60E-17	1.19E-16	1.40E-16	1.31E-16	1.50E-16	1.17E-16	8.70E-17	1.75E-16	1.58E-16
90	4.24E-17	5.40E-17	1.12E-16	1.30E-16	1.25E-16	1.45E-16	1.16E-16	8.80E-17	1.80E-16	1.52E-16
100	4.24E-17	5.15E-17	1.06E-16	1.23E-16	1.20E-16	1.40E-16	1.16E-16	8.90E-17	1.80E-16	1.48E-16
150	4.29E-17	4.15E-17	8.30E-17	1.00E-16	1.03E-16	1.20E-16	1.06E-16	8.50E-17	1.66E-16	1.27E-16
200	4.29E-17	3.50E-17	7.05E-17	8.35E-17	8.80E-17	1.05E-16	9.40E-17	7.90E-17	1.50E-16	1.17E-16
250	3.85E-17	3.00E-17	6.00E-17	7.35E-17	7.85E-17	9.30E-17	8.30E-17	7.00E-17	1.30E-16	1.05E-16
300	3.63E-17	2.65E-17	5.20E-17	6.50E-17	6.80E-17	8.50E-17	7.50E-17	6.40E-17	1.10E-16	9.60E-17
400	3.08E-17	2.15E-17	4.05E-17	5.25E-17	5.83E-17	7.10E-17	6.30E-17	5.55E-17	8.70E-17	8.30E-17
600	2.53E-17	1.65E-17	2.90E-17	3.90E-17	4.40E-17	5.40E-17	4.80E-17	4.50E-17	6.10E-17	6.40E-17
800	2.15E-17	1.35E-17	2.20E-17	3.10E-17	3.55E-17	4.50E-17	3.85E-17	3.65E-17	4.45E-17	5.40E-17
1000	1.82E-17	1.15E-17	1.85E-17	2.65E-17	3.10E-17	3.85E-17	3.30E-17	3.15E-17	3.70E-17	4.60E-17
2000	1.16E-17	6.70E-18					2.00E-17	1.85E-17		2.80E-17
4000	6.82E-18	4.05E-18					1.15E-17	1.05E-17		
6000	5.06E-18	3.10E-18					8.00E-18	7.90E-18		
10000	3.52E-18	2.25E-18					4.90E-18	5.20E-18		

Table 3.2.5. Recommended cross sections for single-electron ionization of singly-charged ions (Cr^+-Kr^+) under electron impact as a function of the electron impact energy (cf. Figs. 3.2.11 and 3.2.12).

Energy [eV]	Cross section [cm^2]								
	Cr^+	Fe^+	Ni^+	Cu^+	Zn^+	Ga^+	Ge^+	Se^+	Kr^+
20	4.45E-17	4.30E-17	1.90E-17		1.05E-17		3.50E-17		
25	6.80E-17	7.30E-17	6.00E-17	6.30E-17	4.20E-17	6.00E-17	6.50E-17	5.10E-17	
30	8.30E-17	8.80E-17	7.90E-17	8.30E-17	5.70E-17	7.30E-17	8.60E-17	1.03E-16	6.50E-17
35	9.15E-17	9.50E-17	8.70E-17	9.25E-17	6.60E-17	8.35E-17	1.02E-16	1.35E-16	1.20E-16
40	9.90E-17	9.90E-17	9.15E-17	9.85E-17	7.20E-17	8.80E-17	1.10E-16	1.50E-16	1.44E-16
50	1.18E-16	1.05E-16	1.00E-16	1.05E-16	7.70E-17	9.10E-17	1.15E-16	1.65E-16	1.72E-16
60	1.21E-16	1.07E-16	1.04E-16	1.09E-16	7.80E-17	9.15E-17	1.15E-16	1.66E-16	1.85E-16
70	1.21E-16	1.08E-16	1.07E-16	1.11E-16	7.80E-17	9.10E-17	1.13E-16	1.64E-16	1.99E-16
80	1.20E-16	1.07E-16	1.08E-16	1.11E-16	7.70E-17	9.05E-17	1.08E-16	1.59E-16	1.97E-16
90	1.18E-16	1.06E-16	1.09E-16	1.10E-16	7.65E-17	8.95E-17	1.02E-16	1.55E-16	1.91E-16
100	1.15E-16	1.05E-16	1.08E-16	1.09E-16	7.60E-17	8.85E-17	9.30E-17	1.49E-16	1.86E-16
150	1.08E-16	9.60E-17	1.03E-16	9.92E-17	7.50E-17	8.20E-17	7.10E-17	1.23E-16	1.55E-16
200	1.01E-16	8.80E-17	9.65E-17	9.05E-17	7.00E-17	7.60E-17	5.60E-17	1.05E-16	1.35E-16
250	9.55E-17	8.30E-17	9.05E-17	8.30E-17	6.60E-17	6.80E-17	5.00E-17		1.20E-16
300	9.10E-17	7.65E-17	8.40E-17	7.55E-17	6.20E-17	6.45E-17	4.20E-17		1.05E-16
400	8.00E-17	6.70E-17	7.40E-17	6.52E-17	5.50E-17	5.56E-17	3.30E-17		8.80E-17
600	6.35E-17	5.30E-17	6.15E-17	5.15E-17	4.60E-17	4.60E-17			6.55E-17
800	5.30E-17	4.55E-17	5.20E-17	4.30E-17	4.00E-17	4.00E-17			5.35E-17
1000	4.55E-17	3.90E-17	4.50E-17	3.75E-17	3.50E-17	3.58E-17			4.50E-17
2000		2.40E-17			2.25E-17	2.47E-17			2.50E-17
4000		1.50E-17			1.45E-17				
6000		1.15E-17			1.10E-17				
10000		8.00E-18			7.80E-18				

Table 3.2.6. Recommended cross sections for single-electron ionization of singly-charged ions (Rb^+-Xe^+) under electron impact as a function of the electron impact energy (cf. Figs. 3.2.13 and 3.2.14).

Energy [eV]	Cross section [cm^2]							
	Rb^+	Sr^+	Mo^+	Cd^+	In^+	Sb^+	Te^+	Xe^+
12.5		1.20E-17						
15		4.00E-17						
20		6.15E-17	9.00E-17	2.20E-17	2.10E-17	8.30E-17	1.20E-17	
25		1.99E-16	1.60E-16	5.40E-17	7.35E-17	1.45E-16	7.50E-17	1.50E-16
30	3.00E-17	2.28E-16	2.15E-16	6.80E-17	1.00E-16	1.80E-16	2.05E-16	2.28E-16
35	8.30E-17	2.35E-16	2.40E-16	8.60E-17	1.18E-16	2.00E-16	2.38E-16	2.49E-16
40	1.09E-16	2.38E-16	2.75E-16	1.03E-16	1.28E-16	2.05E-16	2.45E-16	2.48E-16
50	1.36E-16	2.44E-16	2.95E-16	1.24E-16	1.40E-16	2.05E-16	2.42E-16	2.38E-16
60	1.46E-16	2.49E-16	2.87E-16	1.38E-16	1.51E-16	2.00E-16	2.33E-16	2.29E-16
70	1.52E-16	2.50E-16	2.75E-16	1.42E-16	1.60E-16	1.95E-16	2.22E-16	2.19E-16
80	1.55E-16	2.48E-16	2.58E-16	1.45E-16	1.63E-16	1.80E-16	2.09E-16	2.10E-16
90	1.57E-16	2.40E-16	2.45E-16	1.46E-16	1.61E-16	1.75E-16	2.02E-16	2.02E-16
100	1.56E-16	2.30E-16	2.35E-16	1.45E-16	1.58E-16	1.70E-16	1.90E-16	1.95E-16
150	1.42E-16	1.97E-16	2.00E-16	1.34E-16	1.40E-16	1.40E-16	1.61E-16	1.63E-16
200	1.23E-16	1.76E-16	1.80E-16	1.22E-16	1.20E-16	1.20E-16	1.39E-16	1.42E-16
250	1.10E-16	1.60E-16	1.62E-16	1.18E-16	1.03E-16	1.05E-16		1.26E-16
300	9.80E-17	1.49E-16	1.50E-16	1.14E-16	9.00E-17	9.00E-17		1.13E-16
400	8.30E-17	1.32E-16	1.28E-16	1.06E-16	7.50E-17	7.30E-17		9.35E-17
600	6.35E-17	1.11E-16	1.02E-16	9.00E-17	5.50E-17	5.30E-17		7.00E-17
800	5.00E-17	9.50E-17	8.60E-17	7.55E-17		4.30E-17		5.80E-17
1000	4.30E-17	8.30E-17	7.30E-17	6.20E-17		3.70E-17		4.90E-17
2000	2.40E-17			3.10E-17				3.00E-17
4000								1.80E-17
6000								1.35E-17
10000								9.30E-18

Table 3.2.7. Recommended cross sections for single-electron ionization of singly-charged ions (Cs^+-Bi^+) under electron impact as a function of the electron impact energy (cf. Figs. 3.2.15 and 3.2.16).

Energy [eV]	Cross section [cm^2]							
	Cs^+	Ba^+	La^+	Ta^+	W^+	Hg^+	Tl^+	Bi^+
12.5		7.50E-17	3.50E-17					
15		1.50E-16	8.90E-17					
20		3.80E-16	3.00E-16	9.50E-17	9.40E-17	2.60E-17		7.60E-17
25		4.20E-16	3.85E-16	1.83E-16	1.60E-16	6.15E-17	4.10E-17	1.60E-16
30	1.35E-16	4.25E-16	4.11E-16	2.33E-16	2.03E-16	8.50E-17	8.00E-17	2.10E-16
35	1.86E-16	4.30E-16	4.39E-16	2.48E-16	2.26E-16	1.02E-16	1.08E-16	2.41E-16
40	1.96E-16	4.25E-16	4.26E-16	2.69E-16	2.42E-16	1.18E-16	1.35E-16	2.53E-16
50	2.08E-16	4.25E-16	4.05E-16	2.68E-16	2.52E-16	1.40E-16	1.63E-16	2.65E-16
60	2.11E-16	4.15E-16	4.00E-16	2.58E-16	2.48E-16	1.56E-16	1.72E-16	2.62E-16
70	2.15E-16	4.05E-16	3.98E-16	2.45E-16	2.42E-16	1.64E-16	1.75E-16	2.52E-16
80	2.10E-16	3.85E-16	3.80E-16	2.34E-16	2.34E-16	1.68E-16	1.75E-16	2.42E-16
90	2.09E-16	3.80E-16	3.70E-16	2.23E-16	2.25E-16	1.69E-16	1.73E-16	2.31E-16
100	2.08E-16	3.60E-16	3.60E-16	2.14E-16	2.17E-16	1.68E-16	1.72E-16	2.18E-16
150	1.72E-16	3.20E-16	3.05E-16	1.81E-16	1.85E-16	1.56E-16	1.57E-16	1.80E-16
200	1.46E-16	2.80E-16	2.70E-16	1.58E-16	1.64E-16	1.47E-16	1.48E-16	1.56E-16
250	1.28E-16	2.55E-16	2.40E-16	1.41E-16	1.50E-16	1.35E-16	1.38E-16	1.38E-16
300	1.12E-16	2.25E-16	2.15E-16	1.28E-16	1.36E-16	1.28E-16	1.28E-16	1.23E-16
400	9.40E-17	1.90E-16	1.80E-16	1.11E-16	1.18E-16	1.14E-16	1.15E-16	1.04E-16
600	7.20E-17	1.50E-16	1.40E-16	8.70E-17	9.60E-17	9.80E-17	9.40E-17	7.90E-17
800	5.90E-17	1.25E-16	1.17E-16	7.15E-17	8.25E-17	7.80E-17	8.00E-17	6.50E-17
1000	5.00E-17	1.05E-16	1.00E-16	6.10E-17	7.35E-17	6.20E-17	6.85E-17	5.80E-17
2000	2.85E-17	6.20E-17		3.65E-17		3.60E-17	4.00E-17	
4000	1.75E-17							

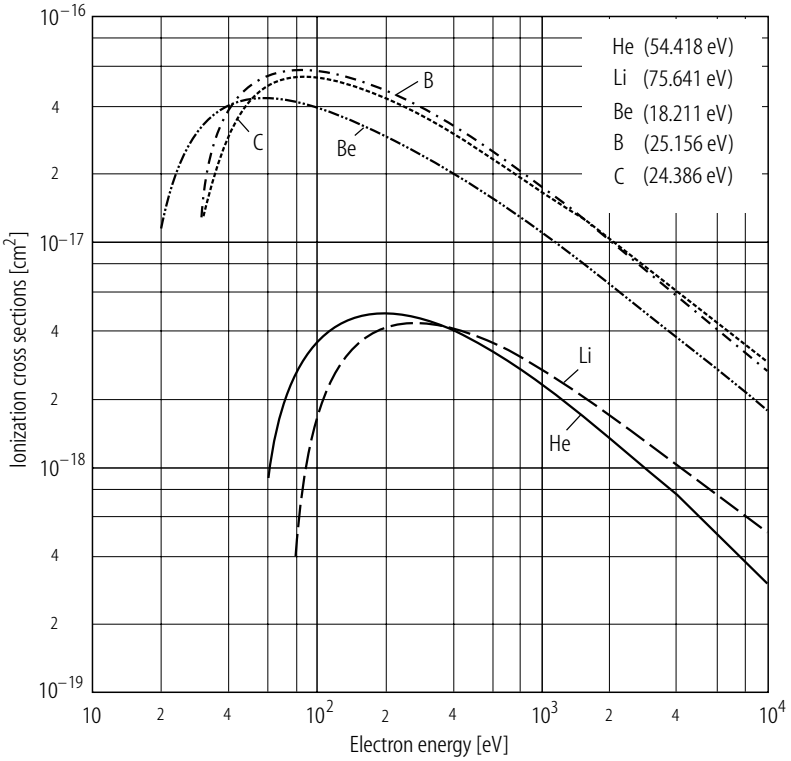

Fig. 3.2.7. Single-electron ionization cross sections for He^+ to C^+ ion plotted as a function of electron impact energy (cf. Table 3.2.3).

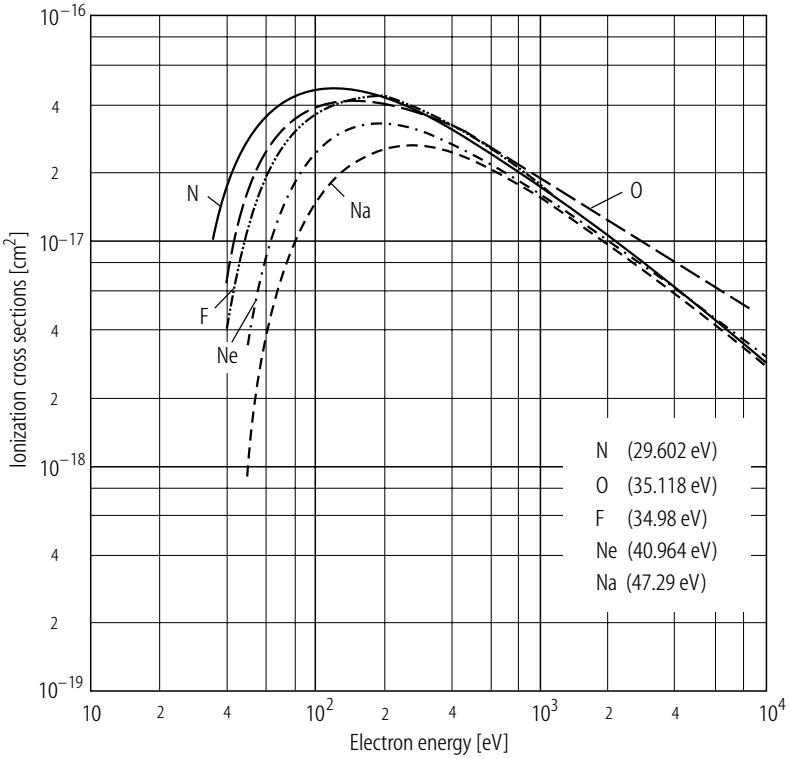

Fig. 3.2.8. Single-electron ionization cross sections for N^+ to Na^+ ion plotted as a function of electron impact energy (cf. Table 3.2.3).

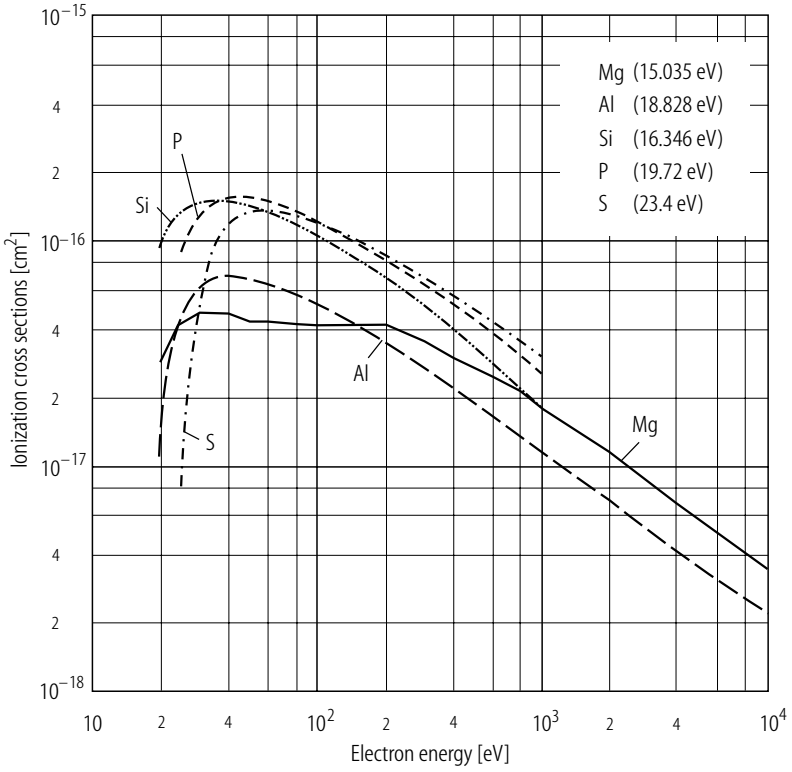

Fig. 3.2.9. Single-electron ionization cross sections for Mg^+ to S^+ ion plotted as a function of electron impact energy (cf. Table 3.2.4).

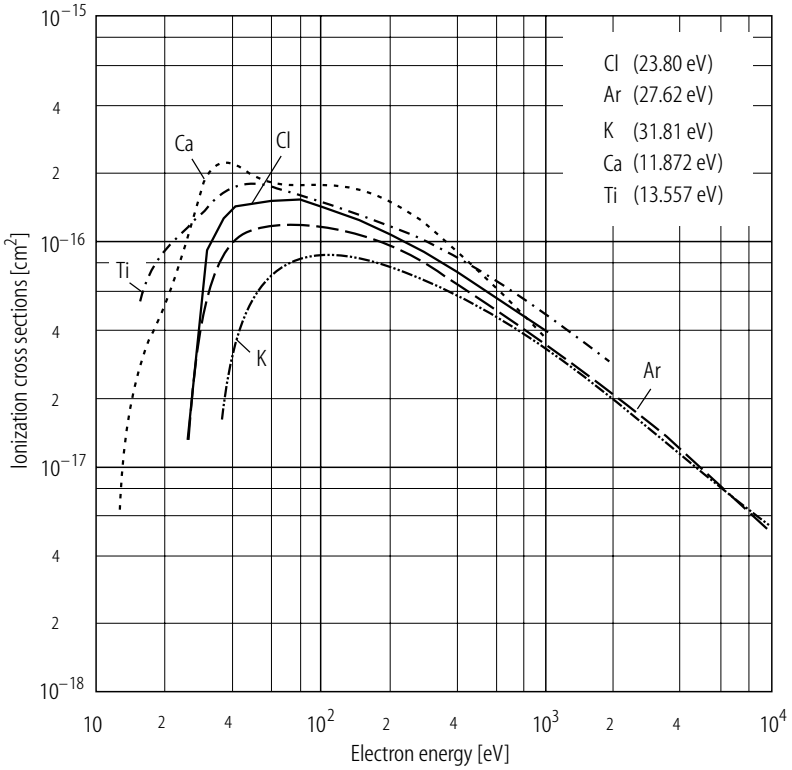

Fig. 3.2.10. Single-electron ionization cross sections for Cl^+ to Ti^+ ion plotted as a function of electron impact energy (cf. Table 3.2.4).

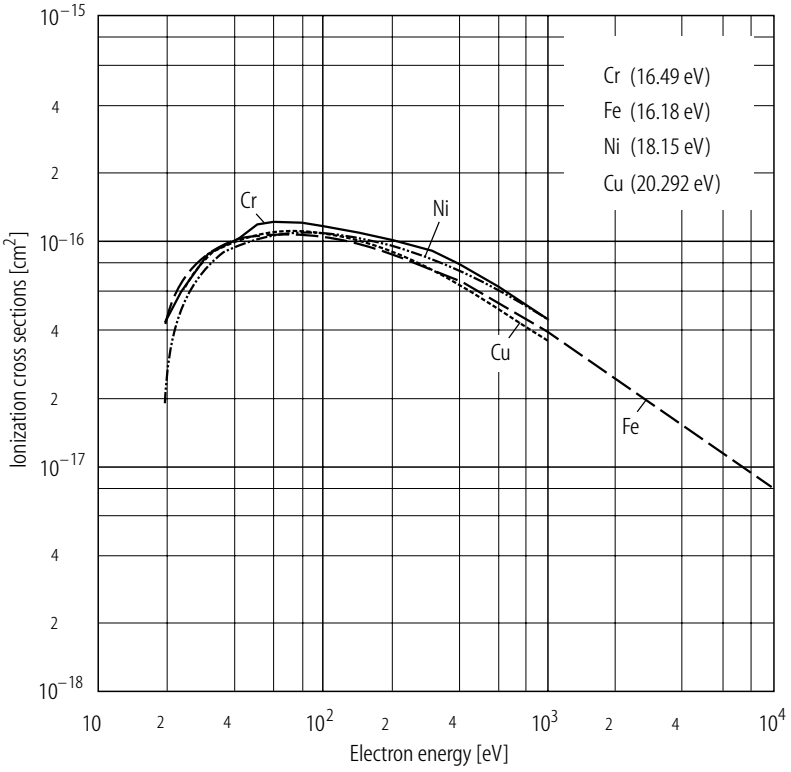

Fig. 3.2.11. Single-electron ionization cross sections for Cr^+ to Cu^+ ion plotted as a function of electron impact energy (cf. Table 3.2.5).

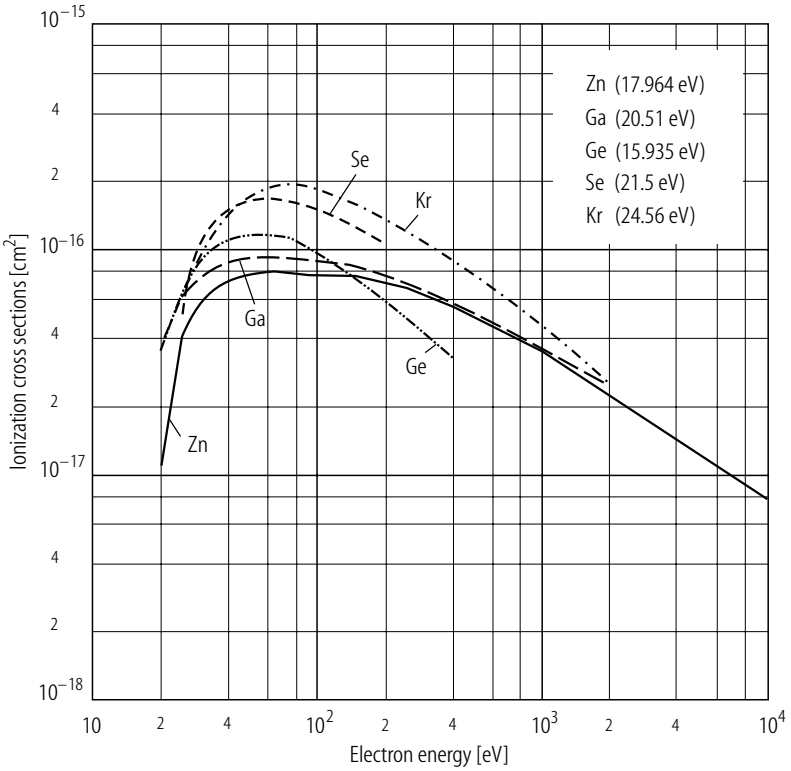

Fig. 3.2.12. Single-electron ionization cross sections for Zn^+ to Kr^+ ion plotted as a function of electron impact energy (cf. Table 3.2.5).

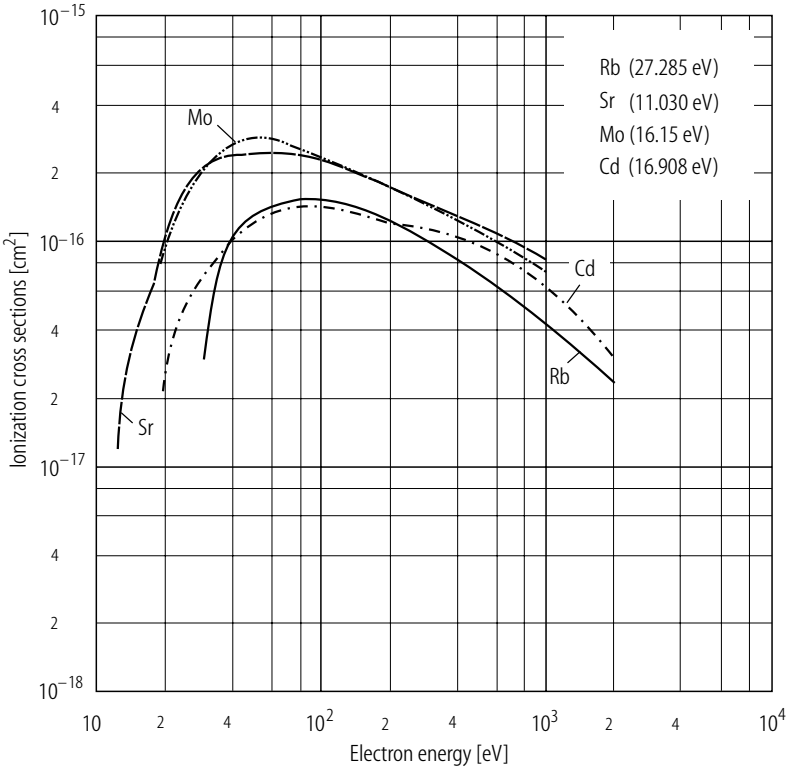

Fig. 3.2.13. Single-electron ionization cross sections for Rb^+ to Cd^+ ion plotted as a function of electron impact energy (cf. Table 3.2.6).

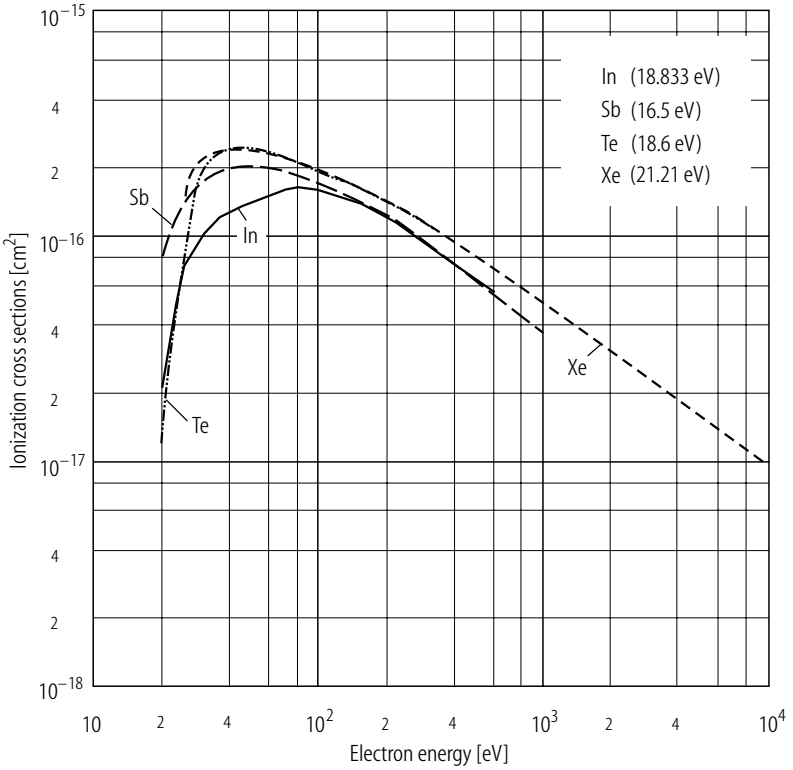

Fig. 3.2.14. Single-electron ionization cross sections for In^+ to Xe^+ ion plotted as a function of electron impact energy (cf. Table 3.2.6).

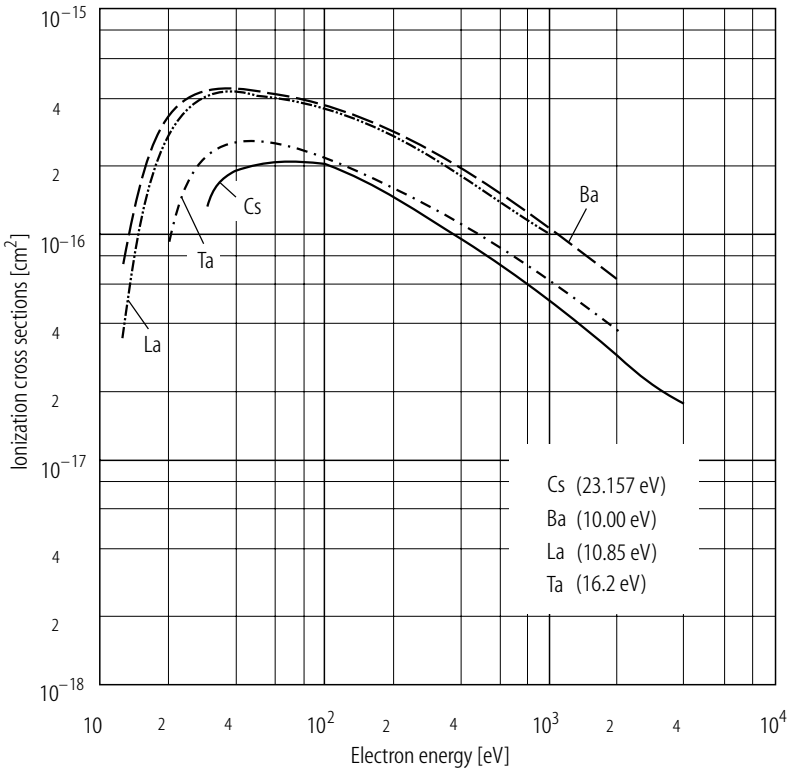

Fig. 3.2.15. Single-electron ionization cross sections for Cs^+ to Ta^+ ion plotted as a function of electron impact energy (cf. Table 3.2.7).

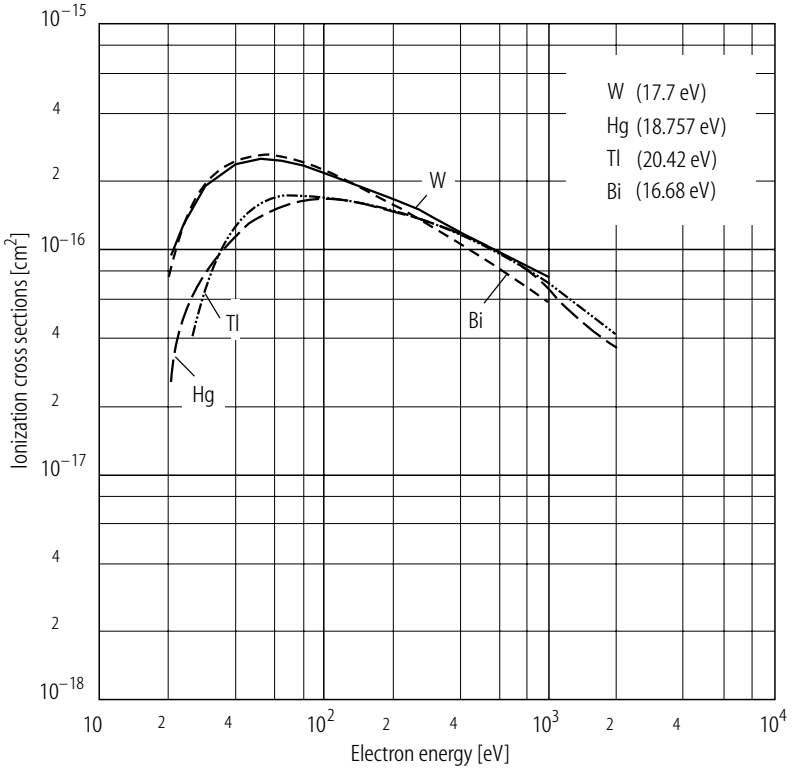

Fig. 3.2.16. Single-electron ionization cross sections for W^+ to Bi^+ ion plotted as a function of electron impact energy (cf. Table 3.2.7).

3.2.7 Empirical formula for ionization cross sections

In a number of applications, it is important to have some empirical formulas to estimate the ionization cross sections. Some critical reviews on the existing empirical formulas exist. The empirical formulas for neutral atom targets, already given in Section 2.6, should be basically valid in most of the ion targets. In fact these empirical formulas can be nicely applied to ions with different charge states, except for the ions where the indirect ionization processes become dominant. Therefore, here we try to describe, in addition to treatments of relatively simple ions such as H-, He- and Li-like ions, some empirical formulas for the collision processes of ions where the indirect processes, namely EA, RERDAI and RERADI, play a role.

3.2.7.1 H- and He-like ions

Recently based upon a series of the distorted-wave Born exchange approximation calculations with the relativistic correction [95Fan1], the following empirical formula, practically the modified Young formula, has been proposed for the ionization cross sections for simple H- and He-like ions up to Cu^{28+} (Z = 29) ions as a function of the incident electron energy E:

$$uI^2\sigma_i = A + B/Z_{eff} \tag{21}$$

where the normalized electron incident energy $u = E/I$ with I being the ionization threshold energy.

For H-like ions, $Z_{eff} = Z$ and for He-like ions, $Z_{eff} = Z - 1$. And the constants A and B are given in the following forms as a function of the normalized electron energy u:

$$A = a_1(1 - 1/u) + a_2(1 - 1/u)^2 + a_3\ln(u) + a_4\ln(u)/u \tag{22}$$

$$B = b_1(1 - 1/u) + b_2(1 - 1/u)^2 + b_3\ln(u) + b_4\ln(u)/u. \tag{23}$$

These parameters, a_n and b_n, are given in their tables [95Fan1].

This empirical formula has also been applied to other electronic systems of Ne^{q+} (q = 1-9) ions and found to be in reasonable agreement with the experimental data by taking into account the outer-most and the next outer-shell electrons. The parameters for these shells have been given [98Sun1].

3.2.7.2 Li-like ions

An empirical formula has been proposed for ionization cross sections of Li-like ions ($1s^22s$) for Z = 6-29, including the contribution of the excitation-autoionization processes based upon the distorted-wave Born exchange calculations with the relativistic correction [96Che1]. The empirical formula of the direct ionization for Li-like ions is practically the same to that for H- and He-like ions shown above, except for different effective charge of the ions, namely $Z_{eff} = Z - 2$. The necessary parameters are given [96Che1]. As mentioned above, it is important to realize that in Li-like ions the excitation-autoionization (EA) processes significantly contribute to the total ionization and thus the EA cross sections for Li-like ions are found to be given as follows:

$$Z^4\sigma_{EA} = a(1 - u^{-40})(u^{-1/3} + bu^{-4/3}) \tag{24}$$

where $u = E/I_{ex}(2s)$, $I_{ex}(2s)$ being the excitation threshold energy of the 2s electron. Here the excitation to $1s2s^2$, 1s2s2p and 1s2s3p states are taken into account but that to $1s^2p2$, 1s2p3s and 1s2p3p states are excluded as their contribution is estimated to be small. Among them, 1s2s2p excitation is the largest contribution to the excitation-autoionization. The parameters, a and b, for various ions are given as a function of Z of the ion in the reference [96Che1].

Then, the total cross sections, σ_i, are given as the sum of the direct and excitation-autoionization cross sections as most of the excited states formed decay via autoionization:

$$\sigma_i = \sigma_{di} + \sigma_{EA}. \tag{25}$$

3.2.7.3 Empirical formula for excitation for many-electron systems

In order to know the contribution of the indirect ionization processes, the excitation cross sections can be empirically fitted to the following formula:

$$\sigma_{ex} = \frac{a + \frac{b}{u} + \frac{c}{u^2} + d\ln(u) + \frac{e\ln(u)}{u}}{E} \tag{26}$$

where $u = E/I_{ex}$, E and I_{ex} being the electron impact energy and excitation threshold energy, respectively, a, b, c and d are constants and, furthermore, d and e are equal to zero for the non-dipole-allowed transitions [88Gri1]. The ionization due to the excitation processes which is followed by autoionization can be given as follows:

$$\sigma_{EA} = \sigma_{ex} B \tag{27}$$

where B represents the branching ratio of autoionization in a particular excited state. Then the total ionization cross sections is given as the sum of two processes, as in eq. (25).

3.2.7.4 Empirical formula for multiple ionization

Multiple-electron ionization processes are much more complicated in many-electron ion systems where it is expected to have the significant contribution from the indirect processes. Recently three different empirical formulas [95Fis1, 95She1, 96Deu1, 97Bel1] for multiple-electron ionization of ions have been proposed and found to provide reasonable agreement (within a factor of two) with the observations even for $m = 13$. The detail of these formulas have been already described in Section 2.6.

3.2.7.5 Ionization rate coefficients

At the same time, the so-called ionization rate coefficients, which are averaged over some distributions of the electron energy or velocity such as the Maxwellian distributions, are also useful, in particular in applications involving plasmas. But it has been recently realized that the original cross section data are more convenient in some cases and indeed there are a number of cases which do not follow the Maxwellian distributions of the energy and then another procedure is necessary to get the rate coefficients if the energy distributions are non-Maxwellian.

A number of different empirical forms for the ionization rate coefficients, namely the cross sections multiplied by the electron velocity, $<\sigma_i v_e>$, averaged over the Maxwellian velocity (energy) distributions have been proposed.

1. One of the most commonly used forms is represented in the following [83Bel1, 88Len1, 89Hig1]:

$$<\sigma_i v_e> = e^{-I_i/kT}\left(\frac{kT}{I_i}\right)^{1/2}\sum \alpha_n \left\{\log\left(\frac{kT}{I_i}\right)\right\}^n \qquad \text{for } I_i/10 \le kT \le 10I_i \tag{28}$$

$$<\sigma_i v_e> = \left(\frac{kT}{I_i}\right)^{-1/2}\left\{\gamma \ln\left(\frac{kT}{I_i}\right) + \sum \beta_n \left(\frac{I_i}{kT}\right)^n\right\} \qquad \text{for } kT > 10I_i. \tag{29}$$

where I_i is the ionization energy. These parameters, α_n, β_n, and γ, are given in the references for a number of atoms and ions in various ionization stages [83Bel1, 88Len1, 89Hig1].

2. Based upon the recommended ionization data [83Bel1, 88Len1, 89Hig1] from H to Ni ions, another simple fitting formula for ionization rate coefficients has been proposed [97Vor1],

$$<\sigma_i v_e> = a\left(1+Pu^{1/2}\right)u^k \frac{e^{-u}}{X+u} \tag{30}$$

where $u = I_i/T$. I_i is the ionization energy (eV) and T the electron temperature. a, k and X are the adjustable parameters which have been determined from the best fit to the recommended data. P is another adjustable parameter to fit the threshold behavior (in most cases P is 0 or 1). These parameters are given in the reference [97Vor1].

3.2.8 References for 3.2

71Ino1 Inokuti, M.: Rev. Mod. Phys. **43** (1971) 297.
83Bel1 Bell, K.L., Gilbody, H.B., Hughes, J.G., Kingston, A.E., Smith, F.J.: J. Phys. Chem. Ref. Data **12** (1983) 891.
85Mär1 Märk, T.D., Dunn, G.H.: Electron Impact Ionization, Wien, New York: Springer 1985.
86Gre1 Gregory, D.C., Howald, A.M.: Phys. Rev. A **34** (1986) 97.
87Gre1 Gregory, D.C., Wang, L.J., Meyer, F.W., Rinn, K.: Phys. Rev. A **35** (1987) 3256.
87Pin1 Pindzola, M.S., Griffin, D.C., Bottcher, C., Younger, S.M., Hunter, H.T.: Special Supplement to Nucl. Fusion (1987), p.21.
87Taw1 Tawara H., Kato, T.: At. Data Nucl. Data Tables **36** (1987) 167; Tawara, H., Koto, M.: NIFS-DATA-51, National Institute for Fusion Science, Toki, Japan 1999.
88Gri1 Griffin, D.C., Pindzola, M.S.: J. Phys. B **21** (1988) 3253.
88Len1 Lennon, M.A., Bell, K.L., Gilbody, H.B., Hughes, J.G., Kingston, A.E., Murray, M.J., Smith, F.J.: J. Phys. Chem. Ref. Data **17** (1988) 1285.
88Wan1 Wang, L.J., Rinn, K., Gregory, D.C.: J. Phys. B **21** (1988) 2117.
89Hig1 Higgins, M.J., Lennon, M.A., Hughes, J.G., Bell, K.L. Gilbody, H.B., Kingston, A.E., Smith, F.J.: CLM-R294, Culham Laboratory, UK, 1989.
90Che1 Chen, M.H., Reed, K.J., Moore, D.L.: Phys. Rev. Lett. **64** (1990) 1350.
90Hof1 Hoffmann, G., Müller, A., Tinchert, K., Salzborn, E.: Z. Phys. D **15** (1990) 113.
91Bad1 Badnell, N.R., Pindzola, M.S.: Phys. Rev. A **43** (1991) 2250.
92Bra1 Bray, I., Stelbovics, A.T.: Phys. Rev. A **46** (1992) 6995.
92Kil1 Kilgus, G., Habs, D., Schwalm, D., Wolf, A., Badnell, N.R., Müller, A.: Phys. Rev. A **46** (1992) 5730.
92Ree1 Reed, K.J., Chen, M.H.: Phys. Rev. A **45** (1992) 4519.
93Bad1 Badnell, N.R, Pindzola, M.S.: Phys. Rev. A **47** (1993) 2937.
93Bra1 Bray, I., Stelbovics, A.T.: Phys. Rev. Lett. **70** (1993) 746.
93Che1 Chen, M.H., Reed, K.J.: Phys. Rev. A **47** (1993) 1874.
93Won1 Wong, K.L., Beiersdorfer, P., Chen, M.H., Marrs, R.E., Reed, K.J., Scofield, J.H., Vogel, D.A., Zasadzinski, R.: Phys. Rev. A **48** (1993) 2850.
94Dol1 Dolder, K.: Adv. At. Mol. Opt. Phys. **32** (1994) 69.
94Moo1 Moore, D.L., Reed, K.J.: Adv. At. Mol. Opt. Phys. **34** (1994) 301.
95Che1 Chen, M.H., Moore, K.J., McWilliams, D.M.: Phys. Rev. A **52** (1995) 2881.
95Fan1 Fang, D., Hu, W., Chen, C., Wang, Y., Lu, F., Tang, J., Yang, F.: At. Data Nucl. Data Tables **61** (1995) 91.
95Fis1 Fisher, V., Ralchenko, Yu., Goldgirsh, A., Fisher, D., Martin, Y.: J. Phys. B **28** (1995) 3027.
95Fon1 Fontes, C.J., Sampson, D.H., Zhang, H.L.: Phys. Rev. A **51** (1995) R12.

2. Based upon the recommended ionization data [83Bel1, 88Len1, 89Hig1] from H to Ni ions, another simple fitting formula for ionization rate coefficients has been proposed [97Vor1],

$$<\sigma_i v_e> = a\left(1+Pu^{1/2}\right)u^k \frac{e^{-u}}{X+u} \tag{30}$$

where $u = I_i/T$. I_i is the ionization energy (eV) and T the electron temperature. a, k and X are the adjustable parameters which have been determined from the best fit to the recommended data. P is another adjustable parameter to fit the threshold behavior (in most cases P is 0 or 1). These parameters are given in the reference [97Vor1].

3.2.8 References for 3.2

71Ino1 Inokuti, M.: Rev. Mod. Phys. **43** (1971) 297.
83Bel1 Bell, K.L., Gilbody, H.B., Hughes, J.G., Kingston, A.E., Smith, F.J.: J. Phys. Chem. Ref. Data **12** (1983) 891.
85Mär1 Märk, T.D., Dunn, G.H.: Electron Impact Ionization, Wien, New York: Springer 1985.
86Gre1 Gregory, D.C., Howald, A.M.: Phys. Rev. A **34** (1986) 97.
87Gre1 Gregory, D.C., Wang, L.J., Meyer, F.W., Rinn, K.: Phys. Rev. A **35** (1987) 3256.
87Pin1 Pindzola, M.S., Griffin, D.C., Bottcher, C., Younger, S.M., Hunter, H.T.: Special Supplement to Nucl. Fusion (1987), p.21.
87Taw1 Tawara H., Kato, T.: At. Data Nucl. Data Tables **36** (1987) 167; Tawara, H., Koto, M.: NIFS-DATA-51, National Institute for Fusion Science, Toki, Japan 1999.
88Gri1 Griffin, D.C., Pindzola, M.S.: J. Phys. B **21** (1988) 3253.
88Len1 Lennon, M.A., Bell, K.L., Gilbody, H.B., Hughes, J.G., Kingston, A.E., Murray, M.J., Smith, F.J.: J. Phys. Chem. Ref. Data **17** (1988) 1285.
88Wan1 Wang, L.J., Rinn, K., Gregory, D.C.: J. Phys. B **21** (1988) 2117.
89Hig1 Higgins, M.J., Lennon, M.A., Hughes, J.G., Bell, K.L. Gilbody, H.B., Kingston, A.E., Smith, F.J.: CLM-R294, Culham Laboratory, UK, 1989.
90Che1 Chen, M.H., Reed, K.J., Moore, D.L.: Phys. Rev. Lett. **64** (1990) 1350.
90Hof1 Hoffmann, G., Müller, A., Tinchert, K., Salzborn, E.: Z. Phys. D **15** (1990) 113.
91Bad1 Badnell, N.R., Pindzola, M.S.: Phys. Rev. A **43** (1991) 2250.
92Bra1 Bray, I., Stelbovics, A.T.: Phys. Rev. A **46** (1992) 6995.
92Kil1 Kilgus, G., Habs, D., Schwalm, D., Wolf, A., Badnell, N.R., Müller, A.: Phys. Rev. A **46** (1992) 5730.
92Ree1 Reed, K.J., Chen, M.H.: Phys. Rev. A **45** (1992) 4519.
93Bad1 Badnell, N.R, Pindzola, M.S.: Phys. Rev. A **47** (1993) 2937.
93Bra1 Bray, I., Stelbovics, A.T.: Phys. Rev. Lett. **70** (1993) 746.
93Che1 Chen, M.H., Reed, K.J.: Phys. Rev. A **47** (1993) 1874.
93Won1 Wong, K.L., Beiersdorfer, P., Chen, M.H., Marrs, R.E., Reed, K.J., Scofield, J.H., Vogel, D.A., Zasadzinski, R.: Phys. Rev. A **48** (1993) 2850.
94Dol1 Dolder, K.: Adv. At. Mol. Opt. Phys. **32** (1994) 69.
94Moo1 Moore, D.L., Reed, K.J.: Adv. At. Mol. Opt. Phys. **34** (1994) 301.
95Che1 Chen, M.H., Moore, K.J., McWilliams, D.M.: Phys. Rev. A **52** (1995) 2881.
95Fan1 Fang, D., Hu, W., Chen, C., Wang, Y., Lu, F., Tang, J., Yang, F.: At. Data Nucl. Data Tables **61** (1995) 91.
95Fis1 Fisher, V., Ralchenko, Yu., Goldgirsh, A., Fisher, D., Martin, Y.: J. Phys. B **28** (1995) 3027.
95Fon1 Fontes, C.J., Sampson, D.H., Zhang, H.L.: Phys. Rev. A **51** (1995) R12.

95Ken1 Kenntner, J., Linkemann, J., Badnell, N.R. Broude, C., Habs, D., Hofmann, G., Müller, A., Pindzola, M.S., Salzborn, E., Schwalm D., Wolf, A.: Nucl. Instr. Meth. B **98** (1995) 142.
95Lin1 Linkemann, J., Müller, A., Kenntner, J., Habs, D., Schwalm, D., Wolf, A., Badnell, N.R., Pindzola, M.S.: Phys. Rev. Lett. **74** (1995) 4173.
95Moo1 Moores, D.L., Reed, K.J.: Phys. Rev. A **51** (1995) R9.
95She1 Shevelko, V.P., Tawara, H.: J. Phys. B **28** (1995) L589.
95Ste1 Stenke, M., Aichele, K., Hithiramani, D., Hoffmann, G., Steidl, M., Vögel, R., Salzborn, E.: Nucl. Instr. Meth. B **98** (1995) 573.
96Che1 Chen, C., Hu, W., Fang, D. Wang, Y., Yang, F., Teng, H.: At. Data Nucl. Data Tables **64** (1996) 301.
96Deu1 Deutsch, H., Becker, K., Märk, T.D.: J. Phys. B **29** (1996) L497.
96Iti1 Itikawa, Y.: At. Data Nucl. Data Tables **49** (1991) 209; ibid. **63** (1996) 315.
96Mül1 Müller, A.: Comm. At. Mol. Phys. **32** (1996) 143.
97Bél1 Bélenger, C., Defrance, P., Salzborn, E., Shevelko, V.P., Tawara, H., Uskov, D.B.: J. Phys. B **30** (1997) 2667.
97Mar1 Marrs, R.E., Elliot, S.R., Scofield, J.H.: Phys. Rev. A **56** (1997) 1338.
97Vor1 Voronov, G.S.: At. Data Nucl. Data Tables **65** (1997) 1.
98Sun1 Sun, Y.S.: International Atomic Energy Agency INDC(NDC)-377 (1998) and private communication 1997.
www1 www at http://dbshino.nifs.ac.jp (accessible after getting the ID) (National Institute for Fusion Science, Toki, Japan).
www2 www at http://wwwndc.tokai.jaeri.go.jp/JEAMDL/index.html (Japan Atomic Energy Research Institute, Tokai, Ibaraki, Japan).
www3 www at http://ornl.gov (Oak Ridge National Laboratory, Oak Ridge, TN, USA).
www4 www at http://iaea.org.at (International Atomic Energy Agency, Wien, Austria).

Appendix

Data sources for the experimental ionization cross sections of atomic ions

Appendix 1 lists the papers reporting experimental data on the cross section for the electron-impact ionization of atomic ions. The list shows the papers published in 1986-1997. The data published before 1986 have been compiled by Tawara and Kato (At. Data Nucl. Data Tables **36** (1987) 167). The listings in Appendix 1 are arranged in groups by year of publication and, within each group, by the name of the first author. For readers' convenience, Appendix 2 gives an index of the papers in Appendix 1 by ion species (*N* being the number of bound electrons of each ion).

Appendix 1. List of papers reporting experimental cross sections for the ionization of atomic ions, published in 1986-1997.

86C D.H. Crandall, R.A. Phaneuf, D.C. Gregory, A.M. Howald, D.W. Mueller, T.J. Morgan, G.H. Dunn, D.C. Griffin, and R.J.W. Henry
Phys. Rev. A **34** (1986) 1757
Electron-impact ionization of B^{2+} and O^{5+}: Excitation-autoionization in Li-like ions

86G1 D.C. Gregory and A.M. Howald
Phys. Rev. A **34** (1986) 97
Electron-impact ionization of multicharged metal ions: Ni^{3+}, Cu^{2+}, Cu^{3+}, and Sb^{3+}

95Ken1 Kenntner, J., Linkemann, J., Badnell, N.R. Broude, C., Habs, D., Hofmann, G., Müller, A., Pindzola, M.S., Salzborn, E., Schwalm D., Wolf, A.: Nucl. Instr. Meth. B **98** (1995) 142.
95Lin1 Linkemann, J., Müller, A., Kenntner, J., Habs, D., Schwalm, D., Wolf, A., Badnell, N.R., Pindzola, M.S.: Phys. Rev. Lett. **74** (1995) 4173.
95Moo1 Moores, D.L., Reed, K.J.: Phys. Rev. A **51** (1995) R9.
95She1 Shevelko, V.P., Tawara, H.: J. Phys. B **28** (1995) L589.
95Ste1 Stenke, M., Aichele, K., Hithiramani, D., Hoffmann, G., Steidl, M., Vögel, R., Salzborn, E.: Nucl. Instr. Meth. B **98** (1995) 573.
96Che1 Chen, C., Hu, W., Fang, D. Wang, Y., Yang, F., Teng, H.: At. Data Nucl. Data Tables **64** (1996) 301.
96Deu1 Deutsch, H., Becker, K., Märk, T.D.: J. Phys. B **29** (1996) L497.
96Iti1 Itikawa, Y.: At. Data Nucl. Data Tables **49** (1991) 209; ibid. **63** (1996) 315.
96Mül1 Müller, A.: Comm. At. Mol. Phys. **32** (1996) 143.
97Bél1 Bélenger, C., Defrance, P., Salzborn, E., Shevelko, V.P., Tawara, H., Uskov, D.B.: J. Phys. B **30** (1997) 2667.
97Mar1 Marrs, R.E., Elliot, S.R., Scofield, J.H.: Phys. Rev. A **56** (1997) 1338.
97Vor1 Voronov, G.S.: At. Data Nucl. Data Tables **65** (1997) 1.
98Sun1 Sun, Y.S.: International Atomic Energy Agency INDC(NDC)-377 (1998) and private communication 1997.
www1 www at http://dbshino.nifs.ac.jp (accessible after getting the ID) (National Institute for Fusion Science, Toki, Japan).
www2 www at http://wwwndc.tokai.jaeri.go.jp/JEAMDL/index.html (Japan Atomic Energy Research Institute, Tokai, Ibaraki, Japan).
www3 www at http://ornl.gov (Oak Ridge National Laboratory, Oak Ridge, TN, USA).
www4 www at http://iaea.org.at (International Atomic Energy Agency, Wien, Austria).

Appendix

Data sources for the experimental ionization cross sections of atomic ions

Appendix 1 lists the papers reporting experimental data on the cross section for the electron-impact ionization of atomic ions. The list shows the papers published in 1986-1997. The data published before 1986 have been compiled by Tawara and Kato (At. Data Nucl. Data Tables **36** (1987) 167). The listings in Appendix 1 are arranged in groups by year of publication and, within each group, by the name of the first author. For readers' convenience, Appendix 2 gives an index of the papers in Appendix 1 by ion species (*N* being the number of bound electrons of each ion).

Appendix 1. List of papers reporting experimental cross sections for the ionization of atomic ions, published in 1986-1997.

86C D.H. Crandall, R.A. Phaneuf, D.C. Gregory, A.M. Howald, D.W. Mueller, T.J. Morgan, G.H. Dunn, D.C. Griffin, and R.J.W. Henry
Phys. Rev. A **34** (1986) 1757
Electron-impact ionization of B^{2+} and O^{5+}: Excitation-autoionization in Li-like ions

86G1 D.C. Gregory and A.M. Howald
Phys. Rev. A **34** (1986) 97
Electron-impact ionization of multicharged metal ions: Ni^{3+}, Cu^{2+}, Cu^{3+}, and Sb^{3+}

86G2 D.C. Gregory, F.W. Meyer, A. Muller, and P. Defrance
Phys. Rev. A **34** (1986) 3657
Experimental cross sections for electron-impact ionization of iron ions: Fe^{5+}, Fe^{6+}, and Fe^{9+}

86H1 T. Hirayama, K. Oda, Y. Morikawa, T. Ono, Y. Ikezaki, T. Takayanagi, K. Wakiya, and H. Suzuki
J. Phys. Soc. Jpn. **55** (1986) 1411
Measurements of cross sections for single and double ionization of Na^+ and K^+ by electron impact

86H2 A.M. Howald, D.C. Gregory, F.W. Meyer, R.A. Phaneuf, A. Muller, N. Djuric, and G.H. Dunn
Phys. Rev. A **33** (1986) 3779
Electron-impact ionization of Mg-like ions: S^{4+}, Cl^{5+}, and Ar^{6+}

86H3 A.M. Howald, D.C. Gregory, R.A. Phaneuf, and D.H. Crandall
Phys. Rev. Lett. **56** (1986) 1675
Observation of multiple-electron processes in ionization of Xe^{6+} by electron impact

87B D.S. Belic, R.A. Falk, C. Timmer, and G.H. Dunn
Phys. Rev. A **36** (1987) 1073
Absolute cross-section measurements for electron-impact ionization of Al^+, Cd^+, and Hg^+

87D P. Defrance, S. Rachafi, J. Jureta, F. Meyer, and S. Chantrenne
Nucl. Instrum. Methods B **23** (1987) 265
Electron impact ionization of Ar^{8+}

87G D.C. Gregory, L.J. Wang, F.W. Meyer, and K. Rinn
Phys. Rev. A **35** (1987) 3256
Electron-impact ionization of iron ions: Fe^{11+}, Fe^{13+}, and Fe^{15+}

87H T. Hirayama, S. Kobayashi, A. Matsumoto, S. Ohtani, T. Takayanagi, K. Wakiya, and H. Suzuki
J. Phys. Soc. Jpn. **56** (1987) 851
Electron-impact double ionization of Ba^+

87M1 K.F. Man, A.C.H. Smith, and M.F.A. Harrison
J. Phys. B **20** (1987) 1351
A measurement of the cross section for ionisation of Mo^+ by electron impact

87M2 K.F. Man, A.C.H. Smith, and M.F.A. Harrison
J. Phys. B **20** (1987) 2571
A measurement of the cross section for ionisation of Cr^+ by electron impact

87M3 K.F. Man, A.C.H. Smith, and M.F.A. Harrison
J. Phys. B **20** (1987) 4895
A measurement of the cross section for ionisation of Ta^+ by electron impact

87M4 K.F. Man, A.C.H. Smith, and M.F.A. Harrison
J. Phys. B **20** (1987) 5865
A measurement of the cross section for electron impact ionisation of Ne^+, Ar^+, Kr^+ and Xe^+

87R K. Rinn, D.C. Gregory, L.J. Wang, R.A. Phaneuf, and A. Müller
Phys. Rev. A **36** (1987) 595
Electron-impact ionization of O^{5+}: Improved measurements

87T1 K. Tinschert, A. Müller, R. Becker, and E. Salzborn
J. Phys. B **20** (1987) 1823
Electron impact multiple ionisation of multiply charged krypton ions

87T2 K. Tinschert, A. Müller, G. Hofmann, C. Achenbach, R. Becker, and E. Salzborn
J. Phys. B **20** (1987) 1121
Electron impact single ionisation of multiply charged krypton ions

88B M.E. Bannister, D.W. Mueller, L.J. Wang, M.S. Pindzola, D.C. Griffin, and D.C. Gregory
Phys. Rev. A **38** (1988) 38
Cross sections for electron-impact single ionization of Kr^{8+} and Xe^{8+}

88D M.J. Diserens, A.C.H. Smith, and M.F.A. Harrison
J. Phys. B **21** (1988) 2129
Ionisation of Ti^{+}, Ti^{2+}, and Ar^{2+} by electron impact

88M1 A. Müller, G. Hofmann, K. Tinschert, and E. Salzborn
Phys. Rev. Lett. **61** (1988) 1352
Dielectronic capture with subsequent two-electron emission in electron-impact ionization of C^{3+} ions

88M2 A. Muller, L. Tinschert, G. Hofmann, E. Salzborn, and G.H. Dunn
Phys. Rev. Lett. **61** (1988) 70
Resonances in electron-impact single, double, and triple ionization of heavy metal ions

88W K.L. Wang, K. Rinn, and D.C. Gregory
J. Phys. B **21** (1988) 2117
Electron impact ionisation of nickel ions

88Y I. Yamada, A. Danjo, T. Hirayama, A. Matsumoto, S. Ohtani, H. Suzuki, H. Tawara, T. Takayanagi, K. Wakiya, and M. Yoshino
J. Phys. Soc. Jpn. **57** (1988) 2699
Electron impact ionization of O^{+}, S^{+}, and S^{2+} ions

89M1 D.W. Mueller, L.J. Wang, and D.C. Gregory
Phys. Rev. A **39** (1989) 2381
Electron-impact double-ionization cross sections for Xe^{8+}

89M2 A. Müller, K. Tinschert, G. Hofmann, E. Salzborn, G. Dunn, S.M. Younger, and M.S. Pindzola
Phys. Rev. A **40** (1989) 3584
Electron-impact ionization of La^{q+} ions (q = 1, 2, 3)

89M3 A. Müller, G. Hofmann, B. Weissbecker, M. Stenke, K. Tinschert, M. Wagner, and E. Salzborn
Phys. Rev. Lett. **63** (1989) 758
Correlated two-electron transitions in electron-impact ionization of Li^{+} ions

89P1 B. Peart, J. R. A. Underwood, and K. Dolder
J. Phys. B **22** (1989) 1679
Autoionisation and threshold ionisation of Ba^{+} by energy-resolved electrons

89P2 B. Peart, J.R.A. Underwood, and K. Dolder
J. Phys. B **22** (1989) 2789
The ionisation of Ca^{+} by energy-resolved electrons

89P3 B. Peart, J.R.A. Underwood, and K. Dolder
J. Phys. B **22** (1989) 4021
The ionisation of Sr^{+} by energy-resolved electrons

89S M. Sataka, S. Ohtani, D. Swenson, and D.C. Gregory
Phys. Rev. A **39** (1989) 2397
Experimental cross sections for electron-impact ionization of chromium ions: Cr^{6+}, Cr^{7+}, Cr^{8+}, and Cr^{10+}

89T1 K. Tinschert, A. Müller, G. Hofmann, K. Huber, R. Becker, D.C. Gregory, and E. Salzborn
J. Phys. B **22** (1989) 531
Experimental cross sections for electron impact ionization of hydrogen-like Li^{2+} ions

89T2 K. Tinschert, A. Muller, R.A. Phaneuf, G. Hofmann, and E. Salzborn
J. Phys. B **22** (1989) 1241
Electron impact double ionization of Ar^{q+} ions (q = 1, 2-7): two-electron processes compared with inner-shell contributions

89Y1 I. Yamada, A. Danjo, T. Hirayama, A. Matsumoto, S. Ohtani, H. Suzuki, T. Takayanagi, H. Tawara, K. Wakiya, and M. Yoshino
J. Phys. Soc. Jpn. **58** (1989) 1585
Electron impact ionization of C^+, N^+, and P^+ ions

89Y2 I. Yamada, A. Danjo, T. Hirayama, A. Matsumoto, S. Ohtani, H. Suzuki, T. Takayanagi, H. Tawara, K. Wakiya, and M. Yoshino
J. Phys. Soc. Jpn. **58** (1989) 3151
Electron impact ionization of F^+, Ne^+, Cl^+ and Ar^+ ions

90C S.J. Chantrenne, D.C. Gregory, M.J. Buie, and M.S. Pindzola
Phys. Rev. A **41** (1990) 140
Experimental and theoretical cross sections for electron-impact ionization of Ti^{5+}

90D P. Defrance, S. Chantrenne, S. Rachafi, D.S. Belic, J. Jureta, D. Gregory, and F. Brouillard
J. Phys. B **23** (1990) 2333
Absolute cross-section measurements for electron impact ionisation of Li-like N^{4+}, O^{5+}, and Ne^{7+} ions

90G1 D.C. Gregory, M.S. Huq, F.W. Meyer, D.R. Swenson, M. Sataka, and S. Chantrenne
Phys. Rev. A **41** (1990) 106
Electron-impact ionization cross-section measurements for U^{10+}, U^{13+}, and U^{16+}

90G2 D.C. Gregory, L.J. Wang, D.R. Swenson, M. Sataka, and S.J. Chantrenne
Phys. Rev. A **41** (1990) 6512
Electron-impact-ionization cross-section measurements for Ti^{11+} and Cr^{13+}

90H G. Hofmann, A. Müller, K. Tinschert, and E. Salzborn
Z. Phys. D **16** (1990) 113
Indirect processes in the electron-impact ionization of Li-like ions

90M1 A. Matsumoto, A. Danjo, S. Ohtani, H. Suzuki, H. Tawara, T. Takayanagi, K. Wakiya, I. Yamada, M. Yoshino, and T. Hirayama
J. Phys. Soc. Jpn. **59** (1990) 902
Measurements of absolute cross sections for electron-impact ionization of doubly charged rare gas ions; Ne^{2+}, Ar^{2+}, Kr^{2+}, and Xe^{2+}

90M2 A. Muller, G. Hofmann, K. Tinschert, B. Weissbecker, and E. Salzborn
Z. Phys. D **15** (1990) 145
Doubly autoionizing capture resonances in e+Mg^+ collisions

90P B. Peart and J.R.A. Underwood
J. Phys. B **23** (1990) 2343
The ionisation of Ga^+ by energy-resolved electrons

91P1 B. Peart, J.W.G. Thomason, and K. Dolder
J. Phys. B **24** (1991) 489
The ionization of Zn^+ by energy-resolved electrons

91P2 B. Peart, J.W.G. Thomason, and K. Dolder
J. Phys. B **24** (1991) 4453
Direct and indirect ionization of Mg^+ by energy-resolved electrons

91R S. Rachafi, D.S. Belic, M. Duponchelle, J. Jureta, M. Zambra, Z. Hui, and P. Defrance
J. Phys. B **24** (1991) 1037
Absolute cross section measurements for electron impact ionization of Ar^{7+}

91T K. Tinschert, A. Müller, G. Hofmann, E. Salzborn, and S.M. Younger
Phys. Rev. A **43** (1991) 3522
Electron-impact single and double ionization of Ba^{2+} and Ba^{3+} ions

91W K.L. Wong, P. Beiersdorfer, D. Vogel, R. Marrs, and M. Levine
Z. Phys. D **21** (1991) S197
Electron impact ionization cross sections measurement of lithium-like Ba

91Z Y. Zhang, C.B. Reddy, R.S. Smith, D.E. Golden, D.W. Mueller, and D.C. Gregory
Phys. Rev. A **44** (1991) 4368
Measurement of electron-impact single-ionization cross sections of Ar^{8+}

92D N. Djuric, E. W. Bell, E. Daniel, and G. H. Dunn
Phys. Rev. A **46** (1992) 270
Absolute cross-section measurements for electron-impact ionization of Cl^{+}

92Z Y. Zhang, C.B. Reddy, R.S. Smith, D.E. Golden, D.W. Mueller, and D.C. Gregory
Phys. Rev. A **45** (1992) 2929
Total cross sections of electron-impact ionization of Ar^{7+}

93B E. W. Bell, N. Djuric, and G.H. Dunn
Phys. Rev. A **48** (1993) 4286
Electron-impact ionization of In^{+} and Xe^{+}

93D1 N. Djuric, E.W. Bell, X.Q. Guo, G.H. Dunn, R.A. Phaneuf, M.E. Bannister, M.S. Pindzola, and D.C. Griffin
Phys. Rev. A **47** (1993) 4786
Absolute cross sections for electron-impact single ionization of Si^{+} and Si^{2+}

93D2 N. Djuric, E.W. Bell, and G.H. Dunn
Int. J. Mass Spectrom. Ion Processes **123** (1993) 187
Crossed-beams measurements of absolute cross sections for electron-impact ionization of S^{+}

93M K.F. Man, A.C.H. Smith, and M.F.A. Harrison
J. Phys. B **26** (1993) 1365
A measurement of the cross section for electron-impact ionization of Ar^{2+}, Kr^{2+} and Xe^{2+}

93P B. Peart, S.J.T. Green, and J.W.G. Thomason
J. Phys. B **26** (1993) 149
The double ionization of Ba^{+} by energy-resolved electrons

93W K.L. Wong, P. Beiersdorfer, M.H. Chen, R.E. Marrs, K.J. Reed, J.H. Scofield, D.A. Vogel, and R. Zasadzinski
Phys. Rev. A **48** (1993) 2850
Electron-impact ionization of lithium-like ions: Ti^{19+}, V^{20+}, Cr^{21+}, Mn^{22+}, and Fe^{23+}

93Z P.A. Zeijlmans van Emmichoven, M.E. Bannister, D.C. Gregory, C.C. Havener, R.A. Phaneuf, E.W. Bell, X.Q. Guo, J.S. Thompson, and M. Sataka
Phys. Rev. A **47** (1993) 2888
Electron-impact ionization of Si^{6+} and Si^{7+} ions

94B M.E. Bannister, X.Q. Guo, and T.M. Kojima
Phys. Rev. A **49** (1994) 4676
Absolute cross sections for electron-impact single ionization Kr^{4+}, Kr^{5+}, and Kr^{7+} ions

94D N. Djuric, E.W. Bell, and G.H. Dunn
Int. J. Mass Spectrom. Ion Processes **135** (1994) 207
Absolute cross-section measurements for electron-impact single ionization of Se^{+} and Te^{+}

94H S.J.T. Hayton and B. Peart
J. Phys. B **27** (1994) 5331
Measurements of cross sections for the ionization of Al^+ and Cd^+ by energy-resolved electrons

94M R.E. Marrs, S.R. Elliott, and D.A. Knapp
Phys. Rev. Lett. **72** (1994) 4082
Production and trapping of hydrogenlike and bare uranium ions in an Electron Beam Ion Trap

94P M.S. Pindzola, T.W. Gorczyca, N.R. Badnell, D.C. Griffin, M. Stenke, G. Hofmann, B. Weissbecker, K. Tinschert, E. Salzborn, A. Muller, and G.H. Dunn
Phys. Rev. A **49** (1994) 933
Dielectronic capture processes in the electron-impact ionization of Sc^{2+}

94T J.S. Thompson and D.C. Gregory
Phys. Rev. A **50** (1994) 1377
Absolute cross-section measurements for electron-impact single ionization of Si^{4+} and Si^{5+}

94Z M. Zambra, D. Belic, P. Defrance, and D.J. Yu
J. Phys. B **27** (1994) 2383
Electron impact double ionization of singly charged ions C^+, N^+, O^+, F^+ and Ne^+

95B M.E. Bannister, F.W. Meyer, Y.S. Chung, N. Djuric, G.H. Dunn, M.S. Pindzola, and D.C. Griffin
Phys. Rev. A **52** (1995) 413
Absolute cross sections for the electron-impact single ionization of Mo^{4+} and Mo^{5+} ions

95D M. Duponchelle, H. Zhang, E.M. Oualim, C. Belenger, and P. Defrance
Nucl. Instrum. Methods A **364** (1995) 159
A crossed electron-ion beam setup for ionization experiments

95K J. Kenntner, J. Linkemann, N.R. Badnell, C. Broude, D. Habs, G. Hofmann, A. Muller, M.S. Pindzola, E. Salzborn, D. Schwalm, and A. Wolf
Nucl. Instrum. Methods B **98** (1995) 142
Resonant electron impact ionization and recombination of Li-like Cl^{14+} and Si^{11+} at the Heidelberg Test Storage Ring

95L1 J. Linkemann, A. Muller, J. Kenntner, D. Habs, D. Schwalm, A. Wolf, N.R. Badnell, and M.S. Pindzola
Phys. Rev. Lett. **74** (1995) 4173
Electron-impact ionization of Fe^{15+} ions: An ion storage ring cross section measurement

95L2 J. Linkemann, J. Kenntner, A. Muller, A. Wolf, D. Habs, D. Schwalm, W. Spies, O. Uwira, A. Frank, A. Liedtke, G. Hofmann, E. Salzborn, N.R. Badnell, and M.S. Pindzola
Nucl. Instrum. Methods B **98** (1995) 154
Electron impact ionization and dielectronic recombination of sodium-like iron ions

95O E.M. Oualim, M. Duponchelle, and P. Defrance
Nucl. Instrum. Methods B **98** (1995) 150
Electron impact ionization of krypton ions (q = 8-13)

95S1 M. Stenke, K. Aichele, D. Harthiramani, G. Hofmann, M. Steidl, R. Volpel, and E. Salzborn
J. Phys. B **28** (1995) 2711
Electron-impact single-ionization of singly and multiply charged tungsten ions

95S2 M. Stenke, K. Aichele, D. Hathiramani, G. Hofmann, M. Steidl, R. Volpel, V.P. Shevelko, H. Tawara, and E. Salzborn
J. Phys. B **28** (1995) 4853
Electron-impact multiple ionization of singly and multiply charged tungsten ions

95S3 M. Stenke, D. Hathiramani, G. Hofmann, V.P. Shevelko, M. Steidl, R. Volpel, and E. Salzborn
Nucl. Instrum. Methods B **98** (1995) 138
Single and multiple ionization of Ni^{q+} ions by electron impact

95S4 M. Stenke, K. Aichele, D. Hathiramani, G. Hofmann, M. Steidl, R. Volpel, and E. Salzborn
Nucl. Instrum. Methods B **98** (1995) 573
A high-current electron gun for crossed-beams electron-ion collision studies at keV energies

95S5 M. Stenke, K. Aichele, D. Hathiramani, G. Hofmann, M. Steidl, R. Volpel, and E. Salzborn
Nucl. Fusion Suppl. **6** (1995) 51
Electron impact ionisation of tungsten ions

96B M.E. Bannister
Phys. Rev. A **54** (1996) 1435
Absolute cross sections for electron-impact single ionization of Ne^{q+} (q = 2, 4-6) ions

96H D. Hathiramani, K. Aichele, G. Hofmann, M. Steidl, M. Stenke, R. Volpel, E. Salzborn, M.S. Pindzola, J.A. Shaw, D.C. Griffin, and N.R. Badnell
Phys. Rev. A **54** (1996) 587
Electron-impact single ionization of low-charged molybdenum ions

97A K. Aichele, U. Hartenfeller, D. Hathiramani, G. Hofmann, F. Melchert, V. Schafer, M. Steidl, M. Stenke, R. Volpel, and E. Salzborn
Phys. Scr. T **73** (1997) 125
Electron impact ionization of the hydrogen-like ions: B^{4+}, C^{5+}, N^{6+} and O^{7+}

97D M. Duponchelle, M. Khouilid, E.M. Oualim, H. Zhang, and P. Defrance
J. Phys. B **30** (1997) 729
Electron-impact ionization of neon ions (q = 4-8)

97G H. Gao, D. Fang, F. Lu, J. Gu, W. Wu, W. Hu, Y. Wang, S. Wu, J. Tang, and F. Yang
Nucl. Instrum. Methods B **132** (1997) 364
Electron impact ionization cross section of Ar^+, Kr^+, In^+ and Ge^+

97H U. Hartenfeller, K. Aichele, D. Hathiramani, G. Hofmann, F. Melchert, V. Schafer, M. Steidl, M. Stenke, and E. Salzborn
Phys. Scr. T **73** (1997) 123
Electron impact ionization of titanium ions

97M R.E. Marrs, S.R. Elliott, and J.H. Scofield
Phys. Rev. A **56** (1997) 1338
Measurement of electron-impact ionization cross sections for hydrogenlike high-Z ions

97S Th. Stöhlker, A. Kramer, S.R. Elliott, R.E. Marrs, and J.H. Scofield
Phys. Rev. A **56** (1997) 2819
Measurement of L-shell electron-impact ionization cross sections for highly charged uranium ions

97T J.W.G. Thomason, B. Peart, and S.J.T. Hayton
J. Phys. B **30** (1997) 749
The double ionization of Cs^+ and Sr^+ by energy-resolved electrons

Appendix 2. Index by ion species.

N **= 1 (H-like)**	
Li III	89T1
B V	97A
C VI	97A
N VII	97A
O VIII	97A
Mo XLII	97M
Dy LXVI	97M
Au LXXIX	97M
Bi LXXXIII	97M
U XCII	94M, 97M
N **= 2 (He-like)**	
Li II	89M3
Ne IX	97D
U XCI	94M
N **= 3 (Li-like)**	
B III	86C, 90H
C IV	88M1, 90H
N V	90D, 90H
O VI	86C, 87R, 90D, 90H
F VII	90H
Ne VIII	90D, 97D
Si XII	95K
Cl XV	95K
Ti XX	93W
V XXI	93W
Cr XXII	93W
Mn XXIII	93W
Fe XXIV	93W
Ba LIV	91W
U XC	97S
N **= 4 (Be-like)**	
Ne VII	96B, 97D
U LXXXIX	97S
N **= 5 (B-like)**	
C II	89Y1, 94Z
Ne VI	96B, 97D
U LXXXVIII	97S
N **= 6 (C-like)**	
N II	89Y1, 94Z
Ne V	96B, 97D
U LXXXVII	97S
N **= 7 (N-like)**	
O II	88Y, 94Z
Si VIII	93Z
U LXXXVI	97S
N **= 8 (O-like)**	
F II	89Y2
Ne III	90M1, 96B
Si VII	93Z
U LXXXV	97S
N **= 9 (F-like)**	
Ne II	87M4, 89Y2, 94Z
Si VI	94T
U LXXXIV	97S
N **= 10 (Ne-like)**	
Na II	86H1
Si V	94T
Ar IX	87D, 91Z, 95D
N **= 11 (Na-like)**	
Mg II	90M2, 91P2
Ar VIII	89T2, 91R, 92Z
Ti XII	90G2
Cr XIV	90G2
Fe XVI	87G, 95L1, 95L2
N **= 12 (Mg-like)**	
Al II	87B, 94H
Si III	93D1
S V	86H2
Cl VI	86H2
Ar VII	86H2, 89T2
N **= 13 (Al-like)**	
Si II	93D1
Ar VI	89T2
Fe XIV	87G
N **= 14 (Si-like)**	
P II	89Y1
S III	88Y
Ar V	89T2
Cr XI	89S
Ni XV	88W

***N* = 15 (P-like)**	
S II	88Y, 93D2
Ar IV	89T2
Fe XII	87G
***N* = 16 (S-like)**	
Cl II	89Y2, 92D
Ar III	88D, 89T2, 90M1, 93M
Cr IX	89S
Ni XIII	88W
***N* = 17 (Cl-like)**	
Ar II	87M4, 89T2, 89Y2, 97G
Ti VI	90C, 97H
Cr VIII	89S
Fe X	86G2, 95S4
***N* = 18 (Ar-like)**	
K II	86H1
Cr VII	89S
***N* = 19 (K-like)**	
Ca II	89P2
Sc III	94P
***N* = 20 (Ca-like)**	
Ti III	88D, 97H
Fe VII	86G2
Ni IX	88W
***N* = 21 (Sc-like)**	
Ti II	88D
Fe VI	86G2
Ni VIII	88W
***N* = 22 (Ti-like)**	
Ni VII	88W
***N* = 23 (V-like)**	
Cr II	87M2
Ni VI	88W, 95S3
Kr XIV	95O
***N* = 24 (Cr-like)**	
Ni V	95S3
Kr XIII	95O
***N* = 25 (Mn-like)**	
Ni IV	86G1, 95S3
Kr XII	95O

***N* = 26 (Fe-like)**	
Ni III	95S3
Cu IV	86G1
Kr XI	95O
***N* = 27 (Co-like)**	
Cu III	86G1
Kr X	95O
***N* = 28 (Ni-like)**	
Kr IX	88B, 95O
***N* = 29 (Cu-like)**	
Zn II	91P1
Kr VIII	94B
***N* = 30 (Zn-like)**	
Ga II	90P
***N* = 31 (Ga-like)**	
Ge II	97G
Kr VI	94B
***N* = 32 (Ge-like)**	
Kr V	87T1, 94B
***N* = 33 (As-like)**	
Se II	94D
Kr IV	87T1, 87T2
***N* = 34 (Se-like)**	
Kr III	87T1, 87T2, 90M1, 93M
Mo IX	96H
***N* = 35 (Br-like)**	
Kr II	87M4, 87T1, 87T2, 97G
Mo VIII	96H
***N* = 36 (Kr-like)**	
Mo VII	96H
***N* = 37 (Rb-like)**	
Sr II	89P3, 97T
Mo VI	95B, 96H
***N* = 38 (Sr-like)**	
Mo V	95B, 96H
***N* = 39 (Y-like)**	
Mo IV	96H

N = 40 (Zr-like)
Mo III 96H

N = 41 (Nb-like)
Mo II 87M1, 96H

N = 46 (Pd-like)
Xe IX 88B, 89M1, 95S4

N = 47 (Ag-like)
Cd II 87B, 94H

N = 48 (Cd-like)
In II 93B, 97G
Sb IV 86G1
Xe VII 86H3

N = 51 (Sb-like)
Te II 94D

N = 52 (Te-like)
Xe III 90M1, 93M

N = 53 (I-like)
Xe II 87M4, 93B
Ba IV 91T

N = 54 (Xe-like)
Cs II 88M2, 97T
Ba III 88M2, 91T, 95S4
La IV 88M2, 89M2

N = 55 (Cs-like)
Ba II 87H, 89P1, 93P
La III 88M2, 89M2

N = 56 (Ba-like)
La II 89M2
Ce III 88M2

N = 57 (La-like)
Ce II 88M2

N = 64 (Gd-like)
W XI 95S1, 95S5

N = 65 (Tb-like)
W X 95S1, 95S5

N = 66 (Dy-like)
W IX 95S1, 95S5

N = 67 (Ho-like)
W VIII 95S1, 95S5

N = 68 (Er-like)
W VII 95S1, 95S2, 95S5

N = 69 (Tm-like)
W VI 95S1, 95S2, 95S5

N = 70 (Yb-like)
W V 95S1, 95S2, 95S5

N = 71 (Lu-like)
W IV 95S1, 95S2, 95S5

N = 72 (Hf-like)
Ta II 87M3
W III 95S1, 95S2, 95S5

N = 73 (Ta-like)
W II 95S1, 95S2, 95S5

N = 76 (Os-like)
U XVII 90G1

N = 79 (Au-like)
Hg II 87B
UXIV 90G1

N = 82 (Pb-like)
U XI 90G1

3.3 Electron ion recombination processes

3.3.1 Introduction

When free electrons encounter charged atomic ions A^{Z+}, in a plasma for example, several things can happen [87Jan]. If the ions are fully stripped of electrons and bare, the projectile electrons can scatter off the ions, or recombine to form a bound state. In this latter case, the free incoming electron can recombine directly with the target ion with emission of a photon and form a bound state, or discharge its excess energy by increasing the kinetic energy of another electron in the continua. On the other hand, if the target contains one or more bound electrons initially, then in addition to the above, the projectile electrons can excite the target ion by pulling one or more bound electrons to upper excited states (see Section 3.1) and to continuum states (see Section 3.2). In the course of the excitation, the continuum electron can give up some of its excess energy and drop into a bound orbital, thus forming a multiply excited state. Such a state can photo-decay, or can contribute to excitation and ionization channels as well. When modelling a plasma, therefore, one has to take into account all these possible processes allowed by the selection rules and conservation laws, in order to determine how a perturbed plasma proceeds to relax and reach a final stable state. Schematically we have for electron-ion collision system [85Hah, 88Hah, 97Hah2]

$$\begin{aligned} e^- + A^{Z+} &\rightarrow e^{-'} + (A^{Z+})' && \text{(excitation – Section 3.1)} && (1a)\\ &\rightarrow e^{-'} + e^{-''} + A^{ZP+} && \text{(ionization – Section 3.2)} && (1b)\\ &\rightarrow (A^{ZM+}) + x && \text{(recombination – Section 3.3)} && (1c) \end{aligned}$$

where $ZP = Z + 1$ and $ZM = Z - 1$, and x denotes photons. All three basic processes mentioned above may be further subdivided to different modes; that is, they proceed directly from the initial to the final states, or indirectly through intermediate resonance states. When the energy and various selection rules are satisfied, the latter indirect modes often dominate over the former. The recombination processes we focus in this chapter have been the subject of study since the early 1920's. Mainly due to its importance in plasma modelling and diagnostics, much work has been done for the past twenty years, and much new insights have been gained by many crucial experimentations and theoretical analyses.

The recombination processes are conveniently subdivided into the direct and indirect modes, where the direct modes are the radiative recombination (RR) with emission of photons and three-body recombination (TBR) without radiation emission. Generally, the RR results in low-lying bound states, while the TBR is more effective in filling high Rydberg states (HRS). The indirect modes are the dielectronic recombination (DR) and radiative DR (RDR). Thus, we schematically describe the various recombination processes as

$$\begin{aligned} e^- + A^{Z+}(i) &\rightarrow A^{ZM+}(f) + x && \text{(RR)} && (2)\\ &\rightarrow A^{ZM+}(d) \rightarrow A^{ZM+}(f') + x' && \text{(DR)} && (3)\\ &\rightarrow A^{ZM+}(d) \rightarrow A^{Z}(i') + e' && \text{(RE)} && (4)\\ &\rightarrow (A^{ZM+})(d'') + x'' && \text{(RDR)} && (5)\\ e + e' + A^{Z+}(i) &\rightarrow e'' + A^{ZM+}(f'') && \text{(TBR)} && (6) \end{aligned}$$

where the target ion $A^{Z+}(i)$ is assumed to have N electrons initially. (N can be zero for RR, but DR and RDR require $N > 0$.) The recombined states f, f' and d contain a total of $N+1$ electrons. The formation of $A^{ZM+}(d)$ in DR and resonant excitation(RE) is via the inverse autoionization process (see Section 3.1). The RE process in (4) describes a two-step resonant excitation process that complements DR, and the RDR stands for a quasi-two-step, correlated recombination process; the final states (d') in the RDR are doubly excited and thus Auger unstable [81LaG]. On the other

hand, states (f) and (f') denote the final bound (ground or singly excited) states reached by recombination, and may further relax only radiatively (but not by Auger emission.) As noted earlier, in the TBR, the excess energy released by the captured electron is carried away by another continuum electron e'', so that no radiation is emitted in the final state, except through subsequent cascades. Thus, this mode of recombination requires at least two interacting electrons in the continua initially, and its rate increases rapidly with electron density.

The recombination processes often involve high Rydberg states (HRS) as either intermediate states or final recombined states. The presence of electric (and/or magnetic) fields inside plasma can seriously affect these HRS, and thus the corresponding rates. This can be a serious problem, and increases the uncertainty in choosing the proper rates that reflect the structure of the particular rate equations employed. Conversely, sensitivity of the rates to field perturbations may be used with advantage in determining field conditions in the interaction zone where recombination takes place. An excellent and insightful historical review of the recombination was given recently by Bates [92Bat], and the current status on the recombination, both in theory and experiment, were summarized by the experts in the field in a recent proceeding edited by Graham et al. [92Gra]. Previously, several review articles were already available [76Sea, 80Dub, 85Hah, 95Hah]. More recently, atomic data for fusion edge plasmas were reviewed in a collection edited by Janev [95Jan], and a comprehensive overview of the subject of recombination was given [97Hah2], to which we refer for additional theoretical developments. Many of the earlier references on recombination may be found in these reviews.

Glossary of the acronyms used:

RR	–	radiative recombination	HRS	–	high Rydberg states
DR	–	dielectronic recombination	LRS	–	low Rydberg states, for $n < 5$
TBR	–	three-body recombination	DWA	–	distorted wave approximation
RDR	–	radiative dielectronic recombination	CCM	–	coupled channel method
			LTE	–	local thermal equilibrium

3.3.2 General discussion

Since the recombination rates are invariably obtained by often extensive theoretical calculations, a brief summary of the theoretical background is given below. The system under study involves one or more electrons and the radiation-electron coupling, so that theoretical treatment requires simplifying approximations, especially when some perturbing fields are present. On the other hand, recombination experiments are difficult and available data are often contaminated by external perturbations. Nevertheless, available data are helpful in testing the theory.

The theoretical methods adopted are varied, and almost all the theoretical data have been obtained by essentially two methods; the distorted wave approximation (DWA), with or without configuration interactions, and the more extensive coupled-channel method (CCM). When elaborate target functions for the ground and excited states are introduced, and some additional pseudostates for the closed channel effect are included, the CCM is probably the most accurate procedure currently available. But, it is very time consuming to run the programs, and its accuracy depends on extent of states included. Representation of target functions is also often crude. On the other hand, the DWA is relatively simple to use and quick when no configuration interactions are included, but of less accuracy than the CCM. (The DWA without configuration interaction may sometimes lead to serious errors when several open shell electrons participate.) Therefore, the DWA is routinely used to generate a large quantities of rates needed in modelling, and both the CCM and experimental data are used to refine the data. The plasma diagnostics usually requires a small subset of data, and these are more reliably generated by the CCM. For ions with charges

larger than 20, the relativistic effects are no longer a small perturbation, and multiconfiguration Dirac-Fock procedure has also been developed.

In the following, we present the recombination amplitudes in the distorted wave approximation (DWA), which may be the simplest of all approximations and yet quite practical in many cases, in generating a large amount of data. As noted above, however, the use of the DWA data requires caution.

3.3.2.1 The recombination amplitudes and cross sections

Starting with the simple one-step processes, the amplitude for the radiative recombination of (2) is given by [85Hah, 88Hah]

$$M_{fi}^{\mathrm{RR}} \simeq \left\langle \tilde{\Psi}_f^R \left| D \right| \tilde{\Psi}_i^P \right\rangle \tag{7}$$

where $D = H - H_0$= the electron-radiation field coupling, and where the continuum wave function in the DWA (marked with tilde) satisfies, for example,

$$(E - H_0 + U_i)\, \tilde{\Psi}_i^P \simeq 0 \tag{8}$$

where U is a suitably chosen effective distortion potential. The superscripts R and P denote the states with one photon and one continuum electron, respectively. Next, the TBR amplitude for process (6) is given by

$$M_{fi}^{\mathrm{TBR}} \simeq \left\langle \tilde{\Psi}_f^P \left| V \right| \tilde{\Psi}_i^{PP} \right\rangle \tag{9}$$

where PP denotes the states with two continuum electrons in the initial state, and V is the electron-electron interaction. The final state has one electron in continuum and another bound to the target ion.

The two-step resonant process of dielectronic recombination is defined in terms of the multiply excited resonance states. Denoting the resonant state space by Q, we have

$$\tilde{\Psi}_i^Q = G^Q V_{QP} \tilde{\Psi}_i^P \tag{10}$$

where the Green's function G^Q has two parts, the on- and off-shell contributions, as

$$G^Q = \bar{G}^Q - i\ \pi\, \delta\left(\left[G^Q \right]^{-1} \right). \tag{11}$$

The first term in (11) is the principal part and its contribution is generally small, but gives the correlated quasi-two-step radiative DR (RDR) and also the polarization potential. The second term in (11) is the on-shell contribution, and gives the DR amplitude, as shown below. Introducing a broadened delta function, as

$$\Lambda_d^Q = (\Gamma/2\pi) / \left[\left(E - E_d^Q \right)^2 + \Gamma(d)^2/4 \right], \quad \int \Lambda_d^Q \, \mathrm{d}E = 1 \tag{12a}$$

$$\Gamma(d) = \Gamma_a(d) + \Gamma_r(d) + \Gamma_{sk}(d) \tag{12b}$$

we have the DR amplitude from the second term of G^Q, as

$$\begin{aligned} M_{fdi}^{\mathrm{DR}} &\simeq \left\langle \tilde{\Psi}_f^R \left| D\, G^Q\, V \right| \tilde{\Psi}_i^P \right\rangle \\ &\simeq \left\langle \tilde{\Psi}_f^R \left| D \right| \Phi_d^Q \right\rangle \Lambda_d^Q \left\langle \Phi_d^Q \left| V \right| \tilde{\Psi}_i^P \right\rangle \end{aligned} \tag{13}$$

for the transition $i \to d \to f$, with the requirement of energy conservations, separately for $i \to d$ and $d \to f$. The subscript d denotes doubly (and multiply) excited states of the recombined ion.

The widths $\Gamma(d)$ of the resonance levels with energies E_d^Q are usually small as compared with the typical level spacings, and the individual states can be handled separately in that case, resulting in the 'isolated resonance' approximation.

Finally, we briefly discuss the RDR, which is the direct extension of the DR process. As mentioned earlier, we take the contribution from the first term $\bar{G}^Q$ in (11), and define the amplitude symmetric in D and V,

$$M_{fi}^{\mathrm{RDR}} = \left\langle \tilde{\Psi}_f^R \left| \left(D\,\bar{G}^Q\,V + V\bar{G}^Q D \right) \right| \tilde{\Psi}_i^P \right\rangle \tag{14}$$

In the case of a singly excited final state, this amplitude may also be regarded as a higher-order RR process in that the initial or final states are further distorted by V. On the other hand, RDR is capable of producing doubly excited 'final' states ($f = d'$), in which case the process is quite distinct from the distorted RR. The discrete energy conservation of the type associated with DR is not required here, and the process may become important when HRS are involved. Due to many-body nature of the process (for the total number of electrons in the target ion initially $N > 1$), the amplitude (14) is difficult to estimate [95Hah]. No extensive data exist at present, and we do not consider this process further in this report.

The recombination cross sections are defined as

$$\sigma_{fi} = (2\pi/\hbar)\,|M_{fi}|^2\,\rho_f/J_i \tag{15}$$

where ρ_f is the density of the final states (of either photons or electrons), and J_i is the initial state flux of the projectile; these quantities are in general dependent on the way the initial and final states are normalized. The final state density ρ_f may be for the emitted photons in the case of RR and DR, or for the emitted electrons in the case of Auger and TBR processes.

The recombination cross sections are given by

$$\sigma_{fi}^{\mathrm{recomb}} = \sigma_{fi}^{\mathrm{RR}} + \sigma_{fi}^{\mathrm{DR}} + \sigma_{fi}^{\mathrm{RR-DR}} + \sigma_{fi}^{\mathrm{RDR}} + \sigma_{fi}^{\mathrm{TBR}} + \ldots\ , \tag{16}$$

where the RR–DR part refers to an interference between the RR and DR amplitudes, in which case both RR and DR must have the same initial and final states. (In this simplified notation in (16), some terms drop out when a particular pair of (f, i) is chosen.) In general, other interference terms must also be present, such as RR–RDR etc., as well as higher order corrections in powers of D and V. They are usually small and are neglected in our discussion below.

The RR cross section for the transition from the initial state of the ion plus the continuum electron with energy e_{c} to a final recombined state of an empty shell with the quantum number (n, l), is given in the case of one electron system, as

$$\sigma_{fi}^{\mathrm{RR}} = \left(\pi/3(k_{\mathrm{c}}a_0)^2\right)\,\alpha_0^3(\hbar\omega_{fi}/\mathrm{Ry})^3\,\left(l(S_{nl}^{l_{\mathrm{c}}=l-1})^2 + (l+1)(S_{nl}^{l_{\mathrm{c}}=l+1})^2\right)\,(\pi a_0^2) \tag{17}$$

where, for consistency, the continuum function obtained from (8) with $E = e_{\mathrm{c}} > 0$ is energy-normalized, as ($p_{\mathrm{c}} = \hbar k_{\mathrm{c}}$)

$$R_{e_{\mathrm{c}}l_{\mathrm{c}}} \to (2/\pi k_{\mathrm{c}})^{1/2}\,\sin\left(p_{\mathrm{c}}r + (Z/k_{\mathrm{c}}a_0)\,\ln(2p_{\mathrm{c}}r) - l_{\mathrm{c}}\pi/2 + \sigma_{l_{\mathrm{c}}} + \delta_{n,l_{\mathrm{c}}}\right) \tag{18}$$

and the radial dipole matrix elements introduced in the 'length form' are

$$S_{nl}^{l_{\mathrm{c}}} = \int \mathrm{d}r\,R_{e_{\mathrm{c}}l_{\mathrm{c}}}(r)\,R_{nl}(r)\,r\ . \tag{19}$$

We also have, in (17), $\hbar\omega_{fi} = e_{\mathrm{c}} + |E_{nl}|$ = transition energy carried by the emitted photon, and $\alpha_0 = e^2/\hbar c = 1/137$. The form (17) is closely related to the spontaneous radiative transition probability between two bound states; therefore RR is also called spontaneous RR, in order to be distinguished from the stimulated RR.

The TBR cross section is related to that for the collisional ionization, by detailed balance as

$$\sigma_{fi}^{\mathrm{TBR}} = \left[\left(g_i\rho_f J_i\right)/\left(g_f\rho_i J_f\right)\right]\,\sigma_{if}^{\mathrm{Ioniz}}\ , \tag{20}$$

where the collisional ionization cross section may be extracted from experimental data, or by a direct calculation. (See Section 3.2.)

Next, the DR cross section can be given as a sum of factored products of probabilities, because there are usually infinitely many resonance intermediate states involved; in the isolated resonance approximation, the width of the doubly excited resonance levels are assumed much smaller than the inter-resonance spacing, in energy. Then, near $E \simeq E_d^Q$,

$$\sigma_{fdi}^{\mathrm{DR}} \simeq \left(4\pi \mathrm{Ry}/(k_{\mathrm{c}} a_0)^2\right) V_{\mathrm{a}}(i,\, c \to d) \tau_0 \Lambda_d^Q(e_{\mathrm{c}}) \omega(d)\, (\pi a_0^2) \ , \tag{21}$$

where $\pi a_0^2 = 8.80 \times 10^{-17} \mathrm{cm}^2$, $\tau_0 = 2.42 \times 10^{-17} \mathrm{s}, V_{\mathrm{a}}(i,\, c \to d) = (g_d/2g_i) A_{\mathrm{a}}(d \to i, c)$ and $\omega(d) = \Gamma_{\mathrm{r}}(d)/\Gamma(d)$ with $\Gamma = \Gamma_{\mathrm{r}} + \Gamma_{\mathrm{a}}$. The g_d and g_i are the degeneracy factors for states d and i, respectively. (The shake-off contribution Γ_{sk} is neglected here.) The total radiative and Auger widths are defined by

$$\Gamma_{\mathrm{r}}(d) = \sum_{f'} A_{\mathrm{r}}(d \to f') = 2\pi \sum_{f'} \left|\langle f' \left|D\right| d\rangle\right|^2 \rho_f \tag{22a}$$

$$\Gamma_{\mathrm{a}}(d) = \sum_{i',c} A_{\mathrm{a}}(d \to i') = 2\pi \sum_{i',c} \left|\langle i', c \left|V\right| d\rangle\right|^2 \rho_{i',c} \tag{22b}$$

where ρ_f is the photon density and $\rho_{i',c}$ is the continuum electron density. The resonance width Γ is usually much less than 0.01 eV, and often dominated by Γ_{a}, except when $Z >> 1$ where Γ_{r} becomes comparable in magnitude to Γ_{a}. When many (isolated or overlapping) levels d occur in a small energy interval, it is convenient in comparing with experiments to define an energy-averaged cross section, over an energy interval Δe_{c}, as

$$\bar{\sigma}^{\mathrm{DR}} \equiv (1/\Delta e_{\mathrm{c}}) \int_{e_{\mathrm{c}-}}^{e_{\mathrm{c}+}} \sigma^{\mathrm{DR}}(e_{\mathrm{c}'})\, \mathrm{d}e_{\mathrm{c}'} \tag{23}$$

where $e_{\mathrm{c}\pm} \equiv e_{\mathrm{c}} \pm \Delta e_{\mathrm{c}}/2$. Choice of Δe_{c} is quite arbitrary; to retain the essential information in σ^{DR}, Δe_{c} may be chosen somewhat smaller than the experimental electron beam energy spread.

3.3.2.2 Rate coefficients, electron velocity distributions and cascades

The cross sections defined above depend on approximations introduced in the evaluation of the various wave functions. On the other hand, atomic reaction rates are strongly dependent on assumptions made on the electrons and photon distributions, so that special models may be needed in comparing the theoretical result with experiments. The usual assumption of a Maxwell-Boltzmann distribution for a plasma in equilibrium may not always be valid. Recombination rates are defined in general as a velocity-weighted average

$$\alpha \equiv \langle v_{\mathrm{c}} \sigma \rangle = \int \sigma \ \mathrm{d}\phi_T\, v_{\mathrm{c}} \tag{24}$$

where $\mathrm{d}\phi_T$ is usually taken to be Maxwellian, as

$$\mathrm{d}\phi_T = \left(4\pi/\left(2\pi k_{\mathrm{B}} T_{\mathrm{e}}\right)^{3/2}\right) \exp(-e_{\mathrm{c}}/k_{\mathrm{B}} T_{\mathrm{e}})\ v_{\mathrm{c}}\ \mathrm{d}e_{\mathrm{c}} \ , \tag{25}$$

where $\mathrm{e}_{\mathrm{c}} = m_{\mathrm{e}} v_{\mathrm{c}}^2/2 = k_{\mathrm{c}}^2 \hbar^2/2m_{\mathrm{e}}$. This form obviously assumes that the system (plasma, gas, or both) is in local thermal equilibrium (LTE).

With the LTE assumption, the DR rates for example may be immediately evaluated as

$$\alpha_{fdi}^{\mathrm{DR}} = (4\pi \mathrm{Ry}/k_{\mathrm{B}} T_{\mathrm{e}})^{3/2}\, a_0^3\ V_{\mathrm{a}}(i,\, c \to d) \omega(d \to f) \exp(-e_{\mathrm{c}}/k_{\mathrm{B}} T_{\mathrm{e}}) \ , \tag{26}$$

a result first derived by Bates and Massey [43Bat]. The RR and TBR rates evaluated with (24) and (25) are discussed in Subsection 3.3.3.

When the distribution is not quite in LTE, the rates may change considerably. For example, a transient electron distribution may be represented approximately by a sum of two Maxwellians with two different temperatures, as

$$\mathrm{d}\phi_T = a\ \mathrm{d}\phi_{T_a} + b\ \mathrm{d}\phi_{T_b} \quad , \quad a+b=1 \tag{27}$$

When $a >> b$ and $T_a << T_b$, the recombination rates turn out to be less sensitive to T_b mixing, while the ionization rates are especially sensitive to the high temperature components. That is, a small mixture of high T component in the normal Maxwell distribution can seriously affect the effective ionization rates, while the effective recombination rates are not very sensitive to such deviations. This in turn can distort ionization balance, increasing the relative population of the lower charge states.

When a plasma is spatially inhomogeneous, a two-temperature formula is sometimes employed, one for the $T_{||}$ and another for $T_\perp$, such as

$$\begin{aligned} \mathrm{d}\phi_T &= \mathrm{d}\phi_{T_{||}} \cdot \mathrm{d}\phi_{T_\perp} = 4\pi \left[\left(2\pi k_\mathrm{B} T_{||}\right)^{1/2} 2\pi k_\mathrm{B} T_\perp \right]^{-1} \cdot \\ &\quad \cdot \exp(-e_{\mathrm{c}_\perp}/k_\mathrm{B}T_\perp)\ \exp(-(e_{\mathrm{c}_{||}} - \Delta_\mathrm{c})/k_\mathrm{B}T_{||})\ v_\mathrm{c}\ \mathrm{d}e_\mathrm{c}\ , \end{aligned} \tag{28}$$

where $\mathrm{d}\phi_{T_{||}}$ is one-dimensional, while $\mathrm{d}\phi_{T_\perp}$ involves two-dimensional velocities. We also introduced in (28) the longitudinal detuning energy Δ_c.

The recombination processes described by eqs. (2) - (6) often lead to final states f and d' which are not stable against further radiative and/or Auger emissions. The distinction between the two kinds of states, one stable against Auger and the other unstable, is important in completing recombination. In order to complete the recombination, we follow the radiative branches of the cascade and require that the final states should be Auger stable. Thus we have to consider carefully the cascades of the recombined ions. The theory of recombination with cascades was developed previously [85Hah] for the DR process, but it should be equally adoptable to other cases. The cascade correction can be sizeable, up to 20% in some cases, and is the largest when a deep inner shell hole is involved. The fluorescence yield is generalized, as

$$\begin{aligned} \omega\left[d(r,m)\right] &= \sum_{f(r+1,m)} \omega\left[d(r,m) \to f(r+1,m)\right] \\ &\quad + \sum_{d(r+1,m)} \sum_{f(r+2,m)} \omega\left[d(r,m) \to d(r+1,m)\right] \cdot \\ &\quad \cdot \omega\left[d(r+1,m) \to f(r+2,m)\right] + \sum\sum\sum \omega\omega\omega \ + \ \ldots \quad , \end{aligned} \tag{29}$$

where r and m denote the number of accumulated photons and electrons, respectively, during the cascades. So long as states $d(r,m')$ with $m' > m$ do not appear in the above cascade chain, we have the recombination. Otherwise, we will have lost one or more electrons to continua during the cascades. The partial fluorescence yields introduced in (29) are defined as

$$\omega\left[d(r,m) \to d(r+1,m)\right] = A_\mathrm{r}\left[d(r,m) \to d(r+1,m)\right] / \Gamma\left[d(r,m)\right] \tag{30a}$$

$$\Gamma\left[d(r,m)\right] = \Gamma_\mathrm{a}\left[d(r,m) \to d(r,m+1)\right] + \Gamma_\mathrm{r}\left[d(r,m) \to d(r+1,m)\right] \tag{30b}$$

The shakeoff effects are important sometimes in evaluation of fluorescence yields [92Oma1, 92Oma2]. All the relevant tables are given at the end of this section.

3.3.3 Direct processes

In this subsection, we summarize the rates for the RR and TBR processes. The resonant recombination process DR will be discussed in Subsection 3.3.4. Although the amplitudes for the direct

processes are relatively simple in structure, reliable estimates are difficult to obtain, except in the case of a one electron system, where the exact cross section is available. (By definition, the TBR involves at least two electrons, and thus the theory is more complex.) In general cases with more than one electron, the cross sections are sensitive to correlation and other perturbative effects, especially when the energies involved are low and the impulse picture fails. We will therefore first discuss the hydrogenic case ($N = 0$ of the bare target ions) in some detail, with emphasis on low energies and HRS with large n (= principal quantum number of the recombined electron). The $N > 1$ cases with more than one electron are best discussed using the approximate scaling properties with respect to the ionic charge Z (with $Z \gtrsim 3$) and the quantum number n. These properties, with an effective charge, may be used in treating complex systems with more than one electron. For a more accurate estimate of the cross sections at low energies, however, detailed computation must be carried out; the nonrelativistic Hartree-Fock program with the DWA for the amplitudes is routinely used for RR [77Hah], and more elaborate CCM approach is also available [59Sea, 62Sea, 75Sea, 83Sea].

3.3.3.1 Radiative recombination (RR)

The earliest and most prominent RR cross section formula is that of Kramers [23Kra], which is given by

$$\sigma_n^{\mathrm{RR-K}}(\eta) = \frac{\left(32/3\sqrt{3}\right)\alpha_0^3\eta^4}{n(\eta^2+n^2)} \ (\pi a_0^2) \ , \tag{31}$$

where $\eta = Z\,/\,k_{\mathrm{c}}a_0$, k_{c} = wave number of the incoming electron, a_0 = Bohr radius, and n = principal quantum number of the recombined ionic state. This expression was derived by a semiclassical consideration of the hydrogenic system with charge Z, where the initial state of the electron has the kinetic energy $e_{\mathrm{c}} = (k_{\mathrm{c}}a_0)^2\,\mathrm{Ry}$, and the final recombined electron assumes the energy $E_n = -Z^2/n^2\,\mathrm{Ry}$. Note first of all that the cross section is summed over the angular momentum of the captured states. Secondly, the Z and e_{c} dependence is combined into one single parameter η, so that presumably the RR cross section can be scaled accordingly, with an effective charge Z_{eff}. The exact cross section in a hydrogenic case also behaves this way.

As noted above, the RR cross section in the nonrelativistic approximation can be evaluated exactly in the pure Coulombic case of single electron system, [30Sto, 64Bur, 91McL]. A relativistic treatment is also possible [76Lee, 83Kim]; as in the case of photoionization, the relativistic and multipole contributions seem to roughly cancel each other. Thus the nonrelativistic dipole approximation works quite well, so long as Z is not too high ($Z \lesssim 30$).

The formula (31) is simple to apply, and thus it is desirable to determine its reliability. We found [97Zer] that the formula is accurate to within 1% for $\eta > 10^2$ and for $n > 10$; a slightly improved form, valid in this region, is given by

$$\sigma_n^{\mathrm{RR-KI}}(\eta) = \sigma_n^{\mathrm{RR-K}}(\eta)\ \left[0.99 + 0.51/y^2 - (0.27 - 2.70/y^2)/n\right] \tag{32}$$

where $y = \ln\eta$. In addition, this formula has been improved for the parameter regions outside the one specified above, extending its applicability to lower n and low η corresponding to higher energies [97Zer].

Obviously, the Kramers' formula is explicitly angular momentum independent. It is extended to include the explicit l dependence. For high $n > 10$, and at low energies, the l dependence turned out to be roughly Gaussian, with the maxima moving out toward $l_{\max} \simeq n/3$ as the energy is lowered and n is raised. Thus the modified formula is

$$\sigma_n^{\mathrm{RR-KII}}(\eta) = \sigma_n^{\mathrm{RR-KI}}(\eta)\, a_0(n,\eta)\, \exp\left[-a_1(n,\eta)\,(l - a_2(n,\eta))^2\right] \ , \tag{33}$$

where

$$\begin{aligned} a_0(n,\eta) &\simeq 0.041 + 1.16/\eta^{1.14} + (1.50 - 94.9/\eta^{1.93})/n \\ a_1(n,\eta) &\simeq 0.0052 + 3.89/\eta^{1.19} + (0.966 - 0.195/y^2)/n \\ a_2(n,\eta) &\simeq -0.917 - 1.88/y^2 + \sqrt{n}(1.17 + 0.521/y^3) + n(0.175 + 0.334/y^2) \end{aligned} \tag{34}$$

When summed over l, (33) of course reduces to (32). A more extensive fit for wider range of the fitting parameters is also available [97Zer].

The RR rates are accurately given by the formula obtained with the Kramers' cross section, in the region $\Theta = k_B T_e/Z^2\mathrm{Ry} < 10^{-4}$ and $n > 0.1/\sqrt{\Theta}$, to within one percent. Thus, the rates are given for the hydrogenic ions

$$\alpha_n^{\mathrm{RR-K}}(\Theta, Z) = \left(4\sqrt{\pi}/\Theta^{3/2}\right) \int_0^\infty d\eta\, \eta^{-5}\, \sigma_n^{\mathrm{RR}}(\eta)\, \exp(-1/\Theta\eta^2)\ \ (a_0^3/\tau_0)\ . \tag{35}$$

Note that α^{RR}/Z scales in terms of one parameter $\Theta = k_B T_e/Z^2\mathrm{Ry}$. For the improved formula at high n and small Θ,

$$\alpha_n^{\mathrm{RR-KI}}(\Theta) \simeq 5.20 \times 10^{-14}(Z/n\sqrt{\Theta})(0.990 - 0.270/n)\ \ \mathrm{cm}^3/\mathrm{s}\ . \tag{36}$$

For the l dependence, the Kramers' improved formula KI is modified again as

$$\begin{aligned} \alpha_n^{\mathrm{RR-KII}}(\Theta, Z) \simeq\ & \left(3.43 \times 10^{-15}/n + 6.03 \times 10^{-14}/n^2\right)(Z/\sqrt{\Theta})\ \cdot \\ & \cdot\ \exp\left(-\frac{(l - (0.711 + 0.372n))^2}{0.308 + 0.431n + 0.0477n^2}\right)\ \mathrm{cm}^3/\mathrm{s}\ , \end{aligned} \tag{37}$$

which is valid in the region $\Theta < 10^{-2}$ and $n > 1/\sqrt{\Theta}$. (We relaxed the parameter regions here.) More extensive formulas that apply to a larger parameter region may be found in Zerrad et al. [97Zer].

For ions with one or more electrons before capture, the scaled formula for the cross sections and rates may be used if a proper formula for the effective Z_{eff} can be found. Considerable effort was expanded previously in deriving such a formula [85Hah]. Of course, in the simplest form, we have approximately

$$Z^a_{\mathrm{eff}} \simeq (Z_c + Z)/2 \ \text{ for } \ Z > Z_c/2, \ \text{ and } Z^b_{\mathrm{eff}} \simeq \sqrt{Z_c Z} \ \text{ for } \ Z < Z_c/2 \tag{38}$$

where Z_c is the nuclear core charge of the ion, and $Z_c = Z + N$. For simplicity, we recommend the form $Z_{\mathrm{eff}} \simeq \sqrt{Z_c Z}$ for all Z; the difference is minimal for our purpose. More elaborate formulas for Z_{eff} are also available [97Zer] which depend on the n and l parameters as well as the incident energy e_c . In all cases, however, the effective charge treatment is reliable at relatively low η and low n.

We present the typical RR rates for the Fe ions in Fig. 1, for four different N values, where N is the number of electrons in the target initially before capture. At low T the rates behaves as $T^{-1/2}$. For ready access to the RR rates for the individual (n, l), Table 1 may be used for n up to 10. It contains the scaled RR rates $\alpha^{\mathrm{RR}}_{n,l}/Z_{\mathrm{eff}}$ for the scaled temperature $\Theta = k_B T_e/Z^2_{\mathrm{eff}}\mathrm{Ry}$. The table contains the values at several temperatures, for interpolation. For the values of n higher than 10, one can use the modified Kramer's formulas, such as (36) and (37). In order to read the RR rates off the table, we summarize the procedure:

Step 1. From the nuclear core charge Z_c and the degree of ionization Z, compute $Z_{\mathrm{eff}} = \sqrt{Z_c Z}$. Using this, evaluate the scaled temperature Θ.

Step 2. From Table 1, read off the rates for the desired state nl, and multiply it by Z_{eff}. This gives the rates in cm^3/s, under the assumption that the particular nl subshell is empty before capture.

Step 3. If the subshell is only partially empty, with the number of electrons N_{nl} already present before capture, then multiply the rates obtained in Step 2 by $w_{nl} = 1 - N_{nl}/(4l + 2)$.

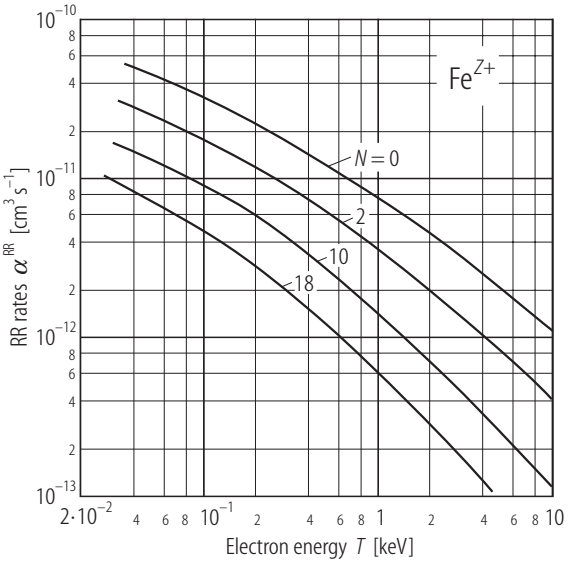

Fig. 1. RR rates for the Fe ions are given, with the number of electrons N in the target ions before capture. For example, $N = 0$ corresponds to a bare Fe ion. This shows the typically smooth behavior of the rates as functions of T, which allows simple scaled empirical formulas of Kramers' and its improvements for low Rydberg states.

Table 2 contains the total RR rates for the scaled hydrogenic target ions, as in Table 1, but summed over all $n > n_0$ and $l > l_0$ for that n. For partially filled inner shells, one has to adjust that part, as with Table 1 above, using w_{nl}. The HRS contribution for $n > 10$ was estimated using the simple n^{-3} dependence; since the HRS contribution is small, the error made is minimal. As discussed in the next subsection, some cutoff is necessary for RR in plasmas. But this is neglected here. With judicious choice of $Z_{\rm eff}$, Tables 1 and 2, together with (36) and (37), may be used to estimate the RR rates, roughly to an accuracy of ±10% in most cases. For more accurate values, there are many codes available [96Hah], some of which adopt the simple distorted wave method and Hartree-Fock wave functions for complex targets.

The experiments on the RR process carried out by the Aarhus group [89And, 90And], with the bare C, O, and F ionic targets and Si^{6+}, agreed well with the theory. However, more recent experiments of Muller et al. [91Mul, 92Mul], Wolf et al. [93Wol], and Gao et al. [95Gao] deviate appreciably from the theoretical predictions, as much as a factor of 20 in some cases. Possible sources of these discrepancies are suggested in terms of nonlinear shielding [01Hah].

There are several empirical formulas for the RR rates available, which are specific to particular ionic species; for example, the fit for the Fe ions are given by Arnaud and Rothenflug [85Arn]. Earlier references may also be found there.

3.3.3.2 Three body recombination (TBR)

In the TBR, as schematically shown by (6), two continuum electrons are involved initially. One of these electrons is captured by the target ion in the final state with $E_{f''}$, and the excess energy released by the recombining electron is carried away by the other outgoing electron e″, with the energy $E_{c''} \simeq E_c + E_{c'} - E_f$. Thus, the TBR does not involve any emission of photons, although the singly excited states f'' can further cascade down radiatively once it is formed by the above collisional process. Evidently, the TBR is the inverse of the electron collisional ionization [83Sea], and this relation is used in deriving the relevant cross section formula, by detailed balance in Eq. (20). In a plasma, the RR process is known to fill predominantly the low-lying Rydberg states, while TBR is mainly responsible in rapidly bringing the HRS into Saha equilibrium (Fig. 2). Therefore, the total TBR rate is expected to be especially sensitive to external perturbations. With the usual choice for $n_{\rm max}$, the Thomson value $n_{\rm max} \simeq n_{\rm T} \simeq (k_{\rm B}T_{\rm e}/Z^2{\rm Ry})^{-1/2}$ associated with the thermal ionization of Rydberg electrons, the density dependent rate parameter is defined,

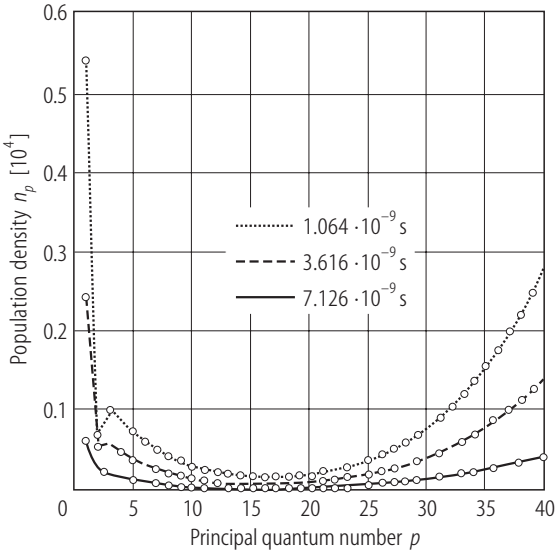

Fig. 2. Relative effectiveness in filling the empty shells by the RR and the TBR processes is illustrated. When an equal number of electrons and ions ($Z = 1$) are mixed at time $t = 0$, the system relaxes by the RR and TBR processes. The population density n_p is given as a function of the principal quantum number p at three different times. The electron temperature is $T = 10^3\,\mathrm{K} \approx 0.1\,\mathrm{eV}$, and the electron density is $n_c = 10^7\,\mathrm{cm}^{-3}$. The population below $p < 18$ is mainly due to RR, while TBR is responsible in filling the levels with $p > 18$.

with the statistical factor $S_n = n^2$, as

$$C^{\mathrm{TBR-T}} \simeq 2.0 \times 10^{-33} N_e^2 N_I Z^{-2} n^4 (1 - \exp(-I_n/T)) g(n, Z)/T[\mathrm{keV}]\ \mathrm{cm}^{-3}/\mathrm{s}\ , \tag{39}$$

where $g(n, Z)$ is the Gaunt factor, which is of the order 2, and the superscript T denotes the thermal average performed in its derivation. The rate given by (39), together with the RR and DR rates, appears as a source term in the rate equation for plasma modelling. Thus, the rates given by Eq. (39) represents the three-body recombination in which two continuum electrons collide to produce a bound electron in the state of principal quantum number n (summed over all the degenerate angular momentum states) as the second electron carries away the excess energy released by the recombined electron. Except for slightly different numerical factors, all the existing TBR formulas exhibit this T and n dependence. Apparently, such a strong n and T dependences predict a nonsensical results at low T and high n. This problem was recently corrected to incorporate the plasma density effects [97Hah1], by introducing a density-dependent HRS cut off $n_D \simeq n_F$, where the subscripts D and F denote the ion density and field effects, respectively. We define the maximum cutoff such that the TBR is to take place for $n < n_{\max}$, where

$$n_{\max} = \min\,(n_F, n_T)\quad , \tag{40}$$

where $n_F \simeq 1.09 \times 10^4 Z^{3/4}/N_I^{1/6}[\mathrm{cm}^{-3}]$ and $n_T \simeq 0.16Z/\sqrt{T[\mathrm{keV}]}$. ($1\,\mathrm{keV} = 73.5\,\mathrm{Ry}$ and $a_0^3 = 1.5 \times 10^{-25}\,\mathrm{cm}^3$). For most cases of interest here, however, at relatively high T, $n_T < n_F$ and thus n_T is the cutoff. We present the TBR rates in units of cm^3/s for ready comparison with the other rates, RR and DR; in this units, the rates are density dependent. Thus, we define

$$\alpha^{\mathrm{TBR}} = C^{\mathrm{TBR}}/N_e N_I\ \ \mathrm{cm}^3/\mathrm{s}\ . \tag{41}$$

We further define the transition probability P,

$$P^{\mathrm{TBR}}(nl) \equiv N_e^{-1}\, C^{\mathrm{TBR}} = \alpha^{\mathrm{TBR}}\, N_I\ \ \mathrm{s}^{-1}\ . \tag{42}$$

Table 3 contains the TBR rates for the electron and ion densities of $N_e = N_I = 10^{11}$ and $10^{14}\,\mathrm{cm}^{-3}$, which are generated by one of the standard formulas [77Pos]. In the table, the parameter $N = Z_c - Z$ is the number of electrons initially, before capture, and $n =$ principal quantum number of the target ion. In view of uncertainty in the statistical factor S_n, we set here $S_n = 1$, rather than the usual $S_n = n^2$ as adopted in (39); this choice may be readily rectified if necessary. The temperature is given in eV, and the parentheses contain the two possible cutoffs, and the smaller

of the two is used as $n_{\max}$ in the calculation. The importance of the different cutoffs is thus illustrated. The TBR in the parameter regions chosen seem to prefer n_T as the lowest upper cutoff for n, but some reversal in the cutoff is seen at low T and high density. As the temperature decreases and the density gets lower, the n_T tends to overestimate the cutoff, and invariably n_F takes over. Since the TBR rates increases rapidly with n, the proper choice of the cutoff is crucial. Finally, the TBR rates for other densities may be obtained easily by multiplying the values from the table by $N_e/10^{14}\,\mathrm{cm}^{-3}$, for example; the rates increase with density. However, the cutoff values are different. When T is very low, say $T < 0.001\,\mathrm{eV}$, and for the two n cutoff values close to each other, the formula (39) with (40) should be used with caution. We estimate that the overall accuracy of the TBR rates given here can be at best within a factor of 10 for high T, and larger as T is lowered. However, the dominance of the contribution of high Rydberg states indicates that the rates are very sensitive to external perturbations. Except for a simple field-ionization cutoff in (40), no field mixing of states and resulting changes in the rates have been treated. Much further work is required to improve the rates.

3.3.4 Indirect processes - dielectronic recombination

Dielectronic recombination is a resonant process in which a continuum electron is first captured as it excites one of the target electrons, thus forming relatively short lived (of the order of 10^{-11} to 10^{-14} s) intermediate states. The initial excitation-capture is mediated by the electron-electron interaction V in the vertex $DG^{QPR}V$, and states d are described by the on-shell part of the Green's function G^{QPR}. The doubly excited states d may subsequently relax by either an electron emission or radiation emission. Recombination is completed when all the cascade intermediate states $d, d', d'', ...$ follow the radiative branches. The partial Auger yield $\xi(d' \to d'')$ and partial fluorescence yields $\omega(d' \to d'')$ describe these branchings. The DR mode of recombination, when energetically allowed, usually dominates over the RR. Because of its very nature, the cross sections are non-zero only for those energies where the resonance conditions plus other necessary selection rules are satisfied. However, once these conditions are met, the cross section can be very large, due to large widths associated with inverse Auger transition.

Much theoretical work has been done to estimate the DR cross sections and rates for a number of important ions for plasma modelling [82McL]. But, the available data are far from complete, and in nearly all cases, the results of the calculations are limited to the ground states of the individual ions. For ready access to these data and to intelligently extrapolate to cases where no data are available, empirical rate formulas are constructed. In particular, an improved fit to the data was obtained [93Hah1]. Extensions to cases with excited initial and final states are discussed recently [98Oma, 01Oma]

Generally, the DR process is divided into three modes of excitation:

(i)	$\Delta n \neq 0$	(e_c high and LRS recombination),
(ii)	$\Delta n = 0$, but $\Delta l \neq 0$	(e_c low and moderate HRS capture),
(iii)	$\Delta n = 0$, and $\Delta l = 0$	(e_c very low and HRS capture).

This classification depends more or less on the magnitude of the excitation energies, and thus by the resonance energy condition on the continuum electron energy e_c. For the initial excitation/capture described by the matrix element $V_a(i, c \to d = d_1\, d_2)$ for DR, we have the approximate resonance condition $E_i + e_c \simeq E_{d_1} + E_{d_2}$, in obvious notation. The excitation energy $\Delta E_{d_1,f} = E_{d_1} - E_i$. Since $e_c = \Delta E_{d_1,f} + E_{d_2}$, the large excitation energy means usually a higher collision energy and $|E_{d_2}|$ can be quite large as well, leading to low Rydberg state (LRS) captures. On the other hand, a small ΔE usually implies a capture to HRS with small $|-E_{d_2}|$ and small e_c.

Some simplifications may be made in the DR rate calculation, that depend on the relative sizes of the transition probabilities A_a and A_r:

(a) $\Gamma_a \gg \Gamma_r$. In this case, we have $\Gamma \simeq \Gamma_a \simeq A_a(d \to i, c)$, and thus $\sigma_{fdi}^{DR} \simeq \Gamma_r$. Therefore, the rate is constant in n. Often, mode (ii) shows this property, in which case, the DR measurement is equivalent to that for the simple A_r for the inner shell electron d_1 which is independent of n , and where $d_2 = nl$. The A_r for the outer shell electron scales as n^{-3} and, for mode (ii), n is high enough to make this part of the contribution small. But for high Z ions, the A_r associated with the outer electron becomes large, mainly because of the Z^4 scaling of A_r. Moreover, the allowed n can be very low even for mode (ii).

(b) $\Gamma_r \gg \Gamma_a$. There are not many cases where this inequality holds, except perhaps when Z is large ($A_r \propto Z^4$) and n is also large in Γ_a. Then $\sigma_{fdi}^{DR} \propto V_a(i, c \to d)$, which is simply the inverse of an Auger transition. Although rare, this situation does occur.

(c) Of practical importance in the evaluation of the DR cross sections and rates is the fact that errors and variations due to approximations introduced in the evaluation of the individual transition probabilities A_r and A_a tend to cancel, because the DR cross sections are given in terms of the ratios of these probabilities $A_a A_r/(A_a + A_r)$. Therefore, a good agreement of the rates calculated by two different approximations does not always reflect the accuracy of the individual probabilities. That is, the DR rates are often not sensitive to errors made in the evaluation of the individual transition probabilities.

There have been some very recent calculation of the DR rates [95Nah1] using an elaborate CCM, which may be more reliable than the previous DWA calculations. For low energy processes where a small number of channels are open, the method is proven to be very effective. However, the CCM has its own intrinsic limitations: (i) a small number of open (and some closed) channels explicitly included, (ii) accuracy of the target ion functions, for the both ground and excited states, and (iii) approximate polarization potentials which must be corrected for possible double counting.

Relativistic calculation of DR cross sections and rate coefficients have been carried out by several groups, including the extensive work of Chen [92Che]. The MCDF codes and their variations are used to generate the relevant wave functions for the evaluation of the individual transition probabilities A_r and A_a. Alternatively, if the nuclear core charge is not too high, $Z_c < 30$, a simpler procedure may be followed a la Cowan [81Cow], by approximately incorporating some of the lowest order relativistic corrections, but still retaining the nonrelativistic framework, with two-component wave functions. For ions of interest here, with the nuclear core charge $Z_c < 30$, the relativistic effect is not expected to be serious, at the level of approximately 30%, especially in view of other uncertainties in the calculations. Some recent calculations for a small number of ionic targets are available, but the overall situation has not improved since 1992.

Thus far, we have limited our discussion to processes which are mediated by one single D or V (or DGV). However, the multiple cascade processes that involve higher powers of D and/or V are sometimes significant, so long as each intermediate state that appears during a cascade is resonant. The higher order terms contribute as strongly as the lower order terms. Thus, the formulas we derived in (29) for cascade processes are followed in practice.

The DR cross sections are often contaminated by weak stray electric fields which may be present in the interaction region. This is the case specially with DR that involves low energy projectile electrons and HRS capture; the stark effect is strong when the energies of the states involved are relatively small in magnitude; therefore mode (iii) DR is most sensitive to external field perturbations.

The DR rates are generated mostly by theoretical calculations. Inspite of much efforts of the past twenty years by many groups, the available data are spotty, as shown in Fig. 3. This is the typical situation throughout the periodic table, especially for $Z_c > 12$. Fig. 4 contains the DR rates for the Fe ions with $Z = 6+$ and $11+$. Curve (1) is for mode (i) excitations, and (2) for mode (ii). Contributions of mode (iii) are not included, but can be sizeable in some cases.

The DR rates given here are generated by a slightly improved version of the earlier empirical formula [93Hah1], which was obtained by fitting all the existing data, as of 1992. Not much additional data have become available since then. The reliability of the calculations varies data to data, and external perturbations can often be sizeable. Tables 4 – 11 contain the rates for different

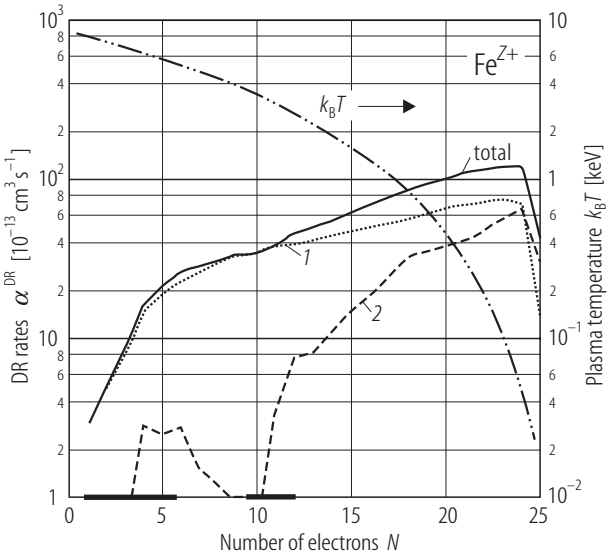

Fig. 3. DR rates for Fe ions are shown, with the initial charge Z and the scaled temperature $k_BT = 11.8\,Z^2$ eV. The k_BT curve indicates the plasma temperature (right-hand scale). N is the number of electrons in the Fe target ions before capture. Curve (1) is for mode (i) excitation contribution, while curve (2) is for mode (ii) excitation. Evidently, mode (2) contribution, with $\Delta n = 0$, is not allowed for ions with $N = 1$, 2, and 10. The regions of N values where some calculated data are available are shown by dark bars along the base scale. This situation is typical of all ions, indicating the need for more data.

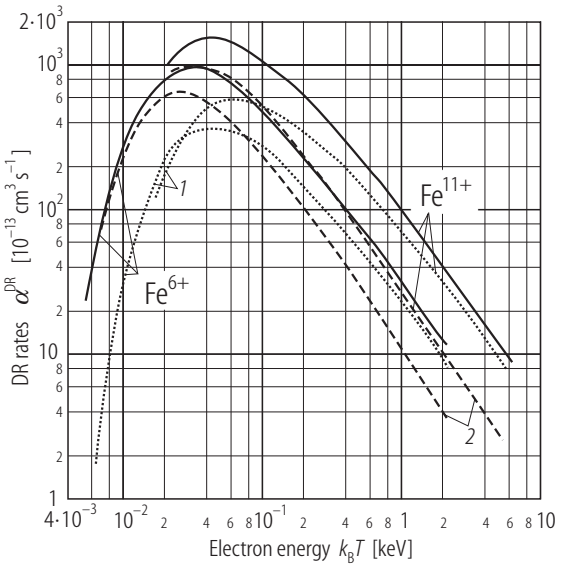

Fig. 4. Typical DR rates are given as functions of electron temperature for the number of electrons $N = 15$ and 20 in the target ions Fe^{11+} and Fe^{6+}, respectively, before capture. Curve (1) corresponds to mode (i) contribution , and (2) for mode (ii) excitations. Evidently, curve (1) peaks at higher temperature than (2). Contributions from mode (iii) excitations are not included, which can be sizeable at lower temperature.

nuclear core charge Z_c , temperature T [keV], and the degree of ionization Z, where $N = Z_c - Z$. (1 eV = 11 600 K.) The rates are associated with the ground states of the ions with Z_c equal to 6, 8, 10, 12, 15, 18, 22, and 26. The number of electrons present in the ions before capture is $N = 1$ to $Z_c - 1$. The rates given here are for the ground states of the ionic species with charge $Z = 1$ to $Z_c - 1$, before capture. All the tables are given at the end of this chapter.

In this connection, we note one important aspect associated with plasma modelling. In almost all cases, the DR process ends in singly excited, Auger stable, states, often in Rydberg states and/or dipole forbidden metastable states. Therefore, the DR rates given here have been obtained with the assumption that these excited states will eventually cascade to the ground states; thus, the final states f in (26) are summed. On the other hand, the rate equations, into which these rates are to be introduced, also contain these singly excited states, and the collisional effects are incorporated, resulting in the effective recombination rates for the ground states. (See also Eqs. (45) and (47)). This apparent inconsistency has been pointed out earlier [97Hah2], but never analyzed in detail. The resulting modifications may not be negligible [92Oma1, 92Oma2].

The empirical formulas published in 1993 [93Hah1] have been slightly adjusted here to incorporate some of the new data [98Hah]. Since the total data used to generate the empirical formula are limited to probably about 10% of the cases contained in Tables 4 – 11, and the rest are obtained by smooth extrapolations, the overall accuracy may be at best at the ±20% level, and often worse. It should be emphasized that the reliability of the calculated data also varies case to case. For more accurate rates, we refer to individual calculations, where a careful assessment of the way they are generated must be made.

For more recent calculation of the DR rates, we refer to the careful evaluation given by Nahar and Pradhan [97Nah] for C and N ions, and [95Nah1, 95Nah2, 97Zha] for Si and S ions. For Fe ions, we refer to the work of Arnaud and Raymond [92Arn] and the data on Be and B by Pindzola and Badnell [92Pin] for the details. Since only a limited number of data is used, the result given here must be used with some caution.

3.3.5 Plasma density effects - field and collisional perturbations

Recombination processes are often strongly affected by (a) time-dependent electric fields, both intrinsic (the plasma ion fields) and extrinsic, and by (b) collisional effects by the plasma particles (mostly plasma electrons). Evidently, an electric field affects HRS more than low-lying Rydberg states (LRS). For RR, low energy continuum electrons are most affected, since the process strongly favors capture to low Rydberg states, as evidenced by the argument that the RR probability may scale as n^{-3}. (However, as noted from Kramers' formula, when collision energy is very low and $\eta = Z/k_c a_0 \gg n$, then the cross section and the rates behave as $1/n$, so that the HRS recombination becomes relatively more important, and distortion of the recombined states by electric field must be taken into account.) In so far as the TBR is concerned, recombined HRS will be affected severely by the field, because, as compared with RR, TBR favors recombination to HRS. According to the general classification of the initial excitation modes in DR, we have the severity of the field effect increased as we go from mode (i) to mode (ii) and then to mode (iii), because of the important role played by HRS in (ii) and (iii). Generally, mode (i) is not much affected by the field, except in low Z ions and relatively high fields.

The source of electric fields may be diverse; the plasma microfield and externally imposed electric field. The field effect on RR has been clarified recently [94Krs1], but the TBR has not been examined in any detail, although by its very nature the effect is expected to be large. The field modified DR cross sections and rate coefficients were first estimated using a full mixing formula for Mg II and C II targets [83LaG1, 83LaG2]. In later works [87LaG], however, diagonalization of the energy matrix formed with $V_{\rm pol} + V_{\rm F}$ was adopted. Some other systems have since been treated by many people [92Gra].

Since it is a nearly impossible task to examine and modify for the field effect all the rates that have been evaluated without field, we formulated a simple procedure in which the existing rates are to be multiplied by overall enhancement factors. These factors for different processes have been given [96Krs, 95Jan]; these results are only preliminary, and further detailed study is necessary. In order to incorporate the plasma collisional effects on the recombination (and ionization) , rate equations for given ionic species may be set up by including all the relevant excited states, and as usual by coupling only two charge states at a time, say Z and $Z+1$. Let $P_n(Z;t)$ denote the population densities of the excited states of the ion with charge Z, and g denotes the ground states of the ions. When the set is solved by setting $\partial P_n/\partial t = 0$ for all $n > g$, and this solution is put into the $\partial P_n/\partial t$ equations. We obtain

$$\mathrm{d}P_g(Z)/\mathrm{d}t = -\beta_{\rm eff} P_g(Z) + \alpha_{\rm eff} P_g(ZP) \tag{43}$$

where $ZP = Z+1$. The ionization balance is calculated by setting $\mathrm{d}P_g/\mathrm{d}t = 0$ in Eq. (43) for each

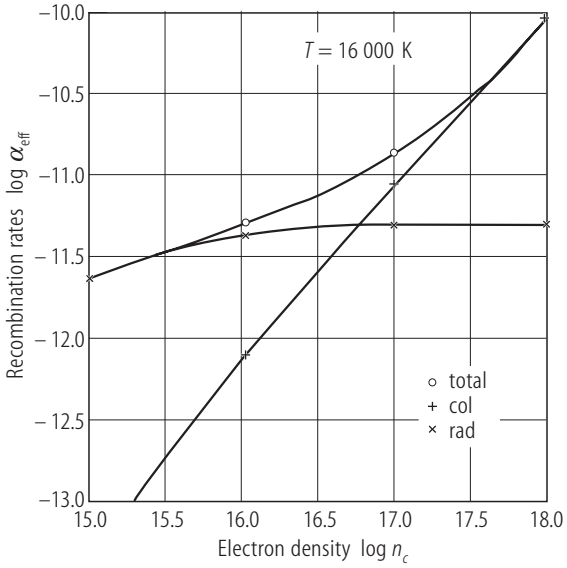

Fig. 5. Variations in the effective recombination (rad) and ionization (col) rates, as deduced from the rate equations in a hydrogen plasma, are illustrated as functions of the electron density n_c in cm^{-3}. The rates are given in cm^3/s. They show a typical density dependence of the effective rates which are inputs to the ionization balance Eq. (44).

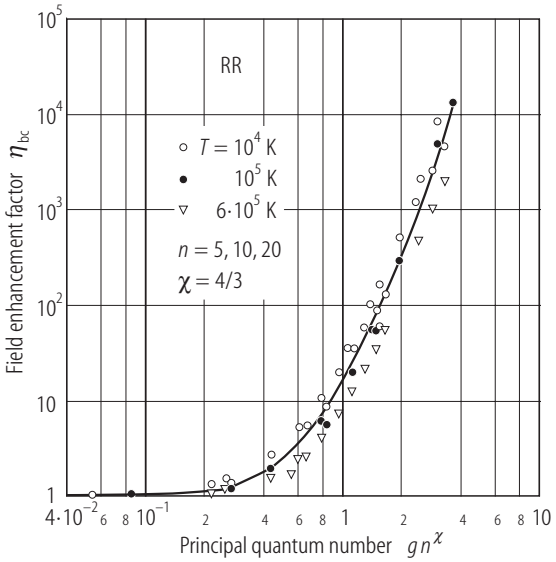

Fig. 6. Field enhancement factor η_{bc} to be multiplied to the existing RR rates is given for different principal quantum number n of the final recombined states. The plasma ion microfield momentum $g \cong 2N_e^{2/3}n^3/Z$, as obtained from the Holtzmark field for ions. n = principal quantum number of the recombined states, and $\chi = 4/3$ is a fitting parameter. The solid curve is a fit.

Z, and

$$P_g(Z)/P_g(ZP) = \alpha_{eff}(Z)/\beta_{eff}(Z) \tag{44}$$

with the constraint $\sum_{Z=0}^{Z_c} P_g(Z) = P_{tot}$ = total density of the ion, normalized by the Saha values. The effective ionization rates β_{eff} and the effective recombination rates α_{eff} are obtained in terms of all the reaction rates, for the ground states as well as the excited states [92Rei, 92Krs, 93Hah2]. Typical values for the effective recombination rates are shown in Fig. 5, for the hydrogenic plasma. The curve (col) is mostly due to TBR, while curve (rad) is mostly due to RR, with the other effects included by the solution of the rate equations. The strong density dependence is indicated, where n_c is the electron density.

Obviously, the individual rates used in determining the effective rate coefficients are presumably field-distorted (e.g. by the ionic microfields). We have recently examined this problem and found that the effect is small until the density becomes quite larger. Fig. 6 shows a typical field dependence of the RR rates; the enhancement factor η_{bc} multiplies the existing RR rates. As expected, it has a strong n dependence, where n is the principal quantum number of the recombined states.

The effective recombination rates that include both the plasma field and collisional effects may be obtained for the ground states of each ion by solving a set of rate equations which contain field-distorted rates. To compactify this procedure, we have constructed [97Hah2] a Fokker-Planck integral operator that contains essentially all the collisional and field distortion information required in evaluating the effective recombination rates. Thus, we have

$$\alpha_{eff}(T) = \alpha_g + \Omega\alpha(n, T) \tag{45}$$

where $\Omega(g, \sum n, T)$ is an integral operator that converts the recombination rates $\alpha(n, T)$ for the states n, to incorporate the plasma collisional effects of all the other n's, summed over n. Thus,

it replaces the need of a rate equation solution. The explicit form of Ω and its applications were given elsewhere [97Hah2].

3.3.6 Conclusion

A complete review of the recombination processes has been given previously in the NATO proceedings [92Gra] by the experts in the field, both experimental and theoretical, where much of the important early references may be found. Our emphasis in this report is to summarize the existing recombination rate data in a user-friendly format.

The RR cross sections and rates given by the Kramers' formula were shown to be quite reliable for HRS with $n > 10$ and for the scaled temperature $\Theta = k_B T_e/Z^2 \mathrm{Ry} < 10^{-2}$. But for the parameter regions outside this, sizeable discrepancies were found between the Kramers' and the exact result. We presented in Subsection 3.3.3 the corrected empirical formulas for the RR rates, for all states and all Z using the approximate scaling and effective charge. In addition, the explicit l dependence is given, which indicates that the high l contribution can be large, and field mixing can also affect this distribution.

The TBR rates are given exclusively from the empirical formula, for ready access. They show the increasing importance of the HRS capture by this mode. Therefore, the high n cutoff, as well as possible field perturbations are important. The n cutoffs are briefly discussed and showed that the T dependent cutoff dominates, but n_F is important at low T.

The DR rates were summarized according to different excitation modes, using the empirical formulas [93Hah1]. They are further upgraded to incorporate the more recent data. The relativistic effect should become important for ions with $Z_c > 20$.

Evidently there are still many areas where future efforts are required. We stress four points of importance:

(1) Completeness of data. In constructing a set of rate equations for plasma modelling, rates of all relevant atomic processes, both for the ground and excited states of all charge states are needed. The situation on availbale data is still far from satisfactory, especially for the M-shell ions. As noted earlier, there are only a handful of recombination rates for excited states. This point is important when the rate equations used in the plasma modelling explicitly contain these excited states. The correlation between the rate data and the structure of the rate equations must be clarified, in order to avoid double counting problems.

(2) Quality of data. Reliability of the existing data depends on the theoretical methods employed, and the accuracy requirement varies with specific applications. For plasma diagnostics, a relatively small number of rates of high accuracy (better than 5 percent) may be desired. On the other hand, a complete set of data for some specific (impurity) ions is needed for plasma modelling. This requires a large number of rates, and can be generated only by an approximate set of empirical formulas, often at reduced accuracy. The theoretical method used must also be relatively simple, such as the distorted wave method. The data presented here are mainly for modelling applications.

(3) We have the improved and compact empirical formulas for all three modes of recombination, the RR, TBR, and DR. The RR formulas are the improved versions of Kramer's, which are applicable for LRS. The TBR formulas are augmented by the two different high n cutoffs, which are important here since the rates increase rapidly with n. Finally, the individual DR rates are given in terms of the different excitation modes, so that all the small contributions are recorded. The rates for each excitation mode are relatively smooth, but the total rates are usually not. These formulas must be periodically upgraded as more data become available.

(4) The plasma density effects must include both plasma ions for field distortions and plasma electrons for collisional re-distribution of ionic excited states. This problem is still in a developing stage, and some recent progress made on this problem has been reviewed elsewhere [97Hah2]. Since

external and intrinsic perturbations on the rates themselves can be sizeable, the values presented here must be taken with some caution.

(5) Finally, the rates must be defined in such a way that they reflect the structure of (and approximations introduced to) the rate equations themselves [97Hah2]. This point has not been stressed enough before. See the discussion near the end of Subsection 3.3.5.

3.3.7 Explanation for the use of tables

In order to facilitate the use of the tables, we further explain the notations introduced, and provide sample cases:

Table 1. Scaled RR rates $\alpha_{nl}^{\mathrm{RR}}/Z_{\mathrm{eff}}$ are given, in units of cm^3/s, for different values of scaled temperature $\Theta = k_{\mathrm{B}}T/Z_{\mathrm{eff}}^2\mathrm{Ry}$. Z_{eff} is given by $Z_{\mathrm{eff}} = \sqrt{Z_{\mathrm{c}}Z}$, where Z_{c} is the nuclear core charge and Z is the degree of ionization before recombination. In general, there can be several different combinations of Z_{c} and Z that give the same Z_{eff}. Example: the RR rates for $Z_{\mathrm{eff}} = 3$ and $k_{\mathrm{B}}T = 4.5\,\mathrm{Ry}$. We first calculate $\Theta = 4.5/9 = 0.5$. Now, for recombination to a completely empty subshell $(n, l) = (3, 1)$, we have from Table 1 the rate $\alpha^{\mathrm{RR}} = 3\times3.591\times10^{-15} = 1.08\times10^{-14}\,\mathrm{cm}^3/\mathrm{s}$. On the other hand, for this shell with two electrons present before capture, we have a slightly different Z_{eff} and the rate must also be reduced further by 2/6.

Table 2. Total RR rates are presented, which are obtained by summing the rates of Table 1 for the individual subshells over all the states which lie above the particular subshell (n_0, l_0). All the subshells below and including the (n_0, l_0) shell are assumed fully filled already before capture. Therefore, the entry $(n_0, l_0) = 0$ represents the bare target ion with no electrons in the target ion before capture. Example: for a target ion with $Z_{\mathrm{eff}} = 5$ and all the subshells up to and including the 2s are fully filled before capture, and the scaled temperature $\Theta = 10$, the total RR rate is $\alpha_{\mathrm{tot}}^{\mathrm{RR}} = 5\times8.29\times10^{-16} = 4.15\times10^{-15}\,\mathrm{cm}^3/\mathrm{s}$. Note that, for the same Θ and Z_{eff}, the difference in the rates for the entry 1s and 2s, in Table 2, for example, is precisely the entry 2s (2,0) in Table 1.

Table 3. TBR rates are presented for two different plasma densities. Unlike RR and DR, the TBR rates are density-dependent. Z_{c} = nuclear core charge, N = number of electrons in the target ion, before capture, and thus $Z = Z_{\mathrm{c}} - N$ = degree of ionization, before the electron capture. Example: for $Z_{\mathrm{c}} = 8$ and $N = 0$ (for a fully stripped oxygen ion) in a plasma with equal electron and ion densities $10^{11}\,\mathrm{cm}^{-3}$ and temperature $k_{\mathrm{B}}T = 0.1\,\mathrm{eV}$, the TBR rate for capture to the state with principal quantum number $n = 60$, summed over the angular degenerate states, is $5.47\times10^{-13}\,\mathrm{cm}^3/\mathrm{s}$. The total TBR rates, summed over all n up $n_{\mathrm{cut}} = n_{\mathrm{T}} = 130$, is $\alpha_{\mathrm{tot}}^{\mathrm{TBR}} = 3.23\times10^{-10}\mathrm{cm}^3/\mathrm{s}$.

Tables 4 to 11. They contain the DR rates, in units of $10^{-13}\,\mathrm{cm}^3/\mathrm{s}$. Example: Mg^{8+}, at $k_{\mathrm{B}}T = 500\,\mathrm{eV}$. We go to Table 7, with the entry $Z_{\mathrm{c}} = 12$ = nuclear core charge, $N = 4$ = number of electrons on the target ion before capture, and the plasma temperature $T = 0.500\,\mathrm{keV}$.The 1s excitation contribution is 9.5, the 2s, $\Delta n = 0$ excitation contribution is 6.1, and the 2s and 2p, $\Delta \neq 0$ excitation contribution is 9.8. The total DR rates is 25.4, in units of $10^{-13}\,\mathrm{cm}^3/\mathrm{s}$. Note that the number of electrons present in the target ion $N = Z_{\mathrm{c}} - Z$.

3.3.8 Tables

Table 1. Scaled RR rates $\alpha_{nl}^{\mathrm{RR}}/Z_{\mathrm{eff}}$ [cm^3/s] for the individual states nl are given as functions of scaled temperature $\Theta = k_{\mathrm{B}}T/Z_{\mathrm{eff}}^2\mathrm{Ry}$. The numbers in brackets are powers of 10.

(n,l)	Θ						
	0.01	0.05	0.10	0.50	1.0	5.0	10.0
(1, 0)	4.1126[-13]	1.793[-13]	1.231[-13]	4.581[-14]	2.752[-14]	6.456[-15]	3.079[-15]
(2, 0)	6.044[-14]	2.652[-14]	1.825[-14]	6.720[-15]	3.980[-15]	8.972[-16]	4.217[-16]
(2, 1)	1.602[-13]	6.258[-14]	3.875[-14]	9.549[-15]	4.544[-15]	6.141[-16]	2.377[-16]
(3, 0)	2.033[-14]	8.871[-15]	6.058[-15]	2.161[-15]	1.261[-15]	2.771[-16]	1.293[-16]
(3, 1)	6.093[-14]	2.383[-14]	1.473[-14]	3.591[-15]	1.699[-15]	2.275[-16]	8.781[-17]
(3, 2)	6.531[-14]	2.115[-14]	1.144[-14]	1.931[-15]	7.887[-16]	8.250[-17]	2.991[-17]
(4, 0)	9.493[-15]	4.085[-15]	2.759[-15]	9.556[-16]	5.519[-16]	1.194[-16]	5.551[-17]
(4, 1)	2.915[-14]	1.132[-14]	6.956[-15]	1.671[-15]	7.865[-16]	1.045[-16]	4.026[-17]
(4, 2)	4.090[-14]	1.324[-14]	7.146[-15]	1.201[-15]	4.896[-16]	5.110[-17]	1.852[-17]
(4, 3)	2.709[-14]	7.045[-15]	3.368[-15]	4.402[-16]	1.668[-16]	1.592[-17]	5.678[-18]
(5, 0)	5.277[-15]	2.231[-15]	1.490[-15]	5.041[-16]	2.890[-16]	6.188[-17]	2.871[-17]
(5, 1)	1.628[-14]	6.249[-15]	3.814[-15]	9.032[-16]	4.234[-16]	5.591[-17]	2.152[-17]
(5, 2)	2.501[-14]	8.052[-15]	4.334[-15]	7.238[-16]	2.947[-16]	3.070[-17]	1.112[-17]
(5, 3)	2.385[-14]	6.196[-15]	2.960[-15]	3.861[-16]	1.463[-16]	1.395[-17]	4.975[-18]
(5, 4)	1.117[-14]	2.345[-15]	1.019[-15]	1.143[-16]	4.187[-17]	3.861[-18]	1.371[-18]
(6, 0)	3.268[-15]	1.356[-15]	8.970[-16]	2.977[-16]	1.698[-16]	3.610[-17]	1.672[-17]
(6, 1)	1.008[-14]	3.816[-15]	2.313[-15]	5.410[-16]	2.528[-16]	3.324[-17]	1.278[-17]
(6, 2)	1.610[-14]	5.146[-15]	2.761[-15]	4.582[-16]	1.863[-16]	1.938[-17]	7.019[-18]
(6, 3)	1.776[-14]	4.600[-15]	2.194[-15]	2.856[-16]	1.081[-16]	1.031[-17]	3.676[-18]
(6, 4)	1.273[-14]	2.670[-15]	1.160[-15]	1.300[-16]	4.762[-17]	4.391[-18]	1.558[-18]
(6, 5)	4.561[-15]	7.934[-16]	3.228[-16]	3.316[-17]	1.196[-17]	1.087[-18]	3.852[-19]
(7, 0)	2.178[-15]	8.873[-16]	5.819[-16]	1.902[-16]	1.081[-16]	2.286[-17]	1.058[-17]
(7, 1)	6.704[-15]	2.503[-15]	1.508[-15]	3.489[-16]	1.626[-16]	2.131[-17]	8.190[-18]
(7, 2)	1.092[-14]	3.461[-15]	1.850[-15]	3.053[-16]	1.240[-16]	1.288[-17]	4.663[-18]
(7, 3)	1.297[-14]	3.345[-15]	1.593[-15]	2.068[-16]	7.828[-17]	7.457[-18]	2.659[-18]
(7, 4)	1.119[-14]	2.342[-15]	1.017[-15]	1.139[-16]	4.170[-17]	3.845[-18]	1.365[-18]
(7, 5)	6.394[-15]	1.112[-15]	4.522[-16]	4.644[-17]	1.675[-17]	1.523[-18]	5.394[-19]
(7, 6)	1.850[-15]	2.761[-16]	1.075[-16]	1.050[-17]	3.757[-18]	3.393[-19]	1.201[-19]
(8, 0)	1.531[-15]	6.129[-16]	3.989[-16]	1.288[-16]	7.297[-17]	1.537[-17]	7.108[-18]
(8, 1)	4.702[-15]	1.731[-15]	1.037[-15]	2.379[-16]	1.106[-16]	1.446[-17]	5.554[-18]
(8, 2)	7.741[-15]	2.430[-15]	1.294[-15]	2.126[-16]	8.624[-17]	8.947[-18]	3.239[-18]
(8, 3)	9.591[-15]	2.461[-15]	1.170[-15]	1.515[-16]	5.733[-17]	5.459[-18]	1.947[-18]
(8, 4)	9.153[-15]	1.912[-15]	8.296[-16]	9.278[-17]	3.397[-17]	3.132[-18]	1.112[-18]
(8, 5)	6.480[-15]	1.126[-15]	4.577[-16]	4.699[-17]	1.694[-17]	1.540[-18]	5.458[-19]
(8, 6)	3.082[-15]	4.600[-16]	1.790[-16]	1.749[-17]	6.257[-18]	5.652[-19]	2.001[-19]

Table 1. Scaled RR rates (continued)

(n,l)	Θ						
	0.01	0.05	0.10	0.50	1.0	5.0	10.0
$(8,7)$	7.494[-16]	9.928[-17]	3.753[-17]	3.560[-18]	1.268[-18]	1.142[-19]	4.040[-20]
$(9,0)$	1.120[-15]	4.412[-16]	2.854[-16]	9.124[-17]	5.155[-17]	1.083[-17]	5.004[-18]
$(9,1)$	3.434[-15]	1.247[-15]	7.433[-15]	1.693[-16]	7.858[-17]	1.025[-17]	3.936[-18]
$(9,2)$	5.686[-15]	1.769[-15]	9.391[-16]	1.536[-16]	6.223[-17]	6.449[-18]	2.335[-18]
$(9,3)$	7.234[-15]	1.846[-15]	8.760[-16]	1.132[-16]	4.281[-17]	4.075[-18]	1.453[-18]
$(9,4)$	7.346[-15]	1.530[-15]	6.633[-16]	7.411[-17]	2.713[-17]	2.501[-18]	8.875[-19]
$(9,5)$	5.877[-15]	1.020[-15]	4.144[-16]	4.252[-17]	1.533[-17]	1.394[-18]	4.939[-19]
$(9,6)$	3.540[-15]	5.281[-16]	2.055[-16]	2.007[-17]	7.180[-18]	6.485[-19]	2.296[-19]
$(9,7)$	1.448[-15]	1.918[-16]	7.250[-17]	6.877[-18]	2.450[-18]	2.205[-19]	7.803[-20]
$(9,8)$	3.047[-16]	3.687[-17]	1.367[-17]	1.274[-18]	4.528[-19]	4.067[-20]	1.439[-20]
$(10,0)$	8.461[-16]	3.283[-16]	2.112[-16]	6.695[-17]	3.776[-17]	7.194[-18]	3.655[-18]
$(10,1)$	2.589[-15]	9.283[-16]	5.510[-16]	1.247[-16]	5.780[-17]	7.528[-18]	2.889[-18]
$(10,2)$	4.301[-15]	1.326[-15]	7.020[-16]	1.143[-16]	4.630[-17]	4.794[-18]	1.735[-18]
$(10,3)$	5.568[-15]	1.413[-15]	6.694[-16]	8.634[-17]	3.263[-17]	3.105[-18]	1.107[-18]
$(10,4)$	5.890[-15]	1.223[-15]	5.298[-16]	5.913[-17]	2.164[-17]	1.995[-18]	7.079[-19]
$(10,5)$	5.095[-15]	8.825[-16]	3.586[-16]	3.677[-17]	1.326[-17]	1.205[-18]	4.270[-19]
$(10,6)$	3.527[-15]	5.257[-16]	2.045[-16]	1.997[-17]	7.145[-18]	6.453[-19]	2.284[-19]
$(10,7)$	1.859[-15]	2.461[-16]	9.303[-17]	8.824[-18]	3.144[-18]	2.830[-19]	1.001[-19]
$(10,8)$	6.701[-16]	8.106[-17]	3.006[-17]	2.801[-18]	9.955[-19]	8.942[-20]	3.163[-20]
$(10,9)$	1.249[-16]	1.411[-17]	5.167[-18]	4.759[-19]	1.689[-19]	1.515[-20]	5.359[-21]

Table 2. Scaled total RR rates $\alpha_{\rm tot}^{\rm RR}(n_0 l_0, \Theta)/Z_{\rm eff}$ [cm^3/s] are given, after summing over all states with $n > n_0$ and $l > l_0$, exclusive of n_0, l_0. For partially filled subshells, the procedure given for Table 1 and w_{nl} must be used. The scaled temperature is $\Theta = k_{\rm B}T/Z_{\rm eff}^2{\rm Ry}$.

$\log\Theta$	$n_0 l_0$						
	0	1s	2s	2p	3s	3p	3d
-2.0	1.23[-12]	8.38[-13]	7.58[-13]	6.24[-13]	5.97[-13]	5.49[-13]	4.72[-13]
-1.5	6.18[-13]	3.97[-13]	3.57[-13]	2.82[-13]	2.69[-13]	2.20[-13]	2.08[-13]
-1.0	2.86[-13]	1.64[-13]	1.43[-13]	1.08[-13]	1.01[-13]	8.73[-14]	7.54[-14]
-0.5	1.21[-13]	5.93[-14]	4.93[-14]	3.51[-14]	3.22[-14]	2.67[-14]	2.33[-14]
0.0	4.60[-14]	1.86[-14]	1.45[-14]	9.97[-15]	8.75[-15]	7.10[-15]	6.32[-15]
0.5	1.52[-14]	5.11[-15]	3.66[-15]	2.55[-15]	2.11[-15]	1.71[-15]	1.55[-15]
1.0	4.33[-15]	1.26[-15]	8.29[-16]	5.93[-16]	4.66[-16]	3.80[-16]	3.51[-16]
1.5	1.05[-15]	2.79[-16]	1.74[-16]	1.27[-16]	9.64[-17]	7.95[-17]	7.42[-17]
2.0	2.22[-16]	5.65[-17]	3.42[-17]	2.50[-17]	1.88[-17]	1.56[-17]	1.47[-17]
2.5	4.27[-17]	1.07[-17]	6.38[-18]	4.62[-18]	3.49[-18]	2.91[-18]	2.74[-19]
3.0	7.81[-18]	1.94[-18]	1.15[-18]	8.32[-19]	6.30[-19]	5.30[-19]	4.97[-19]
	4s	4p	4d	4f	5s	5p	5d
-2.0	4.64[-13]	4.32[-13]	3.95[-13]	3.68[-13]	3.63[-13]	3.46[-13]	3.22[-13]
-1.5	2.02[-13]	1.86[-13]	1.68[-13]	1.58[-13]	1.55[-13]	1.46[-13]	1.35[-13]
-1.0	7.25[-14]	6.54[-14]	5.85[-14]	5.51[-14]	5.37[-14]	4.98[-14]	4.61[-14]
-0.5	2.19[-19]	1.93[-14]	1.72[-14]	1.64[-14]	1.57[-14]	1.42[-14]	1.33[-14]
0.0	5.71[-15]	4.97[-15]	4.45[-15]	4.29[-15]	3.99[-15]	3.57[-15]	3.39[-15]
0.5	1.34[-15]	1.16[-15]	1.06[-15]	1.03[-15]	9.26[-16]	8.24[-16]	7.90[-16]
1.0	2.92[-16]	2.54[-16]	2.34[-16]	2.29[-16]	2.00[-16]	1.78[-16]	1.72[-16]
1.5	6.00[-17]	5.26[-17]	4.39[-17]	4.80[-17]	4.08[-17]	3.67[-17]	3.56[-17]
2.0	1.16[-17]	1.03[-17]	9.60[-13]	9.43[-13]	7.91[-13]	7.15[-18]	6.95[-18]
2.5	2.16[-13]	1.91[-13]	1.79[-13]	1.76[-18]	1.47[-13]	1.33[-13]	1.29[-18]
3.0	3.90[-19]	3.45[-19]	3.24[-19]	3.19[-19]	2.65[-19]	2.40[-19]	2.34[-19]
	5f	5g	6	7	8	9	10
-2.0	2.98[-13]	2.87[-13]	2.23[-13]	1.74[-13]	1.37[-13]	1.11[-13]	9.01[-14]
-1.5	1.25[-13]	1.21[-13]	9.41[-14]	7.37[-14]	5.76[-14]	4.71[-14]	3.81[-14]
-1.0	4.25[-14]	4.15[-14]	3.18[-14]	2.43[-14]	1.94[-14]	1.59[-14]	1.29[-14]
-0.5	1.22[-14]	1.20[-14]	9.15[-15]	7.03[-15]	5.55[-15]	4.51[-15]	3.67[-15]
0.0	3.13[-15]	3.09[-15]	2.34[-15]	1.80[-15]	1.41[-15]	1.14[-15]	9.29[-16]
0.5	7.38[-15]	7.29[-16]	5.48[-16]	4.19[-16]	3.28[-16]	2.64[-16]	2.16[-16]
1.0	1.62[-16]	1.61[-16]	1.20[-16]	9.15[-17]	7.16[-17]	5.76[-17]	4.71[-17]
1.5	3.39[-17]	3.36[-17]	2.48[-17]	1.90[-17]	1.48[-17]	1.19[-17]	9.76[-18]
2.0	6.64[-18]	6.60[-18]	4.82[-18]	3.71[-18]	2.90[-18]	2.33[-18]	1.91[-18]
2.5	1.24[-18]	1.23[-18]	8.93[-19]	6.90[-19]	5.40[-19]	4.35[-19]	3.56[-19]
3.0	2.24[-19]	2.23[-19]	1.61[-19]	1.25[-19]	9.77[-20]	7.87[-20]	6.45[-20]

Table 3. TBR rates α^{TBR} [cm^3/s] are given for the electron and ion densities $N_\mathrm{e} = N_\mathrm{I} = 10^{11}\,\mathrm{cm}^{-3}$ (**a**) and $10^{14}\,\mathrm{cm}^{-3}$ (**b**), where Z_c = nuclear core charge, N = number of electrons in the target ion before capture, and thus $Z = Z_\mathrm{c} - N$ degree of ionization. n = principal quantum number of the recombined state. For reference, the n cutoff values n_T and n_F are shown in parentheses, and the smaller of the two is used as the cutoff in the calculation of the total TBR rates. The electron temperature T is given in eV, (1 eV = 11 600 K), and the individual rates are given for individual n's at every twenty points. The entry TOT shows the total sum over n up to n_max. The numbers in brackets denote powers of 10. The statistical factor is set at $S_n = 1$.

Table 3a. TBR rates α^{TBR} [cm^3/s] for $N_\mathrm{e} = N_\mathrm{I} = 10^{11}\,\mathrm{cm}^{-3}$.

n	α^{TBR}	n	α^{TBR}	n	α^{TBR}	n	α^{TBR}
C^{6+} $Z_\mathrm{c} = 6$, $N = 0$, $Z = 6$						$N_\mathrm{e} = N_\mathrm{I} = 10^{11}\,\mathrm{cm}^{-3}$	
$T = 0.01$ eV (309, 618)		200	0.233[-08]	60	0.806[-12]	$T = 10$ eV (9, 618)	
20	0.111[-12]	220	0.346[-08]	80	0.247[-11]	TOT	0.456[-17]
40	0.229[-11]	240	0.494[-08]	TOT	0.106[-09]	$T = 100$ eV (3, 618)	
60	0.127[-10]	260	0.684[-08]	$T = 1.0$ eV (30, 618)		TOT	0.293[-20]
80	0.436[-10]	280	0.923[-08]	20	0.603[-15]		
100	0.116[-09]	300	0.122[-07]	TOT	0.179[-13]		
120	0.260[-09]	TOT	0.843[-06]				
140	0.511[-09]	$T = 0.1$ eV (97, 618)					
160	0.909[-09]	20	0.967[-14]				
180	0.150[-08]	40	0.157[-12]				
C^{+} $Z_\mathrm{c} = 6$, $N = 5$, $Z = 1$						$N_\mathrm{e} = N_\mathrm{I} = 10^{11}\,\mathrm{cm}^{-3}$	
$T = 0.01$ eV (51, 161)		$T = 0.1$ eV (16, 161)		$T = 1.0$ eV (5, 161)		$T = 10$ eV (1, 161)	
20	0.956[-12]	TOT	0.872[-13]	TOT	0.348[-16]	TOT	0.556[-20]
40	0.132[-10]					$T = 100$ eV (0, 161)	
TOT	0.366[-09]						
O^{8+} $Z_\mathrm{c} = 8$, $N = 0$, $Z = 8$						$N_\mathrm{e} = N_\mathrm{I} = 10^{11}\,\mathrm{cm}^{-3}$	
$T = 0.01$ eV (413, 767)		60	0.809[-11]	180	0.101[-08]	300	0.895[-08]
20	0.530[-13]	80	0.280[-10]	200	0.160[-08]	320	0.117[-07]
40	0.139[-11]	100	0.737[-10]	220	0.242[-08]	340	0.150[-07]
		120	0.165[-09]	240	0.351[-08]	360	0.189[-07]
		140	0.328[-09]	260	0.492[-08]	380	0.235[-07]
		160	0.597[-09]	280	0.672[-08]	400	0.289[-07]

TOT 0.268[-05]

$T = 0.1$ eV (130, 767)

20	0.617[-14]
40	0.100[-12]
60	0.547[-12]
80	0.177[-11]
100	0.431[-11]
120	0.879[-11]
TOT	0.323[-09]

$T = 1.0$ eV (41, 767)

20	0.413[-15]
40	0.519[-14]
TOT	0.532[-13]

$T = 10$ eV (13, 767)

TOT 0.146[-16]

$T = 100$ eV (4, 767)

TOT 0.604[-20]

O^{3+} $Z_c = 8,\ N = 5,\ Z = 3$ $N_e = N_I = 10^{11}\,cm^{-3}$

$T = 0.01$ eV (154, 368)

20	0.392[-12]
40	0.641[-11]
60	0.354[-10]
80	0.119[-09]
100	0.296[-09]
120	0.614[-09]
140	0.113[-08]
TOT	0.517[-07]

$T = 0.1$ eV (48, 368)

20	0.269[-13]
40	0.364[-12]
TOT	0.762[-11]

$T = 1.0$ eV (15, 368)

TOT 0.183[-14]

$T = 10$ eV (4, 368)

TOT 0.418[-18]

$T = 100$ eV (1, 368)

TOT 0.154[-21]

Mg^{12+} $Z_c = 12,\ N = 0,\ Z = 12$ $N_e = N_I = 10^{11}\,cm^{-3}$

$T = 0.01$ eV (619, 1040)

20	0.854[-14]
40	0.603[-12]
60	0.400[-11]
80	0.145[-10]
100	0.388[-10]
120	0.866[-10]
140	0.171[-09]
160	0.311[-09]
180	0.528[-09]
200	0.850[-09]
220	0.131[-08]
240	0.194[-08]
260	0.279[-08]
280	0.388[-08]
300	0.527[-08]
320	0.700[-08]
340	0.911[-08]
360	0.117[-07]
380	0.147[-07]
400	0.183[-07]
420	0.224[-07]
440	0.273[-07]
460	0.328[-07]
480	0.392[-07]
500	0.464[-07]
520	0.545[-07]
540	0.636[-07]
560	0.738[-07]
580	0.851[-07]
600	0.977[-07]
TOT	0.135[-04]

$T = 0.1$ eV (195, 1040)

20	0.308[-14]
40	0.525[-13]
60	0.288[-12]
80	0.996[-12]
100	0.257[-11]
120	0.549[-11]
140	0.103[-10]
160	0.176[-10]
180	0.281[-10]
TOT	0.152[-08]

$T = 1.0$ eV (61, 1040)

20	0.220[-15]
40	0.328[-14]
60	0.149[-13]
TOT	0.212[-12]

$T = 10$ eV (19, 1040)

TOT 0.452[-16]

$T = 100$ eV (6, 1040)

TOT 0.174[-19]

Mg^{7+} $Z_c = 12,\ N = 5,\ Z = 7$ $N_e = N_I = 10^{11}\,cm^{-3}$

$T = 0.01$ eV (361, 694)	
20	0.765[-13]
40	0.177[-11]
60	0.100[-10]
80	0.344[-10]
100	0.910[-10]
120	0.204[-09]
140	0.405[-09]
160	0.731[-09]
180	0.122[-08]
200	0.192[-08]
220	0.288[-08]
240	0.414[-08]
260	0.578[-08]
280	0.784[-08]
300	0.104[-07]
320	0.135[-07]
340	0.172[-07]
360	0.217[-07]
TOT	0.157[-05]

$T = 0.1$ eV (114, 694)	
20	0.762[-14]
40	0.124[-12]
60	0.660[-12]
80	0.208[-11]
100	0.498[-11]
TOT	0.196[-09]

$T = 1.0$ eV (36, 694)	
20	0.497[-15]
TOT	0.342[-13]

$T = 10$ eV (11, 694)	
TOT	0.860[-17]

$T = 100$ eV (3, 694)	
TOT	0.248[-20]

Mg^{2+} $Z_c = 12,\ N = 10,\ Z = 2$ $N_e = N_I = 10^{11}\,cm^{-3}$

$T = 0.01$ eV (103, 271)	
20	0.665[-12]
40	0.108[-10]
60	0.562[-10]
80	0.174[-09]
100	0.412[-09]
TOT	0.997[-08]

$T = 0.1$ eV (32, 271)	
20	0.421[-13]
TOT	0.168[-11]

$T = 1.0$ eV (10, 271)	
TOT	0.488[-15]

$T = 10$ eV (3, 271)	
TOT	0.207[-18]

$T = 100$ eV (1, 271)	
TOT	0.215[-21]

Ar^{18+} $Z_c = 18,\ N = 0,\ Z = 18$ $N_e = N_I = 10^{11}\,cm^{-3}$

$T = 0.1$ eV (293, 1410)	
20	0.135[-14]
40	0.271[-13]
60	0.150[-12]
80	0.514[-12]
100	0.137[-11]
120	0.306[-11]
140	0.598[-11]
160	0.106[-10]
180	0.174[-10]
200	0.270[-10]
220	0.399[-10]
240	0.568[-10]
260	0.785[-10]
280	0.106[-09]
TOT	0.740[-08]

$T = 1.0$ eV (92, 1410)	
20	0.114[-15]
40	0.185[-14]
60	0.933[-14]
80	0.284[-13]
TOT	0.942[-12]

$T = 10$ eV (29, 1410)	
20	0.697[-17]
TOT	0.177[-15]

$T = 100$ eV (9, 1410)	
TOT	0.525[-19]

Ar^{13+} $Z_c = 18,\ N = 5,\ Z = 13$ $N_e = N_I = 10^{11}\,cm^{-3}$

$T = 0.01$ eV (671, 1105)	
20	0.341[-14]
40	0.498[-12]
60	0.343[-11]
80	0.126[-10]
100	0.340[-10]
120	0.762[-10]
140	0.151[-09]
160	0.273[-09]
180	0.463[-09]
200	0.746[-09]
220	0.115[-08]
240	0.171[-08]
260	0.246[-08]
280	0.343[-08]
300	0.468[-08]
320	0.623[-08]
340	0.814[-08]
360	0.105[-07]
380	0.132[-07]
400	0.165[-07]
420	0.203[-07]
440	0.247[-07]
460	0.298[-07]
480	0.357[-07]
500	0.423[-07]
520	0.498[-07]
540	0.582[-07]
560	0.676[-07]
580	0.781[-07]
600	0.897[-07]
620	0.102[-06]
640	0.117[-06]
660	0.132[-06]
TOT	0.186[-04]

$T = 0.1$ eV (212, 1105)	
20	0.265[-14]
40	0.462[-13]
60	0.253[-12]
80	0.877[-12]
100	0.229[-11]
120	0.494[-11]
140	0.934[-11]
160	0.161[-10]
180	0.258[-10]
200	0.392[-10]
TOT	0.211[-08]

$T = 1.0$ eV (67, 1105)	
20	0.193[-15]
40	0.296[-14]
60	0.137[-13]
TOT	0.301[-12]

$T = 10$ eV (21, 1105)	
20	0.101[-16]
TOT	0.632[-16]

$T = 100$ eV (6, 1105)	
TOT	0.158[-19]

Ar^{8+} $Z_c = 18,\ N = 10,\ Z = 8$ $N_e = N_I = 10^{11}\,cm^{-3}$

$T = 0.01$ eV (413, 767)	
20	0.530[-13]
40	0.139[-11]
60	0.809[-11]
80	0.280[-10]
100	0.737[-10]
120	0.165[-09]
140	0.328[-09]
160	0.597[-09]
180	0.101[-08]
200	0.160[-08]
220	0.242[-08]
240	0.351[-08]
260	0.492[-08]
280	0.672[-08]
300	0.895[-08]
320	0.117[-07]
340	0.150[-07]
360	0.189[-07]
380	0.235[-07]
400	0.289[-07]
TOT	0.268[-05]

$T = 0.1$ eV (130, 767)	
20	0.617[-14]
40	0.100[-12]
60	0.547[-12]
80	0.177[-11]
100	0.431[-11]
120	0.879[-11]
TOT	0.323[-09]

$T = 1.0$ eV (41, 767)	
20	0.413[-15]
40	0.519[-14]
TOT	0.532[-13]

$T = 10$ eV (13, 767)	
TOT	0.146[-16]

$T = 100$ eV (4, 767)	
TOT	0.604[-20]

Ar^{3+} $Z_c = 18,\ N = 15,\ Z = 3$ $N_e = N_I = 10^{11}\,cm^{-3}$

$T = 0.01$ eV (154, 368)	
20	0.392[-12]
40	0.641[-11]
60	0.354[-10]
80	0.119[-09]
100	0.296[-09]
120	0.614[-09]
140	0.113[-08]
TOT	0.517[-07]

$T = 0.1$ eV (48, 368)	
20	0.269[-13]
40	0.364[-12]
TOT	0.762[-11]

$T = 1.0$ eV (15, 368)	
TOT	0.183[-14]

$T = 10$ eV (4, 368)	
TOT	0.418[-18]

$T = 100$ eV (1, 368)	
TOT	0.154[-21]

Fe^{26+} $Z_c = 26,\ N = 0,\ Z = 26$ $N_e = N_I = 10^{11}\,cm^{-3}$

$T = 0.1$ eV (424, 1858)	
20	0.516[-15]
40	0.140[-13]
60	0.818[-13]
80	0.283[-12]
100	0.747[-12]
120	0.167[-11]
140	0.332[-11]
160	0.604[-11]
180	0.102[-10]
200	0.163[-10]
220	0.246[-10]
240	0.358[-10]
260	0.503[-10]
280	0.687[-10]
300	0.916[-10]
320	0.120[-09]
340	0.154[-09]
360	0.194[-09]
380	0.242[-09]
400	0.297[-09]
420	0.362[-09]
TOT	0.315[-07]

$T = 1.0$ eV (134, 1858)	
20	0.624[-16]
40	0.101[-14]
60	0.555[-14]
80	0.181[-13]
100	0.441[-13]
120	0.903[-13]
TOT	0.384[-11]

$T = 10$ eV (42, 1858)	
20	0.420[-17]
40	0.533[-16]
TOT	0.609[-15]

$T = 100$ eV (13, 1858)	
TOT	0.150[-18]

Fe^{21+} $Z_c = 26,\ N = 5,\ Z = 21$ $N_e = N_I = 10^{11}\,cm^{-3}$

$T = 0.1$ eV (342, 1583)	
20	0.937[-15]
40	0.207[-13]
60	0.117[-12]
80	0.400[-12]
100	0.106[-11]
120	0.238[-11]
140	0.471[-11]
160	0.847[-11]
180	0.141[-10]
200	0.221[-10]
220	0.329[-10]
240	0.473[-10]
260	0.658[-10]
280	0.890[-10]
300	0.118[-09]
320	0.153[-09]
340	0.195[-09]
TOT	0.135[-07]

$T = 1.0$ eV (108, 1583)	
20	0.887[-16]
40	0.144[-14]
60	0.760[-14]
80	0.237[-13]
100	0.564[-13]
TOT	0.171[-11]

$T = 10$ eV (34, 1583)	
20	0.570[-17]
TOT	0.301[-15]

$T = 100$ eV (10, 1583)	
TOT	0.666[-19]

Fe^{16+} $Z_c = 26,\ N = 10,\ Z = 16$ $N_e = N_I = 10^{11}\,cm^{-3}$

$T = 0.1$ eV (261, 1291)	
20	0.175[-14]
40	0.330[-13]
60	0.181[-12]
80	0.624[-12]
100	0.166[-11]
120	0.367[-11]
140	0.709[-11]
160	0.124[-10]
180	0.202[-10]
200	0.311[-10]
220	0.457[-10]
240	0.648[-10]
260	0.891[-10]
TOT	0.473[-08]

$T = 1.0$ eV (82, 1291)	
20	0.138[-15]
40	0.221[-14]
60	0.108[-13]
80	0.323[-13]
TOT	0.621[-12]

$T = 10$ eV (26, 1291)	
20	0.804[-17]
TOT	0.126[-15]

$T = 100$ eV (8, 1291)	
TOT	0.379[-19]

Fe^{11+} $Z_c = 26,\ N = 15,\ Z = 11$ $N_e = N_I = 10^{11}\,cm^{-3}$

$T = 0.01$ eV (567, 975)	
20	0.153[-13]
40	0.733[-12]
60	0.469[-11]
80	0.168[-10]
100	0.446[-10]
120	0.995[-10]
140	0.197[-09]
160	0.358[-09]
180	0.608[-09]
200	0.980[-09]
220	0.151[-08]
240	0.223[-08]
260	0.318[-08]
280	0.441[-08]
300	0.597[-08]
320	0.789[-08]
340	0.102[-07]
360	0.131[-07]
380	0.164[-07]
400	0.203[-07]
420	0.249[-07]
440	0.302[-07]
460	0.363[-07]
480	0.432[-07]
500	0.511[-07]
520	0.599[-07]
540	0.698[-07]
560	0.809[-07]
TOT	0.947[-05]

$T = 0.1$ eV (179, 975)	
20	0.361[-14]
40	0.603[-13]
60	0.332[-12]
80	0.114[-11]
100	0.290[-11]
120	0.613[-11]
140	0.114[-10]
160	0.194[-10]
TOT	0.110[-08]

$T = 1.0$ eV (56, 975)	
20	0.253[-15]
40	0.365[-14]
TOT	0.157[-12]

$T = 10$ eV (17, 975)	
TOT	0.312[-16]

$T = 100$ eV (5, 975)	
TOT	0.963[-20]

Fe^{6+} $Z_c = 26,\ N = 20,\ Z = 6$ $N_e = N_I = 10^{11}\,cm^{-3}$

$T = 0.01$ eV (309, 618)	
20	0.111[-12]
40	0.229[-11]
60	0.127[-10]
80	0.436[-10]
100	0.116[-09]
120	0.260[-09]
140	0.511[-09]
160	0.909[-09]
180	0.150[-08]
200	0.233[-08]
220	0.346[-08]
240	0.494[-08]
260	0.684[-08]
280	0.923[-08]
300	0.122[-07]
TOT	0.843[-06]

$T = 0.1$ eV (97, 618)	
20	0.967[-14]
40	0.157[-12]
60	0.806[-12]
80	0.247[-11]
TOT	0.106[-09]

$T = 1.0$ eV (30, 618)	
20	0.603[-15]
TOT	0.179[-13]

$T = 10$ eV (9, 618)	
TOT	0.456[-17]

$T = 100$ eV (3, 618)	
TOT	0.293[-20]

Table 3b. TBR rates α^{TBR} [cm^3/s] for $N_\mathrm{e} = N_\mathrm{I} = 10^{14}\,\mathrm{cm}^{-3}$.

n	α^{TBR}	n	α^{TBR}	n	α^{TBR}	n	α^{TBR}
C^{6+} $Z_\mathrm{c} = 6,\ N = 0,\ Z = 6$						$N_\mathrm{e} = N_\mathrm{I} = 10^{14}\,\mathrm{cm}^{-3}$	
$T = 0.01$ eV (309, 195)		140	0.511[-06]	60	0.806[-09]	$T = 10$ eV (9, 195)	
20	0.111[-09]	160	0.909[-06]	80	0.247[-08]	TOT	0.456[-14]
40	0.229[-08]	180	0.150[-05]	TOT	0.106[-06]	$T = 100$ eV (3, 195)	
60	0.127[-07]	TOT	0.788[-04]	$T = 1.0$ eV (30, 195)		TOT	0.293[-17]
80	0.436[-07]	$T = 0.1$ eV (97, 195)		20	0.603[-12]		
100	0.116[-06]	20	0.967[-11]	TOT	0.179[-10]		
120	0.260[-06]	40	0.157[-09]				
C^{+} $Z_\mathrm{c} = 6,\ N = 5,\ Z = 1$						$N_\mathrm{e} = N_\mathrm{I} = 10^{14}\,\mathrm{cm}^{-3}$	
$T = 0.01$ eV (51, 51)		$T = 0.1$ eV (16, 51)		$T = 1.0$ eV (5, 51)		$T = 10$ eV (1, 51)	
20	0.956[-09]	TOT	0.872[-10]	TOT	0.348[-13]	TOT	0.556[-17]
40	0.132[-07]					$T = 100$ eV (0, 51)	
TOT	0.366[-06]						
O^{8+} $Z_\mathrm{c} = 8,\ N = 0,\ Z = 8$						$N_\mathrm{e} = N_\mathrm{I} = 10^{14}\,\mathrm{cm}^{-3}$	
$T = 0.01$ eV (413, 242)		180	0.101[-05]	80	0.177[-08]	$T = 10$ eV (13, 242)	
20	0.530[-10]	200	0.160[-05]	100	0.431[-08]	TOT	0.146[-13]
40	0.139[-08]	220	0.242[-05]	120	0.879[-08]	$T = 100$ eV (4, 242)	
60	0.809[-08]	240	0.351[-05]	TOT	0.323[-06]	TOT	0.604[-17]
80	0.280[-07]	TOT	0.166[-03]	$T = 1.0$ eV (41, 242)			
100	0.737[-07]	$T = 0.1$ eV (130, 242)		20	0.413[-12]		
120	0.165[-06]	20	0.617[-11]	40	0.519[-11]		
140	0.328[-06]	40	0.100[-09]	TOT	0.532[-10]		
160	0.597[-06]	60	0.547[-09]				

O^{3+} $Z_c = 8,\ N = 5,\ Z = 3$ $N_e = N_I = 10^{14}\,cm^{-3}$

$T = 0.01$ eV (154, 116)	
20	0.392[-09]
40	0.641[-08]
60	0.354[-07]
80	0.119[-06]
100	0.296[-06]
TOT	0.126[-04]

$T = 0.1$ eV (48, 116)	
20	0.269[-10]
40	0.364[-09]
TOT	0.762[-08]

$T = 1.0$ eV (15, 116)	
TOT	0.183[-11]

$T = 10$ eV (4, 116)	
TOT	0.418[-15]

$T = 100$ eV (1, 116)	
TOT	0.154[-18]

Mg^{12+} $Z_c = 12,\ N = 0,\ Z = 12$ $N_e = N_I = 10^{14}\,cm^{-3}$

$T = 0.01$ eV (619, 329)	
20	0.854[-11]
40	0.603[-09]
60	0.400[-08]
80	0.145[-07]
100	0.388[-07]
120	0.866[-07]
140	0.171[-06]
160	0.311[-06]
180	0.528[-06]
200	0.850[-06]
220	0.131[-05]
240	0.194[-05]
260	0.279[-05]
280	0.388[-05]
300	0.527[-05]
320	0.700[-05]
TOT	0.482[-03]

$T = 0.1$ eV (195, 329)	
20	0.308[-11]
40	0.525[-10]
60	0.288[-09]
80	0.996[-09]
100	0.257[-08]
120	0.549[-08]
140	0.103[-07]
160	0.176[-07]
180	0.281[-07]
TOT	0.152[-05]

$T = 1.0$ eV (61, 329)	
20	0.220[-12]
40	0.328[-11]
60	0.149[-10]
80	0.208[-08]
100	0.498[-08]
TOT	0.196[-06]

$T = 10$ eV (19, 329)	
TOT	0.452[-13]

$T = 100$ eV (6, 329)	
TOT	0.174[-16]

Mg^{7+} $Z_c = 12,\ N = 5,\ Z = 7$ $N_e = N_I = 10^{14}\,cm^{-3}$

$T = 0.01$ eV (361, 219)	
20	0.765[-10]
40	0.177[-08]
60	0.100[-07]
80	0.344[-07]
100	0.910[-07]
120	0.204[-06]
140	0.405[-06]
160	0.731[-06]
180	0.122[-05]
200	0.192[-05]
TOT	0.118[-03]

$T = 0.1$ eV (114, 219)	
20	0.762[-11]
40	0.124[-09]
60	0.660[-09]

$T = 1.0$ eV (36, 219)	
20	0.497[-12]
TOT	0.342[-10]

$T = 10$ eV (11, 219)	
TOT	0.860[-14]

$T = 100$ eV (3, 219)	
TOT	0.248[-17]

Mg^{2+} $Z_c = 12,\ N = 10,\ Z = 2$ $N_e = N_I = 10^{14}\,cm^{-3}$

$T = 0.01$ eV (103, 85)	
20	0.665[-09]
40	0.108[-07]
60	0.562[-07]
80	0.174[-06]
TOT	0.391[-05]

$T = 0.1$ eV (32, 85)	
20	0.421[-10]
TOT	0.168[-08]

$T = 1.0$ eV (10, 85)	
TOT	0.488[-12]

$T = 10$ eV (3, 85)	
TOT	0.207[-15]

$T = 100$ eV (1, 85)	
TOT	0.215[-18]

Ar^{18+} $Z_c = 18,\ N = 0,\ Z = 18$ $N_e = N_I = 10^{14}\,cm^{-3}$

$T = 0.01$ eV (929, 446)	
20	0.933[-11]
40	0.193[-09]
60	0.172[-08]
80	0.688[-08]
100	0.194[-07]
120	0.445[-07]
140	0.890[-07]
160	0.162[-06]
180	0.274[-06]
200	0.440[-06]
220	0.676[-06]
240	0.100[-05]
260	0.144[-05]
280	0.202[-05]
300	0.277[-05]
320	0.373[-05]
340	0.492[-05]
360	0.639[-05]
380	0.817[-05]
400	0.103[-04]
420	0.128[-04]
440	0.158[-04]
TOT	0.137[-02]

$T = 0.1$ eV (293, 446)	
20	0.135[-11]
40	0.271[-10]
60	0.150[-09]
80	0.514[-09]
100	0.137[-08]
120	0.306[-08]
140	0.598[-08]
160	0.106[-07]
180	0.174[-07]
200	0.270[-07]
220	0.399[-07]
240	0.568[-07]
260	0.785[-07]
280	0.106[-06]
TOT	0.740[-05]

$T = 1.0$ eV (92, 446)	
20	0.114[-12]
40	0.185[-11]
60	0.933[-11]
80	0.284[-10]
TOT	0.942[-09]

$T = 10$ eV (29, 446)	
20	0.697[-14]
TOT	0.177[-12]

$T = 100$ eV (9, 446)	
TOT	0.525[-16]

Ar^{13+} $Z_c = 18,\ N = 5,\ Z = 13$ $N_e = N_I = 10^{14}\,cm^{-3}$

$T = 0.01$ eV (671, 349)	
20	0.341[-11]
40	0.498[-09]
60	0.343[-08]
80	0.126[-07]
100	0.340[-07]
120	0.762[-07]
140	0.151[-06]
160	0.273[-06]
180	0.463[-06]
200	0.746[-06]
220	0.115[-05]
240	0.171[-05]
260	0.246[-05]
280	0.343[-05]
300	0.468[-05]
320	0.623[-05]
340	0.814[-05]
TOT	0.589[-03]

$T = 0.1$ eV (212, 349)	
20	0.265[-11]
40	0.462[-10]
60	0.253[-09]
80	0.877[-09]
100	0.229[-08]
120	0.494[-08]
140	0.934[-08]
160	0.161[-07]
180	0.258[-07]
200	0.392[-07]
TOT	0.211[-05]

$T = 1.0$ eV (67, 349)	
20	0.193[-12]
40	0.296[-11]
60	0.137[-10]
TOT	0.301[-09]

$T = 10$ eV (21, 349)	
20	0.101[-13]
TOT	0.632[-13]

$T = 100$ eV (6, 349)	
TOT	0.158[-16]

Ar^{8+} $Z_c = 18,\ N = 10,\ Z = 8$ $N_e = N_I = 10^{14}\,cm^{-3}$

$T = 0.01$ eV (413, 242)	
20	0.530[-10]
40	0.139[-08]
60	0.809[-08]
80	0.280[-07]
100	0.737[-07]
120	0.165[-06]
140	0.328[-06]
160	0.597[-06]
180	0.101[-05]
200	0.160[-05]
220	0.242[-05]
240	0.351[-05]
TOT	0.166[-03]

$T = 0.1$ eV (130, 242)	
20	0.617[-11]
40	0.100[-09]
60	0.547[-09]
80	0.177[-08]
100	0.431[-08]
120	0.879[-08]
TOT	0.323[-06]

$T = 1.0$ eV (41, 242)	
20	0.413[-12]
40	0.519[-11]
TOT	0.532[-10]

$T = 10$ eV (13, 242)	
TOT	0.146[-13]

$T = 100$ eV (4, 242)	
TOT	0.604[-17]

Ar^{3+} $Z_c = 18,\ N = 15,\ Z = 3$ $N_e = N_I = 10^{14}\,cm^{-3}$

$T = 0.01$ eV (154, 116)	
20	0.392[-09]
40	0.641[-08]
60	0.354[-07]
80	0.119[-06]
100	0.296[-06]
TOT	0.126[-04]

$T = 0.1$ eV (48, 116)	
20	0.269[-10]
40	0.364[-09]
TOT	0.762[-08]

$T = 1.0$ eV (15, 116)	
TOT	0.183[-11]

$T = 10$ eV (4, 116)	
TOT	0.418[-15]

$T = 100$ eV (1, 116)	
TOT	0.154[-18]

Fe^{26+} $Z_c = 26,\ N = 0,\ Z = 26$ $N_e = N_I = 10^{14}\,cm^{-3}$

$T = 0.01$ eV (1342, 587)	
20	0.137[-10]
40	0.179[-10]
60	0.623[-09]
80	0.305[-08]
100	0.938[-08]
120	0.226[-07]
140	0.468[-07]
160	0.870[-07]
180	0.149[-06]
200	0.242[-06]
220	0.372[-06]
240	0.552[-06]
260	0.793[-06]
280	0.111[-05]
300	0.152[-05]
320	0.203[-05]
340	0.268[-05]
360	0.348[-05]
380	0.447[-05]
400	0.565[-05]
420	0.708[-05]
440	0.877[-05]
460	0.108[-04]
480	0.131[-04]
500	0.158[-04]
520	0.189[-04]
540	0.225[-04]
560	0.266[-04]
580	0.312[-04]
TOT	0.348[-02]

$T = 0.1$ eV (424, 587)	
20	0.516[-12]
40	0.140[-10]
60	0.818[-10]
80	0.283[-09]
100	0.747[-09]
120	0.167[-08]
140	0.332[-08]
160	0.604[-08]
180	0.102[-07]
200	0.163[-07]
220	0.246[-07]
240	0.358[-07]
260	0.503[-07]
280	0.687[-07]
300	0.916[-07]
320	0.120[-06]
340	0.154[-06]
360	0.194[-06]
380	0.242[-06]
400	0.297[-06]
420	0.362[-06]
TOT	0.315[-04]

$T = 1.0$ eV (134, 587)	
20	0.624[-13]
40	0.101[-11]
60	0.555[-11]
80	0.181[-10]
100	0.441[-10]
120	0.903[-10]
TOT	0.384[-08]

$T = 10$ eV (42, 587)	
20	0.420[-14]
40	0.533[-13]
TOT	0.609[-12]

$T = 100$ eV (13, 587)	
TOT	0.150[-15]

Fe^{21+} $Z_c = 26,\ N = 5,\ Z = 21$ $N_e = N_I = 10^{14}\,cm^{-3}$

$T = 0.01$ eV (1084, 500)	
20	0.121[-10]
40	0.103[-09]
60	0.117[-08]
80	0.500[-08]
100	0.145[-07]
120	0.339[-07]
140	0.686[-07]
160	0.126[-06]
180	0.214[-06]
200	0.343[-06]
220	0.527[-06]
240	0.780[-06]
260	0.112[-05]
280	0.157[-05]
300	0.215[-05]
320	0.289[-05]
340	0.382[-05]
360	0.496[-05]
380	0.636[-05]
400	0.805[-05]
420	0.101[-04]
440	0.125[-04]
460	0.152[-04]
480	0.185[-04]
500	0.222[-04]
TOT	0.201[-02]

$T = 0.1$ eV (342, 500)	
20	0.937[-12]
40	0.207[-10]
60	0.117[-09]
80	0.400[-09]
100	0.106[-08]
120	0.238[-08]
140	0.471[-08]
160	0.847[-08]
180	0.141[-07]
200	0.221[-07]
220	0.329[-07]
240	0.473[-07]
260	0.658[-07]
280	0.890[-07]
300	0.118[-06]
320	0.153[-06]
340	0.195[-06]
TOT	0.135[-04]

$T = 1.0$ eV (108, 500)	
20	0.887[-13]
40	0.144[-11]
60	0.760[-11]
80	0.237[-10]
100	0.564[-10]
TOT	0.171[-08]

$T = 10$ eV (34, 500)	
20	0.570[-14]
TOT	0.301[-12]

$T = 100$ eV (10, 500)	
TOT	0.666[-16]

Fe^{16+} $Z_c = 26,\ N = 10,\ Z = 16$ $N_e = N_I = 10^{14}\,cm^{-3}$

$T = 0.01$ eV (826, 408)	
20	0.599[-11]
40	0.283[-09]
60	0.224[-08]
80	0.865[-08]
100	0.239[-07]
120	0.543[-07]
140	0.108[-06]
160	0.196[-06]
180	0.332[-06]
200	0.532[-06]
220	0.818[-06]
240	0.122[-05]
260	0.175[-05]
280	0.246[-05]
300	0.337[-05]
320	0.452[-05]
340	0.595[-05]
360	0.770[-05]
380	0.981[-05]
400	0.123[-04]
TOT	0.101[-02]

$T = 0.1$ eV (261, 408)	
20	0.175[-11]
40	0.330[-10]
60	0.181[-09]
80	0.624[-09]
100	0.166[-08]
120	0.367[-08]
140	0.709[-08]
160	0.124[-07]
180	0.202[-07]
200	0.311[-07]
220	0.457[-07]
240	0.648[-07]
260	0.891[-07]
TOT	0.473[-05]

$T = 1.0$ eV (82, 408)	
20	0.138[-12]
40	0.221[-11]
60	0.108[-10]
80	0.323[-10]
TOT	0.621[-09]

$T = 10$ eV (26, 408)	
20	0.804[-14]
TOT	0.126[-12]

$T = 100$ eV (8, 408)	
TOT	0.379[-16]

Fe^{11+} $Z_c = 26,\ N = 15,\ Z = 11$ $N_e = N_I = 10^{14}\,cm^{-3}$

$T = 0.01$ eV (567, 308)	
20	0.153[-10]
40	0.733[-09]
60	0.469[-08]
80	0.168[-07]
100	0.446[-07]
120	0.995[-07]
140	0.197[-06]
160	0.358[-06]
180	0.608[-06]
200	0.980[-06]
220	0.151[-05]
240	0.223[-05]
260	0.318[-05]
280	0.441[-05]
300	0.597[-05]
TOT	0.384[-03]

$T = 0.1$ eV (179, 308)	
20	0.361[-11]
40	0.603[-10]
60	0.332[-09]
80	0.114[-08]
100	0.290[-08]
120	0.613[-08]
140	0.114[-07]
160	0.194[-07]
TOT	0.110[-05]

$T = 1.0$ eV (56, 308)	
20	0.253[-12]
40	0.365[-11]
TOT	0.157[-09]

$T = 10$ eV (17, 308)	
TOT	0.312[-13]

$T = 100$ eV (5, 308)	
TOT	0.963[-17]

Fe^{6+} $Z_c = 26,\ N = 20,\ Z = 6$ $N_e = N_I = 10^{14}\,cm^{-3}$

$T = 0.01$ eV (309, 195)	
20	0.111[-09]
40	0.229[-08]
60	0.127[-07]
80	0.436[-07]
100	0.116[-06]
120	0.260[-06]
140	0.511[-06]
160	0.909[-06]
180	0.150[-05]
TOT	0.788[-04]

$T = 0.1$ eV (97, 195)	
20	0.967[-11]
40	0.157[-09]
60	0.806[-09]
80	0.247[-08]
TOT	0.106[-06]

$T = 1.0$ eV (30, 195)	
20	0.603[-12]
TOT	0.179[-10]

$T = 10$ eV (9, 195)	
TOT	0.456[-14]

$T = 100$ eV (3, 195)	
TOT	0.293[-17]

Table 4. DR rates $\alpha^{\mathrm{DR}}\,[\mathrm{cm}^3/\mathrm{s}]$ are given for the C^{Z+} ions ($Z_c = 6$), as they are generated by the fitted empirical formula. Z_c = nuclear core charge, N = number of electrons before the recombination, degree of ionization before capture $Z = Z_c - N$. T is the plasma temperature. The column 1S denotes the 1s electron excitation of mode (i); 2S denotes the 2s electron excitation of mode (ii), and 2P denotes the 2s and 2p electron excitation mode (i). Similarly, 3S denotes the excitation mode (ii) for the 3s, 3p and 3d electrons where appropriate, while 3P is for excitation mode (i) for all the M-shell electrons. The rates are displayed in fixed point format for ready comparison of the relative magnitudes for the different excitation modes, but at most only the first two digits are significant in all cases.

N	T [keV]	1S	2S	2P	3S	3P	TOTAL
				C^{5+}			
1	0.001	0.0	0.0	0.0	0.0	0.0	0.0
1	0.002	0.0	0.0	0.0	0.0	0.0	0.0
1	0.005	0.0	0.0	0.0	0.0	0.0	0.0
1	0.010	0.0	0.0	0.0	0.0	0.0	0.0
1	0.020	0.0	0.0	0.0	0.0	0.0	0.0
1	0.050	1.8	0.0	0.0	0.0	0.0	1.8
1	0.100	12.3	0.0	0.0	0.0	0.0	12.3
1	0.200	18.9	0.0	0.0	0.0	0.0	18.9
1	0.500	11.6	0.0	0.0	0.0	0.0	11.6
1	1.000	5.5	0.0	0.0	0.0	0.0	5.5
1	2.000	2.2	0.0	0.0	0.0	0.0	2.2
1	5.000	0.6	0.0	0.0	0.0	0.0	0.6
1	10.000	0.2	0.0	0.0	0.0	0.0	0.2
				C^{4+}			
2	0.001	0.0	0.0	0.0	0.0	0.0	0.0
2	0.002	0.0	0.0	0.0	0.0	0.0	0.0
2	0.005	0.0	0.0	0.0	0.0	0.0	0.0
2	0.010	0.0	0.0	0.0	0.0	0.0	0.0
2	0.020	0.0	0.0	0.0	0.0	0.0	0.0
2	0.050	3.7	0.0	0.0	0.0	0.0	3.7
2	0.100	16.7	0.0	0.0	0.0	0.0	16.7
2	0.200	21.0	0.0	0.0	0.0	0.0	21.0
2	0.500	11.4	0.0	0.0	0.0	0.0	11.4
2	1.000	5.2	0.0	0.0	0.0	0.0	5.2
2	2.000	2.1	0.0	0.0	0.0	0.0	2.1
2	5.000	0.6	0.0	0.0	0.0	0.0	0.6
2	10.000	0.2	0.0	0.0	0.0	0.0	0.2
				C^{3+}			
3	0.001	0.0	16.4	0.1	0.0	0.0	16.5
3	0.002	0.0	180.5	8.3	0.0	0.0	188.8
3	0.005	0.0	341.8	57.9	0.0	0.0	399.7
3	0.010	0.0	228.4	61.9	0.0	0.0	290.2
3	0.020	0.0	107.9	38.0	0.0	0.0	145.9
3	0.050	3.9	31.3	13.4	0.0	0.0	48.7
3	0.100	15.5	11.3	5.3	0.0	0.0	32.1
3	0.200	18.2	4.0	2.0	0.0	0.0	24.2

Table 4. DR rates for C^{Z+} (continued)

N	T [keV]	1S	2S	2P	3S	3P	TOTAL
3	0.500	9.5	1.0	0.5	0.0	0.0	11.0
3	1.000	4.3	0.3	0.2	0.0	0.0	4.8
3	2.000	1.7	0.1	0.1	0.0	0.0	1.9
3	5.000	0.5	0.0	0.0	0.0	0.0	0.5
3	10.000	0.2	0.0	0.0	0.0	0.0	0.2
				C^{2+}			
4	0.001	0.0	11.1	0.1	0.0	0.0	11.2
4	0.002	0.0	121.6	8.8	0.0	0.0	130.3
4	0.005	0.0	230.2	61.4	0.0	0.0	291.5
4	0.010	0.0	153.8	65.6	0.0	0.0	219.4
4	0.020	0.0	72.7	40.3	0.0	0.0	113.0
4	0.050	3.2	21.1	14.2	0.0	0.0	38.6
4	0.100	12.0	7.6	5.6	0.0	0.0	25.2
4	0.200	13.7	2.7	2.1	0.0	0.0	18.4
4	0.500	7.0	0.7	0.5	0.0	0.0	8.2
4	1.000	3.1	0.2	0.2	0.0	0.0	3.5
4	2.000	1.2	0.1	0.1	0.0	0.0	1.4
4	5.000	0.3	0.0	0.0	0.0	0.0	0.4
4	10.000	0.1	0.0	0.0	0.0	0.0	0.1
				C^{+}			
5	0.001	0.0	5.2	0.1	0.0	0.0	5.3
5	0.002	0.0	57.0	7.6	0.0	0.0	64.6
5	0.005	0.0	108.0	53.1	0.0	0.0	161.1
5	0.010	0.0	72.1	56.8	0.0	0.0	128.9
5	0.020	0.0	34.1	34.9	0.0	0.0	69.0
5	0.050	1.8	9.9	12.3	0.0	0.0	24.0
5	0.100	6.4	3.6	4.9	0.0	0.0	14.8
5	0.200	7.2	1.2	1.8	0.0	0.0	10.2
5	0.500	3.6	0.3	0.5	0.0	0.0	4.4
5	1.000	1.6	0.1	0.2	0.0	0.0	1.9
5	2.000	0.6	0.0	0.1	0.0	0.0	0.7
5	5.000	0.2	0.0	0.0	0.0	0.0	0.2
5	10.000	0.1	0.0	0.0	0.0	0.0	0.1

Table 5. DR rates α^{DR} [cm^3/s] for the O^{Z+} ions ($Z_c = 8$). Notation as in Table 4.

N	T [keV]	1S	2S	2P	3S	3P	TOTAL
				O^{7+}			
1	0.001	0.0	0.0	0.0	0.0	0.0	0.0
1	0.002	0.0	0.0	0.0	0.0	0.0	0.0
1	0.005	0.0	0.0	0.0	0.0	0.0	0.0

Table 5. DR rates for O^{Z+} (continued)

N	T [keV]	1S	2S	2P	3S	3P	TOTAL
1	0.010	0.0	0.0	0.0	0.0	0.0	0.0
1	0.020	0.0	0.0	0.0	0.0	0.0	0.0
1	0.050	0.1	0.0	0.0	0.0	0.0	0.1
1	0.100	4.2	0.0	0.0	0.0	0.0	4.2
1	0.200	17.0	0.0	0.0	0.0	0.0	17.0
1	0.500	18.4	0.0	0.0	0.0	0.0	18.4
1	1.000	10.6	0.0	0.0	0.0	0.0	10.6
1	2.000	4.8	0.0	0.0	0.0	0.0	4.8
1	5.000	1.4	0.0	0.0	0.0	0.0	1.4
1	10.000	0.5	0.0	0.0	0.0	0.0	0.5
				O^{6+}			
2	0.001	0.0	0.0	0.0	0.0	0.0	0.0
2	0.002	0.0	0.0	0.0	0.0	0.0	0.0
2	0.005	0.0	0.0	0.0	0.0	0.0	0.0
2	0.010	0.0	0.0	0.0	0.0	0.0	0.0
2	0.020	0.0	0.0	0.0	0.0	0.0	0.0
2	0.050	0.2	0.0	0.0	0.0	0.0	0.2
2	0.100	6.6	0.0	0.0	0.0	0.0	6.6
2	0.200	20.5	0.0	0.0	0.0	0.0	20.5
2	0.500	19.0	0.0	0.0	0.0	0.0	19.0
2	1.000	10.4	0.0	0.0	0.0	0.0	10.4
2	2.000	4.6	0.0	0.0	0.0	0.0	4.6
2	5.000	1.3	0.0	0.0	0.0	0.0	1.3
2	10.000	0.5	0.0	0.0	0.0	0.0	0.5
				O^{5+}			
3	0.001	0.0	2.1	0.0	0.0	0.0	2.1
3	0.002	0.0	115.1	0.0	0.0	0.0	115.1
3	0.005	0.0	572.0	12.6	0.0	0.0	584.5
3	0.010	0.0	527.0	52.8	0.0	0.0	579.8
3	0.020	0.0	292.4	64.4	0.0	0.0	356.8
3	0.050	0.3	93.5	34.2	0.0	0.0	127.9
3	0.100	6.2	34.8	15.5	0.0	0.0	56.6
3	0.200	17.7	12.4	6.2	0.0	0.0	36.3
3	0.500	15.7	3.1	1.7	0.0	0.0	20.4
3	1.000	8.4	1.1	0.6	0.0	0.0	10.1
3	2.000	3.7	0.4	0.2	0.0	0.0	4.2
3	5.000	1.0	0.1	0.1	0.0	0.0	1.2
3	10.000	0.4	0.0	0.0	0.0	0.0	0.4
				O^{4+}			
4	0.001	0.0	1.4	0.0	0.0	0.0	1.4
4	0.002	0.0	77.5	0.0	0.0	0.0	77.5
4	0.005	0.0	385.1	13.3	0.0	0.0	398.5
4	0.010	0.0	354.9	56.0	0.0	0.0	410.9

Table 5. DR rates for O^{Z+} (continued)

N	T [keV]	1S	2S	2P	3S	3P	TOTAL
4	0.020	0.0	196.9	68.2	0.0	0.0	265.1
4	0.050	0.2	62.9	36.3	0.0	0.0	99.4
4	0.100	4.6	23.4	16.4	0.0	0.0	44.5
4	0.200	12.6	8.3	6.6	0.0	0.0	27.5
4	0.500	10.8	2.1	1.8	0.0	0.0	14.7
4	1.000	5.8	0.7	0.6	0.0	0.0	7.1
4	2.000	2.5	0.2	0.2	0.0	0.0	3.0
4	5.000	0.7	0.1	0.1	0.0	0.0	0.8
4	10.000	0.3	0.0	0.0	0.0	0.0	0.3
				O^{3+}			
5	0.001	0.0	0.8	0.0	0.0	0.0	0.8
5	0.002	0.0	45.5	0.0	0.0	0.0	45.5
5	0.005	0.0	225.8	14.4	0.0	0.0	240.3
5	0.010	0.0	208.1	60.6	0.0	0.0	268.7
5	0.020	0.0	115.5	73.8	0.0	0.0	189.3
5	0.050	0.1	36.9	39.2	0.0	0.0	76.3
5	0.100	2.8	13.7	17.8	0.0	0.0	34.3
5	0.200	7.4	4.9	7.1	0.0	0.0	19.4
5	0.500	6.3	1.2	1.9	0.0	0.0	9.4
5	1.000	3.3	0.4	0.7	0.0	0.0	4.5
5	2.000	1.4	0.1	0.3	0.0	0.0	1.8
5	5.000	0.4	0.0	0.1	0.0	0.0	0.5
5	10.000	0.2	0.0	0.0	0.0	0.0	0.2
				O^{2+}			
6	0.001	0.0	0.5	0.0	0.0	0.0	0.5
6	0.002	0.0	25.7	0.0	0.0	0.0	25.7
6	0.005	0.0	127.5	15.8	0.0	0.0	143.3
6	0.010	0.0	117.5	66.5	0.0	0.0	184.0
6	0.020	0.0	65.2	81.0	0.0	0.0	146.2
6	0.050	0.1	20.8	43.1	0.0	0.0	64.0
6	0.100	1.4	7.8	19.5	0.0	0.0	28.7
6	0.200	3.7	2.8	7.8	0.0	0.0	14.2
6	0.500	3.1	0.7	2.1	0.0	0.0	5.9
6	1.000	1.6	0.2	0.8	0.0	0.0	2.6
6	2.000	0.7	0.1	0.3	0.0	0.0	1.1
6	5.000	0.2	0.0	0.1	0.0	0.0	0.3
6	10.000	0.1	0.0	0.0	0.0	0.0	0.1
				O^{+}			
7	0.001	0.0	0.2	0.0	0.0	0.0	0.2
7	0.002	0.0	11.1	0.0	0.0	0.0	11.1
7	0.005	0.0	55.2	14.0	0.0	0.0	69.3
7	0.010	0.0	50.9	59.0	0.0	0.0	109.9
7	0.020	0.0	28.2	71.9	0.0	0.0	100.1

Table 5. DR rates for O^{Z+} (continued)

N	T [keV]	1S	2S	2P	3S	3P	TOTAL
7	0.050	0.0	9.0	38.2	0.0	0.0	47.2
7	0.100	0.5	3.4	17.3	0.0	0.0	21.1
7	0.200	1.2	1.2	6.9	0.0	0.0	9.3
7	0.500	1.0	0.3	1.9	0.0	0.0	3.2
7	1.000	0.5	0.1	0.7	0.0	0.0	1.3
7	2.000	0.2	0.0	0.2	0.0	0.0	0.5
7	5.000	0.1	0.0	0.1	0.0	0.0	0.1
7	10.000	0.0	0.0	0.0	0.0	0.0	0.0

Table 6. DR rates α^{DR} [cm^3/s] for the Ne^{Z+} ions ($Z_c = 10$). Notation as in Table 4.

N	T [keV]	1S	2S	2P	3S	3P	TOTAL
				Ne^{9+}			
1	0.001	0.0	0.0	0.0	0.0	0.0	0.0
1	0.002	0.0	0.0	0.0	0.0	0.0	0.0
1	0.005	0.0	0.0	0.0	0.0	0.0	0.0
1	0.010	0.0	0.0	0.0	0.0	0.0	0.0
1	0.020	0.0	0.0	0.0	0.0	0.0	0.0
1	0.050	0.0	0.0	0.0	0.0	0.0	0.0
1	0.100	0.7	0.0	0.0	0.0	0.0	0.7
1	0.200	9.1	0.0	0.0	0.0	0.0	9.1
1	0.500	20.3	0.0	0.0	0.0	0.0	20.3
1	1.000	14.8	0.0	0.0	0.0	0.0	14.8
1	2.000	7.5	0.0	0.0	0.0	0.0	7.5
1	5.000	2.4	0.0	0.0	0.0	0.0	2.4
1	10.000	0.9	0.0	0.0	0.0	0.0	0.9
				Ne^{8+}			
2	0.001	0.0	0.0	0.0	0.0	0.0	0.0
2	0.002	0.0	0.0	0.0	0.0	0.0	0.0
2	0.005	0.0	0.0	0.0	0.0	0.0	0.0
2	0.010	0.0	0.0	0.0	0.0	0.0	0.0
2	0.020	0.0	0.0	0.0	0.0	0.0	0.0
2	0.050	0.0	0.0	0.0	0.0	0.0	0.0
2	0.100	1.2	0.0	0.0	0.0	0.0	1.2
2	0.200	11.9	0.0	0.0	0.0	0.0	11.9
2	0.500	21.9	0.0	0.0	0.0	0.0	21.9
2	1.000	15.0	0.0	0.0	0.0	0.0	15.0
2	2.000	7.4	0.0	0.0	0.0	0.0	7.4
2	5.000	2.3	0.0	0.0	0.0	0.0	2.3
2	10.000	0.9	0.0	0.0	0.0	0.0	0.9

Table 6. DR rates for Ne^{Z+} (continued)

N	T [keV]	1S	2S	2P	3S	3P	TOTAL
				Ne^{7+}			
3	0.001	0.0	0.2	0.0	0.0	0.0	0.2
3	0.002	0.0	52.7	0.0	0.0	0.0	52.7
3	0.005	0.0	623.6	0.7	0.0	0.0	624.3
3	0.010	0.0	767.3	20.8	0.0	0.0	788.1
3	0.020	0.0	492.0	65.5	0.0	0.0	557.4
3	0.050	0.0	171.5	61.5	0.0	0.0	233.0
3	0.100	1.2	65.8	33.7	0.0	0.0	100.6
3	0.200	10.3	23.7	14.8	0.0	0.0	48.8
3	0.500	17.8	5.9	4.3	0.0	0.0	28.0
3	1.000	11.9	2.0	1.6	0.0	0.0	15.6
3	2.000	5.8	0.7	0.6	0.0	0.0	7.1
3	5.000	1.8	0.2	0.1	0.0	0.0	2.1
3	10.000	0.7	0.1	0.1	0.0	0.0	0.8
				Ne^{6+}			
4	0.001	0.0	0.2	0.0	0.0	0.0	0.2
4	0.002	0.0	35.5	0.0	0.0	0.0	35.5
4	0.005	0.0	419.9	0.8	0.0	0.0	420.7
4	0.010	0.0	516.6	22.0	0.0	0.0	538.7
4	0.020	0.0	331.3	69.4	0.0	0.0	400.7
4	0.050	0.0	115.5	65.2	0.0	0.0	180.7
4	0.100	0.8	44.3	35.7	0.0	0.0	80.8
4	0.200	6.9	16.0	15.7	0.0	0.0	38.6
4	0.500	11.5	4.0	4.5	0.0	0.0	20.1
4	1.000	7.7	1.4	1.7	0.0	0.0	10.7
4	2.000	3.7	0.5	0.6	0.0	0.0	4.8
4	5.000	1.1	0.1	0.2	0.0	0.0	1.4
4	10.000	0.4	0.0	0.1	0.0	0.0	0.5
				Ne^{5+}			
5	0.001	0.0	0.1	0.0	0.0	0.0	0.1
5	0.002	0.0	20.8	0.0	0.0	0.0	20.8
5	0.005	0.0	246.2	0.9	0.0	0.0	247.1
5	0.010	0.0	302.9	23.9	0.0	0.0	326.8
5	0.020	0.0	194.2	75.1	0.0	0.0	269.3
5	0.050	0.0	67.7	70.5	0.0	0.0	138.2
5	0.100	0.5	26.0	38.6	0.0	0.0	65.0
5	0.200	3.7	9.4	17.0	0.0	0.0	30.0
5	0.500	6.0	2.3	4.9	0.0	0.0	13.3
5	1.000	4.0	0.8	1.8	0.0	0.0	6.6
5	2.000	1.9	0.3	0.7	0.0	0.0	2.9
5	5.000	0.6	0.1	0.2	0.0	0.0	0.8
5	10.000	0.2	0.0	0.1	0.0	0.0	0.3

Table 6. DR rates for Ne^{Z+} (continued)

N	T [keV]	1S	2S	2P	3S	3P	TOTAL
				Ne^{4+}			
6	0.001	0.0	0.1	0.0	0.0	0.0	0.1
6	0.002	0.0	11.7	0.0	0.0	0.0	11.7
6	0.005	0.0	139.0	0.9	0.0	0.0	139.9
6	0.010	0.0	171.0	26.2	0.0	0.0	197.2
6	0.020	0.0	109.7	82.4	0.0	0.0	192.1
6	0.050	0.0	38.2	77.4	0.0	0.0	115.6
6	0.100	0.2	14.7	42.4	0.0	0.0	57.2
6	0.200	1.6	5.3	18.6	0.0	0.0	25.5
6	0.500	2.5	1.3	5.4	0.0	0.0	9.2
6	1.000	1.7	0.5	2.0	0.0	0.0	4.1
6	2.000	0.8	0.2	0.7	0.0	0.0	1.7
6	5.000	0.2	0.0	0.2	0.0	0.0	0.5
6	10.000	0.1	0.0	0.1	0.0	0.0	0.2
				Ne^{3+}			
7	0.001	0.0	0.0	0.0	0.0	0.0	0.0
7	0.002	0.0	6.4	0.0	0.0	0.0	6.4
7	0.005	0.0	75.3	1.0	0.0	0.0	76.3
7	0.010	0.0	92.6	29.0	0.0	0.0	121.6
7	0.020	0.0	59.4	91.4	0.0	0.0	150.7
7	0.050	0.0	20.7	85.8	0.0	0.0	106.5
7	0.100	0.1	7.9	47.0	0.0	0.0	55.0
7	0.200	0.5	2.9	20.7	0.0	0.0	24.1
7	0.500	0.9	0.7	6.0	0.0	0.0	7.5
7	1.000	0.6	0.2	2.2	0.0	0.0	3.0
7	2.000	0.3	0.1	0.8	0.0	0.0	1.2
7	5.000	0.1	0.0	0.2	0.0	0.0	0.3
7	10.000	0.0	0.0	0.1	0.0	0.0	0.1
				Ne^{2+}			
8	0.001	0.0	0.0	0.0	0.0	0.0	0.0
8	0.002	0.0	3.1	0.0	0.0	0.0	3.1
8	0.005	0.0	37.2	1.2	0.0	0.0	38.3
8	0.010	0.0	45.7	32.4	0.0	0.0	78.2
8	0.020	0.0	29.3	102.1	0.0	0.0	131.4
8	0.050	0.0	10.2	95.9	0.0	0.0	106.1
8	0.100	0.0	3.9	52.5	0.0	0.0	56.4
8	0.200	0.1	1.4	23.1	0.0	0.0	24.7
8	0.500	0.2	0.4	6.7	0.0	0.0	7.3
8	1.000	0.2	0.1	2.5	0.0	0.0	2.7
8	2.000	0.1	0.0	0.9	0.0	0.0	1.0
8	5.000	0.0	0.0	0.2	0.0	0.0	0.3
8	10.000	0.0	0.0	0.1	0.0	0.0	0.1

Table 6. DR rates for Ne^{Z+} (continued)

N	T [keV]	1S	2S	2P	3S	3P	TOTAL
				Ne^{+}			
9	0.001	0.0	0.0	0.0	0.0	0.0	0.0
9	0.002	0.0	1.0	0.0	0.0	0.0	1.0
9	0.005	0.0	11.3	1.0	0.0	0.0	12.3
9	0.010	0.0	13.9	29.2	0.0	0.0	43.1
9	0.020	0.0	8.9	91.8	0.0	0.0	100.7
9	0.050	0.0	3.1	86.3	0.0	0.0	89.4
9	0.100	0.0	1.2	47.2	0.0	0.0	48.4
9	0.200	0.0	0.4	20.8	0.0	0.0	21.2
9	0.500	0.0	0.1	6.0	0.0	0.0	6.1
9	1.000	0.0	0.0	2.2	0.0	0.0	2.3
9	2.000	0.0	0.0	0.8	0.0	0.0	0.8
9	5.000	0.0	0.0	0.2	0.0	0.0	0.2
9	10.000	0.0	0.0	0.1	0.0	0.0	0.1

Table 7. DR rates α^{DR} [cm^3/s] for the Mg^{Z+} ions ($Z_c = 12$). Notation as in Table 4.

N	T [keV]	1S	2S	2P	3S	3P	TOTAL
				Mg^{11+}			
1	0.001	0.0	0.0	0.0	0.0	0.0	0.0
1	0.002	0.0	0.0	0.0	0.0	0.0	0.0
1	0.005	0.0	0.0	0.0	0.0	0.0	0.0
1	0.010	0.0	0.0	0.0	0.0	0.0	0.0
1	0.020	0.0	0.0	0.0	0.0	0.0	0.0
1	0.050	0.0	0.0	0.0	0.0	0.0	0.0
1	0.100	0.1	0.0	0.0	0.0	0.0	0.1
1	0.200	3.3	0.0	0.0	0.0	0.0	3.3
1	0.500	17.3	0.0	0.0	0.0	0.0	17.3
1	1.000	16.8	0.0	0.0	0.0	0.0	16.8
1	2.000	9.9	0.0	0.0	0.0	0.0	9.9
1	5.000	3.4	0.0	0.0	0.0	0.0	3.4
1	10.000	1.3	0.0	0.0	0.0	0.0	1.3
				Mg^{10+}			
2	0.001	0.0	0.0	0.0	0.0	0.0	0.0
2	0.002	0.0	0.0	0.0	0.0	0.0	0.0
2	0.005	0.0	0.0	0.0	0.0	0.0	0.0
2	0.010	0.0	0.0	0.0	0.0	0.0	0.0
2	0.020	0.0	0.0	0.0	0.0	0.0	0.0
2	0.050	0.0	0.0	0.0	0.0	0.0	0.0
2	0.100	0.1	0.0	0.0	0.0	0.0	0.1
2	0.200	4.6	0.0	0.0	0.0	0.0	4.6
2	0.500	19.5	0.0	0.0	0.0	0.0	19.5

Table 7. DR rates for Mg^{Z+} (continued)

N	T [keV]	1S	2S	2P	3S	3P	TOTAL
2	1.000	17.6	0.0	0.0	0.0	0.0	17.6
2	2.000	9.9	0.0	0.0	0.0	0.0	9.9
2	5.000	3.3	0.0	0.0	0.0	0.0	3.3
2	10.000	1.3	0.0	0.0	0.0	0.0	1.3
				Mg^{9+}			
3	0.001	0.0	0.0	0.0	0.0	0.0	0.0
3	0.002	0.0	23.1	0.0	0.0	0.0	23.1
3	0.005	0.0	581.9	0.0	0.0	0.0	581.9
3	0.010	0.0	920.5	4.2	0.0	0.0	924.7
3	0.020	0.0	669.3	44.3	0.0	0.0	713.6
3	0.050	0.0	251.6	85.9	0.0	0.0	337.4
3	0.100	0.1	98.9	59.9	0.0	0.0	158.9
3	0.200	4.0	36.2	29.7	0.0	0.0	69.9
3	0.500	15.6	9.1	9.2	0.0	0.0	33.9
3	1.000	13.8	3.1	3.5	0.0	0.0	20.4
3	2.000	7.7	1.1	1.3	0.0	0.0	10.0
3	5.000	2.6	0.3	0.3	0.0	0.0	3.1
3	10.000	1.0	0.1	0.1	0.0	0.0	1.2
				Mg^{8+}			
4	0.001	0.0	0.0	0.0	0.0	0.0	0.0
4	0.002	0.0	15.6	0.0	0.0	0.0	15.6
4	0.005	0.0	391.8	0.0	0.0	0.0	391.8
4	0.010	0.0	619.8	4.5	0.0	0.0	624.3
4	0.020	0.0	450.7	46.9	0.0	0.0	497.6
4	0.050	0.0	169.4	91.0	0.0	0.0	260.4
4	0.100	0.1	66.6	63.5	0.0	0.0	130.2
4	0.200	2.5	24.3	31.5	0.0	0.0	58.4
4	0.500	9.5	6.1	9.8	0.0	0.0	25.4
4	1.000	8.3	2.1	3.7	0.0	0.0	14.1
4	2.000	4.6	0.7	1.4	0.0	0.0	6.7
4	5.000	1.5	0.2	0.3	0.0	0.0	2.0
4	10.000	0.6	0.1	0.1	0.0	0.0	0.8
				Mg^{7+}			
5	0.001	0.0	0.0	0.0	0.0	0.0	0.0
5	0.002	0.0	9.1	0.0	0.0	0.0	9.1
5	0.005	0.0	229.7	0.0	0.0	0.0	229.8
5	0.010	0.0	363.4	4.8	0.0	0.0	368.3
5	0.020	0.0	264.3	50.8	0.0	0.0	315.0
5	0.050	0.0	99.3	98.5	0.0	0.0	197.8
5	0.100	0.0	39.1	68.7	0.0	0.0	107.8
5	0.200	1.2	14.3	34.1	0.0	0.0	49.6
5	0.500	4.5	3.6	10.6	0.0	0.0	18.6
5	1.000	3.8	1.2	4.0	0.0	0.0	9.1

Table 7. DR rates for Mg^{Z+} (continued)

N	T [keV]	1S	2S	2P	3S	3P	TOTAL
5	2.000	2.1	0.4	1.5	0.0	0.0	4.0
5	5.000	0.7	0.1	0.4	0.0	0.0	1.2
5	10.000	0.3	0.0	0.1	0.0	0.0	0.4
				Mg^{6+}			
6	0.001	0.0	0.0	0.0	0.0	0.0	0.0
6	0.002	0.0	5.2	0.0	0.0	0.0	5.2
6	0.005	0.0	129.7	0.0	0.0	0.0	129.7
6	0.010	0.0	205.2	5.3	0.0	0.0	210.5
6	0.020	0.0	149.2	55.7	0.0	0.0	204.9
6	0.050	0.0	56.1	108.1	0.0	0.0	164.2
6	0.100	0.0	22.1	75.4	0.0	0.0	97.4
6	0.200	0.4	8.1	37.4	0.0	0.0	45.9
6	0.500	1.6	2.0	11.6	0.0	0.0	15.2
6	1.000	1.4	0.7	4.4	0.0	0.0	6.5
6	2.000	0.8	0.2	1.6	0.0	0.0	2.6
6	5.000	0.3	0.1	0.4	0.0	0.0	0.7
6	10.000	0.1	0.0	0.1	0.0	0.0	0.3
				Mg^{5+}			
7	0.001	0.0	0.0	0.0	0.0	0.0	0.0
7	0.002	0.0	2.8	0.0	0.0	0.0	2.8
7	0.005	0.0	70.2	0.0	0.0	0.0	70.3
7	0.010	0.0	111.1	5.9	0.0	0.0	117.0
7	0.020	0.0	80.8	61.8	0.0	0.0	142.6
7	0.050	0.0	30.4	119.9	0.0	0.0	150.2
7	0.100	0.0	11.9	83.6	0.0	0.0	95.5
7	0.200	0.1	4.4	41.5	0.0	0.0	46.0
7	0.500	0.4	1.1	12.9	0.0	0.0	14.4
7	1.000	0.4	0.4	4.9	0.0	0.0	5.6
7	2.000	0.2	0.1	1.8	0.0	0.0	2.1
7	5.000	0.1	0.0	0.5	0.0	0.0	0.6
7	10.000	0.0	0.0	0.2	0.0	0.0	0.2
				Mg^{4+}			
8	0.001	0.0	0.0	0.0	0.0	0.0	0.0
8	0.002	0.0	1.4	0.0	0.0	0.0	1.4
8	0.005	0.0	34.7	0.0	0.0	0.0	34.7
8	0.010	0.0	54.9	6.6	0.0	0.0	61.4
8	0.020	0.0	39.9	69.0	0.0	0.0	108.9
8	0.050	0.0	15.0	133.9	0.0	0.0	148.9
8	0.100	0.0	5.9	93.4	0.0	0.0	99.3
8	0.200	0.0	2.2	46.4	0.0	0.0	48.5
8	0.500	0.1	0.5	14.4	0.0	0.0	15.0
8	1.000	0.1	0.2	5.4	0.0	0.0	5.7
8	2.000	0.0	0.1	2.0	0.0	0.0	2.1

Table 7. DR rates for Mg^{Z+} (continued)

N	T [keV]	1S	2S	2P	3S	3P	TOTAL
8	5.000	0.0	0.0	0.5	0.0	0.0	0.5
8	10.000	0.0	0.0	0.2	0.0	0.0	0.2
				Mg^{3+}			
9	0.001	0.0	0.0	0.0	0.0	0.0	0.0
9	0.002	0.0	0.5	0.0	0.0	0.0	0.5
9	0.005	0.0	13.2	0.0	0.0	0.0	13.2
9	0.010	0.0	20.8	7.4	0.0	0.0	28.2
9	0.020	0.0	15.1	77.6	0.0	0.0	92.8
9	0.050	0.0	5.7	150.6	0.0	0.0	156.3
9	0.100	0.0	2.2	105.0	0.0	0.0	107.2
9	0.200	0.0	0.8	52.1	0.0	0.0	53.0
9	0.500	0.0	0.2	16.2	0.0	0.0	16.4
9	1.000	0.0	0.1	6.1	0.0	0.0	6.2
9	2.000	0.0	0.0	2.2	0.0	0.0	2.3
9	5.000	0.0	0.0	0.6	0.0	0.0	0.6
9	10.000	0.0	0.0	0.2	0.0	0.0	0.2
				Mg^{2+}			
10	0.001	0.0	0.0	0.0	0.0	0.0	0.0
10	0.002	0.0	0.0	0.0	0.0	0.0	0.0
10	0.005	0.0	0.0	0.0	0.0	0.0	0.0
10	0.010	0.0	0.0	7.3	0.0	0.0	7.3
10	0.020	0.0	0.0	76.6	0.0	0.0	76.6
10	0.050	0.0	0.0	148.6	0.0	0.0	148.6
10	0.100	0.0	0.0	103.6	0.0	0.0	103.6
10	0.200	0.0	0.0	51.4	0.0	0.0	51.4
10	0.500	0.0	0.0	15.9	0.0	0.0	16.0
10	1.000	0.0	0.0	6.0	0.0	0.0	6.0
10	2.000	0.0	0.0	2.2	0.0	0.0	2.2
10	5.000	0.0	0.0	0.6	0.0	0.0	0.6
10	10.000	0.0	0.0	0.2	0.0	0.0	0.2
				Mg^{+}			
11	0.001	0.0	0.0	0.0	32.5	264.8	297.3
11	0.002	0.0	0.0	0.0	19.9	410.3	430.2
11	0.005	0.0	0.0	0.0	7.0	251.9	258.9
11	0.010	0.0	0.0	4.7	2.8	119.7	127.1
11	0.020	0.0	0.0	49.5	1.0	49.0	99.6
11	0.050	0.0	0.0	96.0	0.3	13.6	109.8
11	0.100	0.0	0.0	66.9	0.1	4.9	72.0
11	0.200	0.0	0.0	33.2	0.0	1.8	35.0
11	0.500	0.0	0.0	10.3	0.0	0.5	10.8
11	1.000	0.0	0.0	3.9	0.0	0.2	4.1
11	2.000	0.0	0.0	1.4	0.0	0.1	1.5

Table 7. DR rates for Mg^{Z+} (continued)

N	T [keV]	1S	2S	2P	3S	3P	TOTAL
11	5.000	0.0	0.0	0.4	0.0	0.0	0.4
11	10.000	0.0	0.0	0.1	0.0	0.0	0.1

Table 8. DR rates α^{DR} [cm^3/s] for the P^{Z+} ions ($Z_c = 15$). Notation as in Table 4.

N	T [keV]	1S	2S	2P	3S	3P	TOTAL
				P^{14+}			
1	0.001	0.0	0.0	0.0	0.0	0.0	0.0
1	0.002	0.0	0.0	0.0	0.0	0.0	0.0
1	0.005	0.0	0.0	0.0	0.0	0.0	0.0
1	0.010	0.0	0.0	0.0	0.0	0.0	0.0
1	0.020	0.0	0.0	0.0	0.0	0.0	0.0
1	0.050	0.0	0.0	0.0	0.0	0.0	0.0
1	0.100	0.0	0.0	0.0	0.0	0.0	0.0
1	0.200	0.4	0.0	0.0	0.0	0.0	0.4
1	0.500	9.4	0.0	0.0	0.0	0.0	9.4
1	1.000	15.4	0.0	0.0	0.0	0.0	15.4
1	2.000	11.7	0.0	0.0	0.0	0.0	11.7
1	5.000	4.7	0.0	0.0	0.0	0.0	4.7
1	10.000	1.9	0.0	0.0	0.0	0.0	1.9
				P^{13+}			
2	0.001	0.0	0.0	0.0	0.0	0.0	0.0
2	0.002	0.0	0.0	0.0	0.0	0.0	0.0
2	0.005	0.0	0.0	0.0	0.0	0.0	0.0
2	0.010	0.0	0.0	0.0	0.0	0.0	0.0
2	0.020	0.0	0.0	0.0	0.0	0.0	0.0
2	0.050	0.0	0.0	0.0	0.0	0.0	0.0
2	0.100	0.0	0.0	0.0	0.0	0.0	0.0
2	0.200	0.6	0.0	0.0	0.0	0.0	0.6
2	0.500	11.3	0.0	0.0	0.0	0.0	11.3
2	1.000	17.0	0.0	0.0	0.0	0.0	17.0
2	2.000	12.3	0.0	0.0	0.0	0.0	12.3
2	5.000	4.8	0.0	0.0	0.0	0.0	4.8
2	10.000	2.0	0.0	0.0	0.0	0.0	2.0
				P^{12+}			
3	0.001	0.0	0.0	0.0	0.0	0.0	0.0
3	0.002	0.0	7.8	0.0	0.0	0.0	7.8
3	0.005	0.0	487.0	0.0	0.0	0.0	487.0
3	0.010	0.0	1041.6	0.1	0.0	0.0	1041.7
3	0.020	0.0	880.6	12.6	0.0	0.0	893.2
3	0.050	0.0	362.3	96.9	0.0	0.0	459.2

Table 8. DR rates for P^{Z+} (continued)

N	T [keV]	1S	2S	2P	3S	3P	TOTAL
3	0.100	0.0	146.9	106.8	0.0	0.0	253.6
3	0.200	0.5	54.5	66.6	0.0	0.0	121.6
3	0.500	8.9	13.8	23.7	0.0	0.0	46.4
3	1.000	12.9	4.8	9.4	0.0	0.0	27.1
3	2.000	9.2	1.7	3.5	0.0	0.0	14.4
3	5.000	3.6	0.4	0.9	0.0	0.0	4.9
3	10.000	1.5	0.1	0.3	0.0	0.0	1.9
				P^{11+}			
4	0.001	0.0	0.0	0.0	0.0	0.0	0.0
4	0.002	0.0	5.3	0.0	0.0	0.0	5.3
4	0.005	0.0	327.9	0.0	0.0	0.0	327.9
4	0.010	0.0	701.4	0.1	0.0	0.0	701.5
4	0.020	0.0	593.0	13.4	0.0	0.0	606.4
4	0.050	0.0	244.0	102.7	0.0	0.0	346.7
4	0.100	0.0	98.9	113.2	0.0	0.0	212.1
4	0.200	0.3	36.7	70.6	0.0	0.0	107.6
4	0.500	4.9	9.3	25.1	0.0	0.0	39.4
4	1.000	7.0	3.2	10.0	0.0	0.0	20.2
4	2.000	5.0	1.1	3.7	0.0	0.0	9.8
4	5.000	1.9	0.3	1.0	0.0	0.0	3.2
4	10.000	0.8	0.1	0.3	0.0	0.0	1.2
				P^{10+}			
5	0.001	0.0	0.0	0.0	0.0	0.0	0.0
5	0.002	0.0	3.1	0.0	0.0	0.0	3.1
5	0.005	0.0	192.3	0.0	0.0	0.0	192.3
5	0.010	0.0	411.3	0.1	0.0	0.0	411.4
5	0.020	0.0	347.7	14.5	0.0	0.0	362.2
5	0.050	0.0	143.1	111.1	0.0	0.0	254.2
5	0.100	0.0	58.0	122.5	0.0	0.0	180.4
5	0.200	0.1	21.5	76.4	0.0	0.0	98.1
5	0.500	2.0	5.5	27.2	0.0	0.0	34.6
5	1.000	2.8	1.9	10.8	0.0	0.0	15.4
5	2.000	2.0	0.7	4.0	0.0	0.0	6.7
5	5.000	0.8	0.2	1.1	0.0	0.0	2.0
5	10.000	0.3	0.1	0.4	0.0	0.0	0.7
				P^{9+}			
6	0.001	0.0	0.0	0.0	0.0	0.0	0.0
6	0.002	0.0	1.7	0.0	0.0	0.0	1.7
6	0.005	0.0	108.6	0.0	0.0	0.0	108.6
6	0.010	0.0	232.2	0.2	0.0	0.0	232.3
6	0.020	0.0	196.3	15.9	0.0	0.0	212.2
6	0.050	0.0	80.8	121.9	0.0	0.0	202.7
6	0.100	0.0	32.7	134.4	0.0	0.0	167.1

Table 8. DR rates for P^{Z+} (continued)

N	T [keV]	1S	2S	2P	3S	3P	TOTAL
6	0.200	0.0	12.1	83.9	0.0	0.0	96.1
6	0.500	0.6	3.1	29.8	0.0	0.0	33.5
6	1.000	0.8	1.1	11.8	0.0	0.0	13.7
6	2.000	0.6	0.4	4.4	0.0	0.0	5.4
6	5.000	0.2	0.1	1.2	0.0	0.0	1.5
6	10.000	0.1	0.0	0.4	0.0	0.0	0.5
				P^{8+}			
7	0.001	0.0	0.0	0.0	0.0	0.0	0.0
7	0.002	0.0	0.9	0.0	0.0	0.0	0.9
7	0.005	0.0	58.8	0.0	0.0	0.0	58.8
7	0.010	0.0	125.7	0.2	0.0	0.0	125.9
7	0.020	0.0	106.3	17.6	0.0	0.0	123.9
7	0.050	0.0	43.7	135.2	0.0	0.0	178.9
7	0.100	0.0	17.7	149.0	0.0	0.0	166.7
7	0.200	0.0	6.6	93.0	0.0	0.0	99.6
7	0.500	0.1	1.7	33.1	0.0	0.0	34.9
7	1.000	0.2	0.6	13.1	0.0	0.0	13.9
7	2.000	0.1	0.2	4.9	0.0	0.0	5.2
7	5.000	0.0	0.0	1.3	0.0	0.0	1.4
7	10.000	0.0	0.0	0.5	0.0	0.0	0.5
				P^{7+}			
8	0.001	0.0	0.0	0.0	0.0	0.0	0.0
8	0.002	0.0	0.5	0.0	0.0	0.0	0.5
8	0.005	0.0	29.0	0.0	0.0	0.0	29.0
8	0.010	0.0	62.1	0.2	0.0	0.0	62.3
8	0.020	0.0	52.5	19.7	0.0	0.0	72.2
8	0.050	0.0	21.6	151.1	0.0	0.0	172.7
8	0.100	0.0	8.8	166.5	0.0	0.0	175.3
8	0.200	0.0	3.2	103.9	0.0	0.0	107.2
8	0.500	0.0	0.8	37.0	0.0	0.0	37.8
8	1.000	0.0	0.3	14.6	0.0	0.0	15.0
8	2.000	0.0	0.1	5.5	0.0	0.0	5.6
8	5.000	0.0	0.0	1.4	0.0	0.0	1.5
8	10.000	0.0	0.0	0.5	0.0	0.0	0.5
				P^{6+}			
9	0.001	0.0	0.0	0.0	0.0	0.0	0.0
9	0.002	0.0	0.2	0.0	0.0	0.0	0.2
9	0.005	0.0	11.0	0.0	0.0	0.0	11.0
9	0.010	0.0	23.5	0.2	0.0	0.0	23.8
9	0.020	0.0	19.9	22.2	0.0	0.0	42.1
9	0.050	0.0	8.2	169.9	0.0	0.0	178.1
9	0.100	0.0	3.3	187.2	0.0	0.0	190.6
9	0.200	0.0	1.2	116.9	0.0	0.0	118.1

Table 8. DR rates for P^{Z+} (continued)

N	T [keV]	1S	2S	2P	3S	3P	TOTAL
9	0.500	0.0	0.3	41.6	0.0	0.0	41.9
9	1.000	0.0	0.1	16.5	0.0	0.0	16.6
9	2.000	0.0	0.0	6.2	0.0	0.0	6.2
9	5.000	0.0	0.0	1.6	0.0	0.0	1.6
9	10.000	0.0	0.0	0.6	0.0	0.0	0.6
				P^{5+}			
10	0.001	0.0	0.0	0.0	0.0	0.0	0.0
10	0.002	0.0	0.0	0.0	0.0	0.0	0.0
10	0.005	0.0	0.0	0.0	0.0	0.0	0.0
10	0.010	0.0	0.0	0.2	0.0	0.0	0.2
10	0.020	0.0	0.0	21.9	0.0	0.0	21.9
10	0.050	0.0	0.0	167.6	0.0	0.0	167.6
10	0.100	0.0	0.0	184.7	0.0	0.0	184.7
10	0.200	0.0	0.0	115.3	0.0	0.0	115.3
10	0.500	0.0	0.0	41.0	0.0	0.0	41.0
10	1.000	0.0	0.0	16.2	0.0	0.0	16.2
10	2.000	0.0	0.0	6.1	0.0	0.0	6.1
10	5.000	0.0	0.0	1.6	0.0	0.0	1.6
10	10.000	0.0	0.0	0.6	0.0	0.0	0.6
				P^{4+}			
11	0.001	0.0	0.0	0.0	153.1	7.3	160.4
11	0.002	0.0	0.0	0.0	204.7	109.3	314.0
11	0.005	0.0	0.0	0.0	115.0	262.0	377.0
11	0.010	0.0	0.0	0.2	53.1	196.0	249.3
11	0.020	0.0	0.0	17.7	21.4	100.8	139.9
11	0.050	0.0	0.0	135.4	5.9	31.9	173.2
11	0.100	0.0	0.0	149.2	2.1	12.2	163.5
11	0.200	0.0	0.0	93.1	0.8	4.5	98.4
11	0.500	0.0	0.0	33.1	0.2	1.2	34.5
11	1.000	0.0	0.0	13.1	0.1	0.4	13.6
11	2.000	0.0	0.0	4.9	0.0	0.1	5.1
11	5.000	0.0	0.0	1.3	0.0	0.0	1.3
11	10.000	0.0	0.0	0.5	0.0	0.0	0.5
				P^{3+}			
12	0.001	0.0	0.0	0.0	124.5	14.9	139.4
12	0.002	0.0	0.0	0.0	206.4	223.0	429.4
12	0.005	0.0	0.0	0.0	131.9	534.6	666.6
12	0.010	0.0	0.0	0.1	63.5	400.0	463.7
12	0.020	0.0	0.0	14.3	26.2	205.7	246.3
12	0.050	0.0	0.0	109.7	7.3	65.2	182.2
12	0.100	0.0	0.0	120.9	2.7	24.8	148.4
12	0.200	0.0	0.0	75.5	1.0	9.1	85.6
12	0.500	0.0	0.0	26.9	0.2	2.4	29.5

Table 8. DR rates for P^{Z+} (continued)

N	T [keV]	1S	2S	2P	3S	3P	TOTAL
12	1.000	0.0	0.0	10.6	0.1	0.8	11.6
12	2.000	0.0	0.0	4.0	0.0	0.3	4.3
12	5.000	0.0	0.0	1.0	0.0	0.1	1.1
12	10.000	0.0	0.0	0.4	0.0	0.0	0.4
				P^{2+}			
13	0.001	0.0	0.0	0.0	95.9	21.9	117.8
13	0.002	0.0	0.0	0.0	167.7	327.9	495.6
13	0.005	0.0	0.0	0.0	110.7	786.1	896.7
13	0.010	0.0	0.0	0.1	53.9	588.1	642.1
13	0.020	0.0	0.0	11.6	22.4	302.5	336.5
13	0.050	0.0	0.0	89.2	6.2	95.8	191.2
13	0.100	0.0	0.0	98.3	2.3	36.5	137.1
13	0.200	0.0	0.0	61.4	0.8	13.4	75.6
13	0.500	0.0	0.0	21.8	0.2	3.5	25.5
13	1.000	0.0	0.0	8.6	0.1	1.2	10.0
13	2.000	0.0	0.0	3.2	0.0	0.4	3.7
13	5.000	0.0	0.0	0.8	0.0	0.1	1.0
13	10.000	0.0	0.0	0.3	0.0	0.0	0.3
				P^{+}			
14	0.001	0.0	0.0	0.0	42.8	22.0	64.8
14	0.002	0.0	0.0	0.0	76.5	329.4	405.9
14	0.005	0.0	0.0	0.0	51.2	789.6	840.8
14	0.010	0.0	0.0	0.1	25.0	590.8	615.9
14	0.020	0.0	0.0	7.6	10.4	303.8	321.8
14	0.050	0.0	0.0	58.2	2.9	96.2	157.3
14	0.100	0.0	0.0	64.1	1.1	36.7	101.8
14	0.200	0.0	0.0	40.0	0.4	13.5	53.9
14	0.500	0.0	0.0	14.2	0.1	3.5	17.8
14	1.000	0.0	0.0	5.6	0.0	1.2	6.9
14	2.000	0.0	0.0	2.1	0.0	0.4	2.6
14	5.000	0.0	0.0	0.6	0.0	0.1	0.7
14	10.000	0.0	0.0	0.2	0.0	0.0	0.2

Table 9. DR rates α^{DR} [cm^3/s] for the Ar^{Z+} ions ($Z_c = 18$). Notation as in Table 4.

N	T [keV]	1S	2S	2P	3S	3P	TOTAL
				Ar^{17+}			
1	0.001	0.0	0.0	0.0	0.0	0.0	0.0
1	0.002	0.0	0.0	0.0	0.0	0.0	0.0
1	0.005	0.0	0.0	0.0	0.0	0.0	0.0
1	0.010	0.0	0.0	0.0	0.0	0.0	0.0

Table 9. DR rates for Ar^{Z+} (continued)

N	T [keV]	1S	2S	2P	3S	3P	TOTAL
1	0.020	0.0	0.0	0.0	0.0	0.0	0.0
1	0.050	0.0	0.0	0.0	0.0	0.0	0.0
1	0.100	0.0	0.0	0.0	0.0	0.0	0.0
1	0.200	0.0	0.0	0.0	0.0	0.0	0.0
1	0.500	3.6	0.0	0.0	0.0	0.0	3.6
1	1.000	11.0	0.0	0.0	0.0	0.0	11.0
1	2.000	11.5	0.0	0.0	0.0	0.0	11.5
1	5.000	5.6	0.0	0.0	0.0	0.0	5.6
1	10.000	2.4	0.0	0.0	0.0	0.0	2.4
				Ar^{16+}			
2	0.001	0.0	0.0	0.0	0.0	0.0	0.0
2	0.002	0.0	0.0	0.0	0.0	0.0	0.0
2	0.005	0.0	0.0	0.0	0.0	0.0	0.0
2	0.010	0.0	0.0	0.0	0.0	0.0	0.0
2	0.020	0.0	0.0	0.0	0.0	0.0	0.0
2	0.050	0.0	0.0	0.0	0.0	0.0	0.0
2	0.100	0.0	0.0	0.0	0.0	0.0	0.0
2	0.200	0.0	0.0	0.0	0.0	0.0	0.0
2	0.500	4.6	0.0	0.0	0.0	0.0	4.6
2	1.000	12.8	0.0	0.0	0.0	0.0	12.8
2	2.000	12.6	0.0	0.0	0.0	0.0	12.6
2	5.000	5.9	0.0	0.0	0.0	0.0	5.9
2	10.000	2.6	0.0	0.0	0.0	0.0	2.6
				Ar^{15+}			
3	0.001	0.0	0.0	0.0	0.0	0.0	0.0
3	0.002	0.0	3.5	0.0	0.0	0.0	3.5
3	0.005	0.0	418.3	0.0	0.0	0.0	418.3
3	0.010	0.0	1108.3	0.0	0.0	0.0	1108.3
3	0.020	0.0	1042.9	1.7	0.0	0.0	1044.6
3	0.050	0.0	457.6	73.8	0.0	0.0	531.3
3	0.100	0.0	189.5	143.6	0.0	0.0	333.1
3	0.200	0.0	71.0	119.2	0.0	0.0	190.2
3	0.500	3.6	18.1	50.3	0.0	0.0	72.0
3	1.000	9.4	6.3	21.1	0.0	0.0	36.9
3	2.000	9.2	2.2	8.1	0.0	0.0	19.5
3	5.000	4.2	0.5	2.2	0.0	0.0	6.9
3	10.000	1.8	0.2	0.8	0.0	0.0	2.8
				Ar^{14+}			
4	0.001	0.0	0.0	0.0	0.0	0.0	0.0
4	0.002	0.0	2.4	0.0	0.0	0.0	2.4
4	0.005	0.0	281.7	0.0	0.0	0.0	281.7
4	0.010	0.0	746.3	0.0	0.0	0.0	746.3
4	0.020	0.0	702.2	1.9	0.0	0.0	704.1

Table 9. DR rates for Ar^{Z+} (continued)

N	T [keV]	1S	2S	2P	3S	3P	TOTAL
4	0.050	0.0	308.1	78.2	0.0	0.0	386.3
4	0.100	0.0	127.6	152.3	0.0	0.0	279.8
4	0.200	0.0	47.8	126.3	0.0	0.0	174.2
4	0.500	1.8	12.2	53.3	0.0	0.0	67.3
4	1.000	4.7	4.3	22.4	0.0	0.0	31.3
4	2.000	4.5	1.5	8.6	0.0	0.0	14.6
4	5.000	2.1	0.4	2.3	0.0	0.0	4.7
4	10.000	0.9	0.1	0.8	0.0	0.0	1.8
				Ar^{13+}			
5	0.001	0.0	0.0	0.0	0.0	0.0	0.0
5	0.002	0.0	1.4	0.0	0.0	0.0	1.4
5	0.005	0.0	165.2	0.0	0.0	0.0	165.2
5	0.010	0.0	437.6	0.0	0.0	0.0	437.6
5	0.020	0.0	411.8	2.0	0.0	0.0	413.8
5	0.050	0.0	180.7	84.6	0.0	0.0	265.3
5	0.100	0.0	74.8	164.7	0.0	0.0	239.6
5	0.200	0.0	28.1	136.7	0.0	0.0	164.7
5	0.500	0.6	7.2	57.7	0.0	0.0	65.5
5	1.000	1.6	2.5	24.2	0.0	0.0	28.3
5	2.000	1.5	0.9	9.3	0.0	0.0	11.7
5	5.000	0.7	0.2	2.5	0.0	0.0	3.4
5	10.000	0.3	0.1	0.9	0.0	0.0	1.3
				Ar^{12+}			
6	0.001	0.0	0.0	0.0	0.0	0.0	0.0
6	0.002	0.0	0.8	0.0	0.0	0.0	0.8
6	0.005	0.0	93.2	0.0	0.0	0.0	93.2
6	0.010	0.0	247.0	0.0	0.0	0.0	247.1
6	0.020	0.0	232.5	2.2	0.0	0.0	234.7
6	0.050	0.0	102.0	92.9	0.0	0.0	194.9
6	0.100	0.0	42.2	180.8	0.0	0.0	223.0
6	0.200	0.0	15.8	150.0	0.0	0.0	165.8
6	0.500	0.1	4.0	63.3	0.0	0.0	67.5
6	1.000	0.4	1.4	26.5	0.0	0.0	28.3
6	2.000	0.3	0.5	10.2	0.0	0.0	11.0
6	5.000	0.2	0.1	2.7	0.0	0.0	3.0
6	10.000	0.1	0.0	1.0	0.0	0.0	1.1
				Ar^{11+}			
7	0.001	0.0	0.0	0.0	0.0	0.0	0.0
7	0.002	0.0	0.4	0.0	0.0	0.0	0.4
7	0.005	0.0	50.5	0.0	0.0	0.0	50.5
7	0.010	0.0	133.8	0.0	0.0	0.0	133.8
7	0.020	0.0	125.9	2.4	0.0	0.0	128.3
7	0.050	0.0	55.2	103.0	0.0	0.0	158.2

Table 9. DR rates for Ar^{Z+} (continued)

N	T [keV]	1S	2S	2P	3S	3P	TOTAL
7	0.100	0.0	22.9	200.5	0.0	0.0	223.3
7	0.200	0.0	8.6	166.3	0.0	0.0	174.9
7	0.500	0.0	2.2	70.2	0.0	0.0	72.4
7	1.000	0.1	0.8	29.4	0.0	0.0	30.2
7	2.000	0.1	0.3	11.3	0.0	0.0	11.6
7	5.000	0.0	0.1	3.0	0.0	0.0	3.1
7	10.000	0.0	0.0	1.1	0.0	0.0	1.1
				Ar^{10+}			
8	0.001	0.0	0.0	0.0	0.0	0.0	0.0
8	0.002	0.0	0.2	0.0	0.0	0.0	0.2
8	0.005	0.0	24.9	0.0	0.0	0.0	24.9
8	0.010	0.0	66.1	0.0	0.0	0.0	66.1
8	0.020	0.0	62.2	2.7	0.0	0.0	64.9
8	0.050	0.0	27.3	115.1	0.0	0.0	142.3
8	0.100	0.0	11.3	224.0	0.0	0.0	235.3
8	0.200	0.0	4.2	185.9	0.0	0.0	190.1
8	0.500	0.0	1.1	78.4	0.0	0.0	79.5
8	1.000	0.0	0.4	32.9	0.0	0.0	33.3
8	2.000	0.0	0.1	12.7	0.0	0.0	12.8
8	5.000	0.0	0.0	3.4	0.0	0.0	3.4
8	10.000	0.0	0.0	1.2	0.0	0.0	1.2
				Ar^{9+}			
9	0.001	0.0	0.0	0.0	0.0	0.0	0.0
9	0.002	0.0	0.1	0.0	0.0	0.0	0.1
9	0.005	0.0	9.5	0.0	0.0	0.0	9.5
9	0.010	0.0	25.1	0.0	0.0	0.0	25.1
9	0.020	0.0	23.6	3.1	0.0	0.0	26.6
9	0.050	0.0	10.3	129.4	0.0	0.0	139.7
9	0.100	0.0	4.3	251.9	0.0	0.0	256.2
9	0.200	0.0	1.6	209.0	0.0	0.0	210.6
9	0.500	0.0	0.4	88.2	0.0	0.0	88.6
9	1.000	0.0	0.1	37.0	0.0	0.0	37.1
9	2.000	0.0	0.0	14.2	0.0	0.0	14.3
9	5.000	0.0	0.0	3.8	0.0	0.0	3.8
9	10.000	0.0	0.0	1.4	0.0	0.0	1.4
				Ar^{8+}			
10	0.001	0.0	0.0	0.0	0.0	0.0	0.0
10	0.002	0.0	0.0	0.0	0.0	0.0	0.0
10	0.005	0.0	0.0	0.0	0.0	0.0	0.0
10	0.010	0.0	0.0	0.0	0.0	0.0	0.0
10	0.020	0.0	0.0	3.0	0.0	0.0	3.0
10	0.050	0.0	0.0	127.6	0.0	0.0	127.6
10	0.100	0.0	0.0	248.5	0.0	0.0	248.5

Table 9. DR rates for Ar^{Z+} (continued)

N	T [keV]	1S	2S	2P	3S	3P	TOTAL
10	0.200	0.0	0.0	206.2	0.0	0.0	206.2
10	0.500	0.0	0.0	87.0	0.0	0.0	87.0
10	1.000	0.0	0.0	36.5	0.0	0.0	36.5
10	2.000	0.0	0.0	14.0	0.0	0.0	14.0
10	5.000	0.0	0.0	3.7	0.0	0.0	3.7
10	10.000	0.0	0.0	1.3	0.0	0.0	1.3
				Ar^{7+}			
11	0.001	0.0	0.0	0.0	114.4	0.0	114.4
11	0.002	0.0	0.0	0.0	317.5	8.4	325.9
11	0.005	0.0	0.0	0.0	276.6	143.0	419.6
11	0.010	0.0	0.0	0.0	147.7	205.9	353.6
11	0.020	0.0	0.0	2.4	64.2	146.9	213.5
11	0.050	0.0	0.0	103.1	18.4	56.6	178.1
11	0.100	0.0	0.0	200.7	6.8	23.0	230.5
11	0.200	0.0	0.0	166.5	2.4	8.7	177.7
11	0.500	0.0	0.0	70.3	0.6	2.3	73.2
11	1.000	0.0	0.0	29.5	0.2	0.8	30.5
11	2.000	0.0	0.0	11.3	0.1	0.3	11.7
11	5.000	0.0	0.0	3.0	0.0	0.1	3.1
11	10.000	0.0	0.0	1.1	0.0	0.0	1.1
				Ar^{6+}			
12	0.001	0.0	0.0	0.0	83.9	0.0	84.0
12	0.002	0.0	0.0	0.0	325.1	17.1	342.2
12	0.005	0.0	0.0	0.0	345.8	291.8	637.6
12	0.010	0.0	0.0	0.0	197.4	420.1	617.4
12	0.020	0.0	0.0	2.0	88.6	299.7	390.3
12	0.050	0.0	0.0	83.6	25.9	115.5	225.0
12	0.100	0.0	0.0	162.7	9.6	47.0	219.3
12	0.200	0.0	0.0	135.0	3.5	17.8	156.3
12	0.500	0.0	0.0	57.0	0.9	4.7	62.6
12	1.000	0.0	0.0	23.9	0.3	1.7	25.9
12	2.000	0.0	0.0	9.2	0.1	0.6	9.9
12	5.000	0.0	0.0	2.4	0.0	0.2	2.6
12	10.000	0.0	0.0	0.9	0.0	0.1	0.9
				Ar^{5+}			
13	0.001	0.0	0.0	0.0	76.2	0.1	76.2
13	0.002	0.0	0.0	0.0	320.6	25.1	345.7
13	0.005	0.0	0.0	0.0	358.4	429.0	787.5
13	0.010	0.0	0.0	0.0	208.0	617.6	825.6
13	0.020	0.0	0.0	1.6	94.2	440.6	536.4
13	0.050	0.0	0.0	67.9	27.6	169.9	265.4
13	0.100	0.0	0.0	132.3	10.3	69.1	211.6
13	0.200	0.0	0.0	109.7	3.7	26.2	139.7

Table 9. DR rates for Ar^{Z+} (continued)

N	T [keV]	1S	2S	2P	3S	3P	TOTAL
13	0.500	0.0	0.0	46.3	1.0	6.9	54.2
13	1.000	0.0	0.0	19.4	0.3	2.5	22.2
13	2.000	0.0	0.0	7.5	0.1	0.9	8.5
13	5.000	0.0	0.0	2.0	0.0	0.2	2.2
13	10.000	0.0	0.0	0.7	0.0	0.1	0.8
				Ar^{4+}			
14	0.001	0.0	0.0	0.0	66.3	0.1	66.4
14	0.002	0.0	0.0	0.0	289.0	31.5	320.5
14	0.005	0.0	0.0	0.0	329.9	538.7	868.7
14	0.010	0.0	0.0	0.0	192.8	775.6	968.3
14	0.020	0.0	0.0	1.3	87.6	553.3	642.2
14	0.050	0.0	0.0	55.4	25.8	213.3	294.4
14	0.100	0.0	0.0	107.8	9.6	86.8	204.2
14	0.200	0.0	0.0	89.4	3.5	32.9	125.8
14	0.500	0.0	0.0	37.7	0.9	8.7	47.3
14	1.000	0.0	0.0	15.8	0.3	3.1	19.3
14	2.000	0.0	0.0	6.1	0.1	1.1	7.3
14	5.000	0.0	0.0	1.6	0.0	0.3	1.9
14	10.000	0.0	0.0	0.6	0.0	0.1	0.7
				Ar^{3+}			
15	0.001	0.0	0.0	0.0	53.3	0.1	53.4
15	0.002	0.0	0.0	0.0	236.4	35.7	272.1
15	0.005	0.0	0.0	0.0	272.9	609.3	882.3
15	0.010	0.0	0.0	0.0	160.0	877.2	1037.3
15	0.020	0.0	0.0	1.1	72.9	625.8	699.8
15	0.050	0.0	0.0	45.2	21.5	241.3	307.9
15	0.100	0.0	0.0	88.1	8.0	98.2	194.2
15	0.200	0.0	0.0	73.1	2.9	37.2	113.2
15	0.500	0.0	0.0	30.8	0.7	9.8	41.4
15	1.000	0.0	0.0	12.9	0.3	3.5	16.7
15	2.000	0.0	0.0	5.0	0.1	1.3	6.3
15	5.000	0.0	0.0	1.3	0.0	0.3	1.7
15	10.000	0.0	0.0	0.5	0.0	0.1	0.6
				Ar^{2+}			
16	0.001	0.0	0.0	0.0	37.5	0.1	37.6
16	0.002	0.0	0.0	0.0	168.4	37.2	205.6
16	0.005	0.0	0.0	0.0	195.6	635.7	831.3
16	0.010	0.0	0.0	0.0	115.0	915.1	1030.1
16	0.020	0.0	0.0	0.9	52.4	652.9	706.2
16	0.050	0.0	0.0	37.0	15.4	251.7	304.1
16	0.100	0.0	0.0	72.1	5.7	102.4	180.2
16	0.200	0.0	0.0	59.8	2.1	38.8	100.7
16	0.500	0.0	0.0	25.2	0.5	10.2	36.0

Table 9. DR rates for Ar^{Z+} (continued)

N	T [keV]	1S	2S	2P	3S	3P	TOTAL
16	1.000	0.0	0.0	10.6	0.2	3.7	14.4
16	2.000	0.0	0.0	4.1	0.1	1.3	5.5
16	5.000	0.0	0.0	1.1	0.0	0.3	1.4
16	10.000	0.0	0.0	0.4	0.0	0.1	0.5
				Ar^{+}			
17	0.001	0.0	0.0	0.0	15.7	0.1	15.8
17	0.002	0.0	0.0	0.0	70.9	29.0	99.9
17	0.005	0.0	0.0	0.0	82.8	495.6	578.3
17	0.010	0.0	0.0	0.0	48.7	713.4	762.1
17	0.020	0.0	0.0	0.6	22.2	509.0	531.8
17	0.050	0.0	0.0	24.3	6.5	196.2	227.0
17	0.100	0.0	0.0	47.3	2.4	79.8	129.5
17	0.200	0.0	0.0	39.2	0.9	30.3	70.4
17	0.500	0.0	0.0	16.6	0.2	8.0	24.8
17	1.000	0.0	0.0	6.9	0.1	2.9	9.9
17	2.000	0.0	0.0	2.7	0.0	1.0	3.7
17	5.000	0.0	0.0	0.7	0.0	0.3	1.0
17	10.000	0.0	0.0	0.3	0.0	0.1	0.4

Table 10. DR rates α^{DR} [cm^3/s] for the Ti^{Z+} ions ($Z_c = 22$). Notation as in Table 4.

N	T [keV]	1S	2S	2P	3S	3P	TOTAL
				Ti^{21+}			
1	0.001	0.0	0.0	0.0	0.0	0.0	0.0
1	0.002	0.0	0.0	0.0	0.0	0.0	0.0
1	0.005	0.0	0.0	0.0	0.0	0.0	0.0
1	0.010	0.0	0.0	0.0	0.0	0.0	0.0
1	0.020	0.0	0.0	0.0	0.0	0.0	0.0
1	0.050	0.0	0.0	0.0	0.0	0.0	0.0
1	0.100	0.0	0.0	0.0	0.0	0.0	0.0
1	0.200	0.0	0.0	0.0	0.0	0.0	0.0
1	0.500	0.6	0.0	0.0	0.0	0.0	0.6
1	1.000	5.2	0.0	0.0	0.0	0.0	5.2
1	2.000	9.1	0.0	0.0	0.0	0.0	9.1
1	5.000	5.9	0.0	0.0	0.0	0.0	5.9
1	10.000	2.9	0.0	0.0	0.0	0.0	2.9
				Ti^{20+}			
2	0.001	0.0	0.0	0.0	0.0	0.0	0.0
2	0.002	0.0	0.0	0.0	0.0	0.0	0.0
2	0.005	0.0	0.0	0.0	0.0	0.0	0.0
2	0.010	0.0	0.0	0.0	0.0	0.0	0.0

Table 10. DR rates for Ti^{Z+} (continued)

N	T [keV]	1S	2S	2P	3S	3P	TOTAL
2	0.020	0.0	0.0	0.0	0.0	0.0	0.0
2	0.050	0.0	0.0	0.0	0.0	0.0	0.0
2	0.100	0.0	0.0	0.0	0.0	0.0	0.0
2	0.200	0.0	0.0	0.0	0.0	0.0	0.0
2	0.500	0.9	0.0	0.0	0.0	0.0	0.9
2	1.000	6.5	0.0	0.0	0.0	0.0	6.5
2	2.000	10.5	0.0	0.0	0.0	0.0	10.5
2	5.000	6.6	0.0	0.0	0.0	0.0	6.6
2	10.000	3.2	0.0	0.0	0.0	0.0	3.2
				Ti^{19+}			
3	0.001	0.0	0.0	0.0	0.0	0.0	0.0
3	0.002	0.0	1.9	0.0	0.0	0.0	1.9
3	0.005	0.0	379.6	0.0	0.0	0.0	379.6
3	0.010	0.0	1191.0	0.0	0.0	0.0	1191.0
3	0.020	0.0	1219.5	0.0	0.0	0.0	1219.6
3	0.050	0.0	562.9	29.8	0.0	0.0	592.7
3	0.100	0.0	237.1	146.5	0.0	0.0	383.5
3	0.200	0.0	89.6	193.1	0.0	0.0	282.7
3	0.500	0.7	23.0	107.6	0.0	0.0	131.2
3	1.000	4.6	8.0	49.5	0.0	0.0	62.2
3	2.000	7.3	2.8	20.0	0.0	0.0	30.1
3	5.000	4.6	0.7	5.5	0.0	0.0	10.7
3	10.000	2.2	0.2	2.0	0.0	0.0	4.4
				Ti^{18+}			
4	0.001	0.0	0.0	0.0	0.0	0.0	0.0
4	0.002	0.0	1.3	0.0	0.0	0.0	1.3
4	0.005	0.0	255.6	0.0	0.0	0.0	255.6
4	0.010	0.0	802.0	0.0	0.0	0.0	802.0
4	0.020	0.0	821.2	0.0	0.0	0.0	821.2
4	0.050	0.0	379.1	31.6	0.0	0.0	410.6
4	0.100	0.0	159.6	155.3	0.0	0.0	314.9
4	0.200	0.0	60.4	204.7	0.0	0.0	265.1
4	0.500	0.3	15.5	114.1	0.0	0.0	129.8
4	1.000	2.0	5.4	52.5	0.0	0.0	59.9
4	2.000	3.2	1.9	21.2	0.0	0.0	26.2
4	5.000	1.9	0.5	5.8	0.0	0.0	8.2
4	10.000	0.9	0.2	2.1	0.0	0.0	3.2
				Ti^{17+}			
5	0.001	0.0	0.0	0.0	0.0	0.0	0.0
5	0.002	0.0	0.8	0.0	0.0	0.0	0.8
5	0.005	0.0	149.9	0.0	0.0	0.0	149.9
5	0.010	0.0	470.2	0.0	0.0	0.0	470.2
5	0.020	0.0	481.5	0.1	0.0	0.0	481.6

Table 10. DR rates for Ti^{Z+} (continued)

N	T [keV]	1S	2S	2P	3S	3P	TOTAL
5	0.050	0.0	222.3	34.2	0.0	0.0	256.4
5	0.100	0.0	93.6	168.0	0.0	0.0	261.6
5	0.200	0.0	35.4	221.5	0.0	0.0	256.9
5	0.500	0.1	9.1	123.4	0.0	0.0	132.6
5	1.000	0.5	3.2	56.8	0.0	0.0	60.5
5	2.000	0.8	1.1	22.9	0.0	0.0	24.8
5	5.000	0.5	0.3	6.3	0.0	0.0	7.1
5	10.000	0.2	0.1	2.3	0.0	0.0	2.6
				Ti^{16+}			
6	0.001	0.0	0.0	0.0	0.0	0.0	0.0
6	0.002	0.0	0.4	0.0	0.0	0.0	0.4
6	0.005	0.0	84.6	0.0	0.0	0.0	84.6
6	0.010	0.0	265.5	0.0	0.0	0.0	265.5
6	0.020	0.0	271.8	0.1	0.0	0.0	271.9
6	0.050	0.0	125.5	37.5	0.0	0.0	163.0
6	0.100	0.0	52.8	184.4	0.0	0.0	237.2
6	0.200	0.0	20.0	243.1	0.0	0.0	263.0
6	0.500	0.0	5.1	135.4	0.0	0.0	140.6
6	1.000	0.1	1.8	62.3	0.0	0.0	64.2
6	2.000	0.1	0.6	25.1	0.0	0.0	25.9
6	5.000	0.1	0.2	6.9	0.0	0.0	7.1
6	10.000	0.0	0.1	2.5	0.0	0.0	2.6
				Ti^{15+}			
7	0.001	0.0	0.0	0.0	0.0	0.0	0.0
7	0.002	0.0	0.2	0.0	0.0	0.0	0.2
7	0.005	0.0	45.8	0.0	0.0	0.0	45.8
7	0.010	0.0	143.8	0.0	0.0	0.0	143.8
7	0.020	0.0	147.2	0.1	0.0	0.0	147.3
7	0.050	0.0	68.0	41.6	0.0	0.0	109.5
7	0.100	0.0	28.6	204.4	0.0	0.0	233.0
7	0.200	0.0	10.8	269.5	0.0	0.0	280.3
7	0.500	0.0	2.8	150.2	0.0	0.0	152.9
7	1.000	0.0	1.0	69.1	0.0	0.0	70.1
7	2.000	0.0	0.3	27.9	0.0	0.0	28.2
7	5.000	0.0	0.1	7.6	0.0	0.0	7.7
7	10.000	0.0	0.0	2.8	0.0	0.0	2.8
				Ti^{14+}			
8	0.001	0.0	0.0	0.0	0.0	0.0	0.0
8	0.002	0.0	0.1	0.0	0.0	0.0	0.1
8	0.005	0.0	22.6	0.0	0.0	0.0	22.6
8	0.010	0.0	71.0	0.0	0.0	0.0	71.0
8	0.020	0.0	72.7	0.1	0.0	0.0	72.8
8	0.050	0.0	33.6	46.5	0.0	0.0	80.0

Table 10. DR rates for Ti^{Z+} (continued)

N	T [keV]	1S	2S	2P	3S	3P	TOTAL
8	0.100	0.0	14.1	228.5	0.0	0.0	242.6
8	0.200	0.0	5.3	301.2	0.0	0.0	306.5
8	0.500	0.0	1.4	167.8	0.0	0.0	169.2
8	1.000	0.0	0.5	77.2	0.0	0.0	77.7
8	2.000	0.0	0.2	31.1	0.0	0.0	31.3
8	5.000	0.0	0.0	8.5	0.0	0.0	8.6
8	10.000	0.0	0.0	3.1	0.0	0.0	3.1
				Ti^{13+}			
9	0.001	0.0	0.0	0.0	0.0	0.0	0.0
9	0.002	0.0	0.0	0.0	0.0	0.0	0.0
9	0.005	0.0	8.6	0.0	0.0	0.0	8.6
9	0.010	0.0	26.9	0.0	0.0	0.0	26.9
9	0.020	0.0	27.6	0.1	0.0	0.0	27.6
9	0.050	0.0	12.7	52.3	0.0	0.0	65.0
9	0.100	0.0	5.4	256.9	0.0	0.0	262.2
9	0.200	0.0	2.0	338.6	0.0	0.0	340.7
9	0.500	0.0	0.5	188.7	0.0	0.0	189.2
9	1.000	0.0	0.2	86.8	0.0	0.0	87.0
9	2.000	0.0	0.1	35.0	0.0	0.0	35.1
9	5.000	0.0	0.0	9.6	0.0	0.0	9.6
9	10.000	0.0	0.0	3.5	0.0	0.0	3.5
				Ti^{12+}			
10	0.001	0.0	0.0	0.0	0.0	0.0	0.0
10	0.002	0.0	0.0	0.0	0.0	0.0	0.0
10	0.005	0.0	0.0	0.0	0.0	0.0	0.0
10	0.010	0.0	0.0	0.0	0.0	0.0	0.0
10	0.020	0.0	0.0	0.1	0.0	0.0	0.1
10	0.050	0.0	0.0	51.6	0.0	0.0	51.6
10	0.100	0.0	0.0	253.4	0.0	0.0	253.4
10	0.200	0.0	0.0	334.0	0.0	0.0	334.0
10	0.500	0.0	0.0	186.1	0.0	0.0	186.1
10	1.000	0.0	0.0	85.6	0.0	0.0	85.6
10	2.000	0.0	0.0	34.5	0.0	0.0	34.5
10	5.000	0.0	0.0	9.5	0.0	0.0	9.5
10	10.000	0.0	0.0	3.4	0.0	0.0	3.4
				Ti^{11+}			
11	0.001	0.0	0.0	0.0	43.4	0.0	43.4
11	0.002	0.0	0.0	0.0	295.1	0.1	295.2
11	0.005	0.0	0.0	0.0	440.1	33.8	473.9
11	0.010	0.0	0.0	0.0	281.1	157.6	438.7
11	0.020	0.0	0.0	0.1	133.6	202.3	335.9
11	0.050	0.0	0.0	41.6	40.4	110.9	192.9
11	0.100	0.0	0.0	204.7	15.1	50.7	270.6

Table 10. DR rates for Ti^{Z+} (continued)

N	T [keV]	1S	2S	2P	3S	3P	TOTAL
11	0.200	0.0	0.0	269.8	5.5	20.4	295.7
11	0.500	0.0	0.0	150.3	1.4	5.6	157.3
11	1.000	0.0	0.0	69.2	0.5	2.0	71.7
11	2.000	0.0	0.0	27.9	0.2	0.7	28.8
11	5.000	0.0	0.0	7.6	0.0	0.2	7.9
11	10.000	0.0	0.0	2.8	0.0	0.1	2.9
				Ti^{10+}			
12	0.001	0.0	0.0	0.0	25.3	0.0	25.3
12	0.002	0.0	0.0	0.0	277.3	0.1	277.4
12	0.005	0.0	0.0	0.0	550.8	69.0	619.8
12	0.010	0.0	0.0	0.0	387.1	321.5	708.6
12	0.020	0.0	0.0	0.0	192.9	412.7	605.7
12	0.050	0.0	0.0	33.8	60.0	226.3	320.0
12	0.100	0.0	0.0	165.9	22.7	103.5	292.2
12	0.200	0.0	0.0	218.7	8.3	41.6	268.7
12	0.500	0.0	0.0	121.9	2.1	11.4	135.4
12	1.000	0.0	0.0	56.1	0.8	4.1	61.0
12	2.000	0.0	0.0	22.6	0.3	1.5	24.4
12	5.000	0.0	0.0	6.2	0.1	0.4	6.6
12	10.000	0.0	0.0	2.2	0.0	0.1	2.4
				Ti^{9+}			
13	0.001	0.0	0.0	0.0	23.1	0.0	23.1
13	0.002	0.0	0.0	0.0	284.8	0.2	285.0
13	0.005	0.0	0.0	0.0	607.7	101.5	709.2
13	0.010	0.0	0.0	0.0	437.4	472.8	910.1
13	0.020	0.0	0.0	0.0	220.6	606.8	827.4
13	0.050	0.0	0.0	27.4	69.1	332.7	429.2
13	0.100	0.0	0.0	134.9	26.2	152.2	313.3
13	0.200	0.0	0.0	177.8	9.6	61.2	248.6
13	0.500	0.0	0.0	99.1	2.5	16.7	118.3
13	1.000	0.0	0.0	45.6	0.9	6.1	52.5
13	2.000	0.0	0.0	18.4	0.3	2.2	20.9
13	5.000	0.0	0.0	5.0	0.1	0.6	5.7
13	10.000	0.0	0.0	1.8	0.0	0.2	2.1
				Ti^{8+}			
14	0.001	0.0	0.0	0.0	21.6	0.0	21.6
14	0.002	0.0	0.0	0.0	281.0	0.2	281.2
14	0.005	0.0	0.0	0.0	617.8	127.4	745.2
14	0.010	0.0	0.0	0.0	449.1	593.7	1042.7
14	0.020	0.0	0.0	0.0	227.6	761.9	989.6
14	0.050	0.0	0.0	22.4	71.5	417.8	511.6
14	0.100	0.0	0.0	109.9	27.2	191.2	328.3
14	0.200	0.0	0.0	144.9	10.0	76.9	231.8

Table 10. DR rates for Ti^{Z+} (continued)

N	T [keV]	1S	2S	2P	3S	3P	TOTAL
14	0.500	0.0	0.0	80.8	2.6	21.0	104.3
14	1.000	0.0	0.0	37.1	0.9	7.6	45.7
14	2.000	0.0	0.0	15.0	0.3	2.7	18.0
14	5.000	0.0	0.0	4.1	0.1	0.7	4.9
14	10.000	0.0	0.0	1.5	0.0	0.2	1.8
				Ti^{7+}			
15	0.001	0.0	0.0	0.0	20.0	0.0	20.0
15	0.002	0.0	0.0	0.0	266.1	0.2	266.4
15	0.005	0.0	0.0	0.0	594.3	144.1	738.5
15	0.010	0.0	0.0	0.0	434.3	671.5	1105.7
15	0.020	0.0	0.0	0.0	220.7	861.8	1082.5
15	0.050	0.0	0.0	18.3	69.4	472.5	560.2
15	0.100	0.0	0.0	89.8	26.4	216.2	332.4
15	0.200	0.0	0.0	118.4	9.7	87.0	215.0
15	0.500	0.0	0.0	66.0	2.5	23.8	92.2
15	1.000	0.0	0.0	30.3	0.9	8.6	39.9
15	2.000	0.0	0.0	12.2	0.3	3.1	15.6
15	5.000	0.0	0.0	3.4	0.1	0.8	4.2
15	10.000	0.0	0.0	1.2	0.0	0.3	1.5
				Ti^{6+}			
16	0.001	0.0	0.0	0.0	17.9	0.0	17.9
16	0.002	0.0	0.0	0.0	242.5	0.3	242.8
16	0.005	0.0	0.0	0.0	546.7	150.4	697.1
16	0.010	0.0	0.0	0.0	400.8	700.5	1101.2
16	0.020	0.0	0.0	0.0	204.0	899.0	1103.0
16	0.050	0.0	0.0	15.0	64.2	492.9	572.1
16	0.100	0.0	0.0	73.5	24.4	225.5	323.5
16	0.200	0.0	0.0	96.9	9.0	90.7	196.6
16	0.500	0.0	0.0	54.0	2.3	24.8	81.1
16	1.000	0.0	0.0	24.8	0.8	9.0	34.7
16	2.000	0.0	0.0	10.0	0.3	3.2	13.5
16	5.000	0.0	0.0	2.7	0.1	0.8	3.6
16	10.000	0.0	0.0	1.0	0.0	0.3	1.3
				Ti^{5+}			
17	0.001	0.0	0.0	0.0	15.5	0.0	15.5
17	0.002	0.0	0.0	0.0	212.1	0.3	212.4
17	0.005	0.0	0.0	0.0	481.2	146.5	627.7
17	0.010	0.0	0.0	0.0	353.5	682.6	1036.1
17	0.020	0.0	0.0	0.0	180.1	876.1	1056.2
17	0.050	0.0	0.0	12.3	56.7	480.4	549.4
17	0.100	0.0	0.0	60.3	21.6	219.8	301.6
17	0.200	0.0	0.0	79.4	7.9	88.4	175.8
17	0.500	0.0	0.0	44.3	2.0	24.2	70.5

Table 10. DR rates for Ti^{Z+} (continued)

N	T [keV]	1S	2S	2P	3S	3P	TOTAL
17	1.000	0.0	0.0	20.4	0.7	8.8	29.9
17	2.000	0.0	0.0	8.2	0.3	3.1	11.6
17	5.000	0.0	0.0	2.2	0.1	0.8	3.1
17	10.000	0.0	0.0	0.8	0.0	0.3	1.1
				Ti^{4+}			
18	0.001	0.0	0.0	0.0	12.8	0.0	12.8
18	0.002	0.0	0.0	0.0	176.5	0.2	176.7
18	0.005	0.0	0.0	0.0	402.1	134.4	536.5
18	0.010	0.0	0.0	0.0	295.8	626.1	921.9
18	0.020	0.0	0.0	0.0	150.9	803.5	954.4
18	0.050	0.0	0.0	10.1	47.5	440.6	498.2
18	0.100	0.0	0.0	49.5	18.1	201.6	269.2
18	0.200	0.0	0.0	65.2	6.6	81.1	152.9
18	0.500	0.0	0.0	36.3	1.7	22.2	60.2
18	1.000	0.0	0.0	16.7	0.6	8.0	25.4
18	2.000	0.0	0.0	6.7	0.2	2.9	9.8
18	5.000	0.0	0.0	1.8	0.1	0.7	2.6
18	10.000	0.0	0.0	0.7	0.0	0.3	0.9
				Ti^{3+}			
19	0.001	0.0	0.0	0.0	9.9	0.0	9.9
19	0.002	0.0	0.0	0.0	136.7	0.2	136.9
19	0.005	0.0	0.0	0.0	312.5	116.6	429.1
19	0.010	0.0	0.0	0.0	230.2	543.1	773.2
19	0.020	0.0	0.0	0.0	117.4	697.0	814.4
19	0.050	0.0	0.0	8.3	37.0	382.2	427.5
19	0.100	0.0	0.0	40.7	14.1	174.9	229.6
19	0.200	0.0	0.0	53.6	5.2	70.3	129.1
19	0.500	0.0	0.0	29.9	1.3	19.2	50.4
19	1.000	0.0	0.0	13.7	0.5	7.0	21.2
19	2.000	0.0	0.0	5.5	0.2	2.5	8.2
19	5.000	0.0	0.0	1.5	0.0	0.6	2.2
19	10.000	0.0	0.0	0.6	0.0	0.2	0.8
				Ti^{2+}			
20	0.001	0.0	0.0	0.0	6.7	0.0	6.7
20	0.002	0.0	0.0	0.0	93.7	0.2	93.8
20	0.005	0.0	0.0	0.0	214.6	95.9	310.6
20	0.010	0.0	0.0	0.0	158.2	447.0	605.2
20	0.020	0.0	0.0	0.0	80.7	573.7	654.5
20	0.050	0.0	0.0	6.8	25.5	314.6	346.9
20	0.100	0.0	0.0	33.5	9.7	143.9	187.1
20	0.200	0.0	0.0	44.2	3.6	57.9	105.6
20	0.500	0.0	0.0	24.6	0.9	15.8	41.4
20	1.000	0.0	0.0	11.3	0.3	5.7	17.4

Table 10. DR rates for Ti^{Z+} (continued)

N	T [keV]	1S	2S	2P	3S	3P	TOTAL
20	2.000	0.0	0.0	4.6	0.1	2.1	6.7
20	5.000	0.0	0.0	1.2	0.0	0.5	1.8
20	10.000	0.0	0.0	0.5	0.0	0.2	0.6
				Ti^{+}			
21	0.001	0.0	0.0	0.0	2.7	0.0	2.7
21	0.002	0.0	0.0	0.0	38.3	0.1	38.5
21	0.005	0.0	0.0	0.0	88.0	60.1	148.1
21	0.010	0.0	0.0	0.0	64.9	280.0	344.9
21	0.020	0.0	0.0	0.0	33.1	359.3	392.5
21	0.050	0.0	0.0	0.0	10.5	197.0	207.5
21	0.100	0.0	0.0	0.0	4.0	90.2	94.1
21	0.200	0.0	0.0	0.0	1.5	36.3	37.7
21	0.500	0.0	0.0	0.0	0.4	9.9	10.3
21	1.000	0.0	0.0	0.0	0.1	3.6	3.7
21	2.000	0.0	0.0	0.0	0.0	1.3	1.3
21	5.000	0.0	0.0	0.0	0.0	0.3	0.3
21	10.000	0.0	0.0	0.0	0.0	0.1	0.1

Table 11. DR rates α^{DR} [cm^3/s] for the Fe^{Z+} ions ($Z_c = 26$). Notation as in Table 4.

N	T [keV]	1S	2S	2P	3S	3P	TOTAL
				Fe^{25+}			
1	0.001	0.0	0.0	0.0	0.0	0.0	0.0
1	0.002	0.0	0.0	0.0	0.0	0.0	0.0
1	0.005	0.0	0.0	0.0	0.0	0.0	0.0
1	0.010	0.0	0.0	0.0	0.0	0.0	0.0
1	0.020	0.0	0.0	0.0	0.0	0.0	0.0
1	0.050	0.0	0.0	0.0	0.0	0.0	0.0
1	0.100	0.0	0.0	0.0	0.0	0.0	0.0
1	0.200	0.0	0.0	0.0	0.0	0.0	0.0
1	0.500	0.1	0.0	0.0	0.0	0.0	0.1
1	1.000	1.9	0.0	0.0	0.0	0.0	1.9
1	2.000	5.9	0.0	0.0	0.0	0.0	5.9
1	5.000	5.6	0.0	0.0	0.0	0.0	5.6
1	10.000	3.1	0.0	0.0	0.0	0.0	3.1
				Fe^{24+}			
2	0.001	0.0	0.0	0.0	0.0	0.0	0.0
2	0.002	0.0	0.0	0.0	0.0	0.0	0.0
2	0.005	0.0	0.0	0.0	0.0	0.0	0.0
2	0.010	0.0	0.0	0.0	0.0	0.0	0.0
2	0.020	0.0	0.0	0.0	0.0	0.0	0.0

Table 11. DR rates for Fe^{Z+} (continued)

N	T [keV]	1S	2S	2P	3S	3P	TOTAL
2	0.050	0.0	0.0	0.0	0.0	0.0	0.0
2	0.100	0.0	0.0	0.0	0.0	0.0	0.0
2	0.200	0.0	0.0	0.0	0.0	0.0	0.0
2	0.500	0.1	0.0	0.0	0.0	0.0	0.1
2	1.000	2.5	0.0	0.0	0.0	0.0	2.5
2	2.000	7.3	0.0	0.0	0.0	0.0	7.3
2	5.000	6.5	0.0	0.0	0.0	0.0	6.5
2	10.000	3.5	0.0	0.0	0.0	0.0	3.5
				Fe^{23+}			
3	0.001	0.0	0.0	0.0	0.0	0.0	0.0
3	0.002	0.0	1.6	0.0	0.0	0.0	1.6
3	0.005	0.0	387.6	0.0	0.0	0.0	387.6
3	0.010	0.0	1301.2	0.0	0.0	0.0	1301.2
3	0.020	0.0	1378.2	0.0	0.0	0.0	1378.2
3	0.050	0.0	649.2	6.8	0.0	0.0	656.0
3	0.100	0.0	275.3	101.6	0.0	0.0	376.9
3	0.200	0.0	104.4	233.3	0.0	0.0	337.7
3	0.500	0.1	26.9	181.4	0.0	0.0	208.3
3	1.000	1.7	9.4	93.2	0.0	0.0	104.3
3	2.000	4.9	3.2	39.7	0.0	0.0	47.9
3	5.000	4.3	0.8	11.2	0.0	0.0	16.4
3	10.000	2.3	0.3	4.1	0.0	0.0	6.7
				Fe^{22+}			
4	0.001	0.0	0.0	0.0	0.0	0.0	0.0
4	0.002	0.0	1.1	0.0	0.0	0.0	1.1
4	0.005	0.0	261.0	0.0	0.0	0.0	261.0
4	0.010	0.0	876.2	0.0	0.0	0.0	876.2
4	0.020	0.0	928.0	0.0	0.0	0.0	928.0
4	0.050	0.0	437.1	7.2	0.0	0.0	444.4
4	0.100	0.0	185.4	107.7	0.0	0.0	293.1
4	0.200	0.0	70.3	247.4	0.0	0.0	317.7
4	0.500	0.0	18.1	192.3	0.0	0.0	210.4
4	1.000	0.7	6.3	98.8	0.0	0.0	105.8
4	2.000	1.8	2.2	42.1	0.0	0.0	46.2
4	5.000	1.6	0.5	11.9	0.0	0.0	14.1
4	10.000	0.9	0.2	4.4	0.0	0.0	5.4
				Fe^{21+}			
5	0.001	0.0	0.0	0.0	0.0	0.0	0.0
5	0.002	0.0	0.6	0.0	0.0	0.0	0.6
5	0.005	0.0	153.0	0.0	0.0	0.0	153.0
5	0.010	0.0	513.8	0.0	0.0	0.0	513.8
5	0.020	0.0	544.2	0.0	0.0	0.0	544.2
5	0.050	0.0	256.3	7.8	0.0	0.0	264.1

Table 11. DR rates for Fe^{Z+} (continued)

N	T [keV]	1S	2S	2P	3S	3P	TOTAL
5	0.100	0.0	108.7	116.6	0.0	0.0	225.3
5	0.200	0.0	41.2	267.6	0.0	0.0	308.9
5	0.500	0.0	10.6	208.0	0.0	0.0	218.7
5	1.000	0.1	3.7	106.9	0.0	0.0	110.8
5	2.000	0.4	1.3	45.6	0.0	0.0	47.3
5	5.000	0.3	0.3	12.9	0.0	0.0	13.6
5	10.000	0.2	0.1	4.7	0.0	0.0	5.0
				Fe^{20+}			
6	0.001	0.0	0.0	0.0	0.0	0.0	0.0
6	0.002	0.0	0.4	0.0	0.0	0.0	0.4
6	0.005	0.0	86.4	0.0	0.0	0.0	86.4
6	0.010	0.0	290.0	0.0	0.0	0.0	290.0
6	0.020	0.0	307.2	0.0	0.0	0.0	307.2
6	0.050	0.0	144.7	8.6	0.0	0.0	153.3
6	0.100	0.0	61.4	127.9	0.0	0.0	189.3
6	0.200	0.0	23.3	293.7	0.0	0.0	317.0
6	0.500	0.0	6.0	228.3	0.0	0.0	234.3
6	1.000	0.0	2.1	117.3	0.0	0.0	119.5
6	2.000	0.0	0.7	50.0	0.0	0.0	50.8
6	5.000	0.0	0.2	14.2	0.0	0.0	14.4
6	10.000	0.0	0.1	5.2	0.0	0.0	5.3
				Fe^{19+}			
7	0.001	0.0	0.0	0.0	0.0	0.0	0.0
7	0.002	0.0	0.2	0.0	0.0	0.0	0.2
7	0.005	0.0	46.8	0.0	0.0	0.0	46.8
7	0.010	0.0	157.1	0.0	0.0	0.0	157.1
7	0.020	0.0	166.4	0.0	0.0	0.0	166.4
7	0.050	0.0	78.4	9.5	0.0	0.0	87.9
7	0.100	0.0	33.2	141.8	0.0	0.0	175.1
7	0.200	0.0	12.6	325.7	0.0	0.0	338.3
7	0.500	0.0	3.2	253.1	0.0	0.0	256.4
7	1.000	0.0	1.1	130.1	0.0	0.0	131.2
7	2.000	0.0	0.4	55.5	0.0	0.0	55.9
7	5.000	0.0	0.1	15.7	0.0	0.0	15.8
7	10.000	0.0	0.0	5.8	0.0	0.0	5.8
				Fe^{18+}			
8	0.001	0.0	0.0	0.0	0.0	0.0	0.0
8	0.002	0.0	0.1	0.0	0.0	0.0	0.1
8	0.005	0.0	23.1	0.0	0.0	0.0	23.1
8	0.010	0.0	77.6	0.0	0.0	0.0	77.6
8	0.020	0.0	82.1	0.0	0.0	0.0	82.1
8	0.050	0.0	38.7	10.6	0.0	0.0	49.3
8	0.100	0.0	16.4	158.5	0.0	0.0	174.9

Table 11. DR rates for Fe^{Z+} (continued)

N	T [keV]	1S	2S	2P	3S	3P	TOTAL
8	0.200	0.0	6.2	363.9	0.0	0.0	370.1
8	0.500	0.0	1.6	282.9	0.0	0.0	284.5
8	1.000	0.0	0.6	145.4	0.0	0.0	146.0
8	2.000	0.0	0.2	62.0	0.0	0.0	62.2
8	5.000	0.0	0.0	17.5	0.0	0.0	17.6
8	10.000	0.0	0.0	6.4	0.0	0.0	6.5
				Fe^{17+}			
9	0.001	0.0	0.0	0.0	0.0	0.0	0.0
9	0.002	0.0	0.0	0.0	0.0	0.0	0.0
9	0.005	0.0	8.8	0.0	0.0	0.0	8.8
9	0.010	0.0	29.4	0.0	0.0	0.0	29.4
9	0.020	0.0	31.2	0.0	0.0	0.0	31.2
9	0.050	0.0	14.7	12.0	0.0	0.0	26.6
9	0.100	0.0	6.2	178.2	0.0	0.0	184.5
9	0.200	0.0	2.4	409.2	0.0	0.0	411.6
9	0.500	0.0	0.6	318.1	0.0	0.0	318.7
9	1.000	0.0	0.2	163.5	0.0	0.0	163.7
9	2.000	0.0	0.1	69.7	0.0	0.0	69.8
9	5.000	0.0	0.0	19.7	0.0	0.0	19.7
9	10.000	0.0	0.0	7.2	0.0	0.0	7.2
				Fe^{16+}			
10	0.001	0.0	0.0	0.0	0.0	0.0	0.0
10	0.002	0.0	0.0	0.0	0.0	0.0	0.0
10	0.005	0.0	0.0	0.0	0.0	0.0	0.0
10	0.010	0.0	0.0	0.0	0.0	0.0	0.0
10	0.020	0.0	0.0	0.0	0.0	0.0	0.0
10	0.050	0.0	0.0	11.8	0.0	0.0	11.8
10	0.100	0.0	0.0	175.8	0.0	0.0	175.8
10	0.200	0.0	0.0	403.7	0.0	0.0	403.7
10	0.500	0.0	0.0	313.8	0.0	0.0	313.8
10	1.000	0.0	0.0	161.3	0.0	0.0	161.3
10	2.000	0.0	0.0	68.8	0.0	0.0	68.8
10	5.000	0.0	0.0	19.5	0.0	0.0	19.5
10	10.000	0.0	0.0	7.1	0.0	0.0	7.1
				Fe^{15+}			
11	0.001	0.0	0.0	0.0	13.5	0.0	13.5
11	0.002	0.0	0.0	0.0	205.7	0.0	205.7
11	0.005	0.0	0.0	0.0	497.7	4.0	501.7
11	0.010	0.0	0.0	0.0	373.5	83.7	457.2
11	0.020	0.0	0.0	0.0	192.4	228.1	420.5
11	0.050	0.0	0.0	9.5	61.0	196.5	267.1
11	0.100	0.0	0.0	142.0	23.3	104.5	269.8
11	0.200	0.0	0.0	326.1	8.5	45.3	379.9

Table 11. DR rates for Fe^{Z+} (continued)

N	T [keV]	1S	2S	2P	3S	3P	TOTAL
11	0.500	0.0	0.0	253.5	2.2	13.0	268.6
11	1.000	0.0	0.0	130.3	0.8	4.8	135.8
11	2.000	0.0	0.0	55.5	0.3	1.7	57.5
11	5.000	0.0	0.0	15.7	0.1	0.4	16.2
11	10.000	0.0	0.0	5.8	0.0	0.2	6.0
				Fe^{14+}			
12	0.001	0.0	0.0	0.0	6.2	0.0	6.2
12	0.002	0.0	0.0	0.0	174.2	0.0	174.2
12	0.005	0.0	0.0	0.0	607.0	8.1	615.1
12	0.010	0.0	0.0	0.0	514.5	170.7	685.2
12	0.020	0.0	0.0	0.0	281.6	465.4	747.0
12	0.050	0.0	0.0	7.7	92.6	401.0	501.3
12	0.100	0.0	0.0	115.1	35.7	213.3	364.2
12	0.200	0.0	0.0	264.3	13.2	92.5	370.0
12	0.500	0.0	0.0	205.4	3.4	26.5	235.3
12	1.000	0.0	0.0	105.6	1.2	9.7	116.6
12	2.000	0.0	0.0	45.0	0.4	3.5	49.0
12	5.000	0.0	0.0	12.7	0.1	0.9	13.8
12	10.000	0.0	0.0	4.7	0.0	0.3	5.0
				Fe^{13+}			
13	0.001	0.0	0.0	0.0	5.5	0.0	5.5
13	0.002	0.0	0.0	0.0	178.7	0.0	178.7
13	0.005	0.0	0.0	0.0	682.1	11.9	694.0
13	0.010	0.0	0.0	0.0	595.9	251.0	846.9
13	0.020	0.0	0.0	0.0	331.2	684.3	1015.4
13	0.050	0.0	0.0	6.3	109.9	589.6	705.8
13	0.100	0.0	0.0	93.6	42.5	313.6	449.8
13	0.200	0.0	0.0	214.9	15.7	136.0	366.6
13	0.500	0.0	0.0	167.0	4.1	38.9	210.0
13	1.000	0.0	0.0	85.8	1.5	14.3	101.6
13	2.000	0.0	0.0	36.6	0.5	5.2	42.3
13	5.000	0.0	0.0	10.4	0.1	1.3	11.8
13	10.000	0.0	0.0	3.8	0.0	0.5	4.3
				Fe^{12+}			
14	0.001	0.0	0.0	0.0	5.2	0.0	5.2
14	0.002	0.0	0.0	0.0	180.6	0.0	180.6
14	0.005	0.0	0.0	0.0	716.1	15.0	731.1
14	0.010	0.0	0.0	0.0	633.6	315.2	948.8
14	0.020	0.0	0.0	0.0	354.4	859.2	1213.6
14	0.050	0.0	0.0	5.1	118.0	740.4	863.5
14	0.100	0.0	0.0	76.3	45.7	393.8	515.9
14	0.200	0.0	0.0	175.1	16.9	170.8	362.9
14	0.500	0.0	0.0	136.1	4.4	48.8	189.4

Table 11. DR rates for Fe^{Z+} (continued)

N	T [keV]	1S	2S	2P	3S	3P	TOTAL
14	1.000	0.0	0.0	70.0	1.6	18.0	89.5
14	2.000	0.0	0.0	29.8	0.6	6.5	36.9
14	5.000	0.0	0.0	8.4	0.1	1.7	10.2
14	10.000	0.0	0.0	3.1	0.1	0.6	3.7
				Fe^{11+}			
15	0.001	0.0	0.0	0.0	5.0	0.0	5.0
15	0.002	0.0	0.0	0.0	177.9	0.0	177.9
15	0.005	0.0	0.0	0.0	719.7	17.0	736.7
15	0.010	0.0	0.0	0.0	641.0	356.5	997.5
15	0.020	0.0	0.0	0.0	359.7	971.8	1331.6
15	0.050	0.0	0.0	4.2	120.1	837.4	961.6
15	0.100	0.0	0.0	62.3	46.6	445.4	554.3
15	0.200	0.0	0.0	143.1	17.2	193.2	353.5
15	0.500	0.0	0.0	111.2	4.5	55.2	170.9
15	1.000	0.0	0.0	57.2	1.6	20.3	79.1
15	2.000	0.0	0.0	24.4	0.6	7.3	32.3
15	5.000	0.0	0.0	6.9	0.1	1.9	8.9
15	10.000	0.0	0.0	2.5	0.1	0.7	3.2
				Fe^{10+}			
16	0.001	0.0	0.0	0.0	4.7	0.0	4.7
16	0.002	0.0	0.0	0.0	171.2	0.0	171.2
16	0.005	0.0	0.0	0.0	700.9	17.7	718.6
16	0.010	0.0	0.0	0.0	626.8	371.9	998.8
16	0.020	0.0	0.0	0.0	352.5	1013.9	1366.3
16	0.050	0.0	0.0	3.4	117.8	873.6	994.8
16	0.100	0.0	0.0	51.0	45.7	464.7	561.4
16	0.200	0.0	0.0	117.1	16.9	201.5	335.5
16	0.500	0.0	0.0	91.0	4.4	57.6	153.0
16	1.000	0.0	0.0	46.8	1.6	21.2	69.6
16	2.000	0.0	0.0	19.9	0.6	7.7	28.2
16	5.000	0.0	0.0	5.6	0.1	2.0	7.7
16	10.000	0.0	0.0	2.1	0.1	0.7	2.8
				Fe^{9+}			
17	0.001	0.0	0.0	0.0	4.3	0.0	4.3
17	0.002	0.0	0.0	0.0	161.3	0.0	161.3
17	0.005	0.0	0.0	0.0	665.6	17.2	682.8
17	0.010	0.0	0.0	0.0	596.8	362.4	959.2
17	0.020	0.0	0.0	0.0	336.0	988.0	1324.0
17	0.050	0.0	0.0	2.8	112.4	851.3	966.5
17	0.100	0.0	0.0	41.8	43.6	452.8	538.3
17	0.200	0.0	0.0	96.0	16.2	196.4	308.5
17	0.500	0.0	0.0	74.6	4.2	56.2	135.0
17	1.000	0.0	0.0	38.4	1.5	20.7	60.5

Table 11. DR rates for Fe^{Z+} (continued)

N	T [keV]	1S	2S	2P	3S	3P	TOTAL
17	2.000	0.0	0.0	16.4	0.5	7.5	24.3
17	5.000	0.0	0.0	4.6	0.1	1.9	6.7
17	10.000	0.0	0.0	1.7	0.0	0.7	2.4
				Fe^{8+}			
18	0.001	0.0	0.0	0.0	4.0	0.0	4.0
18	0.002	0.0	0.0	0.0	148.8	0.0	148.8
18	0.005	0.0	0.0	0.0	617.5	15.8	633.3
18	0.010	0.0	0.0	0.0	554.7	332.4	887.1
18	0.020	0.0	0.0	0.0	312.6	906.1	1218.8
18	0.050	0.0	0.0	2.3	104.6	780.8	887.7
18	0.100	0.0	0.0	34.3	40.6	415.3	490.3
18	0.200	0.0	0.0	78.8	15.0	180.1	274.0
18	0.500	0.0	0.0	61.3	3.9	51.5	116.7
18	1.000	0.0	0.0	31.5	1.4	19.0	51.9
18	2.000	0.0	0.0	13.4	0.5	6.8	20.8
18	5.000	0.0	0.0	3.8	0.1	1.8	5.7
18	10.000	0.0	0.0	1.4	0.0	0.6	2.1
				Fe^{7+}			
19	0.001	0.0	0.0	0.0	3.6	0.0	3.6
19	0.002	0.0	0.0	0.0	134.3	0.0	134.3
19	0.005	0.0	0.0	0.0	559.6	13.7	573.3
19	0.010	0.0	0.0	0.0	503.4	288.3	791.7
19	0.020	0.0	0.0	0.0	283.9	786.0	1069.9
19	0.050	0.0	0.0	1.9	95.0	677.3	774.2
19	0.100	0.0	0.0	28.2	36.9	360.3	425.4
19	0.200	0.0	0.0	64.8	13.7	156.2	234.7
19	0.500	0.0	0.0	50.4	3.6	44.7	98.6
19	1.000	0.0	0.0	25.9	1.3	16.5	43.6
19	2.000	0.0	0.0	11.0	0.5	5.9	17.4
19	5.000	0.0	0.0	3.1	0.1	1.5	4.8
19	10.000	0.0	0.0	1.1	0.0	0.5	1.7
				Fe^{6+}			
20	0.001	0.0	0.0	0.0	3.1	0.0	3.1
20	0.002	0.0	0.0	0.0	118.2	0.0	118.2
20	0.005	0.0	0.0	0.0	493.9	11.3	505.1
20	0.010	0.0	0.0	0.0	444.7	237.3	682.0
20	0.020	0.0	0.0	0.0	250.9	647.0	897.9
20	0.050	0.0	0.0	1.6	84.0	557.5	643.1
20	0.100	0.0	0.0	23.2	32.6	296.6	352.4
20	0.200	0.0	0.0	53.4	12.1	128.6	194.1
20	0.500	0.0	0.0	41.5	3.1	36.8	81.4
20	1.000	0.0	0.0	21.3	1.1	13.5	36.0
20	2.000	0.0	0.0	9.1	0.4	4.9	14.4

Table 11. DR rates for Fe^{Z+} (continued)

N	T [keV]	1S	2S	2P	3S	3P	TOTAL
20	5.000	0.0	0.0	2.6	0.1	1.3	3.9
20	10.000	0.0	0.0	0.9	0.0	0.4	1.4
				Fe^{5+}			
21	0.001	0.0	0.0	0.0	2.6	0.0	2.6
21	0.002	0.0	0.0	0.0	100.7	0.0	100.7
21	0.005	0.0	0.0	0.0	421.9	8.8	430.7
21	0.010	0.0	0.0	0.0	380.2	185.8	566.0
21	0.020	0.0	0.0	0.0	214.6	506.6	721.1
21	0.050	0.0	0.0	0.0	71.9	436.5	508.4
21	0.100	0.0	0.0	0.0	27.9	232.2	260.1
21	0.200	0.0	0.0	0.0	10.3	100.7	111.0
21	0.500	0.0	0.0	0.0	2.7	28.8	31.5
21	1.000	0.0	0.0	0.0	1.0	10.6	11.6
21	2.000	0.0	0.0	0.0	0.3	3.8	4.2
21	5.000	0.0	0.0	0.0	0.1	1.0	1.1
21	10.000	0.0	0.0	0.0	0.0	0.3	0.4
				Fe^{4+}			
22	0.001	0.0	0.0	0.0	2.2	0.0	2.2
22	0.002	0.0	0.0	0.0	82.1	0.0	82.1
22	0.005	0.0	0.0	0.0	344.7	6.6	351.3
22	0.010	0.0	0.0	0.0	310.8	138.6	449.5
22	0.020	0.0	0.0	0.0	175.5	377.9	553.4
22	0.050	0.0	0.0	0.0	58.8	325.6	384.4
22	0.100	0.0	0.0	0.0	22.8	173.2	196.0
22	0.200	0.0	0.0	0.0	8.5	75.1	83.6
22	0.500	0.0	0.0	0.0	2.2	21.5	23.7
22	1.000	0.0	0.0	0.0	0.8	7.9	8.7
22	2.000	0.0	0.0	0.0	0.3	2.9	3.1
22	5.000	0.0	0.0	0.0	0.1	0.7	0.8
22	10.000	0.0	0.0	0.0	0.0	0.3	0.3
				Fe^{3+}			
23	0.001	0.0	0.0	0.0	1.6	0.0	1.6
23	0.002	0.0	0.0	0.0	62.6	0.0	62.6
23	0.005	0.0	0.0	0.0	263.3	4.7	268.0
23	0.010	0.0	0.0	0.0	237.6	98.7	336.3
23	0.020	0.0	0.0	0.0	134.2	269.0	403.2
23	0.050	0.0	0.0	0.0	45.0	231.8	276.7
23	0.100	0.0	0.0	0.0	17.5	123.3	140.8
23	0.200	0.0	0.0	0.0	6.5	53.5	59.9
23	0.500	0.0	0.0	0.0	1.7	15.3	17.0
23	1.000	0.0	0.0	0.0	0.6	5.6	6.2
23	2.000	0.0	0.0	0.0	0.2	2.0	2.2
23	5.000	0.0	0.0	0.0	0.1	0.5	0.6

Table 11. DR rates for Fe^{Z+} (continued)

N	T [keV]	1S	2S	2P	3S	3P	TOTAL
23	10.000	0.0	0.0	0.0	0.0	0.2	0.2
				Fe^{2+}			
24	0.001	0.0	0.0	0.0	1.1	0.0	1.1
24	0.002	0.0	0.0	0.0	42.4	0.0	42.4
24	0.005	0.0	0.0	0.0	178.4	3.2	181.6
24	0.010	0.0	0.0	0.0	161.0	67.1	228.1
24	0.020	0.0	0.0	0.0	91.0	182.9	273.8
24	0.050	0.0	0.0	0.0	30.5	157.6	188.1
24	0.100	0.0	0.0	0.0	11.8	83.8	95.7
24	0.200	0.0	0.0	0.0	4.4	36.4	40.7
24	0.500	0.0	0.0	0.0	1.1	10.4	11.5
24	1.000	0.0	0.0	0.0	0.4	3.8	4.2
24	2.000	0.0	0.0	0.0	0.1	1.4	1.5
24	5.000	0.0	0.0	0.0	0.0	0.4	0.4
24	10.000	0.0	0.0	0.0	0.0	0.1	0.1
				Fe^{+}			
25	0.001	0.0	0.0	0.0	0.4	0.0	0.4
25	0.002	0.0	0.0	0.0	17.2	0.0	17.2
25	0.005	0.0	0.0	0.0	72.4	1.7	74.0
25	0.010	0.0	0.0	0.0	65.4	34.9	100.2
25	0.020	0.0	0.0	0.0	36.9	95.1	132.0
25	0.050	0.0	0.0	0.0	12.4	81.9	94.3
25	0.100	0.0	0.0	0.0	4.8	43.6	48.4
25	0.200	0.0	0.0	0.0	1.8	18.9	20.7
25	0.500	0.0	0.0	0.0	0.5	5.4	5.9
25	1.000	0.0	0.0	0.0	0.2	2.0	2.2
25	2.000	0.0	0.0	0.0	0.1	0.7	0.8
25	5.000	0.0	0.0	0.0	0.0	0.2	0.2
25	10.000	0.0	0.0	0.0	0.0	0.1	0.1

3.3.9 References for 3.3

23Kra Kramers, H. A.: Philos. Mag. 46 (1923) 836

30Sto Stobbe, M.: Ann. Phys. (New York) 7 (1930) 661

43Bat Bates, D.R., Massey, H.S.W.: Philos. Trans. R. Soc. London A239 (1943) 269

59Sea Seaton, M.J.: Mon. Not. R. Astron. Soc. 119 (1959) 81

62Sea Seaton, M.J., in: At. Mol. Proc. (Bates, D.R., et al., eds.), New York: Academic Press (1962) p. 375

64Bur Burgess, A.: Mem. R. Astron. Soc. 69 (1964) 1-20

76Lee Lee, C.M., Pratt, R.H.: Phys. Rev. A14 (1976) 990

75Sea Seaton, M.J., in: Adv. At. Mol. Phys. (Bates, D.R., Bederson, B., eds.), New York: Academic Press, Vol. 11 (1975) pp. 83-142

76Sea Seaton, M.J., Storey, P.J., in: Atomic Processes and Applications (Burke, P.G., Moiseiwitsch, B.L., eds.), Amsterdam: North-Holland (1976) pp. 133-197

77Hah Hahn, Y., Rule, D.W.: J. Phys. B10 (1977) 2689

77Pos Post, D.E., et al.: At. Data Nucl. Data Tables 20 (1977) 397

80Dub Dubau, J., Volonte, S.: Rep. Prog. Phys. 43 (1980) 199-251

81Cow Cowan, R.D.: Theory of Atomic Structure and Spectra, Berkeley: Univ. Calif. Press (1981)

81LaG LaGattuta, K., Hahn, Y.: Phys. Rev. A24 (1981) 2273

82McL McLaughlin, D.J., Hahn, Y.: Phys. Lett. A88 (1982) 394

83Kim Kim, Y.S., Pratt, R.H.: Phys. Rev. A27 (1983) 2913

83LaG1 LaGattuta, K., Hahn, Y.: Phys. Rev. Lett. 50 (1983) 668-671

83LaG2 LaGattuta, K., Hahn, Y.: Phys. Rev. Lett. 51 (1983) 558

83Sea Seaton, M.J.: Rep. Prog. Phys. 46 (1983) 167-257

85Arn Arnaud, M., Rothenflug, R.: Astron. Astrophys. Suppl. 60 (1985) 425

85Hah Hahn, Y., in: Adv. At. Mol. Phys. (Bates, D.R., Bederson, B., eds.), New York: Academic Press, Vol. 21 (1985) pp. 123-196

87Jan Janev, R.K., Langer, W.D., Evans Jr., K., Post Jr., D.E.: Elementary Processes in Hydrogen-Helium Plasmas: Cross sections and reaction rate coefficients, Berlin: Springer-Verlag (1987)

87LaG LaGattuta, K., Nasser, I., Hahn, Y.: J. Phys. B20 (1987) 1577

88Hah Hahn, Y., LaGattuta, K.: Phys. Rep. Vol. 166, Amsterdam: North-Holland (1988) 195

89And Andersen, L.H., Hvelplund, P., Knudsen, H., Kvistgaard, P.: Phys. Rev. Lett. 62 (1989) 2656

90And Andersen, L.H., Bolko, J., Kvistgaard, P.: Phys. Rev. Lett. 64 (1990) 729

91Mul Muller, A., et al.: Phys. Scr. T37 (1991) 62

91McL McLaughlin, D.J., Hahn, Y.: Phys. Rev. A43 (1991) 1313; Errata: Phys. Rev. A45 (1992) 5317

92Arn Arnaud, M., Raymond, J.: Astrophys. J. 398 (1992) 394

92Bat Bates, D.R., in: Recombination of Atomic Ions (Graham, W.G., Fritsch, W., Hahn, Y., Tanis, J.A., eds.), NATO ASI Series B: Phys. Vol. 296, New York: Plenum (1992), p. 3

92Che Chen, M.H., in: Recombination of Atomic Ions (Graham, W.G., Fritsch, W., Hahn, Y., Tanis, J.A., eds.), NATO ASI Series B: Phys. Vol. 296, New York: Plenum (1992), p. 61

92Gra Graham, W.G., Fritsch, W., Hahn, Y., Tanis, J.A. (eds.): Recombination of Atomic Ions, NATO ASI Series B: Phys. Vol. 296, New York: Plenum (1992)

92Mul Muller, A., et al., in: Recombination of Atomic Ions, (Graham, W.G., Fritsch, W., Hahn, Y., Tanis, J.A., eds.), NATO ASI Series B: Phys. Vol. 296, New York: Plenum (1992) p. 155
92Oma1 Omar, G., Hahn, Y.: Z. Phys. D25 (1992) 41-46
92Oma2 Omar, G., Hahn, Y.: Z. Phys. D25 (1992) 31-39
92Pin Pindzola, M.S., Badnell, N.R.: Nucl. Fus. Suppl. 3 (1992) 101
92Rei Reisenfeld, D.B.: Astrophys. J. 398 (1992) 386
93Hah1 Hahn, Y.: J. Quant. Spectros. Radiat. Transfer 49 (1993) 81; Errata: J. Quant. Spectros. Radiat. Transfer 51 (1994) 663
93Hah2 Hahn, Y., Krstic, P.: J. Phys. B26 (1993) L297
92Krs Krstic, P., Hahn, Y.: Phys. Rev. A48 (1993) 4515
93Wol Wolf, A., Habs, D., Lampert, A., Neumann, R., Schramm, U., Schussler, T., Schwalm, D.: At. Phys. (H. Walther, et al., eds.), New York: American Institute of Physics, Vol. 13 (1993) p. 228
94Hah Hahn, Y., Krstic, P.: J. Phys. B27 (1994) L509
94Krs1 Krstic, P., Hahn, Y.: Phys. Rev. A50 (1994) 4629
94Krs2 Krstic, P., Hahn, Y.: Phys. Lett. A192 (1994) 47
95Gao Gao, H., DeWitt, D.R., Schuch, R., Zong, W., Asp, S., Pajek, M.: Phys. Rev. Lett. 75 (1995) 4381
95Hah Hahn, Y., in: Atomic and Molecular Processes in Fusion Edge Plasmas (Janev, R.K., ed.), New York: Plenum (1995) pp. 91-117.
95Jan Janev, R.K. (ed.): Atomic and Molecular Processes in Fusion Edge Plasmas, New York: Plenum (1995)
95Nah1 Nahar, S.N.: Astrophys. J. Suppl. 101 (1995) 423
95Nah2 Nahar, S.N., Pradhan, A.K.: Astrophys. J. 447 (1995) 966
96Hah Hahn, Y.: Computer program - the improved MTRX (unpublished)
96Krs Krstic, P., Hahn, Y.: J. Quant. Spectros. Radiat. Transfer 55 (1996) 499
97Hah1 Hahn, Y.: Phys. Lett. A231 (1997) 82-88
97Hah2 Hahn, Y.: Rep. Progr. Phys. 60 (1997) 691-759
97Nah Nahar, S.N., Pradhan, A.K.: Astrophys. J. Suppl. 111 (1997) 339
97Zer Zerrad, E., Hahn, Y.: J. Quant. Spectros. Radiat. Transfer (1997) 637
97Zha Zhang, H.L., Pradhan, A.K.: Phys. Rev. Lett. 78 (1997) 195
98Hah Hahn, Y.: (unpublished) 1998
98Oma Omar, G., Hahn, Y.: Phys. Rev. E62 (1998) 1
01Hah Hahn Y.: J. Phys. B Letters (to be published) (2001)
01Oma Omar, G., Hahn, Y.: Phys. Rev. E (to be published) (2001)

3.4 Electron detachment from negative ions

3.4.1 Introduction

Nowadays most of the elements, except for the rare gas atoms and a few others, in the periodic table are known to form negative ions. In Table 3.4.1 a list of typical negative ions, stable and metastable, is shown whose features such as the electron affinity, electronic configurations and terms are summarized [76Mas1, 82Smi1, 85Hot1, 95Blo1, 97And1].

Still only a limited number of the experimental and theoretical investigations have been performed for negative ions colliding with electrons. This is mostly due to the fact that the electron detachment from negative ions under electron impact has to be experimentally investigated through so-called crossed-beams techniques which need some advanced techniques such as the ultra-high vacuum system [67Dan1]. Theoretical studies even on the single-electron detachment processes are limited and practically no theoretical analysis for multiple-electron detachment has been reported. Only some empirical treatments of single- and double-electron detachment processes are available and found to reproduce reasonably well the observed cross sections.

Table 3.4.1. A list of the negative ions and their features (electronic configuration, term, electron affinity). The asterisks indicate the negative ions in the metastable state.

Z	Element	Negative ion			Z	Element	Negative ion		
		Config.	Term	Affinity [eV]			Config.	Term	Affinity [eV]
1	H	$1s^2$	^1S	0.75421	21	Sc	$3d4s^24p$	$^{1,3}D$	0.188
2	He	1s2s2p	^4P	0.0774*				$^{3,1}D$	0.041
3	Li	$[He]2s^2$	^1S	0.6180	22	Ti	$3d^34s^2$	^4F	0.079
4	Be	$2s2p^2$	^4P	≈ 0.26*	23	V	$3d^44s^2$	^5D	0.525
5	B	$2s^2p^2$	^3P	0.277	24	Cr	$3d^54s^2$	^6S	0.666
6	C	$2s^2p^3$	^4S	1.2629	25	Mn	non		< 0
			^2D	0.033	26	Fe	$3d^74s^2$	^4F	0.163
7	N	$2s^22p^4$	^3P	– 0.07	27	Co	$3d^84s^2$	^3F	0.661
8	O	$2s^22p^5$	^2P	1.46112	28	Ni	$3d^94s^2$	^2D	1.156
9	F	$2s^22p^6$	^1S	3.399	29	Cu	$3d^{10}4s^2$	^1S	1.228
10	Ne	non		< 0	30	Zn	$4s4p^2$	^4P	> 0*
11	Na	$[Ne]3s^2$	^1S	0.54793	31	Ga	$4s^24p^2$	^3P	0.30
12	Mg	$3s3p^2$	^4P	≈ 0.35*	32	Ge	$4s^24p^3$	^4S	1.2
13	Al	$3s^23p^2$	^3P	0.441				^2D	0.4
			^1D	0.109	33	As	$4s^24p^4$	^3P	0.81
14	Si	$3s^23p^3$	^4S	1.385	34	Se	$4s^24p^5$	^2P	2.02069
			^2D	0.523	35	Br	$4s^24p^6$	^1S	3.365
			^2P	0.029	36	Kr	non		
15	P	$3s^23p^4$	^3P	0.7465	37	Rb	$5s^2$	^1S	0.48592
16	S	$3s^23p^5$	^2P	2.07712	38	Sr	$5s5p^2$	^4P	– *
17	Cl	$3s^23p^6$	^1S	3.617	39	Y	$4d5s^25p$	^1D	0.307
18	Ar	$3p^54s4p$	^4S	> 0*				^3D	0.164
19	K	$[Ar]4s^2$	^1S	0.50147	40	Zr	$4d^35s^2$	^4F	0.426
20	Ca	$4s^24p$	^2P	0.018	41	Nb	$4d^45s^2$	^5D	0.893
		$4s4p^2$	^4P	– *	42	Mo	$4d^55s^2$	^6S	0.746

43	Tc	$4d^6 5s^2$	^5D	0.55	71	Lu	non		
44	Ru	$4d^7 5s^2$	^4F	1.05	72	Hf	$5d^3 6s^2$	^4F	
45	Rh	$4d^8 5s^2$	^3F	1.137	73	Ta	$5d^4 6s^2$	^5D	0.322
46	Pd	$4d^{10} 5s$	^2P	0.557	74	W	$5d^5 6s^2$	^6S	0.815
		$4d^9 5s^2$	^2D	0.421	75	Re	$5d^6 6s^2$	^4D	0.15
47	Ag	$4d^{10} 5s^2$	^1S	1.30	76	Os	$5d^7 6s^2$	^4F	1.1
48	Cd	$5s5p^2$	^4P	– *	77	Ir	$5d^8 6s^2$	^3F	1.565
49	In	$5p^2$	^3P	0.3	78	Pt	$5d^9 6s^2$	^2D	2.128
50	Sn	$5p^3$	^4S	1.2	79	Au	$5d^{10} 6s^2$	^1S	2.3086
			^2D	0.4	80	Hg	$6s6p^2$	^4P	– *
51	Sb	$5p^4$	^3P	1.07	81	Tl	$6p^2$	^3P	0.2
52	Te	$5p^5$	^2P	1.9708	82	Pb	$6p^3$	^4S	0.363
53	I	$5p^6$	^1S	3.0591	83	Bi	$6p^4$	^3P	0.946
54	Xe	non			84	Po	$6p^5$	^2P	1.9
55	Cs	$6s^2$	^1S	0.47163	85	At	$6p^6$	^1S	2.8
56	Ba	$6s6p^2$	^4P	– *					
57	La	$5d^2 6s^2$	^3F	0.5					

3.4.2 Electron detachment cross sections

3.4.2.1 Negative hydrogen ions

Among various negative ions, the collision processes of the simplest negative hydrogen ions, $H^-(1s,1s')$, have been investigated relatively well. The cross sections for the single- and double-electron detachment from H^- ions into continuum under electron impact

$$e + H^- \rightarrow e + H^0 + e \quad (1)$$

$$e + H^- \rightarrow e + H^+ + 2e \quad (2)$$

have been measured. The observed single-electron detachment cross sections of the outer 1s' electron with the binding energy of 0.75 eV seem to be in a reasonable agreement with each other [67Dan1, 68Tis1, 70Pea1]. The cross sections near the threshold region have carefully been measured in details [95And1, 96Vej1] using the H^- ion beam colliding with a cooler electron beam in a storage ring (see Section 3.2). In contrast to those observed previously [73Pea1], no resonance formation of the doubly charged negative hydrogen ions, resulting in the production of neutral hydrogen atoms via two-electron emission, has been observed. The cross sections evaluated by the present author are shown in Fig. 3.4.1 as a function of the electron impact energy and the numerical data of the recommended cross sections are given in Table 3.4.2 which also includes those for other negative ions.

From Fig. 3.4.1, it is easily noted that the cross sections for single-electron detachment processes, plotted as a function of the electron impact energy, are much wider than those in double-electron detachment as well as in neutral atoms and positive ions (see Sections 2.6 and 3.2). This feature has never been discussed in detail so far. But it can be due to the fact that the low energy (< 10 eV in particular) incident electrons near the threshold energy region are significantly deflected away from the target electrons and, therefore, the cross sections near the threshold of the electron detachment from negative ions are drastically reduced. As the electron energy increases, this deflection becomes small. Then, the behavior at higher energies shows the trends similar to those in single-electron ionization from neutral atoms and positive ions. Thus, the combined features are expected to show the observed wider energy dependence in the single-electron detachment from the negative ions [98She1]. Similar features are also observed in other negative ions (see Subsect. 3.4.2.2).

On the other hand, it should also be noted that the single-electron detachment cross sections at higher energy electron impact seem to be in good agreement with those in proton impact over 80 keV/amu, which velocity is equivalent to 40 eV electrons, indicating that the (at least single-) electron detachment cross sections are in principle independent of the sign of the (singly charged) projectile charge, either positive or negative, as well as of its mass at higher impact energies [76Pea1].

Some theoretical treatments have been also reported for the single-electron detachment from H^- ions [96Bel1, 96Kaz1, 96Lin1, 96Pin1]. Recent calculations based upon the close-coupling theory, taking into account the Coulomb repulsive trajectory of the incident electrons, result in good agreement with the observed data even near the threshold energies [96Lin1].

Serious discrepancies still exist in the observed double-electron detachment cross sections even at relatively high energies [82Def1, 92Yu1]. No reasons have been known in such discrepancies as well as in some structures observed at 200 eV. So far no theoretical analysis of the double-electron detachment has been reported. An empirical formula in estimating the double-electron detachment cross sections has been proposed and found to be able to reproduce reasonably the observed data at high energies [97Bél1] (see Subsect. 3.4.4).

It is noted in Fig. 3.4.1 that the electron impact energy dependence at higher electron energies is only slightly different in both the single- and double-electron detachment cross sections, suggesting strong inter-correlation between the two electrons in H^- ions. This is in sharp contrast with the simple expectation of the independent electron model where the double-electron detachment cross sections decrease much faster than those for the single-electron detachment as the incident electron energy increases.

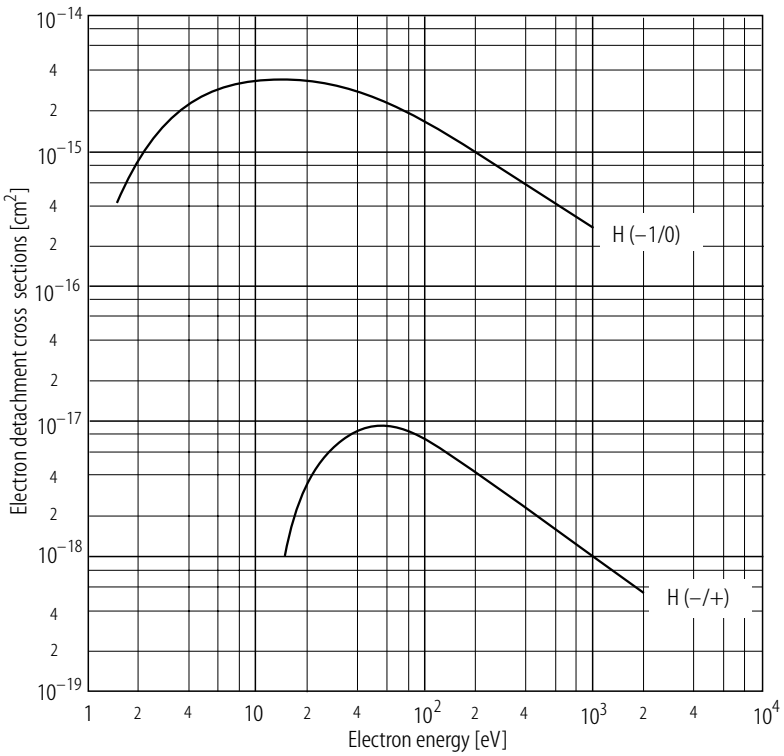

Fig. 3.4.1. Recommended single- and double-electron detachment cross sections from H^- ions under electron impact as a function of the electron energy.

Table 3.4.2. Recommended cross sections for single- and double-electron detachment from negative ions (H^-, C^-, O^- and F^-) by electron impact as a function of the electron energy. H(–/0) and H(–/+), for example, represent the single- and double-electron detachment from negative hydrogen ions resulting in neutral and positive (singly charged) particles, respectively.

Energy [eV]	Cross section [cm^2]							
	H(–1/0)	C(–/0)	O(–/0)	F(–/0)	H(–/+)	C(–/+)	O(–/+)	F(–/+)
1.50	4.30E-16							
2.00	8.40E-16		2.40E-17					
2.50	1.30E-15		6.80E-17					
3.00	1.75E-15		1.02E-16					
4.00	2.35E-15		1.75E-16					
5.00	2.70E-15		2.30E-16					
6.00	3.00E-15		2.85E-16					
8.00	3.25E-15		3.80E-16					
10.00	3.45E-15	1.82E-15	4.45E-16					
15.00	3.50E-15	1.85E-15	5.40E-16	1.30E-16	1.00E-18	4.20E-18	2.70E-19	5.00E-19
20.00	3.45E-15	1.83E-15	5.85E-16	1.75E-16	3.10E-18	1.10E-17	1.75E-18	1.78E-18
25.00	3.35E-15	1.75E-15	6.13E-16	2.05E-16	5.50E-18	2.85E-17	6.50E-18	4.10E-18
30.00	3.25E-15	1.68E-15	6.20E-16	2.30E-16	6.80E-18	3.80E-17	1.02E-17	6.75E-18
35.00	3.05E-15	1.61E-15	6.20E-16	2.50E-16	8.00E-18	5.20E-17	1.76E-17	9.60E-18
40.00	2.90E-15	1.55E-15	6.15E-16	2.60E-16	8.76E-18	5.95E-17	2.35E-17	1.23E-17
50.00	2.55E-15	1.39E-15	6.00E-16	2.70E-16	9.45E-18	7.20E-17	3.30E-17	1.76E-17
60.00	2.35E-15	1.29E-15	5.75E-16	2.75E-16	9.45E-18	7.90E-17	4.05E-17	2.12E-17
80.00	1.95E-15	1.10E-15	5.30E-16	2.72E-16	8.75E-18	7.80E-17	4.85E-17	2.60E-17
100.00	1.70E-15	9.70E-16	4.85E-16	2.65E-16	7.60E-18	7.25E-17	5.20E-17	2.70E-17
150.00	1.25E-15	7.60E-16	4.10E-16	2.35E-16	5.45E-18	5.90E-17	5.20E-17	2.55E-17
200.00	9.90E-16	6.25E-16	3.45E-16	2.05E-16	4.40E-18	4.80E-17	4.80E-17	2.35E-17
300.00	7.20E-16	4.65E-16	2.60E-16	1.65E-16	3.05E-18	3.35E-17	3.85E-17	2.01E-17
400.00	5.65E-16	3.65E-16	2.15E-16	1.35E-16	2.35E-18	2.65E-17	3.20E-17	1.65E-17
600.00	4.25E-16	2.60E-16	1.62E-16	1.05E-16	1.65E-18	1.75E-17	2.35E-17	1.30E-17
800.00	3.35E-16	2.05E-16	1.30E-16	8.50E-17	1.25E-18	1.35E-17	1.90E-17	1.10E-17
1000.00	2.85E-16	1.70E-16	1.12E-16	7.30E-17	1.02E-18	1.10E-17	1.60E-17	9.70E-18
2000.00					5.70E-19	5.80E-18	9.00E-18	
3000.00						4.00E-18	6.20E-18	

3.4.2.2 Heavier negative ions

There are a limited number of the investigations for heavy negative ions colliding with electrons. The single-electron detachment cross sections have been reported for negative ions (C^-, O^-, F^-) and found to generally decrease as the electron affinity of the negative ions (see Table 3.4.1) increases (see Fig. 3.4.2) [68Tis1, 79Pea1, 79Pea2].

Here those for H^- ions are again shown for comparison. Most of the cross sections observed in the single-electron detachment are in a reasonably good agreement with each other. The most recent observation of the single-electron detachment from O^- ions has been performed near the threshold energy region using a storage ring [70Pea1, 95And1] which has been found to be well reproduced theoretically [96Pin1]. The recommended cross sections of the single- and double-electron detachment from these negative ions are also given in Table 3.4.2.

But the observed double-electron detachment cross sections [93Def1, 95Ste1, 95Bél1] are still in some disagreement among the experiments, particularly at low electron energy region. The general trend indicates that the double-electron detachment cross sections decrease, especially near the threshold region, as the total binding energy required to detach two-electrons increases (12.5, 15.1 and 20.8 eV for C^-, O^- and F^- ions, respectively) (see Fig. 3.4.3). Also those for H^- ions are included for comparison. Note that the number of so-called innershell electrons is significantly different among H^- and other negative ions (C^-, O^- and F^-). However, it is easily noted that the electron impact energy dependence is the same at higher impact energy which can be represented with the well-known form of $(\ln E)/E$ where E is the incident electron energy.

So far no experimental as well as theoretical investigations of the multiple (more than three-electron) detachment processes have been reported yet, though such multiple-electron detachment processes colliding with gases at high energy (MeV) region are well known in applications to tandem accelerators for a long time. Only an empirical formula for the double-electron detachment has been proposed and found to reproduce the observed data within a factor of two for these heavy negative ions [97Bél1].

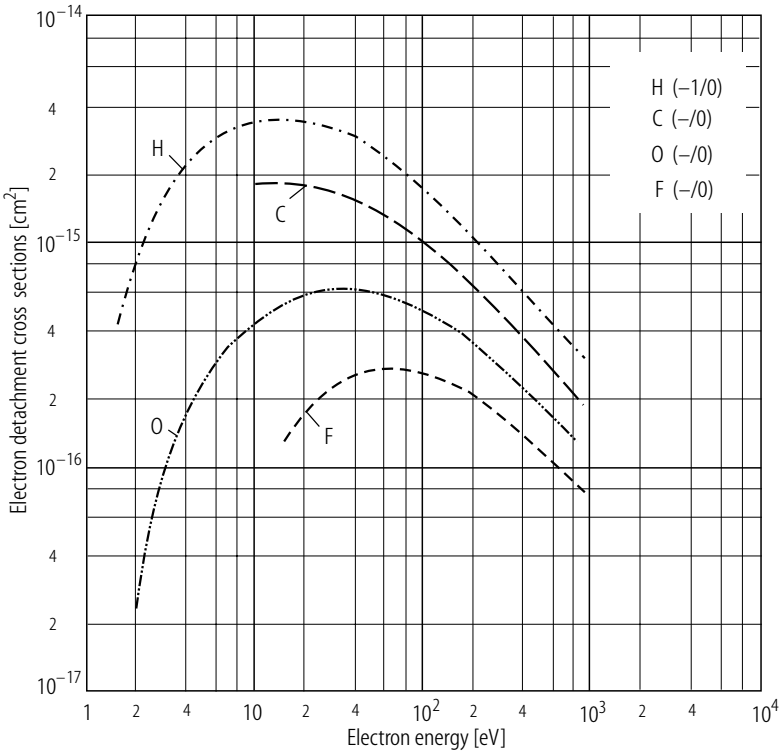

Fig. 3.4.2. Recommended cross sections for single-electron detachment from C^-, O^- and F^- ions under electron impact as a function of the electron impact energy. Those for H^- ions are also included for comparison.

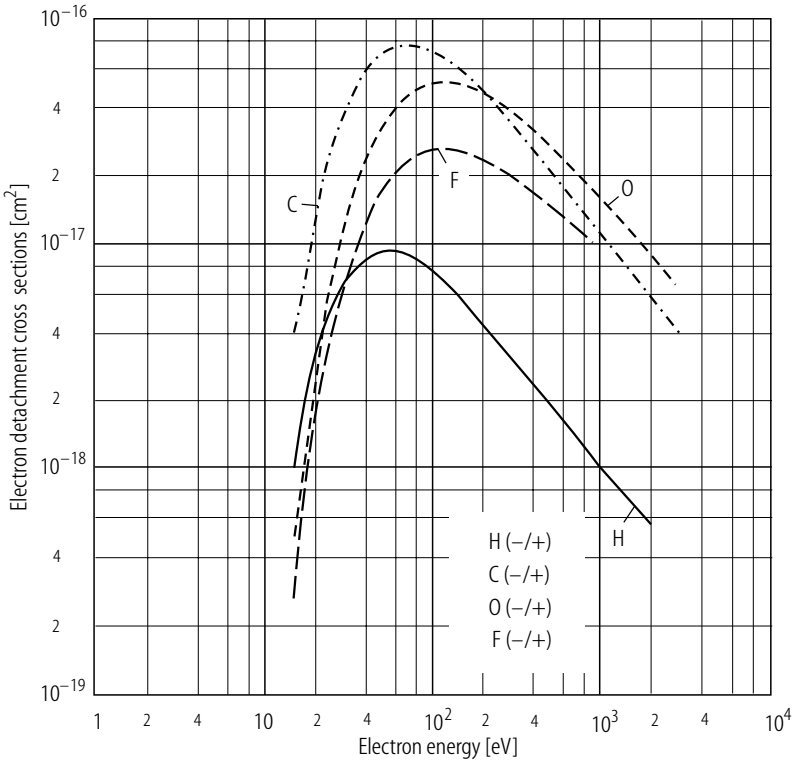

Fig. 3.4.3. Recommended cross sections for double-electron detachment from C^-, O^- and F^- ions under electron impact as a function of the electron impact energy. Those for H^- ions are also included.

3.4.3 Theoretical treatments

3.4.3.1 Single-electron detachment

Theoretically the single-electron detachment can be treated as ionization process. Indeed the quantum-mechanical distorted-wave calculations for the single-electron detachment cross sections have recently been performed based upon the direct ionization theories [96Pin1]. The calculated results with the exchange effect for $1s1s'\ ^1S \rightarrow 1s\ ^2S$ ionization of H^- ions resulting in forming the ground state atomic hydrogen atoms have been shown to be very sensitive to the choice of the polarization potential which reduces the cross sections by roughly 40 % in the electron detachment from H^- ions near the threshold. The calculated results are roughly 30 % larger than those obtained through storage ring experiments.

Similar calculations have been extended to the single-electron detachment from O^- ions where the calculated results show that the $2p^5\ ^2P \rightarrow 2p^4\ ^3P$ ionization process is found to be far dominant (roughly 65 %) over other processes such as $2p^5\ ^2P \rightarrow 2p^4\ ^1D$ (30 %) and $2p^5\ ^2P \rightarrow 2p^4\ ^1S$ (5 %) processes, indicating that the single-electron detachment from O^- ions results mostly in the formation of the ground state O atoms. The calculated total single-electron detachment cross sections near the threshold are found to be in good agreement with the results observed in the storage ring experiment [96Vej1].

3.4.3.2 Double-electron detachment

So far no critical analysis of the double-electron detachment from negative ions colliding with electrons has been reported. Indeed it is known that the strong electron-electron correlation plays a significant role in the double-electron detachment and, therefore, rigorous treatments are crucial in understanding the double electron processes in H^- ion collisions with electrons.

3.4.4 Empirical formulas for electron detachment

3.4.4.1 Single-electron detachment

So far no empirical formulas for estimating the single-electron detachment cross sections have been proposed. The following empirical formula can be used for single-electron detachment cross section, σ_1, and are found to reproduce the observed results within a factor of two, though the discrepancy becomes significantly large at low impact energy (in units of 10^{-18} cm^2) [98She1]:

$$\sigma_1 = \frac{200}{I_1^2}\left(\frac{u}{u+7.8}\right)^{2.0}\frac{\ln(u+1)}{u+1} \tag{3}$$

where I_1 represents the minimal ionization energy (in Rydberg units) required to remove the outermost electron from the negative ion and the reduced electron energy $u = (E/I_1) - 1$, E being the incident electron energy in Rydberg units.

3.4.4.2 Double-electron detachment

Only the following empirical treatment, which has been applied successfully to the double-electron detachment, can provide the important understanding of the double-electron detachment from negative ions (in units of 10^{-18} cm^2) [97Bél1]:

$$\sigma_2 = \frac{14.0N^{1.08}}{I_2^2}\left(\frac{u}{u+1}\right)^{0.75}\frac{\ln(u+1)}{u+1} \tag{4}$$

where N represents the number of target electrons, I_2 the minimal ionization energy (in Rydberg units) required to remove two outermost electrons from the negative ions and the reduced electron energy $u = (E/I_2) - 1$, E being the incident electron energy in Rydberg units.

As seen in Fig. 3.4.4, the agreement seems to be only qualitative, though the tendencies at higher impact energies seem to show an agreement between the observation and the empirical formula [97Bél1].

3.4.5 Resonance states in electron detachment under electron impact

Some measurements had indicated the possibility of the resonance state formed through the triply excited H^{2-} ($nln'l'n''l''$) state in the single electron detachment in e + H^- collisions [73Pea1] which was seen in the resonance-like enhancement of the single electron detachment. Recent detailed experiments at the storage ring facility have confirmed that there is no such resonance state of the formation of H^{2-} ions in e + H^- collisions [95And1, 96Tan1]. Resonances have been observed in negative molecular ions such as C_2^-, B_2^-, BN^- and O_2^- ions colliding with slow electrons. These phenomena, though interesting themselves, seem to be outside the present scope. The readers should refer the references [96And1, 96And2, 97Ped1].

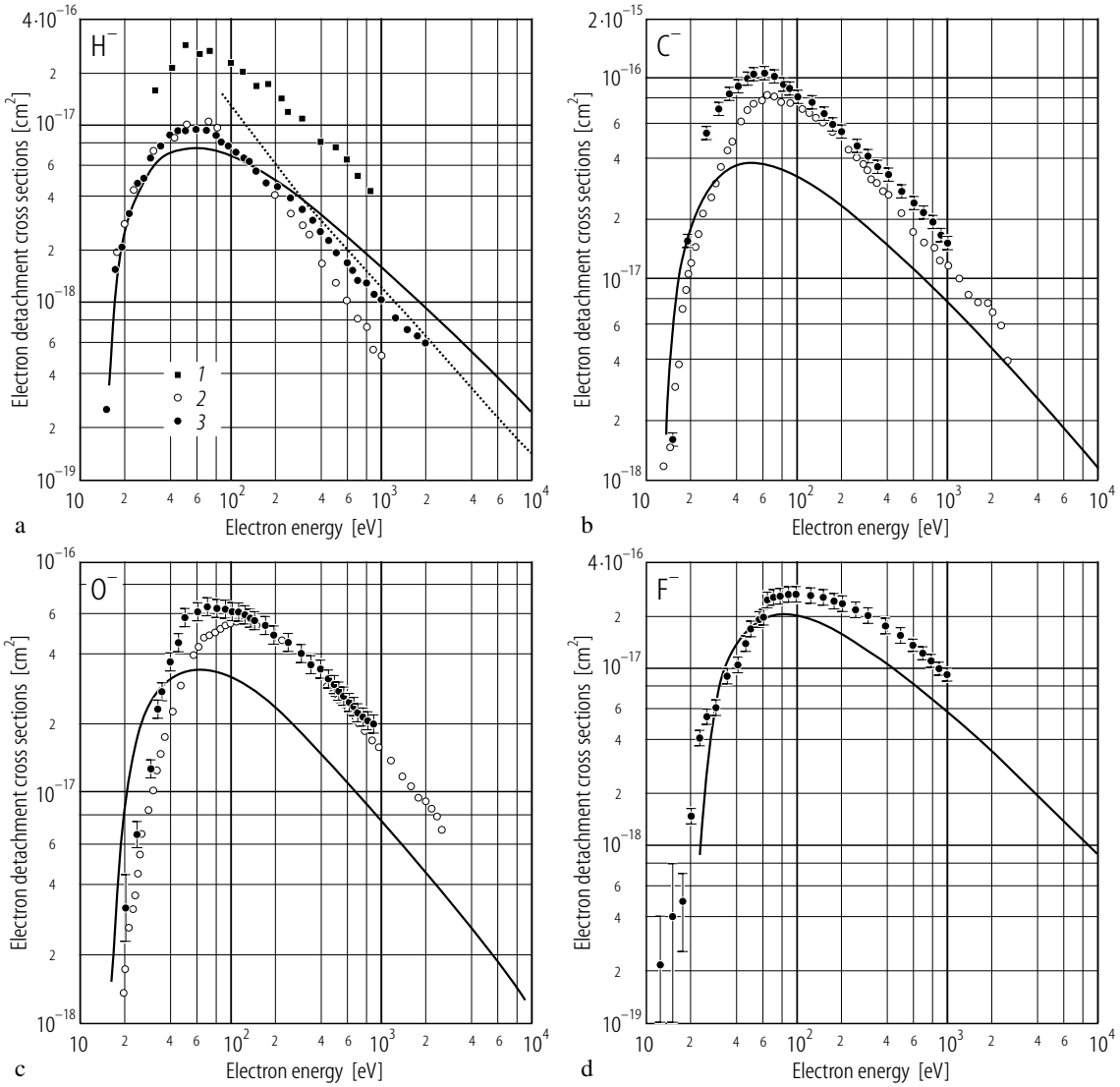

Fig. 3.4.4. Comparison of the observed double-electron detachment cross sections from (**a**) H^-, (**b**) C^-, (**c**) O^- and (**d**) F^- ions with the empirical formula (4). (**a**): *1* [71Pea1], *2* [82Def1], *3* [92Yu1]; (**b**) – (**d**): solid circles [95Ste1], open circles [95Bél1], dotted curve asymptotic.

3.4.6 References for 3.4

67Dan1 Dance, D.F., Harrison, M.F.A., Rundel, R.D.: Proc. R. Soc. A **299** (1967) 525.

68Tis1 Tisone, G.C., Branscomb, L.M.: Phys. Rev. **170** (1968) 169.

69Bel1 Belly, O., Schwartz, S.B.: J. Phys. B **2** (1969) 159.

70Pea1 Peart, B., Walton, D.S., Dolder, K.T.: J. Phys. B **3** (1970) 1346.

73Pea1 Peart, B., Dolder, K.T.: J. Phys. B **6** (1973) 1497.

76Mas1 Massey, H.: Negative ions, Cambridge: University Press 1976.

76Pea1 Peart, B., Forrest, R., Dolder, K.T.: J. Phys. B **9** (1976) 3047.

79Pea1 Peart, B., Forrest, R., Dolder, K.T.: J. Phys. B **12** (1979) 847.

79Pea2 Peart, B., Forrest, R., Dolder, K.T.: J. Phys. B **12** (1979) L115.

82Def1 Defrance, P., Claeys, W., Brouillard, F.: J. Phys. B **15** (1982) 3509.

82Smi1 Smirnov, B.M.: Negative ions, New York, London: McGraw-Hill 1982.

85Hot1 Hotop, H., Lineberger, W.C.: J. Phys. Chem. Ref. Data **14** (1985) 731.

92Yu1 Yu, D.J., Rachafi, S., Jureta J., Defrance, P.: J. Phys. B **25** (1992) 4593.

93Def1 Defrance, P., Yu, D.J., Belic, D., in: Abstract of XVIII-th International Conference on Physics of Electronic and Atomic Collisions (Andersen, T., Fastrup, B., Folkmann, F., Knudsen, H., Andersen, N., eds.), New York: AIP (1993), p. 370.

95And1 Andersen, L.H., Mathur, D., Schmidt, H.T., Vejby-Christensen, L.: Phys. Rev. Lett. **74** (1995) 892.

95Bél1 Bélenger, C., Yu, D.J., Defrance, P.: unpublished (1995).

95Blo1 Blondel, C.: Phys. Scr. T **58** (1995) 31.

95Ste1 Steidl, M. Hathiramani, D., Hofmann, G., Stenke, M. Völpel, R. Salzborn, E., in: Abstract of XIX-th International Conference on Physics of Electronic and Atomic Collisions (Mitchell, J.B.A., McConkey, J.W., Brion, C.E., eds.), (1995), p.564.

96And1 Andersen, L.H.: Comm. At. Mol. Phys. **33** (1996) 111.

96And2 Andersen, L.H., Hvelplund, P., Kella, D., Mokler, P.H., Pedersen, H.B., Schmidt H.T., Vejby-Christensen, L.: J. Phys. B **29** (1996) .

96Kaz1 Kazansky, A.K., Taulbjerg, K.: J. Phys. B **29** (1996) 4465.

96Lin1 Lin, J.T., Jiang, T.F., Lin, C.D.: J. Phys. B **29** (1996) 6175.

96Pin1 Pindzola, M.S.: Phys. Rev. A **54** (1996) 3671.

96Tan1 Tanabe, T., Katayama, I., Kamegaya, H., Chida, K., Watanabe, T. Araki, Y., Yoshizawa, M., Haruyama, Y., Saito, M., Honma, T., Hosono, K., Hatanaka, K., Noda, K.: Phys. Rev. A **54** (1996) 4069.

96Vej1 Vejby-Christensen, L. Kella, D., Petersen, H.B., Schmidt, H.T., Andersen, L.H.: Phys. Rev. A **53** (1996) 2371.

97And1 Andersen, T., Andersen, H.H., Balling, P., Kristensen, P., Petrunin, V.V.: J. Phys. B **30** (1997) 3317.

97Bél1 Bélenger, C.B., Defrance, P., Salzborn, E., Shevelko, V.P., Tawara H., Usko, D.B.: J. Phys. B **30** (1997) 2667.

97Ped1 Pedersen, H.B., Jensen, M.J., Kella, D., Schmidt, H.T., Vejby-Christensen, L., Andersen, L.H., in: Abstract of XX-th International Conference on Physics of Electronic and Atomic Collisions (Aumayer, F., Winter, H.P., eds.), (1997), p. MO165.

98She1 Shevelko, V.P., Tawara, H.: private communication 1998.